

Geology and Gold Mineralization of the Gold Basin-Lost Basin Mining Districts, Mohave County, Arizona

U.S. GEOLOGICAL SURVEY PROFESSIONAL PAPER 1361



**GEOLOGY AND GOLD MINERALIZATION OF THE
GOLD BASIN-LOST BASIN MINING DISTRICTS,
MOHAVE COUNTY, ARIZONA**



Placer gold nugget about 1 cm wide showing gold molded partly against rounded fragment of clear vein quartz. Collected from King Tut placer workings, Lost Basin mining district.

Geology and Gold Mineralization of the Gold Basin-Lost Basin Mining Districts, Mohave County, Arizona

By TED G. THEODORE, WILL N. BLAIR, *and* J. THOMAS NASH

With a section on K-AR CHRONOLOGY OF MINERALIZATION AND
IGNEOUS ACTIVITY

By EDWIN H. McKEE

and a section on IMPLICATIONS OF THE COMPOSITIONS OF LODGE
AND PLACER GOLD

By J.C. ANTWEILER *and* W.L. CAMPBELL

U.S. GEOLOGICAL SURVEY PROFESSIONAL PAPER 1361



UNITED STATES GOVERNMENT PRINTING OFFICE, WASHINGTON : 1987

DEPARTMENT OF THE INTERIOR

DONALD PAUL HODEL, *Secretary*

U.S. GEOLOGICAL SURVEY

Dallas L. Peck, *Director*

Library of Congress Cataloging-in-Publication Data

Theodore, Ted G.

Geology and gold mineralization of the Gold Basin-Lost Basin mining districts, Mohave County, Arizona.

(U.S. Geological Survey Professional Paper 1361)

Bibliography

Supt. of Docs. No.: I 19.16:1361

1. Geology—Arizona—Mohave County. 2. Gold ores—Arizona—Mohave County. I. Blair, Will N. II. Nash, J. Thomas (John Thomas), 1941— . III. Title. IV. Series: Geological Survey Professional Paper 1361. V. Title: Gold Basin-Lost Basin mining districts, Mohave County, Arizona.

QE86.M63T48 1987

557.91'59

87-600286

**For sale by the Books and Open-File Reports Section,
U.S. Geological Survey, Federal Center, Box 25425, Denver, CO 80225**

CONTENTS

	Page		Page
Abstract	1	Gold deposits and occurrences	70
Introduction	1	Proterozoic veins	71
Acknowledgments	2	Late Cretaceous and (or) early Tertiary veins	74
History of mining activity	3	Disseminated gold in episyenite	82
General geology of the districts	9	Petrography	84
K-Ar chronology of mineralization and igneous activity,		Paragenetic relations of gold	87
by Edwin H. McKee	14	Chemistry	88
Cretaceous plutonic rocks	15	Discussion	91
Cretaceous veins	15	Veins along the Miocene detachment fault	93
Proterozoic(?) vein	16	Placer gold deposits	93
Tertiary volcanic rocks	17	Implications of the compositions of lode and placer gold,	
Petrochemistry of crystalline rocks and their relation to		by J.C. Antweiler and W.L. Campbell	100
mineralization	18	Introduction	100
Pelitic metamorphic rocks	20	Variations in gold composition	101
Muscovite-biotite schist	21	Comparison of composition of placer gold in Lost Basin	
Tourmaline schist and gneiss	23	with that of possible lode sources	103
Almandine-biotite ± staurolite schist and gneiss	25	Composition of lode gold from the Lost Basin district	105
Kyanite-bearing gneiss	27	Composition of gold from mines in Gold Basin	105
Sillimanite- and cordierite-bearing gneiss and schist	29	Similarity of signatures of gold samples from some	
Petrogenetic implications of mineral relations	32	localities in the districts to that of gold samples from	
Quartzofeldspathic gneiss	33	some porphyry copper deposits	105
Amphibolite	35	Fluid-inclusion studies	108
Metachert, banded iron formation, and metarhyolite	43	Types of fluid inclusions	109
Marble, calc-silicate marble, and skarn	44	Homogenization temperatures and salinities	111
Proterozoic igneous and metaigneous rocks	46	Fluid inclusions in the episyenitic alteration pipes	
Leucogranite	47	containing disseminated gold	115
Gneissic granodiorite	48	Fluid inclusions in a quartz-fluorite-white mica vein that	
Feldspathic gneiss	49	cuts the Late Cretaceous two-mica monzogranite	117
Biotite monzogranite	49	Comparison of fluids in a quartz-fluorite-white mica vein	
Leucocratic monzogranite	50	and in gold-bearing episyenitic pipes	120
Porphyritic monzogranite of Garnet Mountain	51	Estimates of the pressure-temperature environment of	
Granodiorite	60	mineralization	120
Diabase	61	Discussion	122
Cretaceous crystalline rocks	61	Suggestions for exploratory programs	125
Two-mica monzogranite	61	References	126
Episyenite	69		

ILLUSTRATIONS

	Page
FRONTISPIECE. Placer gold nugget about 1 cm wide showing gold molded partly against rounded fragment of clear vein quartz.	
PLATE 1. Localities for commodities and compositional analyses in the Gold Basin-Lost Basin mining districts	In pocket
FIGURE 1. Index map showing area of study	2
2. Sketch map of area of Gold Basin-Lost Basin mining districts showing geology, major mines credited with production of metal(s), known occurrences of gold, and major placer workings	4
3. Schematic east-west cross sections showing inferred geologic relations	8
4. Scanning electron micrograph and X-ray spectra of an unknown mineral	17
5. Photographs showing typical exposures of paragenetic sequences	19
6. Photograph showing coarse-grained quartz-feldspar leucogranite crosscutting schistosity in amphibolite and filling fracture opened between blocks of amphibolite	20
7. Chart of inferred mineral changes and corresponding metamorphic facies in pelitic rocks from the Early Proterozoic gneiss terrane	21
8. Photograph of laminated muscovite-biotite-quartz schist showing fabric composed of three distinct s surfaces reflecting three superposed deformations	21

	Page
FIGURES 9-14. Photomicrographs showing:	
9. Schist containing relatively abundant concentrations of muscovite and (or) biotite - - - - -	22
10. Structural and textural relations of tourmaline in metamorphic rocks- - - - -	25
11. Textural relations among minerals in garnet-bearing gneiss - - - - -	26
12. Textural relations of kyanite - - - - -	28
13. Textural relations of sillimanite - - - - -	30
14. Textural relations of cordierite - - - - -	32
15. Thompson (1957) AFM diagrams for medium-pressure progressive metamorphism- - - - -	33
16. Equilibrium curves generated from thermodynamic data- - - - -	34
17. Graph showing plot of SiO ₂ versus CaO in four samples of quartzofeldspathic gneiss - - - - -	35
18. Photomicrographs of structure and textures in amphibolite - - - - -	36
19-21. Graphs showing:	
19. Niggli 100 <i>mg, c</i> , and <i>al-alk</i> values for amphibolite, diabase, and pyroxene-banded gneiss - - - - -	41
20. Niggli <i>c</i> versus <i>mg</i> values for amphibolite, diabase, and pyroxene-banded gneiss - - - - -	42
21. Niggli <i>c</i> versus <i>al-alk</i> values for amphibolite, diabase, and pyroxene-banded gneiss - - - - -	42
22. Photomicrograph of oxide facies, banded iron formation - - - - -	44
23. Schematic diagram of sequence of mineral assemblages developed in zones near the contact between medium-grained schist and fine-grained calc-silicate rock - - - - -	46
24. Ternary diagram showing modes of Proterozoic igneous and metagneous rocks- - - - -	47
25. Photographs of porphyritic monzogranite of Garnet Mountain - - - - -	53
26. Photomicrographs showing textural relations in gneiss immediately adjacent to porphyritic monzogranite and in porphyritic monzogranite itself- - - - -	54
27. Graph showing fluorine and cerium contents versus differentiation index of analyzed samples of Early Proterozoic porphyritic monzogranite of Garnet Mountain and Early Proterozoic biotite monzogranite - - - -	57
28. Graph showing total alkalis and CaO plotted against weight percent SiO ₂ for analyzed samples of Early Proterozoic porphyritic monzogranite and Early Proterozoic biotite monzogranite - - - - -	58
29. Ternary chemical and normative diagrams of analyzed Early Proterozoic porphyritic monzogranite and biotite monzogranite- - - - -	59
30. Photomicrographs showing textural relations in Early Proterozoic granodiorite border phase of the porphyritic monzogranite of Garnet Mountain - - - - -	60
31. Map showing occurrences of Phanerozoic muscovite-bearing plutonic rocks in Western United States - - - - -	62
32. Photograph of Tertiary(?) composite, partly chloritized, porphyritic biotite dacite dike containing septum of Cretaceous two-mica monzogranite- - - - -	63
33. Ternary diagram showing modes of Cretaceous two-mica monzogranite - - - - -	64
34. Photomicrographs showing textural relations in Cretaceous two-mica monzogranite - - - - -	65
35-37. Graphs showing:	
35. Ratio of Al ₂ O ₃ : (K ₂ O + Na ₂ O + CaO) versus SiO ₂ from a Cretaceous two-mica monzogranite - - - - -	68
36. Na ₂ O plus K ₂ O versus Al ₂ O ₃ from a Cretaceous two-mica monzogranite - - - - -	68
37. Normative corundum versus SiO ₂ from a Cretaceous two-mica monzogranite - - - - -	69
38. Ternary diagram showing normative proportion of albite, orthoclase, and quartz in Cretaceous two-mica monzogranite- - - - -	69
39. Map showing areas reported to contain gold mineralization in the general area of the Black Mountains volcanic province of Liggett and Childs (1977) - - - - -	71
40. Photographs showing microscopic and megascopic relations in apparently Proterozoic veins- - - - -	72
41. Scanning electron micrographs showing relations of gold in apparently Proterozoic veins at locality 735 in the Senator Mountain 15-minute quadrangle - - - - -	73
42. Photographs of selected mine workings, quartz veins, and quartz-cored pegmatite- - - - -	74
43. Equal-area projection showing orientation of poles to veins - - - - -	75
44. Photographs showing typical veins- - - - -	76
45. Photomicrographs showing relations between quartz-ferroan calcite veins and sericitically altered Proterozoic granitic gneiss - - - - -	77
46. Scanning electron micrographs of lode gold collected from Golden Gate mine - - - - -	78
47. Diagrammatic summary of alteration surrounding typical feldspar-stage vein including albite-quartz-calcite-barite-pyrite-gold composite assemblage - - - - -	80
48. AKFC diagram showing mineral assemblages in altered wall rock adjacent to typical feldspar-bearing vein - - - -	80
49. Schematic stability relations among minerals as function of (Mg ²⁺)/(2H ⁺) and (K ⁺)/(H ⁺) cation activity ratios in coexisting fluid- - - - -	81
50. Geologic sketch map of immediate vicinity of occurrence of visible disseminated gold - - - - -	83
51. Photographs of gold-bearing episyenitic rock- - - - -	84
52. Graph showing variation in volume percent of potassium feldspar and quartz along section line A-A' of figure 50 - - - - -	84
53. Photomicrographs and scanning electron micrograph of mineralogic relations in episyenitic rock - - - - -	86
54. Scanning electron micrographs showing gold disseminated in episyenitic rock - - - - -	88
55. Photomicrographs of coarse-grained episyenite containing visible gold- - - - -	89

	Page
FIGURE 56. Photomicrograph showing morphology of intergrown fluorite and gold -----	89
57. Plot showing normative potassium feldspar, normative albite, and normative quartz in analyzed samples of Late Cretaceous and (or) early Tertiary episyenite, contact zone of the episyenite, and sample of Early Proterozoic biotite monzogranite -----	91
58-60. Photographs showing:	
58. Relations along Miocene detachment fault in general area of Cyclopic mine -----	94
59. Placer gold from Lost Basin mining district -----	95
60. Small, hand-operated dry washer -----	95
61. Scanning electron micrographs of placer gold nuggets -----	96
62. Photograph of relatively large placer gold nugget from Lost Basin mining district -----	97
63. Scanning electron micrographs of silver-gold relations in placer gold nugget obtained from northern part of Lost Basin mining district -----	97
64. Graphs of weight percent silver versus number of gold occurrences -----	104
65. Graphs of mean fineness versus number of gold occurrences in lode and placer gold -----	104
66. Photomicrograph and scanning electron micrographs showing relations among liquid carbon dioxide-bearing fluid inclusions -----	112
67. Photomicrographs showing relations among liquid carbon dioxide-bearing fluid inclusions -----	113
68. Graph of fluid-inclusion homogenization temperature and salinity data for various precious- and base-metal districts and deposits -----	115
69. Photomicrographs of fluid inclusions in samples from gold-bearing episyenitic rock -----	116
70-72. Histograms showing:	
70. Salinities of primary and pseudosecondary and secondary fluid inclusions in fluorite from gold-bearing episyenitic rocks -----	118
71. Filling temperatures in fluorite from gold-bearing episyenitic rocks -----	118
72. Salinity and filling-temperature data obtained from selected quartz-fluorite-white mica vein -----	119
73. Schematic cross sections showing inferred relations among Early Proterozoic mafic and ultramafic rocks, Late Cretaceous two-mica monzogranite, fluids evolved from monzogranite, and episyenite -----	123

TABLES

	Page
TABLE 1. Descriptions of gold-quartz mills in the Gold Basin-Lost Basin mining districts -----	10
2. Production of gold, silver, copper, and lead from lode deposits in the Gold Basin and Lost Basin mining districts, 1901-42 -----	11
3. K-Ar analytical data and ages -----	15
4. Chemical analyses of selected schist and gneiss from the Gold Basin-Lost Basin mining districts compared with analyses of slate, argillite, shale, graywacke, and arkose -----	24
5. Composite assemblages in sillimanite- and cordierite-bearing gneiss and schist in the Early Proterozoic metamorphic rocks in the general area of the Gold Basin-Lost Basin mining districts -----	29
6. Composite mineral assemblages in amphibolite and altered amphibolite from the Gold Basin-Lost Basin mining districts -----	38
7. Analyses of mafic rocks from the Early Proterozoic terrane in the Gold Basin-Lost Basin mining districts -----	39
8. Analyses for minor metals in selected samples of amphibolite and associated soil from the general area of the Bluebird mine in the Lost Basin mining district -----	40
9. Average major-element compositions of Gold Basin-Lost Basin amphibolite and various groups of igneous rocks and other amphibolites -----	41
10. Analyses of metachert, banded iron formation, metarhyolite, and calc-silicate marble in various Early Proterozoic metamorphic units from the Gold Basin-Lost Basin mining districts -----	43
11. Notable occurrences of commodities in the Gold Basin-Lost Basin mining districts -----	135
12. Modal data for Proterozoic igneous and metaigneous rocks from the Gold Basin-Lost Basin mining districts -----	48
13. Analytical data of Early Proterozoic biotite monzogranite -----	50
14. Analytical data from the Early Proterozoic porphyritic monzogranite of Garnet Mountain -----	56
15. Analytical data from the Cretaceous two-mica monzogranite -----	66
16. Occurrences of episyenitic and syenitic rocks known in the Gold Basin-Lost Basin mining districts -----	70
17. Modal analyses of thin sections from rocks in the general area of the occurrence of visible, disseminated gold cropping out in the southeastern part of the Gold Basin mining districts -----	85
18. Analytical data of Late Cretaceous and (or) early Tertiary episyenite, of the contact zone of the episyenite, and of the adjoining host Early Proterozoic biotite monzogranite -----	90
19. Chemical analysis of average episyenite from Gold Basin and chemical analyses of other syenitic and episyenitic rocks from elsewhere -----	92

	Page
TABLE 20. Semiquantitative spectrographic analyses for minor metals in heavy-mineral concentrates from a selected lode occurrence and previously worked placer deposits and occurrences in the Gold Basin-Lost Basin mining districts -----	99
21. Compilation of signatures of placer gold samples, Lost Basin mining district -----	102
22. Variation of silver and copper content of lode gold samples from Lost Basin and Gold Basin mining districts as shown by replicate emission-spectrographic analyses -----	103
23. Comparison of signatures of placer gold and possible lode gold sources -----	104
24. Compilation of signatures of lode gold, Lost Basin mining district -----	106
25. Compilation of lode gold signatures, Gold Basin mining district -----	108
26. Signatures of gold from Lost Basin and Gold Basin mining districts that are somewhat similar to those of gold from porphyry copper deposits in other areas -----	110
27. Homogenization temperatures and salinity data from fluid-inclusion studies in the Gold Basin-Lost Basin mining districts -----	114

CONVERSION FACTORS

1 micrometer (μm) = 1×10^{-6} meter (m)
1 meter (m) = 3.281 feet (ft)
1 kilometer (km) = 0.6214 mile (mi)
1 gram (g) = 0.0022 pound, avoirdupois (lb avdp)
1 gram (g) = 0.035 ounce, avoirdupois (oz avdp)
1 kilogram (kg) = 2.205 pounds, avoirdupois (lb avdp)
1 tonne (t) = 1.102 tons, short (2,000 lb)
1 tonne (t) = 0.9842 ton, long (2,240 lb)
1 kilogram per square centimeter (kg/cm^2) = 0.98 bar (0.9869 atm)
1×10^6 pascals (MPa) = 10 bars
degree Celsius ($^{\circ}\text{C}$) = $1.8 (\text{temp } ^{\circ}\text{C}) + 32$ degrees Fahrenheit ($^{\circ}\text{F}$)

GEOLOGY AND GOLD MINERALIZATION OF THE GOLD BASIN-LOST BASIN MINING DISTRICTS, MOHAVE COUNTY, ARIZONA

By TED G. THEODORE, WILL N. BLAIR, and J. THOMAS NASH

ABSTRACT

The Gold Basin and adjacent Lost Basin mining districts are in northwestern Arizona, south of Lake Mead and just west of the Grand Wash Cliffs. Gold in quartz veins was apparently first discovered in the area in the 1870's. Recorded production from the districts between 1901 and 1942 includes 13,508 oz gold and 6,857 oz silver and has a value of about \$359,000, of which 98 percent is credited to gold. Most recorded production from lode deposits was from mines in the Gold Basin district, which is in the southern White Hills, whereas the bulk of placer production was along the east flank of the Lost Basin Range, about 16 km to the northeast across Hualapai Valley. The districts have been idle since about 1942, except for very small scale placer mining.

Most known occurrences of lode gold in the districts are associated with widespread quartz-cored pegmatite vein systems that were probably emplaced episodically during Early Proterozoic, Middle Proterozoic, and Late Cretaceous time into Early Proterozoic metamorphic and igneous rocks. Most of the veins apparently were emplaced during the Late Cretaceous, and they were localized along both high- and low-angle structures in the Early Proterozoic rocks. These veins are associated spatially and possibly genetically with two-mica magmatism of presumed Late Cretaceous age. A Late Cretaceous two-mica monzogranite, which includes some episyenite, crops out in an area of 4 to 5 km² in the southern part of the Gold Basin district. Some gold is found also in small episyenitic alteration pipes and in veins along a regionally extensive, low-angle detachment surface that has been traced for at least 30 km along the western flank of the White Hills and crops out conspicuously in their southern part.

Hydrothermal micas from selected veins in the districts give K-Ar ages of 822, 712, 69, 68, and 65 Ma, and those from pipes give ages of 130 and 127 Ma. The oldest ages (822 and 712 Ma) may reflect resetting of veins emplaced penecontemporaneously with the 1,400-m.y.-old granite of Gold Butte, which crops out just to the north of Lake Mead. The ages from pipes (130 and 127 Ma) must reflect either the presence of excess radiogenic argon in the hydrothermal environment of the evolving pipes or contamination of the dated mineral separates by Proterozoic mica and (or) feldspar. Primary white mica from the two-mica monzogranite gives a K-Ar age of 72 Ma.

Most occurrences of gold in the veins and pipes probably reflect either remobilization of gold from gold-bearing, near-surface Proterozoic metabasite or anatectic incorporation of gold into Late Cretaceous, two-mica magmas from very deep gold-bearing Proterozoic sources. Deposition of gold occurred in a mesothermal environment during the galena-, chalcopyrite-, and ferroan-carbonate-bearing stages of the veins. Homogenization studies of fluid inclusions prominent in the veins and pipes yield temperatures mostly in the range 150 to 280 °C. Early-stage trapping temperatures in the pipes were probably about 330 °C, and pressures in the range 50 to 70 MPa can be inferred. Fluids were moderately saline, mostly 4 to 16 weight percent NaCl equivalent, non-boiling, and contained appreciable amounts of carbon dioxide and, in

places, fluorine. Such fluids associated with the deposition of gold in these districts largely bridge the fluid-composition interval between fluids associated with other epithermal precious-metal and porphyry copper deposits.

Approximately 350 compositional analyses of samples of native gold from 20 mines in the Gold Basin district and from 48 veins in the Lost Basin district show silver contents from 6 to approximately 50 weight percent, and copper contents from 0.01 to 0.5 weight percent. Metal zonation and a possible relation to a porphyry copper system at depth can be inferred from some of these chemical data. Differences between the composition of placer gold from 24 occurrences in the Lost Basin district and that of gold in nearby lode sources suggest that other sources contributed gold to the placers or that locally derived grains were enriched by oxidation and weathering of the lodes.

INTRODUCTION

The Gold Basin-Lost Basin mining districts of northwestern Arizona are in Mohave County, 120 km southeast of Las Vegas, Nev., and about 95 km north of Kingman, Ariz. (fig. 1). These districts comprise primarily gold-bearing vein deposits containing minor byproduct lead, silver, and copper, and placer gold deposits. Gold was first discovered there in the 1870's. The districts lie adjacent to each other south of Lake Mead and west of the Grand Wash Cliffs, which mark the boundary of the Colorado Plateau. The Gold Basin district is mostly in the southern White Hills, and the Lost Basin district is to the east, across Hualapai Wash; they are mostly in the Garnet Mountain 15-minute quadrangle (fig. 2). In this report, we follow a broadly defined, strictly geographic assembly of mineral deposits and occurrences into mining districts. Our Gold Basin mining district includes the Gold Basin, Cyclopic, and Gold Hill mineral districts of Welty and others (1985), and our Lost Basin mining district includes the Lost Basin and Garnet Mountain mineral districts of Welty and others (1985). In their classification, Welty and others (1985) grouped known metallic mineral occurrences and deposits according to metallogenic criteria. This report summarizes field and laboratory investigations in which a remarkable suite of gold-bearing samples were collected from wide-ranging localities in these districts. Included are discussions of the environment(s) and age

of gold deposition based on geochemical studies, fluid-inclusion studies, and K-Ar isotopic dating, all supplemented by observations with the scanning electron microscope (SEM). For our investigations, lode and placer samples containing visible gold were collected from more than 30 localities.

ACKNOWLEDGMENTS

The preceding geologic investigations of P.M. Blacet (1975) of the U.S. Geological Survey in the Garnet Mountain quadrangle during the late 1960's and early 1970's and of E.J. Krish (1974) and A.J. Deaderick (1980) pro-

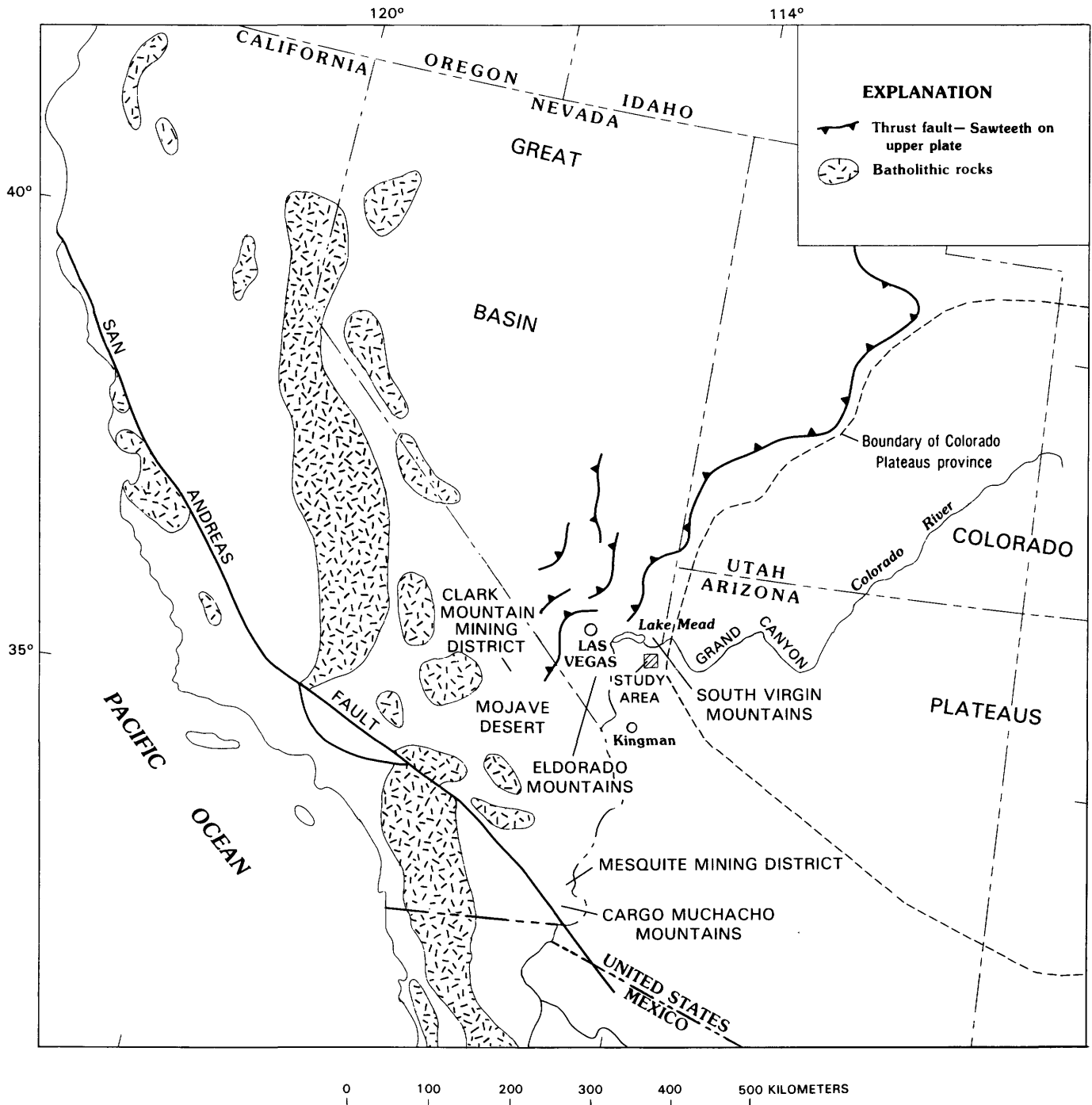


FIGURE 1.—Index map showing location of study area containing Gold Basin-Lost Basin mining districts. Modified from Haxel and others (1984).

vided the geologic framework upon which we built much of our studies. Further, Blacet collected many of the gold-bearing samples used in this study. R.L. Oscarson introduced us to the scanning electron microscope methods needed in the development of electron micrographs and aided our usage of the X-ray detector (EDAX) during the qualitative chemical analyses of selected mineral grains. Fluid-inclusion studies were conducted in the laboratory of W.E. Hall, U.S. Geological Survey.

HISTORY OF MINING ACTIVITY

The Gold Basin district is situated mostly in the eastern part of the White Hills and is bounded on the east by Hualapai Wash (fig. 2). Gold in quartz veins apparently was discovered in the district in the early 1870's, and most of the production until 1932 came from a small group of mines, including the El Dorado, Excelsior, Golden Rule, Jim Blaine, Never-Get-Left, O.K., and Cyclopic (fig. 3). About 1880 there was a small boom in the area, and by 1881 the ores were being worked in two stamp mills (Burchard, 1882, p. 253); in 1882 the El Dorado mine produced 26,000 tons of developed ore (Burchard, 1883, p. 305). Table 1 summarizes information concerning the mills previously operated in the Gold Basin-Lost Basin districts. The first stamp mill, a cooperative venture by the miners, was built about 1880 at "Grass Springs" near the present (1986) headquarters of the Diamond Bar Ranch, and in 1881 a second five-stamp mill was constructed, probably at Red Willow Spring, 4.0 km southwest of the Cyclopic mine. By 1883, most of the important mines in the district had been located, were developed, and had produced relatively small tonnages of free-milling, gold-quartz ores ranging from 0.5 to 3.0 oz gold per ton.

A third stamp mill was built along Hualapai Wash about 1886 and soon became the nucleus of a settlement called Gold Basin. About this time the gold-bearing veins in the Lost Basin district were discovered, and the centrally located Gold Basin mill soon became the most important in the region. Several years of relative inactivity preceded and followed the burning of the Gold Basin mill in 1893, but in 1896 it was rebuilt with 10 stamps and a cyanide plant. Water was piped about 10 km from water tunnels at Patterson's well (SW $\frac{1}{4}$ sec. 36, T. 29 N., R. 17 W.), because two wells drilled at Gold Basin had penetrated nothing but dry alluvial gravels to depths of 150 and 230 m (Lee, 1908, p. 78). Most of the mines in both districts had passed their peaks of production when the second burning of the Gold Basin mill occurred in 1906; in June 1907 the post office at "Basin" was discontinued, and postal service was transferred entirely to a post office established in 1905 at the Cyclopic mine.

In 1904, the Cyclopic mine was purchased by the Cyclopic Gold Mining Company, and the next year a

40-ton-per-day cyanide mill was built along Cyclopic Wash just below the mine. From this time on, "Cyclopic" was the main population center of the district, supporting a post office until 1917. After several years of idleness, intermittent production began again at the Cyclopic in 1919, and the old mill was remodeled in 1923 after the mine was taken over by the Gold Basin Exploration Company. In 1926 a new ore body was discovered, so the mill was again remodeled and its daily capacity increased to 100 tons.

Although the Cyclopic was one of the earliest discoveries and also was one of the largest overall producers of ore in the district, it was apparently inactive during the late 1920's. However, in 1929 the Kiowa Gold Mining Company built the San Juan mill about 1.6 km north of Cyclopic. Water for this then-new 60-ton mill evidently was obtained from the Cyclopic pumping station, previously built about 1905 to pipe water to an earlier mill at the same site. The actual source of the water was a well 5 km to the southwest (S $\frac{1}{2}$ sec. 35, T. 28 N., R. 19 W.). About this time there was renewed interest in the Harmonica (Climax) mine, 3.2 km north of the San Juan mill. This mill may have processed ore from several small nearby mines until the Cyclopic mill was reactivated about 1932. The Cyclopic mine produced intermittently during 1932-34, when the shallow underground workings were abandoned in favor of a large-volume open-cut operation. By late 1933 a cyanide mill operated at a daily capacity of 125 tons, and a total of about 40 men were employed at the mine and mill. Much of the ore mined in 1934 reportedly averaged 0.2 oz gold per ton (Wilson and others, 1934, p. 77). In 1936 the Cyclopic property was acquired by Manta de Oro Mines, Inc., and the mine produced somewhat steadily through 1940. From 1941 to about 1967 the mine was idle, and all mine buildings are now (1986) gone. Exploration drilling in 1968 failed to locate any additional ore. However, some attempts to heap-leach at the site of the Cyclopic mine apparently were undertaken in 1981. In 1984-85 Saratoga Mines Inc. of Blackhawk, Colo. apparently conducted some additional exploration near the Cyclopic mine (Engineering and Mining Journal, 1984; Saratoga Mines, Inc. Quarterly Report to Stockholder, March 31, 1984).

In addition to the Cyclopic, O.K., and Excelsior mines, which were relatively steady producers over the years, the following mines had intermittent production during the Depression-era mining revival from 1930 to 1942: Harmonica, Eldorado, Fry, Gold Hill, Golden Link, Golden Rule, M.O., Morning Star, and San Juan. Most of the ore from these and several smaller mines and prospects was treated at the Cyclopic or Malco mills. In 1942, four lode mines in the Gold Basin district had a recorded production of 108 oz gold and 24 oz silver from 249 short tons of treated ore (Woodward and Luff, 1943). The district

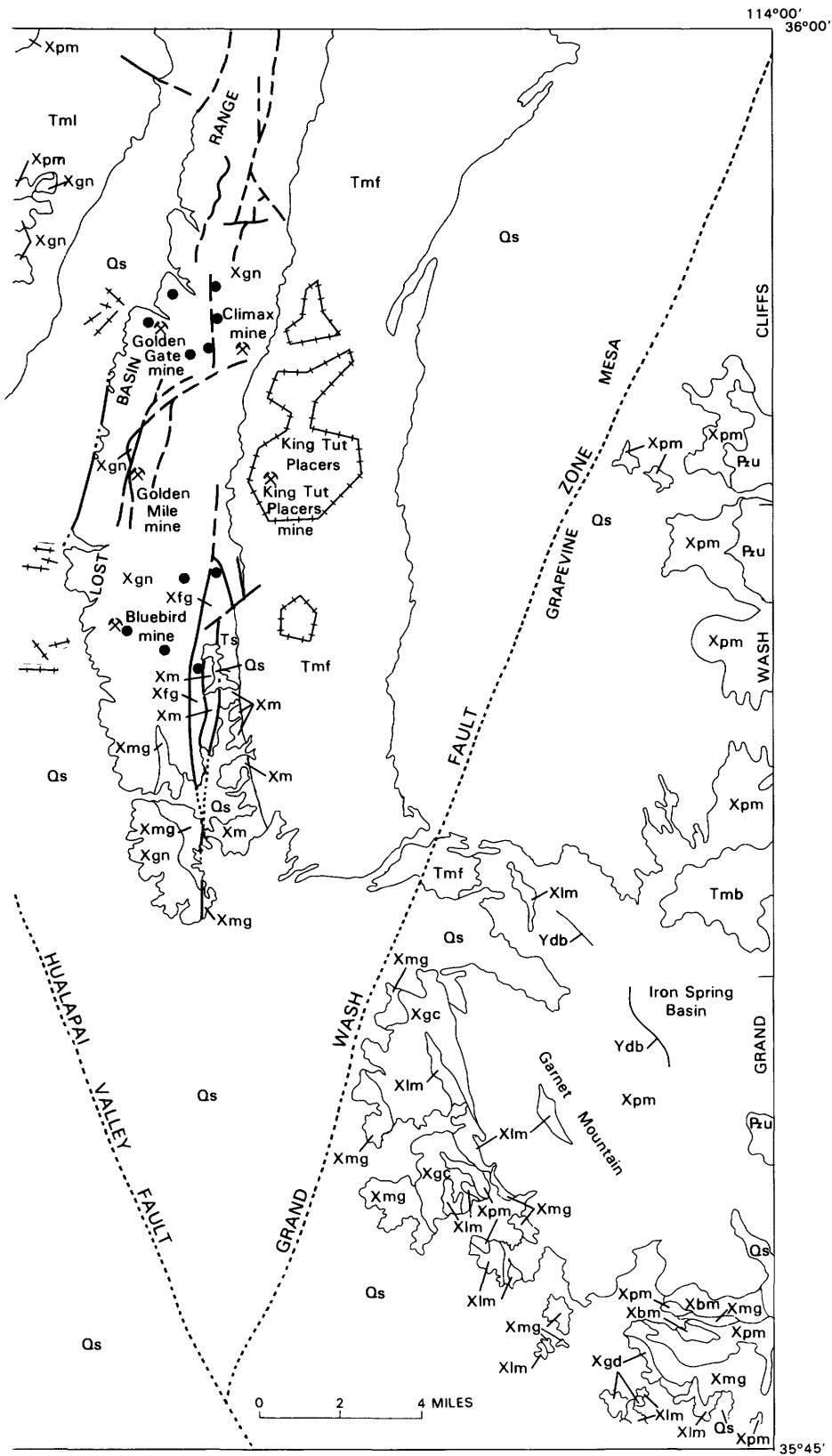
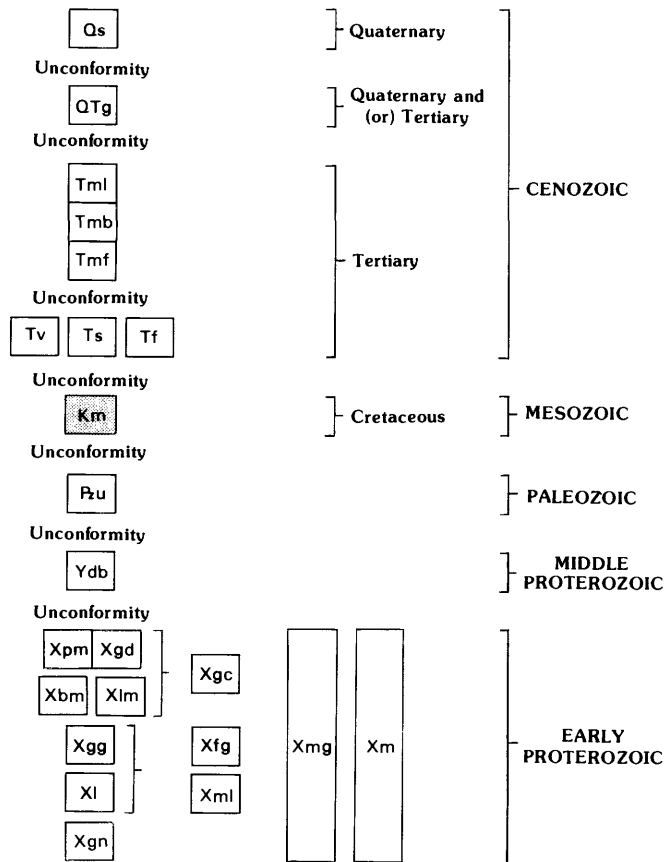


FIGURE 2.—Continued.

CORRELATION OF MAP UNITS



DESCRIPTION OF MAP UNITS

- Qs** Sedimentary deposits (Quaternary)—Includes sand and gravel along active stream washes, talus, colluvium, poorly consolidated fanglomerate currently being dissected, and landslide deposits; also may include extensive high-level fanglomeratic deposits, west of Grand Wash Cliffs in general area of Grapevine Mesa, that may be Tertiary and (or) Quaternary in age
- QTg** Fanglomerate (Quaternary and (or) Tertiary)—Locally derived fanglomerate deposits that include mostly clasts of metamorphic rock south-southeast of Senator Mountain and that do not contain clasts of rapakivi granite or any interbedded tuffs
- Muddy Creek Formation (Tertiary)**
- Tml** Hualapai Limestone Member—Includes limestone interbedded with thin beds of limy claystone, mudstone, and siltstone. Weathered limestone beds have a predominantly reddish color and form steep cliffs where they are dissected by Hualapai Wash
- Tmb** Basalt—As shown, flows at Senator Mountain, near west edge of map area, and at Iron Spring Basin, near east edge. Basalt in these two areas correlates probably with basalt flows (not shown) that conformably underlie the Hualapai Limestone Member and also are interbedded with fanglomerate of the Muddy Creek Formation near northwest corner of map area. Whole-rock K-Ar age determination of basalt from this area yields age of 10.9 Ma (see section by E.H. McKee, this report)

- Tmf** Fanglomerate—Alluvial fanglomeratic deposits that include conglomerate, sandstone, siltstone, mudstone, and locally abundant gypsum lenses. Locally includes lenses and beds of rhyolitic tuff and, as shown near southwest corner of map area, fanglomerate mapped previously by Blacet (1975) as unit Tf. Unit is also intruded by minor basalt dikes, especially in general area of Senator Mountain. Near northwest corner of map area, unit includes well-exposed flows of basalt
- Tv** Volcanic rocks (Tertiary)—Includes mostly andesite. Map unit near northwest corner of map area internally is highly broken by numerous faults, and near here, unit also includes air-fall tuff and reddish-brown sandstone interbedded with chaotic sedimentary breccia composed of fragments of Early Proterozoic gneiss. In places, unit also includes massive porphyritic hornblende andesite and basalt flows and breccia and overall minor amounts of tightly cemented volcanoclastic rocks. Flow layering and bedding generally dip at angles of 35° in contrast with shallow dips of about 5° in unconformably overlying basal fanglomerate of the Muddy Creek Formation. Age ranges of 11.8 to 14.6 Ma are reported near type section of the Mount Davis Volcanics (Anderson and others, 1972), whereas K-Ar age determination on sanidine from air-fall tuff near Salt Creek Wash in northwestern part of area yields age of 15.4 Ma. The volcanic rocks may be equivalent of the Mount Davis Volcanics or the Patsy Mine Volcanics (see section by E.H. McKee, this report).
- Ts** Rhyolitic tuffaceous sedimentary rocks and fanglomerate (Tertiary)—Includes well-bedded mudflows and rhyolitic tuffaceous sedimentary rocks and minor amounts of fanglomerate. Crops out as steeply dipping sequence of rocks, bounded by north-striking faults, near south end of Lost Basin Range. Possibly equivalent to the Mount Davis Volcanics
- Tf** Fanglomerate (Tertiary)—Coarse fanglomeratic deposits that locally include landslide or mudflow breccia. Overlain unconformably by fanglomeratic deposits of the Muddy Creek Formation, and apparently intercalated with andesite possibly equivalent to the Mount Davis Volcanics
- Km** Two-mica monzogranite (Cretaceous)—Includes mostly highly leucocratic muscovite-biotite monzogranite and some minor amounts of felsic muscovite granodiorite and episyenitic-altered muscovite-biotite monzogranite. Some facies are fluorite bearing. Porphyritic variants contain as much as 5 percent quartz phenocrysts. In places, contains very weakly defined primary layering of dimensionally oriented potassium feldspar and biotite
- Pzu** Sedimentary rocks, undivided (Paleozoic)—Includes Cambrian Tapeats Sandstone, Bright Angel Shale, and Muav Limestone
- Ydb** Diabase (Middle Proterozoic)—Includes normally zoned laths of plagioclase set in very fine grained matrix of granules of opaque mineral(s) and clinopyroxene. Close to chilled margins of some fresh outcrops of undeformed diabase, olivine is found in concentrations of as much as 10 volume percent. Small masses of fine-grained diabase crop out sporadically in Early Proterozoic igneous and metamorphic rocks. Most extensive exposures are about 2 km east of Garnet Mountain. Subophitic textures are dominant. Lower chilled margins of some sills contain sparse hornblende and biotite microveinlets. Presumed to be correlative with the diabase of Sierra Ancha, Ariz., having an emplacement age of 1,150 Ma (Silver, 1963)
- Xpm** Porphyritic monzogranite of Garnet Mountain (Early Proterozoic)—Includes conspicuous, large potassium feldspar phenocrysts, set in a light-pinkish-gray, coarse-grained hypidiomorphic groundmass. Many exposures show tabular phenocrysts as much as 10 cm long. Some phases are predominantly subporphyritic seriate and show an almost continual gradation in size of their euhedral potassium feldspar phenocrysts. Most widely exposed mass crops out in the general area of Garnet Mountain, in the southeastern part of the area, and extends discontinuously from there to north along the low hills leading to Grand Wash Cliffs. Dated by Wasserburg and Lanphere (1965) to be about 1,660 Ma

FIGURE 2.—Continued.

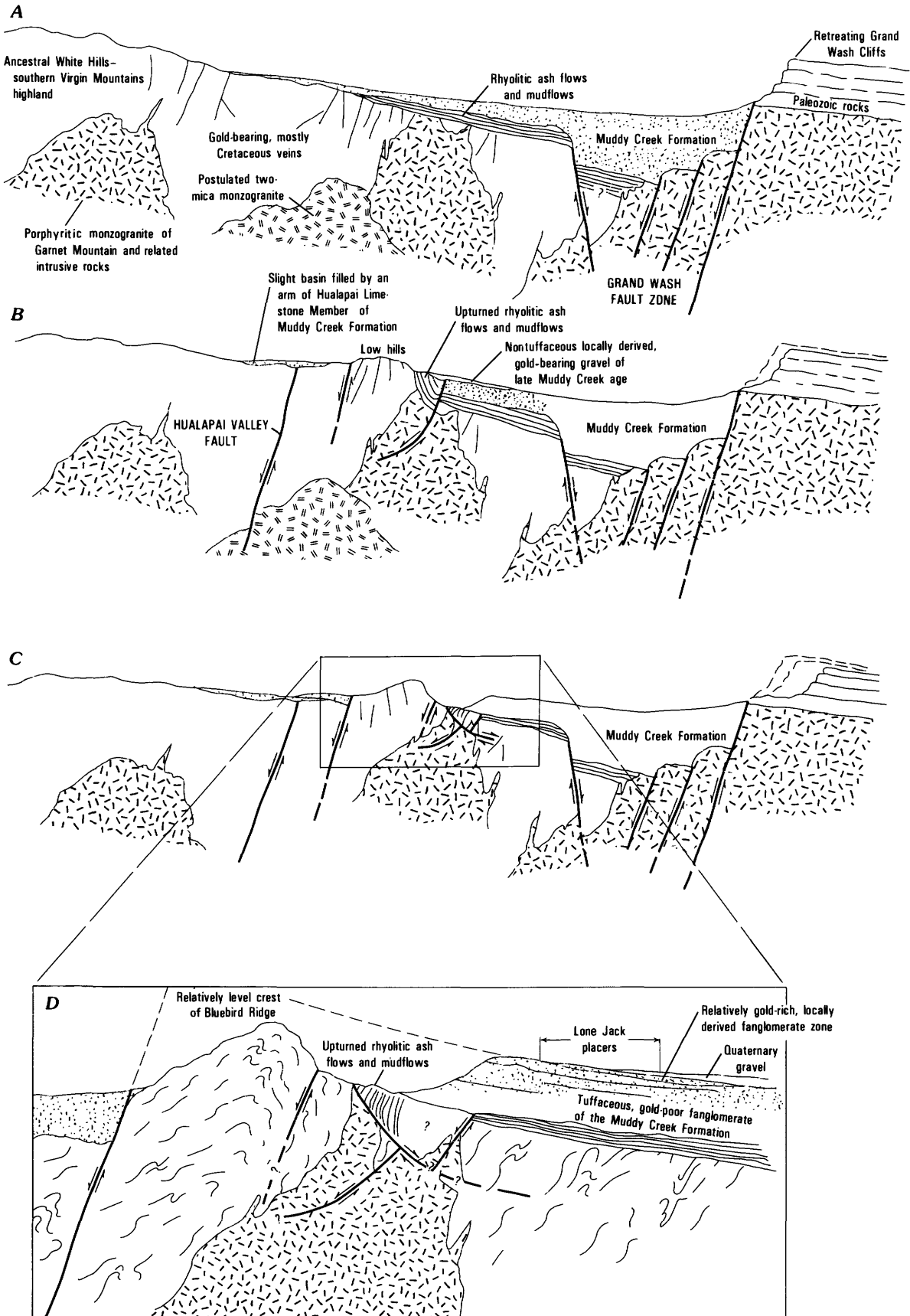
has been idle generally from about 1942 to the mid-1970's, except for small-scale placer mining that recovered a little detrital gold. In 1985-86 at least three major mining companies were active in the district; some relatively closely spaced drill holes were put down in the general area of the Owens mine.

The Lost Basin district contains a wide-ranging group of placer and lode mines in a belt lying between Hualapai Wash on the west and the Grand Wash Cliffs on the east (fig. 3). It extends from the Colorado River at the mouth of the Grand Canyon southward through the Grand Wash Cliffs for a total length of about 32 km. This district, although much larger in areal extent, has not been as active nor as productive as the adjacent Gold Basin district. The principal gold veins were discovered in 1886,

and the production of the district was reported by Schrader (1909) to be "many thousand dollars," chiefly in gold. Placers apparently were first worked in 1931 and resulted in a minor local boom. However, recorded production in copper, gold, and silver during 1904-32 was valued at less than \$45,000 (Hewett and others, 1936). The King Tut placers, discovered in 1931, were the most important placers in the Lost Basin district. Systematic sampling of the King Tut placers by G.E. Pitts in 1932 delineated approximately 90,000 tons of indicated reserves and 250,000 tons of probable reserves before mining operations on a relatively large scale began (Mining Journal, 1933, p. 10). All of this was confined to approximately one section of land. In the last four months of 1933 the King Tut yielded 117 oz of gold (Gerry and

- Xgd** Granodiorite border facies of porphyritic monzogranite (Early Proterozoic)—Gray granodiorite that includes variable proportions of biotite, hornblende, quartz, plagioclase, and potassium feldspar. Includes less abundant porphyritic granodiorite and porphyritic monzogranite phases. Locally coarse grained and sparsely porphyritic. Porphyritic phases show potassium feldspar phenocrysts set in coarse-grained hornblende-biotite hypidiomorphic granular matrix that is very magnetite rich. Crops out along west and southwest flanks of Garnet Mountain as mafic border facies of porphyritic monzogranite of Garnet Mountain. Found as homogeneous discrete bodies and also in the mixed granodiorite complex (Xgc)
- Xbm** Biotite monzogranite (Early Proterozoic)—Includes a homogeneous light-gray, fine-grained monzogranite and some porphyritic facies containing potassium-feldspar and quartz phenocrysts. Crops out south-southeast of Garnet Mountain and in the southern part of the Gold Basin mining district. In southern Gold Basin district, forms host rock for numerous fluorite-bearing, quartz-carbonate veins, presumably Late Cretaceous in age, some of which contain visible gold
- Xlm** Leucocratic monzogranite (Early Proterozoic)—Typically light-yellowish-gray rock and generally nonporphyritic. Partly chloritized biotite makes up less than 5 percent of most outcrops. Crops out as discontinuous, lensoid masses along western front of Garnet Mountain. Where well exposed, contacts with porphyritic monzogranite of Garnet Mountain (Xpm) show irregular dike offshoots of porphyritic monzogranite of Garnet Mountain cutting leucocratic monzogranite
- Xgc** Mixed granodiorite complex (Early Proterozoic)—Composite unit that includes mainly granodiorite (Xgd), some of which is porphyritic, and porphyritic monzogranite of Garnet Mountain (Xpm). Also includes some leucocratic monzogranite (Xlm)
- Xgg** Gneissic granodiorite (Early Proterozoic)—Generally, well-foliated, medium-gray-green rock containing highly variable alkali feldspar to plagioclase ratios. Biotite makes up about 20 volume percent of unit. Crops out in elongate body in southern White Hills
- Xl** Leucogranite (Early Proterozoic)—Includes coarse-grained leucogranite to pegmatitic leucogranite that contains potassium feldspar phenocrysts as much as 8 cm wide. Largest mass is 1-km-long sill cropping out 3 km northeast of Cyclopic mine. Stringers several centimeters wide parallel layering throughout much of the gneiss (Xgn). Fabrics grade from relatively undeformed to intensely mylonitic. Northeast of Gold Hill mine, large sills of pegmatitic leucogranite increase in abundance and eventually grade into complexes of migmatitic leucogranite (Xml). Most facies show modal compositions that plot in the field of granite; some outcrops of gneissic leucogranite contain garnet
- Xfg** Feldspar gneiss (Early Proterozoic)—Generally, light gray to light pinkish gray; compositionally homogeneous and typified by a strongly lineated fabric. Includes minor amounts of amphibolite, mafic gneiss, highly crenulated quartz tourmaline schist, and tourmalinite. Crops out in a 5-km-long and 0.8-km-wide sliver, bounded by faults in southern Lost Basin Range. Cut by quartz-feldspar veins, some of which contain gold
- Xml** Migmatitic leucogranite complex (Early Proterozoic)—Composite unit that includes swarms of leucogranite (Xl), aplite, and pegmatite dikes, together with pegmatoid quartz veins all cutting gneiss (Xgn). Complex and highly deformed by a ductile (mylonitic and gneissic) style of deformation
- Xgn** Gneiss (Early Proterozoic)—Includes variably metamorphosed gneiss and some metaquartzite in northern parts of the Lost Basin Range, and in northern White Hills. Exposed sequence of gneiss in southern parts of the Lost Basin Range includes abundant metabasite and amphibolite consisting partly of metagabbro, metaclinopyroxenite, metawehrlite, metadiabase, and metabasalt. Intruded to varying degrees by porphyritic monzogranite of Garnet Mountain (Xpm), biotite monzogranite (Xbm), leucocratic monzogranite (Xlm), leucogranite (Xl), and diabase (Ydb)
- Xmg** Migmatitic gneiss (Early Proterozoic)—Composite unit that includes mostly gneiss (Xgn) intruded to varying degrees by porphyritic monzogranite of Garnet Mountain (Xpm), biotite monzogranite (Xbm), and granodiorite (Xgd)
- Xm** Migmatite (Early Proterozoic)—Composite unit that includes mostly medium-grained, sparsely porphyritic monzogranite of Garnet Mountain (Xpm) complexly intruded into gneiss (Xgn)
- ?Contact—Queried where location uncertain
 - - - Fault—Dashed where approximately located; dotted where concealed
 -▲-▲-? Detachment fault—Dashed where approximately located; dotted where concealed; queried where uncertain. Sawteeth on upper plate
 ● Lode-gold locality—Collected for this report or observed (see Blacet, 1975; and section by J.C. Antweiler and W.L. Campbell, this report)
 - - - - -? Fluorite occurrence—Outer limit observed either in veins or disseminated in the Late Cretaceous two-mica monzogranite; dashed where approximately located; queried where uncertain
-  Area of placer deposit and (or) mine

FIGURE 2.—Continued.



Miller, 1935). By 1936 the gold output from the King Tut was 450 oz, which represented the bulk of the entire production from the Lost Basin district. In 1939 Mr. Charles Duncan placered 13 oz of gold in 16 days, using only a sluice box and wash tub, near the King Tut placers (Engineering and Mining Journal, 1939), whereas the King Tut placers themselves were only worked intermittently until 1942. Eventually, placer mining of unconsolidated gravel from the upper reaches of present-day arroyos extended across approximately 25 km² in the general area of the King Tut placers (Blacet, 1969). Nonetheless, by 1942 no additional production was recorded from the Lost Basin district. However, in the middle and late 1960's several small operators using dry washers were active intermittently in the general area of the King Tut placers. These washers were powered by small portable gasoline motors. Because of the surge in the price of gold during 1978-80, small-scale placer operations and extensive exploration efforts, centered on an area just to the north of the King Tut placers, began again. These efforts were continuing intermittently through 1986.

A summary of the recorded metal production from the lode mines in the Gold Basin-Lost Basin districts between 1901 and 1942 reveals that 13,508 oz gold, 6,857 oz silver, 5,918 lb (2,684 kg) copper, and 43,652 lb (19,797 kg) lead were produced from a total of 69,189 tons of treated ore (table 2). The value of these metals was approximately \$359,000, and approximately 98 percent of the dollar value is credited to gold. Recorded production from the Gold Basin district in the period 1904 to 1932 was 15,109 tons of ore yielding 6,244.91 oz gold, 5,059 oz silver, 4,738 lbs copper, and 1,765 lb lead, valued in all at \$133,014 (Hewett and others, 1936; table 2). Most of this production, excluding 4,711 lb copper produced during 1918, came from the Eldorado mine. The 4,711 lb of copper is assigned questionably to an unknown mine in the Gold Basin district. A total of 19 oz of placer gold was also recovered from the Gold Basin district in 1942 (Woodward and Luff, 1943).

GENERAL GEOLOGY OF THE DISTRICTS

The Gold Basin-Lost Basin mining districts are in the Basin and Range province, just south of Lake Mead and west of the Colorado Plateau. The west edge of the Colo-

rado Plateau is approximately 3 km west of the east edge of the Garnet Mountain quadrangle (fig. 1), where the generally gently east dipping to flat-lying lower Paleozoic basal formations of the Colorado Plateau crop out along the Grand Wash Cliffs. The districts are present in an uplifted region near the leading edge of the North American platform (see Burchfiel, 1979; Dickinson, 1981) and straddle several north-trending ranges of mostly Proterozoic basement rocks from which the rocks of the Paleozoic stable platform have been removed by erosion. Lake Mead occupies a structurally complex area to the north marked by the junction of several regionally extensive major geologic features (see Anderson and Laney, 1975; Angelier and others, 1985). These features include the boundary between the Paleozoic miogeocline and stable platform, the Mesozoic Sevier orogenic belt, and the Las Vegas shear zone. Further, the districts are present along the southern extension of the Virgin Mountains structural block of Longwell (1936) and Anderson and Laney (1975). The districts include two ranges of mostly Early Proterozoic metamorphic and igneous rocks, the White Hills and the next range to the east, herein termed the Lost Basin Range but referred to as the Infernal Range by Lucchitta (1966), and two intervening valleys filled by Tertiary and Quaternary deposits (Blacet, 1975). These two valleys are drained by Hualapai Wash and Grapevine Wash, and the latter valley also cuts through Grapevine Mesa. The Grapevine geomorphic trough includes the Grand Wash fault zone, a N. 10°-15° E.-striking system of Miocene normal faults (west block down) now covered by Tertiary fanglomerate and Quaternary gravel (see Longwell, 1936; Lucchitta, 1966, 1979). The trace of the Grand Wash fault zone is inferred to pass between Lost Basin Range and Garnet Mountain, southwest of which the Grand Wash fault zone is inferred on the basis of relations apparent in satellite imagery (Goetz and others, 1975, fig. IV-B-2) to terminate against a younger northwest-striking structure, herein named the Hualapai Valley fault. The Hualapai Valley fault is inferred to change its strike gradually to almost north-south as it passes west of the Lost Basin Range along the main drainage of Hualapai Wash (Liggett and Childs, 1977). Major offsets along the Hualapai Valley fault may be penecontemporaneous with deposition of the uppermost sequences of the upper Miocene limestone. However, along the Grand Wash trough basin-and-range faulting was active during the early stages of basin fill, although movement(s) along some faults apparently continued after deposition of the upper Miocene limestone, (Lucchitta, 1972; also note displacements shown along the Wheeler fault in figure 6 of Lucchitta, 1979). Similarly, initial movements along the Hualapai Valley fault may have contributed toward local development of an embayment in which the limestone was deposited.

FIGURE 3.—Schematic east-west cross section from ancestral highland of the White Hills-southern Virgin Mountains to Grand Wash Cliffs showing inferred geologic relations. Arrows, direction of relative movement; dashed line, previous position or approximate location; query, where uncertain. Modified from P.M. Blacet (unpub. data, 1967-72) and Deaderick (1980). A, About 15-18 Ma. B, About 8 Ma. C, About 5 Ma. D, Present day.

TABLE 1.—Descriptions of gold-quartz mills in the Gold Basin-Lost Basin mining districts, Arizona

Name of site	Type of mill	Location	History and remarks
Willow mill (Gold Spring)	Arrastre and stamp	Red Willow Spring, NW1/4 sec. 12, T. 27 N., R. 19 W.	Possibly the location of the first arrastre in the district, built in the early 1870's. A stamp mill was built here prior to 1915, perhaps as early as 1881.
Grass Springs (Grass Valley)	Stamp	At the headquarters of the Diamond Bar Ranch, NW1/4 sec. 27, T. 29 N., R. 16 W.	An inefficient four- or five-stamp mill, the first for the district, was constructed at Grass Springs about 1880 as a cooperative venture by the early miners.
Patterson's well	Arrastre	SE1/4 sec. 36, T. 29 N., R. 17 W.	Robert Patterson, a pioneer rancher and miner, built an arrastre near his well (water tunnels) in 1883.
Butcher Camp O.K. mill (Gold Basin or Burnt mill)	Arrastre Arrastre and stamp	NW1/4 sec. 7, T. 27 N., R. 18 W. Along Hualapai Wash, NE1/4 sec. 13, T. 28 N., R. 18 W.	Two arrastres at shallow well. History unknown. This stamp mill operated intermittently at the settlement of Gold Basin from 1887 to 1890; it burned in 1893, but was rebuilt in 1896 and its 10 stamps and cyanide plant ran intermittently until it burned again in 1906 (Schraeder, 1909, p. 120-121).
Old Senator mill	Stamp	Near the Colorado River east of the mouth of Salt Springs Wash, SW1/4 sec. 5, T. 30 N., R. 18 W.	A 10-stamp mill was built here about 1892, operating for about 6 months on low-grade ore hauled 16 mi from the Senator Mine.
Salt Springs mill	Stamp	At Salt Springs near center of sec. 18, T. 30 N., R. 18 W.	History uncertain, probably built by the Salt Springs Mining Co. about 1900. This mill apparently operated as late as 1917.
Cyclopic mill	Cyanide	At Cyclopic mine, SW1/4 sec. 30, T. 28 N., R. 18 W.	A 40-ton-per-day mill was built in 1905 by the Cyclopic Gold Mining Co., producing considerable bullion during the next few years. In 1923, the Gold Basin Exploration Co. acquired the property and remodeled the mill. After discovery of a new ore body in 1926, the mill was again remodeled, and its capacity increased to 100 tons per day. The mill operated intermittently during 1932-40 and was enlarged to 125 tons daily capacity in late 1933.
San Juan mill	Amalgamating and cyanide	In canyon 1 mi north of Cyclopic mine, SE1/4 sec. 19, T. 28 N., R. 18 W.	In 1929, the Kiowa Gold Mining Co. built a 60-ton-per-day amalgamating and cyanide mill to process ore from the San Juan group of claims. This plant may have provided custom milling for several small miners during the early 1930's (Mining Journal, 1929).
Lost Basin mill (Scanlon)	Ball mill with flotation and cyanide	About 1 mi northeast of the Golden Gate mine, SW1/4 sec. 28, T. 30 N., R. 17 W.	In the mid-1930's, the Lost Basin Gold Mining Co. was apparently operating a diesel-powered 50-ton-per-day ball mill at the old Scanlon mine. Prior to the filling of Lake Mead, this company may have operated a mill near the Colorado River along Hualapai Wash.
Malco mill (Excelsior, Eldorado)	Ball mill with flotation and cyanide(?)	At Excelsior mine, NW1/4 sec. 22, T. 28 N., R. 18 W.	A 35-ton-per-day diesel-powered ball mill was built in 1938 by the Malco Mining Co. (Mining Journal, 1938). About 1908, a stamp mill may have been built at this site by the Arizona-Minnesota Gold Mining Co.

Early Proterozoic rocks crop out widely in both the Gold Basin and Lost Basin mining districts. These rocks consist mostly of gneiss that presumably is 1,750 Ma and that includes both paragneiss and orthogneiss, the coarse-grained porphyritic monzogranite of Garnet Mountain, and relatively small masses of medium-grained leucocratic monzogranite that crop out as part of the plutonic complex of Garnet Mountain (fig. 2). In this report, we use the classification of Streckeisen and others (1973). As such, the porphyritic monzogranite of Garnet Mountain and the leucocratic monzogranite correspond to the porphyritic quartz monzonite and leucocratic quartz monzonite of Blacet (1975), who followed the classification of Bateman (1961). The porphyritic monzogranite of Garnet Mountain intrudes gneiss and most likely was emplaced about 1,660 Ma (Wasserburg and Lanphere, 1965). The Proterozoic terrane in the quadrangle also includes small bodies of granodiorite, gneissic granodiorite, alaskite, various mappable migmatite units, feldspathic gneiss, amphibolite derived from igneous and sedimentary protoliths, and other metasedimentary rocks, including some fairly widespread metaquartzite. In addition, some minor amounts of diabase that presumably is of Middle Proterozoic age are exposed mostly as thin northwest-striking dikes in the general area of Iron Spring Basin (fig. 2).

The most widespread unit of Early Proterozoic age to crop out in the districts is the gneiss unit (Xgn, fig. 2).

TABLE 2.—*Production of gold, silver, copper, and lead from lode deposits in the Gold Basin-Lost Basin mining districts, 1901-42*

[Quantities furnished by the U.S. Bureau of Mines; ---, no production recorded]

Year	Ore treated (short tons)	Gold (ounces)	Silver (ounces)	Copper (pounds)	Lead (pounds)
1901----	30	59	15	---	---
1902----	3,900	260	810	---	---
1903----	4,723	2,361	300	---	---
1904----	2,000	1,429	351	---	---
1905----	360	1,356	209	---	---
1906----	903	380	115	---	---
1907----	101	27	15	---	---
1908----	55	29	10	---	---
1910----	412	203	68	27	149
1911----	431	197	47	---	---
1913----	600	228	41	---	---
1914----	600	280	42	---	---
1915----	600	300	70	---	---
1917----	560	280	50	---	---
1918----	639	248	827	4,711	---
1919----	2,813	270	784	---	1,616
1920----	800	275	50	---	---
1922----	3	2	---	---	---
1923----	5	6	1	---	---
1929----	9	4	4	---	---
1933----	3,425	371	77	16	243
1934----	3,306	317	5	---	---
1935----	502	209	114	310	---
1936----	2,231	326	94	---	---
1937----	13,354	923	275	---	1,373
1938----	7,968	370	809	310	9,033
1939----	3,170	655	307	25	6,724
1940----	14,299	1,453	973	283	7,114
1941----	1,141	582	370	236	17,400
1942----	249	108	24	---	---
Total—	69,189	13,508	6,857	5,918	43,652

As such, it hosts most of the known gold-quartz vein deposits. These deposits are concentrated in a belt that trends approximately N. 15°-20° E. and that spans the Gold Basin and Lost Basin districts. The deposits are found mostly in the western half of the Garnet Mountain quadrangle (fig. 3). The remaining gold-quartz veins are concentrated mostly in the southern part of the Gold Basin district, east of the Cyclopic mine. The veins here are hosted by gneissic granodiorite and porphyritic monzogranite of Garnet Mountain.

The Early Proterozoic gneiss, and here we paraphrase Blacet's (1975) descriptions for the most part, consists of an assemblage of metasedimentary rocks, mostly quartzofeldspathic gneiss interlayered with subordinate cordierite gneiss, biotite-garnet-sillimanite schist, and amphibolite. Locally, dark-gray to black amphibolite forms a large part of the gneiss unit, especially in the southern part of the Lost Basin Range where the amphibolite sequence consists of metagabbro, metadiabase, metaclinopyroxenite, and metawehrlite. Generally, the amphibolite crops out discontinuously in lensoid masses of various sizes. In addition, thin lenses of marble, calc-silicate gneiss, banded iron formation, and metachert crop out sporadically within the gneiss. All these metamorphic rocks have been deformed intensely during several episodes of deformation in Early Proterozoic time (Blacet, 1975). The presence of Paleozoic rocks in the eastern part of the study area and their absence in the western part results from regional downward tilting to the northeast and consequent erosional stripping of the Paleozoic rocks. As pointed out by Lucchitta (1966), the tilt results from a belt of uplift southwest of the present-day edge of the Colorado Plateau. This uplift is presumably of early to middle Tertiary (or Laramide) age and predated the basin-and-range rifting in the area, exemplified by the Grand Wash fault zone. Displacements along the Grand Wash fault zone are estimated to range from 1,000 to more than 5,000 m (Lucchitta, 1966). However, north of the Colorado River, the Grand Wash fault zone apparently has displaced 6.9-Ma basalt by as much as 305 m (Hamblin, 1984). These studies by Hamblin suggest that the eastern block(s) has been elevated, whereas the western block(s) remained relatively stationary.

East of the Lost Basin district, well-exposed Paleozoic formations crop out at the base of the Grand Wash Cliffs, near the east boundary of the Garnet Mountain quadrangle. These Cambrian formations include the conformable Tapeats Sandstone, Bright Angel Shale, and Muav Limestone (Blacet, 1975). The Tapeats Sandstone rests unconformably on the porphyritic monzogranite of Garnet Mountain. All of these formations are included within the Paleozoic undivided unit of figure 2.

An undeformed leucocratic two-mica monzogranite intrudes gneiss about 1.5 km north of the Cyclopic mine in

the southern part of the Gold Basin district (fig. 2). The two-mica monzogranite crops out across an area of about 4 to 5 km² and is Late Cretaceous in age (Blacet, 1972); it includes some zones of episyenite, with minor aplite and pegmatite. The two-mica monzogranite in the Gold Basin district is part of the Wilderness "strato-tectonic" assemblage of Keith and Wilt (1985), which apparently makes up the most widespread and most voluminous type of magmatism during the Late Cretaceous and (or) early Tertiary in Arizona (see also Keith, 1984).

Three types of lode gold deposits are known in the Gold Basin-Lost Basin districts (Blacet, 1969, 1975). Most lode gold deposits in the districts are present as veins, presumably of Late Cretaceous age, and are localized along preexisting structures in Early Proterozoic rocks. In addition, some of the gold-bearing quartz veins probably are of Proterozoic age. A minor yet geologically significant type of lode gold deposit in the Gold Basin district consists of small masses of Late Cretaceous fluorite-bearing episyenite containing macroscopically visible disseminated gold (Blacet, 1969). Most likely, the emplacement of these episyenite bodies is related genetically to the intrusion of Late Cretaceous two-mica monzogranite. The third type of lode gold deposit, exemplified by the Cyclopic mine, consists of Late Cretaceous gold-quartz veins that may have been originally deposited as cap-rock silica breccias and then brecciated further as they were caught up along a regionally extensive Miocene low-angle fault. This fault crops out in the southern part of the Gold Basin district and has been traced to the north along the west flank of the White Hills (fig. 2).

The oldest Tertiary rocks in the general area of the districts are volcanic rocks presumably equivalent to the Tertiary Mount Davis Volcanics or Patsy Mine Volcanics as mapped by Longwell (1963) and Anderson and others (1972; unit Tv, fig. 2), rhyolitic tuffaceous sedimentary rocks and fanglomerate (unit Ts), and Tertiary fanglomerate (unit Tf). The volcanic rocks include mostly andesite. Their base in the general area of the districts is not exposed but instead is marked apparently by a low-angle detachment surface. In the Eldorado Mountains, Nev., just west of the Colorado River and south-southwest of Lake Mead, andesite and rhyolite lavas of the Patsy Mine Volcanics are overlain successively by rhyolitic ash-flow tuff of the tuff of Bridge Spring and by basaltic and rhyodacitic lavas of the Mount Davis Volcanics (Anderson and others, 1972). A sequence of tuffaceous mudflows and rhyolitic water-laid tuffaceous sedimentary rocks and fanglomerate crops out near the south end of the Lost Basin Range (fig. 2) and was mapped in detail by Deaderick (1980). This sequence is steeply dipping, is partly bounded by north-striking faults on the west, and possibly is equivalent in age to the Tertiary volcanic rocks; on the east, the sequence is overlain unconformably by con-

glomerates belonging to the Muddy Creek Formation (Blacet, 1975). In addition, Deaderick (1980) reported that the mudflows and rhyolitic tuffaceous sedimentary rocks locally are in depositional contact with Early Proterozoic migmatitic gneiss and that the mudflows and tuffaceous sedimentary rocks may be equivalent in age to the Miocene Patsy Mine Volcanics (or formerly the Golden Door Volcanics of Longwell, 1963). In the northwest corner of the study area (fig. 2), Tertiary fanglomerate (unit Tf) apparently is intercalated with the Tertiary volcanic rocks. These coarse fanglomeratic deposits locally include landslide or mudflow breccia and are overlain unconformably by younger fanglomeratic deposits (unit Tmf).

Although the stratigraphic nomenclature for nonmarine Tertiary sedimentary rocks in the Lake Mead area has been modified recently by Bohannon (1984), the nomenclature used for purposes of this report follows that of Longwell (1936), Lucchitta (1966, 1972, 1979), Blacet (1975), and Blair (1978). The Muddy Creek Formation of Miocene age in the study area consists of conglomerate, claystone, mudstone, and gypsum; basalt, possibly equivalent to the Fortification Basalt Member of the Muddy Creek Formation, at Senator Mountain and Iron Spring Basin near the Grand Wash Cliffs; and an upper carbonate member that has been called the Hualapai Limestone Member. The conglomerate appears to have been deposited in small basins and topographic lows in an environment of interior drainage. Small patches of landslide or mudflow breccia containing Proterozoic clasts occur within the fanglomerate of the Muddy Creek Formation southeast of the Lost Basin Range. Stratigraphically, much of the Fortification Basalt Member and the Hualapai Limestone Member of the Muddy Creek Formation occupies approximately the same position near the top of the section (Longwell, 1936; Lucchitta, 1979), although Anderson (1977, 1978) shows lenses of the Fortification Basalt Member cropping out throughout the entire sequence of the Muddy Creek Formation. The Hualapai Limestone Member may have been deposited in a marine environment (Blair, 1978; Blair and Armstrong, 1979), although Lucchitta (1979) has reinterpreted Blair's data to suggest that the Hualapai Limestone Member was deposited in saline lakes at or below sea level. Further, the low contents of bromide, six to seven parts per million in salt from the Muddy Creek Formation near Overton, Nev. (85 km northwest of the study area), suggested to Holser (1970) that these salts could have been derived from evaporites on the Colorado Plateau. Nonetheless, some paleontological and chemical evidence at least suggests that the Hualapai Limestone Member may reflect deposition at the north end of an extended embayment of the Gulf of California beginning more than 8.9 Ma (Blair and others, 1977) or 5 to 6 Ma according to Lucchitta (1979). The type locality for the Hualapai Limestone

Member is along Hualapai Wash, and the thickest part of the limestone at the type locality is almost 300 m. Some beds of this limestone cover the Grand Wash fault zone near the base of the Grand Wash Cliffs where the Colorado River emerges from the Grand Canyon (Longwell, 1936; Lucchitta, 1966). Thus, apparently no major movement occurred along this fault zone after the last several hundred meters of deposition of the Muddy Creek Formation. However, northwest of the Cyclopic mine, rocks assigned to the Muddy Creek Formation apparently have been faulted against Proterozoic metamorphic and igneous rocks and the Late Cretaceous two-mica monzogranite along the regionally extensive low-angle Miocene fault, which crops out there (fig. 2; see also Blacet, 1975). Exposures of the actual surface of this low-angle detachment fault are extremely difficult to find. Locally, nevertheless, indurated conglomerate of the Muddy Creek Formation containing boulders of coarse-grained porphyritic monzogranite of Garnet Mountain are faulted against crushed migmatitic gneiss and crushed porphyritic monzogranite of Garnet Mountain. This detachment fault borders the White Hills along the entire west margin and thus establishes an eastern leading edge for low-angle detachment terranes in the Lake Mead area (see Anderson, 1971; Davis and others, 1979, fig. 1).

The overall tectonic history of this low-angle structure is still poorly resolved. The detachment fault does not appear, however, to be similar to dislocation surfaces (decollement) immediately associated spatially with closely underlying cordilleran metamorphic core complexes, owing to the absence of pervasive penetrative linear structures associated with widespread mylonitic or cataclastic fabrics (see Crittenden and others, 1980). The fabric of the two-mica monzogranite is not mylonitic or cataclastic. In addition, such core-complex-associated dislocation surfaces typically show an underlying microbreccia about 1 m thick, which is in turn underlain by a zone of chlorite breccia. Furthermore, the detachment fault, which crops out along the west margin of the White Hills and at the Cyclopic mine, must not reflect the eastern distal effect of near-surface distension associated with the emplacement of plutons coeval with the Miocene Mount Davis Volcanics (see Anderson, 1971; Anderson and others, 1972). The detachment fault apparently is younger than the Mount Davis Volcanics because it cuts rocks assigned to the Muddy Creek Formation (fig. 2). The overall extension associated with this structure appears to have an azimuthal bearing of approximately east-west based on the roughly north-south trend of its trace along the west flank of the White Hills. In the general area of the Cyclopic mine, some sequences of conglomerate assigned to the Muddy Creek Formation crop out in the upper plate of the detachment fault; however, as mapped, parts of the Muddy Creek Formation apparently crop out also in the

lower plate of the detachment fault farther to the northwest (fig. 2). Several splays of the detachment fault are well exposed in the general area of the Cyclopic mine. Some additional field relations along this fault are provided in the section "Veins Along the Miocene Detachment Fault." Nonetheless, the geologic relations shown on figure 2 must be amplified by studies beyond the intended scope of this present report. As pointed out by Lucchitta (1979; written commun., 1983) only the lowermost basin-fill deposits are substantially deformed and cut by detachment-type faults elsewhere in the region. Rarely in the region have such faults been reported to cut basin-fill rocks of Muddy Creek age. To the west near the Eldorado Mountains, south of Boulder City, Nev., Anderson (1971) provided some of the first comprehensive descriptions of thin-skin Tertiary distension. There, along the northwest flank of the Eldorado Mountains, some of the flat-lying Muddy Creek Formation rests unconformably across some of the listric normal faults. However, just to the northeast of Boulder City, rocks of the Muddy Creek are cut by a number of high-angle faults (Anderson, 1977), and the Muddy Creek Formation in the eastern part of the Eldorado Mountains is involved significantly in detachment-type faulting, particularly in its lowermost sequences (Anderson, 1978).

Displacements along the low-angle fault may have occurred in response to either of two other tectonic phenomena. First, the low-angle displacements may reflect the near-surface uplift of the White Hills associated with strike-slip offsets along a southeast-striking fault postulated to go through Lake Mead (Anderson, 1973, fig. 8), south of the Virgin Mountains. Second, the possibility of local gravity sliding off the White Hills cannot be discounted.

The next younger sequence of rocks in the Gold Basin-Lost Basin districts includes some unconsolidated sediment (Blacet, 1975), but because of their patchy distribution, they are not shown as separate map units on the geologic sketch map (fig. 2). Well-rounded cobbles and gravels derived from the Colorado Plateau lie scattered unconformably on the Hualapai Limestone Member and some ridges of the Muddy Creek Formation. These cobbles and gravels probably represent Pliocene high-level remnants of the ancestral Colorado River (Lucchitta, 1966).

Some late Tertiary gravels are present as dissected alluvial fan remnants along Grapevine Wash at the base of the Grand Wash Cliffs and are included with the Quaternary sedimentary deposits of figure 2 (unit Qs).

The Grand Wash fault zone near the base of the Grand Wash Cliffs has had a profound impact on the overall geomorphic evolution of the region. However, any viable regional interpretation must include the critical geologic relations mapped by Blacet (1975) at the Lost Basin

Range, approximately 10 km west of the Grand Wash Cliffs and almost at the very center of the Garnet Mountain quadrangle. Our hypotheses of the geologic-geomorphic history of the region during the past 18 to 15 m.y. is shown schematically, in an east-west cross section (fig. 3). Inferred structural relations are shown extending from the ancestral highland of the White Hills-southern Virgin Mountains on the west, through the rocks of the Lost Basin Range, and finally to the Grand Wash Cliffs on the east.

Prolonged but episodic regional extensional tectonism in the late Tertiary seems to have affected the predominantly Early Proterozoic crystalline terrane of the districts, and this in turn apparently contributed toward the eventual distribution of the productive placer gold deposits. The development of the relatively deep middle to late Tertiary basin along the Grand Wash fault zone was apparently controlled primarily by regional east-west extension (fig. 3A; Lucchitta, 1966). This extension must also be reflected in the low-angle detachment surfaces at the base of the volcanic rocks possibly equivalent in age to the Mount Davis Volcanics and through the general area of the Cyclopic mine workings and along the west margin of the White Hills, described previously (fig. 2). Sediment was shed into the basin along the Grand Wash trough mostly from a highland at the ancestral White Hills and southern Virgin Mountains as suggested previously by Longwell (1936) and Lucchitta (1966). Sometime after deposition of the lowermost sequences of tuffaceous gold-poor fanglomerate belonging to the Muddy Creek Formation into the basin, local tilting toward the east in response to movements along the Grand Wash fault zone may have occurred during the late Tertiary in the general area of the Lost Basin Range to yield the steeply dipping and partly overturned sequence of mudflows and rhyolitic tuffaceous sedimentary rocks (fig. 3B). Early Proterozoic gneiss, migmatitic gneiss, feldspathic gneiss, and amphibolite in turn may have been faulted against this sequence of steeply dipping and locally overturned mudflows and rhyolitic tuffaceous sedimentary rocks and fanglomerate (fig. 2, unit Ts; see also Deaderick, 1980, pl. 1). Such late Tertiary faulting must have been a near-surface phenomenon and contributed to the development of low hills at and ancestral to the present-day Lost Basin Range. Continued east-west extension is reflected by steeply west dipping normal faults (west side down) along both the east and west range fronts of the Lost Basin Range. These north-south normal faults seem to reflect a westward migration in extensional phenomena away from the Grand Wash fault zone (see Longwell, 1936; Lucchitta, 1966). Some of the past major normal displacements here were concentrated along the Hualapai Valley fault and predated deposition of the nearby Hualapai Limestone Member.

The initiation of block faulting at the Lost Basin Range probably occurred at nearly the same time as deposition

of nontuffaceous locally derived gold-bearing gravels of late Muddy Creek age. These gravels, which contain gold in noneconomic concentrations, most likely were derived in part from the now-eroded upper portions of veins exposed along Lost Basin Range and uplifted possibly as a result of faulting during the late Tertiary. However, continued movements along the normal fault inferred to bound Lost Basin Range immediately on the west, together with the deep post-Muddy Creek erosion just to the west of Lost Basin Range led to the relative uplifting of the gold-bearing gravels at the leading edge of Grapevine Mesa and the reworking of these gravels during the Quaternary into important placer deposits (Lone Jack placers, SW $\frac{1}{4}$ sec. 15, T. 29 N., R. 17 W.). These gold-bearing placers are now perched approximately 500 m above the main drainage of Hualapai Wash, about 5 km to the west.

The relations between the detachment fault, which crops out just east and southeast of Senator Mountain and along the west margin of the White Hills (fig. 2), and the Lost Basin Range are difficult to resolve. The detachment fault probably continues to the southeast from the area of the Cyclopic mine, where it last crops out before being covered by Quaternary gravels (P.M. Blacet, unpub. data, 1967-72). The trace of the detachment fault probably lies to the east of Table Mountain Plateau, approximately 10 km to the southeast of the Cyclopic mine area.

K-AR CHRONOLOGY OF MINERALIZATION AND IGNEOUS ACTIVITY

By EDWIN H. MCKEE

A total of 11 samples were dated by the K-Ar method. These samples include 10 purified mineral separates (eight white mica, one biotite, and one sanidine) and one whole-rock sample (table 3). Sample preparation and argon and potassium analyses were done in the U.S. Geological Survey laboratories, Menlo Park, Calif. Potassium analyses were performed by a lithium metaborate flux fusion-flame-photometry technique, and argon analyses were performed by standard isotope-dilution procedures. Nine of the samples were analyzed using a 60° sector 15.2-cm-radius Neir-type¹ mass spectrometer operated in the static mode in which six manual scans of ⁴⁰Ar, ³⁸Ar, ³⁶Ar peaks were made during a time interval of about 10 minutes. Two samples (table 3, samples 837, 999) were analyzed on a five-collector, first-order, direction-focusing, 22.9-cm-radius mass spectrometer controlled by a PDP8/3 mini-computer that takes peak heights simultaneously from the

¹Any use of trade names and trademarks in this publication is for descriptive purposes only and does not constitute endorsement by the U.S. Geological Survey.

three argon collectors. The constants used in age calculations are:

$$\lambda_e = 0.581 \times 10^{-10}/\text{yr}, \lambda_\beta = 4.963 \times 10^{-10}/\text{yr}, \text{ and}$$

$$^{40}\text{K}/\text{K}_{\text{total}} = 1.167 \times 10^{-4} \text{ mole/mole.}$$

The precision or analytical reproducibility reported as a \pm value is at σ . In a general way, it reflects the relative amount of $^{40}\text{Ar}_{\text{rad}}$ to $^{40}\text{Ar}_{\text{total}}$, the higher percent of $^{40}\text{Ar}_{\text{rad}}$ the smaller the \pm . The \pm value is determined by assessment of the various analytical procedures, including flame-photometer and spectrometer reproducibility and standard and argon tracer calibration. The precision of the eight ages reported ranges from 0.7 to 6.5 percent of the calculated age.

CRETACEOUS PLUTONIC ROCKS

Several small two-mica leucocratic monzogranite plutons crop out in the southwestern part of the study area (fig. 2). Muscovite from a sample of one of these bodies about 2 km north of the Cyclopic mine was dated at 72.0 ± 2.1 Ma, which is Late Cretaceous (Laramide) and

typical of many granitic rocks in central and western Arizona.

Biotite from a sample of Proterozoic gneiss from about 2 km east of this pluton was dated to see what effect, if any, the Cretaceous plutons have had on surrounding rocks. A number of dikes of presumed and (or) known Cretaceous age intrude the gneiss and much or most of the hydrothermal alteration and mineralization is also of Cretaceous age. Radiogenic ^{40}Ar in biotite in the gneiss, which is easily lost at moderately low temperatures, would hopefully reflect the extent of pervasive regional heating during the Late Cretaceous. The biotite yielded an age of 76.3 ± 3.0 Ma, which is very near that of the pluton and substantiates the widespread character of the Laramide event.

CRETACEOUS VEINS

Three quartz-muscovite veins were sampled for age determination. Two of the veins cut granitic rocks known or assumed to be Late Cretaceous in age, and one cuts gneissic rocks of Proterozoic age. Sample 923 (table 3)

TABLE 3.—K-Ar analytical data and ages

Sample and location	Unit name	Mineral dated	K ₂ O percent	⁴⁰ Ar _{rad} 10 ⁻¹¹ mol/g	⁴⁰ Ar _{rad} percent	Apparent age (Ma)
733C 35°59'54" 114°17'40"	Basalt flow in Muddy Creek Formation	Whole-rock basalt	1.045 1.067	1.6619	17.1	10.9±0.6
728A 35°52'00" 114°07'00"	Air-fall tuff	Sanidine	8.48	11.9251	77.2	15.4±0.2
837 35°46'00" 114°14'00"	Quartz-muscovite-fluorite-pyrite vein	Muscovite	10.75	103.001	21.1	65.4±2.6
278A 35°53'15" 114°08'04"	Quartz vein containing hydrothermal muscovite	Muscovite	10.95	108.991	79.4	67.8±2.0
923 35°48'22" 114°15'15"	Muscovite from quartz-muscovite-fluorite-pyrite vein cutting two-mica monzogranite	Muscovite	10.73 10.75	108.465	88.5	68.8±1.8
884 35°48'22" 114°15'15"	Two-mica monzogranite	Muscovite	10.67	112.823	76.9	72.0±2.1
999 35°48'03" 114°12'44"	Gneissic granodiorite	Biotite	9.06	101.666	85.1	76.3±3.0
79GM8b 35°46'42" 114°11'07"	Episyenitic alteration pipe, gold-bearing	Sericite	11.64	220.225	90.8	126.9±3.8
79GM8b 35°46'42" 114°11'07"	Episyenitic alteration pipe, gold-bearing	Sericite	11.64	226.550	87.8	130.3±3.9
735 35°58'45" 114°15'42"	Secondary mica in quartz	Muscovite	10.62	1.3342×10 ⁻⁸	98.0	712±5.0
735-1 35°58'45" 114°15'42"	Secondary mica in quartz	Muscovite	10.67	1.6007×10 ⁻⁸	95.0	822±6.0

cuts the leucocratic monzogranite dated at 72.0 ± 2.1 Ma—it yielded an age of 68.8 ± 1.8 Ma, which is the same as the pluton (within the overlap of the \pm values). The second vein in granitic rock is 4 km southeast of the dated pluton and vein described above. Its K-Ar age is 65.4 ± 2.6 Ma, the same, considering the analytical precision, as the first vein.

Both veins contain fluorite and pyrite as well as white mica and quartz as major components. Gold in trace amounts is also present in the veins and is the metal most sought after in the numerous prospects and small abandoned mines throughout the area. On the basis of these age determinations, mineralization is considered to be Late Cretaceous in age and to be a late stage of the period of Laramide plutonism prevalent throughout the Basin and Range region of Arizona.

The third dated vein (sample 287A) cuts Proterozoic gneiss about 1 km east of the Bluebird mine in the center of the study area. Hand samples of this vein contain what appears to be hydrothermal white mica along with trace amounts of gold. The white mica yields a K-Ar age of 67.8 ± 2.0 Ma and is within the age span of the two veins reported above and about the same as the age of primary muscovite from the leucocratic monzogranite. This age substantiates the thesis that Laramide igneous activity was associated with significant gold mineralization throughout the Gold Basin-Lost Basin area, approximately at the same time as the widespread Laramide porphyry copper deposits formed elsewhere in the Southwest.

Two ages were determined on fine muscovite from a gold-bearing episyenitic alteration pipe in Proterozoic biotite monzogranite about 5 km southeast of the dated Late Cretaceous two-mica leucocratic pluton. This alteration pipe is in the same general area as the dated Late Cretaceous veins, and its mineral assemblage and geologic setting suggest that it is related to and probably the same age as the other veins in the area. The ages from this pipe are 126.9 ± 3.8 and 130.3 ± 3.9 Ma, or twice as old as expected. If the pipe is Late Cretaceous, as field evidence indicates, some type of contamination has affected the sample. Two possibilities that seem most likely include: Excess radiogenic Ar picked up by hydrothermal solutions passing through the surrounding Proterozoic rocks was incorporated into the hydrothermal-vein sericite during its formation, or mineral contamination was caused by inclusion of some Proterozoic muscovite or feldspar from the host gneiss during collection of the vein sample. From the data available, the mechanism that accounts for the anomalously old age of the pipe's muscovite is impossible to verify.

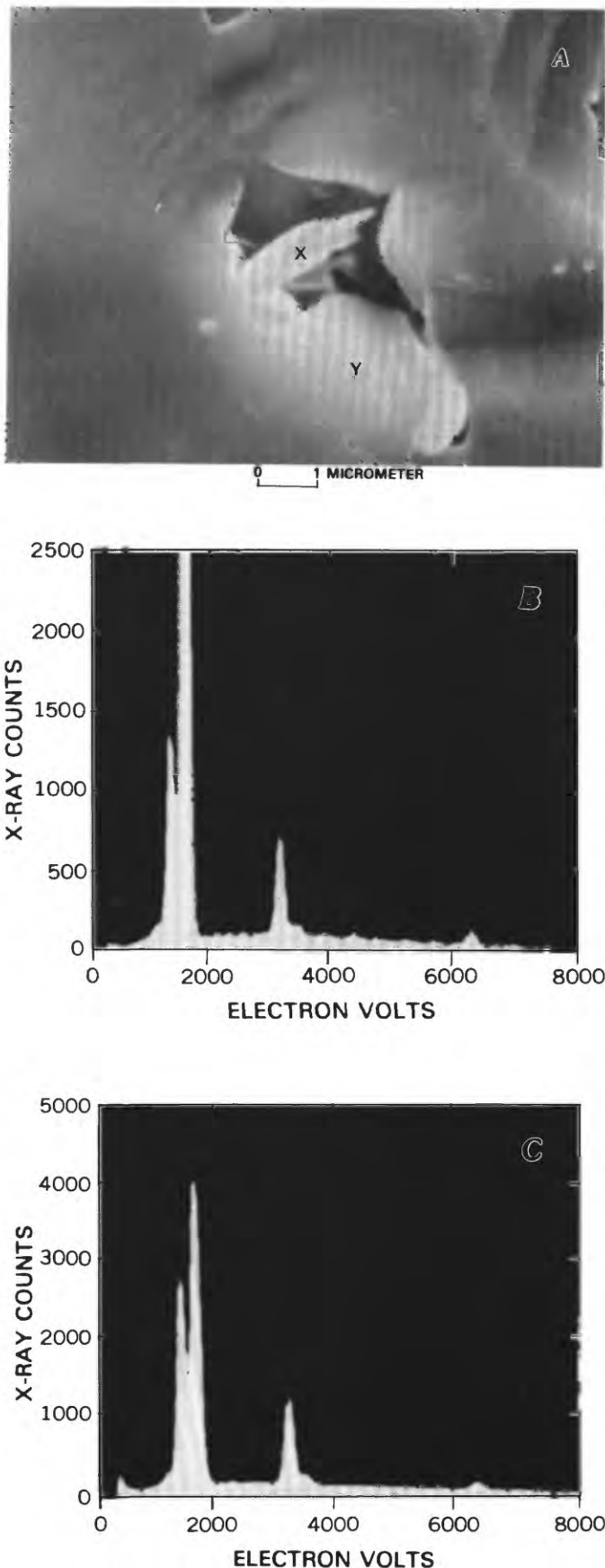
PROTEROZOIC(?) VEIN

Two samples of secondary coarse-grained hydrothermal white mica from a gold-bearing quartz vein about 3 km southwest of Salt Spring Bay on Lake Mead (15 km north

of the study area) were dated. The vein, which cuts Proterozoic gneiss, looks like the other veins in the region, some of which yielded Late Cretaceous or Laramide ages. This vein was thought to be Laramide in age as well; however, the apparent ages are discordant— 712 ± 5 and 822 ± 6 Ma. Interpretation of these values is difficult. Proterozoic gneiss of similar appearance as the host rock of the vein described here is intruded by porphyritic monzogranite that was dated by Rb-Sr methods (a well-defined isochron) at 1,660 Ma (Wasserburg and Lanphere, 1965, p. 746 and fig. 4). This age is similar to many ages of Proterozoic rocks in central and western Arizona and is considered an established age for major regional igneous events in this region (Silver, 1964, 1966, 1967; Ludwig, 1973). The discordant K-Ar ages on the vein white mica could represent partial and different amounts of argon loss from a Proterozoic vein related either to the widespread 1,660-Ma event or a less well documented gold mineralization event at 1,440 Ma. The partial argon loss and accompanying partial resetting of the so-called K-Ar clock may have been caused by slight heating during the Late Cretaceous or early Tertiary Laramide event documented elsewhere in the area. If the rocks near the vein were not heated sufficiently to release all the radiogenically produced ^{40}Ar , the age would be some indeterminate amount less than the original 1,660-Ma age—the 711 and 822 Ma determined here. Alternatively, the partial argon loss could also represent small but continuous argon diffusion from the white mica caused by general regional geothermal elevation throughout the past 1,660 m.y. In either case a reset age that does not record the time of any single event is the result. The vein was assumed to be about the same age as the dated gneiss, or approximately 1,660 Ma.

The possibility exists that the white mica mineral separate from the vein contained a small amount of Proterozoic muscovite from the enclosing host gneiss. A small and different amount of 1,660-Ma contaminant muscovite with a larger amount of Late Cretaceous vein white mica could cause the two aberrant ages. The possibility of this mechanism causing the 711- and 822-Ma ages is impossible to evaluate. Assumedly, the ages do not represent the time of vein emplacement. We believe, however, that the overwhelming bulk of the white mica composing these two mineral separates dated by the K-Ar method crystallized during the vein's emplacement.

Textural relations between white mica and vein quartz from the sample site at locality 735, yielding the 711- and 822-Ma ages, were studied using the scanning electron microscope (SEM; fig. 4). These studies strongly suggest that the white mica there composing the dated samples is secondary. An initially unknown 1.5- μm -long bladed mineral (fig. 4A) was chemically verified by its SEM X-ray spectra as having the same overall proportions of aluminum, silicon, potassium, and iron as a known muscovite standard (compare fig. 4B and C). In addition, some of



these very fine grained bladed crystals, which can reasonably be assumed to be white mica, appear to be growing into 3- to 5- μm irregularly shaped cavities in vein quartz. This relation suggests the white mica is secondary; that is, it crystallized initially during vein formation. These small crystals of mica are probably not daughter minerals but are instead trapped or captured mineral grains (see Roedder, 1972, p. JJ24).

TERTIARY VOLCANIC ROCKS

Samples 733C, basalt, and 728A, rhyolite ash-flow tuff, were dated to aid in establishing the chronology of Tertiary rocks and tectonic events in the Gold Basin-Lost Basin area. The ages were used in conjunction with stratigraphic relations for correlation between units in the complex lenticular sequences of Tertiary basin and sub-aerial deposits of the region. They also provide limits on the age of low-angle faulting (regional sliding) that has displaced most of the Tertiary rocks in the region.

The 15.4 ± 0.2 -Ma age on sanidine from a rhyolite welded ash-flow tuff from a large tectonic block along Salt Creek Wash suggests correlation with the middle part of the Patsy Mine Volcanics or possibly the lower part of the Mount Davis Volcanics as described by Anderson and others (1972). The Patsy Mine Volcanics are composed of more than 1,000 m of lenticular volcanogenic rock including a variety of rhyolitic to dacitic lava flows and tuff beds. The type section for the Patsy Mine Volcanics is in the Eldorado Mountains of Nevada about 70 km due west of the sample site of the tuff reported here. Unspecified Tertiary volcanic rocks, of which the Patsy Mine Volcanics are a part, are shown on figure 2 of Anderson and others (1972) as extending into the Gold Basin-Lost Basin area. Because the middle part of this composite volcanic unit is rhyolite lavas and interstratified tuffaceous sedimentary rocks with K-Ar ages in the range of 14.5 to 18.6 Ma, the correlation with our 15.4 ± 0.2 -Ma rhyolite tuff seems good. In fact, Anderson and others (1972, table 1 and appendix, samples 36-40) record three rhyolite flows with ages that are the same, within analytical uncertainty, as the tuff reported here. Furthermore, sanidine mineral separates used to date the Patsy Mine rocks and the Gold Basin-Lost Basin ash flow have a similar unusually low K_2O content, suggesting a genetic relation.

A sample of basalt collected from the lower of two flows beneath the late Miocene Hualapai Limestone Member of the Muddy Creek Formation near the north-central edge

FIGURE 4.—Scanning electron microscope (SEM) photograph and X-ray spectra. A, SEM photograph of sample collected from locality 735 (pl. 1) showing approximately 1.5- μm -long blade of an unknown mineral (X) projecting into open cavity in vein quartz (Y). B, SEM-produced X-ray spectra for unknown mineral. C, X-ray spectra for known muscovite. B and C were both generated under 20 kV for 100 s.

of the study area and 6.8 km south of Temple Bar yields a K-Ar age of 10.9 ± 0.6 Ma. This age is the same (11.3 ± 0.3 , 11.1 ± 0.5 , and 10.6 ± 1.1 Ma), within the analytical uncertainty, as that of the Fortification Basalt Member of the Muddy Creek Formation as reported by Anderson and others (1972). These ages were subsequently discarded and a new set of ages of 4.9, 5.8, and 5.9 Ma were adopted for the age of the Fortification Basalt Member of the Muddy Creek Formation (Lucchitta, 1979). The locality south of Temple Bar is at least 30 km east of Fortification Hill and 45 and 50 km east-southeast of the collection sites of the other basalt samples, so these samples are probably not from the same lava flow. The concordant ages on basalts indicate that basaltic volcanism was widespread and from a number of vents in the region from 11 Ma to 5–6 Ma.

All of the silicic and intermediate volcanic rocks in the Gold Basin-Lost Basin area (those correlated with the Patsy Mine Volcanics or Mount Davis Volcanics) are in fault contact with surrounding older rocks. This low-angle fault is apparently some type of regional slide surface and not a thrust fault. Other areas in southern Arizona, southeastern California, western Utah, and eastern Nevada in which the terrane is characterized by large slide blocks of Tertiary rocks have almost universally been related to metamorphic core complexes. Gravity tectonics caused by doming of the core complex is the driving force that causes movement of these large slide blocks. In the Gold Basin-Lost Basin area, sliding postdates the rhyolite unit dated at 15.4 ± 0.2 Ma. A second period of sliding is recorded by low-angle fault surfaces between Tertiary conglomerate of the Muddy Creek Formation that is dated about 10.9 Ma and older rocks including Proterozoic gneiss and the Late Cretaceous two-mica monzogranite (see fig. 2). This second period of sliding is probably not much younger than about 10.9 Ma because the Hualapai Limestone Member of the Muddy Creek Formation, a thick carbonate unit in the region about 8 Ma (Blair, 1978), is somewhat younger (Lucchitta, 1979), is largely undeformed, and is not in low-angle fault contact with older rocks.

PETROCHEMISTRY OF CRYSTALLINE ROCKS AND THEIR RELATION TO MINERALIZATION

Metamorphic rocks in the Gold Basin-Lost Basin mining districts have been derived from igneous and sedimentary protoliths that were regionally metamorphosed to as high as upper-amphibolite-facies (Miyashiro, 1973) assemblages and complexly deformed syntectonically during the older Early Proterozoic Mazatzal orogeny (see Wilson, 1939, 1962). This orogeny occurred 1,650 to 1,750 Ma (Silver, 1967). The Mazatzal orogeny thus correlates temporally with the upper half of the Hudsonian orogeny in the Canadian Shield, with final metamorphism in the Front Range,

Colorado, and with the pre-Belt basement, Montana (King, 1969). Early Proterozoic metamorphic rocks in Arizona broadly compose three tectonic belts, of which the northwesternmost one, in the general region of the Gold Basin-Lost Basin mining districts, is mostly gneiss derived largely from an epiclastic protolith (Anderson and Guilbert, 1979); it also includes schist in the Vishnu Complex of Brown and others (1979) derived from shale and graywacke protoliths and some thick sequences of gneiss and amphibolite derived from mafic and, very locally, ultramafic protoliths. Metamorphic rocks in the districts also include metaquartzite, thin lenses of marble, calc-silicate gneiss, banded iron formation, and metachert. The protolith(s) of these metamorphic rocks is difficult to correlate convincingly with specific well-studied sequences of Proterozoic rocks in central Arizona (see Donnelly and Hahn, 1981, for descriptions of these sequences). The Early Proterozoic Bagdad Belt of Donnelly and Hahn (1981) includes relatively thick sequences of coarse- to fine-grained metamorphosed wackes near the top of the overall metamorphic pile there. Some of these metamorphosed wackes may be correlative with quartzofeldspathic gneiss at Gold Basin-Lost Basin.

The gneiss exposed in the Gold Basin-Lost Basin mining districts contains highly deformed and lithologically complex sequences that commonly grade or change abruptly into one another across short distances. Although a quartz-plagioclase (oligoclase or andesine) or quartzofeldspathic gneiss is probably the predominant rock type overall of the gneiss unit, quartzofeldspathic gneiss is complexly interlayered with other lithologies in many outcrops (fig. 5A). In addition, moderately thick, layered sequences of predominantly quartzofeldspathic gneiss may grade into sequences consisting mostly of amphibolite by subtle yet marked changes in the relative proportions of quartzofeldspathic gneiss and amphibolite along strike. Some of the amphibolite in the districts will be shown, in the following section, to have an igneous protolith. In some sequences within the gneiss unit, rather abrupt transitions are also present across conformable contacts, perpendicular to lithologic layering between predominantly quartzofeldspathic gneiss and mixed zones of amphibolite and associated gneissic, pegmatoid leucogranite dikes and thin sills (fig. 5B). However, most of these contacts could not be laterally extended sufficiently to be shown at a scale of 1:48,000, the scale of the map published by Blacet (1975). Further, many outcrops show an overall banded aspect resulting from complex and close interlamination and interlayering of quartzofeldspathic gneiss and amphibolite. In fact, many outcrops in the gneiss unit contain abundant 0.3- to 5.0-cm, highly planar and continuous bands of amphibolite, some bands reaching thicknesses as great as 40 cm. Many such outcrops commonly show a pulling apart or boudinage of the amphibolite layers. In

these outcrops, the foliation in the surrounding quartzofeldspathic gneiss converges dramatically in the necked domains of the amphibolite, suggesting the preferred concentration of ductile flow in the quartzofeldspathic gneiss during deformation. Additional evidence for the brittle behavior of blocks of layered amphibolite during igneous injection includes the infilling of leucogranite along fractures between separated blocks of amphibolite (fig. 6). Some further evidence for the complexity of the prolonged deformation(s) to affect the Early Proterozoic gneiss terrane is reflected in highly contorted and isoclinally folded sequences of gneiss containing locally pervasive cataclasite and mylonite, and mylonitized coarse-grained leucogranite cutting amphibolite and quartz-plagioclase gneiss. The cataclastically deformed rocks must reflect a brittle-type deformation, whereas the largely recrystallized mylonite, including mylonitic schist and mylonitic gneiss, must reflect syntectonic recrystallization accompanying ductile flow.

Widespread and pervasive injection of the gneiss by Early Proterozoic granitic magmas yielded migmatitic

complexes now concentrated mostly along the lower west flanks of Garnet Mountain and near the southernmost extent of Lost Basin Range (fig. 2, units Xgc, Xmg, Xm, and Xml). Migmatitic gneiss (Xmg) and migmatite (Xm) were mapped separately mostly on the basis of the relative proportion of granitic injecta. Migmatitic gneiss includes mostly pelitic gneiss and lesser amounts of, but nonetheless relatively abundant, granitic material; whereas migmatite (Xm) contains mostly Proterozoic granitic rock (fig. 5C). Swarms of leucogranite, aplite, and pegmatite dikes, including varying amounts of pegmatoid quartz veins and irregular quartz masses, cut gneiss locally in the northwestern part of the Garnet Mountain quadrangle and together compose a migmatitic leucogranite complex (Xml).

Approximately 200 thin sections, prepared from metamorphic rocks showing wide-ranging overall bulk chemistries, were studied petrographically. These Proterozoic metamorphic rocks host many of the lode gold deposits known in the districts. For the most part, the metamorphic rocks show prograde mineral assemblages of upper

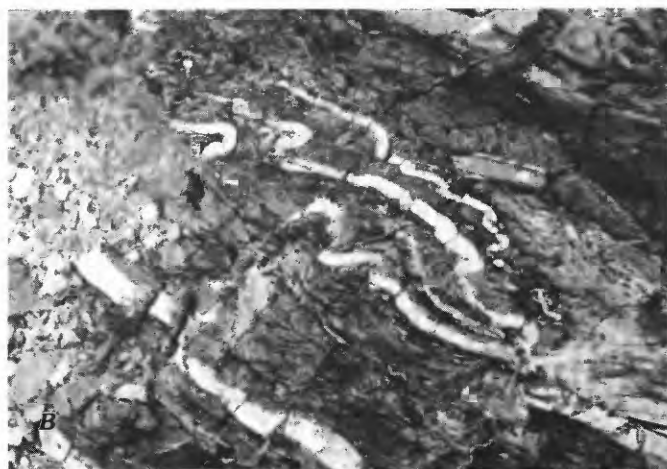


FIGURE 5.—Outcrops of gneiss sequences at various localities in the Lost Basin Range and in the White Hills. *A*, Typical exposure of distinctly layered gneiss showing similar well-developed folds plunging about N. 35°-75° W. Quartz vein cuts gneiss near base of photograph. Note pocket knife near upper center for scale. *B*, Zone of folded thin leucogranite layers confined to 30-cm sequence of chloritized amphibolite within uniformly dipping paragneiss. View toward west approximately parallel to moderately plunging (25°) fold axes. Shearing locally concentrated near axial planes of folds. *C*, Ribboned and spotted migmatitic gneiss containing abundant wispy and discontinuous leucogranitic segregations. Dark bands consist of early garnet-biotite (greenish-brown, Z axis)-minor muscovite-quartz-opaque mineral(s) assemblage that is replaced in part by epidote-chlorite fine-grained muscovite-opaque mineral(s) assemblage. Some blades of chlorite are porphyroblastic and cut schistose fabric of earlier mineral assemblage at high angles. Note pocket knife near upper center of photograph for scale.

amphibolite facies that have been retrograded partly or completely to greenschist assemblages; approximately 70 percent of our thin-sectioned samples contain such retrograde assemblages. In addition to greenschist-facies mineral assemblages locally developed syntectonically during recrystallization of a fabric showing strong crystallographic and dimensional preferred orientation of quartz and various phyllosilicate minerals, some of the metamorphic rocks also are altered deuterically to propylitic assemblages and even phyllic and potassic (see Creasey, 1966; Beane and Titley, 1981) assemblages. The propylitic assemblages are especially well developed in the general area of the major north-striking faults in the southern Lost Basin Range (Deaderick, 1980, pl. 1), and

phyllic and potassic assemblages are present in rocks very close to many of the gold-bearing quartz veins (see following section). However, several areas in the districts have not been affected strongly by retrograde metamorphic effects. These areas include the gneiss south-southeast of the Cyclopic mine, the gneiss exposed near the base of the Grand Wash Cliffs, the migmatitic rocks exposed on Garnet Mountain, and an area of about 15 km² in the northern part of the Lost Basin Range near the north edge of the Garnet Mountain quadrangle (P.M. Blacet, unpub. data, 1967-72).

PELITIC METAMORPHIC ROCKS

Pelitic metamorphic rocks are widespread throughout the gneiss terrane in the Gold Basin-Lost Basin districts. From our studies, however, we were not able to establish an areal distribution of prograde mineral zones in these rocks because of the extensive and locally intense disruptions in metamorphic grade caused by superimposed dynamic retrograde event(s) and somewhat passive hydrothermal phenomena associated with gold mineralization. Most of the pelitic gneiss rocks include composite metamorphic assemblages that reflect disequilibrium or metastability generally between relict, prograde, high-metamorphic-grade assemblages and a subsequent lower grade one. Incomplete metamorphic reactions are recorded in most of the rocks which now contain both product and reactant minerals. Nonetheless, we describe in the following sections petrographic details of the early assemblages in the metamorphic rocks in accordance with increasing grade of characteristic assemblages inferred from classic studies in zoned metamorphic terranes elsewhere (see Miyashiro, 1973; Winkler, 1974). The pelitic metamorphic rocks in the Gold Basin-Lost Basin districts include the following rocks, grouped by dominant characteristic mineral(s): Biotite-muscovite schist, tourmaline schist, almandine-biotite ± staurolite schist and gneiss, kyanite gneiss and schist, and sillimanite- and cordierite-bearing gneiss and schist. Inferred mineral changes and the corresponding metamorphic facies in the pelitic rocks are shown schematically in figure 7. For example, some of the pelitic metamorphic rocks record at least three superposed deformations, one prograde upper amphibolite event, and two retrograde lower amphibolite(?) events (fig. 8). As seen in figure 8, the predominant structure in the rock is a foliation (s_2) which developed penecontemporaneously with the crystallization of muscovite, biotite, and quartz after the metamorphic peak was reached during crystallization of garnet, biotite, and quartz (s_1). The last deformation to affect the rock resulted in a moderately well developed strain-slip cleavage (s_3) that cuts s_2 at angles of about 30°.



FIGURE 6.—Coarse-grained quartz-feldspar leucogranite crosscutting schistosity in 40-cm-thick amphibolite layer in quartzofeldspathic-amphibolite sequence of gneiss and filling a fracture opened between blocks of amphibolite. Some clots of chlorite found as schlieren in leucogranite probably reflect altered amphibolite xenoliths torn from wall rock of leucogranite. Photograph taken on west flank of southern Lost Basin Range. Ruler is 11 cm long.

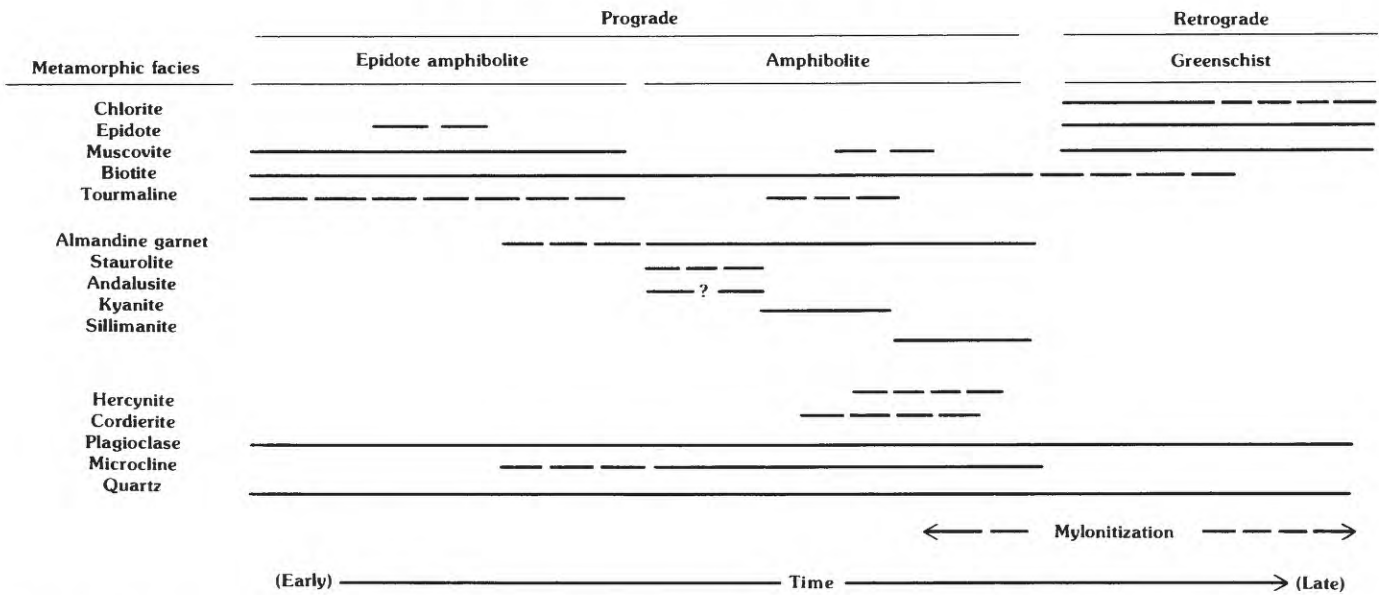


FIGURE 7.—Inferred mineral changes and corresponding metamorphic facies in pelitic rocks from the Early Proterozoic gneiss terrane of Gold Basin-Lost Basin mining districts. Solid line, ubiquitous mineral presence; dashed line, sporadic mineral presence; queried where mineral distribution uncertain.

MUSCOVITE-BIOTITE SCHIST

Muscovite-biotite schist that presumably dates from the prograde metamorphism of the area is sporadically present as layers within other lithologies in the gneiss. Samples of these rocks contain mostly a muscovite-biotite-quartz assemblage wherein the biotite is typically dark brown (Z axis) under the microscope. Potassium feldspar is notably absent from this assemblage. Muscovite and biotite in some of the more pelitic of these rocks show apparently compatible relations with minor amounts of tourmaline, oligoclase, opaque minerals, and apatite (fig. 9A). Further, where some of the schist is retrograded slightly, it shows incipient neocrystallization of very fine grained quartz and muscovite along 0.1- to 1.0-mm-wide zones of axial-plane cleavage, which cut the dominant foliation in the rock at high angles (fig. 9B). Such retrograded schist also contains sparse porphyroblasts of disseminated chlorite, showing a strong preferred orientation of its {001} cleavage, which parallels also the axial-plane cleavage in the rock. We infer from the very wide ranging proportions of phyllosilicates and tourmaline in the muscovite-biotite schist that this unit may grade locally into tourmaline-rich rocks, described in the following section.

These white mica (presumably muscovite)-biotite assemblages are not particularly useful indicators of barometric conditions during metamorphism, but they can be used to estimate approximately the upper limit of temperatures in the rocks during the early stages of the prograde event. The absence of stilpnomelane in these rocks suggests that

the metamorphic event occurred at a grade higher than the stilpnomelane isoreaction grad (Winkler, 1974), which has been placed at temperatures slightly greater than 425 to 460 °C using the experimental studies of Nitsch (1970). Nitsch studied the breakdown of stilpnomelane + phengite

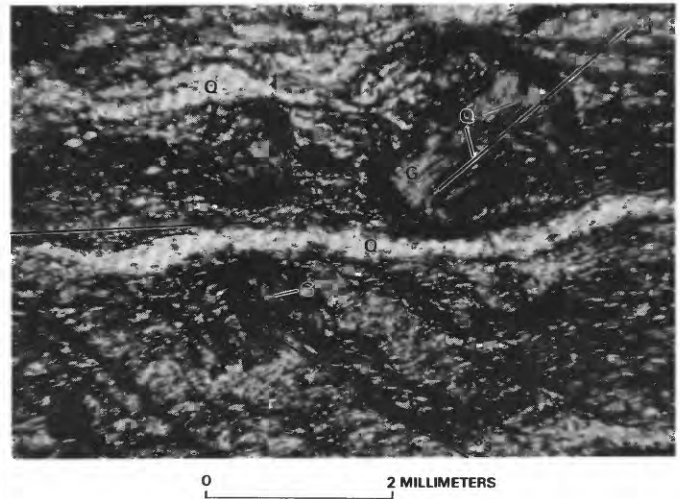
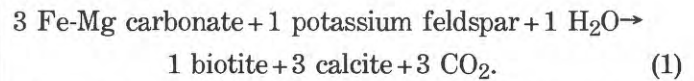


FIGURE 8.—Laminated muscovite-biotite-quartz schist showing fabric composed of three distinct *s* surfaces reflecting three superposed deformations. Oldest surface (*s*₁) has weakest preferred orientation over all the rock and is defined by aligned trains of wispy quartz (Q) inclusions in garnet (G) porphyroclasts. *s*₂, dominant foliation in rock, is defined by strong preferred crystallographic orientation of muscovite and biotite and dimensional orientation of additional quartz. *s*₃, strain-slip cleavage; cuts *s*₂ at angles of about 30° and contains increased abundances of muscovite and biotite relative to *s*₂. Sample GM-73.

to biotite + chlorite + quartz + H₂O. However, these temperature estimates are based on the assumption that the partial pressure of water (P_{H_2O}) equalled total pressure (P_{tot}) during the prograde event. This assumption probably is not valid, however, as will be discussed subsequently. Therefore, the 425 to 460 °C temperature range should be considered only as the highest temperatures one would infer for the onset of such white mica-biotite assemblages. Miyashiro (1973) notes that stilpnomelane may occur in high-pressure metamorphic terranes and very rarely in low-pressure ones, a relation that may further constrain the thermal implications of the absence of stilpnomelane.

Some of the mica schists also show textural relations suggesting compatibility between biotite and carbonate, probably calcite, during the prograde metamorphism of the area (fig. 9C). From the absence of talc and tremolite as the first silicate minerals to crystallize in this assemblage and the appropriate experimentally determined carbonate-silicate equilibria (Skippen, 1971; Winkler,

1974, p. 113), we infer that the molecular fraction of carbon dioxide, at least locally, must have been very high in the fluid(s) associated with metamorphism. Winkler (1974) further suggests that such a high molecular fraction of carbon dioxide in the fluid(s) may have been maintained by a reaction such as



However, the early biotite (dark brown, Z axis)-carbonate-quartz assemblage in the fine-grained schist, exemplified by sample GM-339 (fig. 9C), has been replaced significantly by a retrograde greenschist assemblage of chlorite, epidote (clinzoisite), white mica, and minor rutile. The white mica probably is mostly muscovite, but it may include some margarite. Where ductile flow was concentrated in these micaceous rocks during the biotite-destructive greenschist metamorphic event, the rocks were converted into chlorite-rich phyllonitic schist. Such changes commonly occur across sharp boundaries and are reflected by marked modal differences. These changes are primarily an increased abundance of chlorite and white mica, whereas there are sharply decreased amounts of biotite. Further, in these domains of chlorite-rich

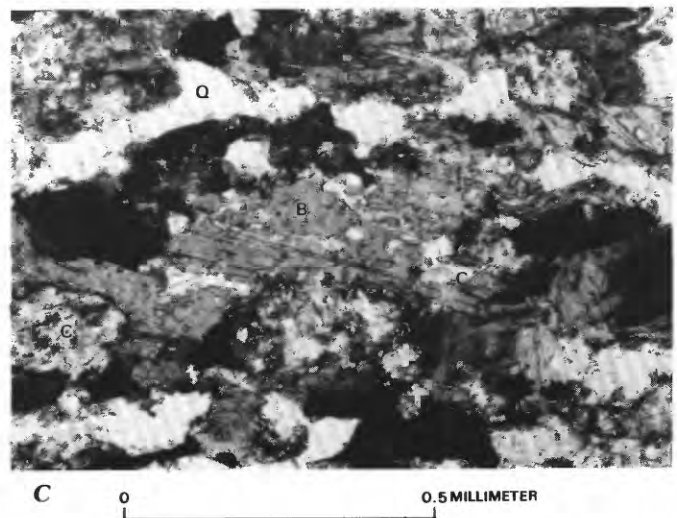
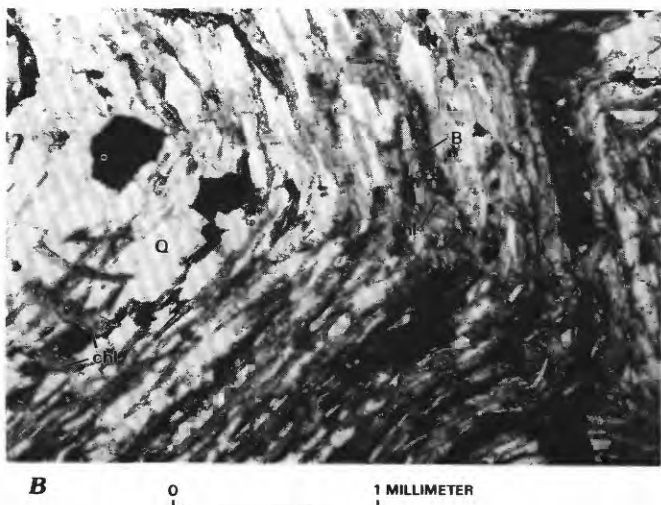
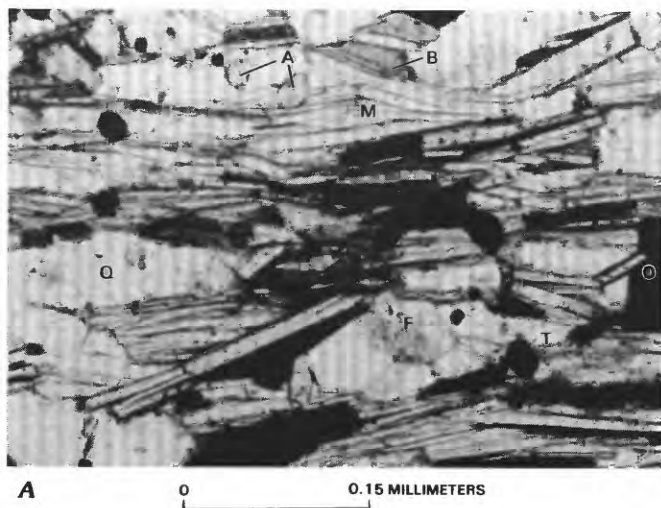


FIGURE 9.—Schist containing relatively abundant concentrations of muscovite (M) and (or) biotite (B). Plane-polarized light. Q, quartz. A, Unretrograded quartz-biotite-muscovite schist containing minor tourmaline (T), apatite (A), opaque minerals (O), and oligoclase feldspar (F). Sample GM-233. B, Crenulated quartz-biotite-muscovite schist showing incipient neocrystallization of quartz and muscovite along zones of axial-plane cleavage, which cut dominant foliation in rock at high angles. Sparse porphyroblasts of chlorite (chl) aligned with their {001} cleavage traces parallel to the axial-plane cleavage. Sample GM-273. C, Apparently compatible relict biotite (B) and carbonate (C) in a highly retrograded biotite-chlorite-white mica-epidote (clinzoisite) schist. Sample GM-339.

phyllonitic schist, calcite is a conspicuous relict from the earlier biotite-stable metamorphic event, and it shows mostly an intensification of its dimensional orientation wherein the short axes of the calcite grains are transverse to the trace of the foliation. A chemical analysis of a sample of heavily retrograded biotite-carbonate schist shows a very low Na_2O content of 0.1 weight percent, a CO_2 content of 3.1 weight percent, and a relatively high TiO_2 content of 1.9 weight percent (table 4, analysis 1).

TOURMALINE SCHIST AND GNEISS

Tourmaline, a complex boron-bearing silicate typically containing 8 to 10 weight percent B_2O_3 (Deer and others, 1962a), is present in significant concentrations at several localities in the gneiss terrane. However, within most of the gneiss, tourmaline is a relatively sparse mineral that crystallized during the early metamorphism of the area. In those rocks containing tourmaline in relatively abundant concentrations of perhaps as much as 30 volume percent, the prismatic crystals of tourmaline show a very strong preferred orientation that defines the metamorphic foliation or *s* surface. Generally, the known tourmaline schists or tourmalinites form zones that may be several centimeters thick, mostly in sequences of quartzofeldspathic gneiss. Many of these zones show well-developed, small-scale, composite folds that reflect a combination of shear along an axial-plane cleavage and buckling due to lateral compression (fig. 10A). In such folded rocks, the leucocratic layers include mostly quartz, muscovite, tourmaline, and sparse oligoclase. These leucocratic layers show a more ductile behavior during deformation than the dark, tourmaline-rich layers. Under the microscope, the tourmaline-rich layers are composed of aggregates of fine-grained crystals that measure approximately 0.1 mm across their basal sections. The tourmaline is strongly pleochroic from very pale light olive gray to dark greenish blue. Such a pleochroic scheme suggests that the tourmaline in these rocks is the iron-containing variety known as schorl (Deer and others, 1962a). However, the identification of the compositional variety of tourmaline primarily by color may be misleading (Jones, 1979). In addition, tourmaline in these rocks shows apparently stable compatibilities with a broad spectrum of the characteristic minerals used typically as zonal indicators in pelitic metamorphic terranes. As described above, it is present in sparse concentrations with prograde quartz-muscovite-biotite assemblages. Tourmaline is also present in epidote-quartz-microcline-muscovite-plagioclase-opaque mineral assemblages that compose the wispy banded layers within quartzitic sequences of the gneiss. Tourmaline is also abundant in somewhat higher grade schists containing a muscovite-biotite-almandine(?) garnet-quartz-sparse potassium feldspar assemblage. The tex-

tural relations and crystal forms of the garnets in this assemblage suggest they are in their initial stages of crystallization (fig. 10B). Some quartz-kyanite clots in the metamorphic rocks, which will be discussed fully in a following section describing kyanite relations, also contain tourmaline. However, tourmaline was not found to be associated with sillimanite, cordierite, or staurolite. Nonetheless, it has been reported to occur with staurolite in mica schist of the Alto Adige region, Italy (Gregnanin and Piccirillo, 1969), with garnet and staurolite in the eastern Alps, Austria (Ackermann and Morteani, 1977), with staurolite and sillimanite in metamorphic rocks of the Kamchatka Peninsula, U.S.S.R. (Lebedev and others, 1967), and with staurolite and kyanite in the Black Mountain area, New Hampshire (Rumble, 1978). A tourmaline-quartz association is also present in some rocks of the Early Proterozoic Yavapai Series (Anderson and others, 1971) of the Jerome, Ariz., area (S.C. Creasey, oral commun., 1979), and tourmaline is a common accessory in amphibolite-facies micaceous and quartzofeldspathic schist of the Early Proterozoic Vishnu Complex in the Grand Canyon (Brown and others, 1979).

Experimental studies further substantiate the wide-ranging, pressure-temperature stability of tourmaline. Reynolds (1965) showed that a marked redistribution of boron occurs at metamorphic conditions near the greenschist facies. He concluded that boron typically is expelled from a boron-bearing, 1 Md lattice of illite in sedimentary rocks when recrystallized during metamorphism to the 2 M polymorph and that the expelled boron is fixed finally in tourmaline. However, the extremely high concentrations of boron required locally by these stratiform occurrences of tourmaline schist (fig. 10A), or tourmalinite in the usage of Nicholson (1980), indicate that boron-bearing clays could not have been the primary source of boron here (see Ethier and Campbell, 1977). Further, the tourmaline in the tourmaline schist obviously reflects recrystallization dating from the prograde metamorphism of the area. Although detrital tourmaline grains commonly act as nuclei for any newly crystallized tourmaline, careful petrographic examination of these tourmaline-bearing rocks revealed that the tourmaline does not now show overgrowths, broken crystals, or any variably rounded crystal forms. Thus, the tourmaline-bearing biotite-stable schists in the Gold Basin-Lost Basin districts are well beyond the lower stability limit of tourmaline. At the high metamorphic end of the spectrum, the experimental studies of Robbins and Yoder (1962) in the system dravite- H_2O suggest temperatures greater than 800 °C at pressures ($P_{\text{H}_2\text{O}}$) greater than 50 MPa are needed to decompose dravite, the Fe-free Mg-bearing tourmaline, into mostly cordierite bearing assemblages.

The provenance of the protolith and the overall petrogenesis of the tourmaline schist remain nonetheless

TABLE 4.—*Chemical analyses of selected schist and gneiss from the Gold Basin-Lost Basin mining districts compared with analyses of slate, argillite, shale, graywacke, and arkose*

[Chemical analyses by rapid-rock methods; analysts, P.L.D. Elmore and S. Botts. Methods used are those described by Shapiro (1967). Spectrographic analyses by Chris Heropoulos. Results are identified with geometric brackets whose boundaries are 1.2, 0.88, 0.56, 0.38, 0.26, 0.18, 0.12, and so forth, but are reported arbitrarily as midpoints of these brackets, 1, 0.7, 0.5, 0.3, 0.2, 0.15, 0.1, and so forth. The precision of a reported value is approximately plus or minus one bracket at 68-percent confidence or two brackets at 95-percent confidence. Looked for but not found: Ag, As, Au, B, Be, Bi, Cd, Mo, Pd, Pt, Sb, Sn, Te, V, W, Zn, Ge, Hf, In, Li, Re, Ta, Th, Tl, Eu; ---, not detected; N.D., not determined; Tr, trace]

Analysis -----	1	2	3	4	5	6	7	8	9	10	11
Sample -----	GM-339	GM-555	GM-312b	GM-255	GM-295	GM-498					
Chemical analyses (weight percent)											
SiO ₂ -----	50.9	66.8	76.3	75.4	75.0	72.3	60.6	66.9	60.2	66.7	77.1
Al ₂ O ₃ -----	13.6	17	12.3	12.4	12.7	14	17.3	15.4	16.4	13.5	8.7
Fe ₂ O ₃ -----	3.4	1.2	1	1.6	1.7	2.8	2.3	2.8	4	1.6	1.5
FeO -----	10.4	4.4	.68	1.9	1.7	2.2	3.7	1.9	2.9	3.5	.7
MgO -----	5	1.7	.6	1.7	.4	.7	2.6	2.4	2.3	2.1	.5
CaO -----	5.7	.90	3.3	2.1	3	4.3	1.5	.34	1.4	2.5	2.7
Na ₂ O -----	.1	1.4	3	2.7	3	3	1.2	1.2	1	2.9	1.5
K ₂ O -----	2.4	4	1.3	1.3	1	.7	3.7	6.6	3.6	2	2.8
H ₂ O+ -----	3.4	1.8	.87	.98	1	1.1	3.5	1.4	3.8	2.4	.9
H ₂ O- -----	.05	.08	.02	.02	.05	.04	.62	.00	.89	.6	N.D.
TiO ₂ -----	1.9	.74	.08	.13	.12	.01	.73	.47	.76	.6	.3
P ₂ O ₅ -----	.24	.05	.00	.01	.04	.07	N.D.	.23	.15	.2	.1
MnO -----	.06	.12	.02	.06	.09	.06	N.D.	.05	Tr	.1	.2
CO ₂ -----	3.1	<.05	.05	.05	.15	.05	1.5	.28	1.5	1.2	3
Total -----	100	100	100	100	100	101	99	100	99	100	100
Semiquantitative spectrographic analyses (weight percent)											
Ba -----	0.05	0.15	0.1	0.07	0.1	0.07					
Co -----	.005	.0015	----	.0005	.0003	.001					
Cr -----	.007	.007	----	.0002	.0002	.0005					
Cu -----	.005	.001	.0001	.001	.0005	.0005					
La -----	----	.007	----	----	----	----					
Mo -----	.001	----	----	----	----	----					
Nb -----	.001	.0015	----	----	----	----					
Ni -----	.005	.003	----	.0002	----	.0003					
Pb -----	----	----	.0015	.001	.0007	----					
Sc -----	.005	.0015	.001	.001	.001	.002					
Sr -----	.02	.02	.03	.015	.03	.05					
V -----	.05	.007	----	.0007	.002	.0005					
Y -----	.002	.003	.0015	.001	----	.0015					
Zr -----	.007	.02	.007	.007	.01	.003					
Ce -----	----	.02	----	----	----	----					
Ga -----	.003	.003	.0015	.001	.001	.0015					
Yb -----	.0003	.0003	.0002	.0001	.0001	.0002					

1. Highly retrograded biotite-carbonate-chlorite-white mica-epidote schist (unit Xgn, of fig. 2); NE1/4 sec. 7, T. 29 N., R. 17 W.
2. Schist showing an assemblage of biotite, chlorite, white mica, clinozoisite, and quartz superposed on an earlier garnet-bearing one (unit Xgn); UTM, 753,600 m E., 3,987,050 m N.
3. Quartz-rich quartzofeldspathic gneiss (unit Xgn); NE1/4 sec. 19, T. 29 N., R. 17 W.
4. Quartzofeldspathic gneiss (unit Xgn); SW1/4 sec. 20, T. 29 N., R. 17 W.
5. Quartzofeldspathic gneiss (unit Xgn); SE1/4 sec. 17, T. 29 N., R. 17 W.
6. Quartzofeldspathic gneiss (unit Xgn); NE1/4 sec. 33, T. 30 N., R. 17 W.
7. Average of 16 analyses of slate (Pettijohn, 1949, p. 344).
8. Argillite, Precambrian Fern Creek Formation, Dickinson County, Mich. (Pettijohn, 1949, p. 345).
9. Composite sample of 51 Paleozoic shales (Clarke, 1924, p. 552).
10. Mean composition of 61 analyses of graywacke (Pettijohn, 1963, table 12). Also includes 0.3 weight percent SO₃, 0.1 S and 0.1 C.
11. Mean composition of 32 analyses of arkose (Pettijohn, 1963, table 12).

problematical, especially the rocks that are rich in quartz. In these rocks, tourmaline and quartz form the predominant mineral association, a common association as noted above. Elsewhere, quartz-tourmaline clasts are present in the Late Proterozoic Torridonian Group of northwest Scotland (Allen and others, 1974). These authors infer

such rocks to be derived from contact aureoles of high-level granites in the source area of the Torridonian Group. Rarely, however, quartz has been reported to be found also as a replacement of tourmaline (McCurry, 1971). The provenance of the tourmaline-quartz schist in the Gold Basin-Lost Basin districts appears to be different in that

the schist composes wispy stratiform zones containing sparse concentrations of other minerals that also have relatively high specific gravities. The specific gravity of tourmaline is approximately 3.00 to 3.20 (Deer and others, 1962a). These relations suggest that the tourmaline schist or tourmalinite may reflect local syngenetic exhalative emanations of boron-rich fluids onto the sea floor, where the protolith of the Proterozoic metamorphic rocks occurred. Such a syngenetic model for similar rocks elsewhere has been proposed recently (Ethier and Campbell, 1977; Nicholson, 1980; Plimer, 1980; Slack, 1980). The exploration implications of these rocks will be discussed in the section entitled "Suggestions for Exploratory Programs."

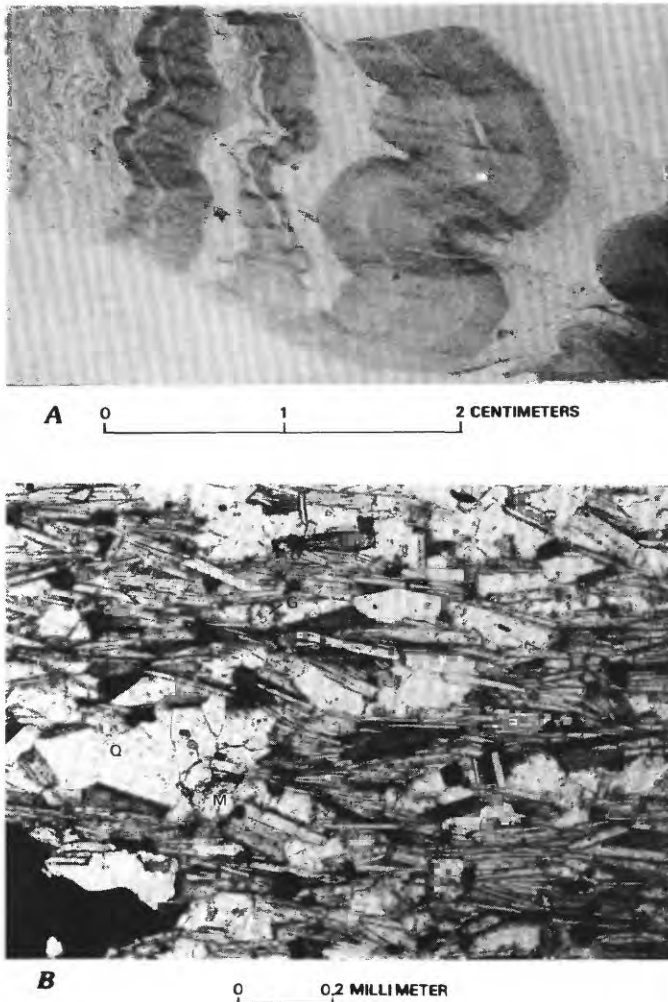
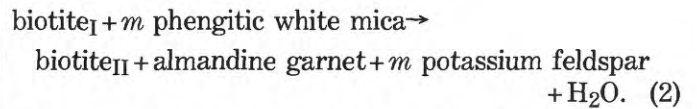


FIGURE 10.—Structural and textural relations of tourmaline in metamorphic rocks. Plane-polarized light. A, Composite small-scale folds in tourmaline schist. Sample GM-296. B, Disseminated euhedral crystals of fine-grained garnet in a tourmaline-biotite-muscovite schist. T, tourmaline; Q, quartz; G, garnet; M, microcline. Sample GM-297a.

ALMANDINE-BIOTITE±STAUROLITE SCHIST AND GNEISS

Pelitic schist and gneiss in the Proterozoic metamorphic terrane also include almandine-biotite-quartz-potassium feldspar-plagioclase assemblages. The potassium feldspar is mostly microcline, and the plagioclase is mostly oligoclase or andesine, although some of these rocks rarely contain albite. Minor accessory minerals include apatite, opaque mineral(s), and rutile. Some of the initial crystallization stages of almandine are recorded by rocks still containing muscovite and biotite, as described in the preceding section. In such a mineral association, almandine garnet is present as euhedral 0.1-mm-wide porphyroblasts in a fabric wherein the schistosity and subsequent strain-slip cleavage are defined by muscovite and biotite. Textural relations suggesting specific reactions that controlled the crystallization and growth of almandine are very difficult to ascertain. Generally, however, increased modal abundances of almandine and microcline appear to have been compensated by (1) a decrease in overall abundance and eventual disappearance of muscovite and (2) a change in the color of biotite from dark brown (Z axis) to reddish brown (Z axis). These changes are accompanied also by an apparent increase in grain size. The first crystallization of almandine-rich garnet in these rocks is not sharply defined areally and is not marked by the disappearance of a phyllosilicate phase. Instead, we infer from our petrographic observations that the initial crystallization of garnet reflects a reaction such as



We suggest that early dark-brown (Z axis) biotite_I is an iron-rich variety and that the ensuing red-brown (Z axis) biotite_{II} is a variety containing more magnesium than biotite_I. If reaction (2) is mostly correct for the onset of the biotite_{II}-almandine-potassium feldspar compatibility, then the magnesium content of biotite_{II} may be derived principally from the breakdown of phengitic white mica, which may have magnesium substituted for aluminum in its octahedral structural sites (Deer and others, 1962b). Further, *m* in reaction (2) may be greater than one, thus reflecting a preferred consumption of white mica relative to biotite_I. In addition, reaction (2) provides a mechanism whereby biotite_{II} in the rocks becomes more magnesian and thus stable to higher temperatures than biotite_I.

Staurolite (ideally Fe₂Al₉Si₄O₂₃(OH)) was found at only one locality (GM-922), near the south edge of the Gold Basin district, approximately 5 km south of the Cyclopic mine. Ribboned and spotted migmatitic gneisses there are retrograded partly to a chlorite-white mica greenschist assemblage. However, the melanosomes of these rocks

contain a well-developed, garnet-biotite-staurolite-quartz-andalusite(?) assemblage with an absence of potassium feldspar and plagioclase. Andalusite is possibly present in the rock in trace amounts as crystals apparently compatible with garnet during the prograde event, but subsequently highly altered to white mica during the retrograde event. Equant to stubby-prismatic crystals of staurolite measure typically 0.5 to 1.0 mm wide and they form, in places, 120° dihedral angles against euhedral porphyroblasts of garnet (fig. 11A). Under the microscope, the staurolite is strongly pleochroic from colorless (X axis) to pale golden yellow (Z axis); some crystals are twinned. In the melanosomes of these staurolite-bearing rocks, chlorite and white mica partly replace mostly biotite as fine-grained porphyroblasts at high angles to the trace of the foliation defined by the biotite. Many of the staurolite crystals are also rimmed by aggregates of very fine

grained white mica. However, the crystals of garnet here are remarkably free of replacement phenomena related to the retrograde event.

The presence of staurolite in the almandine-biotite schist and gneiss allows us to make some inferences concerning the prograde metamorphism of the area during the Early Proterozoic. The onset of the crystallization of staurolite is generally accepted to be at temperatures somewhat higher than almandine garnet (Miyashiro, 1973) and to indicate thereby that regionally metamorphosed rocks have reached at least a medium grade, or temperatures in the 500 to 550 °C range (Winkler, 1974). Although staurolite can apparently form across a broad spectrum of pressure environments (Miyashiro, 1973), its maximum stability determined experimentally in the presence of quartz, muscovite, and biotite appears to be about 675 °C at 550 MPa and about 575 °C at 200 MPa, $P_{H_2O} = P_{tot}$ and $Mg/(Mg+Fe) = 0.4$ (Hoschek, 1969). G. Hoschek further found that a relatively high Fe/(Mg + Fe) ratio will expand the stability field of staurolite. Thus, the very restricted presence of staurolite in contrast with the very wide distribution of cordierite in the Proterozoic terrane of the Gold Basin-Lost Basin districts may reflect such chemical controls. Although staurolite is present here in an assemblage questionably containing andalusite, staurolite-bearing assemblages elsewhere are

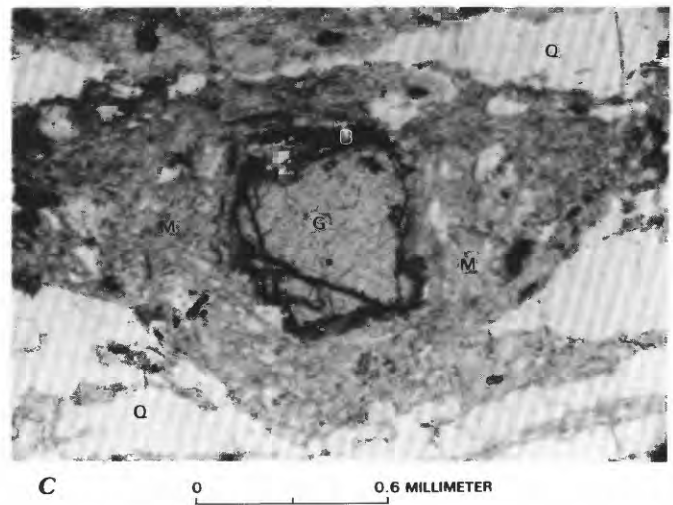
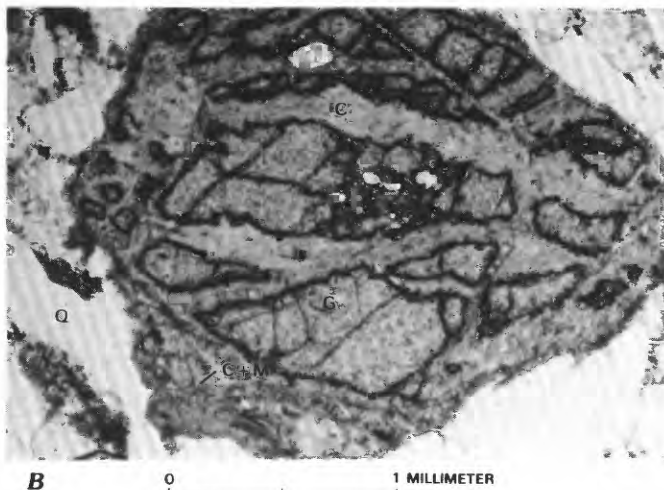
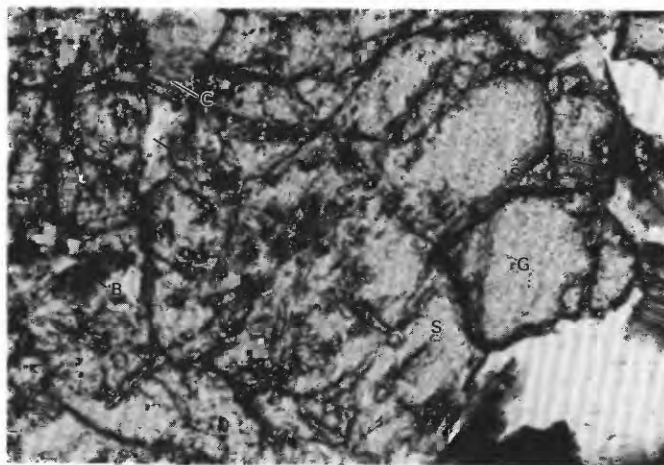


FIGURE 11.—Textural relations among minerals in garnet-bearing gneiss. G, garnet; S, staurolite; B, biotite; C, chlorite; M, white mica; Q, quartz. Plane-polarized light. A, Textural relations in garnet-staurolite-biotite gneiss relict from prograde event. Chlorite and white mica crystallized during subsequent greenschist retrograde event. Sample GM-922a. B, Rounded and highly altered crystals of garnet in retrograded garnetiferous leucogneiss. Partially chloritized garnets are replaced by aggregates of very fine grained white mica. Sample GM-462. C, Mylonitic fabric consisting of biotite-chlorite-white mica-clinozoisite-quartz assemblage superposed during greenschist retrograde event on an earlier garnet-bearing assemblage. Sample GM-555.

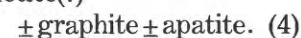
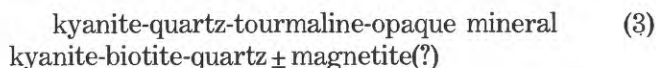
reported commonly to include all three aluminosilicate polymorphs (Hietanen, 1973; Carmichael, 1978; Dusel-Bacon and Foster, 1983).

Almandine-biotite prograde assemblages are also present in some rocks intermediate in composition between the pelitic and quartzofeldspathic gneisses. However, many of these rocks are retrograded intensely, as exemplified by garnet-bearing leucogneiss that is interlayered with quartzofeldspathic and amphibolite gneisses (fig. 11B). In the garnet-bearing leucogneiss, partially chloritized crystals of garnet are as much as 1 cm across in some of the layers. The cores of many of the garnets host rounded fine-grained crystals of quartz, engulfed possibly by rapid growth of garnet during its early stages of crystallization. Further, the garnets are replaced at their margins and along fractures by pale-green chlorite and some white mica. The light-colored matrix of the rocks consists of quartz, clouded feldspar, and a few relicts of biotite now replaced largely by interlayered chlorite. Most oligoclase grains are partly replaced by white mica and clinozoisite and (or) epidote. The almandine, which is present in some gneiss, is intermediate chemically between the pelitic and quartzofeldspathic end members and shows excellent textural relations indicating the crystallization of some retrograde biotite (fig. 11C). In these rocks, fractured crystals of garnet contain alteration rims of biotite. In addition, the garnets are microveined by biotite, chlorite, and white mica, which together with clinozoisite and quartz make up the predominant minerals in the mylonitic fabric that developed contemporaneously with retrograde metamorphism and isoclinal folding of some sequences of gneiss. Chemical analysis of such a rock shows contents of Al_2O_3 , of total alkalis ($\text{K}_2\text{O} + \text{Na}_2\text{O}$), and ratios of $\text{SiO}_2/\text{Al}_2\text{O}_3$ similar to fine-grained detrital rocks (table 4, compare analysis 2 with analyses 8–10).

KYANITE-BEARING GNEISS

Kyanite (Al_2SiO_5) is present in at least three localities in the Early Proterozoic gneiss terrane of the Gold Basin-Lost Basin districts, and it has been reported only from about 12 widespread localities across all three Proterozoic metamorphic belts of Arizona (Espenshade, 1969; Galbraith and Brennan, 1970). However, kyanite may occur more commonly in the Proterozoic rocks of Arizona than believed previously because systematic petrographic examination of some relatively highly metamorphosed Early Proterozoic Pinal Schist at Mineral Mountain southeast of Phoenix (Theodore and others, 1978) revealed its presence there also (T.G. Theodore, unpub. data, 1979). Indeed, the anhydrous chemistry of kyanite and its polymorphs, sillimanite and andalusite, make parageneses involving these minerals excellent diagnostic pressure-temperature indicators for moderate temperature region-

ally metamorphosed pelitic assemblages (Kepezhinskas and Khlestov, 1977; and many others). As described below, one can make certain barometric inferences from kyanite and sillimanite parageneses using the appropriate thermodynamically generated equilibrium curves and the appropriate experimentally determined phase relations (Helgeson and others, 1978, fig. 49). Early prograde assemblages in kyanite-bearing pelitic paragneiss in the Gold Basin-Lost Basin districts include:



The kyanite-bearing assemblages (3) and (4) were found at three widely separated localities in the districts. Assemblage (3) is present in gneissic schlieren within a mixed granodioritic complex (unit Xmg of figure 2) on the lower west flanks of Garnet Mountain (SW $\frac{1}{4}$ sec. 15, T. 28 N., R. 17 W.). Assemblage (4) is present in samples collected from two localities: the first is in a thin layer of pelitic biotite schist within foliated and lineated hornblende amphibolite on the west flank of the Lost Basin Range (SE $\frac{1}{4}$ sec. 18, T. 29 N., R. 17 W.), and the second locality is in migmatitic gneiss that crops out in Grapevine Wash, approximately 2.5 km southwest of the Grand Wash Cliffs. This last sample locality containing kyanite assemblage (4) falls well within the projected outer limit of the suite of Early Proterozoic plutonic igneous rocks exposed predominantly in the general area of Garnet Mountain. Thus, two of the kyanite-bearing assemblages are related spatially with the igneous rocks of Garnet Mountain.

The kyanite-bearing assemblages known in the Garnet Mountain quadrangle now appear to be of two genetic types. The first includes locally preserved relicts initially crystallized prior to and separately from the enclosing schist and possibly shed detritally into the metamorphic terrane's protolith or, more likely, preserved in situ from an earlier stage of the metamorphic event. The other kyanite-bearing assemblage crystallized syntectonically, penecontemporaneous with development of the enclosing schistose fabric, which is strongly lineated. The first assemblage in fact shows textural relations strongly suggesting physicochemical incompatibility with its enclosing phyllosilicate-dominant fabric. Kyanite in assemblage (4) thus is present in 0.6- to 1.0-mm, sieve-textured clots containing minute, highly rounded crystals of quartz. These crystals of quartz are aligned in trains defining *s* surfaces at very high angles to the schistosity in a quartz-muscovite-chlorite-albite-cordierite(?) fine-grained schist. In addition, the kyanite is altered partially along its rims to white mica, probably muscovite (fig. 12A). Kyanite in one of the two samples of assemblage (4) shows a very strong preferred orientation of its *c* axis which lies in, and

partly defines, the foliation of sample GM-283 (fig. 12*B*). Kyanite and biotite are apparently compatible in this sample because they are juxtaposed along sharp, straight crystal contacts showing at high magnifications no indication in either mineral of replacement by the other (fig. 12*B*). In addition, the kyanite in this rock shows relations indicative of partial replacement by two subsequent generations of muscovite. The two generations of muscovite comprise (1) large single crystals and (2) very fine grained crystals of muscovite aggregated into microveinlets that cut the earlier crystallized kyanite. We want

to emphasize again that the important feature of sample GM-283 is its apparent hosting of syntectonically crystallized kyanite. Finally, two of the kyanite-bearing samples studied (samples GM-283 and GM-1010c) contain another Al_2SiO_5 polymorph, sillimanite. However, the two minerals in these samples do not show textural relations of apparent mutual compatibility. Sillimanite appears to postdate crystallization of kyanite. In sample GM-1010c, fibrous sillimanite partly replaces kyanite as a direct nucleation product, but more commonly sillimanite replaces an intervening muscovite, possibly by a paired or

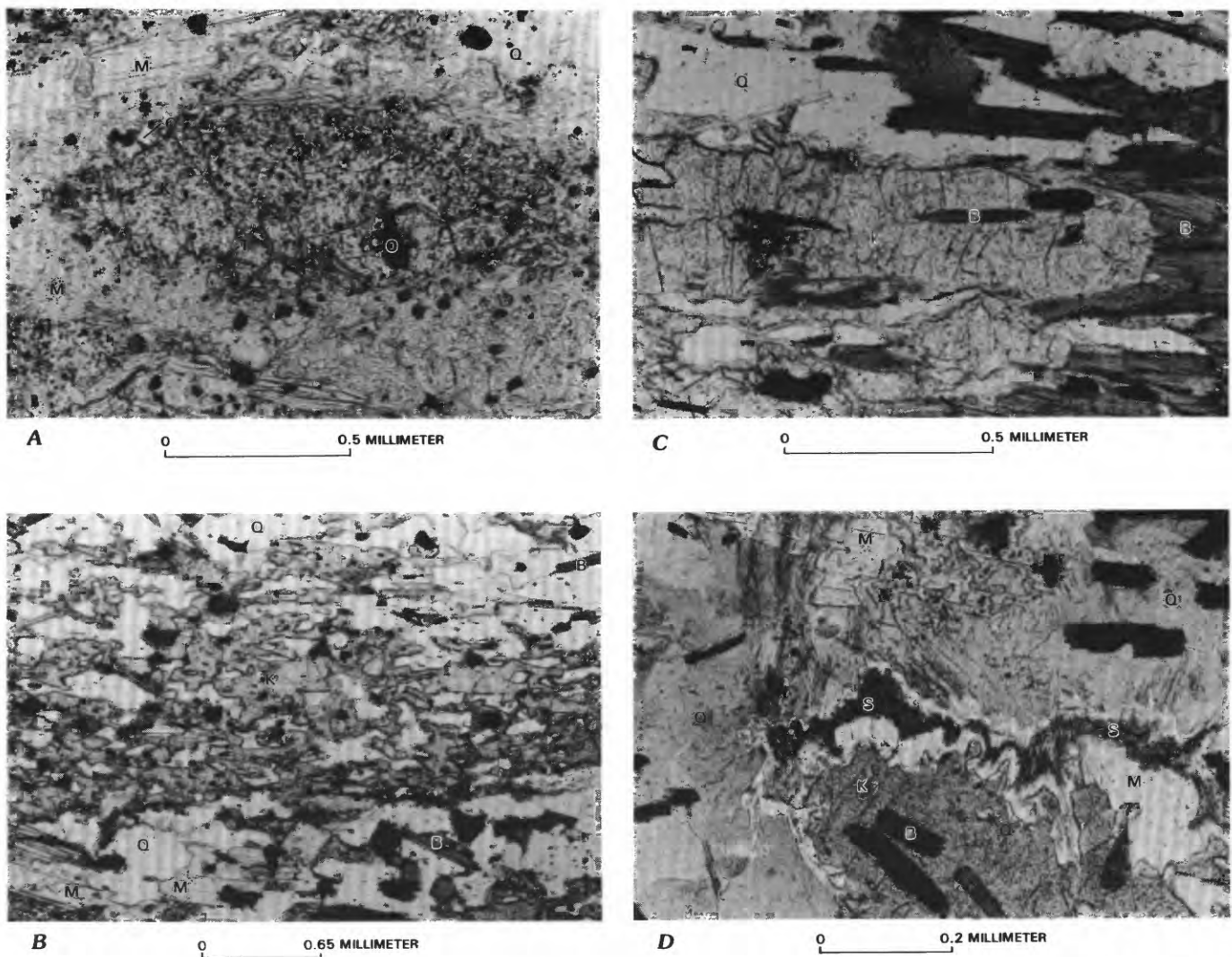


FIGURE 12.—Textural relations of kyanite. Plane-polarized light. B, biotite; K, kyanite; O, opaque mineral; Q, quartz; S, sillimanite; T, tourmaline. A, Clot of kyanite containing quartz, tourmaline, and opaque mineral. Kyanite is partially altered along its rim to white mica (M, probably muscovite). Sample GM-235; SW¼ sec. 15, T. 28 N., R. 17 W. B, Foliation defined partly by very strong preferred orientation of kyanite *c* axes that lie in plane of foliation and by dimensionally oriented flakes of biotite; M, postkyanite white mica porphyroblast

(probably muscovite). Sample GM-283, SE¼ sec. 18, T. 29 N., R. 17 W. C, Kyanite and biotite in contact with each other and showing no visible signs of mutual incompatibility. Sample GM-283, SE¼ sec. 18, T. 29 N., R. 17 W. D, Assemblage of kyanite, quartz, and biotite showing partial replacement of kyanite by white mica (M, probably muscovite), which is in turn partially replaced by fibrous sillimanite. Sample GM-1010e, NW¼ sec. 21, T. 29 N., R. 16 W.

cyclic reaction (Carmichael, 1969). In sample GM-283, fibrous sillimanite partly replaces biotite in a quartz-rich domain of the rock that contains no kyanite.

SILLIMANITE- AND CORDIERITE-BEARING GNEISS AND SCHIST

Sillimanite- and cordierite-bearing gneiss and schist in the Early Proterozoic metamorphic rocks show complex compatibilities, many of which are confined to very small domains (table 5). Textural and field relations documented during our petrologic studies suggest that some initially very high grade assemblages developed in these rocks, including:

- garnet-sillimanite(?)-biotite-quartz ± potassium feldspar ± plagioclase ± opaque mineral(s) ± hercynite (5)
- biotite-sillimanite-quartz-opaque mineral (6)
- sillimanite-quartz ± muscovite ± rutile (7)
- cordierite-biotite-quartz ± garnet ± plagioclase ± potassium feldspar ± rutile (8)
- cordierite-sillimanite-hercynite-quartz-potassium feldspar-plagioclase. (9)

Garnet, presumably rich in the almandine molecular end member, in muscovite-free assemblage (5) contains isolated apparently stable inclusions of biotite, quartz, opaque mineral(s), plagioclase (in trace amounts), and hercynite (in trace amounts), thereby corroborating our judgment that these minerals together constitute one of the

TABLE 5.—Composite assemblages in sillimanite- and cordierite-bearing gneiss and schist in the Early Proterozoic metamorphic rocks in the general area of the Gold Basin-Lost Basin mining districts

[X, mineral present; Tr, mineral present in trace amounts; ---, not observed; ?, identification uncertain]

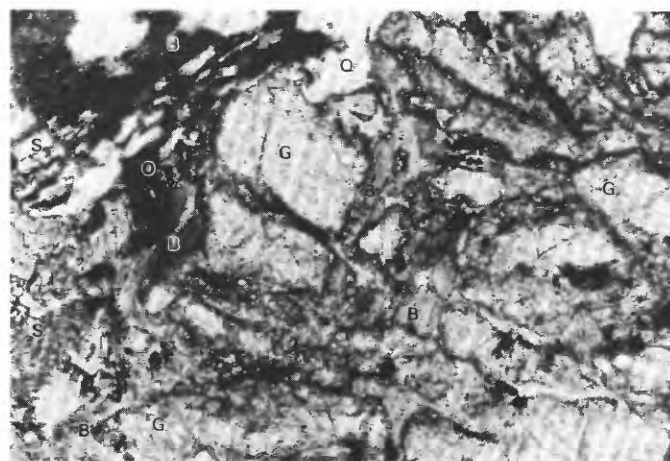
Sample	GM-83-1	GM-125	GM-126a	GM-126b	GM-394	GM-406	GM-1010c	¹ GM-1010e	GM-1077
Quartz	X	X	X	X	X	X	X	X	X
Biotite	X	X	X	X	---	X	X	X	X
Garnet	X	X	X	---	---	² X	---	---	X
Sillimanite	X	X	X	X	X	X	X	X	X
Potassium feldspar	---	X	X	X	---	X	X	X	X
Plagioclase	Tr	X	X	X	---	X	X	X	X
White mica	Tr	---	Tr	³ X	X	---	X	X	X
Cordierite	---	X	X	X	---	---	X	---	---
Hercynite	---	X	X	X	---	---	---	---	---
Opaque mineral(s)	Tr	X	X	X	Tr	X	Tr	Tr	X
Rutile	Tr	---	---	---	X	---	---	---	---
Apatite	---	---	---	---	---	---	---	---	X
Zircon	Tr	Tr	Tr	Tr	---	Tr	Tr	Tr	Tr

Sample	GM-412e	GM-51	GM-116	GM-116b	GM-126a-1	GM-135	GM-1010b	GM-1113a	GM-126c
Quartz	X	X	X	X	X	X	X	X	X
Biotite	X	X	X	X	X	X	X	X	X
Garnet	X	X	X	X	X	---	X	X	X
Sillimanite	X	---	---	---	---	---	---	X	---
Potassium feldspar	X	X	Tr	X	X	X	---	X	X
Plagioclase	X	---	X	X	X	X	Tr	Tr	X
Whitw mica	---	³ X	³ X	³ X	---	⁴ X	³ Tr	³ X	---
Cordierite	---	X	X	X	X	X	Tr?	X	X
Hercynite	---	X	---	---	---	---	---	---	---
Opaque mineral	X	X	Tr	X	X	Tr	X	X	X
Rutile	---	Tr	---	Tr	---	?	---	---	---
Apatite	Tr	---	---	Tr	---	---	Tr	---	---
Zircon	Tr	Tr	Tr	Tr	Tr	Tr	Tr	Tr	Tr

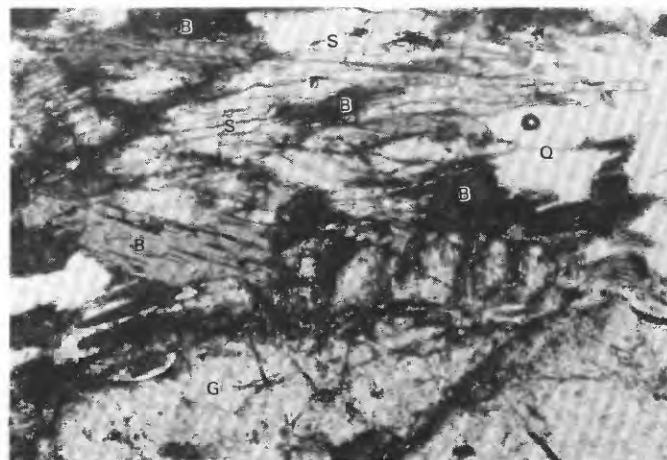
¹Includes kyanite partly replaced by white mica and sillimanite.
²Altered partly to chlorite along grain boundaries and microfractures.
³Fine-grained alteration of feldspar and (or) cordierite.
⁴Almost complete replacement of cordierite.

earliest stable assemblages in the gneiss. However, the paragenetic position of sillimanite in garnet-biotite assemblage (5) is problematical. Careful examination of garnet-sillimanite textural relations reveals the crystals of garnet to be corroded marginally and embayed locally by stout crystals of sillimanite (fig. 13A). Further, excellent textural evidence in such rocks shows that garnet is veined and partially replaced by assemblage (6). Nonetheless, many garnet crystals contain swarms of very fine grained needlelike crystals of sillimanite aligned parallel to the trace of the flowlines in the enclosing matrix of gneiss. Such sillimanite elsewhere has been interpreted by others

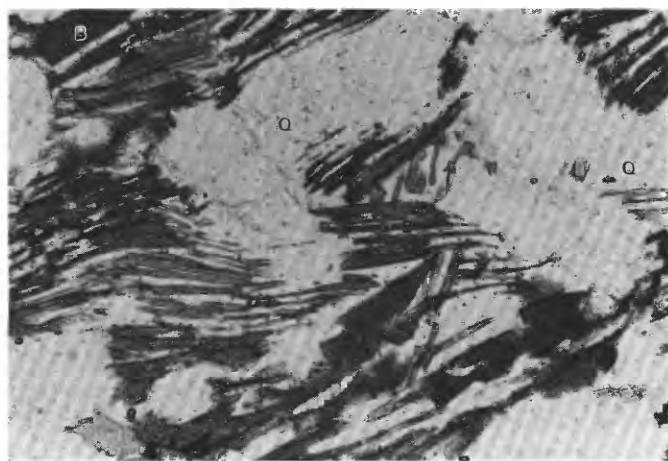
(Reinhardt, 1968) as an early relict phase initially stable with its host garnet as a two-phase subsystem. However, the overall fabric of such needles of sillimanite in garnet here suggests to us that crystallization of these needles occurred penecontemporaneously with the crystallization of the surrounding stout sillimanite, which in places embays and thus somewhat postdates the paragenetically earlier garnet. Nonetheless, because textural criteria are highly interpretive as to compatibilities and because some biotite seems to have replaced an early sillimanite (fig. 13B), we assign sillimanite tentatively as a queried phase in early assemblage (5).



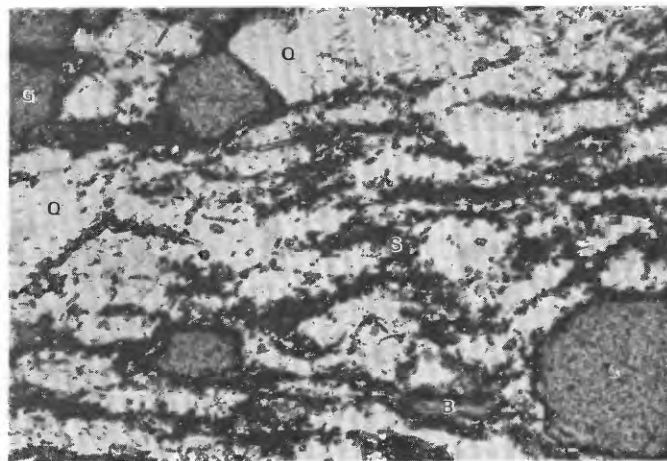
A 0 0.25 MILLIMETER



C 0 0.2 MILLIMETER



B 0 0.2 MILLIMETER

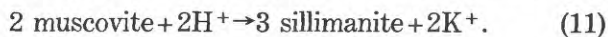
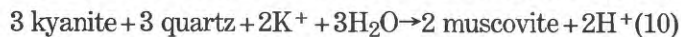


D 0 0.5 MILLIMETER

FIGURE 13.—Textural relations of sillimanite. Plane-polarized light. A, Embayed and highly corroded crystal of garnet (G) showing replacement and microveining by assemblage of biotite (B), sillimanite (S), quartz (Q), and opaque mineral (O). Sample GM-406. B, Greenish-brown biotite (B) completely replacing pseudomorphically earlier crystallized sillimanite in 1-cm-long lensoid domains within an assemblage of

garnet, biotite (red-brown, Z axis), cordierite, plagioclase (An_{15}), and quartz, where biotite is partially replaced by serpentine. Sample GM-125. C, Sillimanite (S) partially replaced by biotite (B). Sample GM-406. D, Rounded porphyroclasts of garnet (G) in a quartz (Q)-sillimanite (S) mylonitic schist. Sillimanite is apparently replacing both garnet and biotite (B). Sample GM-83-1.

Sillimanite shows additional apparently metastable relations with biotite and muscovite in the gneiss and schist. Some sillimanite appears to be in the initial stages of replacement by biotite (fig. 13C). Most of this biotite that partly or wholly replaces sillimanite is various shades of greenish brown (Z axis) under plane light in contrast to the more typical reddish-brown (Z axis) colors of the other biotites. We have already briefly described the growth of sillimanite in muscovite, which previously had replaced kyanite (fig. 12D). Such textural relations among these three minerals may be interpreted most simply as reflecting the following cyclic or paired reactions wherein muscovite occurs as an intermediate phase (Carmichael, 1969):



A critical implication of reactions (10) and (11) is the apparent immobility of Al^{3+} (Carmichael, 1969). However, as pointed out by Glen (1979), if overall volumetric changes and half reactions in physically separate domains of the rocks during metamorphism also are considered in such metapelites, then some elements (Al^{3+} , Si^{4+}) may indeed be relatively mobile.

The metamorphic rocks thus contain textural evidence documenting repeated and possibly prolonged periods of sillimanite crystallization after the onset of crystallization of a biotite-garnet-quartz \pm potassium feldspar \pm plagioclase \pm opaque minerals \pm hercynite assemblage. The pelitic gneiss also may have included sillimanite as an early phase.

Some high-grade-metamorphic rocks host an assemblage of quartz and sillimanite, (7), which together make up the bulk of the blastomylonitic matrix of these rocks (fig. 13D). These mylonitic rocks crop out discontinuously in the metamorphic terrane, and the white mica in them is present as poorly developed coronas that surround sillimanite. In these rocks, which also contain previously crystallized porphyroclasts of garnet and biotite, the phyllonitic structure is defined mostly by sillimanite, which crystallized preferentially along the mylonitic *s* surface. In addition, quartz shows a strong crystallographic and dimensional orientation wherein the orientations of its 0001 axes coincide closely with the *s* surface of the mylonite. Although quartz in the matrix of the blastomylonitic rocks shows complex and highly sutured boundaries, the bulk of the quartz is strain free and triple junctions of 120° dihedral angles are common. In some mylonitic rocks, white mica partly replaces sillimanite and may reflect continued late-stage mylonitization under hydrous conditions. Thus, local mylonitization apparently occurred initially during the metamorphic peak of the region at upper-amphibolite-facies conditions, and perhaps continued sporadically into the subsequent greenschist metamorphism (see fig. 7).

The cordierite-bearing rocks most commonly include a cordierite-biotite-garnet-potassium feldspar association, (8) (table 5), which does not contain white mica that is paragenetically the same age as the cordierite. The bulk of the white mica in the cordierite-bearing assemblage (table 5) is a very late mineral that partly replaces feldspar and (or) cordierite in the rocks. Thus, the progressive and consistent decrease in the modal abundance of early white mica in these rocks suggests that the peak of the prograde metamorphism occurred at physical conditions wherein the white mica-quartz assemblage was not stable. Although cordierite isograds elsewhere commonly have been mapped fairly concisely as halos around intrusive rocks emplaced into metapelitic terranes (Loomis, 1979; and many others), we have established only a very approximate boundary for the distribution of cordierite in the Gold Basin-Lost Basin districts. Cordierite in the districts seems generally to be confined to relatively fresh non-retrograded metamorphic rocks associated spatially with the suite of Early Proterozoic igneous rocks that crop out in the general area of Garnet Mountain east of the trace of the Grand Wash fault zone and northeast of the intersection of the inferred traces of the Grand Wash and Hualapai Valley faults. In these rocks, cordierite does not reflect thermal recrystallization during a relatively dry nondynamic contact event related primarily to final emplacement of nearby igneous rocks. Cordierite in many of these rocks forms an integral part of the gneissic fabric of the garnet-biotite assemblage(s). Many of the rocks containing cordierite are metamorphic schlieren and pendants of metapelites engulfed by more widespread igneous rocks. However, many pelitic rocks in these schlieren and pendants do not contain cordierite very close to their contacts with adjoining plutonic igneous rocks. Some pelitic migmatitic gneiss within 3 m of very large Early Proterozoic igneous bodies show quartz + biotite + plagioclase (oligoclase to even albite, in places) + microcline \pm white mica \pm garnet composite assemblages but also include carbonate and clinozoisite-epidote alteration of earlier plagioclase. The only contact phenomena noted are the porphyroblastic growths of white mica and feldspar (both albite and microcline) and the alteration of plagioclase.

Cordierite, as listed in reactions (8) and (9), is present in at least two parageneses in nonretrograded pelitic gneiss and migmatite. The more common, and probably early, association is with biotite and garnet (table 5), an association (8) that partly defines the schistose fabric of the host pelitic gneiss. Presumably early cordierite is also present with biotite and garnet in the melanosome (Mehnert, 1968), or dark portion of migmatites, against which the light micropegmatitic portion, or leucosome, apparently has advanced (fig. 14A). We herein use the terms melanosome and leucosome in a purely descriptive sense. It is beyond the intended scope of our present study to

attempt a full documentation of the overall genesis of these extremely complex rocks. For example, we have not established whether the melanosomes reflect simply an in situ residue from the parent rock (paleosome of Mehnert, 1968) or whether the melanosomes are chemically transformed even partially. However, modal analyses of adjoining layers of melanosomes and leucosomes in these rocks show approximately equivalent abundances of the felsic minerals (quartz and feldspars). The major difference between the two is the almost complete absence of biotite from the leucosome whereas the melanosome

typically includes about 25 volume percent biotite. Further, in the melanosome some cordierite is concentrated in biotite-potassium feldspar (mostly microcline)-plagioclase (An_{20-25}) domains away from garnet-quartz domains. Within these latter domains, xenoblastic garnet also commonly shows highly irregular skeletal outlines resulting from its growth along quartz crystal boundaries. In the melanosomes, garnet appears to be associated stably with biotite. Biotite shows invariably an increased abundance within about 0.2 mm of the sharply adjoining leucosome, especially along fronts convex toward the melanosome. The leucosomes of these migmatitic rocks commonly contain a cordierite-sillimanite-hercynite assemblage (9) (fig. 14B). Contents of Al_2O_3 and K_2O , calculated from modal abundances and inferred ideal compositions of constituent minerals, locally show several-fold increases in the leucosomes versus the adjoining melanosomes. The increase of Al_2O_3 is primarily a reflection of strong concentrations of sillimanite in many leucosomes and appears to document at least very local mobility of Al_2O_3 . Overall, however, Al_2O_3 probably remained fairly constant during prograde development of the migmatites, provided these rocks behaved similarly to migmatitic terranes elsewhere (Wenk, 1954; Suk, 1964; Busch, 1966; Mehnert, 1968).

The cordierite- and sillimanite-bearing assemblages correspond to assemblages in the classic Barrovian region, which are indicative of medium-pressure regional metamorphism (fig. 15). Generally accepted rough estimates of geothermal gradients during such metamorphism are about 20 °C per kilometer (Miyashiro, 1973). From what we can assemble of the prograde metamorphism of the region by "looking through" the subsequent greenschist event, the rocks appear to show transitions from garnet-biotite, staurolite, and kyanite assemblages to ones dominated by cordierite and (or) sillimanite. We infer these latter assemblages to reflect the thermal peak of the Proterozoic metamorphism in the area. The cordierite-sillimanite assemblages seem to be best preserved in the general area of the widespread Early Proterozoic plutonism at Garnet Mountain.

PETROGENETIC IMPLICATIONS OF MINERAL RELATIONS

The established relations between kyanite- and sillimanite-bearing assemblages rank among the most critical of all petrogenetic relations, especially taking into account their experimentally and theoretically determined stability fields (Helgeson and others, 1978). An early kyanite-stable metamorphic event (fig. 7) must have occurred at pressure-temperature (PT) conditions greater than the kyanite-andalusite-sillimanite triple point (fig. 16) because the transition recorded in the rocks is kyanite to sillimanite and not to andalusite. Helgeson and others (1978) now

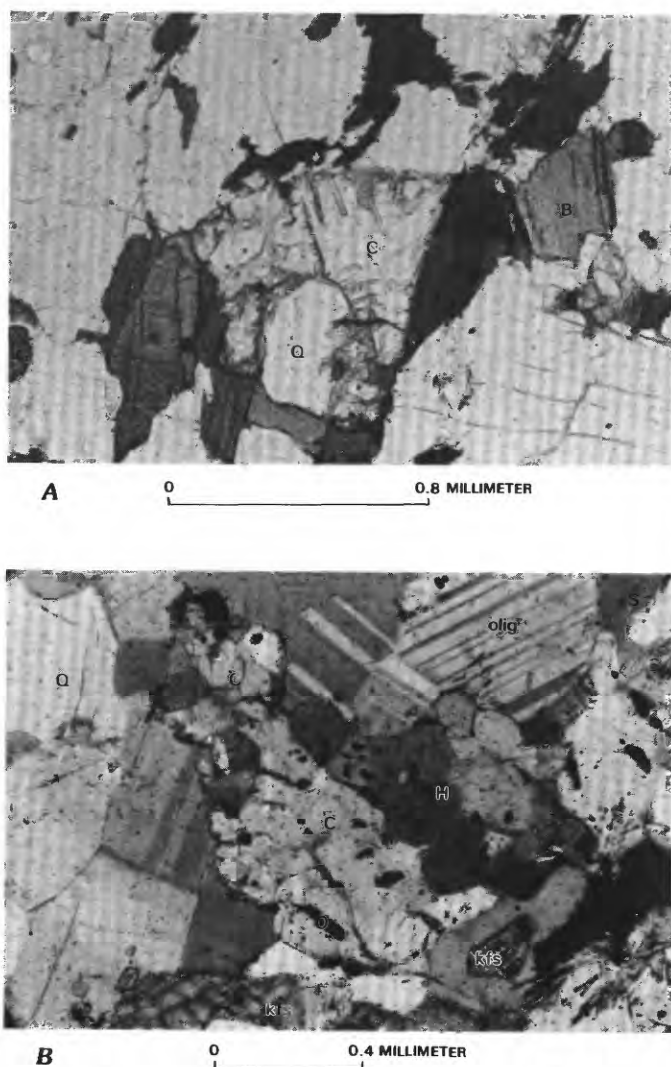


FIGURE 14.—Textural relations of cordierite. A, Early cordierite (C) associated with biotite (B), garnet (G), and quartz (Q) in the melanosome of migmatitic gneiss. Plane-polarized light. Sample GM-126a. B, Subsequent cordierite (C) associated with sillimanite (S), hercynite (H), and opaque minerals (O) concentrated in a 1- to 2-cm-wide leucosome rich in quartz (Q) and feldspar-microcline (kfs) and oligoclase (olig). Partly crossed nicols. Sample GM-125.

place the triple point in the system $\text{Al}_2\text{O}_3\text{-SiO}_2\text{-H}_2\text{O}$ at approximately 370 MPa and 500 °C, or close to the 510 °C and 400 MPa coordinates of the triple point proposed by Newton (1966) and Holdaway (1971). We cannot ascertain how far beyond the kyanite-sillimanite transition the kyanite initially crystallized. However, this crystallization may not have been far from the transition, because kyanite was found to occur only sparingly, although unknown amounts of kyanite may have been destroyed during the widespread retrograde metamorphism of the area. Further, Kepezhinskas and Khlestov (1977) cautioned that the boundaries of the *PT* stability regions of naturally occurring aluminosilicates may in fact be not so well defined. They envision the boundaries to contain a field in *PT* space rather than a line. Nonetheless, the overall transition from kyanite to sillimanite must reflect an increase in the geothermal gradient that created the regional metamorphic maximum for the area. Assemblages of Fe-Mg cordierite that include potassium feldspar and that occurred at *PT* conditions of muscovite-quartz instability define extremely wide ranging stability fields that also are a function of $P_{\text{H}_2\text{O}}$ (Holdaway and Lee, 1977). Holdaway and Lee (1977) showed that under such conditions and at $P_{\text{H}_2\text{O}} = P_{\text{tot}}$ but still below the granite solidus, Mg cordierite + potassium feldspar + vapor is stable to a maximum pressure of about 500 MPa whereas at $P_{\text{H}_2\text{O}} = 0.4 P_{\text{tot}}$, this assemblage is stable to about 600 MPa. These pressures are probably reasonable upper pressure limits to the cordierite- and sillimanite-bearing assemblages created during the prograde Early Proterozoic regional metamorphic event in the districts. Last, the absence of hypersthene from the cordierite-bearing assemblages suggests that the upper-temperature stability limit of cordierite here did not exceed a biotite + quartz breakdown reaction (see Hess, 1969).

QUARTZOFELDSPATHIC GNEISS

Epiclastic rocks, best termed quartzofeldspathic gneiss, are probably the most common rock type in the mapped Early Proterozoic gneiss. However, quartzofeldspathic gneiss typically does not make up extensive monolithic sequences of gneiss throughout the unit. Instead, the quartzofeldspathic gneiss is interlayered with many other lithologies, including amphibolite and marble. Locally, thin layers of quartzofeldspathic gneiss are present within larger masses of amphibolite; some of these masses of amphibolite are large enough to be shown as separate map units (see Blacet, 1975), and others are included within the rocks mapped as paragneiss by him. In the amphibolite, the quartzofeldspathic gneiss ranges from sharply defined layers a few millimeters to as much as 20 cm thick. However, either of these rocks, quartzofeldspathic gneiss or amphibolite, locally may grade into the other by interbedding across an interval of 2 to 3 m. In fact, quartzofeldspathic gneiss and amphibolite together impart a banded aspect to many outcrops within the gneiss unit. These outcrops may be nearly homoclinal sequences of rock, or they may be complexly isoclinally folded at the outcrop scale. In addition, some of the thicker sequences of quartzofeldspathic gneiss show sporadic pegmatoid clots, inferred to be "sweatouts," that formed during the peak of prograde regional metamorphism. These clots consist of, in decreasing abundance, feldspar, quartz, and biotite, and they show gradational boundaries with the surrounding more uniformly sized quartzofeldspathic gneiss. Further, layering throughout the quartzofeldspathic gneiss provided the local structural controls that determined the attitude and geometry of subsequently introduced quartz + sulfide lenses and (or) veins that will be discussed in the section "Gold Deposits and Occurrences."

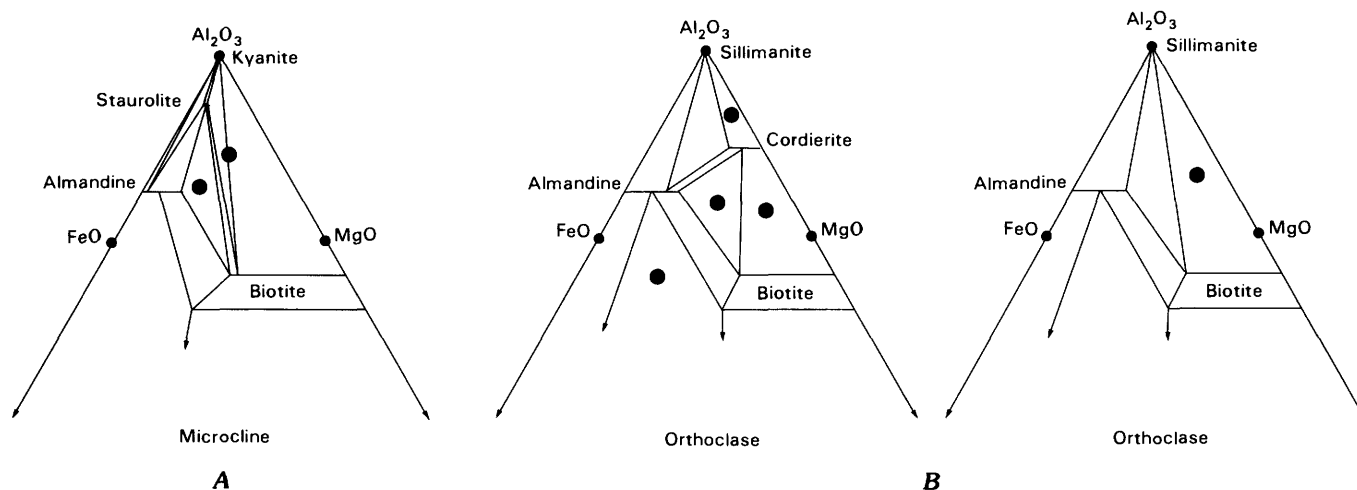


FIGURE 15.—Thompson (1957) projected AFM diagrams for medium-pressure progressive metamorphism. Small dots at Al_2O_3 (A), FeO (F), and MgO (M). Large dots, assemblages observed in metamorphic rocks from Gold Basin-Lost Basin districts. A, Kyanite zone. B, Sillimanite zone.

By using a microscope, visual estimates of representative samples of quartzofeldspathic gneiss reveal that many samples may have consisted of mostly quartz and oligoclase prior to metamorphism. Polycrystalline quartz grains that are round to subround are fairly common in the size range 0.1 to 0.4 mm. These relations suggest that the protolith of the quartzofeldspathic gneiss consisted of fine-grained arkosic to possibly subarkosic sandstone, on the basis of the classification of McBride (1963). We have not recognized any lithic fragments in the samples studied. The polycrystalline quartz grains show very complex sutured intragranular crystal boundaries for the most part, but many grains have retained their overall subrounded to well-rounded detrital outlines through the superposed metamorphic events. Although oligoclase was probably the predominant feldspar in most samples prior to metamorphism, it now has been replaced variably in most samples by a very finely crystallized shreddy aggregate of white mica, chlorite, actinolite, sphene (trace), and opaque minerals (including some ilmenite), with or without epidote-clinozoisite, calcite, and albite. This assemblage of minerals, predominantly reflecting the retrograde

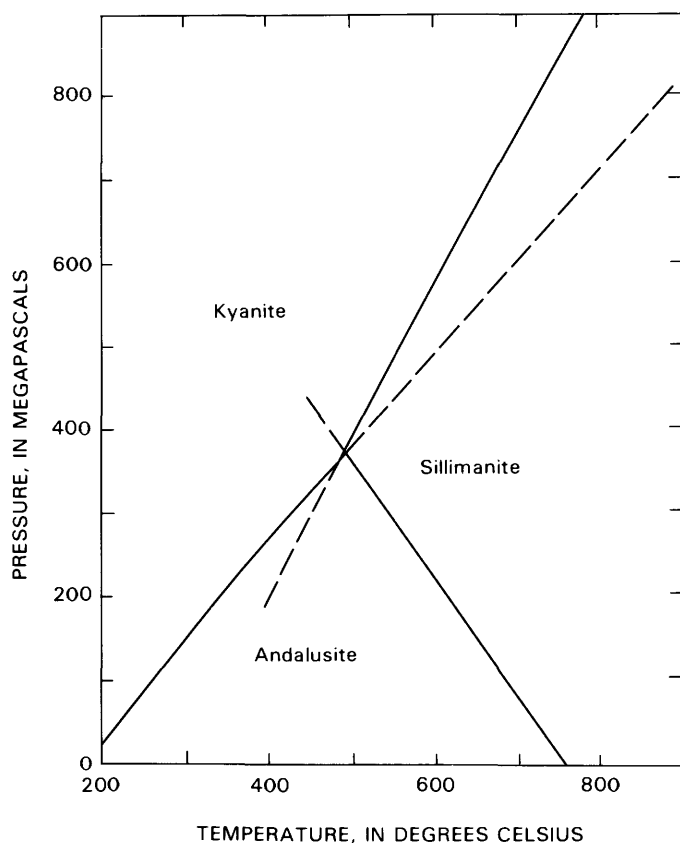


FIGURE 16.—Equilibrium curves generated from thermodynamic data by Helgeson and others (1978) in system $\text{Al}_2\text{O}_3\text{-SiO}_2\text{-H}_2\text{O}$ at high pressures and temperatures. Dashed lines indicate metastable projections of equilibrium curves.

metamorphic event, is also present as a matrix which supports the quartz and feldspar framework minerals. However, the intense development of retrograde assemblages in the plagioclase feldspars and matrix generally obscures significantly the premetamorphic textural relations in the rocks between framework feldspars and matrix. In fact, the matrix may have consisted of very fine granules of plagioclase, including varying amounts of diagenetic phyllosilicate minerals and minor amounts of calcite cement. Although relict oligoclase grains are the only recognizable feldspar in many samples of the quartzofeldspathic gneiss, overall plagioclase to potassium feldspar ratios are inferred to have varied highly prior to metamorphism. Some samples contain oligoclase to potassium feldspar ratios of approximately 10 to 1. The potassium feldspar, including both perthite and locally abundant microcline, typically has not been replaced by mineral assemblages diagnostic of the retrograde event. Heavy minerals in the quartzofeldspathic gneiss include 0.01- to 0.05-mm-wide subrounded prisms to well-rounded ellipsoids of zircon and, less commonly, sphene and apatite.

Chemical analyses of four samples of quartzofeldspathic gneiss (table 4, analyses 3-6) reveal compositions most similar to published analyses of eugeoclinal sandstone or graywacke. The content of SiO_2 in these analyzed samples of quartzofeldspathic gneiss ranges from 72.3 to 76.3 weight percent, only slightly higher than the 71 weight percent geometric mean determined for the eugeosynclinal graywackes by Middleton (1960). However, the mean SiO_2 content of 61 graywackes (table 4, analysis 10) compiled by Pettijohn (1963) is 66.7 weight percent. Further, the analyses of quartzofeldspathic gneiss show low K_2O to Na_2O ratios that range from 0.23 to 0.48 (table 4). Such low ratios are a feature common to graywackes (Middleton, 1960; Pettijohn, 1963, fig. 2), but they are somewhat lower than the 0.69 ratio of K_2O to Na_2O in the average graywacke (table 4, analysis 10), and significantly lower than the 1.9 ratio in the average arkose (table 4, analysis 11). The low ratios of less than one confirm our petrographic estimates for the overall low ratio of potassium feldspar to plagioclase in the detrital framework minerals. In addition, the content of Al_2O_3 in these rocks ranges from 12.3 to 14.0 weight percent, which is close to the mean value of 13.5 (Pettijohn, 1963) but is significantly higher than the 8.7 weight percent mean Al_2O_3 content of arkose (table 4, analysis 11). The contents of CaO in the four rocks range from 2.1 to 4.3 weight percent; thus they are not much different from the 2.5 and 2.7 weight percent content of CaO in the average graywacke and arkose. Such contents of CaO in the four samples of quartzofeldspathic gneiss are somewhat higher than the contents of CaO reported for the Early Proterozoic Vishnu Complex by Brown and others (1979; fig. 17). MgO in the quartzofeldspathic gneiss analyzed ranges

from 0.4 to 1.7 weight percent and is thus less than the mean MgO composition of 61 graywackes (2.1 weight percent; table 4, analysis 10). Such low contents of MgO may reflect the very low content of lithic volcanic detritus shed into the protolith of the gneiss. Although these chemical analyses of quartzofeldspathic gneiss from the Gold Basin-Lost Basin mining districts show similarities generally to graywacke, all of these samples have been affected moderately to strongly by retrograde alteration phenomena. The rocks have been subjected to several intense and prolonged metamorphic events and weathering phenomena that contributed to the final chemical composition of the gneiss. The chemical changes, if any, that accompanied each of the events cannot be ascertained.

AMPHIBOLITE

Amphibolite bodies of varying sizes are present throughout the Proterozoic metamorphic terrane in the Gold Basin-Lost Basin mining districts. However, only a few of these amphibolite bodies are shown as separate

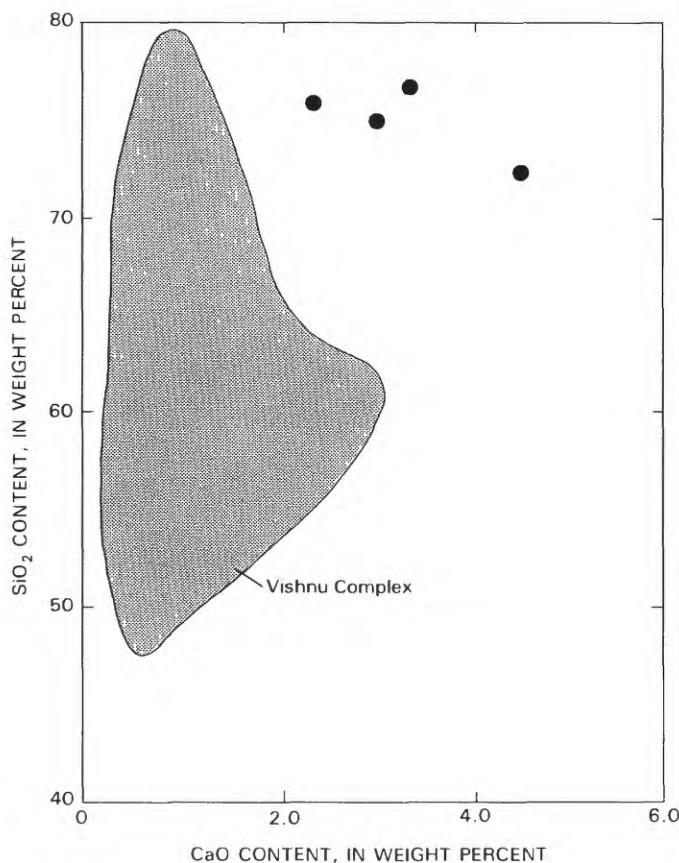


FIGURE 17.—SiO₂ versus CaO in four samples (dots) of quartzofeldspathic gneiss (analyses 3-6, table 4); field (shaded area) established by Brown and others (1979) for 16 analyses of metasedimentary rocks from the Early Proterozoic Vishnu Complex of Brown and others (1979).

map units in the district-wide geologic map by Blacet (1975) because of the scale of the quadrangle map, their discontinuous structure, and the overall highly irregular size distribution of many individual outcrops. Most amphibolite is present within the gneiss (fig. 2, unit Xgn), which includes mainly quartzofeldspathic gneiss as described previously. Lesser amounts of amphibolite are present in the migmatitic units and also scattered as pendants in the various Early Proterozoic igneous rocks. In the gneiss unit, some outcrops consist of 30-m-thick layers that are as much as 80 to 90 percent dark-green-gray to dark-greenish-black to black amphibolite (see fig. 5B). Such masses of amphibolite may grade across several meters into quartzofeldspathic gneiss by decreased numbers of layers of amphibolite along strike of the foliation. Layers of amphibolite also may terminate abruptly or be crosscut by coarse-grained, quartz-feldspar-rich leucogranite which in turn then grades into the surrounding quartzofeldspathic gneiss. The overall abundance of amphibolite in the Proterozoic terrane here in the Gold Basin-Lost Basin mining districts is much greater than in similar metamorphic terranes just to the north around Lake Mead (P.M. Blacet, unpub. data, 1967-72). However, even within the districts themselves there is a wide variation in the proportion of amphibolite in the Early Proterozoic gneiss map unit (fig. 2). Near the south end of the Lost Basin Range, amphibolite is derived largely from igneous protoliths, an assessment based on the occurrence of widespread relict gabbroic and diabasic textures. Careful examination of outcrops there further reveals that rarely some amphibolite definitely crosscuts the lithologic layering in the enclosing paraschist and paragneiss and clearly shows preserved chilled margins against these rocks.

Amphibolite in the Proterozoic terrane is either massive, showing no readily apparent macroscopic structure, or more commonly it contains a well-developed fabric. Generally, the fabric consists of at least one obvious foliation and possibly a less well-developed lineation. The principal foliation (s_1) is defined by millimeter-size layers of different compositions and by differences in grain size between adjoining domains of similar mineralogy (fig. 18A). Most commonly, the attitude of s_1 in the amphibolite is the same as that in the surrounding gneiss, and s_1 may be better developed near the margins of the amphibolite bodies. Lineation in the amphibolite locally is defined by a strong preferred orientation of amphibole crystals within s_1 . In addition, other types of lineation in amphibolite include minor fold axes and well-developed mullion structures consisting of aggregates of hornblende showing a strong preferred orientation of their [001] axes parallel to the mullions. The fold axes and mullion structures commonly are coaxial. Isoclinally folded amphibolite interlayered with quartzofeldspathic gneiss is especially

abundant along the west flank of the Lost Basin Range. Lamination in amphibolite may also be defined by the intersection of a subsequent fracture cleavage (s_2) with s_1 . Locally, in amphibolite, ripplelike corrugations on s_1 plunge shallowly (about 10°) and reflect the intersection of s_1 with the s_2 fracture cleavage. Typically, such s_2 fracture cleavages are more widely spaced than the s_1 layering. In addition, chloritization occurred concurrently with the development of s_2 , and thus the fracture cleavage

most probably dates from the widespread retrograde metamorphic event described above. Nonetheless, relatively fresh amphibolite, fresh to the unaided eye anyway, is present in small core domains between the traces of the s_2 fracture cleavage. Lastly, some amphibolitic schist is lineated locally on s_1 because of the crystallization of elongate splotches of white mica, also most probably dating from the retrograde event. These splotches of white mica parallel the hornblende lineation in the rocks.

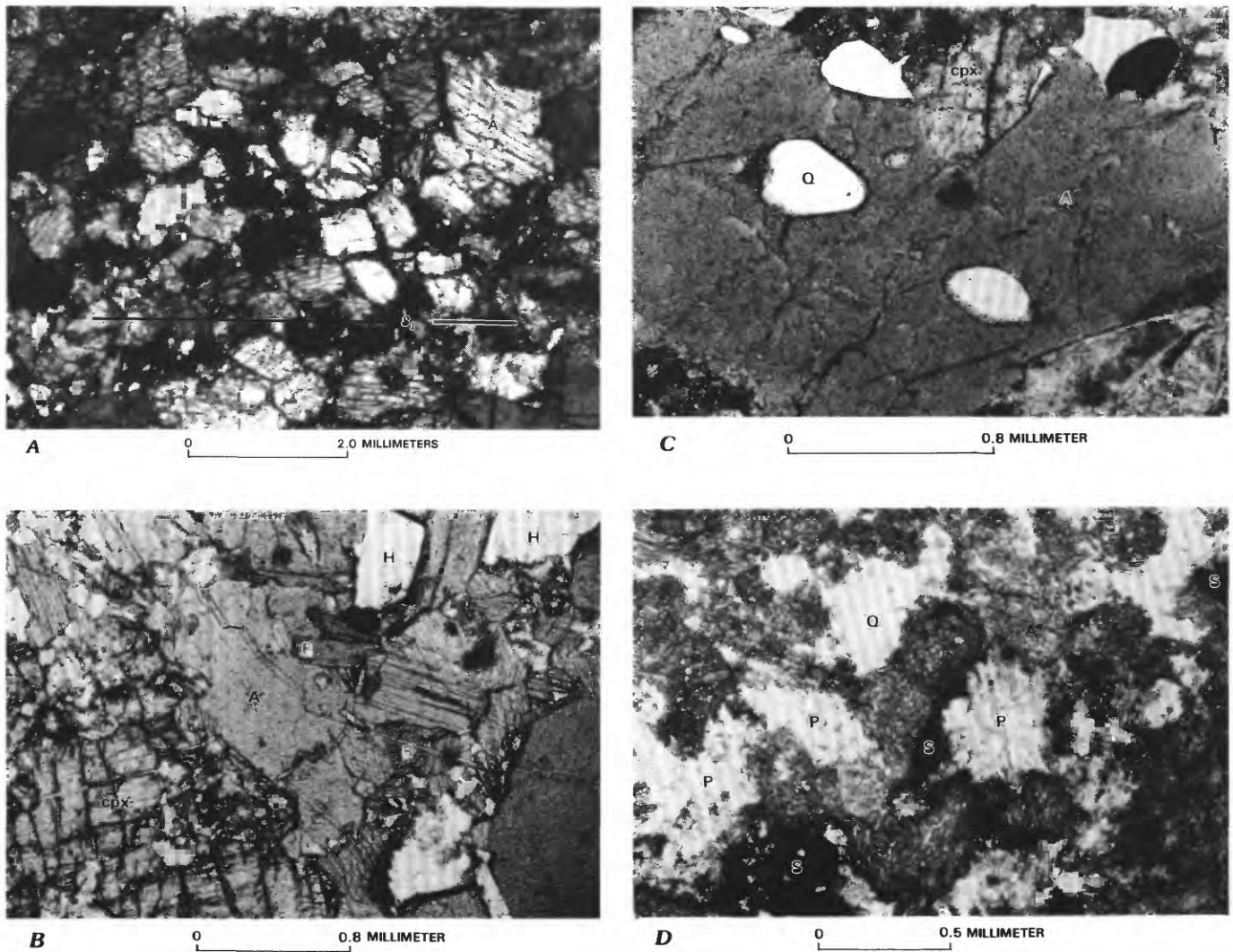


FIGURE 18.—Structure and textures observed in amphibolite. A, amphibole; Q, quartz; P, plagioclase or retrograde alteration products of plagioclase, including white mica, carbonate, and clay(s). A, Principal foliation (s_1) defined by lithologic layering of varying compositions. Sample GM-290, SE $\frac{1}{4}$ sec. 18, T. 29 N., R. 17 W. B, Fabric of hornblende-clinopyroxene-plagioclase (An_{70})-quartz-biotite (B) amphibolite crystallized at upper-amphibolite-facies conditions and, among samples studied, judged to have been least modified by subsequent geologic events. H, hole in thin section. Sample GM-1117. C, Well-rounded grains of strained, monocrystalline quartz included within brown to olive-green-brown hornblende (Z axis) in a hornblende-

plagioclase(?) quartz-clinopyroxene-opaque mineral assemblage. Clinopyroxene (cpx) altered partially to epidote-group mineral, chlorite, and minor white mica. Plagioclase has been completely replaced by a very fine grained aggregate of white mica, chlorite, epidote, tremolite, actinolite, and opaque mineral(s). Sample GM-1063, NE $\frac{1}{4}$ sec. 3, T. 28 N., R. 17 W. D, Fabric of amphibolite showing effects of contact metamorphism related to emplacement of Late Cretaceous two-mica monzogranite of Gold Basin. S, sphene. Sample GM-1103a, collected 3 m from two-mica monzogranite; SE $\frac{1}{4}$ sec. 12, T. 28 N., R. 19 W.

The protolith for many individual outcrops of amphibolite or cluster of outcrops can be ascertained primarily using relict textures or geologic field relations with other lithologies of known provenance. In addition, we have supplemented and refined these observations by extensive microscopic examination of thin sections of amphibolite and chemical analyses of a few selected samples of amphibolite in this report and reported elsewhere (Page and others, 1986). However, some of the amphibolite exposed in the districts cannot be classified as to protolith because of the absence of diagnostic macroscopic, microscopic, or chemical criteria. Locally, amphibolite in the gneiss derived from a sedimentary protolith includes relict beds which consist of calc-silicate minerals and marble and is finer grained than amphibolite derived from igneous rocks. Some of these beds reach a maximum thickness of about 30 cm along a continuously exposed strike length of about 15 m. The calc-silicate beds are conformable with the layering in the adjoining amphibolite, and in places they neck down to about 2.5 cm or less. The delicate interlayering of many amphibolite layers with quartzofeldspathic beds a few millimeters to approximately 20 cm thick is additional evidence for a sedimentary origin. This evidence for a sedimentary protolith for some amphibolite in the gneiss is especially convincing if we recall from our descriptions above that the quartzofeldspathic gneiss shows abundant textural and chemical evidence for a sedimentary protolith. Lastly, we will show below that many hornblende crystals in this type of amphibolite have trapped well-rounded to ovoid grains of quartz that obviously had been through a sedimentary cycle.

In all, 37 samples of amphibolite from 27 localities were studied petrographically (table 6). Almost all of these samples contain mixed mineral assemblages, which reflect crystallization during the Early Proterozoic upper-amphibolite-facies metamorphism and retrograde metamorphism at greenschist conditions. The amphibolite locally includes some cataclastic or mylonitic fabrics and finally some local thermal and (or) hydrothermal alteration phenomena associated with Cretaceous plutonism and vein-type gold mineralization. The latter mineralogic changes in a selected suite of amphibolite samples will be discussed in the section entitled "Gold Deposits and Occurrences." Nonetheless, the mineral assemblage formed during any one of the above events is relatively simple. For example, amphibolite that shows the least modification by subsequent events contains a greenish-brown to brown (Z axis) hornblende-plagioclase (An_{70})-quartz-clinopyroxene-biotite (trace)-opaque mineral assemblage that includes apatite and sphene as minor accessories (fig. 18B). In outcrop, this 5- to 6-m-thick zone of amphibolite shows a sparkling fresh granoblastic fabric and is present within some garnet-biotite migmatitic

gneiss. Red-brown (Z axis) biotite in trace amounts is apparently compatible with the other minerals in the assemblage. Normally zoned very calcic plagioclase (An_{70}) is present as generally untwinned, stubby to equant prisms. Miyashiro (1973) and Mason (1978), and many others, have noted the general tendency for the calcium content of plagioclase to increase and the color of hornblende to go from blue green to various shades of brown during an increase in the grade of metamorphism of metabasites from the lower to the upper amphibolite facies. These relations are present in amphibolite from the Gold Basin-Lost Basin districts (table 6) and suggest the amphibolite reached prograde metamorphic peaks similar perhaps to zone-C metabasites in the low-pressure central Abukuma Plateau, Japan (Miyashiro, 1958), or to zone-B metabasites in the medium-pressure Broken Hill area, Australia (Binns, 1965a, b, c).

Quartz makes up a significant proportion of many of the samples of amphibolite and is present in all but five of the samples studied (table 6). Quartz in these rocks is of several different parageneses. Some quartz is premetamorphic and is from the protolith of the amphibolite, whereas the bulk of the quartz crystallized either during the prograde or the retrograde events. The hornblende in some samples includes abundant, small, well-rounded, monocrystalline grains of quartz and much lesser quantities of rounded grains of plagioclase. Such quartz in places is rimmed partially by an extremely fine grained unknown silicate. Many such grains of quartz were strained moderately and are inferred to reflect relict detrital quartz grains engulfed by a subsequent overgrowth of hornblende during the upper-amphibolite-facies metamorphism of the area (fig. 18C). The fabric of much of the quartz that recrystallized during either the early amphibolite-facies metamorphism or the subsequent greenschist and contact events differs markedly from these grains of quartz showing well-rounded outlines. Such metamorphic quartz typically has a blebby or shredded overall aspect and is associated very closely with blue-green (Z axis) hornblende and (or) tremolite-actinolite that replaces partially the early green or brown hornblende. The quartz-quartz boundaries in such associations are very complexly sutured. Further, contact effects are notable in outcrops of some amphibolite as much as 3 m from the Cretaceous two-mica monzogranite that crops out in the southern part of the Gold Basin district. Under the microscope, such rock shows a well-developed granoblastic texture of tightly intergrown fine-grained crystals of mostly blue green (Z axis) hornblende and quartz (fig. 18D).

Some quartz-free metabasite in the gneiss was probably derived from clinopyroxenite. Such metabasite includes black, dense, highly magnetic rocks that locally are layered and that crop out predominantly along a strike

TABLE 6.—Composite mineral assemblages in amphibolite and altered amphibolite from the Gold Basin-Lost Basin mining districts

[Color of amphibole under microscope is down Z axis using plane-polarized light. Biotite is present as primary and (or) secondary mineral. Tremolite-actinolite, epidote group, chlorite, white mica, and carbonate minerals are present mostly as part of regional greenschist retrograde assemblage and (or) local hydrothermal assemblage adjacent to mineralized veins. X, mineral present; Tr, present in trace amounts; 50, An content of plagioclase; ---, not found; ?, presence uncertain]

Sample	Amphibole											White mica	Carbonate	
	Blue green	Gray green to olive-gray green	Green brown to brown	Quartz	Plagioclase	Clinopyroxene	Biotite	Opaque minerals	Apatite	Sphene	Tremolite actinolite			Epidote group
GM-92a	---	X	---	X	Tr	---	---	X	---	---	---	X	---	---
GM-124	---	X	---	X	X	X	X	X	---	---	---	X	X	---
GM-191	X	---	---	---	---	---	---	X	X	---	---	---	---	X
GM-191a	X	---	---	Tr	X	---	---	---	---	---	---	---	---	---
GM-209	---	X ¹	---	---	---	---	---	Tr ²	---	---	---	---	---	---
GM-213	---	X ¹	---	---	---	---	---	X ²	---	---	---	---	---	---
GM-213a	---	X	---	---	---	---	---	---	X	---	---	---	---	---
GM-242	---	X	---	---	---	---	---	X	X	---	---	---	---	Tr
GM-246	---	X	---	X	40	---	---	X	X	---	---	---	---	?
GM-254	---	X	---	X	30	---	---	X	X	---	---	---	---	---
GM-290a	---	---	X	---	X	---	---	---	---	---	---	---	---	X
GM-290	---	---	X	---	---	---	---	---	---	---	---	---	---	---
GM-298a	---	---	X	---	---	---	---	---	---	---	---	---	---	---
GM-3714	X	---	---	---	---	---	---	---	---	---	---	---	---	---
GM-382a ⁵	X	---	---	X	30	---	---	---	X	---	---	---	---	---
GM-382b ⁵	X	---	---	---	---	---	---	---	---	---	---	---	---	X
GM-382c ⁵	X	---	---	---	---	---	---	---	---	---	---	---	---	X
GM-392d ⁵	---	---	---	---	---	---	---	---	---	---	---	---	---	X
GM-382e ⁵	---	---	---	---	---	---	---	---	---	---	---	---	---	X
GM-412f	X	---	---	---	---	---	---	---	---	---	---	---	---	---
GM-461b	---	---	X	---	---	---	---	---	---	---	---	---	---	---
GM-468	X	---	---	X	---	---	---	---	---	---	---	---	---	---
GM-529	X	---	---	X	35	---	---	---	---	---	---	---	---	---
GM-529a	X	---	---	X	---	---	---	---	---	---	---	---	---	---
GM-539	X	---	---	---	---	---	---	---	---	---	---	---	---	---
GM-634a	X	---	---	---	---	---	---	---	---	---	---	---	---	---
GM-634a ¹	X	---	---	---	---	---	---	---	---	---	---	---	---	---
GM-665	---	X	---	---	X	---	---	---	---	---	---	---	---	X
GM-669	---	X	---	---	---	---	---	---	---	---	---	---	---	X
GM-697	X	---	---	---	---	---	---	---	---	---	---	---	---	---
GM-699	X	---	---	---	---	---	---	---	---	---	---	---	---	---
GM-855	---	X	---	---	---	---	---	---	---	---	---	---	---	---
GM-962	---	X	---	---	65	---	---	---	---	---	---	---	---	---
GM-1063	---	---	X	---	---	---	---	---	---	---	---	---	---	---
GM-1063b	---	---	X	---	---	---	---	---	---	---	---	---	---	---
GM-1103a	X	---	---	---	---	---	---	---	---	---	---	---	---	---
GM-1117	---	---	X	---	70	---	---	---	---	---	---	---	---	---

¹Cummingtonite.
²Includes green spinel, and probable chromite.
³Includes serpentine.
⁴Includes potassium feldspar in hairline microveinlets cutting metamorphic fabric of amphibolite; biotite is secondary.
⁵Sample included in alteration suite studied near a vein (see text and fig. 47).

length measuring about 100 m, as exemplified by locality 213 (pl. 1, see table 11). Here the contacts of these rocks with the enclosing gneiss are obscured by rubble. However, close examination of these rocks reveals that they are unquestionably pods of metamorphosed ultramafic rocks. These rocks are very magnesian in composition (Page and others, 1986). They show marked petrologic differences from the bulk of the amphibolite in the gneiss. Under the microscope, no evidence of an ophitic or subophitic texture common to most of the amphibolite derived from gabbroic protoliths can be seen. The amphibole in the metamorphosed ultramafic rocks is colorless to very

weakly pleochroic in contrast to the more common blue-green and brown hornblende in most amphibolite (table 6). In addition, the amphibole that typically makes up about 40 to 50 volume percent of the rock is optically positive, a relation that further suggests it is a Mg-rich cummingtonite (ideally $(Mg)_7[Si_8O_{22}](OH)_2$). Cummingtonite is the dominant mineral in the early metamorphic assemblage and appears to be compatible with clinopyroxene, green spinel, magnetite, and only traces of plagioclase. The cummingtonite-rich assemblage is in turn replaced partially by a late tremolite-serpentine-talc composite assemblage most likely related to greenschist metamorphism of the area. The overall fabric of the rock nonetheless suggests that the protolith was a clinopyroxenite (N.J. Page, oral commun., 1980). Our study thus substantiates the prior recognition by Wyman (1974) that ultramafics occur among the early Proterozoic rocks of the districts.

Major- and minor-element analyses of three samples of amphibolite (analyses 1-3), a diabase, and a pyroxene banded gneiss from the districts are presented in table 7, together with calculated Niggli values. Minor-element analyses of another six samples of amphibolite and one sample of iron-oxide-rich soil along a fault cutting amphibolite are listed in table 8. The latter minor-element analyses all were obtained from samples collected from the general area of the Bluebird mine in the Lost Basin district. The composite mineral assemblages of analyses 1 to 3 (table 7) are included in table 6, listed under the appropriate sample number, and these assemblages show that all three samples have been affected by the retrograde metamorphism. In fact, much of the plagioclase in these rocks is altered. Further, all three samples contain some modal quartz. The overall proportion of quartz in the samples ranges from trace amounts (table 7, sample GM-190a; 46.0 weight percent SiO_2) to approximately 20 volume percent (table 7, sample GM-529; 55.2 weight percent SiO_2). An additional 16 chemical analysis of amphibolite are included in Page and others (1986).

The average major-element composition of the three analyzed amphibolite samples was compared with the average concentration of these elements in various igneous-rock series and other selected amphibolite (table 9). Thus, from table 9, simply by comparing the major-element compositions of the amphibolite analyzed from Gold Basin-Lost Basin to similar averages of various igneous-rock series, one might suggest that these analyzed amphibolite samples have igneous protoliths. The average of these three analyses (table 9, sample 1) corresponds closely to the average continental basalt of Manson (1967, p. 222) or the average tholeiite of Le Maitre (1976). Further, these analyses are not much different from an analyzed sample of diabase collected from the main drift of the Golden Gate mine (table 7, sample 4). However, the

TABLE 7.—Analyses of mafic rocks from the Early Proterozoic terrane in the Gold Basin-Lost Basin mining districts

[Chemical analyses by rapid-rock methods; analysts, P.L.D. Elmore and S. Botts. Methods used are those described in Shapiro and Brannock (1962), supplemented by atomic absorption (Shapiro, 1967). Spectrographic analyses by Chris Heropoulos. Results are reported to the nearest number in the series 1, 0.7, 0.5, 0.3, 0.2, 0.15, 0.1, 0.70, and so forth, which represents approximate midpoints of interval data on a geometric scale. The precision of a reported value is approximately plus or minus one series interval at 68-percent confidence or two intervals at 95-percent confidence. Looked for but not found: Ag, As, Au, B, Bi, Cd, Mo, Ni, Pd, Pt, Sb, Sn, Te, U, W, Zn, Hf, In, Li, Re, Ta, Th, Tl, Pr, Sm, Eu]

Analysis -----	1	2	3	4	5
Sample -----	GM-290a	GM-242	GM-529	GM-578	GM-245
Chemical analyses (weight percent)					
SiO_2 -----	46.0	49.6	55.2	47.5	45.0
Al_2O_3 -----	15	15.4	13.7	17.2	15.9
Fe_2O_3 -----	3.2	3.2	6.5	6.7	5.8
FeO -----	9.7	8.5	7.4	3	9.3
MgO -----	8.4	5.7	3.9	6	5.7
CaO -----	10.5	10.5	8.3	10.1	10.9
Na_2O -----	2.1	2	2	2.7	1.5
K_2O -----	.70	1	.8	.40	.50
H_2O^+ -----	1.3	1.1	1.5	1.2	1.9
H_2O^- -----	.03	.08	.06	1.3	.13
TiO_2 -----	1.3	1	1.4	1.2	1.7
P_2O_5 -----	.15	.12	.24	.24	.16
MnO -----	.15	.22	.22	.12	.21
CO_2 -----	.11	.12	<.05	1.9	.05
Total -----	99	99	101	100	99
Semiquantitative spectrographic analyses (weight percent)					
Ba -----	0.05	0.03	0.02	0.05	0.03
Co -----	.007	.005	.005	.005	.007
Cr -----	.1	.05	.001	.02	.02
Cu -----	.007	.0015	.01	.007	.01
Ni -----	.03	.01	.005	.01	.01
Sc -----	.005	.005	.005	.005	.005
Sr -----	.03	.05	.05	.07	.03
V -----	.02	.03	.03	.015	.05
Y -----	.003	.002	.002	.003	.002
Zr -----	.007	.005	.007	.01	.003
Ga -----	.0015	.0015	.002	.0015	.002
Yb -----	.0003	.0003	.0003	.0003	.0003
Niggli values					
al -----	19	22	22	25	21
fm -----	51	44	47	41	48
c -----	25	27	24	27	27
alk -----	5	6	7	7	4
si -----	101	121	151	118	103
k -----	.18	.25	.21	.09	.18
mg -----	.41	.47	.34	.54	.41

1. Amphibolite, interlayered with quartzofeldspathic banded gneiss in feldspathic gneiss (Xfg); SW1/4 sec. 17, T. 29 N., R. 17 W.
2. Amphibolite 3 cm thick, interlayered with biotite quartzofeldspathic gneiss on contact between migmatitic gneiss unit (Xmg) and gneiss unit (Xgn); NW1/4 sec. 5, T. 28 N., R. 17 W.
3. Amphibolite in gneiss unit (Xgn); NW1/4 sec. 16, T. 30 N., R. 17 W.
4. Diabase collected from main drift, Golden Gate mine; NW1/4 sec. 32, T. 30 N., R. 17 W.
5. Pyroxene banded gneiss in migmatitic gneiss unit (Xmg); NE1/4 sec. 32, T. 29 N., R. 17 W.

TABLE 8.—Analyses for minor metals in selected samples of amphibolite and associated soil from the general area of the Bluebird mine in the Lost Basin mining district

[Spectrographic analyses by Leon A. Bradley. Results are reported to the nearest number in the series 1, 0.7, 0.5, 0.3, 0.2, 0.15, 0.1, 0.07, and so forth, which represent approximate midpoints of interval data on a geometric scale. The precision of a reported value is approximately plus or minus one series interval at 68-percent confidence or two intervals at 95-percent confidence. Looked for but not found: Ag, As, Au, Bi, Cd, Mo, Pd, Pt, Sb, Sn, Te, U, W, Hf, In, Li, Re, Ta, Th, Tl, Pr, Sm, Eu; L, less than determination value; --, not detected; N.D., not determined. Chemical analyses by Joseph Haffty, A.W. Haubert, and J. McDade using techniques of Haffty and Riley (1968) for Pd, Pt, and Rh; and Haffty, Haubert, and Page (1980) for Ir and Ru]

Analysis ----- Sample -----	1 79GM-1	2 79GM-2	3 79GM-3	4 79GM-4	5 79GM-5	6 79GM-6	7 79GM-7	8 79GM-7a
Semiquantitative spectrographic analyses (weight percent)								
B -----	0.002	--	--	L	--	--	--	N.D.
Ba -----	.015	0.015	0.007	0.02	0.015	0.02	0.015	N.D.
Co -----	.007	.005	.003	.0007	.005	.003	.003	N.D.
Cr -----	.1	.3	.05	.007	.2	.07	.15	N.D.
Cu -----	.00015	.0007	.015	.0015	.007	.02	.015	N.D.
Mn -----	.15	.15	.1	.05	.07	.15	.1	N.D.
Ni -----	.007	.02	.01	.0015	.07	.015	.03	N.D.
Pb -----	.0015	--	--	.003	--	--	.0015	N.D.
Sc -----	.007	.005	.003	.001	.002	.003	.003	N.D.
Sr -----	.02	.01	.007	.015	.0015	.007	.01	N.D.
V -----	.07	.02	.015	.005	.01	.02	.015	N.D.
Y -----	L	.003	.0015	.0015	L	.0015	.0015	N.D.
Zr -----	--	.003	.0015	.0015	.0015	.003	.003	N.D.
Ga -----	.0015	.0015	.002	.0015	.001	.002	.0015	N.D.
Chemical analyses (parts per million)								
Pd -----	0.029	<0.001	<0.001	<0.001	0.003	0.001	0.001	0.004
Pt -----	.027	.033	.032	.015	.024	.029	.013	.021
Rh -----	<.001	<.001	<.001	<.001	<.001	<.001	<.001	<.001
Ir -----	<.02	<.02	<.02	<.02	<.02	<.02	<.02	<.02
Ru -----	<.1	<.1	<.1	<.1	<.1	<.1	<.1	<.1

1. Amphibolite, composite sample; NE1/4 sec. 20, T. 29 N., R. 17 W.
2. Amphibolite, composite sample of several centimeter-sized layers in quartzofeldspathic gneiss; NE1/4 sec. 20, T. 29 N., R. 17 W.
3. Amphibolite, composite sample assembled from several centimeter- to meter-sized discontinuous pods; NE1/4 sec. 20, T. 29 N., R. 17 W.
4. Soil along fault cutting amphibolite, iron oxide stained; NE1/4 sec. 20, T. 29 N., R. 17 W.
5. Amphibolite, composite samples containing 1- to 2-volume-percent pyrite disseminated as 1- to 2-mm blebs; NW1/4 sec. 20, T. 29 N., R. 17 W.
6. Amphibolite, composite sample; SW1/4 sec. 17, T. 29 N., R. 17 W.
7. Amphibolite, composite sample; SE1/4 sec. 18, T. 29 N., R. 17 W.
8. Amphibolite, composite sample; SE1/4 sec. 18, T. 29 N., R. 17 W.

Al₂O₃ content of the diabase (17.2 weight percent) is somewhat higher than the 14.7 weight percent average content of Al₂O₃ in the amphibolite, probably reflecting the higher content of modal plagioclase in the diabase than in the amphibolite. However, Leake (1964) suggested that a comparison of trends of certain elements in amphibolite with similar trends in sedimentary and igneous rocks might be more useful in establishing a sedimentary or igneous protolith than a comparison of average concentrations of elements. For example, an elongation of data points along a Karroo dolerite trend at high angles to the trend for varying mixtures of calcium carbonate, magnesium carbonate, and shale would suggest an igneous parentage. Thus, from the major-element data of table 6, plots of Niggli 100 *mg*, *c*, and *al-alk* values; Niggli *c* versus *mg*; and Niggli *c* versus *al-alk* were prepared (figs. 19-21).

Plots of various Niggli values yield results that are not particularly diagnostic primarily because of the small number of analyses of amphibolite available. Niggli values in a 100 *mg*, *c*, and *al-alk* ternary plot for the amphibolite show that they form a cluster slightly off the trendline established for Karroo dolerites by Evans and Leake (1960) but also well within the field of values expected for various shale-carbonate mixtures (fig. 19). The analyzed diabase (table 7, analysis 4) also plots slightly off the trendline in this ternary diagram. A plot of the Niggli values for the pyroxene-banded gneiss (table 7, analysis 5), however, falls within the small cluster established by the data from the amphibolite samples. On the other hand, the plot of Niggli *mg* versus *c* shows data from the amphibolite to plot in the field for the Karroo dolerites and to follow a trendline approximately parallel to the differentiation trendline of the dolerites (fig. 20). On such

TABLE 9.—Average major-element compositions, in weight percent, of Gold Basin-Lost Basin amphibolite and various groups of igneous rocks and other amphibolites
[N.D., not determined]

Analysis	1	2	3	4	5	6	7	8
SiO ₂	50.3	49.9	49.58	57.94	48.87	52.8	49.3	55.5
Al ₂ O ₃	14.7	16.2	14.79	17.02	12.26	14.7	16.3	16.1
Fe ₂ O ₃	4.3	3	3.38	3.27	¹ 11.89	4.5	2.5	2.8
FeO	8.5	7.8	8.03	4.04	N.D.	6.6	8.5	5
MgO	6	6.3	7.30	3.33	10.13	6.5	6	5.7
CaO	9.8	9.8	10.36	6.79	9.84	8.8	10.7	6.9
Na ₂ O	2	2.8	2.37	3.48	1.91	2.5	3.1	3.4
K ₂ O	.83	1.1	.43	1.62	1.90	.68	.59	1.7
H ₂ O ⁺	1.3	1	.91	.83	N.D.	1.2	1.2	1.3
H ₂ O ⁻	.06	N.D.	.50	.34	N.D.	.39	.10	.10
TiO ₂	1.2	1.6	1.98	.87	.62	1.1	1.1	.78
P ₂ O ₅	.17	.30	.24	.21	.09	.15	.23	.32
MnO	.19	.17	.18	.14	.34	.19	.17	.12
CO ₂	.09	N.D.	.03	.05	N.D.	.04	.18	.04
Total	99	100	100.08	99.93	97.85	100.2	100	100

¹Total Fe calculated as Fe₂O₃.

1. Average amphibolite, analyses 1-3 (table 6), this report.
2. Average continental basalt (Manson, 1967, table III, p. 222).
3. Average tholeiite (LeMaitre, 1976, No. 28).
4. Average andesite (LeMaitre, 1976, No. 16).
5. Selected amphibolite from Early Proterozoic Vishnu Schist in the Grand Canyon (Clark, 1979, table II, analysis 4).
6. Average of five amphibolites in Early Proterozoic Pinal Schist from the Mineral Mountain area, Arizona (T.G. Theodore, unpub. data, 1982).
7. Average of 12 amphibolites from Condrey Mountain, Klamath Mountains, Calif. (Hotz, 1979, table 5, p. 16).
8. Average amphibolite, central Beartooth Mountains, Montana-Wyoming (Armbrustmacher and Simons, 1977).

a diagram, the analyzed diabase appears to be less differentiated than the three analyzed amphibolite samples. On a Niggli *c* versus Niggli *al-alk* diagram, the data for the amphibolite again cluster and fall just outside the values most expected for shale-carbonate mixtures but still within a field of possible values for shale-carbonate mixtures (fig. 21). Again, the clustering of the small number of data points (three amphibolite, and one pyroxene-banded gneiss) follow clearly neither a sedimentary nor an igneous trend. Therefore, only one of the plots (fig. 20) yields a trend for the amphibolite that might be interpreted as an igneous one. The minor-element data, particularly the concentration of chromium and nickel in some of the samples of amphibolite analyzed (tables 7, 8), also suggest derivation from igneous protoliths. Further, the presence of detectable platinum-group metals in eight samples of amphibolite analyzed from the general area of the Bluebird mine (table 8), in the Lost Basin Range, implies an igneous protolith, as does the relict igneous fabric in these samples and in most other metabasites throughout the southern part of the Lost Basin Range. Plots of all available chemical analyses of amphibolite from the districts (Page and others, 1986) suggest that igneous

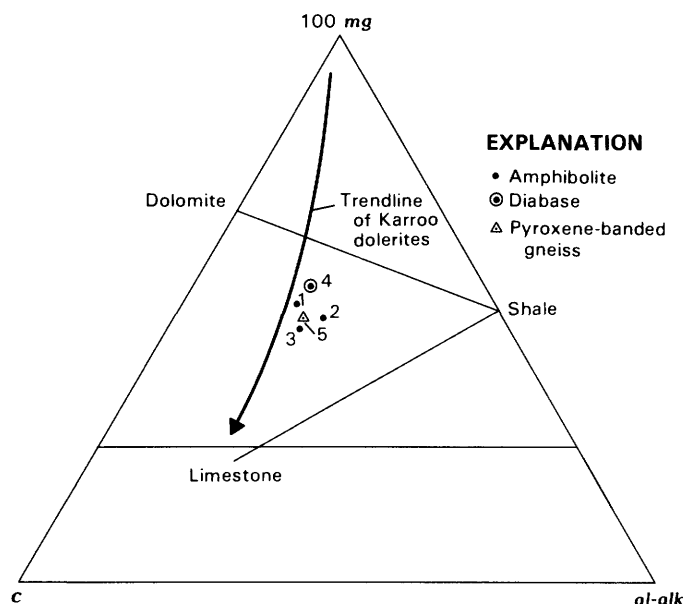


FIGURE 19.—Niggli 100 mg, *c*, and *al-alk* values for amphibolite, diabase, and pyroxene-banded gneiss from Gold Basin-Lost Basin mining districts. Analysis numbers same as in table 7. Solid lines indicate tielines between end-member compositions for dolomite, shale, and limestone.

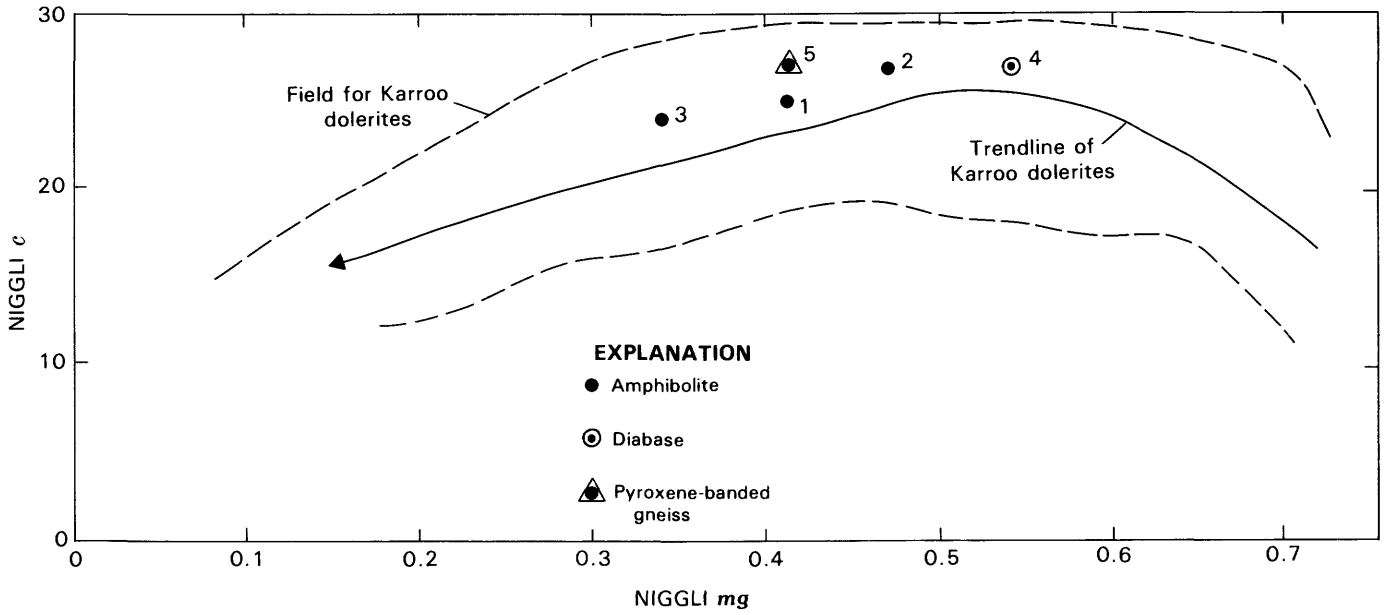


FIGURE 20.—Niggli *c* versus *mg* values for amphibolite, diabase, and pyroxene-banded gneiss from Gold Basin-Lost Basin mining districts. Analysis numbers same as in table 7. Field and trendline for Karroo dolerites are from Evans and Leake (1960).

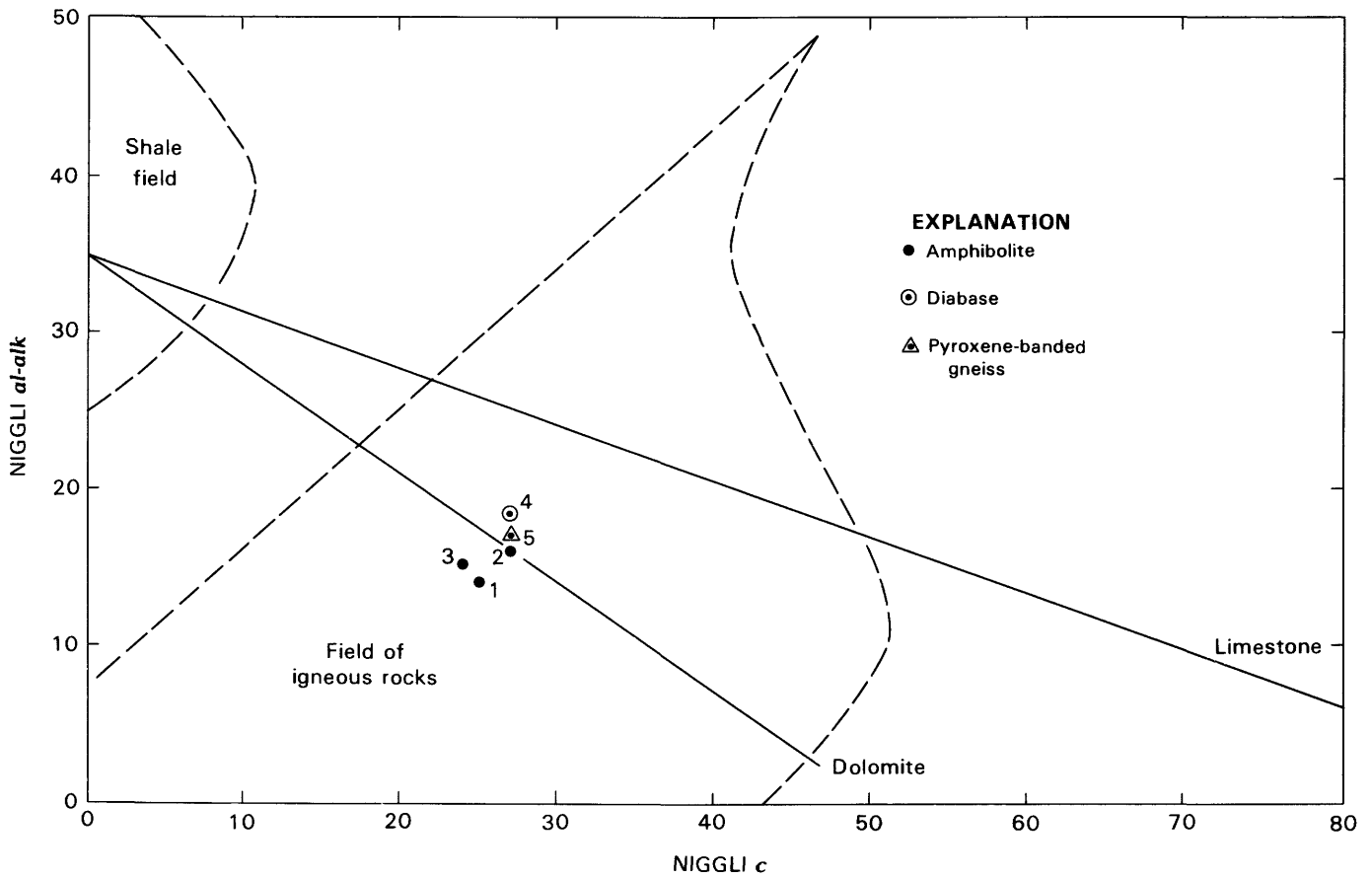


FIGURE 21.—Niggli *c* versus *al-alk* values for amphibolite, diabase, and pyroxene-banded gneiss from Gold Basin-Lost Basin mining districts. Analysis numbers same as in table 7. Solid lines, potential trends of variation in mixtures of shale and carbonate (van de Kamp, 1969).

protoliths of amphibolite varied from ultramafic komatiite to basaltic komatiite to tholeiite in the classification scheme of Jensen (1976). Eight of the samples analyzed by Page and others (1986) contain as much as 1,000 ppm chromium and 300 ppm nickel. However, these observations and geologic relations together with those in the quartz-rich, sedimentary-derived amphibolite suggest very strongly that amphibolite in the districts was derived from both igneous and sedimentary protoliths.

METACHERT, BANDED IRON FORMATION, AND METARHYOLITE

Thin lenses of metachert, discontinuous beds of banded iron formation (see Stanton, 1972), and scattered outcrops of metarhyolite are found in the Proterozoic metamorphic rocks of the districts. Most of these rocks are in the gneiss (fig. 2, unit Xgn) and the three types commonly are associated spatially with one another. They are rarely present in the migmatitic gneiss unit. Most are quite thin, generally 20 to 90 cm thick. Metachert typically is well laminated, probably reflecting relict bedding. The metachert consists of irregularly banded quartz- and feldspar-containing laminae that in places are conformable and interlayered with amphibolite. The feldspar-containing laminae have been altered mostly to various phyllosilicate and epidote-group minerals. Metachert also is associated spatially with several other lithologies, including complexly scrambled calc-silicate rocks, amphibolitic calc-silicate rocks, and marble. Chemical analysis of a grab sample of a slightly pinkish micaceous or argillaceous metachert gives an SiO₂ content of 79.5 weight percent (table 10, analysis 1). Examination of a thin section of this metachert shows a quartz-biotite-cordierite-plagioclase prograde assemblage that has been replaced intensely during the retrograde regional metamorphic event. The retrograde assemblage includes chlorite, white mica, albite, and rutile. These thin sequences of metachert grade locally into iron formation, which consists of alternating hematite- and magnetite-rich laminae and finely crystalline quartz-rich laminae. Chemical analysis of a ferruginous sample which is intermediate between metachert and typical iron formation shows a content of about 14 weight percent total iron as FeO (table 10, analysis 2). In addition, this particular sample contains 100 ppm copper and 200 ppm zinc. Quartz, magnetite, and hematite are the dominant minerals in the rock, and the iron oxide-rich laminae include a composite assemblage of clinopyroxene, amphibole, apatite, white mica, and abundant paragenetically late needles of probable minnesotaite, an iron analog of talc (see Deer and others, 1962c). These samples (table 9, analyses 1, 2) are interbedded with a metaquartzite most likely derived from a pebbly, limy siltstone. Under the microscope the metaquartzite shows 1.0-cm elongate clasts of monocrystalline

to polycrystalline quartz set in an equigranular 0.08- to 1.0-mm-size matrix of mostly quartz and epidote. The clasts of quartz are tightly sutured into the matrix across several millimeters of intergrown quartz and epidote.

Well-developed oxide-facies banded iron formation is present in at least five localities in the districts (table 11, locs. 216, 303, 664, 973, and 1086). All five of these occurrences of iron formation are associated closely with at least some metabasites, including amphibolite, sequences of amphibolitic gneiss, and mafic schist. The best developed iron formation probably crops out at locality 303 (table 11). Here, a 60- to 90-cm-thick sequence of laminated hematitic but highly magnetic iron formation (fig. 22) strikes approximately N. 30° W. and dips about 50° SW. It can be traced more than 200 m along strike primarily by using float. Further, the iron formation at

TABLE 10.—Analyses of metachert, banded iron formation, metarhyolite, and calc-silicate marble in various Early Proterozoic metamorphic units from the Gold Basin-Lost Basin mining districts

[Chemical analyses by rapid-rock methods; analysts P.L.D. Elmore and S. Botts. Methods used are those described in Shapiro and Brannock (1962), supplemented by atomic absorption (Shapiro, 1967). Spectrographic analyses by Chris Heropoulos. Results are reported to the nearest number in the series 1, 0.7, 0.5, 0.3, 0.2, 0.15, 0.1, 0.07, and so forth, which represent approximate midpoints of interval data on a geometric scale. The precision of a reported value is approximately plus or minus one series interval at 68-percent confidence or two intervals at 95-percent confidence. Looked for but not found: Ag, As, Au, B, Bi, Cd, Mo, Pd, Pt, Sb, Sn, Te, U, W, Hf, In, Li, Re, Ta, Th, Tl, Pr, Sm, Eu; —, not detected]

Analysis -----	1	2	3	4	5
Sample -----	GM-216a	216	303	303a	290b
Chemical analyses (weight percent)					
SiO ₂ -----	79.5	81.3	45.8	71.4	17.8
Al ₂ O ₃ -----	11.5	1.1	1.3	13.9	1.9
Fe ₂ O ₃ -----	1	11	42.4	.80	1.2
FeO -----	1.5	4.8	4.6	3.6	3.3
MgO -----	2.6	.50	—	2.6	2.3
CaO -----	.2	.60	2.4	1.5	43.1
Na ₂ O -----	.5	—	—	3.8	—
K ₂ O -----	1.6	—	—	.90	—
H ₂ O ⁺ -----	2.2	.58	1.1	1.8	.68
H ₂ O ⁻ -----	.05	.07	.09	.04	.11
TiO ₂ -----	.17	.08	.02	.18	.08
P ₂ O ₅ -----	—	.24	.43	.12	.02
MnO -----	.06	.12	—	—	.12
CO ₂ -----	<.05	<.05	.42	<.05	30.4
Total -----	101	100	98.6	100.7	101.0
Semiquantitative spectrographic analyses (weight percent)					
Ba -----	0.07	0.015	0.007	0.05	0.002
Co -----	—	.0005	.0005	.0007	.0015
Cr -----	.00015	.0002	.0005	.005	.007
Cu -----	.0005	.01	.0007	.00015	.002
Ni -----	.0002	.0007	.0005	.001	.002
Pb -----	—	—	—	.001	—
Sc -----	.001	—	—	.001	.0015
Sr -----	.002	—	.003	.01	.02
V -----	—	.0015	.0015	.005	.005
Y -----	—	.001	.002	—	.0015
Zn -----	—	.02	—	—	—
Zr -----	.007	.001	—	.007	—
Ga -----	.001	—	—	.0015	.0003
Yb -----	—	.00015	.0002	—	.00015

1. Quartzite or argillaceous metachert, in migmatitic gneiss unit (Xmg) of figure 2; SE1/4 sec. 32, T. 29 N., R. 17 W.
2. Magnetite-bearing banded metachert, in migmatitic gneiss unit (Xmg) of figure 2; SE1/4 sec. 32, T. 29 N., R. 17 W.
3. Iron formation, in gneiss unit (Xgn) of figure 2; NW1/4 sec. 16, T. 29 N., R. 17 W.
4. Metarhyolite, in gneiss unit (Xgn) of figure 2; NW1/4 sec. 16, T. 29 N., R. 17 W.
5. Calc-silicate marble, in feldspathic gneiss unit (Xfg) of figure 2; SW1/4 sec. 17, T. 29 N., R. 17 W.

locality 303 has been prospected by use of an approximately 20-m-deep vertical shaft. Near the shaft, the iron formation is very closely associated with laminated fine-grained amphibolite. Approximately 100 m to the west-northwest, an exposed sequence of banded amphibolite and quartzofeldspathic gneiss is heavily stained by various iron oxides. However, these iron oxides are associated with highly manganese-rich gossanlike stringers in brecciated quartz and highly altered granitoid pegmatite. The major minerals in these oxide-facies iron formations are maghemite (magnetic hematite derived from magnetite) and quartz, which are present in alternating bands. Granoblastic quartz typically shows complexly sutured boundaries and may have long dimensions of about 4 mm in some quartz-rich bands about 5 mm thick. However, such grains of quartz include swarms of extremely fine grained aligned crystals of maghemite that parallel the trace of the maghemite-quartz bands. Therefore, recrystallization of these rocks must have involved a tremendous increase in grain size as has been reported in metamorphosed bedded iron formations elsewhere (see James, 1981). We infer that these thinly banded maghemite-quartz rocks in the Gold Basin-Lost Basin districts were initially deposited as chemical precipitates related to sporadic volcanic activity during the largely epiclastic deposition of the protoliths of the surrounding metamorphic rocks. Kimberley (1983) reported that approximately 85 percent of Early Proterozoic iron formations examined contain more than 5 volume percent chert and thus would be classified as cherty in his scheme. However, a more useful classification is one that relates the iron formation to a tectonic or depositional environment. Gross (1980) proposed that iron formations may be classed as epeirogenic (Superior type) or orogenic (Algoma type). The depositional environment of the iron formation in the Gold Basin

and Lost Basin mining districts is probably more closely related to the Algoma type because of the association of the iron formation here with a presumably arc-related, graywacke-rich protolith. Indeed, some of the nearby iron formation enclosing rocks in the Gold Basin-Lost Basin districts also include detrital magnetite (Deaderick, 1980, p. 16-19). Chemical analysis of a representative sample from the iron formation shows a content of about 43 weight percent total iron as FeO and an SiO₂ content of 45.8 weight percent (table 10, analysis 3). However, the high content of hematite in this sample is reflected in its high ratio of Fe₂O₃ to FeO, about 9 to 1 (table 10).

Porphyritic to seriate, foliated metarhyolite also crops out in the general area of the iron formation at locality 303 (table 11). Phenocrysts and crystal fragments of albite-oligoclase (An₁₀) and quartz make up about 20 to 25 volume percent of the rock. These phenocrysts and crystal fragments range from 0.3 to 3.5 mm in size and probably average about 1.5 mm in their largest dimension. Some of the albite-oligoclase is present in glomeroporphyritic aggregates, some of which include small ovoid lithic clots of very fine grained granule quartz plus chlorite. About one-third of the phenocrysts are quartz. Many of the quartz crystals are embayed, and several of them are obviously bipyramids. In addition, they are highly strained, showing a ribbon-type extinction under crossed nicols. Where the originally monocrystalline quartz phenocrysts have recrystallized, the newly grown crystals of quartz are associated with recrystallization of chlorite, which is moderately abundant throughout the matrix. The matrix is poorly but nonetheless distinctly foliated, a textural relation that is one of the most diagnostic features of the rock. The laths of albite have poorly defined crystal boundaries with the surrounding matrix and are aggregated with quartz, chlorite, biotite, and additional granoblastic albite. Light- to medium-brown (Z axis) biotite is paragenetically earlier than chlorite. Minor accessories include apatite, zircon, and fine-grained granules of epidote. Chemical analysis of a grab sample from the metarhyolite shows an SiO₂ content of 71.4 weight percent and an Na₂O plus K₂O content of 4.7 weight percent (table 10, analysis 4), which plots in the rhyolite field using the chemical classification of Middlemost (1980).

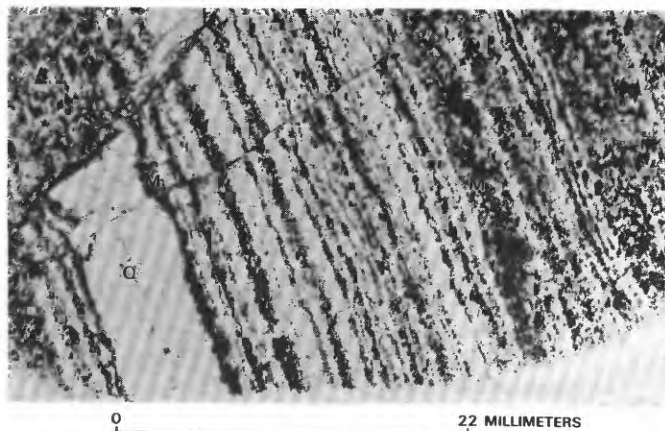


FIGURE 22.—Oxide facies, banded iron formation. Q, quartz; M, maghemite. Plane-polarized light. Sample GM-303, NW $\frac{1}{4}$ sec. 16, T. 29 N., R. 17 W.

MARBLE, CALC-SILICATE MARBLE, AND SKARN

Beds generally less than 2 m thick of marble, calc-silicate marble, and skarn crop out sporadically throughout much of the gneiss and feldspathic gneiss units (fig. 2). In detail, many individual beds of these carbonate or replaced carbonate beds are also spatially associated very closely with amphibolite. Most of the marble is impure and

in places it is squeezed into the cores of very tightly appressed recumbent and overturned folds that measure as much as 1 to 2 m across. Typically, wide-ranging overall proportions of silicate minerals are present in these rocks both along individual beds and among different nearby beds. The best replacement phenomena between carbonate and silicate minerals are recorded in some of the most calcite-rich calc-silicate marble, as exemplified by sample GM-290b (table 10, analysis 5). A relatively silica deficient calc-silicate marble (17.8 weight percent SiO_2) contains a composite assemblage of actinolite, diopside-salite (trace), quartz, and sphene, which shows excellent textural relations documenting multiple crystallization events. The earliest assemblage probably consisted of calcite, and diopside-salite. Then, medium-grained calcite crystals, approximately 2.0 mm across, show incipient patchy replacement by early pale-apple-green (Z axis) actinolite. Reaction fronts between unreplaced calcite and partially replaced calcite are exceptionally sharp and seem to be confined to select crystals of calcite scattered through the rock rather than defining planes cutting across the calcite's crystal boundaries. Further, aligned fine-grained crystals of less strongly pleochroic actinolite (and thus probably more magnesian, see Deer and others, 1963) define foliations through the calc-silicate marble by their strong preferred dimensional orientation. Increased abundances of the fine-grained crystals of actinolite are concentrated mostly peripheral to lensoid clots of finely crystalline quartz. In addition, there is some dimensional orientation of calcite in these domains. In some of the more heavily retrograded calc-silicate marbles, and also more siliceous than sample GM-290b, carbonate has been completely replaced by an assemblage of zoisite and clinozoisite, chlorite, white mica (possibly chloritoid), sphene, and quartz, and including relict plagioclase and various opaque minerals in trace amounts.

Some calc-silicate marble contains garnet as one of its diagnostic minerals. Isotropic garnet, probably rich in the grossular molecular end member, in these calc-silicate marbles typically includes medium-grained crystals of diopside-salite, a relation suggesting crystallization of diopside-salite preceded crystallization of garnet. Where foliated, the schistosity is confined primarily to the quartz- and calcite-rich domains of the rock. Minor accessories include sphene and slightly rounded crystals of zircon.

Some pods of calc-silicate minerals in generally migmatitic-gneiss sequences of rock show the development of zoned reaction rims with an adjoining pelitic schist. These reaction rims are millimeter sized and probably developed by a predominantly diffusion-dominant process (for discussion of diffusion phenomena, see Vidale, 1969; Hewitt, 1973; Vidale and Hewitt, 1973). Where the pelitic schist has not apparently reacted with the enclosed carbonate-rich pods, it contains a typical biotite-quartz-

plagioclase (about An_{45})-apatite-opaque mineral assemblage (fig. 23, zone I). However, within about 13 mm of the approximate original boundary between the pelitic schist and the carbonate-rich rock, the first mineralogical changes are present. These changes are (1) the sporadic nucleation of newly crystallized clinozoisite that either envelopes an opaque mineral (probably magnetite) or is very close to an opaque mineral, (2) a marked decrease in the average maximum dimension of biotite from about 0.5 mm in zone I to about 0.12 mm in zone II, and (3) a progressive decrease in the grain size of biotite and a concomitant increase in the modal abundance of largely untwinned plagioclase (approximately An_{50}). The boundary of zone II on the side of the calc-silicate pod is placed at the point of final disappearance of biotite. However, a bladed opaque mineral, which is most likely ilmenite, appears initially about two-thirds of the way into zone II and continues through zone III; the ilmenite disappears finally about one-quarter of the way through zone IV (fig. 23). A weakly pleochroic amphibole in zone III, probably tremolite-actinolite, is present as stubby crystals that have an overall shredded aspect and make up about 10 to 15 volume percent of the zone. From the specific mineral assemblage and modal composition of zone III, we infer it as having the lowest K_2O content of the three reaction zones (II-IV) developed in rock that formerly had the same overall bulk composition as the unreacted pelitic schist. Relative to zones III and VI, the phyllosilicates biotite (now mostly retrograded to chlorite) and white mica are more abundant in zones IV and V. This increase in abundance is confined mostly to a domain near the original approximate boundary between pelitic rock and carbonate-rich rock. The modal concentration of sphene is highest in zone I, on the carbonate side of the original boundary between the carbonate and pelitic rocks. Thus, all these relations above suggest that the following chemical changes occurred across the pelitic-carbonate contact during metamorphism: (1) a depletion of potassium in the pelitic rocks immediately adjacent to the carbonate, (2) a concomitant flow of calcium from the carbonate out into the pelitic rock, (3) possibly a fixation of some of the potassium released from the pelitic rock into biotite and white mica along the original boundary between pelite and carbonate, and (4) a possible flow of titanium from the breakdown of biotite into the recrystallizing carbonate. Vidale (1969) documented experimentally the differential movement of potassium, calcium, and magnesium across juxtaposed pelite and carbonate assemblages. In her experiments, however, potassium and calcium moved away from the carbonate. Thus, the nucleation of newly grown biotite and white mica in zones IV and V (fig. 23) most likely reflects circulation of a second pulse of fluids primarily along the former pelitic schist and calc-silicate contact.

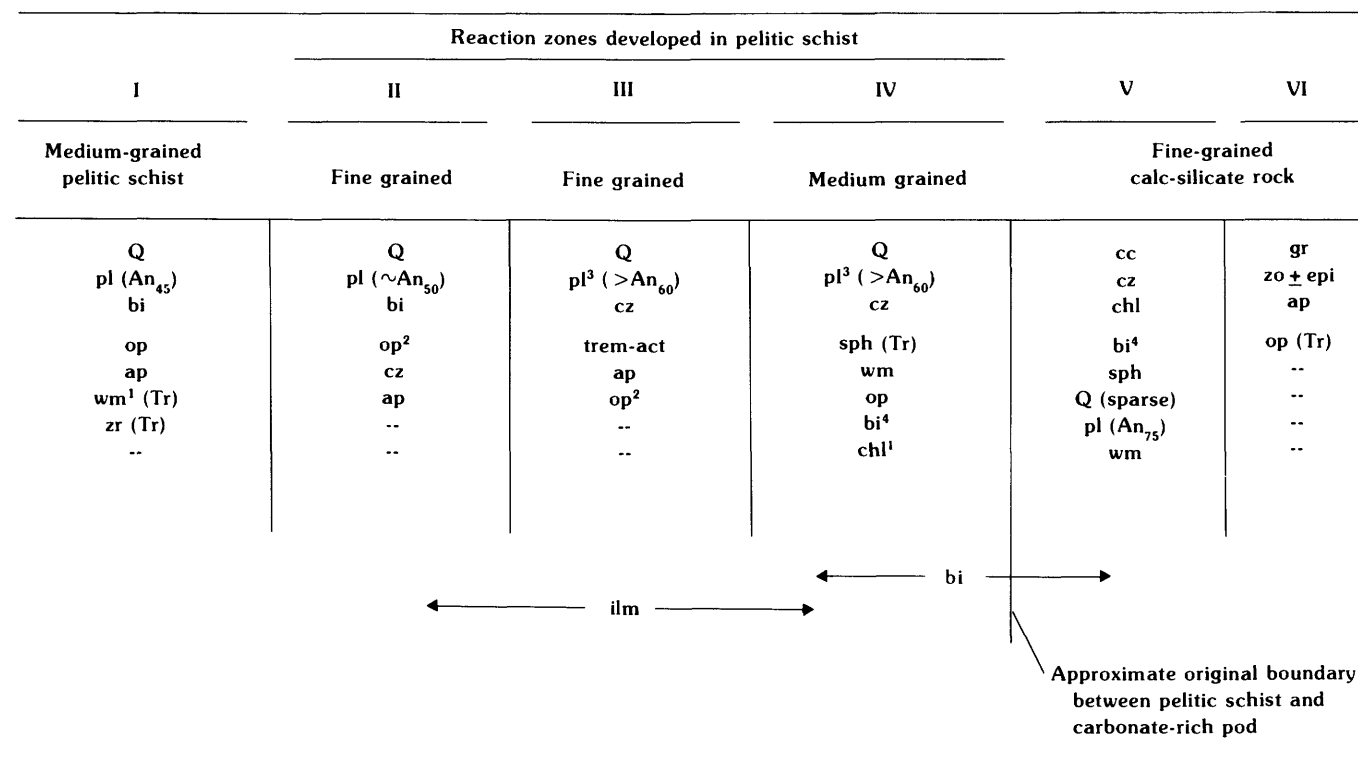
Zone VI contains a relatively simple composite assemblage consisting of isotropic garnet, zoisite or epidote, sparse apatite, and an opaque mineral in trace amounts (fig. 23). The garnet apparently replaced mostly the fine-grained intergrowths of clinozoisite, calcite, and chlorite of zone V. Further, the crystallization of garnet appears to have overstepped that of zoisite because crystals of zoisite typically have been enveloped by a primarily grain-boundary-controlled growth of garnet. The garnet-zoisite assemblage in zone VI is similar to assemblages in zoned calc-silicate rocks in kyanite-grade regionally metamorphosed rocks described by Vidale (1969).

Small bodies of skarn, measuring several meters across, crop out sporadically in many of the Proterozoic metamorphic and igneous units of figure 2. Generally, the skarn consists of discontinuous layers of coarse intergrowths of garnet, dark fibrous amphibole, and quartz; or garnet, epidote, and quartz with or without pyrite and calcite. Locally, some skarn has been prospected for scheelite (tungsten), which is present as crystals as coarse as 2.5

cm in maximum dimension in podlike masses of skarn related probably to nearby thin pegmatite dikes (table 11, loc. 25).

PROTEROZOIC IGNEOUS AND METAIGNEOUS ROCKS

Early Proterozoic igneous and metaigneous rocks in the districts range greatly in size and include leucogranite (unit XI), gneissic granodiorite (Xgg), feldspathic gneiss (Xfg), biotite monzogranite (Xm), leucocratic monzogranite (Xlm), porphyritic monzogranite (Xpm), and granodiorite (Xgd, fig. 2). In addition, varying proportions of igneous and metasedimentary rocks combine to yield a variety of migmatitic rocks in the exposed basement of the districts. The most widely exposed migmatitic rocks are along the lower west flanks of Garnet Mountain. Furthermore, another igneous rock in the districts, presumably Middle Proterozoic in age, is present as scattered undeformed diabase dikes, sills, and small intrusive masses. In addition to small bodies of all of these Pro-



¹Retrograde.

²Includes both bladed and equant varieties; probably ilmenite and mostly magnetite, respectively.

³Mostly untwinned plagioclase.

⁴Altered mostly to chlorite.

FIGURE 23.—Schematic diagram of sequence of mineral assemblages developed in zones near contact between medium-grained pelitic schist and fine-grained calc-silicate rock. Q, quartz; pl, plagioclase; bi, biotite; chl, chlorite; op, opaque mineral; ap, apatite; wm, white mica; zr, zir-

con; Tr, trace; cz, clinozoisite; trem-act, tremolite-actinolite; sph, sphene; cc, carbonate, mostly calcite; gr, garnet, completely isotropic; zo, zoisite; epi, epidote; ilm, opaque mineral, bladed habit, probably ilmenite; --, not found.

terozoic igneous rocks, the gneiss also includes locally some conspicuously exposed hornblende-biotite orthogneiss that has the composition of monzonite (fig. 24).

LEUCOGRANITE

Masses of gneissic leucogranite (unit al of Blacet, 1975) range in size from several-centimeter-wide stringers parallel to compositional layering in the gneiss to the 1-km-long sill that crops out about 3 km northeast of the Cyclopic mine. This sill strikes north-south and dips to the west, approximately conformable with foliation in the surrounding gneiss (unit XI, fig. 2). On the south, the sill of leucogranite appears to be truncated by the large mass

of gneissic granodiorite that crops out in the Gold Basin district. Throughout the gneiss, the fabrics of individual bodies of leucogranite texturally may grade from coarse-grained granitoid to pegmatitic, containing potassium feldspar phenocrysts as much as 8 cm wide. In addition, leucogranite ranges from relatively undeformed to intensely mylonitized rock. Although mylonitized coarse-grained leucogranite is generally conformable with its surrounding rocks, locally it cuts amphibolite and garnetiferous gneiss. Nonetheless, the two diagnostic overall features of the Early Proterozoic leucogranite are (1) its sill-like concordant relation with the gneiss and (2) its commonly gneissic to intensely mylonitic fabric. In addition, many of these leucogranite sills contain bluish-gray, highly

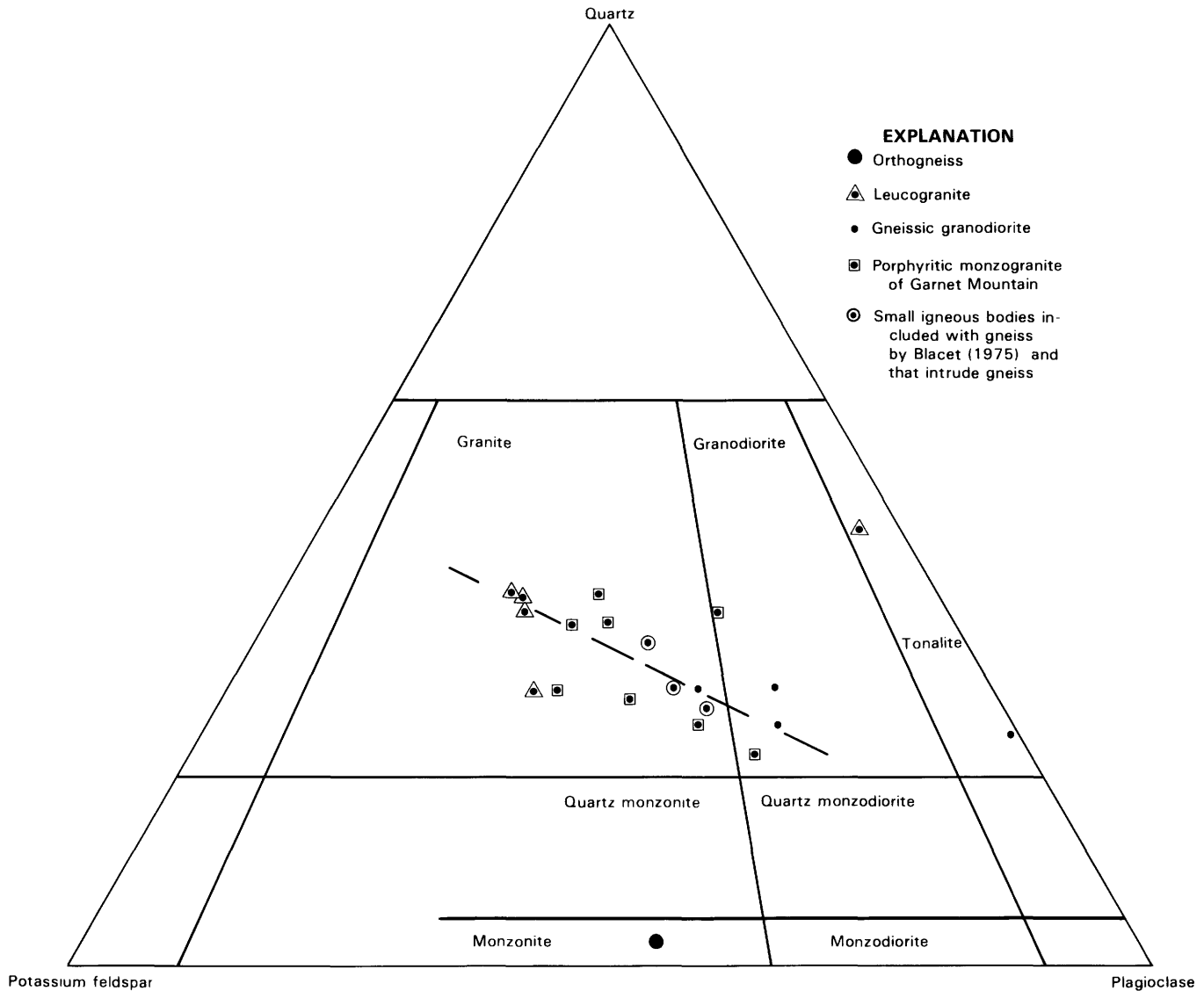


FIGURE 24.—Modes of Proterozoic igneous and metaigneous rocks from Gold Basin-Lost Basin mining districts. Data from table 12. Compositional fields from Streckeisen and others (1973). Dashed line, visually estimated regression line.

vitreous quartz, which is found in wispy segregation lenses. Northeast of the Gold Hill mine, large sills of pegmatitic leucogranite increase in abundance and eventually grade into complexes of highly deformed migmatitic leucogranite (unit mal of Blacet, 1975). These complexes include swarms of leucogranite, aplite, and pegmatite dikes, together with pegmatoid quartz veins, all cutting gneiss. All of the relations indicate that initial emplacement of leucogranite into gneiss occurred during the intense ductile deformation of the gneiss. Although we infer that the mapped body of leucogranite is older than all other Proterozoic igneous rocks, some leucogranite in the Proterozoic terrane probably was emplaced synchronously with all other Early Proterozoic igneous rocks here. Garnetiferous gneissic leucogranite, which ranges widely in grain size, locally becomes very strongly foliated and mylonitic near some minor tungsten (scheelite) prospects. This tungsten mineralization may be Proterozoic in age. In addition, the pink garnet in some of the leucogranite is concentrated near the walls of the leucogranite, especially where the leucogranite is in contact with biotite- or garnet-rich gneiss. Plots of modal data (table 12) for five samples of leucogranite show that four samples fall within the compositional field of granite (fig. 24). The other sample plots within the compositional field for tonalite.

GNEISSIC GRANODIORITE

An elongate body trending N. 25° E. of Early Proterozoic medium-grained gneissic granodiorite crops out across approximately 10 km² in the Gold Basin district

(fig. 2; unit ggd of Blacet, 1975). The southernmost exposures of the gneissic granodiorite body crop out about 2 km northeast of the Cyclopic mine. The gneissic granodiorite apparently intrudes gneiss and some leucogranite and is in turn intruded by Early Proterozoic porphyritic monzogranite of Garnet Mountain and Middle Proterozoic diabase, and presumably even younger pegmatitic leucogranite and gold-bearing veins. Some samples of typical gneissic granodiorite contain approximately 25 to 30 volume percent quartz and plot in the compositional field for granodiorite (fig. 24). However, other samples show wide-ranging alkali feldspar to plagioclase proportions yielding modal compositions that fall in the granite and tonalite compositional fields. Mafic minerals, mostly biotite, make up about 20 volume percent of the rocks. Plagioclase (approximately An₂₀) generally is altered intensely to white mica ± carbonate ± clinozoisite assemblages, whereas the potassium feldspar is remarkably fresh and includes both microcline and perthitic varieties. Accessory minerals are sphene, apatite, and opaque minerals. Gneissic granodiorite may be a mafic, less siliceous variety of igneous rock more or less isochronous with feldspathic gneiss (Xfg, fig. 2).

Numerous shallow prospect pits and mine workings are scattered throughout the gneissic granodiorite. However, the east contact between the gneissic granodiorite and the surrounding gneiss appears to have acted as a very important conduit for the circulation of fluids associated with gold mineralization. Prospects and productive mines, including the Malco mine in the SE¼ sec. 21, T. 28 N., R. 18 W., are especially concentrated along the strike of this contact for approximately 2 km.

TABLE 12.—Modal data for Proterozoic igneous and metaigneous rocks from the Gold Basin-Lost Basin mining districts

Sample	Total points counted	Quartz (volume percent)	Potassium feldspar (volume percent)	Plagioclase (volume percent)	Mafic minerals (volume percent)	Comments	Location
GM-98 -----	1,468	37.3	38.4	22.7	1.6	Foliated leucogranite dike in mixed granodioritic complex	NE1/4 sec. 15, T. 28 N., R. 16 W.
GM-98a -----	1,609	38.8	38.2	20.4	2.6	Porphyritic leucogranite inclusion in sample 98, showing 3-cm crystals of potassium feldspar	NE1/4 sec. 15, T. 28 N., R. 16 W.
GM-126a -----	3,535	19.6	22.2	34.5	23.6	Biotite-hornblende granite of unit Xgn	NW1/4 sec. 24, T. 28 N., R. 16 W.
GM-638z -----	1,798	2.2	33.4	40	24.4	Orthogneiss included in gneiss unit Xgn of Gold Hill mine, T. 29 N., R. 18 W.	Approximately 1.7 km west-northwest of Gold Hill Mine
GM-824 -----	1,479	39.1	38.4	21.4	1	Garnet-bearing pegmatoid leucogranite in gneiss unit Xgn	SW1/4 sec. 4, T. 27 N., R. 18 W.
GM-830 -----	1,344	21.4	24.9	49.8	3.9	Aplite dike, shallow dipping, presumably cogenetic with Xpm unit	NW1/4 sec. 4, T. 27 N., R. 18 W.
GM-848 -----	1,726	24.3	16.2	40.7	18.8	Biotite granodiorite, slightly porphyritic, locally gneissic, in gneiss (Xgn)	NW1/4 sec. 3, T. 27 N., R. 18 W.
GM-874 -----	1,790	22.6	21.1	32.7	23.7	Gneissic granite in gneiss (Xgn); presumably correlative with gneissic granodiorite (Xgd)	NE1/4 sec 23, T. 30 N., R. 19 W.
GM-893 -----	1,338	21.1	21.2	35.1	22.6	Granite in gneiss (Xgn)	NW1/4 sec. 29, T. 28 N., R. 18 W.
GM-894 -----	1,660	28.9	41.6	28.2	1.3	Leucogranite dike, 10 m thick, cutting gneiss (Xgn)	SW1/4 sec. 29, T. 28 N., R. 18 W.
GM-927 -----	1,767	28.6	28.5	39.2	3.8	Gneissic granite in gneiss (Xgn)	NE1/4 sec. 17, T. 28 N., R. 18 W.
GM-945a -----	1,850	20.7	17.5	42.2	19.6	Gneissic granodiorite (Xgd)	SE1/4 sec. 21, T. 28 N., R. 18 W.
GM-1000 -----	1,427	20.7	.4	61.9	17	Gneissic tonalite variant of gneissic granodiorite (Xgd)	NE1/4 sec. 21, T. 28 N., R. 18 W.
GM-1027 -----	1,086	32.7	28.5	27.8	11	Porphyritic biotite granite of porphyritic monzogranite (Xpm)	NE1/4 sec. 16, T. 30 N., R. 18 W.
GM-1051 -----	1,425	33.6	28.6	35.1	2.7	Granite in gneiss (Xgn)	SE1/4 sec. 15, T. 29 N., R. 19 W.
GM-1063 -----	1,398	44.6	3.9	48.1	3.4	Undeformed garnet-bearing leucogranite dike cutting gneiss (Xgn)	NE1/4 sec. 3, T. 28 N., R. 16 W.
GM-1081 -----	1,602	27.2	32.8	36.8	3.1	Porphyritic granite from migmatite terrane (unit Xm)	SW1/4 sec. 33, T. 29 N., R. 17 W.

FELDSPATHIC GNEISS

Early Proterozoic feldspathic gneiss crops out in an approximately 5-km-long and 0.8-km-wide sliver bounded by faults in the southern part of the Lost Basin Range (fig. 2; unit fgn of Blacet, 1975). These faults include both deep-seated mylonitic structures and shallow-seated structures marked by gouge. Generally, the feldspathic gneiss is light gray to light pinkish gray, fine to medium grained, and has a compositionally homogeneous and strongly lineated fabric. The feldspathic gneiss contains few mafic schlieren and inclusions. Locally, foliation in the feldspathic gneiss is highly contorted, and near the northern margins of the sliver, the attitude of foliation gradually converges with the mylonitic rock that is present along its contact with the surrounding gneiss. The gneiss just west of the west boundary fault of the feldspathic gneiss contains abundant slickensides and short discontinuous shear zones, as well as iron oxide staining and increased abundances of chlorite.

The feldspathic gneiss is cut by quartz-feldspar veins, some of which are gold bearing, and sparse occurrences of syenitic aplite. Prospect pits and abandoned shafts and adits are especially abundant near the north end of the feldspathic gneiss. Generally, these workings follow copper (chalcopyrite, chrysocolla, malachite), lead (galena), and native gold shows along quartz plus yellow-brown carbonate veins. In places, the veins are about 0.5 m thick and attenuate downdip to stringers of about 1 to 2 cm thick. No indications of copper, lead, or gold mineralization were found to be associated with the syenitic aplite (P.M. Blacet, unpub. data, 1967-72), although the pits dug on some of the outcrops of syenitic aplite include quartz and orange-brown carbonate vein material and clear crystalline calcite.

BIOTITE MONZOGRANITE

Three bodies of equigranular to sparsely porphyritic Early Proterozoic biotite monzogranite are mapped in the Garnet Mountain quadrangle: (1) an approximately 1-km² west-trending mass near Rattlesnake Spring, which is about 5 km southeast of Garnet Mountain; (2) an approximately 0.1-km² body, about 2 km southwest of Rattlesnake Spring; and (3) a north-trending dikelike mass which has been traced discontinuously for about 4.5 km in the southern part of the Gold Basin district (fig. 2; unit qm of Blacet, 1975). The biotite monzogranite is in contact mostly with porphyritic monzogranite of Garnet Mountain. Age relations between the biotite monzogranite and porphyritic monzogranite of Garnet Mountain cannot be established conclusively because their contact typically is not exposed and can be located only within about 10 m. Nonetheless, the porphyritic monzogranite of Garnet Mountain near the contact is altered more than

the biotite monzogranite and also contains narrow discontinuous cataclastic or protoclastic zones. Near Rattlesnake Spring, however, the biotite monzogranite is associated spatially with moderately abundant rose quartz-bearing pegmatite and other pegmatite. Some similar pegmatites are present definitely as inclusions in the adjoining porphyritic monzogranite of Garnet Mountain (P.M. Blacet, unpub. data, 1967-72), relations from which we infer that the biotite monzogranite may be older than the porphyritic monzogranite of Garnet Mountain. In addition, the biotite monzogranite is intruded by small numbers of diabase dikes, some of which also include leucocratic differentiates.

The biotite monzogranite, which crops out in the southern part of the Gold Basin district, is a rather homogeneous light-gray body and shows only minor variations in overall composition and in igneous fabric. The biotite monzogranite is mostly a fine-grained rock, ranging typically between 0.5 and 1.0 mm in average grain size. Regardless, some facies of this rock in places become medium grained and contain euhedral potassium-feldspar phenocrysts as much as 8 cm in their long dimension and sparse quartz phenocrysts as much as 1.5 cm wide. Other rocks are foliated. Thin sections of six representative samples of fine-grained biotite quartz monzonite show predominantly equigranular hypidiomorphic-granular textures and minor porphyritic, seriate, and glomeroporphyritic textures. Modally, these rocks would plot in the compositional field of granite, using the classification of Streckeisen and others (1973). Some phenocrystic quartz, perhaps 1 to 2 percent by volume, is aggregated into approximately 2.5-mm-wide clots. Primary biotite (dark brown, Z axis) makes up typically about 5 to 10 volume percent and has been altered sparingly to chlorite with or without epidote. Plagioclase (mostly An₁₅₋₂₀) shows varying degrees of replacement by white mica and epidote. The intensity of replacement is highest adjacent to Cretaceous(?) episyenitic rocks which largely developed from the biotite monzogranite. Potassium feldspar, mostly microcline but including also some untwinned but perthitic varieties, is generally quite fresh. Minor accessories include apatite, sphene, and opaque minerals. Locally, pyrite is disseminated in the biotite monzogranite where it is intergrown with coarsely crystalline anhedral fluorite.

The biotite monzogranite, which crops out in the southern Gold Basin district, hosts numerous fluorite-bearing quartz-carbonate veins, some of which contain visible gold. In addition, this body of biotite monzogranite is also cut by several very small masses of Cretaceous(?) episyenite, one of which near the east edge of the biotite-quartz monzonite contains fluorite and disseminated gold (Blacet, 1969; see below).

Chemical data on three representative samples of biotite monzogranite from the Gold Basin district are presented

in table 13. The major-element analyses are generally similar to the average granite of Le Maitre (1976), also listed in table 13 for comparison. However, these three samples of biotite monzogranite are richer in K_2O than the average granite of Le Maitre (1976), and the samples are also lower in Na_2O . The average of total alkalis (sum of K_2O and Na_2O) in the three samples is 8.3 weight percent, which is close to the 7.75 value for total alkalis in the average granite of Le Maitre (1976). Minor elements in the three samples of biotite monzogranite are typical of those commonly associated with granitic rocks, with

TABLE 13.—Analytical data of Early Proterozoic biotite monzogranite

[Chemical analyses of 1 and 2 by rapid-rock methods; analysts, P.L.D. Elmore and S. Botts. Methods used are those described in Shapiro and Brannock (1962), supplemented by atomic absorption (Shapiro, 1967). Spectrographic analyses of 1 and 2 by Chris Heropoulos. Results are reported to the nearest number in the series 1, 0.7, 0.5, 0.3, 0.2, 0.15, 0.1, 0.07, and so forth, which represent approximate midpoints of interval data on a geometric scale. The precision of a reported value is approximately plus or minus one series interval at 68-percent confidence or two intervals at 95-percent confidence. Looked for but not found: Ag, As, Au, B, Bi, Cd, Mo, Ni, Pd, Pt, Sb, Sn, Te, U, W, Zn, Hf, In, Li, Re, Ta, Th, Ti, Pr, Sm, Eu. Chemical analysis of sample 3: major oxides by X-ray spectroscopy; J.S. Wahlberg, J. Taggart, and J. Baker, analysts; partial chemical analyses by standard methods; P.R. Klock and J. Rivielo, analysts. Spectrographic analyses of sample 3 by Judith Kent. Looked for but not found: Ag, As, Au, Bi, Cd, Sb, Sc, W, Ge, In, Re, Ti, and Hg; —, not detected; N.D., not determined]

Analysis -----	1	2	3	4
Sample -----	GM-19	GM-19c	79GM12	
Chemical analyses (weight percent)				
SiO ₂ -----	72.9	70.7	72.9	71.3
Al ₂ O ₃ -----	14	14	13.4	14.32
Fe ₂ O ₃ -----	1.4	2.1	2.15	1.21
FeO -----	1.4	2	1.05	1.64
MgO -----	.10	.40	.36	.71
CaO -----	1.2	2.4	.85	1.84
Na ₂ O -----	2.6	2.6	2.54	3.68
K ₂ O -----	5.6	5.5	6.08	4.07
H ₂ O ^a -----	.68	.74	.64	.64
H ₂ O -----	.04	.08	.06	.13
TiO ₂ -----	.35	.51	.31	.31
P ₂ O ₅ -----	.07	.14	.06	.12
MnO -----	.06	.06	.04	.05
CO ₂ -----	<.05	.05	.06	.05
F -----	.15	.45	.07	N.D.
Cl -----	N.D.	N.D.	.004	N.D.
S -----	N.D.	N.D.	.17	N.D.
Subtotal -----	100.6	101.7	100.74	100.07
Less O = F -----	.06	.19	.03	N.D.
Total -----	100.54	101.51	100.71	N.D.
Semiquantitative spectrographic analyses (weight percent)				
B -----	—	—	0.0007	N.D.
Ba -----	0.07	0.15	.026	N.D.
Be -----	.0003	.0003	.0007	N.D.
Co -----	—	.0005	.0003	N.D.
Cr -----	.0003	.0007	.0002	N.D.
Cu -----	.0001	.0003	.0002	N.D.
La -----	.02	.02	.024	N.D.
Mo -----	—	—	.0003	N.D.
Nb -----	.003	.003	.0054	N.D.
Pb -----	.007	.007	.0058	N.D.
Sc -----	.0005	.001	—	N.D.
Sn -----	—	—	.0008	N.D.
Sr -----	.015	.03	.0013	N.D.
V -----	.001	.002	.0015	N.D.
Y -----	.003	.007	.0036	N.D.
Zr -----	.02	.03	.002	N.D.
Zn -----	—	—	.02	N.D.
Ce -----	.05	.05	.047	N.D.
Ga -----	.002	.002	.0019	N.D.
Yb -----	.0003	.0007	.0003	N.D.
Nd -----	.015	.015	—	N.D.

some exceptions. The contents of fluorine in the biotite monzogranite appear to be atypically high, 0.07 to 0.45 weight percent (table 13). However, the bulk of the fluorine may have been introduced during the development of episyenite sometime during the Cretaceous (see section "Cretaceous Crystalline Rocks"). The estimates by Vinogradov (1962) and Turekian and Wedepohl (1961) for the abundance of minor elements in granitic rocks suggest low-calcium granites and felsic granites and granodiorites to contain 4.0 and 0.5 ppm cerium, respectively. The three samples of biotite monzogranite show cerium contents of 50 ppm (table 13). Thus, this body of biotite monzogranite may be more fractionated than the average granite.

LEUCOCRATIC MONZOGRANITE

The bulk of the Early Proterozoic leucocratic monzogranite (unit lqm of Blacet, 1975) crops out as discontinuous, lensoid masses across a 4-km-wide and 12-km-long belt that trends N. 20°–25° W. along the west front of Garnet Mountain (fig. 2). Two other very small exposures of leucocratic monzogranite crop out near the intersection of Grapevine Wash with the Grand Wash Cliffs at the east edge of the Garnet Mountain quadrangle.

TABLE 13.—Analytical data of Early Proterozoic biotite monzogranite—Continued

Analysis -----	1	2	3	4
Sample -----	GM-19	GM-19c	79GM12	
CIPW norms (weight percent)				
Q -----	33.7	29.7	32.8	29.06
C -----	2	1	1.5	.92
or -----	32.9	31.9	35.7	24.5
ab -----	21.9	21.6	21.4	31.13
an -----	4.4	7.4	3.0	8.04
en -----	.25	.98	.89	13.37
fs -----	.94	1.2	—	N.D.
mt -----	2	3	2	1.75
hm -----	—	—	.8	—
il -----	.66	.95	.59	.58
ap -----	.17	.33	.14	.28
fr -----	.29	.88	.13	N.D.
pr -----	—	—	.32	—
cc -----	—	.11	.14	.12
Total -----	99.2	99	99.4	99.75
Salic -----	94.9	91.6	94.4	93.65
Femic -----	4.3	7.4	5	6.1
² D.I. -----	88.5	83.3	89.9	84.24

¹Hypersthene.
²Differentiation index of Thornton and Tuttle (1960), defined as the total of normative quartz plus normative orthoclase plus normative albite.

1. Biotite monzogranite, fine grained, SE 1/4 sec. 27, T. 28 N., R. 18 W.
2. Biotite monzogranite, medium grained, slightly porphyritic; SE 1/4 sec. 27, T. 28 N., R. 18 W.
3. Biotite monzogranite, medium grained, SE 1/4 sec. 27, T. 28 N., R. 18 W.
4. Granite, average of 2,485 analyses, from LeMaitre (1976).

The leucocratic monzogranite probably has a total outcrop area of about 5 to 6 km² and normally is within the more widespread porphyritic monzogranite of Garnet Mountain. Contacts between leucocratic monzogranite and the porphyritic monzogranite of Garnet Mountain locally are quite sharp, but the transition between the two rock types can also be gradational across 8 to 10 cm or as much as 0.5 m. Further, the abundance of potassium feldspar phenocrysts increases in the leucocratic monzogranite nearest the porphyritic monzogranite. Although the actual contact between these two rocks may be highly irregular in detail at the scale of a single outcrop, the overall attitude of the contact maintains a generally northwest strike. In addition, the potassium feldspar phenocrysts, which are concentrated on the leucocratic monzogranite side of the contact with porphyritic monzogranite of Garnet Mountain, also are commonly oriented with their long dimensions trending northwesterly. Locally, where the contact between these rocks is well exposed, offshooting dikes of porphyritic monzogranite of Garnet Mountain definitely cut leucocratic monzogranite, and in places both rocks are cut in turn by fine-grained dikes of granite. On the other hand, some exposures of the contact between leucocratic monzogranite and porphyritic monzogranite of Garnet Mountain show complexly mixed flowage structures involving both rocks. These relations suggest that initial emplacement of the leucocratic monzogranite to the levels currently exposed was followed very closely by intrusion of the porphyritic monzogranite of Garnet Mountain—so closely that the leucocratic monzogranite in places probably was only partially crystalline. We infer that initial emplacement of the leucocratic monzogranite predates the biotite monzogranite.

In outcrop, the leucocratic monzogranite is typically a light-yellowish-gray rock, which most commonly is medium-grained hypidiomorphic granular in overall texture. Compositionally, these rocks are granite and generally are nonporphyritic although they can grade into slightly porphyritic micropegmatitic varieties. Partly chloritized dark-red-brown (Z axis) biotite makes up less than 5 volume percent of the equigranular varieties. In addition, very fine granules of opaque mineral(s) are concentrated in chlorite which replaces the earlier primary biotite, whereas granules of primary opaque mineral(s) (probably magnetite mostly) are relatively sparse and somewhat coarser grained than the secondary opaque mineral(s). Plagioclase (An₁₅₋₂₅) makes up 30 to 40 volume percent of the rocks and is moderately clouded by a dense intergrowth of clay mineral(s), white mica, and sparse epidote. Potassium feldspar is relatively fresh and contains patches of microcline twinning, which is concentrated usually in the cores of the potassium feldspar crystals. The potassium feldspar also includes irregularly developed bead perthite. Myrmekite is developed

sparsely along potassium feldspar-plagioclase grain boundaries. Primary quartz makes up about 20 to 25 volume percent of the leucocratic monzogranite and in some samples the primary quartz hosts relatively abundant and conspicuous fluid inclusions. These fluid inclusions are concentrated along secondary and pseudo-secondary annealed microfractures through the primary quartz. At room temperature, the fluid-inclusion population consists of a two-phase liquid-rich type, a three-phase type containing liquid carbon dioxide, and a third type which contains from one to three nonopaque daughter minerals. One of these daughter minerals is undoubtedly halite and another is probably sylvite. The third daughter mineral is highly birefringent and shows equant to rod-shaped habits. Heating and freezing tests were not performed on these samples from the leucocratic monzogranite. However, the relative proportions of the daughter minerals in many of the inclusions suggest that highly saline carbon dioxide-rich fluids containing as much as 60 weight percent NaCl equivalent at some time must have circulated through some of the leucocratic monzogranite.

The leucocratic monzogranite contains locally some narrow 1- to 2-m-wide zones of very well foliated gneissic rock of nearly the same composition as the nonfoliated equigranular leucocratic monzogranite. These zones crop out near contacts between leucocratic monzogranite and porphyritic monzogranite of Garnet Mountain and have attitudes that parallel closely the attitude of the contact between the two rocks. The foliation is defined principally by (1) a preferred concentration of stubby crystals of dark-brown (Z axis) biotite into highly discontinuous 0.2-mm-wide lepidoblastic domains and by (2) a preferred dimensional orientation of highly strained ribboned quartz. The extreme freshness of these zones (the biotite is not chloritized, and the plagioclase is not clouded) suggests that they may have been generated protoclastically.

Pegmatite in the leucocratic monzogranite previously has been prospected for sheet mica, as exemplified by the M.P. Mica mine, which is in the SE¹/₄ sec. 26, T. 28 N., R. 17 W. (table 11, see locs. 138, 139). At several places in the general area of the M.P. Mica mine, muscovite books are present in approximately N. 10° W.-striking discontinuous pegmatite dikes and lenses. These dikes and lenses range from 2 to 5 m in width. The pegmatite shows well-developed quartz cores and includes some sparse concentrations of red-brown garnet near its margins with the leucocratic monzogranite.

PORPHYRITIC MONZOGANITE OF GARNET MOUNTAIN

The porphyritic monzogranite of Garnet Mountain (unit pqm of Blacet, 1975) crops out in three main areas in the districts: (1) east of Hualapai Valley and east of Grapevine

Mesa, near the Grand Wash Cliffs, (2) near the northwest corner of the area, in the White Hills, and (3) in the southern White Hills near the southwest corner of the area where it hosts several of the gold-bearing quartz veins (fig. 2). The largest exposed body of the porphyritic monzogranite crops out east of Hualapai Valley, nearly centered on Garnet Mountain itself. Here the porphyritic monzogranite is the principal rock unit exposed in an area of about 60 km². Several northwest-striking dikes and irregularly shaped small bodies of diabase intrude the porphyritic monzogranite in this general area. About 4 km east of Garnet Mountain, the porphyritic monzogranite is overlain unconformably by the Cambrian Tapeats Sandstone, and at Iron Mountain, about 5 km northeast of Garnet Mountain, the porphyritic monzogranite and the diabase are capped unconformably by flat-lying rocks including the Tapeats Sandstone, Tertiary gravel, and Tertiary basalt. From Garnet Mountain, the porphyritic monzogranite can be traced to the north fairly continuously cropping out in progressively smaller areas east of Grapevine Mesa and in the low hills leading to the Grand Wash Cliffs. Near the northwest corner of the area, the porphyritic monzogranite crops out in three irregularly shaped bodies which total approximately 5 km² in area. Finglomeratic sequences of the Tertiary Muddy Creek Formation, the upper Miocene Hualapai Limestone Member of the Muddy Creek Formation, Tertiary ancestral Colorado River deposits (not delineated separately on fig. 2), and various types of Quaternary unconsolidated deposits all rest unconformably on some part of these three bodies of porphyritic monzogranite. As mapped in the southern White Hills, the porphyritic monzogranite crops out in an approximately triangular area of about 10 km². Its maximum inferred dimension at the surface is about 6 km in an approximately N. 40° E. direction.

The age of emplacement of the porphyritic monzogranite was established by Wasserburg and Lanphere (1965) to be about 1,660 Ma using the potassium-argon and rubidium-strontium techniques. Samples of porphyritic monzogranite and pegmatite were obtained by them from several localities in the SW¹/₄ sec. 27, T. 28 N., R. 16 W., near the Boyd Tenney Ranch in the Quartermaster Canyon SW 7¹/₂-minute quadrangle. These localities are approximately 3.2 km north-northeast of the southeast corner of the Garnet Mountain quadrangle, and from them, the porphyritic monzogranite can be traced continuously to Garnet Mountain itself. Hornblende from a sample of porphyritic monzogranite, described by Wasserburg and Lanphere (1965, p. 746) as "coarse-grained biotite-hornblende quartz monzonite characterized by abundant microcline phenocrysts," yielded a K-Ar age of 1,630 Ma. The initial ⁸⁷Sr/⁸⁶Sr ratio for the porphyritic monzogranite is 0.702. Abundant dikes of pegmatite cut the porphyritic monzogranite and the metamorphic rocks, which include garnet-biotite-potassium feldspar gneiss and diopside-hornblende gneiss, at these

localities. Comprehensive analytical results on various minerals from these pegmatites plot on a well-defined isochron of 1,660 Ma showing an initial ⁸⁷Sr/⁸⁶Sr ratio equal to 0.704 (Wasserburg and Lanphere, 1965). Apparently, plutonism here forms part of a northeast-trending magmatic arc that ranges in age from 1,610 to 1,700 Ma (Silver and others, 1977). Such plutonism in the districts occurred well within a broad Proterozoic province of 1,720- to 1,800-Ma apparently supracrustal rock and may reflect magmatism associated with the accretion of another 1,650- to 1,720-Ma terrane outboard to the southeast (Condie, 1982).

Large, abundant, conspicuous potassium feldspar phenocrysts are the most characteristic feature of the porphyritic monzogranite of Garnet Mountain. The phenocrysts are typically pinkish gray to pale pinkish cream and are set in a light-pinkish-gray, coarse-grained, hypidiomorphic-granular groundmass. Many exposures of porphyritic monzogranite show tabular phenocrysts as long as 10 cm. Textures elsewhere in the porphyritic monzogranite are predominantly subporphyritic seriate, and such rocks show an almost continual gradation in size of euhedral potassium feldspar phenocrysts from about 1.5 cm to 10 cm in their long dimension (fig. 25A). In addition, some of the potassium feldspar phenocrysts show evidence of partial rounding. Generally in the porphyritic monzogranite, near its contact with the leucocratic monzogranite, tablets of phenocrystic potassium feldspar show a well-developed preferred orientation. Where oriented, the phenocrysts are aligned with their long axes parallel to the general strike of the contact. In addition, the phenocrysts are subparallel to dimensionally oriented schlieren and inclusions of leucocratic monzogranite. However, the border zone of the porphyritic monzogranite is not everywhere typified by aligned phenocrysts of potassium feldspar. Locally, in the Gold Basin district this border zone between porphyritic monzogranite and gneiss is marked by a conspicuous display of randomly oriented blocks of included biotite-rich and garnet-bearing schist and gneiss. Nonetheless, the contact between gneiss and porphyritic monzogranite is conformable generally with the trend of foliation in the gneiss as exemplified by relations in sec. 29, T. 28 N., R. 18 W. Yet on a scale of a large outcrop, the contact between porphyritic monzogranite and gneiss cuts the schistosity in the gneiss at a high angle, and there is no evidence for shearing along the contact. In places, the contact can be located to within about 1 cm. Elsewhere in the Gold Basin district, the porphyritic monzogranite becomes very distinctly porphyritic as its contact with the surrounding schist and gneiss is approached. In such border areas, the porphyritic monzogranite includes both euhedral and ovoid phenocrysts that may be mantled by plagioclase. However, such rapakivi textures are not restricted exclusively to widespread exposures of the porphyritic monzogranite. In the Gold Basin mining district (fig. 2), the porphyritic monzogranite

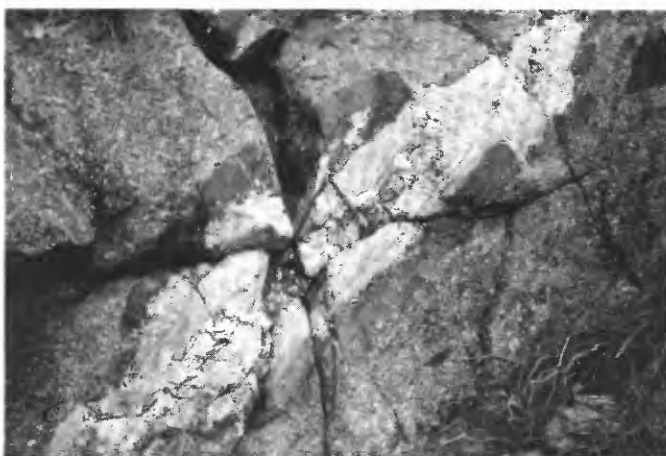
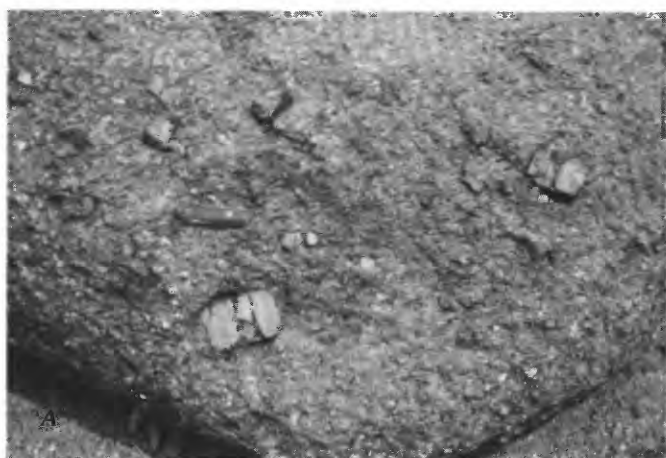
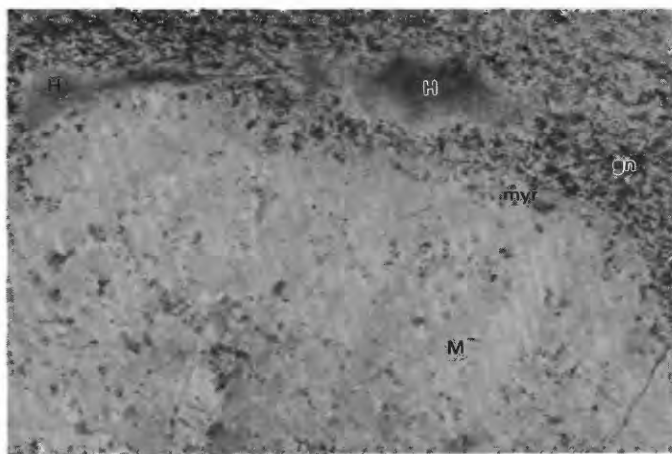


FIGURE 25.—Porphyritic monzogranite of Garnet Mountain. *A*, Large microcline phenocrysts in somewhat seriate-textured, porphyritic monzogranite in southern White Hills; NW $\frac{1}{4}$ sec. 34, T. 28 N., R. 18 W. *B*, Microcline mantled by rims of myrmekite (note relations at head of arrow) in rapakivi dikelike mass that cuts pendant of mostly biotite gneiss within porphyritic monzogranite in southern White Hills. Feldspars crystallized largely in matrix of gneiss. (See fig. 26*A*, *B* for larger scale view of microcline-myrmekite relations.) Scale is 18 cm long. *C*, Pegmatite-cored pod as inclusion in porphyritic monzogranite in SW $\frac{1}{4}$ sec. 20, T. 28 N., R. 16 W. Note rock hammer in center of photograph for scale.

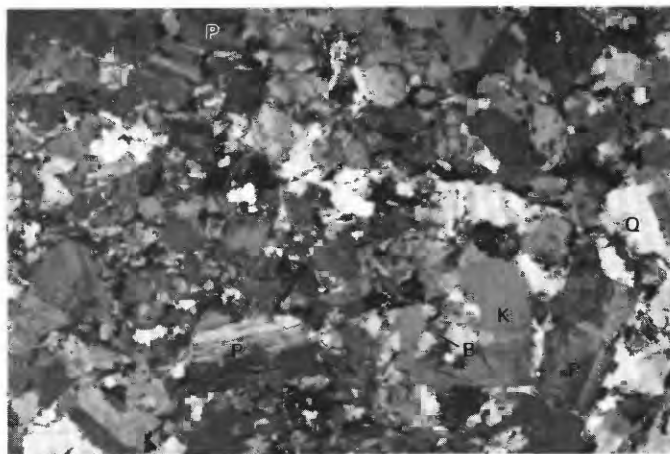
also includes some irregularly shaped areas approximately 0.1 to 0.2 km² in size, too small to show on the map, which consist of mixtures of porphyritic monzogranite and gneiss. In some exposures within these areas, large crystals apparently of completely mantled microcline are very common (fig. 25*B*) and define irregularly bounded dikelike masses of rock that have a matrix of mostly biotite-epidote gneiss. In addition, these areas of mixed rock, which undoubtedly are very close to a local roof of the porphyritic monzogranite, also contain quartz-cored, graphic-granite pegmatite, probably associated genetically with the porphyritic monzogranite. However, relatively deep seated parts of the porphyritic monzogranite in the general area of Garnet Mountain also contain pegmatite. Some of this pegmatite is earlier than porphyritic monzogranite, owing to the presence of pegmatite as pods totally engulfed by subsequently crystallized porphyritic monzogranite (fig. 25*C*).

In thin section, the large porphyroblastic crystals of mantled potassium feldspar are seen to consist of twinned microcline, which is mantled by approximately 0.2- to 2.0-mm-wide rims of oligoclase-dominant myrmekite (fig. 26*A*). The rims of these microcline porphyroblasts also host some crystals of albite. In places, optically continuous microcline extends through the rims and is in contact with the biotite-epidote gneiss. Further, such microcline also engulfs very small fragments of biotite-epidote gneiss and shows no development of a rim of myrmekite between the fragment and the microcline. Although myrmekite and rapakivi textures are difficult to interpret (see Smith, 1974), textural relations in these samples (fig. 26*A*, *B*) suggest that the mantles are a postmicrocline phenomenon and thus possibly reflect a simultaneous coupling of (1) calcium migration toward the microcline and (2) subsolidus exsolution of sodium-rich plagioclase.

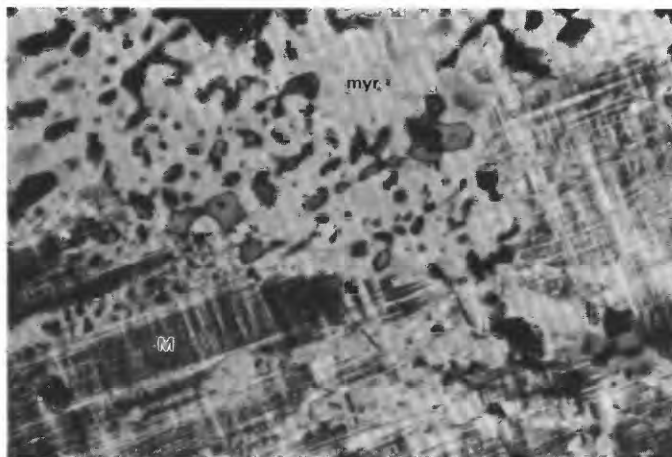
In thin section, the porphyritic monzogranite of Garnet Mountain shows an extremely varied fabric (fig. 26*C-F*). Although most of the groundmass of fresh porphyritic monzogranite is hypidiomorphic granular, even the least deformed hornblende-biotite porphyritic facies (fig. 26*C*) and biotite equigranular facies (fig. 26*D*) of this unit show minor amounts of postcrystalline strain exemplified by mildly bent biotite cleavage lamellae and by undulose quartz. Nonetheless, plagioclase, generally in the range An₃₅ to An₄₀, in much of the porphyritic monzogranite is quite fresh, showing only slight alteration to white mica. Some plagioclase is zoned normally and includes rims as sodic as oligoclase, An₂₀₋₂₅. In addition, hornblende, typically blue green (*Z* axis), and biotite are remarkably fresh locally, especially in the porphyritic monzogranite cropping out in the general area of Garnet Mountain. Although the most conspicuous potassium feldspar in these rocks is perthitic microcline, the range in size of these crystals is quite wide. The size of perthitic microcline in the groundmass of much of the porphyritic monzogranite seems to decrease with decreasing abundance of



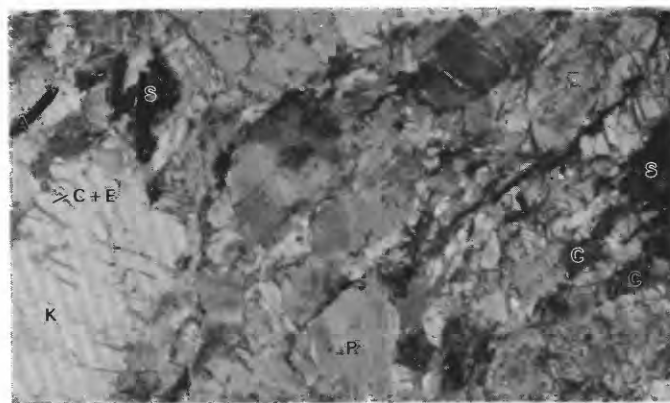
A 0 12 MILLIMETERS



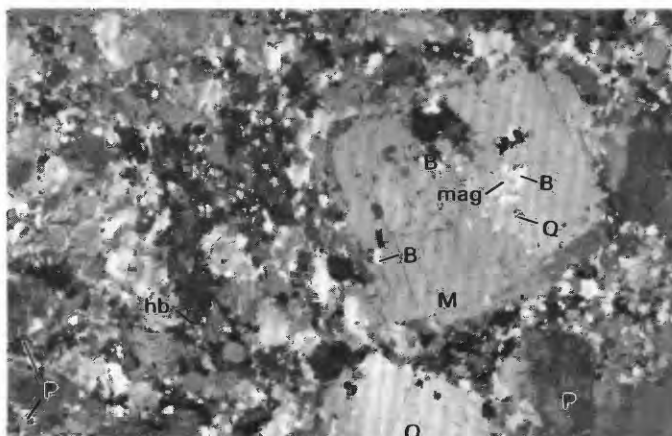
D 0 7 MILLIMETERS



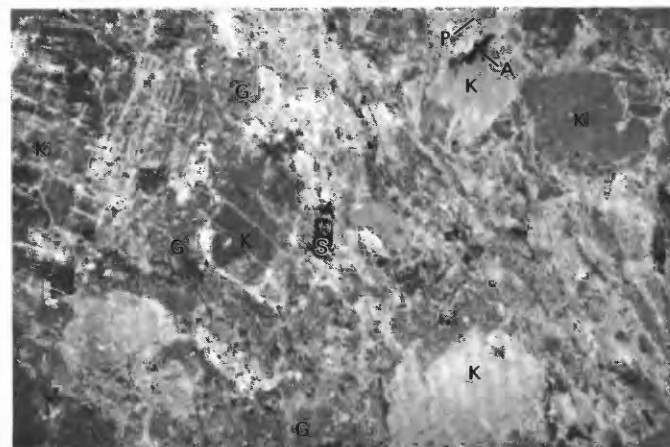
B 0 0.1 MILLIMETER



E 0 8 MILLIMETERS



C 0 12 MILLIMETERS



F 0 8 MILLIMETERS

microcline in the rock. Accessory minerals in the porphyritic monzogranite include zircon, apatite, allanite, sphene, and various opaque minerals. Pyrite and rutile are very minor accessory minerals that are present sporadically in the porphyritic monzogranite.

Although the exposed levels of the porphyritic monzogranite of Garnet Mountain were not deformed syntectonically with the early upper-amphibolite-facies metamorphism of the area, some of the porphyritic monzogranite has been deformed intensely during the retrograde greenschist event. Porphyritic monzogranite, for example, which crops out about 1 km north of Iron Mountain, shows an intensely crushed and chlorite-rich metamorphic overprint (fig. 26*E, F*). The intense deformation of these greenish-gray rocks is indicated by their bent kink-banded plagioclase (oligoclase-andesine, about An_{30}) and the replacement of all primary biotite by chlorite and secondary sphene. These folia in turn show neocrystallization of even later minute undeformed porphyroblasts of greenish biotite, which have grown with their {001} cleavage lamella traces at high angles to the foliation defined by chlorite. Large crystals of primary sphene in the rocks are broken, veined, and altered to leucoxene.

FIGURE 26.—Textural relations in gneiss immediately adjacent to porphyritic monzogranite and in porphyritic monzogranite itself. Crossed nicols. *A*, Microcline (M) mantled by myrmekite (myr), showing porphyroblastic development in matrix of biotite-epidote gneiss (gn). From pendant engulfed by porphyritic monzogranite in southern White Hills. H, hole in thin section. Sample GM-813. *B*, Myrmekite microveining microcline (M) across and along twin planes in microcline. Sample GM-813. *C*, Porphyritic monzogranite showing only slight evidence of deformation, including bent biotite crystals and a slight ribbing and undulation of quartz (Q). Plagioclase (P) is andesine (An_{40}) and partly altered to white mica. Mafic minerals are clustered tightly into mostly hornblende-biotite aggregates (hb). Optically unzoned microcline phenocrysts (M) include flakes of biotite (B) and possibly titaniferous magnetite (mag). Sample GM-50, same as analysis 6, table 14. *D*, Equigranular biotite monzogranite facies of porphyritic monzogranite. K, perthitic microcline; P, plagioclase (An_{35}). Includes accessory allanite, sphene, magnetite, apatite, zircon, and sparse secondary white mica. Sample GM-70, same as analysis 7, table 14. *E*, Porphyritic monzogranite deformed during greenschist metamorphism of area. Plagioclase (P) is partly altered to epidote and white mica. All primary biotite is partly altered to epidote and white mica and is replaced by chlorite (C). Perthitic potassium feldspar (K) is microveined by chlorite and epidote (C+E) and by other veins showing quartz-chlorite-white mica-epidote assemblages. Large crystals of sphene (S) are broken, veined, and altered partly to leucoxene. Accessory minerals in rock include relatively large crystals of allanite (A). Sample GM-29 from approximately 1 km north of Iron Mountain. *F*, Intensely deformed porphyritic monzogranite. Crosshatch-twinned potassium feldspar (K) is veined by white mica, epidote, and quartz. Epidote-rich groundmass (G) also contains chlorite, white mica, and quartz. Fairly large crystals of sphene (S) are altered heavily to leucoxene and are veined by chlorite, quartz, epidote (trace), and white mica. Sparse plagioclase (P) in rock is altered partly to white mica. Allanite (A) is accessory. Sample GM-29a, locality same as *E*.

The large crystals, as long as 2 cm, of perthitic potassium feldspar are brecciated, are cut by microveinlets of quartz, epidote, chlorite, and white mica, and are replaced by patches of deformation-related albite.

As revealed by petrographic studies, the modal compositions of unmetamorphosed porphyritic monzogranite range from monzogranite to granodiorite (fig. 24). Most of these modally analyzed samples, however, plot in the compositional field of monzogranite; only two of the samples plot in the field of granodiorite, very close to the field of monzogranite. The color index of the porphyritic monzogranite ranges from about 5 to about 24 (tables 12, 14).

Modal content of potassium feldspar in the samples of porphyritic monzogranite is among the highest of the Early Proterozoic igneous rocks in the districts (fig. 24). This relation may be interpreted to be the result of differentiation. Projection of this trendline toward the quartz-plagioclase sideline suggests differentiation away from a region close to the plagioclase corner of the ternary diagram. In addition, most of the analyzed samples of Early Proterozoic leucogranite plot near the potassium feldspar-rich domain of the trendline, whereas samples of gneissic granodiorite plot near the plagioclase-rich parts of the trendline. However, these modes may not be accurate because of the relatively large size of the potassium feldspar phenocrysts. Also, many phenocrysts may have crystallized initially from a magma that was different from that represented by the matrix of the rocks (see Wilcox, 1979).

Chemical analyses of eight rock samples from the porphyritic monzogranite of Garnet Mountain suggest that the rocks are chemically quite uniform (table 14). These analyses include a sample from a medium-grained mafic pod (table 14, analysis 4) hosted by the porphyritic monzogranite. Contents of SiO_2 in the eight samples are between 64.4 and 71.9 weight percent and average 69.5 weight percent. The K_2O contents range from 3.3 to 6.1 weight percent, and the Na_2O contents are remarkably consistent, ranging from 2.5 to 2.9 weight percent. The ratio of K_2O to Na_2O ranges from 1.3 to 2.4; the content of K_2O is lowest (table 14, 3.3 weight percent, analysis 6) in the sample containing the most CaO (4.0 weight percent). This sample (table 14, analysis 6) includes significant amounts of hornblende, and the analysis shows the highest ferrous- to ferric-iron ratio determined and the lowest content of SiO_2 . Relatively mafic phases of the porphyritic monzogranite, exemplified by analysis 8 (table 14), which is of a rock determined to have a color index of 18, only differ slightly from leucocratic phases (table 14, analysis 2, color index 4.7). These differences consist primarily of less SiO_2 and K_2O , but more total Fe, CaO, and TiO_2 . Much of the increased content of TiO_2 reflects probably an increase in the amount of sphene in the rock.

TABLE 14.—Analytical data from the Early Proterozoic porphyritic monzogranite of Garnet Mountain

[Chemical analyses by rapid-rock methods; analysts, P.L.D. Elmore and S. Botts. Methods used are those described in Shapiro and Brannock (1962), supplemented by atomic absorption (Shapiro, 1967). Spectrographic analyses by Chris Heropoulos. Results are reported to the nearest number in the series 1, 0.7, 0.5, 0.3, 0.2, 0.15, 0.1, 0.07, and so forth, which represent approximate midpoints of interval data on a geometric scale. The precision of a reported value is approximately plus or minus one series interval at 68-percent confidence or two intervals at 95-percent confidence. Looked for but not found: Ag, As, Au, B, Bi, Cd, Mo, Ni, Pd, Pt, Sb, Sn, Te, U, W, Zn, Hf, In, Li, Re, Ta, Th, Tl, Pr, Sm, Eu. —, not detected; N.D., not determined]

Analysis ----- Sample -----	1 GM-34	2 GM-553	3 GM-562	4 GM-566	5 GM-573	6 GM-50	7 GM-70	8 GM-120	9	10	11
Chemical analyses (weight percent)											
SiO ₂ -----	71.6	71.9	69.8	69.4	70.8	64.4	70.4	67.7	69.5	71.30	72.2
Al ₂ O ₃ -----	14.1	14.3	13.8	14.2	13.8	15.4	14.6	14.3	14.3	14.32	13.8
Fe ₂ O ₃ -----	1.4	1.7	2.3	2.4	1.2	2	1.6	2.1	1.8	1.21	1.9
FeO -----	2.2	1.2	2.1	2.4	2.3	4.7	3.3	3.5	2.7	1.64	1.5
MgO -----	.60	.40	.80	.80	.50	1.2	1.1	.80	.78	.71	.29
CaO -----	1.9	1	2.2	2.6	1.5	4	2.5	3	2.3	1.84	1.5
Na ₂ O -----	2.5	2.5	2.8	2.8	2.9	2.6	2.5	2.8	2.7	3.68	2.6
K ₂ O -----	5.2	6.1	4.9	4.6	5	4	3.3	4.2	4.7	4.07	5.7
H ₂ O ⁺ -----	.84	1.4	1	1	1	.70	.77	.66	.92	.64	.69
H ₂ O -----	.06	.04	.7	.02	.04	.03	.06	.04	.05	.13	.06
TiO ₂ -----	.60	.39	.62	.74	.52	1.3	.74	.95	.73	.31	.39
P ₂ O ₅ -----	.23	.17	.28	.30	.24	.50	.15	.36	.28	.12	.09
MnO -----	.00	.00	.09	.08	.03	.09	.00	.09	.05	.05	.05
CO ₂ -----	.08	.15	.11	<.05	<.05	.05	.06	.15	.10	.05	.06
F -----	.12	.06	.14	.13	.17	N.D.	N.D.	N.D.	.12	N.D.	.22
Subtotal -----	101.43	101.31	101.01	101.47	100	100.97	101.08	100.65	101.03	100.07	101.05
Less O = F -----	.05	.03	.06	.05	.07	N.D.	N.D.	N.D.	.05	N.D.	.13
Total -----	101.38	101.28	100.95	101.42	99.93	100.97	101.08	100.65	100.98	100.07	100.92
Semiquantitative spectrographic analyses (weight percent)											
Ba -----	0.15	0.1	0.2	0.15	0.1	0.2	0.15	0.2	N.D.	N.D.	N.D.
Be -----	.00015	--	.0002	.0002	.0003	.0002	.00015	.0002	N.D.	N.D.	N.D.
Co -----	.0005	.0003	.0007	.0007	.0005	.001	.0007	.001	N.D.	N.D.	N.D.
Cr -----	.0007	.0005	.0007	.0007	.0005	.001	.003	.001	N.D.	N.D.	N.D.
Cu -----	.0003	.00015	.0007	.001	.0005	.001	.0015	.0015	N.D.	N.D.	N.D.
La -----	.015	.015	.005	.02	.015	.007	.02	.01	N.D.	N.D.	N.D.
Nb -----	.0015	.0015	.002	.003	.002	.003	.002	.002	N.D.	N.D.	N.D.
Ni -----	--	.0002	--	.0002	--	.0005	.001	.0003	N.D.	N.D.	N.D.
Pb -----	.003	.007	.002	.002	.005	.0015	.003	.002	N.D.	N.D.	N.D.
Sc -----	.001	.0005	.0015	.001	.001	.003	.0015	.002	N.D.	N.D.	N.D.
Sr -----	.05	.02	.03	.03	.02	.07	.03	.05	N.D.	N.D.	N.D.
V -----	.003	.002	.005	.005	.003	.005	.003	.005	N.D.	N.D.	N.D.
Y -----	.005	.003	.007	.015	.005	.007	.002	.007	N.D.	N.D.	N.D.
Zr -----	.02	.02	.05	.03	.03	.03	.03	.03	N.D.	N.D.	N.D.
Ce -----	.03	.03	.015	.05	.03	.03	.03	.02	N.D.	N.D.	N.D.
Ga -----	.002	.003	.002	.002	.002	.003	.002	.002	N.D.	N.D.	N.D.
Yb -----	.0005	.0002	.0005	.0015	.0005	.001	.0001	.0007	N.D.	N.D.	N.D.
Nd -----	.01	.015	.01	.02	.015	.015	.015	.015	N.D.	N.D.	N.D.
CIPW norms (weight percent)											
Q -----	32.1	31.8	29.5	28.9	30.9	22.7	34.9	27.5	N.D.	29.06	N.D.
C -----	1.9	2.6	1.1	.87	1.9	.83	2.8	.90	N.D.	.92	N.D.
or -----	30.3	35.6	28.7	26.8	29.6	23.4	19.3	24.7	N.D.	24.5	N.D.
ab -----	20.9	20.9	23.5	23.4	24.5	21.8	20.9	23.5	N.D.	31.13	N.D.
an -----	6.6	2.5	7.5	10	4.8	16.1	10.9	11.5	N.D.	8.04	N.D.
en -----	1.5	.98	2	2	1.2	3	2.7	2	N.D.	1.37	N.D.
fs -----	1.9	.15	1.1	1.3	2.4	5	3.4	3.3	N.D.	N.D.	N.D.
mt -----	2	2.4	3.3	3.4	1.7	2.9	2.3	3	N.D.	1.75	N.D.
il -----	1.1	.73	1.2	1.4	.99	2.4	1.4	1.8	N.D.	.58	N.D.
ap -----	.54	.40	.66	.70	.57	1.2	.35	.85	N.D.	.28	N.D.
fr -----	.20	.09	.23	.21	.31	--	--	--	N.D.	N.D.	N.D.
cc -----	.18	.34	.25	--	--	.11	.14	.34	N.D.	.12	N.D.
Total -----	99.1	98.5	98.9	98.9	98.9	99.3	99.2	99.3	N.D.	99.75	N.D.
Salic -----	91.7	93.4	90.3	89.9	91.6	84.8	88.9	88.1	N.D.	93.65	N.D.
Femic -----	7.4	5.1	8.6	9.	7.3	14.5	10.3	11.2	N.D.	6.1	N.D.
² D.I. -----	83.3	88.3	81.7	79	85	67.9	75.1	75.7	N.D.	84.24	N.D.
Modes (volume percent)											
Quartz -----	34.8	27.8	N.D.	N.D.	30.7	N.D.	N.D.	31.0	N.D.	N.D.	N.D.
Potassium feldspar -----	27.6	39.2	N.D.	N.D.	29.9	N.D.	N.D.	17.7	N.D.	N.D.	N.D.
Plagioclase -----	25.7	28.3	N.D.	N.D.	24.3	N.D.	N.D.	33.3	N.D.	N.D.	N.D.
Mafic minerals -----	12	4.7	N.D.	N.D.	15	N.D.	N.D.	18	N.D.	N.D.	N.D.

¹Hypersthene.

²Differentiation index of Thornton and Tuttle (1960), defined as the total of normative quartz plus normative orthoclase plus normative albite.

1. Porphyritic monzogranite; NW1/4 sec. 16, T. 28 N., R. 16 W.
2. Porphyritic monzogranite, fine-grained border facies.
3. Porphyritic monzogranite, biotite-rich mafic facies.
4. Medium-grained mafic pod in porphyritic monzogranite.
5. Porphyritic monzogranite.
6. Porphyritic monzogranite, hornblende bearing; SE1/4 sec. 12, T. 28 N., R. 17 W.
7. Porphyritic monzogranite; SE1/4 sec. 19, T. 28 N., R. 16 W.
8. Porphyritic monzogranite, in mixed granodioritic complex; NW1/4 sec. 26, T. 28 N., R. 17 W.
9. Average porphyritic monzogranite, from analyses 1-8 of this table, excluding detected values below limits of determination.
10. Granite, average of 2,485 analyses, from LeMaitre (1976).
11. Average biotite monzogranite (from table 13, this report).

Five of the samples of porphyritic monzogranite were analyzed for fluorine; the average content of fluorine is 0.12 weight percent (table 14). Also, a slight correlation may exist between the cerium contents of these samples and their differentiation indices (fig. 27). Generally the analyses of porphyritic monzogranite are very like the average granite of Le Maitre (1976), listed in table 14 as analysis 10 for comparison. Similarly, the analyses of porphyritic monzogranite are not much different from the analyses of biotite monzogranite (table 13), the average of which is also listed in table 14 (analysis 11). The "degree of alkalinity" of this suite of rocks from the porphyritic monzogranite and biotite monzogranite, as indicated using the alkali-lime index of Peacock (1931), is calc-alkalic (fig. 28).

The limited number of available analyses of the porphyritic monzogranite preclude our establishing well-documented variation trends. In the AlkFM diagram (fig. 29A), the trend appears to be away from a region near the F corner to a point along the AlkF sideline, approximately one-third of the distance from the Alk corner. However, the two analyzed samples of biotite monzogranite, which apparently is older than the porphyritic monzogranite, plot near the terminus of such a variation trend. The ACF diagram (fig. 29B) also shows a poorly developed variation trend projected toward the A corner of the diagram. The AKF diagram (fig. 29C) shows more scatter than the two preceding diagrams and suggests a variation trend projected away from the midpoint of the

AK sideline. Figure 29D shows normative proportions of quartz, orthoclase, and albite in the analyzed samples from the porphyritic monzogranite and the biotite monzogranite. All these samples contain greater than 80 percent Ab + Or + An + Q; and all but one of the analyses (table 14, analysis 6—a hornblende-rich facies of the porphyritic monzogranite) contain greater than 75 percent Ab + Or + Q. The An contents of all analyzed samples of porphyritic monzogranite and biotite monzogranite, normalized to 100 percent Q + Or + Ab + An, range from 2.8 to 19.2 percent. However, if analysis 6 (table 14) is excluded, the range is 2.8 to 13.2 percent, and the average value of the normalized An contents is 8.2 percent. The normative proportions of quartz, orthoclase, and albite in all but one of the analyzed rocks cluster tightly in an area showing either an increased K_2O/Na_2O ratio relative to a trendline connecting the ternary minimum at $P_{H_2O} = P_{total} = 100$ MPa for contents of An varying from 3 to 7.5, or decreased ratios of $Q/(Ab + Or)$ relative to these minimums (fig. 29D). However, this cluster of normative proportions of quartz, orthoclase, and albite coincides with, and apparently is elongate along, the ternary minimum for $P_{H_2O} = P_{total} = 2,000$ kg/cm² projected onto the anhydrous base of the Ab-Or-Q-H₂O tetrahedron determined by Tuttle and Bowen (1958). The plot of these data from the porphyritic monzogranite and biotite monzogranite thus suggests that the rocks are highly differentiated and that they may have crystallized from a magma at $P_{H_2O} = P_{total} =$ about 200 MPa, assuming that (1) the samples analyzed reflect minimum melt compositions (see above, and Anderson and Cullers, 1978) and (2) the magma(s) was saturated with respect to H₂O (Steiner and others, 1975). The abundance of aplite dikes and pegmatites associated with the porphyritic monzogranite and biotite monzogranite suggests their magma(s) was saturated with respect to H₂O (see Luth, 1969), at least during the final stages of their primary crystallization.

Analytical data based on the chemical composition of the Early Proterozoic porphyritic monzogranite of Garnet Mountain and Early Proterozoic biotite monzogranite in the districts appear to have the characteristics ascribed by Petro and others (1979) to continental magmatic arcs generated at compressional plate boundaries. This relation is especially true when the data from the districts are compared with that for the central Sierra Nevada batholith. The data from table 14 include (1) a nearly unimodal distribution of differentiation indices (total range 67.9 to 88.3), (2) unimodal distributions of normative anorthite (average 28 weight percent), and (3) a calc/alkali index, which is defined as the value of SiO₂ for which $CaO/(Na_2O + K_2O)$ equals 1.00 (Christiansen and Lipman, 1972), greater than 60 (actually 60.5 from fig. 28). The alkali-lime index of Peacock (1931) for the central Sierra Nevada batholith is 60 (Kistler, 1974). Further,

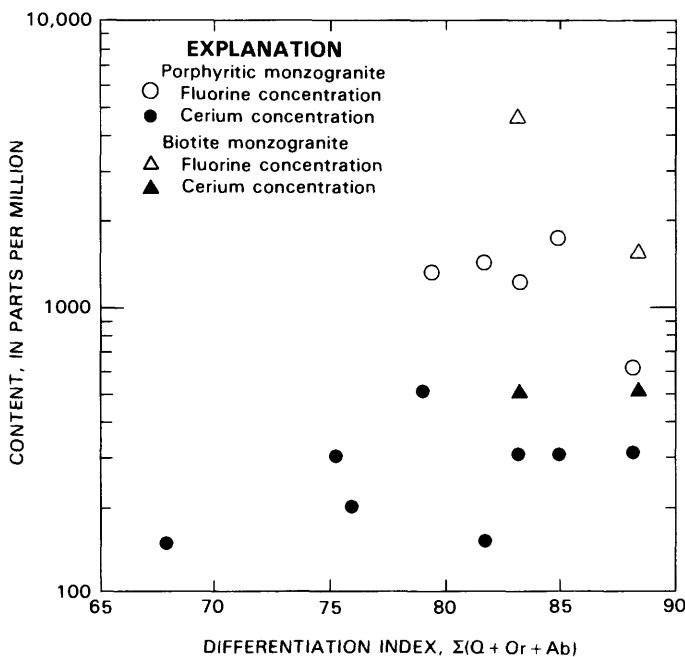


FIGURE 27.—Fluorine and cerium contents versus differentiation index, $\Sigma(Q + Or + Ab)$, of analyzed samples of Early Proterozoic porphyritic monzogranite of Garnet Mountain and Early Proterozoic biotite monzogranite.

the high K_2O/Na_2O ratios and the high ratio of $(FeO + Fe_2O_3)/MgO$ in these rocks from the Gold Basin-Lost Basin districts suggest the rocks have continental rather than island-arc affinities (see Jakes and White, 1972). If these analytical data were to be interpreted using the $K-h$ (K_2O versus depth to the top of a seismic zone) techniques of Dickinson and Hatherton (1967), Hatherton and Dickinson (1969), and Dickinson (1975), a plot of percent K_2O at a projected 57.5 percent SiO_2 for these data would show that the depth inferred to the top of an inclined seismic zone would be anywhere from 160 to 270 km. Such values result from the data for continental margin arcs as modified from Dickinson (1975) by Keith (1978). However, the average dip of seismic zones or subducted slabs associated with compressional continental margins is perhaps 40° (Dickinson, 1975, p. 56). In addition to the possibility of variably dipping seismic zones (Coney and Reynolds, 1977; Keith, 1978), a significant unknown in the region is the position of the paleotrench approximately 1,660 Ma (see Condie, 1982). Further, Wyllie (1981) notes that the composition of magma becomes depleted in SiO_2

with increasing depth and that high- SiO_2 granitic magmas cannot be generated by anatexis of crustal rocks at depths greater than about 30 km, and Glazner (1983) points out several additional problems in relations derived between slab dip and convergence rates.

The porphyritic monzogranite of Garnet Mountain, which crops out in the southern White Hills of the Gold Basin district, hosts several gold-bearing quartz veins. The bulk of these veins strike north-northeast and nearly parallel the trend of the mapped bodies of gneissic granodiorite and the biotite monzogranite, which crop out north and east, respectively, of the main mass of porphyritic monzogranite (fig. 2). However, a few gold-bearing quartz veins in the porphyritic monzogranite have northwesterly strikes. One of these veins crops out about 1.5 km south-southeast of the Malco mine. Another consists of the swarm of veins that made up the deposit at the Cyclopic mine. At the Cyclopic mine, one of the earliest discoveries and the largest overall producer of lode gold in the districts (see above), the ore is found in a northwest-striking zone of gold-bearing, brecciated

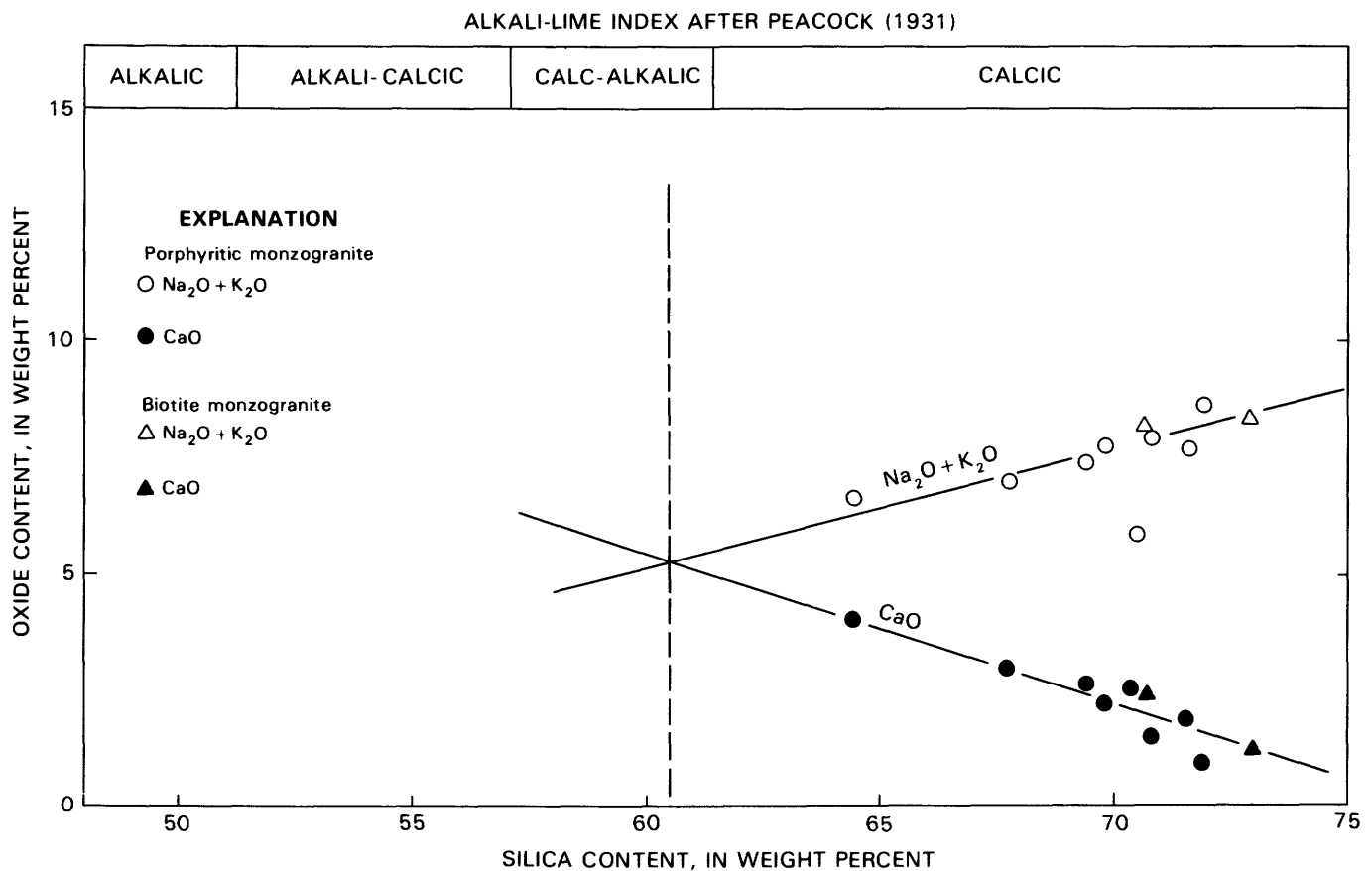


FIGURE 28.—Total alkalis (Na_2O plus K_2O) and CaO plotted against SiO_2 for analyzed samples of Early Proterozoic porphyritic monzogranite and Early Proterozoic biotite monzogranite in general area of Gold Basin-Lost Basin districts. Solid lines, visually estimated regression lines through $Na_2O + K_2O$ and CaO data points used to establish an estimated silica content of 60.5 for the igneous suite at the point where $Na_2O + K_2O$ equals CaO. Thus, the suite is calc-alkalic (dashed line) after Peacock (1931).

quartz veins, most of which probably were emplaced tectonically near a contact between porphyritic monzogranite and metamorphic rocks older than the porphyritic monzogranite. The dips of these veins are mostly to the northeast and range from shallow angles (15° to 25°) to steep (60° to 70°) (P.M. Blacet, unpub. data, 1967-72). The bulk of the ore at the Cyclopic mine consisted of quartz-vein material and not the unconsolidated gouge associated with the major Tertiary detachment fault which cuts the porphyritic monzogranite in the general area of the Cyclopic mine (see below). Some minor amounts of gold mineralization may be associated with localized intense ferric and

argillic alteration along the detachment fault (Myers and Smith, 1984). This Tertiary fault dips gently to the southwest. Crushed and brecciated porphyritic monzogranite crops out extensively near the Cyclopic mine, and locally the porphyritic monzogranite is highly stained by iron oxides. The porphyritic monzogranite near here is also sericitized and even strongly silicified in those areas where it is flooded by numerous veins and veinlets. The unconsolidated gouge, which reflects movements along the Tertiary fault, also locally includes several large blocks of vein quartz. In addition, striations and tectonic polish are present on many blocks of porphyritic monzogranite and

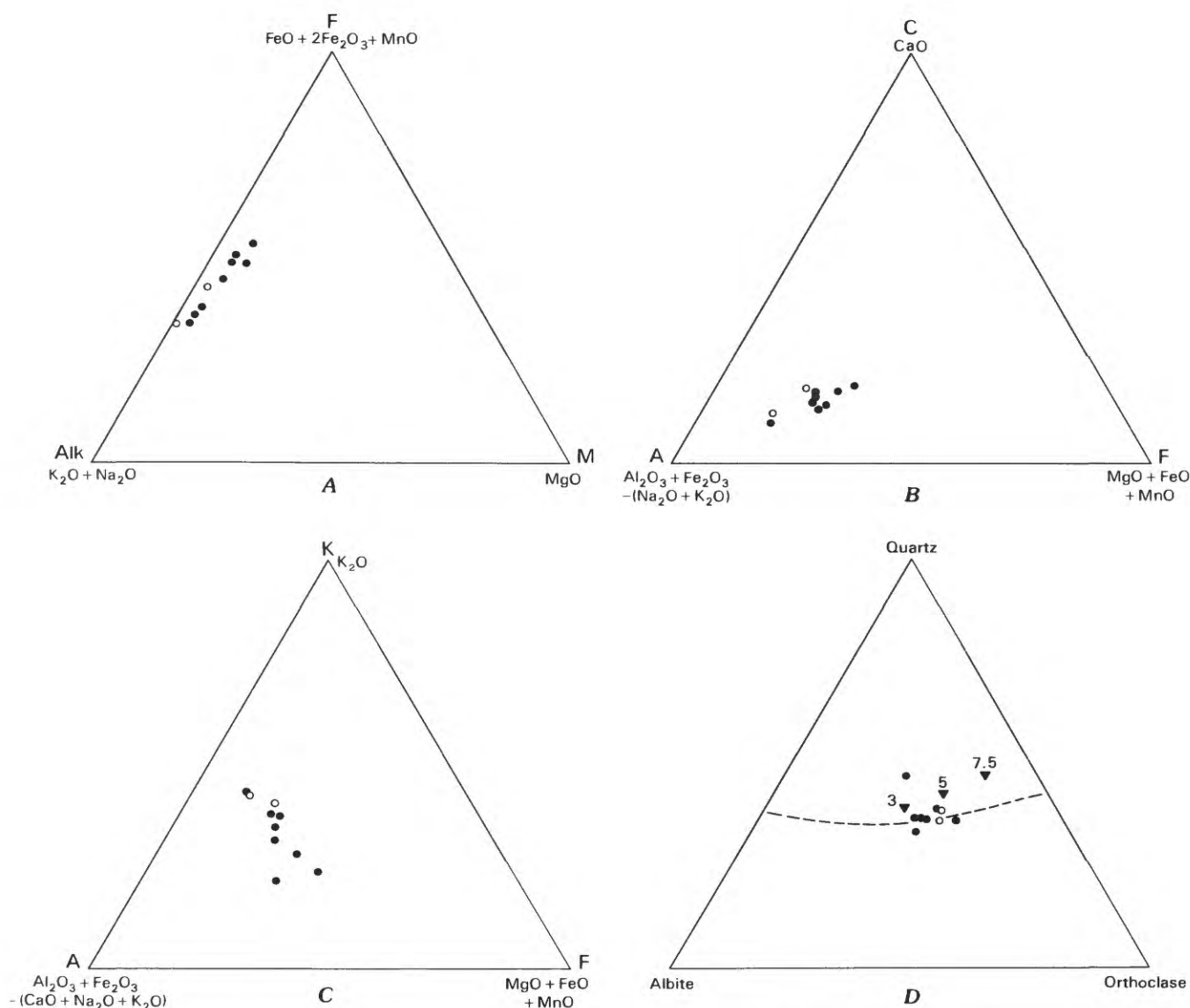


FIGURE 29.—Ternary chemical and normative diagrams of analyzed Early Proterozoic porphyritic monzogranite (dots) and biotite monzogranite (circles) from general area of Gold Basin-Lost Basin mining districts. Data from tables 13 and 14. A, AlkFM diagram. B, ACF diagram. C, AKF diagram. D, Normative proportions of albite, ortho-

clase, and quartz. Triangles, ternary minimum from James and Hamilton (1969) at designated weight percent An for $P_{total} = P_{H_2O} = 1,000$ bars. Dashed line, locus of ternary minimum temperatures projected onto anhydrous base of Ab-Or-Q-H₂O tetrahedron for $P_{H_2O} = P_{total} = 2,000$ kg/cm² from Tuttle and Bowen (1958).

vein quartz in the fault zone, thus documenting the age of the bulk of the mineralization at the Cyclopic mine as predating movement(s) along the Tertiary fault.

GRANODIORITE

Gray granodiorite (unit *gd* of Blacet, 1975) crops out along the western and southwestern flanks of Garnet Mountain as a mafic border facies of the porphyritic monzogranite of Garnet Mountain (fig. 2). The granodiorite is present both as rather homogeneous discrete bodies and in a unit termed by Blacet (1975) "a mixed granodioritic complex" which includes mostly granodiorite and lesser amounts of porphyritic granodiorite and porphyritic monzogranite. All of these rocks are approximately coeval and comagmatic with one another. Contacts between granodiorite and porphyritic monzogranite are gradational. However, the mixed granodioritic complex also includes some of the leucocratic monzogranite, which is definitely older than the granodiorite as indicated by crosscutting relations. Locally, the granodiorite is coarse grained and sparsely porphyritic, with perhaps 20 phenocrysts of potassium feldspar scattered across an exposure of about 0.1 m². Mostly, these phenocrysts are set in a coarse-grained, hornblende-biotite hypidiomorphic-granular matrix that is rich in magnetite. Magnetite clots as much as 1.5 cm wide are quite common in the granodiorite, and magnetite-rich sands are very characteristic of present-day arroyo bottoms that drain areas underlain by outcrops of granodiorite.

In thin section, samples of the granodiorite are seen to consist of somewhat varying proportions of biotite, hornblende, quartz, plagioclase, and potassium feldspar, and the minor accessory minerals magnetite, apatite, and zircon. Plagioclase is more abundant than potassium feldspar. The major overall texture of some of the medium-grained facies of this unit is hypidiomorphic granular, yet subporphyritic, seriate, and slightly gneissic fabrics are present locally. Fabric of a representative sample of medium-grained granodiorite is shown in figure 30A. The color index of the granodiorite ranges from about 10 to about 25 and probably averages about 20. Plagioclase in the equigranular varieties of the granodiorite probably has an anorthite percentage of about 30 to 35, whereas early crystallized plagioclase, which is included within some 2- to 3-cm-wide equant and euhedral phenocrysts of potassium feldspar, has anorthite percentages of about 40. In addition, plagioclase in the granodiorite generally is sparsely altered to white mica. Nevertheless, parts of some crystals of plagioclase are almost completely replaced by sheathlike aggregates of white mica and clay mineral(s), with or without traces of clinozoisite and carbonate. Blue-green (Z axis) hornblende ranges from 0 to perhaps 15 volume percent of the granodiorite. In those

facies of the granodiorite that include both hornblende and biotite, the biotite is red-brown (Z axis), whereas the hornblende-free facies show biotites that are dark brown (Z axis). Mafic minerals tend to form clusters in the granodiorite, which in places contain very abundant concentrations of apatite (fig. 30B). Some samples of granodiorite show sparse concentrations of 4- to 5-mm-wide ovoid aggregates of highly strained, polycrystalline quartz, possibly reflecting incorporation of some material from the gneiss.

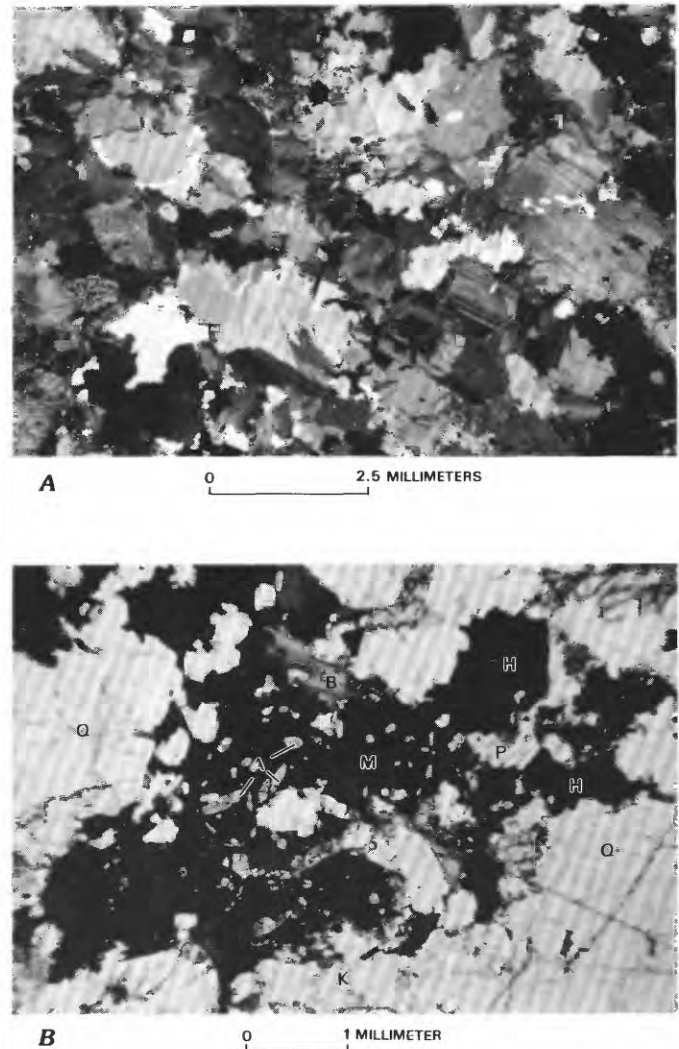


FIGURE 30.—Textural relations in Early Proterozoic granodiorite border phase of the porphyritic monzogranite of Garnet Mountain. Sample GM-1131, SE¼ sec. 25, T. 28 N., R. 17 W. A, Overall fabric of a representative sample of granodiorite. Crossed nicols. B, Textural relations among apatite-rich portions of predominantly mafic-mineral domains of granodiorite. P, plagioclase; A, apatite; Q, quartz, K, potassium feldspar; B, biotite; H, hornblende; M, magnetite. Plane-polarized light.

Fluid inclusions are abundant in some of the primary quartz crystals. Isolated, approximately 6- to 10- μ m-long fluid inclusions are concentrated in subhedral to ovoid crystals of quartz hosted by essentially unaltered phenocrysts of potassium feldspar. Some of these fluid inclusions are rich in carbon dioxide because at room temperature they show the presence of three phases composed mainly of liquid water, liquid carbon dioxide, and carbon dioxide vapor. The proportion of liquid carbon dioxide to carbon dioxide vapor is very high, perhaps two or three to one, which suggests a high trapping pressure at the time of the circulation of these carbon dioxide-rich fluids. Such carbon dioxide-rich fluids are apparently not associated with any gold mineralization in the general area of Garnet Mountain. Nonetheless, we will document in the section "Fluid-Inclusion Studies" that fluids related to gold mineralization, of both the disseminated and vein variety, contained appreciable amounts of carbon dioxide in the districts.

DIABASE

Relatively small masses of fine-grained diabase (unit db of Blacet, 1975) crop out sporadically in the Early Proterozoic metamorphic and igneous terranes (fig. 2). The most extensive exposures are southeast of the Lost Basin district, about 2 km east of Garnet Mountain where an approximately 2- to 3-km-long, northwest-striking dike of diabase cuts porphyritic monzogranite of Garnet Mountain. The bulk of the diabase in and near the districts is undeformed and is found in thin planar dikes that crosscut both the igneous fabric of 1,660-Ma rock and all structural features in complexly folded metamorphic and migmatitic rocks. In addition, about 4 km north-northeast of the southeast corner of the Garnet Mountain quadrangle, an approximately 10-m-thick diabase, dipping about 15° NW., is truncated unconformably by Cambrian Tapeats Sandstone (P.M. Blacet, unpub. data, 1967-72). This diabase shows excellently developed chilled margins against porphyritic monzogranite. We presume all this undeformed diabase described above to be Middle Proterozoic in age, correlative with the diabase of Sierra Ancha, Ariz., first dated by Silver (1960) to have a minimum age of $1,075 \pm 50$ Ma and a probable age of 1,200 Ma or greater, and then further refined by Silver (1963) as having an original age of $1,150 \pm 30$ Ma. Nonetheless, some metadiabase in the Early Proterozoic terrane of the districts is apparently older than 1,150 Ma. Such metadiabase has a superposed metamorphic fabric, is cut sharply by narrow granitic pegmatite, and also very probably is cut by coarse-grained, slightly porphyritic, rapakivi-textured granite.

In thin section, undeformed diabase shows typical diabasic textures. Subophitic texture is dominant in the

chilled margins where normally zoned laths of labradorite (generally An₅₅ to An₆₀) are about 0.3 to 0.35 mm long and are set in a very fine grained matrix of granules of opaque mineral(s) and clinopyroxene. The lower chilled margins of some sills of undeformed diabase also contain rare, discontinuous, wispy, hairline microveinlets of blue-green (Z axis) hornblende and red-brown (C axis) biotite. Ophitic texture is dominant in domains of the diabase interior to the chilled margins. Grain size increases to about 0.8 mm about 2 m from the chilled margins, plagioclase is somewhat more sodic, and sporadic crystals of red-brown (Z axis) biotite form part of the igneous fabric of the diabase. Nonpleochroic pale-grayish-brown clinopyroxene crystals are coalesced into more or less equant plates enclosing the stout laths of plagioclase. Finally, about 6 m from the chilled margins, some of the freshest samples of undeformed diabase show concentrations of olivine reaching as much as 10 volume percent. A chemical analysis of a sample of diabase collected from the main drift of the Golden Gate mine is included in table 7.

CRETACEOUS CRYSTALLINE ROCKS

TWO-MICA MONZOGANITE

Cretaceous two-mica monzogranite, dated at 72.0 Ma in this report by E.H. McKee using the K-Ar method, crops out north-northwest of the Cyclopic mine (fig. 2). This body of rock crops out mostly in the Senator Mountain quadrangle, where Blacet (unpub. data, 1967-72) shows it to have a maximum inferred surface dimension of about 4.0 km across the trace of the lowermost strand of the low-angle detachment surface. As shown (fig. 2), the largest exposed body of two-mica monzogranite has been faulted against fanglomerate of the Muddy Creek Formation. Further, the two-mica monzogranite in the districts is part of a regionally extensive inner-cordilleran belt of muscovite-bearing granitic rocks defined by Miller and Bradfish (1980; fig. 31). In many areas, the granitic rocks are associated spatially with middle Mesozoic to early Tertiary metamorphic rocks that have been referred to as the eastern cordilleran metamorphic belt by Miller (1980) and Haxel and others (1984; compare figs. 1 and 31). The two-mica monzogranite in the Gold Basin mining district belongs to a late Cretaceous-early Tertiary igneous rock series empirically linked by Keith (1984, 1986) to a widespread stratotectonic assemblage of rocks termed the Wilderness assemblage. S.B. Keith has further subdivided the igneous rocks associated with the Wilderness assemblage into a Gold Basin facies and a Sweetwater facies. However, in marked contrast to many of the two-mica granitic rocks along this belt, the two-mica monzogranite in the Gold Basin district does not

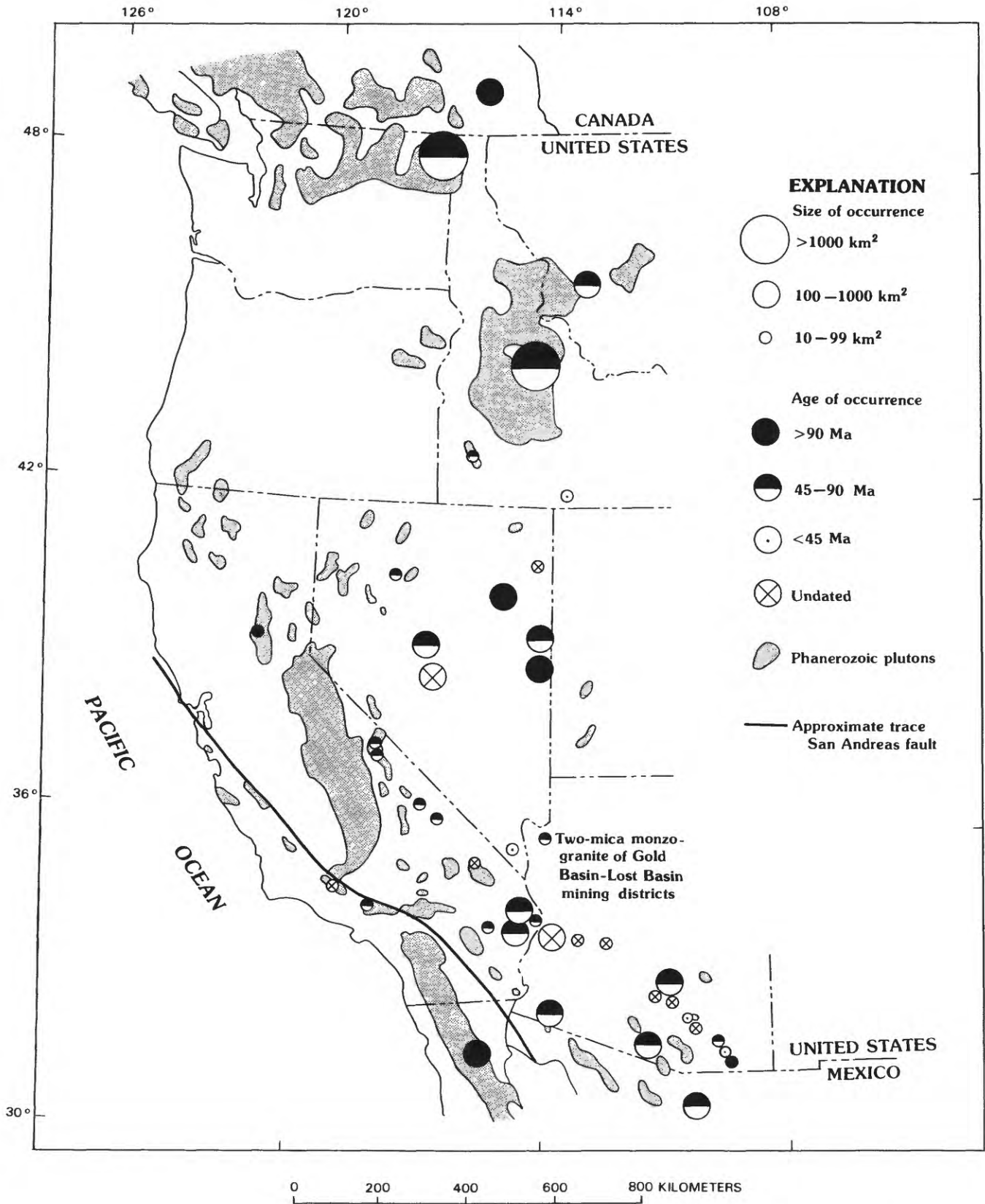


FIGURE 31.—Occurrences of Phanerozoic muscovite-bearing plutonic rocks in the Western United States (modified from Miller and Bradfish, 1980).

exhibit pervasive cataclastic or mylonitic fabrics. The two-mica monzogranite, which is fine to medium grained, shows locally sharp contacts with surrounding amphibolitic gneiss. In the vicinity of these contacts, the grain size of the two-mica monzogranite does not progressively decrease, the overall abundance of mafic minerals does not increase, and inclusions of wall rock are absent. The two-mica monzogranite generally has an equigranular fabric, and overall its area of outcrop is remarkably homogeneous lithologically, showing a strong affinity to the compositionally restricted granite series of Pitcher (1979). In some localities, however, the two-mica monzogranite is porphyritic or slightly foliated. The porphyritic variants contain as much as 5 percent quartz phenocrysts that reach sizes of about 5 cm wide. The foliated aspect is imparted by a weakly defined primary layering of dimensionally oriented potassium feldspar and biotite, probably reflecting a flow fabric. Within the main body of the two-mica monzogranite, locally sharp contacts are present between a fine-grained, sparsely porphyritic biotite monzogranite facies and a muscovite-biotite monzogranite facies. Close examination of these relations suggests that this muscovite-rich facies of the monzogranite is not a metasomatic replacement of biotite-rich monzogranite.

The two-mica monzogranite contains some syenitic zones. This syenitic rock probably reflects subsolidus episyenitization or fenitization, judging from the associated enrichments in muscovite, fluorite, and potassium feldspar and depletion of primary quartz adjacent to local swarms of quartz-, pyrite-, and muscovite-bearing veins. In places, such veins also include some carbonate and fluorite and appear genetically related to the two-mica monzogranite, because the veins cut the two-mica monzogranite and are in places cut by the two-mica monzogranite. Sparse concentrations of chalcopyrite and specular hematite also were noted by Blacet (unpub. data, 1967-72) to be associated with some of the veins which cut the two-mica monzogranite.

Veins and irregular quartz segregations also appear to be concentrated in gneiss in the general vicinity of the two-mica monzogranite. The irregular quartz segregations are associated spatially with aplite and muscovite-bearing pegmatite, an association giving the appearance that the quartz segregations are also related genetically to the two-mica monzogranite.

The two-mica monzogranite shows fairly clear-cut contact relations with two other lithologies. The two-mica monzogranite is cut by some unmapped Tertiary dikes, one of which is shown in figure 32. Most such dikes are partly chloritized, porphyritic biotite dacite, probably related to the Mount Davis Volcanics. On the southwest, the largest body of two-mica monzogranite (fig. 2) is in fault contact with Tertiary(?) fanglomeratic rock of the

Muddy Creek Formation. Crude striae are developed on the topmost surfaces of unweathered two-mica monzogranite where it was excavated by Blacet (unpub. data, 1967-72) along the trace of the fault. The trend of these striae is approximately N. 60° W. Further, immediately above the poorly striated pavement of two-mica monzogranite, a highly comminuted 10- to 15-cm-thick zone of red sandy-clay gouge contains clasts less than 1 cm in diameter. P.M. Blacet traced this low-angle fault to the southeast where it crops out in the immediate area of the Cyclopic mine and to other nearby areas where it juxtaposes Tertiary(?) fanglomerate and Early Proterozoic porphyritic monzogranite of Garnet Mountain (fig. 2).

Examinations of 10 thin sections of the Cretaceous two-mica monzogranite reveal a wide range of textures and compositions. Modal compositions of nine samples range from a biotite-free felsic muscovite granodiorite to muscovite-biotite monzogranite (fig. 33). The samples of



FIGURE 32.—Tertiary (?) composite, partly chloritized, porphyritic biotite dacite dike containing a septum of Late Cretaceous two-mica monzogranite. Note rock hammer in central part of photograph for scale.

muscovite granodiorite are typified by approximately 2.0-mm grain sizes and well-developed hypidiomorphic-granular textures. The muscovite granodiorite includes as much as 47 percent by volume euhedral, tabular crystals of normally zoned plagioclase (oligoclase, An_{15-20}). The plagioclase typically is extremely fresh and shows only sparse dusting by minute crystals of white mica. Some samples, however, show crystallization of 0.2- to 0.4-mm-long books of white mica demonstrably subsequent to crystallization of plagioclase. Biotite in the more common two-mica monzogranite facies of this body of rock is generally dark brown (Z axis), showing slight tints of green under the microscope, and is present in very wide ranging proportions (from 0 to about 10 percent by volume). Quartz is also highly varied in the two-mica monzogranite, both texturally and modally. Rare quartz bipyramids were noted in some rocks, but more commonly the quartz is present in 2- to 3-mm-wide ovoid aggregates of polycrystalline quartz. Such quartz generally is interstitial to plagioclase and potassium feldspar. Potassium feldspar, making up 25 to 35 volume percent of the rocks studied, is extremely fresh and shows the well-developed crosshatch twinning of microcline. Some potassium feldspar crystals poikilitically include numerous oriented crystals of oligoclase (fig. 34A). Minor accessory minerals include zircon, opaque minerals (both equant and prismatic varieties), rutile (in places clustered in books of white mica, and elsewhere as needles in quartz), and rare garnet. Some extremely sparse relatively large crystals of apatite show euhedral 0.8-mm-wide basal sections containing euhedral laths of biotite.

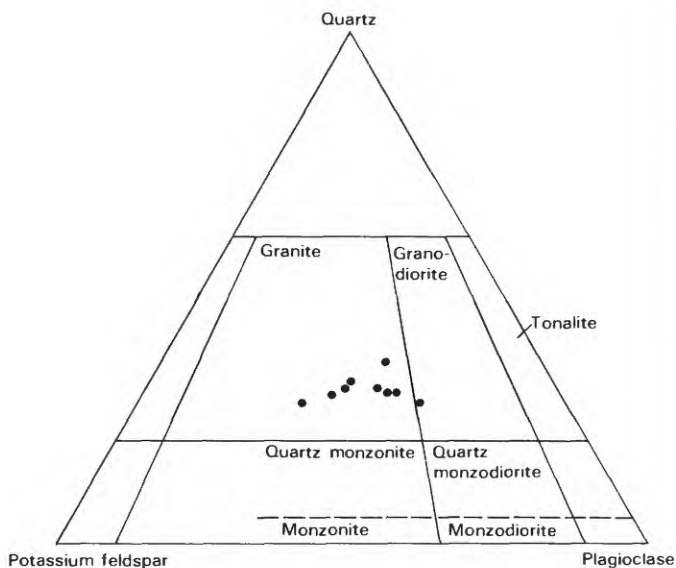


FIGURE 33.—Modes of Late Cretaceous two-mica monzogranite in Gold Basin mining district. Compositional fields from Streckeisen and others (1973).

Muscovite in the two-mica monzogranite is present in many textural associations with various light and dark minerals. In this report, we use the term “muscovite” to describe relatively coarse white micas, generally subhedral to euhedral, that are terminated sharply and cleanly against primary biotite, primary plagioclase, and (or) primary potassium feldspar. Such muscovites show no secondary replacement textures relative to these three minerals that commonly are the same size as the muscovite. Most likely, however, the muscovite in the two-mica monzogranite is far from ideal and probably contains a significant celadonite $[K(Mg, Fe^{2+})_2Si_4O_{10}(OH)_2]$ component (see Davis and others, 1979; Anderson and Rowley, 1981; C.F. Miller, E.F. Stoddard, L.J. Bradfish, and W.A. Dollase, unpub. data, 1981). Some coarse-grained white mica in the two-mica monzogranite obviously formed after the plagioclase and crystallized largely as an open-space filling of a mostly plagioclase supported network or framework (fig. 34B). In this association, {001} lamella traces commonly impinge the euhedral crystal boundaries of the earlier crystallized plagioclase at high angles. Furthermore, alteration of the plagioclase, where it is in contact with the white mica, is not seen. In another relation, stout books of white mica about 0.5 to 1.0 mm wide show sharp contacts with dark-greenish-brown (Z axis) biotite, and again, at high magnifications, the biotite adjacent to the white mica (fig. 34C) does not appear to be bleached. Some coarse plates of white mica are totally engulfed by larger books of unaltered biotite measuring approximately 2.0 to 3.0 mm in length, relations which are not diagnostic as to relative ages of crystallization between white mica and biotite. Some rocks, however, show obvious primary crystals of biotite cut by similar-sized crystals of white mica, which in turn is rarely cut by somewhat finer grained crystals of biotite (fig. 34D). Shredded wormy intergrowths of very fine grained white mica preferentially concentrated at and along the edges of medium-grained plates of white mica must reflect crystallization during the circulation of postmagmatic hydrothermal fluids in the rocks. Such intergrowths of fine-grained white mica also locally replace some primary biotite in the two-mica monzogranite. Where this is present, the adjoining biotite is bleached and partly altered to chlorite. Throughout the two-mica monzogranite, the coarse books of white mica appear to be the preferred nucleation sites for the definitely secondary hydrothermal-related white mica.

Chemical analyses of seven samples from the Cretaceous two-mica monzogranite are given in table 15. Five of the samples show a striking chemical homogeneity; the two exceptions (table 15, analyses 5, 7) are from, respectively, an episyenite zone within the two-mica monzogranite and a two-mica monzogranite partly altered by nearby quartz-fluorite-white mica veins. The five un-

altered samples of the two-mica monzogranite show SiO₂ contents that range from 70.9 to 71.9 weight percent, Al₂O₃ contents that range from 14.9 to 15.5 weight percent, and total alkalis (K₂O plus Na₂O) that range from 8.03 to 8.96 weight percent. The mean ratio of Na₂O to K₂O in weight percent is 1.00 for the five samples. A plot showing the ratio of Al₂O₃:(K₂O + Na₂O + CaO) in molecular percent versus SiO₂ in weight percent for the analyzed samples of the two-mica monzogranite reveals the extent of alumina saturation in these rocks (fig. 35). For comparative purposes, we show also on this figure a field for selected Late Cretaceous to Eocene two-mica

granitoids from elsewhere within the cordillera, compiled by Keith and Reynolds (1980). The two samples of altered two-mica monzogranite (fig. 35, analyses 5, 7) plot significantly away from the field of two-mica granitoids, whereas the samples of unaltered two-mica monzogranite compare favorably with the field.

The two-mica monzogranite from the Gold Basin district is peraluminous. Five samples of unaltered monzogranite show values for Al₂O₃:(K₂O + Na₂O + CaO) in molecular percent that range from 1.09 to 1.21 (fig. 35). Although four of these five values of Al₂O₃:(K₂O + Na₂O + CaO) plot in the strongly peraluminous field (>1.10), two-mica

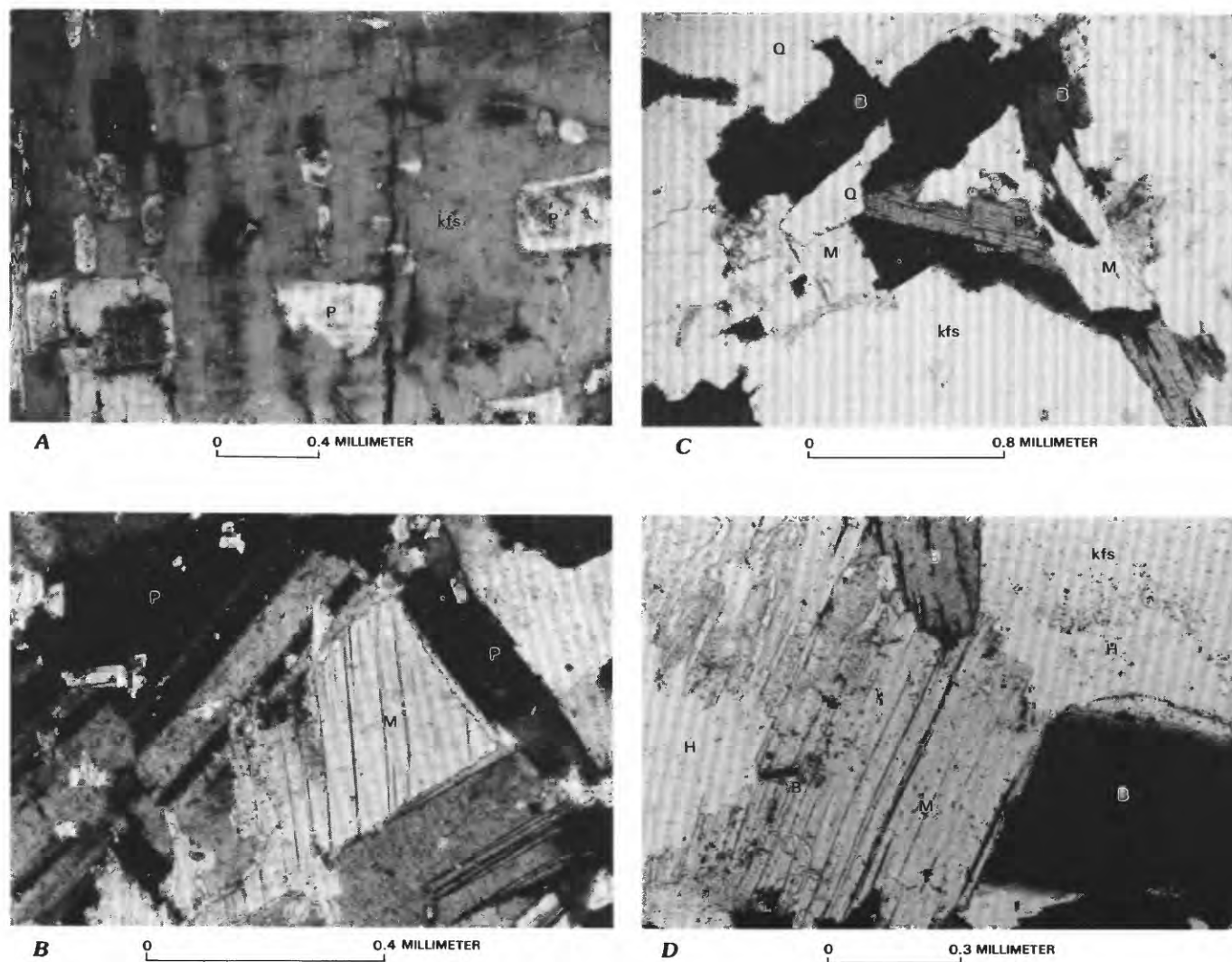


FIGURE 34.—Textural relations in Late Cretaceous two-mica monzogranite. *A*, Subhedral crystals of oscillatory-zoned, perthitic potassium feldspar (kfs) showing inclusion of numerous, small, oriented, euhedral to subhedral crystals of partly sericitized oligoclase (An₁₅₋₂₀). In addition, crystal of included primary biotite (B) shows marginal development of secondary white mica (M). Sample GM-1090a. *B*, Coarsely crystalline white mica (M) filling interstices among framework-

supported network of euhedral plagioclase (P). Sample GM-917c. *C*, Knife-edge contact between muscovite (M) and biotite (B) showing no alteration effects in either mineral. Q, quartz; kfs, potassium feldspar. Sample GM-1089. *D*, Biotite (B) cut by muscovite (M) that has in turn been cut by subsequently crystallized, somewhat finer grained generation of biotite. All biotite is greenish brown (Z axis). H, hole in thin section; kfs, potassium feldspar. Sample GM-1089.

TABLE 15.—Analytical data from the Late Cretaceous two-mica monzogranite

[Chemical analyses: major oxides by X-ray spectroscopy, J.S. Wahlberg, J. Taggart, and J. Baker, analysts; partial chemical analyses by standard methods, D. Shepard and P.T. Klock, analysts; Au, Hg, W, and Zn, P. Briggs and J. Thomas, analysts. Spectrographic analyses by Chris Heropoulos. Results are reported to the nearest number in the series 1, 0.7, 0.5, 0.3, 0.2, 0.15, 0.1, 0.07, and so forth, which represent midpoints of interval data on a geometric scale. The precision of a reported value is approximately plus or minus one series interval at 68-percent confidence and two intervals at 95-percent confidence. Looked for but not found: Ag, As, Au, Bi, Cd, Pd, Pt, Sb, Te, U, and W. —, not detected]

Analysis -----	1	2	3	4	5	6	7
Sample -----	GM-1089a	GM-1089b	GM-880	GM-1088	GM-877	GM-1103	GM-923b
Chemical analyses (weight percent)							
SiO ₂ -----	71.5	71.5	70.9	71.6	62.1	71.9	69.0
Al ₂ O ₃ -----	15.3	15.3	15.5	14.9	20.5	15	17.3
Fe ₂ O ₃ -----	1.3	1.19	1.33	1.31	1.35	1.06	.4
FeO -----	.2	.21	.54	.15	.19	.28	.13
MgO -----	.23	.20	.36	.26	.32	.22	.11
CaO -----	1.09	.99	1.50	.26	.63	1.18	.56
Na ₂ O -----	4.3	4.21	4.43	3.72	5.69	4.33	5.69
K ₂ O -----	4.25	4.19	3.60	5.24	6.35	4.09	4.96
H ₂ O ⁺ -----	.49	.46	.36	.64	.89	.43	.36
H ₂ O ⁻ -----	.1	.1	.06	.04	.04	.04	----
TiO ₂ -----	.21	.2	.25	.17	.23	.16	----
P ₂ O ₅ -----	.06	.06	.09	.06	.1	----	.05
MnO -----	----	----	----	----	.03	----	.02
CO ₂ -----	.13	----	----	.12	.36	.19	.17
F -----	.07	.06	.06	.12	.3	.04	.07
Cl -----	----	----	----	----	----	----	----
S -----	.025	----	.018	.012	----	.026	.005
Subtotal -----	99.26	98.67	99	98.6	99.08	98.95	98.83
Less O=F -----	.03	.03	.03	.05	.13	.02	.03
Total -----	99.23	98.64	98.97	98.55	98.95	98.93	98.8
Semiquantitative spectrographic analyses (weight percent)							
B -----	.0003	.0003	----	.0003	.0002	.0002	----
Ba -----	.1	.15	.15	.1	.15	.1	.015
Be -----	.0003	.0003	.0003	.0003	.0005	.0005	.0005
Co -----	.0002	.0002	.0003	.0002	.0002	.0002	----
Cr -----	.0002	.0002	.00015	.0002	.0002	.0002	.0002
Cu -----	.0005	.0005	.0005	.0005	.001	.0007	.0003
La -----	.005	.005	.01	.005	.007	.007	----
Mn -----	.015	.02	.015	.02	.03	.02	.02
Mo -----	----	----	----	----	.0005	----	----
Nb -----	.0007	.0007	.0007	.0007	.0015	.0007	.005
Ni -----	.0001	.0001	.00015	.0003	.0001	.00007	.0001
Pb -----	.003	.003	.003	.002	.005	.005	.005
Sc -----	.0003	.0003	.0002	----	.0003	.0003	----
Sn -----	.0007	----	----	----	----	----	----
Sr -----	.05	.07	.1	.02	.03	.07	.007
V -----	.002	.002	.003	.0015	.002	.0015	.0007
Y -----	.001	.0007	.0007	.0007	.001	.001	.0007
Zr -----	.01	.01	.015	.007	.007	.007	.0015
Ce -----	.007	.007	.015	.01	.015	.01	----
Ga -----	.003	.003	.003	.003	.005	.003	.007
Ge -----	----	----	----	----	----	----	.0007
Yb -----	.00007	.0001	.00007	----	.00007	.0001	----
Chemical analyses (parts per million)							
Au -----	----	----	----	.06	----	.05	----
Hg -----	.04	.01	.01	.01	.03	.04	----
W -----	2	1	----	3	2	----	----
Zn -----	53	49	67	34	72	52	23

monzogranite from the Gold Basin district is significantly less peraluminous than many other peraluminous granites (Keith, 1986). In addition, a plot of Na₂O + K₂O in molecular percent versus Al₂O₃ in molecular percent

shows a strong clustering of the five samples of unaltered two-mica monzogranite in the peraluminous field, approximately at 10 molecular percent Al₂O₃ (fig. 36). Such values of alumina saturation are similar to values reported

TABLE 15.—Analytical data from the Late Cretaceous two-mica monzogranite—Continued

Analysis -----	1	2	3	4	5	6	7
Sample -----	GM-1089a	GM-1089b	GM-880	GM-1088	GM-877	GM-1103	GM-923b
CIPW norms (weight percent)							
Q -----	28.5	29.3	28.3	30.1	4.7	29.2	16.6
C -----	2.3	2.4	2	3.2	4.3	1.9	2.3
or -----	25.3	25.1	21.5	31.4	37.9	24.4	29.7
ab -----	36.7	36.2	37.9	32	48.7	37.1	48.7
an -----	3.8	4.2	6.5	----	----	4.4	.9
en -----	.58	.51	.91	.41	.1	.55	.28
mt -----	----	.10	.95	----	.04	.33	.45
hm -----	1.3	1.1	.69	1.3	1.3	.84	.09
il -----	.36	.39	.48	.3	.44	.31	----
ru -----	.03	----	----	.02	----	----	----
ap -----	.14	.14	.22	.14	.24	----	.12
fr -----	.13	.11	.11	.24	.61	.08	.14
pr -----	.06	----	.04	.02	----	.06	.02
cc -----	.30	----	----	.02	.12	.44	.39
mg -----	----	----	----	.22	.59	----	----
Total -----	99.5	99.6	99.6	99.4	99.0	99.6	99.7
Salic -----	96.6	97.2	96.2	96.7	95.6	97.	98.2
Femic -----	2.9	2.4	3.4	2.7	3.4	2.6	1.5
¹ D.I. -----	90.6	90.6	87.7	93.5	91.3	90.6	95

¹Differentiation index of Thornton and Tuttle (1960), defined as the total of normative quartz plus normative orthoclase plus normative albite.

- 1-4. Two-mica monzogranite.
- 5. Episyenite facies of two-mica monzogranite; NE1/4 sec. 24, T. 28 N., R. 19 W.
- 6. Two-mica monzogranite.
- 7. Two-mica monzogranite, partly altered by nearby quartz-fluorite-white mica veins; NW1/4 sec. 10, T. 28 N., R. 18 W.

for the Australian S-type granites by Chappell and White (1974) and Hine and others (1978). The two-mica monzogranite in the district shows CIPW normative corundum to be generally more than two weight percent (fig. 37; table 15) and in this regard corresponds to an S-type granite according to some of the criteria used by Chappell and White (1974). However, the two-mica monzogranite in the Gold Basin district shows some major-element chemistry that is significantly different from the Australian S-type granites. The alumina saturation in the two-mica monzogranite is largely a reflection of its depletion in CaO. In this regard, the two-mica monzogranite differs from the Australian S-type granites because their alumina saturation results apparently from a depletion in Na₂O during weathering of the source rocks of the S-type granites (Chappell and White, 1974). The two-mica monzogranite is not depleted in Na₂O (table 15) as are most other well-studied suites of two-mica granitoids in the southern cordillera (fig. 38; see also Keith and Reynolds, 1980). In fact, relative to S-type granites in Australia, most peraluminous granites in southwestern North America are notably enriched in sodium and some have relatively high concentrations of strontium (White and others, 1986). White and others (1986) have concluded

from their studies that S-type granites, that is, granites whose chemical characteristics primarily reflect their crustal sedimentary or metasedimentary protolith(s), do not exist in southwestern North America. As shown on figure 38, the five samples of unaltered two-mica monzogranite from Gold Basin straddle the mutual boundary between the compositional fields defined by major-element data obtained from the Paleocene two-mica Pan Tak Granite of southern Arizona (see Wright and Haxel, 1982) and Late Cretaceous two-mica granitoids from the Whipple Mountains, Calif. (Anderson and Rowley, 1981). Data from the Pan Tak Granite, the Whipple Mountains, and the two-mica monzogranite in the Gold Basin district plot on the albite-orthoclase side of the quartz-feldspar join at 500 kg/cm², a relation which also clearly contrasts with that of the Australian S-type granites (fig. 38). Further, in the Australian S-type granites, Na₂O is generally less than 3.2 weight percent for rocks showing K₂O contents of about 5 weight percent (Chappell and White, 1974), whereas the minimum content of Na₂O in the two-mica monzogranite from Gold Basin is 3.72 weight percent (table 15). Haxel and others (1984) have proposed an elegant model to account for the genesis of early Tertiary two-mica granites (their compositionally restricted, silica-

rich, crustal-anatectic granites) in southernmost central Arizona. Their model includes anomalous heat flux from the mantle together with an upper crustal buildup of heat owing to the thermal blanketing effects of a tectonically overthrust, regionally extensive sheet of rocks. The applicability of such a model to the rocks in the Gold Basin

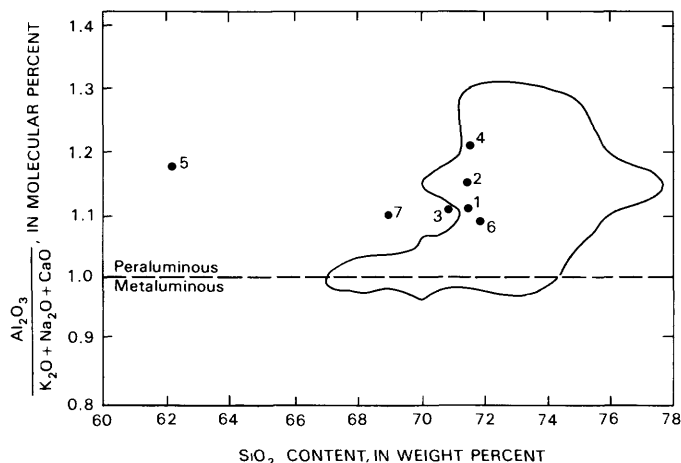


FIGURE 35.—Ratio of $\text{Al}_2\text{O}_3:(\text{K}_2\text{O} + \text{Na}_2\text{O} + \text{CaO})$ versus SiO_2 content from a Late Cretaceous two-mica monzogranite in Gold Basin district. Analysis numbers same as in table 15. Field for selected Late Cretaceous to Eocene peraluminous two-mica granitoids from elsewhere in cordillera also shown, modified from Keith and Reynolds (1980, fig. 5-1).

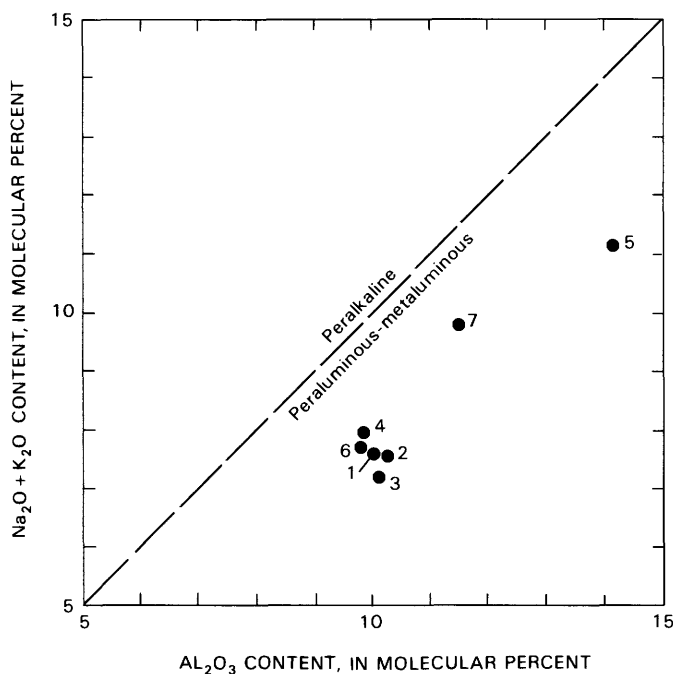


FIGURE 36.— $\text{Na}_2\text{O} + \text{K}_2\text{O}$ content versus Al_2O_3 content from a Late Cretaceous two-mica monzogranite in Gold Basin district. Analysis numbers same as in table 15.

and Lost Basin mining districts is questionable, however, because of the apparent absence of a thrust sheet approximately the same age as the two-mica monzogranite and the apparent absence of clearly demonstrable Cretaceous or younger regional metamorphic event. The Cambrian rocks that overlie the early Proterozoic porphyritic monzogranite of Garnet Mountain are not metamorphosed.

Fluorine is present in the analyzed samples of the two-mica monzogranite from Gold Basin at concentrations in the range 0.04 to 0.12 weight percent (table 15). We do not have a significant number of analyses to document geochemical trends very well, but fluorine contents in these rocks appear to show some variation with other analytical data. The sample of unaltered two-mica monzogranite containing the highest concentration of fluorine (table 15, analysis 4) also is the most highly differentiated (table 15, 93.5 D.I.) and the most strongly peraluminous (fig. 35). This particular sample also shows the lowest content of strontium (200 ppm, table 15, analysis 4), which suggests it may be among the most highly evolved of the analyzed samples. Nonetheless, the content of strontium in these samples to as much as 1,000 ppm suggests that the bulk of the two-mica monzogranite in the Gold Basin district is not that highly evolved. The most weakly peraluminous sample (fig. 35; table 15, analysis 6), however, shows the lowest content of fluorine (0.04 weight percent). Fluorine contents of other suites of two-mica granitic rocks in the southern cordillera appear to be extremely low (S.J. Reynolds, oral commun., 1982). However, the fluorine contents of two-mica granites elsewhere compare favorably with the fluorine contents obtained from the two-mica monzogranite at Gold Basin. Two-mica-bearing granitic rocks from the southern part of peninsular Thailand show fluorine contents in the range 0.09 to 0.25 weight percent (Ishihara and others, 1980). A two-mica granite of the Marukh-Teberdin massif, Caucasus, U.S.S.R., shows fluorine contents of 0.04 to 0.05 weight percent (Odikadze, 1971). Fluorine contents of muscovite-biotite granite in southwest England are reported by Bailey (1977, table VI) to be 0.16 weight percent. Muscovite-biotite granites in the Devonian Blue Tier batholith, Tasmania, contain 0.06 to 1.02 weight percent fluorine (Groves and McCarthy, 1978).

Muscovite-bearing peraluminous granitic rocks contain world-class deposits of tin in Malaysia and Thailand, significant deposits of uranium in France (Leroy, 1978), and significant concentrations of Li, Rb, Cs, Be, Nb, Ta, W, Mo, and F elsewhere (Tischendorf, 1977). However, gold has heretofore generally not been recognized as being associated with this type of igneous rock (see Boyle, 1979). Keith (1986) showed combined production and reserve values for gold suggesting his Gold Basin facies two-mica granites are associated genetically with approximately 180,000 kg gold in 25 mining districts. S.B. Keith further

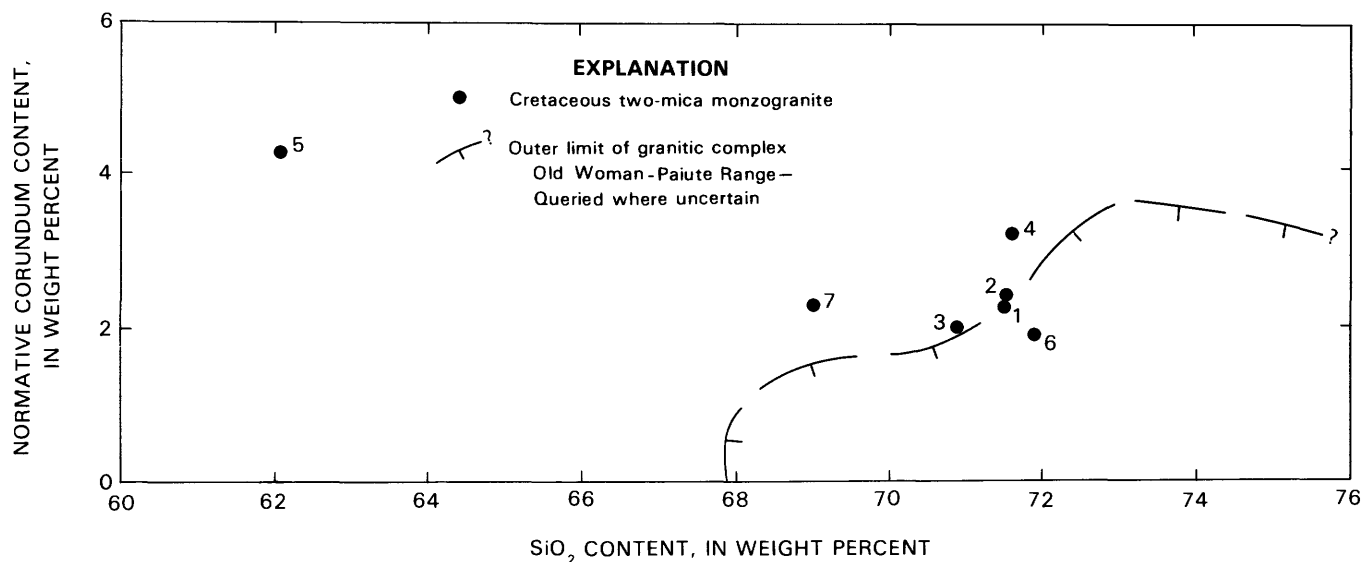


FIGURE 37.—Normative corundum versus SiO₂ content from a Late Cretaceous two-mica monzogranite in Gold Basin district. Analysis numbers same as in table 15. Outer limit of data points from strongly peraluminous granitic complex in Old Woman-Paiute Range, Calif., also shown, modified from Miller (1981).

assigns the largest of these concentrations of gold (115,000 kg) to two mining districts in southeastern California, Mesquite and Cargo Muchacho, that apparently are associated with “peraluminous calcic biotite alaskite” (two-mica granite) systems. However, the Mesquite, California, deposit may in fact largely reflect gold mineralization that postdates any two-mica granites there. In the Gold Basin-Lost Basin districts, much of the known gold mineralization appears to be related temporally with emplacement of the Cretaceous two-mica monzogranite. As will be amplified fully in the following section, one of the diagnostic features of the lode gold deposits in the Gold Basin-Lost Basin districts is the high CO₂ content of the fluid inclusions in quartz and fluorite gangue. Such CO₂-rich fluid inclusions are also locally very abundant in primary quartz crystals in the two-mica monzogranite.

EPISYENITE

Several small bodies of episyenite were found by P.M. Blacet in the Gold Basin-Lost Basin mining districts. We herein apply the term “episyenite” according to the usage of Leroy (1978) to describe rocks that were desilicated and metasomatized hydrothermally under subsolidus conditions. These rocks now resemble syenite. All of these bodies crop out across very small areas and could not be shown on the geologic map. Nonetheless, because one of these bodies of episyenite contains disseminated visible gold (Blacet, 1969), we have tabulated all occurrences of syenitic rock known to us in the districts (table 16).

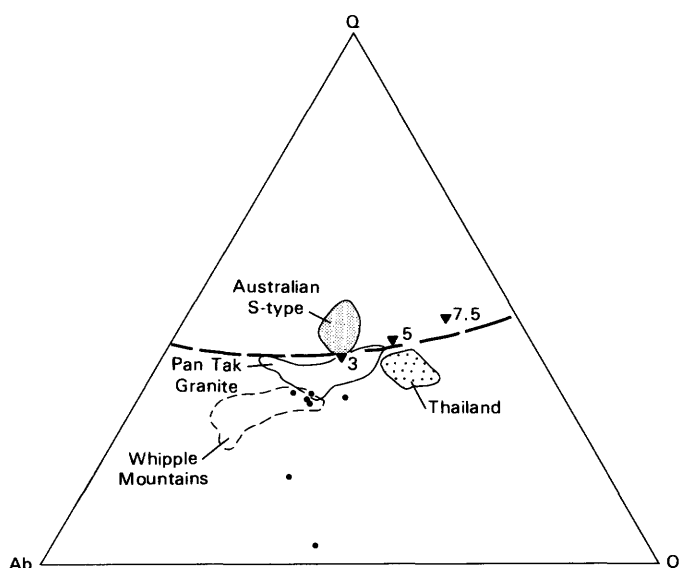


FIGURE 38.—Normative proportion of albite (Ab), orthoclase (Or), and quartz (Q). Data points of Late Cretaceous two-mica monzogranite from table 15 shown as dots. Field of Australian S-type granites modified from White and others (1977). Field of granites showing a “predominantly S-type nature” from southern part of peninsular Thailand modified from Ishihara and others (1980). Field of the two-mica Pan Tak Granite, Coyote Mountains, Ariz. (see Wright and Haxel, 1982), modified from Gordon Haxel (unpub. data, 1982). Field of Late Cretaceous, two-mica granitoids from Whipple Mountains, Calif., modified from Anderson and Rowley (1981). Triangles, ternary minimums from James and Hamilton (1969) at designated weight percent An for $P_{total} = P_{H_2O} = 1,000$ bars. Bold dashed line, locus of ternary minimum temperatures projected onto anhydrous base of Ab-Or-Q-H₂O tetrahedron for $P_{H_2O} = P_{total} = 500$ kg/cm² from Tuttle and Bowen (1958).

TABLE 16.—Occurrences of episyenitic and syenitic rocks known in the Gold Basin-Lost Basin mining districts

[Modified from P.M. Blacet, unpub. data, 1967-72]

Description	Locality (from pl. 1)	Commodities present	Comments
Series of four nearby coarse- and fine-grained, fluorite-bearing potassium feldspar episyenitic bodies. Locally abundant pyrite; some carbonate. Probably reflects alteration of Proterozoic rock during the Cretaceous.	19	Au, F	Muscovite yields K-Ar ages of 128 and 129 Ma. The episyenite bodies are ovoid shaped, have maximum individual outcrop dimensions of about 10 m, and crop out for approximately 70 m along a N. 50° W. trendline.
Medium- to coarse-grained episyenitic body. Contains fluffy, orange carbonate and some iron oxide.	800	Au?	Episyenitic body measures approximately 55 by 20 m and is elongate in a N. 60° E. direction. Ringed by an apparently genetically associated zone made up of stringers of quartz.
Syenitic aplite dike. Abundant quartz and red-brown carbonate associated with this pyrite-bearing dike.	297	Cu stain (trace)	A N. 35° E.-striking dike, approximately 8 to 10 m thick, poorly exposed.
Episyenitic aplite. Some disseminated pyrite. Sparse carbonate.	308	Au?	Exposed in area approximately 3 m long on south slope of small hill.
Muscovite episyenite facies of Late Cretaceous two-mica monzogranite. Abundant quartz, muscovite, and colorless fluorite veins are associated spatially.	877	F	Veins associated with episyenite are as much as 8 cm thick. Sparse quartz fills cavities and selectively replaces potassium feldspar. Quartz encloses abundant fluid inclusions containing high proportions of liquid carbon dioxide.

Indeed, because of the genetic and possibly economic importance of this occurrence, we include its petrographic details and chemistry in the section "Gold Deposits and Occurrences." Primarily because the Late Cretaceous two-mica monzogranite includes some episyenitic facies, we infer that episyenite distant from the Late Cretaceous two-mica monzogranite to be Cretaceous in age also.

GOLD DEPOSITS AND OCCURRENCES

Lode and placer gold deposits and occurrences are widespread throughout the Gold Basin-Lost Basin mining districts (table 11). These reported lode deposits and occurrences include numerous veins, one occurrence of disseminated gold, and veins caught up along the Miocene detachment fault. The most productive placers occur along the east flank of the Lost Basin Range. Relatively minor placer deposits were worked along the west flank of the Lost Basin Range and south-southeast of the Golden Rule Peak in the Gold Basin district. In addition, relatively significant shows of secondary copper minerals are present in the general area of locality 1357 (pl. 1; table 11). This area was geochemically studied in detail by Krish (1974), who concluded that the geochemical associations in rock there most likely reflect those to be found very high in a buried porphyry copper system, beyond even the outermost extent of the dispersed propylitic or advanced argillic halo. However, a careful review of available evidence for and against the presence of a porphyry-copper system at depth led Deaderick (1980) to conclude that its presence could not be substantiated.

The gold-bearing vein deposits and occurrences in the Gold Basin-Lost Basin mining districts appear to have been emplaced episodically over a very long timespan that ranges from the Early Proterozoic to the Late Cretaceous and (or) Paleocene. Indeed, Schrader (1909) recognized that the veins in the Gold Basin-Lost Basin districts contrasted sharply with those in the Black Mountains volcanic province (fig. 39). He grouped the veins in these districts with those of the Cerbat Mountains, about 50 km south of Gold Basin, and noted that they appeared to be associated with "post-Cambrian intrusions of granite porphyry" (Schrader, 1909, p. 48). Schrader further noted that the fissure veins of the Black Mountains cut Tertiary volcanic rocks and probably formed at depths shallower than those of the Cerbat Mountains. Blacet (1975, and unpub. data, 1967-72) documented the presence of visible gold or the inferred presence of gold at more than 100 sites throughout the crystalline terranes of the Gold Basin-Lost Basin districts (table 11). Emplacement of these veins took place during at least three periods. First, hydrothermal emplacement apparently occurred rarely sometime during the Early Proterozoic, most likely concurrently with the regional greenschist metamorphism. Some of the veins in the districts may have been emplaced synchronously with the apparently Middle Proterozoic mineralization in the southern Virgin Mountains. In the southern Virgin Mountains, 50 km north of Lake Mead, vein-type gold mineralization is probably related to the emplacement of the Middle Proterozoic Gold Butte Granite of Longwell (1936) (Longwell and others, 1965). After a long gap in the mineralization record, the emplacement of gold-

bearing veins occurred most likely during the Late Cretaceous and early Tertiary (Laramide). The most widespread introduction of gold-bearing veins was during this period; many of these veins were localized along both high- and low-angle faults and fractures within the Early Proterozoic metamorphic and igneous rocks. Finally, some of this vein-type mineralization also has been localized tectonically along the trace of the regionally extensive Miocene detachment fault where it crops out near the southwestern part of the Gold Basin district. The detachment fault in this part of the district produced low-angle gouge zones that locally contain fault blocks of gold-bearing quartz veins.

Gold mineralization in the Gold Basin-Lost Basin mining districts thus contrasts strongly with gold mineralization in much of the surrounding region. The bulk of the precious metal mineralization in the Black Mountains volcanic province of Liggett and Childs (1977) appears to be related with spatially associated Cenozoic volcanic centers; this relation is probably best exemplified by mineralization in the Searchlight district, Nevada

(Callaghan, 1939) and in the Oatman district, Arizona (Lausen, 1931; Clifton and others, 1980). Gold mineralization in the Oatman district is probably younger than about 10 Ma (Thorson, 1971). Some other nearby areas outside the Black Mountains volcanic province also have been described recently as hosting significant gold mineralization older than the volcanism in the province. A gold-bearing breccia pipe in the Clark Mountain mining district, 72 km southwest of Las Vegas, Nev., has been dated at 100 Ma (Sharp, 1980). In addition, the copper-nickel-cobalt-platinum ores associated with hornblendite intrusions at the Key West mine in the Bunkerville mining district, northern Virgin Mountains, Nevada, contained locally as much as 0.25 oz per ton gold (Beal, 1965, p. 69). Most early workers in the district (see Lindgren and Davy, 1924) believed the mineralization there to be Proterozoic in age. However, Beal (1965) suggested that hypogene copper (chalcopyrite) there may have been superposed on a nickel-cobalt-platinum metal association during the Late Cretaceous and (or) early Tertiary. The unquestionably Early Proterozoic massive-sulfide deposits at Jerome, Ariz., produced substantial amounts of copper ore containing byproduct gold and silver (Anderson, 1968). The United Verde deposit is reported to have produced 34 million tons of ore grading 5 percent copper, 1.7 ounces per ton silver, and 0.045 ounces per ton gold (Anderson and Guilbert, 1979, p. 42).

PROTEROZOIC VEINS

At least two occurrences of gold-bearing quartz veins are believed to be Proterozoic in age. One consists of irregular centimeter-size stringers of quartz together with much less abundant calcite, chlorite, galena, chalcopyrite, and pyrite, and trace amounts of gold visible along the associated iron oxide-stained fractures through the quartz stringers. Secondary minerals along the veins include cerussite, wulfenite, and some green and blue secondary copper minerals. These veins, concentrated in a zone several meters across, have unquestionably been involved in the ductile deformation that has affected the enclosing mafic gneiss. In outcrop, individual veins appear to subparallel the local schistosity. However, thin-section examination of vein-wall rock relations shows that some veins here locally crosscut the schistose fabric of their walls as they pinch and swell through the gneiss (fig. 40A). In addition, quartz in these veins has a recrystallized granoblastic texture wherein the [0001] axes of quartz appear to have a fabric similar to the fabric of quartz in the enclosing gneiss. Furthermore, quartz in the veins is relatively free of fluid inclusions, and quartz-quartz crystal boundaries typically form 120° angles. The minor amounts of chlorite in the veins are concentrated along the medial portions of many individual veins, whereas

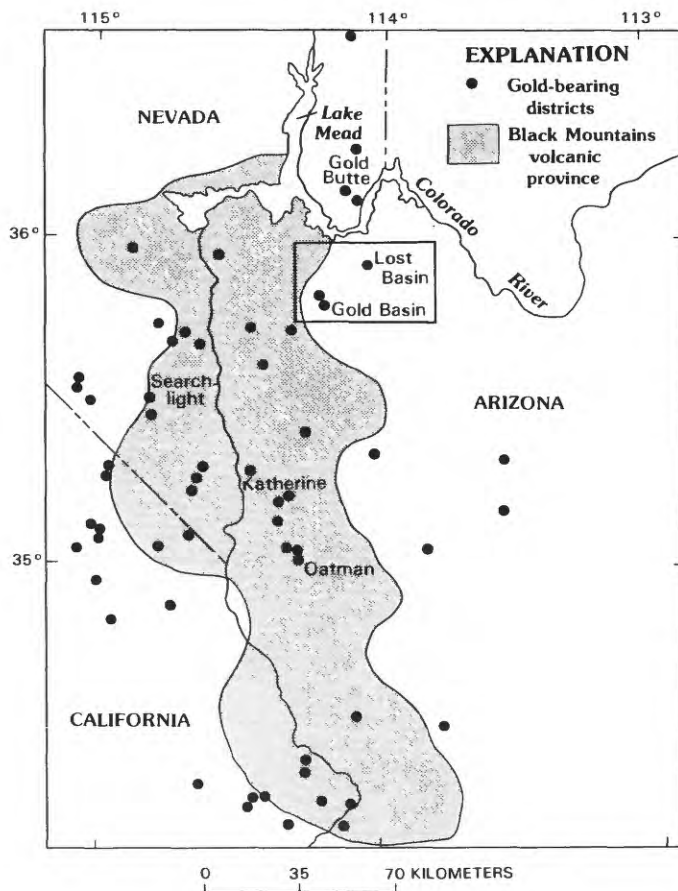
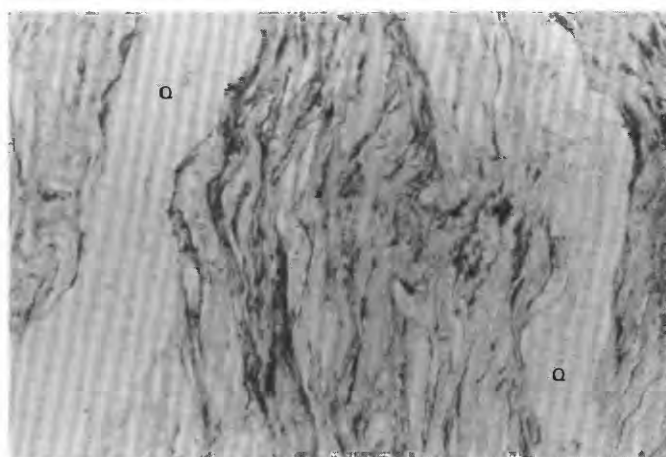


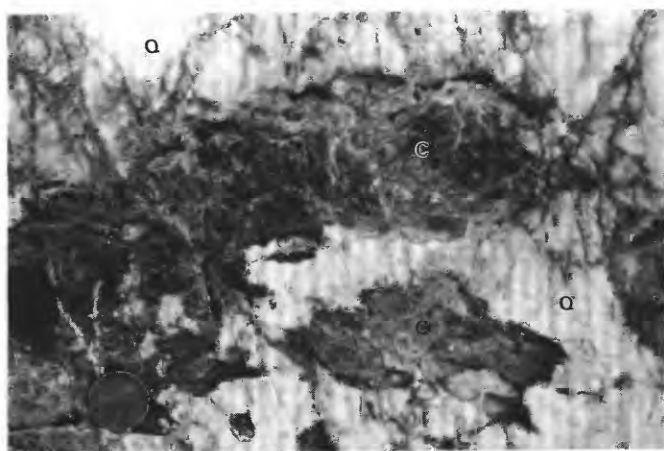
FIGURE 39.—Areas reported by Liggett and others (1974) to contain gold mineralization in general area of the Black Mountains volcanic province of Liggett and Childs (1977). Only prominent mining districts named.

biotite immediately adjacent to the veins has not been altered to chlorite. Calcite is a paragenetically late mineral in the veins and is present interstitially with the tightly interlocking quartz crystals.

The second occurrence of gold-bearing quartz veins that may be Proterozoic in age is in the general area of Salt Spring Wash, near the northeast corner of the Senator Mountain 15-minute quadrangle (pl. 1, loc. 735; table 11). Gold mineralization here, however, is only provisionally assigned to the Proterozoic on the basis of two Proterozoic ages (712 and 822 Ma) obtained from white mica separates



A 0 13 MILLIMETERS

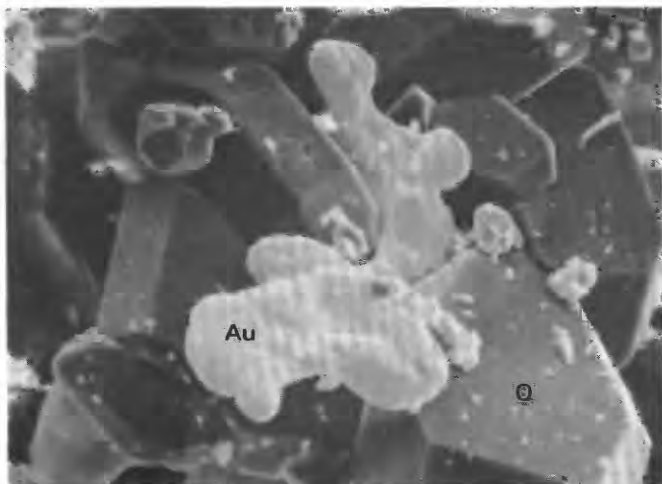


B

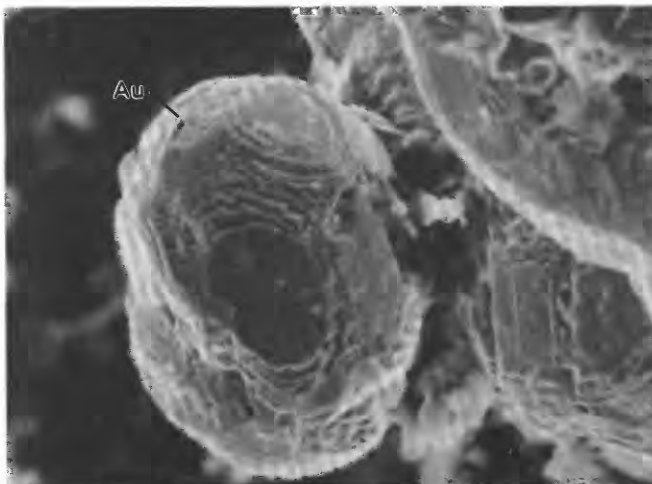
FIGURE 40.—Microscopic and megascopic relations in apparently Proterozoic veins. *A*, Vein deformed along with biotite-dominant schistose fabric of its enclosing gneiss. Primary assemblage of vein includes quartz (Q), calcite, chlorite, galena, chalcopyrite, and pyrite. Gold was found along iron oxide-stained fractures. Secondary vein minerals include cerrusite and wulfenite. Plane-polarized light. Sample GM-911. *B*, Ferroan(?) gray-brown calcite (C) in gold-bearing quartz (Q) at locality 735 (table 11). Note coin at lower left corner of photograph for scale.

from a vein at this locality. In contrast to the well-developed metamorphic fabric of the veins at the first locality of Proterozoic veins, these gold-bearing veins from the general area of Salt Springs Wash apparently have not been involved in the regional metamorphism of the area and may have been emplaced sometime during the middle Proterozoic, penecontemporaneous with the Gold Butte Granite. Altered amphibolite makes up the walls of the veins, and the rocks show some evidence of shearing and brecciation along both the footwall and the hanging wall of the most persistent of the veins. In fact, the veins at this locality appear to have been broken into a series of pods and segmented quartz veins along a steeply dipping shear zone, which strikes about N. 10° W. (P.M. Blacet, unpub. data, 1967–72). The primary assemblage in the veins at this locality includes milky-white quartz, carbonate, galena, chalcopyrite, white mica(?), and gold. The carbonate is distributed sparsely and erratically through the quartz as grayish-brown irregularly shaped masses of ferroan(?) calcite (fig. 40*B*). Pyrite, some cubes reaching dimensions as much as 2.5 cm wide, is typically replaced by coarsely to finely cellular boxworks that are very siliceous. The bulk of the gold appears to have been deposited very late during the overall paragenesis of the veins and is present mostly as approximately 0.5-mm flakes at the interface between milky-white quartz and very late clear quartz, which lines some vugs and cavities together with drusy quartz. In addition, the pyrite here is possibly auriferous. Traces of very delicate flowerlike clusters of gold are present in some of the siliceous boxworks that replace pyrite. Indeed, our collections from these veins, together with Blacet's earlier sampling, yielded a suite of samples showing generally nodular masses of paragenetically very late gold, some possibly even supergene, in various textural relations with earlier and subsequently crystallized quartz (fig. 41*A–F*).

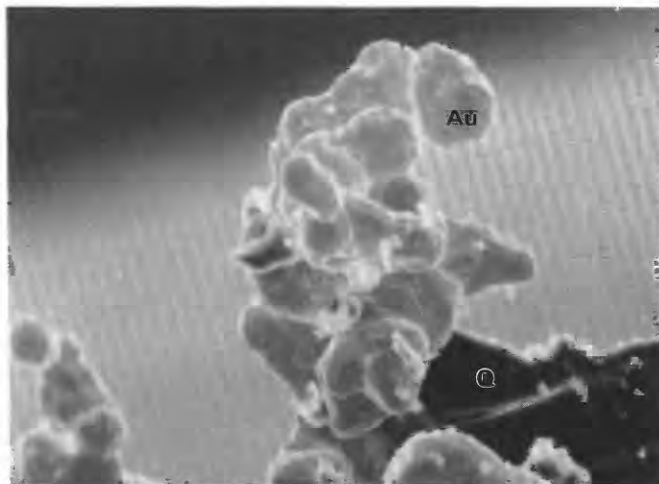
FIGURE 41.—Scanning electron micrographs showing relations of gold in apparently Proterozoic veins at locality 735 (pl. 1) in Senator Mountain 15-minute quadrangle. Au, gold; Q, quartz. *A*, Blebby nodular gold deposited on euhedrally terminated quartz projecting into an open cavity. Sample GM-735-1. *B*, Cluster of small nodules of gold perched on quartz crystals deposited along walls of cubic mold inferred to reflect paragenetically earlier crystal of pyrite. Sample GM-735-1c. *C*, Relatively large mass of nodular gold on and intergrown with quartz. Rectangular area shown in *D*. Sample number GM-735-4. *D*, Closeup view of nodule of gold from rectangular area outlined in *C* showing repeated twinning on {111} and poorly preserved dodecahedral faces. Sample GM-735-4. *E*, Paragenetically late, doubly terminated crystal of quartz on a surface of gold. Sample GM-735-1b. *F*, Quartz crystal at head of arrow associated with nodules of gold, all of which rest on matrix of gold. Sample GM-735-1d.



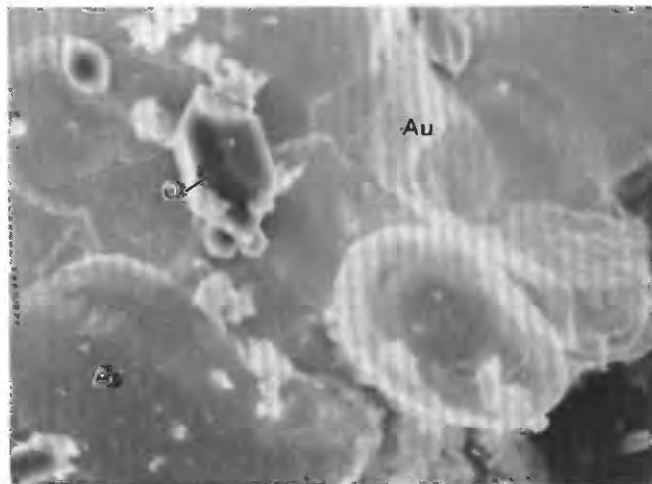
A 0 30 MICROMETERS



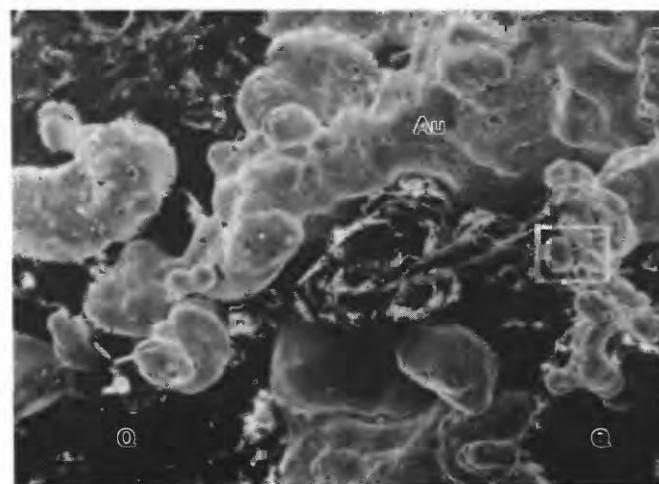
D 0 3 MICROMETERS



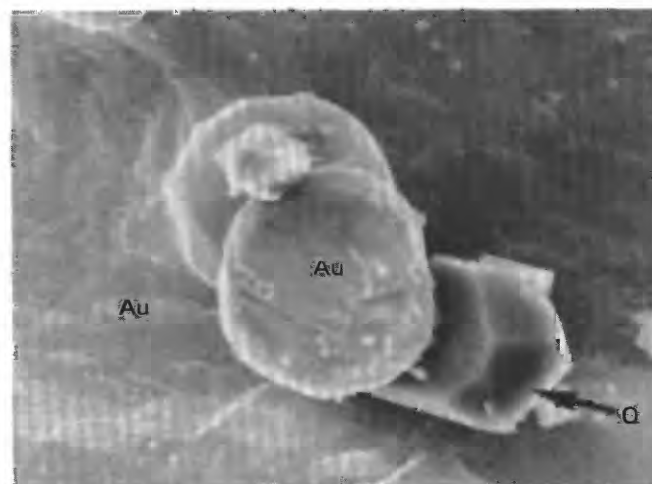
B 0 30 MICROMETERS



E 0 10 MICROMETERS



C 0 30 MICROMETERS



F 0 10 MICROMETERS

LATE CRETACEOUS AND (OR) EARLY TERTIARY VEINS

The vast majority of the gold-bearing veins in the Gold Basin-Lost Basin mining districts presumably are Late Cretaceous and (or) early Tertiary in age. These veins fill fissures and display sharply defined contacts with the country rock. Furthermore, they are locally quite persistent and in places have been traced for approximately 0.25 km by surface and underground workings (fig. 42A). The greatest concentrations of veins are in the southern part of the Gold Basin district and in the central part of the Lost Basin Range (fig. 2). Generally, in both of these areas many veins crop out individually and have northerly strikes, although a few have east-west strikes, their attitudes are controlled mostly by the attitudes of the surrounding schist and gneiss. Previously, Schrader (1917)

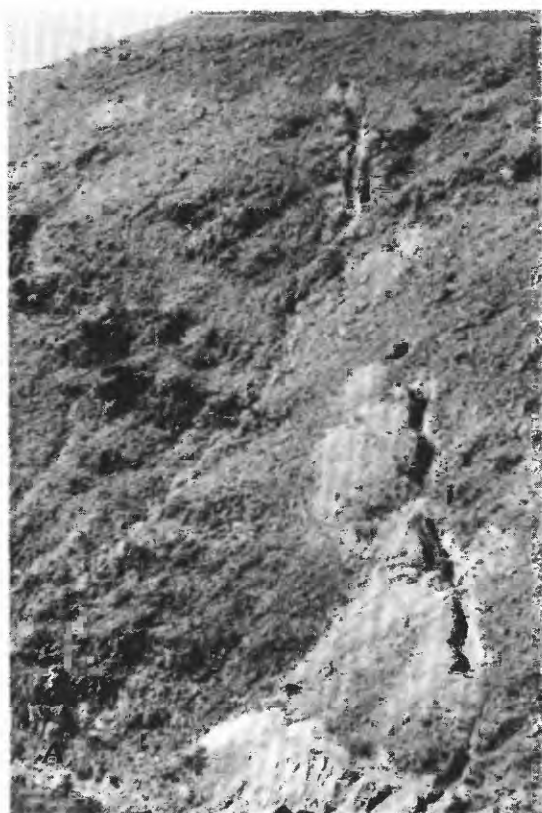


FIGURE 42.—Selected mine workings, quartz veins, and quartz-cored pegmatite from the Gold Basin-Lost Basin districts. A, Surface workings along north-striking, quartz-carbonate-chalcopryrite-galena (trace)-gold vein at Ford mine. View toward N. 10° W. Workings are approximately 2 m wide. B, Quartz-albite-calcite-barite-pyrite-galena (trace) vein at locality 382 (table 11, pl. 1). Note pocket knife near lower right corner of photograph for scale. Coarsely crystalline albite crystals, greater than 3 cm across, and cubes of limonite replacing pyrite are concentrated along border zones of vein. Dark-brown ferruginous calcite is present in deeply corroded pits in central parts of vein. C, Vertical quartz-cored pegmatite including sericitically altered potassium feldspar in general area of Salt Springs Wash. Note felt marker pen in upper central part of photograph for scale.

suggested that most of the gold-bearing veins in the Lost Basin Range strike north, whereas the copper-bearing veins strike northwest. However, the preferred orientation of the strike of the bulk of the veins measured in both districts is northeasterly. Orientation of 325 veins in the Gold Basin-Lost Basin districts is shown in projection in figure 43. Poles to veins in this diagram show double maximums that plunge to approximately N. 25° W. and N. 65° W. at concentrations greater than 3 and 4 percent per 1-percent area. The orientation of these maximums is compatible with the bulk of the veins in the districts having been emplaced into a regional stress field wherein crustal extension during the Late Cretaceous and early Tertiary was oriented north-northwest to south-southeast. As such, crustal extension in the districts during the Late Cretaceous and early Tertiary appears to have been oriented similar to that prevailing across much of the Basin and Range province of Arizona (Rehrig and Heidrick, 1976), with some notable exceptions, however. Late Cretaceous and early Tertiary veins in the Wallapai mining district, which includes the Mineral Park porphyry copper deposit approximately 16 km northwest of Kingman, Ariz., show strong preferred concentrations of their strikes in a northwest direction (Thomas, 1949).

The predominant association of gold in the quartz veins of the Gold Basin-Lost Basin districts is with ferroan calcite, pyrite, and lesser amounts of galena and chalcopryrite in varying proportions. Free gold also is present

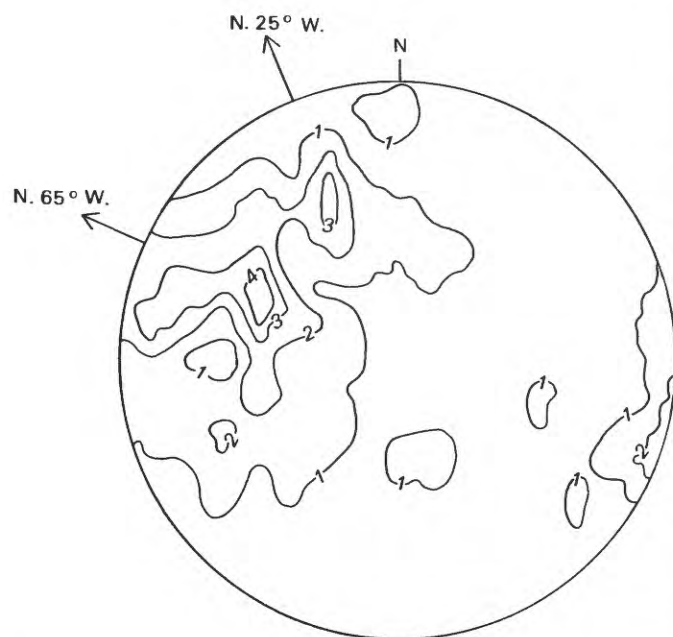


FIGURE 43.—Orientation of poles to veins in Gold Basin-Lost Basin districts. Lower hemisphere, equal-area projection. Contours: 1, 2, 3, and 4 percent per 1-percent area. Data modified from P.M. Blacet (unpub. data, 1967-72).

in two of the fluorite-bearing veins in the Gold Basin district and was noted to be present elsewhere in the districts in veins that include minor amounts of chlorite, topaz, and albite. An association between gold and albite was reported by Gallagher (1940) for many other districts. However, the apparent diversity in mineralogy is largely a reflection of gradual transitions in mineralogy as the veins and their cogenetic pegmatites evolved. For example, many veins in the districts show concentrations of coarsely crystalline albite and pyrite along their walls, along with increased abundances of ferruginous calcite in their central portions (fig. 42B). However, the overwhelming bulk of these veins most likely reflects the final stages of a mineralization event initiated by the emplacement of Late Cretaceous and (or) early Tertiary pegmatites and two-mica monzogranite into the Proterozoic rocks. Pegmatites having quartz cores (fig. 42C) are relatively abundant throughout the districts. Although the pegmatites may crosscut the metamorphic fabric of the Proterozoic rocks at high angles, the clusters of pegmatites locally appear to give way across a distance of about several hundred meters to quartz-dominant veins that closely parallel the schistosity in the surrounding metamorphic rocks. The overall dips of these veins vary widely in the districts from shallow to steep (fig. 44A-C).

The cogenetic association between the quartz-cored pegmatites and the gold-bearing quartz-ferroan calcite veins was established at several localities where critical relations are well exposed and well developed (P.M. Blacet, unpub. data, 1967-72). At these outcrops, 1- to 2-m-thick quartz-microcline-muscovite pegmatites give way internally to a well-defined central portion consisting of quartz, ferroan calcite, and some blades of white mica. However, in a few of these pegmatites small stringers of quartz plus orange-brown ferroan calcite project out from the pegmatite's quartz core and into the surrounding Proterozoic gneiss. The quartz plus ferroan calcite stringers also pinch out away from the pegmatite. These relations strongly suggest that the fluids associated with the quartz-ferroan calcite veins are related genetically to the quartz-cored pegmatites. Pyrite is not present in these well-exposed pegmatites but rather in the quartz-ferroan calcite stringers where they cut the Proterozoic gneiss. Alteration to a chlorite-carbonate assemblage in the gneiss parallels both the pegmatite and the quartz-ferroan calcite stringers. Last, the alteration is confined tightly to rocks in the very immediate area of the pegmatite.

Elsewhere, however, the relations between quartz-cored pegmatites and quartz-ferroan calcite veins suggest a somewhat greater time span between emplacement of pegmatites and the spatially separate veins. Pegmatites locally fill jointlike fractures in gneiss, and somewhat later quartz-ferroan calcite-pyrite-gold veins were emplaced along the same joint system. The veins locally crosscut

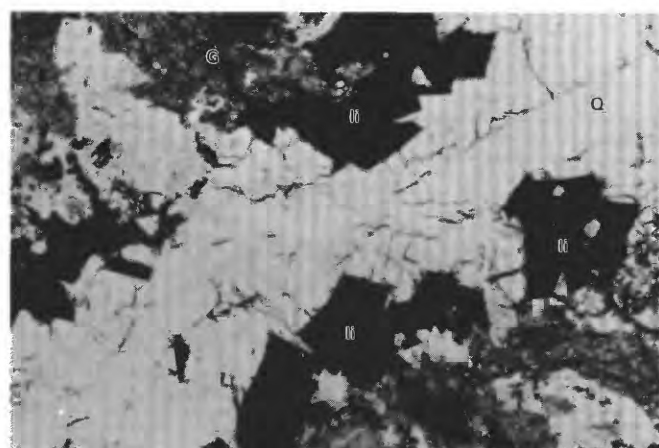


FIGURE 44.—Typical veins in Gold Basin-Lost Basin mining districts. A, Unbrecciated, shallow-dipping, quartz-galena-pyrite-gold-chalcopyrite vein containing secondary malachite, chrysocolla, and wulfenite at Eldorado mine workings. Vein is in intensely sheared zone wherein hanging wall and footwall consist of gneissic granodiorite. Note rock hammer in central part of photograph for scale. B, Gently east dipping vein approximately 1.0 m thick exposed in one working at Eldorado mine. C, Steeply dipping vein in prospect in northern part of Gold Basin district.

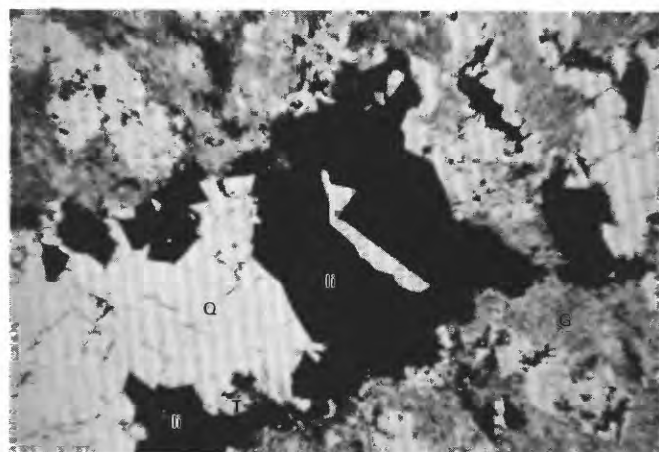
the pegmatite and visibly alter the earlier pegmatite and the enclosing granitic gneiss. Relations between such quartz-ferroan calcite veins and sericitically altered granitic gneiss are shown in figure 45. Ferroan calcite, secondarily altered to orange-brown limonite, was one of the first deposited and lines the walls of the larger veins; it also is present as gash fillings in some of the more granoblastic portions of the gneiss. The veins cut the granitic gneiss at very high angles. Another series of conspicuous echelon pods or veins, which crop out approximately 0.4 km east of the Golden Mile mine in the Lost Basin district, also documents well the transition from feldspathic pegmatite to quartz vein. The veins at this locality have an approximately 20-cm-thick border zone containing coarsely crystalline albite, potassium feldspar, and smaller crystals of greenish-white mica. In places, single crystals of albite are as long as 18 cm. Milky-white quartz and some feldspar and irregular masses of ferroan calcite make up the cores of these veins. The cores pinch and swell along the outcrop of the veins and in places reach widths of about 1 m, where the cores show relatively sharp transitions into the border zones.

In an attempt to document more fully the relations of gold to other minerals in these veins, a suite of gold-bearing samples from an approximately 1-m-thick vein at the Golden Gate mine, which is in the NW $\frac{1}{4}$ sec. 32, T. 30 N., R. 14 W. in the northern part of the Lost Basin district (pl. 1; table 11, loc. 11), was examined in detail using the scanning electron microscope. These studies revealed that the surface textures and forms of the free gold within even a single vein vary greatly (fig. 46A-F). Filliform gold drapes across drusy quartz which is dominated by rhombohedron crystal terminations (fig. 46A). Such gold, however, has also been followed paragenetically by the crystallization of sparse amounts of extremely fine grained, doubly terminated crystals of quartz (fig. 46B). Some gold is present also in a rather delicate dendritic form on prismatic crystals of quartz that line some cavities (fig. 46C), whereas other masses of gold show a nodular form containing moderately well developed dodecahedral faces (fig. 46D). Some irregularly shaped masses of gold are present in very close spatial association with equally sized partially oxidized crystals of pyrite (fig. 46E). This relation suggests that at least some of the gold in the vein was not derived from the breakdown of earlier crystallized auriferous pyrite. The surface of the gold in this association shows a very irregular almost pitted aspect. Although qualitative spot analysis of many of these particles of gold using the energy dispersive analyzer revealed they also contain silver and iron, the iron detected may in fact come from a thin partial dusting of nearby limonite on some of the gold. Such limonite may have been derived from pyrite, which commonly is an important primary mineral. Finally, our SEM studies revealed the presence in the veins

of small wedge-shaped stubby crystals containing significant amounts of vanadium, lead, and copper, and trace amounts of iron (fig. 46F). This unknown mineral may be a copper-rich mottramite, which ideally has the formula $Pb(Cu,Zn)(VO_4)(OH)$ (Roberts and others, 1974). The mottramite(?) obviously crystallized subsequent to the bulk of the gold in the sample studied. SEM studies of other gold-bearing samples showed that gold crystallized in them prior to the deposition of cerussite ($PbCO_3$), which was found by Blacet (unpub. data, 1967-72) to be a fairly common secondary mineral throughout the districts.



A 0 1.0 MILLIMETER



B 0 1.8 MILLIMETERS

FIGURE 45.—Relations between quartz-ferroan calcite veins and sericitized Proterozoic granitic gneiss. Q, quartz; li, limonite replacing ferroan calcite and pyrite(?); G, sericitized granitic gneiss. Sample GM-637. A, General crosscutting relations between veins and gneiss. Note microstreaks of limonite concentrated in granoblastic domains of gneiss away from large vein and roughly parallel with vein. Plane-polarized light. B, Closeup view showing textural relations within quartz-ferroan calcite vein containing minor amounts of topaz (T). Not shown are minor amounts of albite that very locally are found along walls of this particular vein. Crossed nicols.

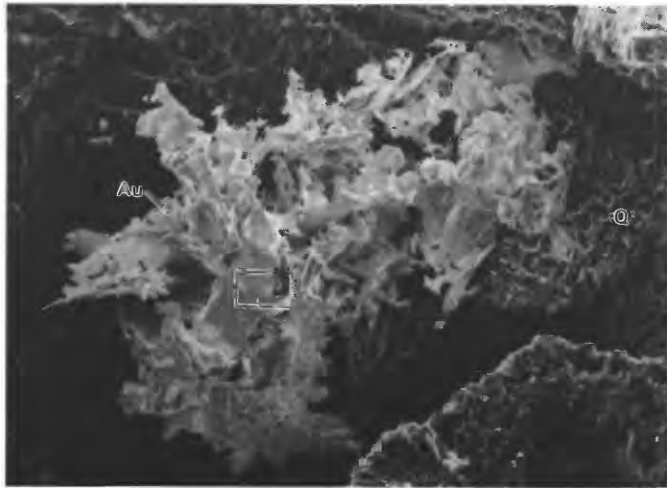
Wulfenite ($PbMoO_4$), another secondary mineral, was found in 19 veins in the districts, and 9 of these veins also contain visible gold, thereby emphasizing the strong association between lead, molybdenum, and gold there. Approximately two-thirds of the wulfenite occurrences are in the southern part of the Gold Basin district; the bulk of the remaining occurrences are clustered about 1.5 km east-northeast of the Golden Gate mine (table 11). On the other hand, none of the veins was noted to contain molybdenite (see also Deaderick, 1980, fig. 22), thus suggesting a supergene cumulative derivation of molybdenum in the wulfenite from many relatively widespread and distant sources. Williams (1963) noted that wulfenite is abundant in many mining districts in the southwestern United States, but only rarely can it be related to hypogene sulfides. He further showed that molybdenum can be extracted fairly easily from wall rocks by oxidizing meteoric fluids. Furthermore, Wilt (1980) and Wilt and Keith (1980) have shown that molybdenite in porphyry copper systems and wulfenite in Pb-Ag-Zn deposits are almost mutually exclusive.

The very strong association between lead (galena) and gold in the primary assemblages of 49 veins shown to contain visible gold in the districts is reflected in the following breakdown of specific, primary assemblages in these veins:

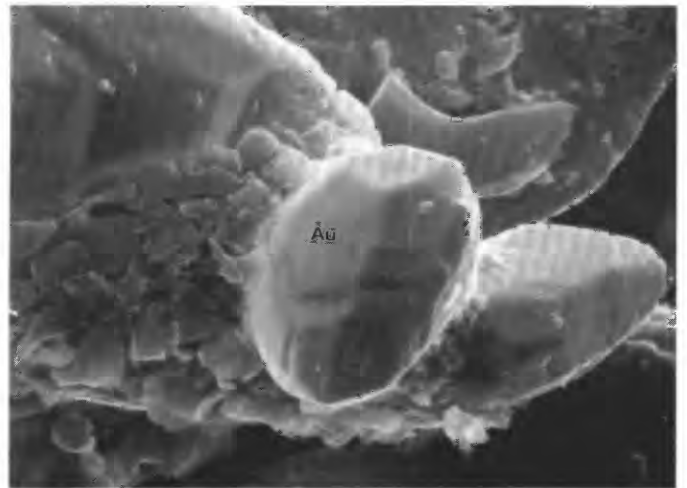
Group I	Group II	Group III
quartz	quartz	quartz
galena	ferroan calcite	feldspar
gold	chalcocopyrite	pyrite
± ferroan calcite	gold	gold
± chalcocopyrite	± pyrite	± ferroan calcite
± pyrite		± topaz
± sphalerite (trace)		± chlorite (trace)
± chlorite		
± albite		
± fluorite		

Group I includes approximately 85 percent of the veins that contain visible gold, group II about 14 percent, and group III about 1 percent. About one-third of the group I veins contain carbonate, mostly as an iron-rich or ferroan calcite. Although a strong overall spatial association exists between fluorite-bearing veins and the distribution of occurrences of visible gold in the southern part of the Gold Basin district, only two veins there were found specifically to contain both visible gold and fluorite. This strong association between lead and gold in the Gold Basin-Lost Basin districts contrasts with the apparent strong association of gold with zinc, and silver with lead in the Cerbat Mountains, 75 km to the south (Hernon, 1938).

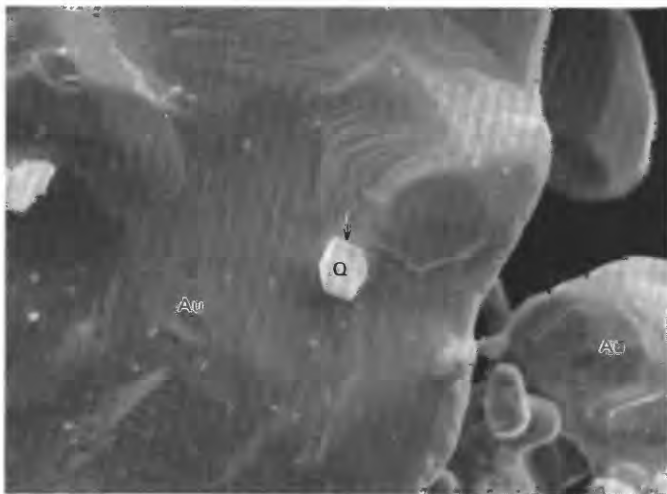
The preceding specific vein assemblages reflect mostly the final stages of a Late Cretaceous and (or) early Tertiary event that began with the widespread introduction of pegmatite or granitic micropegmatite concurrently with the emplacement of the two-mica monzogranite. The pegmatites include both potassium feldspar-rich and



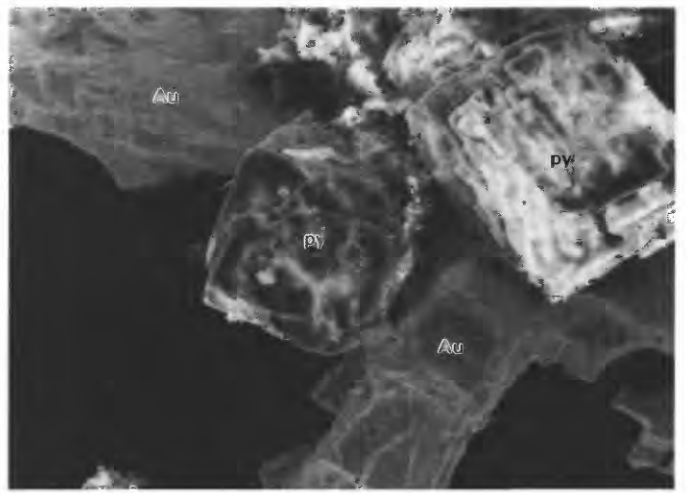
A 0 100 MICROMETERS



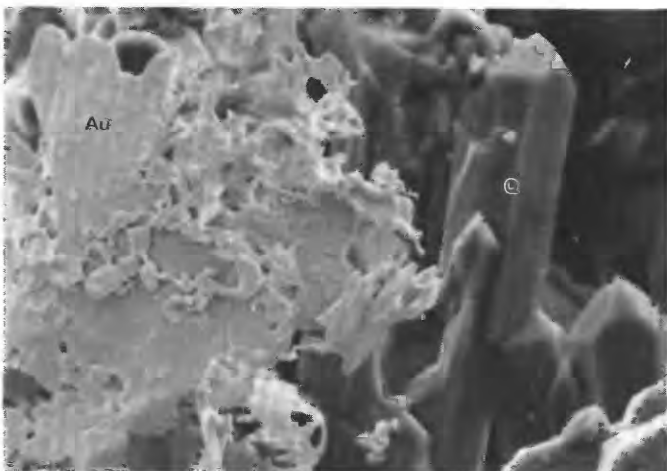
D 0 3 MICROMETERS



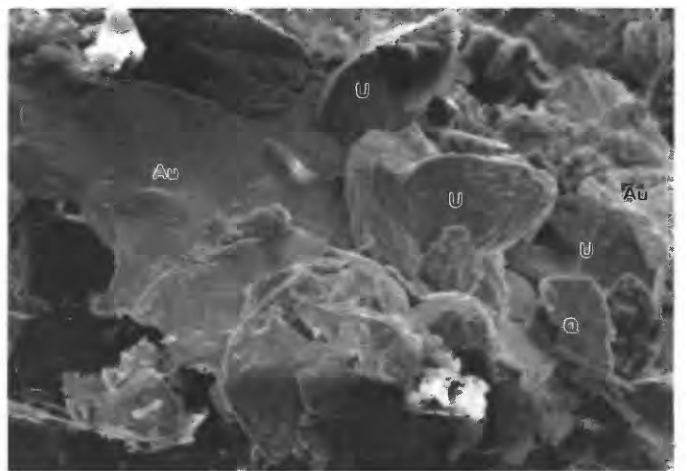
B 0 6 MICROMETERS



E 0 60 MICROMETERS



C 0 30 MICROMETERS



F 0 60 MICROMETERS

albite-rich types and include a feldspar-dominant early stage in the evolution of these pegmatite-vein systems. The feldspar-dominant part of these systems is reflected primarily by the feldspar-rich border zones of the quartz-cored pegmatites. These border zones also include varying but generally minor amounts of quartz, carbonate (usually iron rich), barite, apatite, pyrite, white mica, galena, and chalcopyrite. Barite locally is quite abundant in some of these pegmatite veins, whereas galena and chalcopyrite are present sparsely in and near some feldspar-dominant border zones. This latter relation suggests minor deposition of these minerals (together with traces of gold, as in the group III gold-bearing assemblages listed above) early in the overall evolution of some of the pegmatite-vein systems. Quartz typically is present in concentrations of about one-third to one-fourth of that of the feldspar (potassium feldspar and (or) albite) in the border zones. Further, as the pegmatite-vein systems evolved there appears to be a general decrease in the ratio pyrite:(galena + chalcopyrite) reflected primarily by a substantial increase in the amounts of galena and chalcopyrite late in the paragenesis. This change coincides with the increase in the amount of largely ferroan calcite deposited and with a cessation in the crystallization of feldspar. As we discussed briefly above, fluorite locally is a very important accessory mineral during this predominantly quartz-sulfide-carbonate stage of the pegmatite-vein systems, especially in the southern part of the Gold Basin district. Therefore, for descriptive purposes, we use a two-fold classification of the veins: (1) a feldspar-dominant type (group III, above) and (2) a mostly quartz-sulfide-carbonate type (groups I and II), which includes the majority of the occurrences of visible gold known throughout the districts.

FIGURE 46.—Scanning electron micrographs of lode gold collected from Golden Gate mine in Garnet Mountain 15-minute quadrangle. Au, gold; Q, quartz. *A*, Filliform gold in cavity lined by drusy quartz terminated mostly by rhombohedrons. Rectangular area shown in *B*. Sample GM-11. *B*, Enlargement of area enclosed by rectangle in *A*. At head of arrow an extremely small, doubly terminated crystal of quartz rests on surface of gold. Striations on surface of gold probably reflect repeated twinning on {111}. *C*, Dendritic gold associated with prismatic crystals of quartz, which line a cavity in vein quartz. Qualitative analysis of gold using energy-dispersive X-ray microanalyzer indicates that gold contains detectable amounts of silver and iron. Sample GM-11h. *D*, Nodule of gold in quartz cavity. Gold shows moderately well developed dodecahedral faces and contains detectable amounts of silver and iron. Sample GM-11d. *E*, Irregularly shaped, roughly textured particles of gold associated with partially oxidized cubes of pyrite (py). Sample GM-11-1. *F*, Unknown mineral (U) showing a wedge-shaped habit and containing detectable amounts of vanadium, lead, copper, and iron (in trace amounts). Unknown mineral may be copper-rich mottramite, which ideally has formula $Pb(Cu,Zn)(VO_4)(OH)$ (Roberts and others, 1974). Sample GM-11-1a.

The intensity, type(s), and lateral extent of alteration related to the emplacement of most veins are mostly a function of the chemistry of the surrounding country rock and the chemistry of the fluids involved. A typical approximately 0.5-m-thick vein, which includes a well-developed feldspar (albite) stage, will show alteration phenomena visible in outcrop for about 1 m away from its generally sharp walls. Alteration of amphibolite adjacent to one such well-studied vein clearly reveals the potassic character of some of the early fluids associated with vein emplacement (fig. 47). The effects of alteration were studied in a suite of samples of amphibolite collected 6 m, slightly over 1 m, 0.6 m, 8 cm, and 3 cm from the vein.

Amphibolite 6 m from the vein shows only crystallization and recrystallization effects related to the Early Proterozoic metamorphic events. The amphibolite here contains a generally granoblastic fabric consisting of closely packed crystals of blue-green (Z axis) hornblende that show marginal recrystallization to epidote + carbonate, chlorite + quartz, and actinolite + chlorite assemblages. All of these latter, superposed assemblages presumably reflect the Early Proterozoic retrograde metamorphic event.

Just beyond the alteration halo visible in outcrop, at a distance barely over 1 m from the vein's wall, thin-section study of amphibolite reveals a marked increase in the abundance of chlorite, actinolite, epidote, and quartz, and the first appearance of sphene in the matrix. Here the hornblende takes on a ragged crystal outline and a generally rounded aspect when viewed under the microscope. We suggest that this increased growth of a chlorite-actinolite assemblage centralized in the preexisting matrix reflects a narrow subtle propylitic halo superposed on the earlier greenschist assemblages, and this halo thus marks the outer limit of alteration related to vein emplacement.

At a distance of about 0.6 m, the blue-green hornblende has been replaced almost totally by greenish-brown (Z axis) biotite in a rock showing a suite of superposed assemblages. Only the former crystal outlines of hornblende remain. These outlines are well defined by granoblastic clusters of equant crystals of biotite, some of which show traces of their {001} cleavage planes following locally the directions of {110} cleavage relict from the replaced hornblende. Biotite in very small domains of the rock appears to be compatible with carbonate (probably a very iron rich ankerite), opaque mineral (probably magnetite), quartz, and very minor amounts of apatite. The crystallization of biotite as an almost complete replacement of earlier hornblende and its greenschist and propylitic assemblage breakdown products suggest a significant influx of potassium to yield the assemblage biotite-ankerite-magnetite (fig. 48, assemblage I). However, assemblage I is replaced partially in this rock by an epidote-chlorite-carbonate assemblage (fig. 48, II), and extremely small

domains in the rock show incipient development of the apparently stable assemblage white mica-epidote-chlorite (fig. 48, III). Both of these latter two assemblages also

include quartz. The very sparse presence of albite in the matrix of the rock may reflect incipient development of assemblage IV, which is the same as the early assemblage

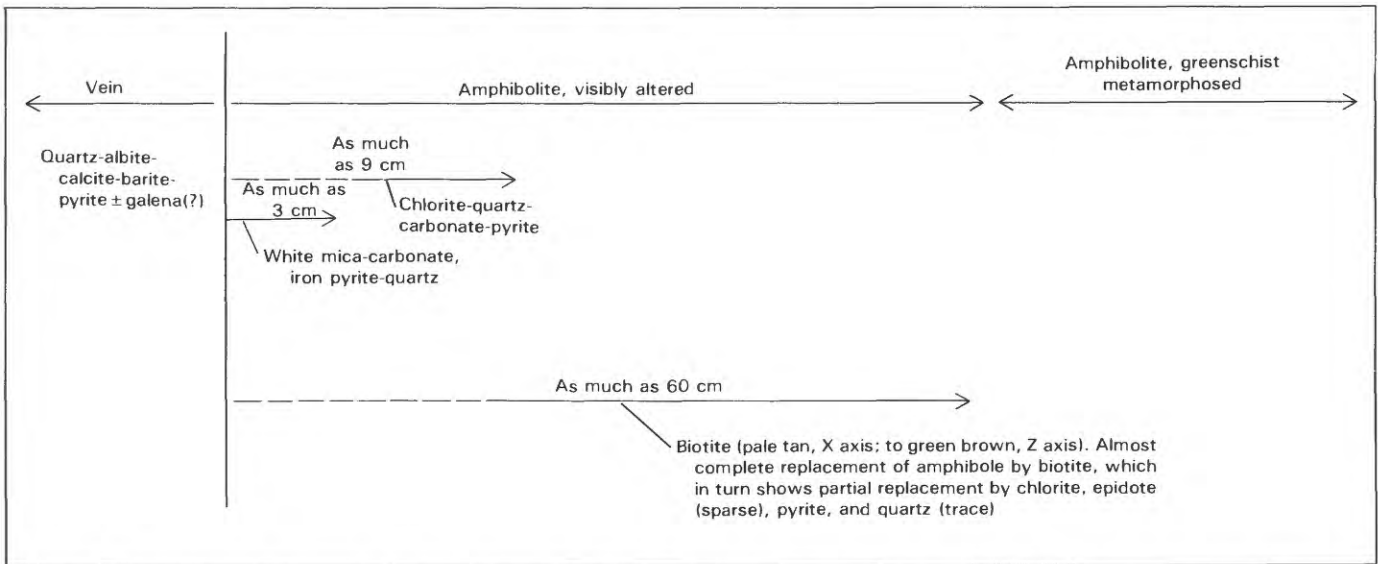


FIGURE 47.—Diagrammatic summary of alteration surrounding typical feldspar-stage vein including quartz-albite-calcite-barite-pyrite ± galena(?) composite assemblage. Dashed lines, sparse concentrations of chlorite-quartz-carbonate-pyrite assemblage or sparse relict biotite.

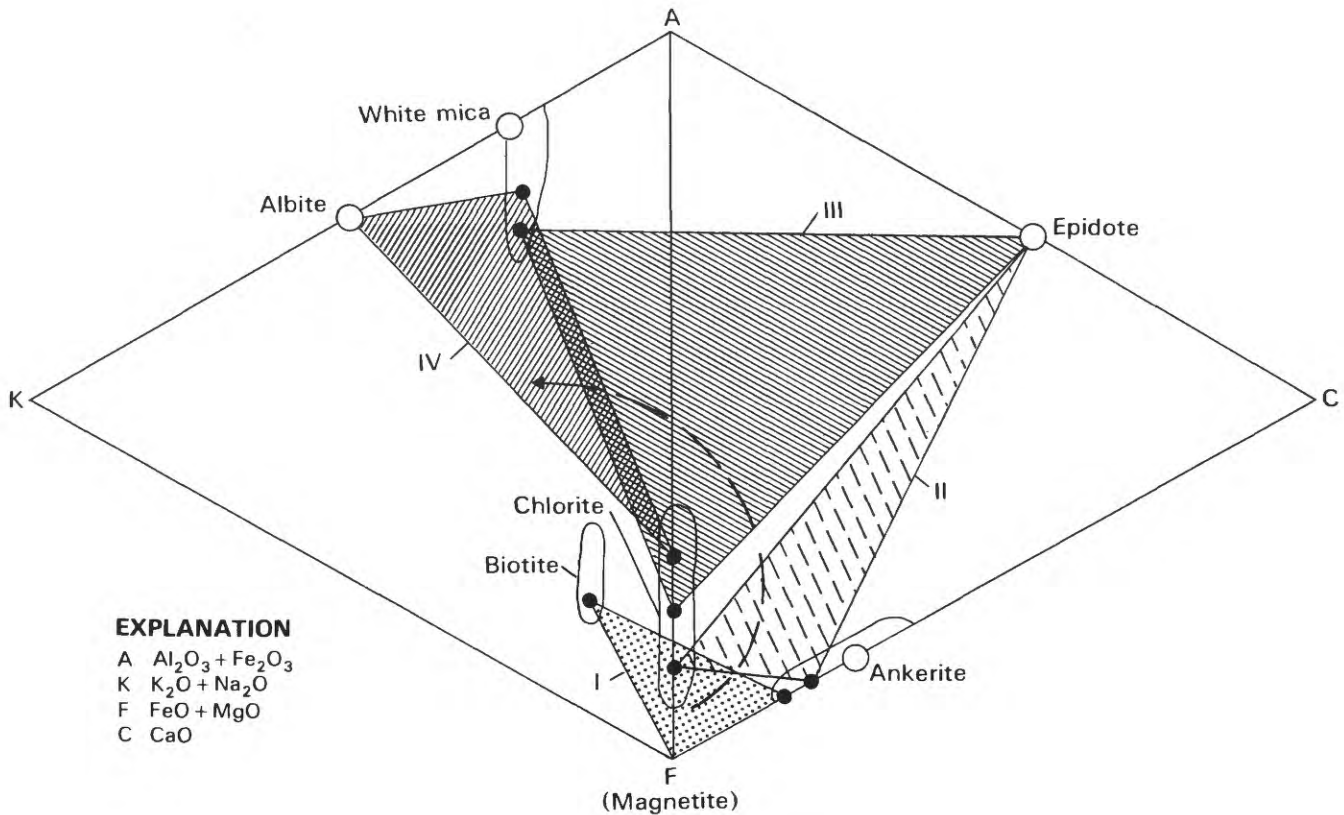


FIGURE 48.—Mineral assemblages in altered wall rock (assemblages I, II, and III) adjacent to typical feldspar-bearing vein (assemblage IV). Quartz and apatite also commonly present. Compositional fields for white mica, biotite, and chlorite from Beane and Titley (1981).

Compositional field for ankerite from Deer and others (1962b). Dots, inferred compositions. Arrow indicates inferred, approximate paragenetic evolution of assemblages with time; early, tail of dashed line; late, head of arrow.

in the vein itself. Thus, the parageneses of these assemblages (fig. 48, I–IV) apparently reflect an initial potassium metasomatism, probably fissure controlled, that was in turn followed by a complex suite of assemblages related to final emplacement of the sodium (albite)-rich vein. These relations imply that an early buildup in the ratio $(K^+)/(H^+)$ of the first fluids to circulate along the fissure was followed by a decrease in this ratio, an increase in $(Ca^{2+})/(2H^+)$, and then the actual emplacement of the vein was accompanied by fluids having a relatively high $(Na^+)/(H^+)$ ratio.

Amphibolite collected 8 cm from the vein shows a wispy microfolded fabric defined by schistose domains of a relict greenish-brown (Z axis) biotite assemblage (I) heavily altered to a chlorite-ferroan carbonate-pyrite assemblage which includes some quartz. The rock shows an increased abundance of chlorite and disseminated ferroan carbonate relative to the previously described samples and also marks the first appearance of sulfide in the wall rock. Some plagioclase remains in the rock relict from the Proterozoic metamorphism(s). Furthermore, the amount of quartz in the rock is significantly greater than that in altered amphibolite farther out in the alteration envelope. This increase in the content of quartz and pyrite may result from a release of SiO_2 from biotite during sulfidation reaction(s) to yield a chlorite-dominant assemblage.

White mica is the dominant silicate gangue mineral approximately 3 cm from the vein. A white mica-ferroan calcite-quartz-pyrite assemblage is superposed here on a suite of minerals including chlorite, biotite (partly altered to chlorite), oligoclase, and opaque minerals—all relict from earlier recrystallization reactions related to passage of fluids associated with the emplacement of the vein. We envision the white mica assemblage adjacent to the vein to be the end product of a complex series of coupled reactions in the country rock controlled primarily by a concomitant decline toward the vein in at least two cation activity ratios of the associated fluid(s). A simultaneous decline in the $(Mg^{2+})/(2H^+)$ and $(K^+)/(H^+)$ activity ratios of the fluid(s) may explain the relations observed among assemblages in this potassium- and magnesium-bearing alteration envelope (fig. 49; see Beane and Titley, 1981). The absence of talc from the biotite-bearing assemblage, which apparently was the earliest prograde assemblage to develop, suggests that initial values of $(Mg^{2+})/(2H^+)$ in the fluid(s) were less than those required to form talc. Finally, the absence of potassium feldspar from any of the observed assemblages suggests that the cation activity ratios of $(Mg^{2+})/(2H^+)$ and $(K^+)/(H^+)$ in the fluids remained outside the field of potassium feldspar.

Three samples of Early Proterozoic quartzofeldspathic gneiss were collected approximately 1.1 m, 0.5 m, and 5 cm from the vein to compare their alteration assemblages with those in the adjacent amphibolite just described. The

prograde regional metamorphic assemblage in the gneiss probably consisted of quartz, oligoclase (An_{15}), garnet, biotite, apatite, and opaque mineral(s). However, garnet and biotite are extremely rare in these samples because the rocks show moderate to heavy partial replacement by an assemblage of chlorite, epidote, white mica, carbonate, quartz, and opaque mineral. This chlorite- and epidote-rich assemblage is concentrated mostly in domains originally including abundant oligoclase. Indeed, as the vein is approached across this approximately 1-m distance, the quartzofeldspathic gneiss shows a progressive increase in the concentrations of white mica and epidote in the plagioclase. Very close to the vein, in the sample collected at a distance of 5 cm, a very well developed phyllonitic or ribboned texture in the quartz-rich domains suggests some ductile flow in the country rock accompanied vein emplacement. This ductile flow may result from a hydrolytic weakening of quartz (see Griggs and Blacic, 1965). In addition, the country rock as much as 5 cm from the vein shows (1) fresh albitic overgrowths on the white mica- and epidote-altered plagioclase and (2) rutile as a common minor accessory. Thus, our petrologic studies of the quartzofeldspathic gneiss failed to document a strong early potassic alteration stage comparable to that found in the amphibolite. However, the few shreds of biotite relict now in the white mica- and (or) chlorite-dominant rocks might be interpreted to reflect such a potassic stage during the process of alteration, although this does not seem probable. Instead, potassium feldspar is a more likely product in rocks of this overall chemistry as a result of an increase in the cation activity ratio of

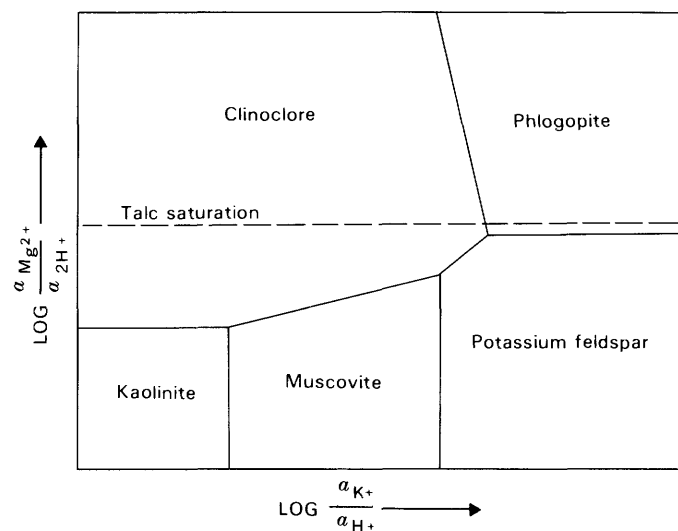


FIGURE 49.—Schematic stability relations among minerals as a function of $(Mg^{2+})/(2H^+)$ and $(K^+)/(H^+)$ cation activity ratios in coexisting fluid (from Beane and Titley, 1981). Pressure 500 bars, temperature near 300 °C. Excess quartz and H_2O . a , activity of subscripted species.

(K⁺)/(H⁺) of the associated fluids. For some reason such early K⁺-enriched fluids did not circulate through the layer of quartzofeldspathic gneiss. However, the predominant type of alteration associated with the majority of veins throughout the districts appears to be propylitic.

Examination in the field (P.M. Blacet, unpub. data, 1967-72) and in thin section shows that the propylitic alteration associated with these veins includes several specific assemblages together with wide-ranging intensities of development and depths of penetration into the surrounding country rock. Some quartz-albite veins measuring 0.5 to 1.0 m in thickness show visible pyrite-carbonate impregnations as much as 8 to 10 cm from the vein wall. As we described above, the ferroan carbonate together with some quartz in places fills tightly spaced irregular microfractures at high angles to the foliation in the country rock. Generally, the ferroan carbonate-filled microfractures are discontinuously confined mostly to the granoblastic parts of the gneiss. Other feldspathic veins about 15 cm thick show in outcrop an inner alteration zone of orange-brown carbonate as much as 10 cm thick in turn mantled by an outer 15-cm-thick zone of well-developed chloritization, which may include epidote and white mica with or without clinozoisite as specific assemblages. However, visible ferroan carbonate plus pyrite alteration in outcrop is only several millimeters thick locally adjacent to some veins, whereas elsewhere along the same vein the alteration may expand markedly into widespread zones of chloritization and flooding by ferroan carbonate. Feldspathic veins that include variable amounts of barite may also show some albite disseminated in the adjacent country rock. Quartz-fluorite veins including either feldspar, or muscovite, or sulfides and gold, generally are characterized by white mica-dominant assemblages in their alteration envelopes.

The mineralogy of a small number of other veins in the districts appears to have been controlled significantly by the adjoining wall rocks. Where such veins cut quartzofeldspathic gneiss, the mineralogy of the vein consists of almost 100 percent quartz. However, where the same vein cuts hydrothermally altered amphibolite, the mineralogy of the vein includes abundant irregularly shaped knots of ferroan calcite. The hydrothermal alteration in the amphibolite adjacent to such veins is predominantly propylitic and shows mostly a chlorite-carbonate assemblage.

The mineralized quartz veins in the districts mostly predate emplacement of thin, presumably Tertiary, biotite lamprophyre dikes which crop out sporadically throughout the crystalline terranes (P.M. Blacet, unpub. data, 1967-72). In many prospects, pits, and underground workings, such as those at the Eldorado mine (table 11, loc. 17), biotite lamprophyre is consistently fine grained along its margins because of rapid chilling against the mineralized veins. In addition, at several other localities

the biotite lamprophyre was found by P.M. Blacet to actually cut quartz-pyrite-muscovite veins. However, not all of the mafic dikes postdate the mineralized veins in the districts. Some mafic dikes clearly were intruded, contorted, and sheared during a postmetamorphic shear deformation (Laramide?) that involved local crumpling and shear folding of the Early Proterozoic metamorphic rocks. Furthermore, an at least 1-m-thick biotite lamprophyre at the L.P.M. mine (table 11, loc. 12) contains a ferroan calcite alteration assemblage possibly related to emplacement of the quartz-pyrite-gold vein there. This relation again suggests that the biotite lamprophyre at the L.P.M. mine may have been present before emplacement of the veins.

DISSEMINATED GOLD IN EPISYENITE

An occurrence of visible gold disseminated in several small alteration pipes was recognized by P.M. Blacet during the initial stages of his regional mapping studies in the districts (table 11, loc. 19). Blacet (1969) described this occurrence as follows:

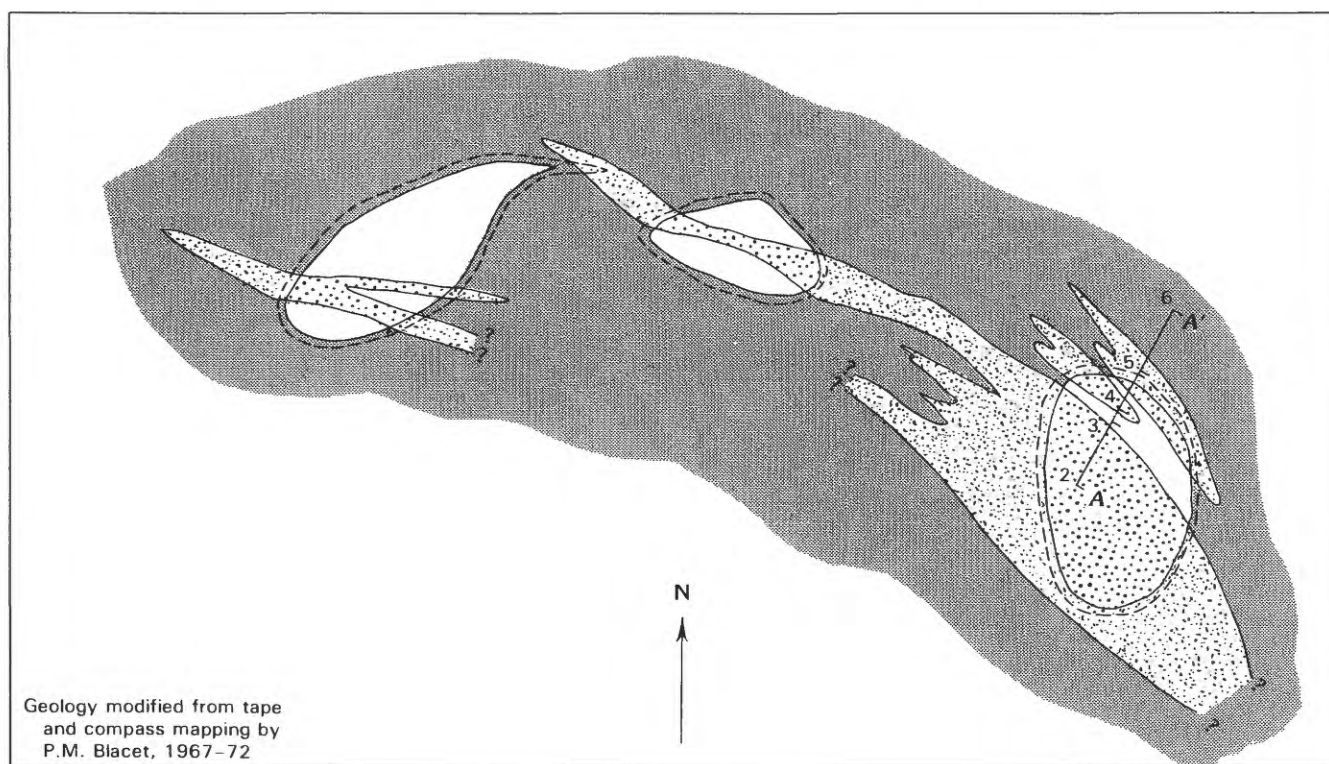
The second type of lode deposit consists of small intrusive bodies of gold-bearing medium-grained, porphyritic leucosyenite containing several percent of interstitial fluorite. Mirolitic cavities in this leucosyenite contain small euhedral crystals of parisite [(Ce, La)₂Ca(CO₃)₃F₂]. Megascopically visible gold is disseminated throughout the leucosyenite and appears to be primary. The leucosyenite is tentatively considered to have crystallized in small pipelike conduits during late magmatic escape of highly potassic residual liquids that were enriched in H₂O, HF, CO₂, SO₂, Zr, Au, and rare earths***.

The largest of the pipes measures at the surface about 8 m across in its longest dimension (fig. 50), but only three pipes of episyenitic (see Leroy, 1978) rock are shown. However, another very small episyenitic body, approximately 3 m in longest dimension, crops out about 40 m southeast of section line A-A' (fig. 50). The alteration pipes consist of coarse-grained and fine-grained episyenitic rocks that cut across Early Proterozoic fine-grained biotite monzogranite and a coarse-grained dike of Early Proterozoic (?) monzogranite. Apparently, the coarse-grained monzogranite dike acted as a structural conduit to funnel fluids that generated the episyenitic rock. The episyenitic rock contains unevenly distributed concentrations of pyrite that is now oxidized to limonite and specular hematite. In places, the original pyrite content of the episyenitic rock probably was as high as 5 to 10 volume percent. Undoubtedly, the resulting color anomaly on the pipes first attracted prospectors, who explored the occurrence with two shallow prospect pits. The prospect pits are on the northernmost and the southernmost of the three pipes shown.

In outcrop, the coarse-grained facies of the gold-bearing episyenitic rock locally shows a quartz-poor igneous rock

fabric that contains well-developed potassium feldspar megacrysts and that shows relatively sharp contact relations with its enclosing quartz-rich host (fig. 51). These relatively large megacrysts of potassium feldspar probably are relict from initial crystallization at magmatic conditions during Early Proterozoic time. Significant removal of silica and potassium metasomatism accompanied by subsolidus crystallization and (or) reequilibration of the megacrysts occurred during Late Cretaceous and (or) early Tertiary. Late-stage fluids associated with this episyenitization finally deposited the gold. The interstitial

matrix among the large potassium feldspar megacrysts is mostly potassium feldspar, but also includes rare secondary quartz, fluffy orange and red-brown limonite and specular hematite (both replacing pyrite), purple fluorite, sparse carbonate, unevenly distributed flakes of free gold, and somewhat sporadic concentrations of white mica. As we described previously, study of two white mica separates from the gold-bearing episyenite pipes yielded ages of 127 and 130 Ma, undoubtedly reflecting the presence of excess radiogenic argon derived from the Early Proterozoic host for the episyenite or minor contaminant of



0 10 20 30 FEET

EXPLANATION

-  Episyenitic rocks (Cretaceous?)—Stippled where coarse grained
-  Monzogranite (Early Proterozoic)—Coarse grained
-  Biotite monzogranite (Early Proterozoic)—Fine grained
-  ? Contact—Queried where continuation uncertain
-  Approximate outer limit of silicified and sericitically altered rocks surrounding the episyenitic rock
-  Line of section (see fig. 52)—Numbers correspond to modal analyses listed in table 17

FIGURE 50.—Geologic sketch map of area in immediate vicinity of occurrence of visible disseminated gold in episyenitic rock cropping out in southeastern part of Gold Basin mining district.

Proterozoic muscovite or Proterozoic feldspar in the mineral separate. These episyenite pipes also could be termed feldspathic fenite in the classification of Sutherland (1965b) or microcline as used by Hanekom and others (1965).

PETROGRAPHY

The episyenitic pipes include very sparse quartz and significant concentrations (generally more than 90 percent) of modal potassium feldspar, which decreases sharply through the approximately 1-m-wide contact zone surrounding the pipes. The variation in modal potassium feldspar and quartz across one of the pipes is shown in figure 52. Quartz in the central part of this studied episyenitic pipe makes up about 4 volume percent of the rock, but decreases to much less than 1 volume percent near

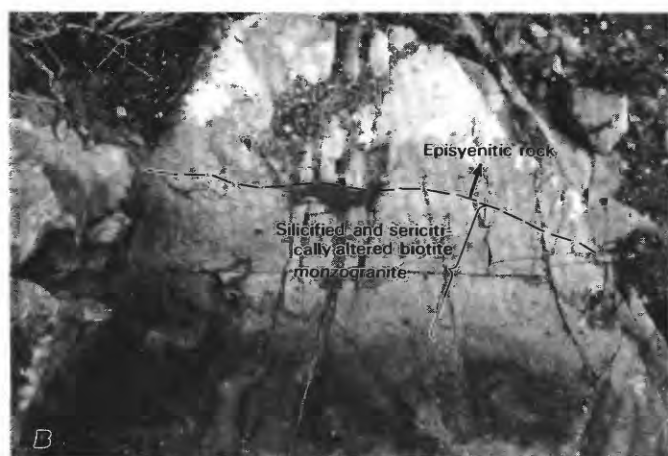
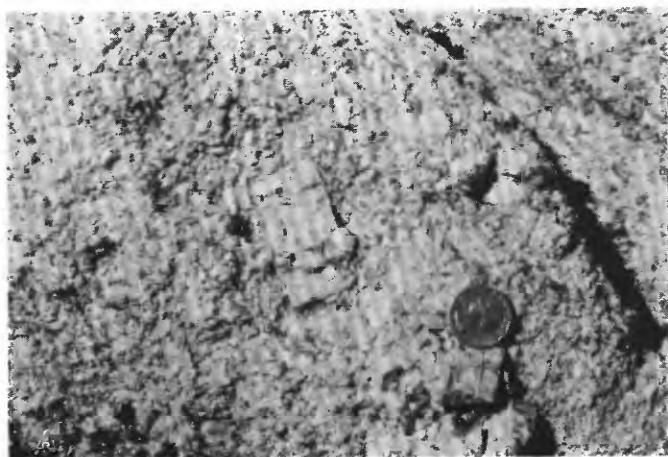


FIGURE 51.—Gold-bearing episyenitic rock. *A*, Medium- to coarse-grained episyenitic rock containing probable mixed phenocrystic and porphyroblastic megacrysts of potassium feldspar. *B*, Contact relations between episyenitic rock and its mantle of silicified and sericitized Early Proterozoic biotite monzogranite.

the outer limit of the episyenitic rock (see table 17 for the complete modal analyses of these samples). In contrast, quartz occurs in concentrations of about 35 volume percent in a representative sample from the silicified and sericitically altered halo which surrounds the episyenitic rock. Potassium feldspar in the episyenitic rock ranges from about 84 to 92 volume percent and makes up about 42 volume percent of altered biotite monzogranite approximately 4 m from the episyenitic contact (fig. 52 and table 17, analysis 6).

Thin sections from approximately 20 rocks were studied from the immediate area of the gold-bearing episyenitic alteration pipes. Fresh complexly twinned potassium feldspar, which makes up typically 85 to 90 volume percent of the central parts of the episyenitic pipes, shows wide-ranging textures. The bulk of these rocks have seriate textures and contain many zoned potassium feldspar megacrysts whose margins are completely sutured. Some megacrysts of potassium feldspar consist of non-turbid crosshatch-twinned potassium feldspar ovoid cores that are mantled by thin, approximately 0.4- to 0.5-mm-wide, borders of additional potassium feldspar. These borders comprise an inner zone of very complexly sutured potassium feldspar that appears to be developing at the expense of the crosshatch-twinned core and an outer zone of potassium feldspar that (1) is very turbid (largely because of the presence of numerous minute crystals of opaque mineral(s)) and that (2) forms a crustified lining for definitely paragenetically very late quartz and (or) fluorite. We presume the borders of potassium feldspar grew in a predominantly hydrothermal postmagmatic

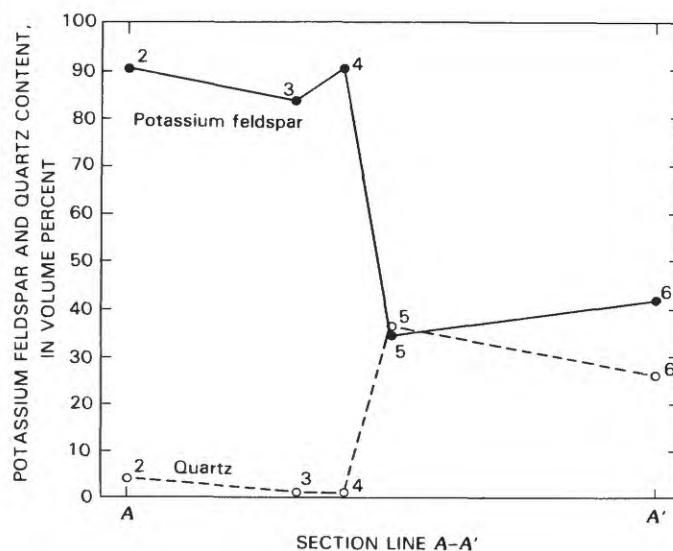


FIGURE 52.—Variation in potassium feldspar and quartz along section line A-A' of figure 50. Numbers indicate analysis and location (see table 17, fig. 50).

environment. However, such turbid versus nonturbid textural relations in the megacrysts do not persist throughout the episyenitic rocks. Other samples include microcline megacrysts showing ovoid turbid cores that are mantled by wide nonturbid borders. All of these specific textural relations impart an overall granoblastic fabric to the rocks. Other episyenitic rocks that formed from fine-grained Early Proterozoic biotite monzogranite show, in places, wispy irregularly shaped comminuted domains of approximately 0.05-mm highly strained crystals of potassium feldspar. These fine-grained discontinuous domains are interstitial among fairly equant 0.4-mm crystals of potassium feldspar whose crystal boundaries initially were complexly sutured. In many of the episyenitic rocks studied, broken angular fragments of potassium feldspar, approximately 0.1 mm in their longest dimension, have been torn from some of the larger potassium feldspar megacrysts and are now included within secondary strain-free quartz which fills cavities. Elsewhere, rocks altered to episyenite are commonly reported as showing cataclastic phenomena (see Viladkar, 1980). In other samples at Gold Basin, some megacrysts of potassium feldspar are present as isolated crystals set in a fine-grained mesostasis of mostly potassium feldspar. Such megacrysts are largely strain free and show evidence of interrupted crystal growth wherein euhedral outer growth zones

mantle ovoid cores (fig. 53A). Hairline microveinlets of carbonate and white mica cut the megacryst, and open spaces at the edge of the megacryst are filled locally by iron oxide that has replaced earlier pyrite. High-magnification examination of the edges of the megacrysts reveals that they are complexly intergrown with the groundmass. In addition, many megacrysts show no compelling systematic textural relations with the groundmass from which their relative ages might be established confidently.

Two generations of quartz are apparently present in the episyenitic rocks. An early stage consists of very sparse rounded possibly resorbed inclusions of quartz that occur only in potassium feldspar crystals. The rounded quartz crystals generally are about 0.1 mm in their longest dimension and are set in equant potassium feldspar, some of which measure approximately 0.7 to 0.9 mm wide. In addition, some of the megacrysts of potassium feldspar larger than this include rounded quartz crystals together with other extremely small unidentifiable crystals all distributed unevenly around the periphery of former growth zones of the megacrysts. The most common textural relation between early-stage quartz and potassium feldspar is for the central parts of the feldspar to poikilitically host clusters of rounded quartz. These clusters are relict from a much earlier, presumably Early Proterozoic, weakly developed graphic texture in the biotite monzo-

TABLE 17.—Modal analyses, in volume percent, of thin sections from rocks in the general area of the occurrence of visible, disseminated gold cropping out in the southeastern part of the Gold Basin mining district

[Analysis number same as location number of figure 50; —, not found; total counts: 600 per sample]

Analysis -----	1	2	3	4	5	6
Sample -----	GM-1136d	GM-1134h	GM-1134k	GM-1134l	GM-1134m	GM-1134q
Potassium feldspar ---	91.7	90.3	83.8	90.2	34.1	47.6
Quartz -----	1	4.2	.3	.2	35.9	¹ 25.5
Plagioclase -----	—	—	—	—	—	15.3
Fluorite -----	.2	1.3	.2	1	—	—
White mica -----	1.3	.3	3.7	.3	17.5	² 11.3
Biotite -----	—	—	.2	—	—	1.8
Chlorite -----	—	—	—	—	—	³ 2.6
Opaque mineral(s) ⁴ ---	3.5	3	10.5	4.3	12.5	.4
Epidote -----	—	—	—	—	—	1.2
Carbonate -----	1.8	.3	.3	3.3	—	—
Apatite -----	.3	.5	.5	.3	—	.2
Zircon -----	.2	—	.5	.3	—	.2
Total -----	100	99.9	100	99.9	100	100.1

¹Quartz contains moderately abundant concentrations of rutile.

²Bulk of the white mica replaces plagioclase.

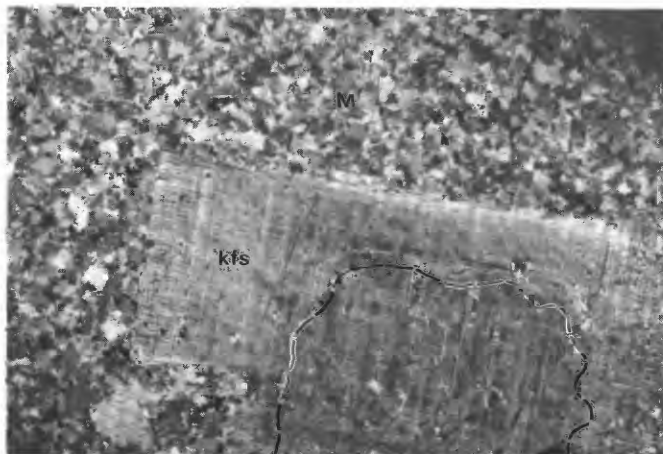
³Chlorite occurs as replacement of primary biotite.

⁴Mostly specular hematite and limonite after pyrite.

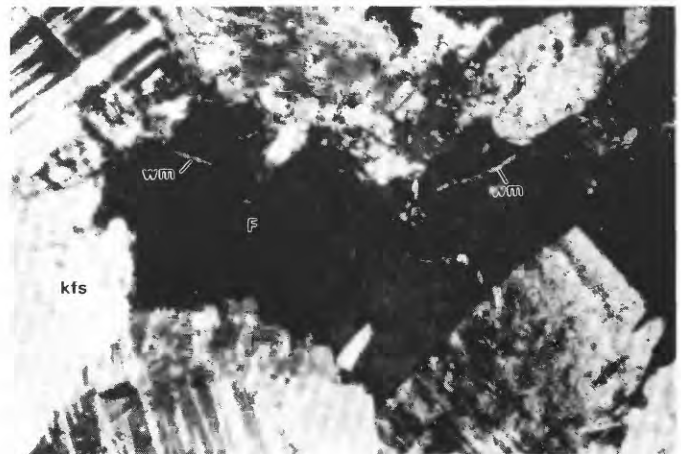
1. Episyenitic rock, coarse grained.
2. Episyenitic rock, coarse grained.
3. Episyenitic rock, fine grained.
4. Episyenitic rock, coarse grained.
5. Silicified and sericitized rock at margin of episyenitic rocks.
6. Biotite monzogranite, partly altered.

granite. Furthermore, relatively stout crystals of rutile are conspicuous in some of this early quartz. Relatively abundant rutile is present in some of these early-stage quartz crystals. A mass of rutile crystals remained in the residue from episyenitic rock digested in hydrofluoric acid (fig. 53B). Primary medium-grained quartz in the biotite monzogranite that surrounds the episyenite also contains abundant rutile. The presence of rutile may be used to differentiate between primary and secondary quartz in the contact zone of the episyenite.

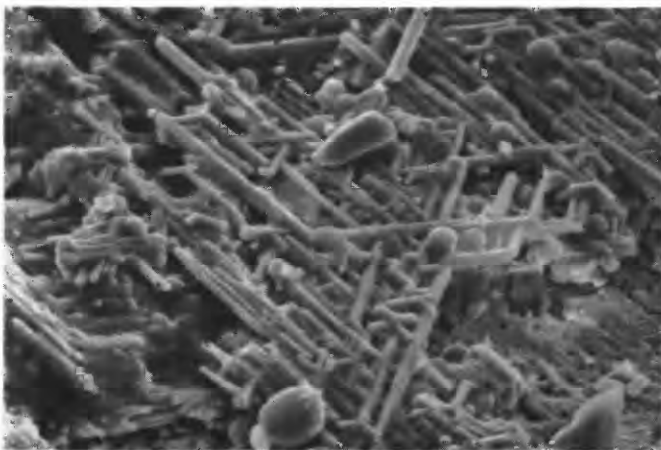
Most of the quartz in the episyenite is a late mineral which partly fills the spaces between euhedrally terminated potassium feldspar crystals. Other minerals in these spaces which are paragenetically about the same age as the late quartz include white mica, apatite, fluorite, pyrite (now altered mostly to limonite and (or) specular hematite), and native gold. Typically in the episyenite, white mica and carbonate are intergrown with each other interstitial to fresh potassium feldspar. A cavity filled mostly by fluorite is shown in figure 53C. Many of the



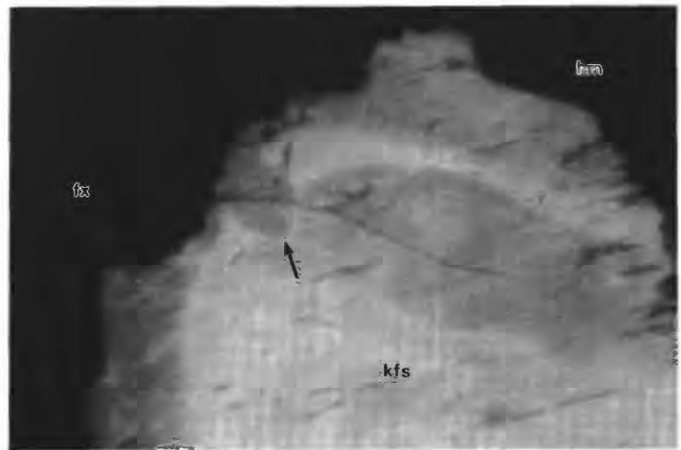
A 0 10 MILLIMETERS



C 0 0.3 MILLIMETER



B 0 20 MICROMETERS



D 0 1 MILLIMETER

FIGURE 53.—Photomicrographs and scanning electron micrograph of relations in episyenitic rock. *A*, Megacryst of crosshatch-twinned potassium feldspar (kfs) set in fine-grained (average size 0.4 mm) mesostasis (M) of mostly potassium feldspar, but including sparse amounts of carbonate, iron oxide(s), and white mica. Megacryst contains ovoid core (dashed outline) that is mantled by euhedral potassium feldspar. Partly crossed nicols. Sample GM-280b (I). *B*, Scanning electron micrograph showing mat of rutile needles in residue remaining after decomposing episyenitic rocks in hydrofluoric acid. Sample

GM-280-51. *C*, Cavity in episyenitic rock filled by fluorite (F) and sparse amounts of white mica (wm). kfs, potassium feldspar. Crossed nicols. Sample GM-280b. *D*, Cathodoluminescent zonation in potassium feldspar (kfs) from episyenitic rock. Crystal of potassium feldspar is mantled partly by specular hematite (hm) and other iron oxide-stained potassium feldspar (fx). At head of arrow, zonation crosscuts regular growth zones in potassium feldspar and is scalloped toward core of potassium feldspar.

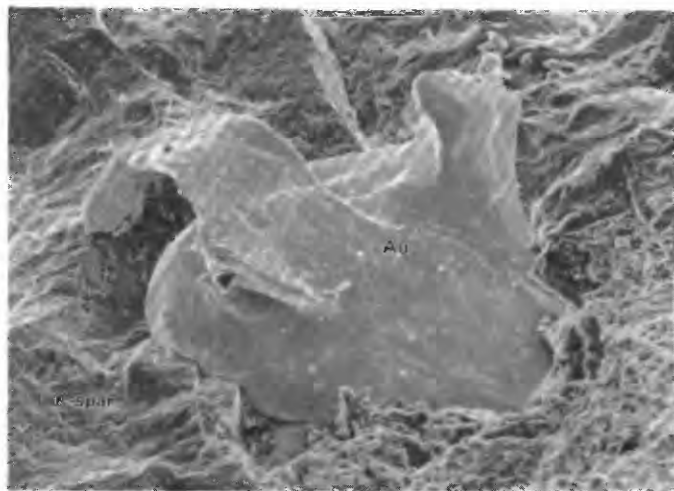
potassium feldspar crystals in direct contact with the minerals in the spaces, mostly quartz, show no visible signs of alteration when examined in ordinary light under the microscope. However, when such boundaries were examined using cathodoluminescence on polished thick sections it was seen that the typically regular and oscillatory growth zones in the potassium feldspar megacrysts marginally have been significantly disrupted by zones that luminesce (fig. 53D). These zonations are scalloped toward the cores of the potassium feldspar megacrysts and are apparently related to adjacent areas of potassium feldspar which are heavily stained by iron oxide and thus do not luminesce because of their high iron content. The scalloped zonations may reflect domains of base leaching or base exchange (sodium for potassium) related chemically either to the final filling of the interstitial spaces, to the enrichment of Fe^{3+} in the late-stage fluids and its substitution structurally in the potassium feldspar (Mariano, 1979), or to subsequent alteration in the zone of oxidation.

The approximately 1-m-thick zone of silicified and sericitized rocks which surrounds the episyenitic rocks shows significant variation in modal abundance and textures. In the silicified zone, which probably averages about 35 volume percent quartz in contrast to less than 5 volume percent in the episyenitic rock (table 17), subhedral almost tabular crystals of potassium feldspar about 6 to 8 mm long show combined Carlsbad and crosshatch twinning. These relatively large crystals appear to have grown as porphyroblasts in a largely subsolidus environment and to have been replaced partly by white mica concentrated in irregular patches. Such crystals also show inclusions of fine-grained ovoid quartz crystals similar to the primary quartz in the potassium feldspar megacrysts of the episyenite. However, the overall size of individual quartz crystals ranges widely in these silicified rocks and probably averages about 2.0 mm in the most quartz-rich domains. In these domains, textures are largely granoblastic, and quartz-quartz boundaries are highly sutured. Similar to the sparse primary quartz in the episyenitic rocks, quartz in the silicified zone is also strongly rutiled, which suggests that primary quartz (rutile bearing) was the site of nucleation for silica flooding marginal to the episyenite. Fluid inclusions are very abundant in the quartz and are mostly concentrated along annealed microfractures that cut the quartz grains. Many of these fluid inclusions contain liquid CO_2 at room temperature. In addition, the silicified and sericitized rocks contain fairly high concentrations of iron oxides that replace earlier crystallized pyrite. As shown in table 17, a typical sample from these altered rocks contains about 13 volume percent iron oxide(s). Paragenetically, the sulfide (probably pyrite) from which the iron oxide(s) has been derived is the same age as the white mica.

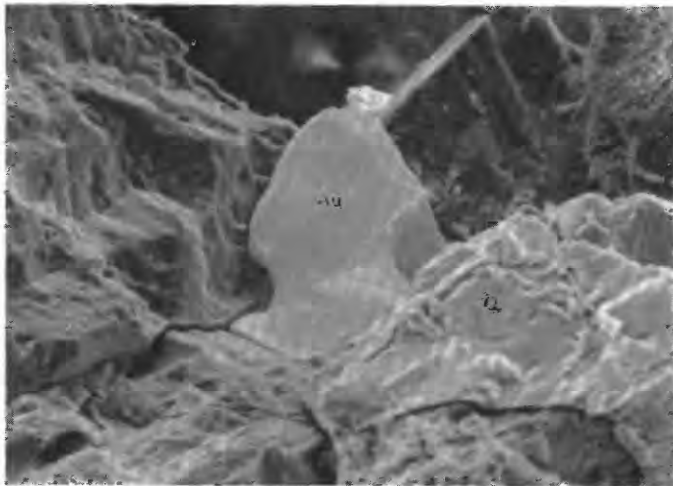
Minor sericitic alteration effects extend at least 4 m beyond the mapped outer limit of the silicified and sericitized halo. A sample of fine-grained Early Proterozoic biotite monzogranite from this general area (table 17 and fig. 52, analysis 6) shows a weakly developed gneissic fabric resulting from a dimensional orientation of primary quartz and biotite. The minimum content of plagioclase (sodic oligoclase, An_{10-15}) in these rocks is about 15 volume percent, but much of the white mica in the mode actually is present with or without epidote as a partial but ubiquitous replacement of plagioclase. Some of the individual crystals of white mica that replace plagioclase are fairly large, reaching lengths of about 0.4 to 0.5 mm. Dark-brown (Z axis) primary biotite is heavily altered to chlorite, with or without epidote and opaque minerals, including possibly magnetite and ilmenite. However, potassium feldspar in these rocks is quite fresh and contains abundant crosshatch twinning. Quartz, which here is obviously part of the igneous fabric of the rocks, contains conspicuous concentrations of needles of rutile. Minor accessories include apatite, zircon, and allanite. The presence of primary biotite, sericitized plagioclase, and abundant primary quartz provides a substantial mineralogical contrast with the potassium feldspar and fluffy orange carbonate-dominant mixed mineralogical assemblages in the episyenite.

PARAGENETIC RELATIONS OF GOLD

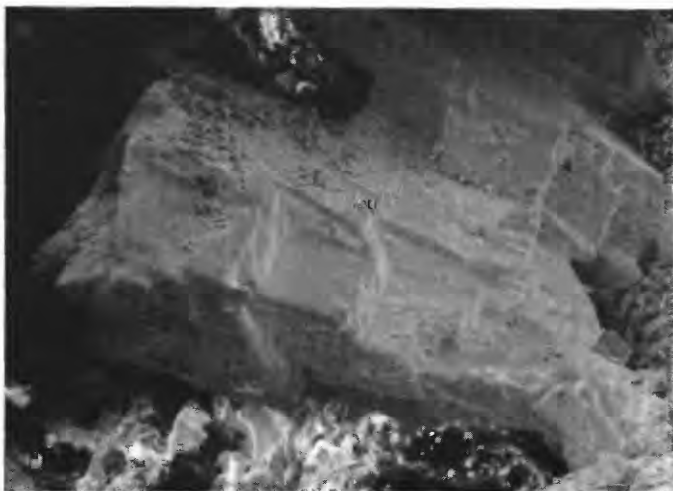
Textural relations of gold in the episyenitic rock were studied using the SEM and standard optical methods. Examination of artificially broken surfaces of episyenitic rock revealed that small nodules of gold in places rest either on potassium feldspar or quartz in the episyenitic rock (fig. 54A, B). Many of these nodules of gold are featureless in the episyenitic rocks, whereas others (fig. 54C) show forms suggesting that they had been molded against a cubic mineral, most likely pyrite. Thus, at least some of the gold in the episyenite must have been introduced quite late paragenetically, that is, after the pyrite. Some of the pyrite in the episyenite pipes also contained gold because some of the cubic vugs are now fringed by limonite and sparse amounts of free gold. Qualitative analyses of many nodules of gold from the pipes using an energy dispersive X-ray microanalyzer on the SEM revealed that in places they contain some silver and apparently some unknown amounts of iron. The relatively late introduction of native gold into the episyenitic pipes is suggested also by the inclusion in these rocks of some gold in carbonate, probably ferroan calcite (fig. 55A, B). As can be seen in polished sections (fig. 55A-C), specular hematite is locally quite abundant. In addition, small amounts of episyenite, ranging from about 9 to 200 g, were digested in hydrofluoric acid using the techniques of Neuerburg



A 0 120 MICROMETERS



B 0 60 MICROMETERS



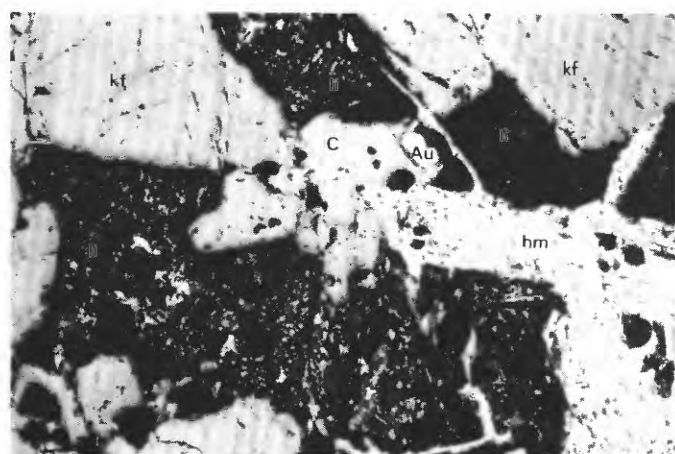
C 0 100 MICROMETERS

(1961, 1975). Residue from these procedures contained some intergrown purple fluorite and gold (fig. 56), thus documenting their penecontemporaneous, late-stage emplacement in the episyenite. Fluorite in the episyenite fills cavities most likely created during the leaching of primary quartz and plagioclase from biotite monzogranite.

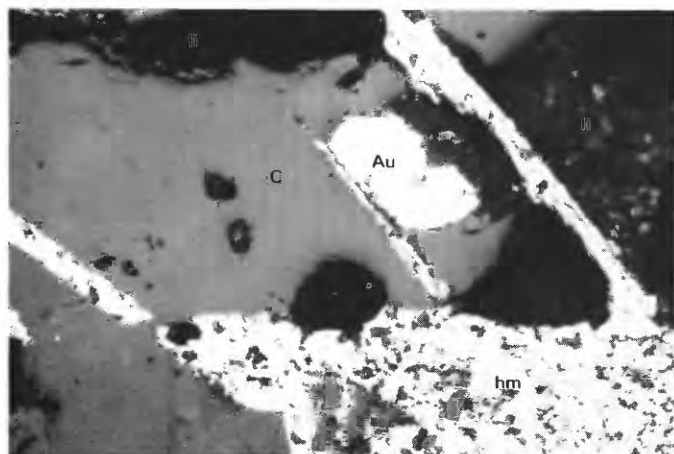
CHEMISTRY

Chemical analyses are available for four fist-size samples of episyenite (table 18, analyses 1–4), three adjoining samples of the contact zone surrounding one of the pipes (table 18, analyses 5–7), and, as a comparison, a sample of fine-grained Early Proterozoic biotite monzogranite (table 18, analysis 8) collected about 15 m southwest of the westernmost episyenite pipe (fig. 50). One of the samples of episyenite (table 18, analysis 1) is from the westernmost pipe. The three remaining samples of episyenite (table 18, analyses 2–4) and the three samples analyzed from the contact zone are all from the episyenitic pipe on the east (fig. 50). Precise quantitative values of metasomatic additions and subtractions of all elements involved during the entire process of episyenitization are difficult to calculate because of the dynamic chemistry and numerous stages of the event. However, the early stages of episyenitization involved (1) addition of potassium and probably barium and removal of silica, sodium, magnesium, and calcium and (2) an overall increase of the porosity of the rock. The samples of episyenite contain more than 14 weight percent K_2O and approximately 0.4 weight percent Na_2O . The content of normative potassium feldspar in the four samples of analyzed episyenite is in the range 83 to 91 weight percent; normative albite is in the range 1.7 to 4.3 weight percent (table 18). These values of normative potassium feldspar are quite similar to the modal contents of 84 to 92 volume percent found in the episyenite (table 17). Silica contents in the four analyzed samples of episyenite are in the range 56 to 65 weight percent. These values contrast significantly with the 1-m-wide contact zone of silicification and sericitization surrounding the episyenitic pipes and with nearby

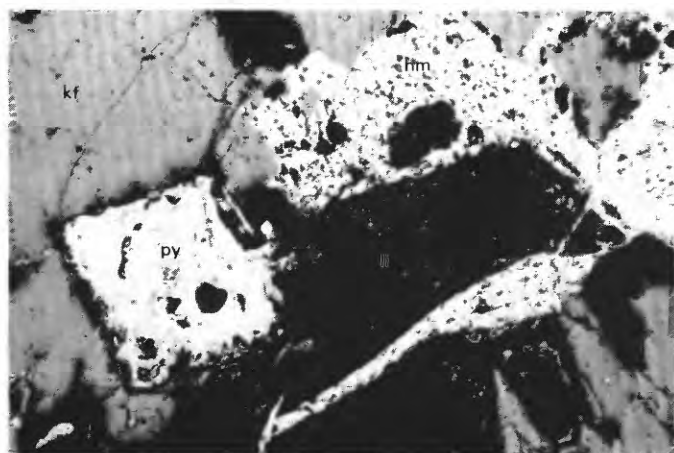
FIGURE 54.—Scanning electron micrographs showing gold disseminated in episyenitic rock from Gold Basin mining district (loc. 19, table 11). *A*, Small nodule of gold (Au) containing some silver and iron resting on potassium feldspar (K-spar). Upper surface of gold nodule apparently was abraded when rock was fractured before mounting sample in microscope. *B*, Small mass of gold (Au) resting against groundmass of secondary quartz (Q) that is present locally in minor amounts in episyenitic rock. Gold is featureless and shows no apparent crystal form. *C*, Small mass of gold (Au) obtained from heavy-mineral concentrate collected from episyenite. Gold appears to have been formed against cubic mineral, most probably pyrite. Silver was detected in gold using X-ray analyzer.



A 0 0.3 MILLIMETER



B 0 0.1 MILLIMETER

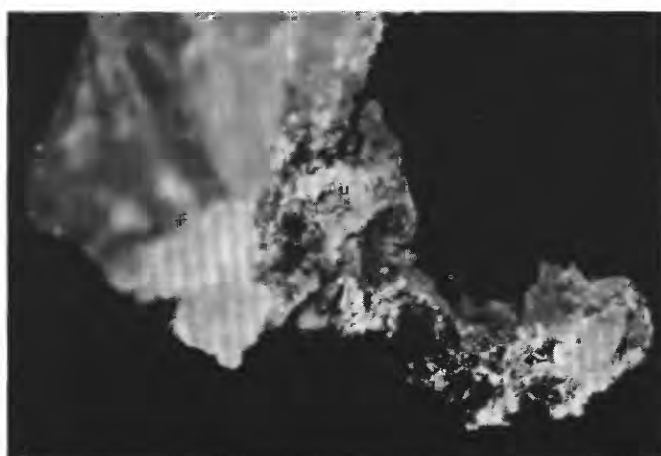


C 0 0.5 MILLIMETER

FIGURE 55.—Coarse-grained episyenite containing visible gold. Sample GM-280b. Plane-polarized reflected light of polished section. A, Textural relations of gold (Au), carbonate (C), potassium feldspar (kf), specular hematite (hm), and limonite (li) in A. B, Closeup view showing details of relations among gold (Au), carbonate (C), specular hematite (hm), and limonite (li) in A. C, Slightly oxidized cube of pyrite (py), potassium feldspar (kf), specular hematite (hm), and limonite (li).

Early Proterozoic biotite monzogranite (table 18) that forms the protolith of much of the episyenite. A graphic comparison of normative potassium feldspar, normative albite, and normative quartz among the episyenite, the contact zone, and the biotite monzogranite is shown in figure 57. Initially, episyenitization involved leaching of primary quartz, simultaneous breakdown and removal of many chemical constituents composing plagioclase and biotite, and metasomatic addition of potassium. Total iron (as Fe_2O_3) makes up about 1 weight percent of the three samples of episyenite most deficient in CO_2 (table 18, analyses 1, 2, 4), whereas Fe_2O_3 makes up almost 2.8 weight percent of the sample (table 18, analysis 2) of episyenite which has the highest content of CO_2 (3.6 weight percent). Most of the Fe_2O_3 in this particular sample must be in late-stage ferroan carbonate, which fills vugs. Some iron also may have been fixed finally as limonite or specular hematite that replaced an early epigenetic stage of pyrite. More realistic estimates of the overall distribution of iron in the episyenitic pipes may be inferred from table 17, which shows modal opaque mineral(s) in episyenite to range from about 3 to 11 percent by volume.

Apparently no major metasomatic addition of alumina occurred to the pipes during episyenitization. The analyzed sample (table 18, analysis 8) from the biotite monzogranite is peraluminous and shows a 1.09 value for $\text{Al}_2\text{O}_3:(\text{K}_2\text{O} + \text{Na}_2\text{O} + \text{CaO})$ in molecular percent. The sample is also corundum normative (1.5 weight percent C, table 18). This degree of alumina saturation may reflect removal of some calcium accompanying partial alteration of plagioclase during the Proterozoic greenschist metamorphic event. Such alumina saturation seemingly has been preserved during the Late Cretaceous and (or) early



0 2 MILLIMETERS

FIGURE 56.—Morphologic relations of intergrown fluorite (F) and gold (Au), which are residues separated from small (about 9 g) sample of episyenite by decomposing episyenite in hydrofluoric acid (see text).

TABLE 18.—Analytical data of Late Cretaceous episyenite, of the contact zone of the episyenite, and of the adjoining host Early Proterozoic biotite monzogranite

[Chemical analyses: 1 and 2, P.L.D. Elmore and S. Botts, analysts. Methods used are those described in Shapiro and Brannock (1962), supplemented by atomic absorption (Shapiro, 1967). 3-8, major oxides by X-ray spectroscopy, J.S. Wahlberg, J. Taggart, and J. Baker, analysts; partial chemical analyses by standard methods, P.R. Kloock and J. Rivello, analysts. Chemical analysis for gold (1 and 2) by a combined fire-assay atomic-absorption technique; Leung Mei, analyst. Spectrographic analyses by Chris Heropoulos (1, 2) and J. Kent (3-8). Results are reported to the nearest number in the series 1, 0.7, 0.5, 0.3, 0.2, 0.15, 0.1, 0.07, and so forth, which represent midpoints of interval data on a geometric scale. The precision of a reported value is approximately plus or minus one series interval at 68-percent confidence and two intervals at 95-percent confidence. Looked for but not found: As, Bi, Cd, Pd, Pt, Sb, Te (1, 2), U (1, 2), W (1, 2), Ge (3-8), Hf, In, Li (1, 2), Re, Ta (1, 2), Th (1, 2), Tl (1, 2), Pr (1, 2), Sm (1, 2), Eu (1, 2). —, not detected; N.D., not determined]

Analysis -----	1	2	3	4	5	6	7	8
Sample -----	GM-280	GM-280b	GM-1134k	GM-1134l	GM-1134m	GM-1134n	GM-1134o	79GM12
Chemical analyses (weight percent)								
SiO ₂ -----	62.2	64.4	56.1	60.8	75.2	76.9	76.0	72.9
Al ₂ O ₃ -----	17.7	18.4	16.7	17.6	10.9	10.1	9.94	13.4
Fe ₂ O ₃ -----	.90	1	2.77	.97	2.31	1.78	2.63	2.15
FeO -----	.12	.44	.03	.03	.26	.17	.70	1.05
MgO -----	.00	.00	.20	<.10	.24	.17	.34	.36
CaO -----	1.8	.30	4.41	1.83	.35	.72	.49	.85
Na ₂ O -----	.50	.40	.21	.28	.28	<.15	<.15	2.54
K ₂ O -----	14.5	14.3	14.1	15.2	7.84	7.80	7.3	6.08
H ₂ O ⁺ -----	.43	.54	.50	.18	.56	.38	.47	.64
H ₂ O -----	.00	.02	.04	.06	.08	.08	.12	.06
TiO ₂ -----	.44	.66	.57	.58	.34	.33	.54	.31
P ₂ O ₅ -----	.00	.12	.12	<.05	.09	.09	.13	.06
MnO -----	.02	.03	.05	<.02	<.02	<.02	<.02	.04
CO ₂ -----	.08	<.05	3.60	.84	.12	.46	.29	.06
F -----	1.1	.06	.15	.53	.21	.13	.16	.07
Cl -----	N.d.	N.d.	.010	.006	.004	.005	.004	.004
S -----	N.d.	N.d.	.001	<.001	.019	.028	.022	.17
Subtotal -----	99.79	100.67	99.56	98.91	98.80	99.14	99.14	100.74
Less O=F, Cl -----	.46	.03	.06	.22	.09	.05	.07	.03
	99.33	100.64	99.50	98.69	98.71	99.09	99.07	100.71
Semiquantitative spectrographic analysis (weight percent)								
Ag -----	<.00007	<.00007	---	---	---	---	---	---
B -----	---	---	.0006	---	.0012	.0006	.0007	.007
Ba -----	.3	.3	.1	.31	.095	.097	.13	.026
Be -----	---	---	---	---	---	---	.0003	.0007
Co -----	---	---	.0002	---	.0002	---	.0003	.0003
Cr -----	.0005	.001	.0019	.0009	.0005	.0007	.0008	.0002
Cu -----	.0002	.0015	.0024	.0016	.0007	.0067	.0037	.0002
La -----	.01	.03	.03	.032	.0097	.016	.023	.024
Mo -----	.0005	.001	.003	.0007	.0009	.0009	.0009	.0003
Nb -----	.0015	.005	.0076	.0059	.0038	.0038	.0069	.0054
Ni -----	---	---	.0003	---	.0003	.0002	.0003	---
Pb -----	.05	.003	.11	.034	.032	.0052	.0046	.0058
Sc -----	---	.0005	---	---	---	---	---	---
Sn -----	---	---	.0011	.0006	.0009	.0007	.0014	.0008
Sr -----	.02	.015	.01	.008	.0058	.0073	.0072	.0093
V -----	.0007	.001	.0023	.0042	.0036	.0018	.0033	.0015
Y -----	.002	.01	.0072	.0069	.0075	.013	.012	.0036
Zn -----	---	---	.018	.0022	.0014	.0022	.0031	.002
Zr -----	.02	.03	.055	.068	.011	.02	.051	.02
Ce -----	.02	.07	.065	.05	.011	.027	.047	.047
Ga -----	.002	.0015	.0016	.0012	.0017	.0012	.0016	.0019
Yb -----	.0002	.001	.0009	.0006	.0005	.0007	---	.0003
Nd -----	.007	.02	---	---	---	---	---	---
Chemical analyses (parts per million)								
Au -----	0.8, 1.1	1.6, 1.4						
Hg -----	N.D.	N.D.						
Zn -----	N.D.	N.D.						

Tertiary emplacement of the episyenite pipes. The mean of those three analyzed samples of episyenite having minimal contents of CO₂ (table 19, analysis 1) shows that the episyenite is saturated similarly with respect to alumina. The value of Al₂O₃:(K₂O + Na₂O + CaO) in molec-

ular percent for the average analysis of episyenite is 0.95. However, if the content of CaO is adjusted to account for the late-stage fluorine and carbonate in the rock, then the average of the episyenite samples analyzed has a 1.04 value for Al₂O₃:(K₂O + Na₂O + CaO) in molecular percent.

TABLE 18.—Analytical data of Late Cretaceous episyenite, of the contact zone of the episyenite, and of the adjoining host Early Proterozoic biotite monzogranite—Continued

Analysis -----	1	2	3	4	5	6	7	8
Sample -----	GM-280	GM-280b	GM-1134k	GM-1134l	GM-1134m	GM-1134n	GM-1134o	79GM12
CIPW norms (weight percent)								
Q -----	3.7	7.3	0.98	1.1	43.9	46.5	47.4	32.8
C -----	1.1	2.2	1.1	.71	2.	1.4	1.8	1.5
or -----	86.3	83.9	83.8	91	47	46.5	43.5	35.7
ab -----	4.3	3.4	1.7	2.3	2.4	1.3	1.3	21.4
an -----	.37	.03	---	---	---	---	---	3
hl -----	---	---	.02	.02	---	---	---	---
en -----	---	---	---	---	.33	.13	.37	.89
mt -----	---	---	---	---	---	---	.69	2
hm -----	.91	.99	2.8	.98	2.3	1.8	2.2	.76
il -----	.3	.99	.17	.11	.55	.33	1	.59
ru -----	.29	.14	.48	.53	.05	.16	---	---
ap -----	---	.28	.29	.12	.22	.22	.31	.14
fr -----	2.3	.10	.29	1.1	.33	.25	.31	.13
pr -----	---	---	---	---	.04	.06	.04	.32
cc -----	.18	.11	7.3	1.8	---	.76	.18	.14
mc -----	---	---	.42	.02	.23	.25	.41	---
Total	99.7	99.4	99.4	99.8	99.4	99.7	99.5	99.4
Salic -----	95.6	96.8	87.6	95.1	95.3	95.7	94.	94.4
Femic -----	4.1	2.6	11.8	4.7	4.1	4	5.5	5
¹ D. I.	94.3	94.6	86.5	94.4	93.3	94.3	92.2	89.9

¹Differentiation index of Thornton and Tuttle (1960), defined as the total of normative quartz plus normative orthoclase plus normative albite.

1. Episyenite, loc. 19, table 11 and plate 1; obtained from the westernmost pipe shown on figure 50.
2. Episyenite, loc. 19, table 11 and plate 1; obtained from the easternmost pipe shown on figure 50.
3. Episyenite, loc. 19, table 11 and plate 1; obtained from the westernmost pipe shown on figure 50.
4. Episyenite, loc. 19, table 11 and plate 1; obtained from the westernmost pipe shown on figure 50.
- 5-7. Contact zone surrounding easternmost episyenite pipe (see fig. 50).
8. Fine-grained Early Proterozoic biotite monzogranite collected 15 m southwest of westernmost pipe on figure 50.

DISCUSSION

The mineral assemblages, chemistry, and genetically associated two-mica monzogranite of the episyenite pipes in the Gold Basin district closely resemble similar rocks elsewhere hosted by an assortment of geologic environments. Uranium-bearing episyenite and unmineralized episyenite are present in upper Paleozoic two-mica granite of the Central France Massif (Moreau and Ranchin, 1973). Emplacement of the mineralized episyenite there included (1) an almost total removal of primary plagioclase and primary quartz from the two-mica granite, (2) conversion of primary biotite to chlorite, (3) subsolidus crystallization of additional white mica, and (4) an increased porosity of the rock. Viladkar (1980) also found a substantial reduction in silica during the development of the fenitized or episyenitized aureole around the Newmania carbonatite, Rajasthan, India. The final stages of mineralization in the episyenite pipes in the Central France Massif

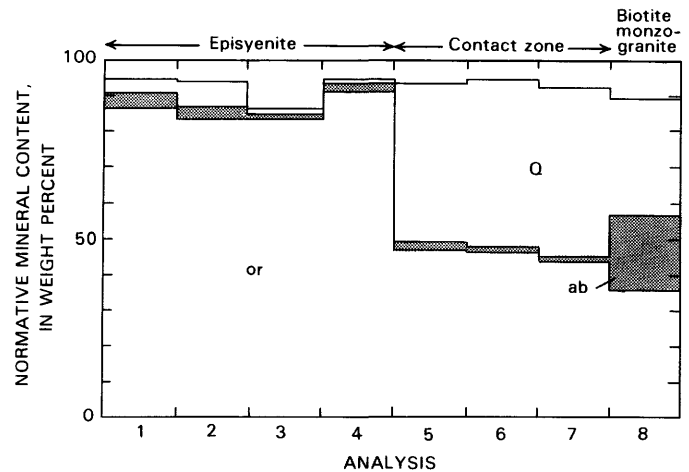


FIGURE 57.—Normative potassium feldspar (or), normative albite (ab), and normative quartz (Q) in analyzed samples of Late Cretaceous and early Tertiary episyenite, contact zone of episyenite, and nearby sample of Early Proterozoic biotite monzogranite. Data from table 18.

resulted in the partial filling of the leached cavities by carbonate(s), hematite, pitchblende, and some secondary quartz (Moreau and Ranchin, 1973). The chemistry of other episyenitic alteration zones or fenites associated with some carbonatite complexes is very similar to the chemical makeup of the episyenites at Gold Basin. This relation is shown in the analyses of selected samples of potash trachyte and fenitized granitic rock from an area of carbonatites at Toror Hills, Uganda, feldspar-rock xenoliths in carbonatite from Amba Dongar, India, and microcline from the Palabora, South Africa, carbonatite area listed in table 19 (compare analysis 1 with analyses 4-7). These latter analyses show K_2O contents that range from about 10 to 15 weight percent and extremely high K_2O to Na_2O ratios. The partial analysis for SiO_2 , Na_2O , and K_2O of a sample of fenitized granitic basement (table 19, analysis 4) and the average sample of episyenite analyzed from the Gold Basin district are similar. In addition, fluorite, apatite, and pyrite are common late-stage accessory minerals in many episyenitic rocks or fenitic rocks associated with carbonatite complexes (Smirnov, 1976), and fluorite even is present in economically important tonnages and grades in some of them (Deans and others, 1972). Parisite, a mineral ideally having the composition $(Ce,La)_2Ca(CO_3)_3F_2$ (Roberts and others, 1974),

also was reported by Blacet (1969) to be present rarely in these episyenitic rocks in the Gold Basin district. Parisite is considered by Smirnov (1976) to be one of the accessory minerals typically developed in carbonatite complexes, but important concentrations of gold are not generally known to be associated with such complexes (see Smirnov, 1976; Boyle, 1979). Some carbonatites, however, contain measurable amounts of gold. Copper concentrate from the Palabora, South Africa, carbonatite is reported to contain 0.05 troy ounces gold and 24.5 troy ounces silver per ton (Hanekom and others, 1965, p. 158). Furthermore, Rubie and Gunter (1983) report that potassic episyenite, as opposed to sodic episyenite, is only found to be associated with carbonatite. Owing largely to the fact that we have not recognized any carbonatite of Late Cretaceous and (or) early Tertiary age in the Gold Basin and Lost Basin mining districts, we conclude tentatively that a fairly unique set of geologic circumstances may have contributed to the development of the gold-mineralized episyenite there.

Our study of the gold-bearing episyenitic pipes suggests a protracted passage of potassium-charged and silica-deficient fluids initially occurred through a narrowly confined series of vents. This streaming of fluids eventually culminated in the late-stage deposition of gold there.

TABLE 19.—*Chemical analysis of average episyenite from Gold Basin and chemical analyses of other syenitic and episyenitic rocks from elsewhere*
[---, not detected; N.D., not determined or not listed]

Analysis -----	1	2	3	4	5	6
Chemical analyses (weight percent)						
SiO_2 -----	62.5	58.58	58.43	62.73	67.52	63.62
Al_2O_3 -----	17.9	16.64	17.84	N.D.	13.58	18.27
Fe_2O_3 -----	.96	3.04	5.09	N.D.	4.71	1.18
FeO -----	.20	3.13	---	N.D.	.20	.09
MgO -----	---	1.87	.43	N.D.	1.03	.10
CaO -----	1.31	3.53	.80	N.D.	1.62	.80
Na_2O -----	.39	5.24	.38	.38	.40	.63
K_2O -----	14.7	4.95	13.9	14.97	10	14.38
H_2O^+ -----	.38	.99	1.05	N.D.	1.04	.18
H_2O^- -----	.03	.23	.11	N.D.	N.D.	N.D.
TiO_2 -----	.56	.84	.34	N.D.	.09	.11
P_2O_5 -----	.03	.29	.35	N.D.	.33	.12
MnO -----	.02	.13	.42	N.D.	N.D.	.02
CO_2 -----	.31	.28	N.D.	N.D.	.20	.26
F -----	.56	N.D.	N.D.	N.D.	.30	N.D.
Subtotal ----	99.85	99.74	99.32	N.D.	100.89	99.94
Less O=F ----	.24	N.D.			.13	
Total -----	99.61	99.74			100.76	

1. Episyenite (loc. 19, table 11). Average of analyses 1, 2, and 4 (table 18).
2. Syenite of LeMaitre (1976).
3. Potash trachyte, Toror Hills, Uganda (Sutherland, 1965a, p. 370).
4. Partial analysis, fenitized granitic basement, Toror Hills, Uganda (Sutherland, 1965a, p. 371).
5. Feldspar rock xenoliths in carbonatite, Amba Dongar, India (Deans and others, 1972, p. B5).
6. Microcline, Palabora, South Africa (Hanekom and others, 1965).

These episyenitic pipes are further envisaged as representing structurally deeper levels of mineralization than the veins in the districts. We infer that the early-stage fluids increased porosity and thereby enhanced permeability at the sites of the vents primarily by leaching primary quartz and primary plagioclase from the rocks. This facilitated a continued circulation of late-stage fluid(s) associated with the introduction of gold and its accompanying pyrite, fluorite, hematite, secondary quartz, carbonate, and white mica. Although two determinations of the age of white mica from the episyenite yielded anomalously old ages (127 and 130 Ma), we nonetheless maintain that the process of episyenitization and the introduction of gold into the episyenitic rocks is related temporally and genetically to a Late Cretaceous, two-mica magmatic event. As discussed in the section "K-Ar Chronology of Mineralization and Igneous Activity" these anomalously old ages may reflect contamination of the evolving episyenite by radiogenic argon relict from the enclosing Early Proterozoic rocks or contamination of the samples dated by Proterozoic mica and (or) feldspar. As will be shown in the section "Fluid-Inclusion Studies," the late-stage fluids in the fluorite-bearing and gold-bearing episyenitic rocks are the same chemically and approximately the same temperatures as those in a well-studied fluorite-bearing vein, which cuts the Late Cretaceous two-mica monzogranite north of the Cyclopic mine as well as many other veins throughout the districts. This vein has been dated at 68 Ma, and white mica from the two-mica monzogranite yields an age of 72 Ma.

VEINS ALONG THE MIOCENE DETACHMENT FAULT

Blocks of presumed Late Cretaceous and (or) early Tertiary mineralized quartz veins crop out along the Miocene detachment fault in the open-cut and underground workings at the Cyclopic mine (P.M. Blacet, unpub. data, 1967-72). The workings at the Cyclopic mine, the deposit showing the largest production of lode gold from the districts to date, consist of a series of open-cuts and shallow underground drifts along a strand of Miocene detachment fault that has been shown to be post-Muddy Creek Formation in age (Blacet, 1975). Some displacements along the detachment fault may have been localized by shallow-dipping zones of weakness dating from Late Cretaceous or early Tertiary time. The blocks of vein quartz, which are present sporadically in gouge of mostly the uppermost splay of the detachment zone, constitute the ore in the deposit. In the general area of the Cyclopic mine, the detachment zone in places consists of at least three stacked plates (Blacet, 1975). Here, the detachment zone shows an approximately N. 50° W. strike, although individual splays along the zone show marked departures from the general trend. Further, some of the individual

splays at the surface crop out across at least 40 m in some of the open-cuts of the mine and can be traced at the surface as much as 1.2 km, as noted previously by Schrader (1909). However, the lowermost surface of some of these splays locally forms a very sharp, almost planar contact with the underlying metamorphic rocks (fig. 58A). In such well-exposed outcrops, the hard yellow-brown gouge zone resting immediately on the metamorphic rocks shows very faint striations that trend subparallel to the northwesterly trend of the trace of the detachment fault. Although dips within the detachment fault zone generally are quite gentle, some open-cuts through individual splays reveal dips of approximately 50° to 55° in varicolored gouge zones that surround some of the large blocks of brecciated vein quartz caught up within the zone (fig. 58B). Some blocks of brecciated vein quartz are very resistant to weathering (fig. 58C) and together with the strong iron oxide staining form excellent markers along the individual fault splays that make up the overall Miocene detachment zone. The mineralogy of these mineralized tectonically bounded blocks of veins is the same as the Late Cretaceous and (or) early Tertiary veins. However, as pointed out by Schrader (1909, p. 125), the blocks of vein material at the Cyclopic mine apparently are not continuous to any great depth nor do they "have any definite fissure wall, but usually at a short distance below the surface [instead] give way to less firm material." Although the deposit at the Cyclopic is the only one known in the districts along the trace of the detachment fault, some dislocation surfaces elsewhere are reported to contain gold ore. Detachment surfaces associated with some cordilleran metamorphic core complexes in western Arizona and eastern California in places contain a chrysocolla-chalcopyrite-specular hematite-pyrite association, together with some barite and fluorite, that locally yielded values in gold (Reynolds, 1980; Wilkins and Heidrick, 1982).

PLACER GOLD DEPOSITS

Placer gold deposits in the Gold Basin-Lost Basin mining districts are primarily present in three areas. The most important deposits are within a 10-km by 3-km area along the east flank of the Lost Basin Range. Many reports refer to this area as the King Tut placer area. Some placer deposits were worked also in the northern part of the Gold Basin district where they are clustered in an approximately 6-km² area, about 2 km south-southeast of Golden Rule Peak (Blacet, 1975). In the Gold Basin district, the placers are reported to have contained gold in erratically distributed channels (U.S. Geological Survey, unpub. data, 1967). Finally, a few occurrences of placer gold were worked from the upper reaches of Quaternary gravel deposits along the west flank of the Lost Basin Range. Although the overall areal extent of

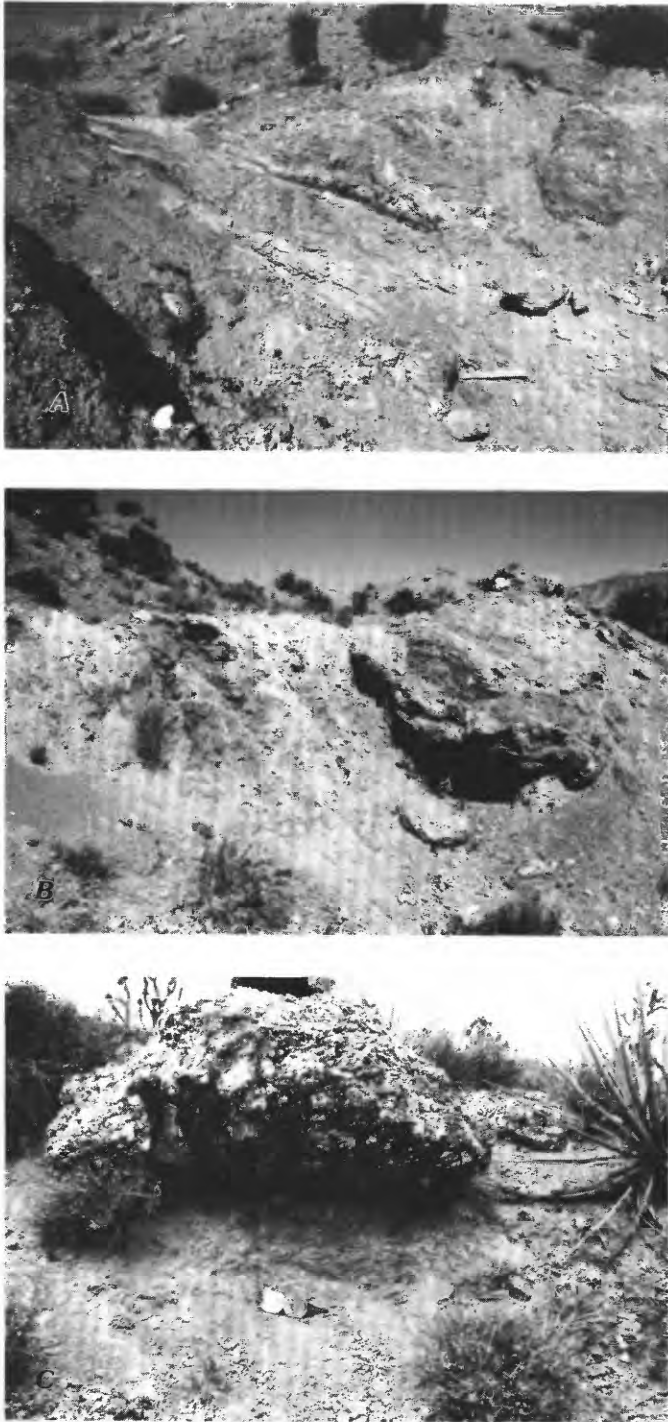


FIGURE 58.—Relations along Miocene detachment fault in general area of Cyclopic mine. *A*, South-dipping low-angle fault between Proterozoic metamorphic rocks on north and gouge along Miocene detachment surface. Hammer for scale. *B*, Discontinuous brecciated and unbrecciated blocks and fragments of mineralized vein quartz at extreme northwest end of large open-cut. Hammer on rock for scale. *C*, Large isolated block of brecciated vein quartz in flat-lying gouge zone between Early Proterozoic porphyritic monzogranite in hanging wall and mixed Early Proterozoic metamorphic rocks and Late Cretaceous two-mica monzogranite in footwall. Pocket compass for scale.

the deposits and occurrences along the west side of the Lost Basin Range is about the same as that along the east side of the range, by far the largest production is credited to the King Tut placer area on the east side of the range. Koschmann and Bergendahl (1968, p. 40) estimate that total minimum gold production of the Gold Basin district was about 15,000 oz. Most of this production was from lode deposits. Johnson (1972, pl. 1) appraises the total production of placer gold at 1,000 oz for each district, Gold Basin and Lost Basin.

The most economic concentrations of gold-bearing gravels were found in the placer deposits along the east flank of the Lost Basin Range. The highest grade gold-bearing gravels there are generally less than 1 m thick and are confined to present-day arroyo bottoms, where they have been concentrated above caliche-cemented false bed rock after having been reworked primarily out of the Muddy Creek Formation (J.D. Love, written commun., 1966, 1967; P.M. Blacet, unpub. data, 1967–72). The richest gold-bearing gravels were apparently concentrated along the upper reaches of these arroyos (Blacet, 1975). Concentrations of placer gold nuggets obtained mostly from the King Tut placer area include coarse and angular nuggets, many showing sharp ragged edges (fig. 59A), indicating that the nuggets have not traveled very far. In addition, some of the placer nuggets enclose rounded to angular granules of vein quartz (frontispiece; fig. 59B), suggesting that some solution and reprecipitation of gold may have taken place in the environment of the placer gravels. Heavy minerals also are relatively abundant in the gold-bearing alluvial sand and gravel (fig. 59B). Deaderick (1980) also reports that an abundance of black sand is associated with the placer gold; this black sand consists largely of partially oxidized cubes of pyrite, magnetite, garnet, ilmenite, hematite, and limonite. In addition, he notes that placer operations in the late 1970's recovered gold nuggets containing a significant amount of attached chalcedonic matrix, partly as inclusions within some of the nuggets.

The surface morphology of selected placer nuggets collected by a hand-operated dry washer (fig. 60) was examined using the SEM. A nugget from the King Tut placer area (fig. 61A) appears to be more worn than most from that general area, and this particular nugget shows, at very high magnifications, extremely well developed surface striae created during transport (fig. 61B). Such a nugget, in contrast to the more ragged and angular nuggets in the same general area, may have undergone major transport during a period of flash flooding in an otherwise generally arid type erosion cycle, or it may have been transported farther than the more angular nuggets. Yeend (1975) showed experimentally that most physical changes in placer gold nuggets occur by exposure to a turbulent high-energy environment. He further documented

that most physical changes reflect the effects of cobbles rather than sand and that gold is abraded faster by wet sand than by dry sand. Overall aspects of a "less worn appearing" nugget obtained from the northern Gold Basin mining district are shown in figure 61C. Many of the nuggets examined by the SEM show that the gold typically contains numerous cubic molds, indicating the former presence of pyrite or galena (fig. 61D), both of which are common minerals in the gold-bearing veins throughout

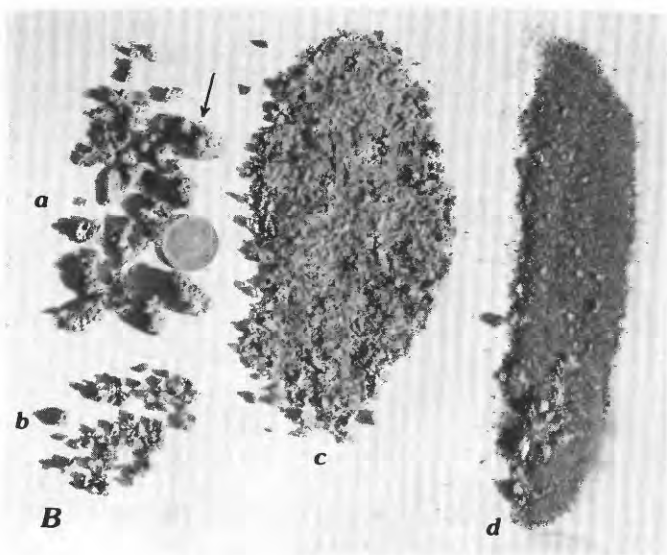
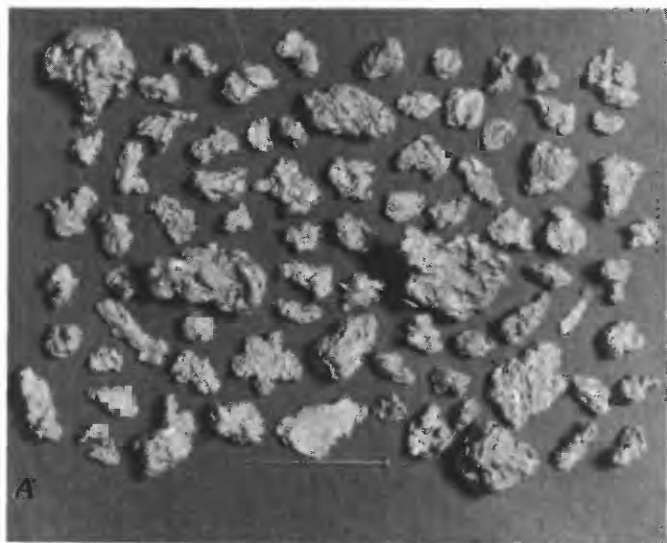


FIGURE 59.—Placer gold from Lost Basin mining district (J. David Love, written commun., 1966). *A*, Coarse angular nuggets of gold. Note 27-mm pin for scale at bottom of photograph. *B*, Varied sizes of concentrations of placer gold. U.S. dime for scale. *a*, coarsest nuggets showing an approximately 1.2-cm-wide composite nugget at head of arrow with gold partly enclosing a rounded granule of quartz; *b*, medium-size nuggets; *c*, small nuggets; *d*, nonmagnetic heavy-mineral concentrate in which all large fragments are gold.

the districts. Spot qualitative analyses of placer nuggets using the energy-dispersive X-ray microanalyzer on the SEM revealed commonly detectable silver and iron. The iron probably is a local surface coating.

Some nuggets contain relicts indicating the former presence of carbonate in their hypogene assemblage. A large, irregularly shaped, 11.9-g nugget obtained from placer workings in the NW $\frac{1}{4}$ sec. 3, T. 29 N., R. 17 W., approximately 2 km northeast of the main workings of the King Tut placers, shows extremely well developed rhombic molds (fig. 62). Measurement of the interfacial angles of these molds suggests that the carbonate may have been ankerite (R.C. Erd, written commun., 1969), which is common together with siderite in the quartz-carbonate \pm base metals \pm gold stages of the pegmatite-vein systems throughout the districts.

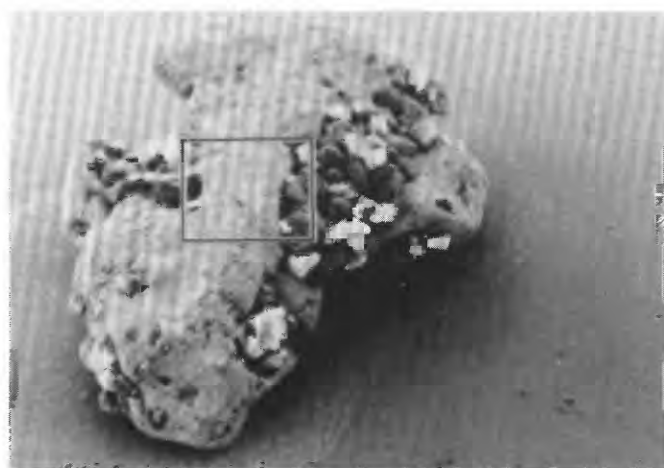
Although the overall geometry and concentrations of placer nuggets reflect fluvial processes, some microscopic features together with physical and chemical relations indicate limited remobilization has taken place locally in the placer environment. A sequence of scanning electron micrographs (fig. 63) at successively larger scales shows textural relations found between native silver and gold in a small nugget collected near the Golden Gate mine.



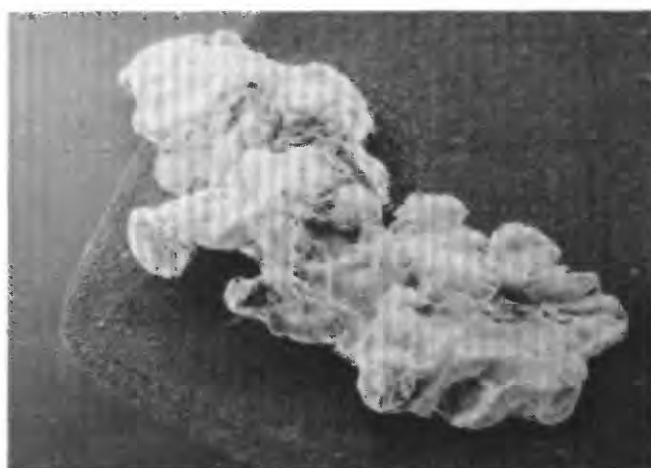
FIGURE 60.—Small, hand-operated dry washer used to collect heavy-mineral concentrates from unconsolidated sand and gravel in arroyo bottoms.

These relations between native silver and native gold were evaluated partly because Diman (1976) had determined previously that the association native silver-native gold is "forbidden" because of widely separate stability fields at elevated temperatures. The two metals can occur together under nonequilibrium conditions or at low temperature(s). Furthermore, Desborough (1970) has shown that most placer gold grains include a relatively thin rim of low silver content. Examination of this particular nugget at very high magnifications reveals that

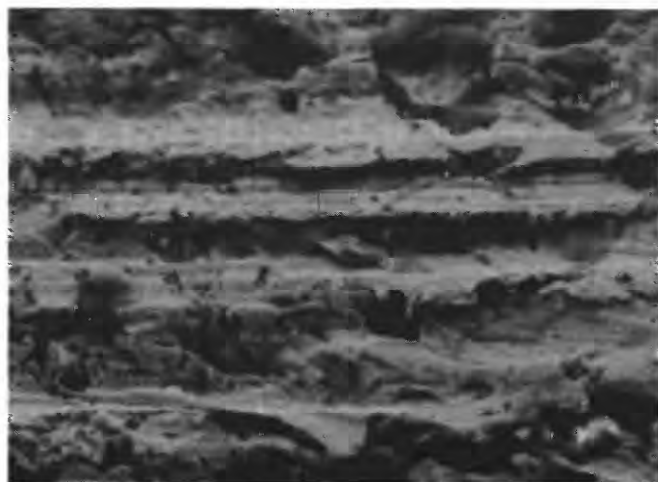
small oriented triangular facets of native silver, many approximately $5\ \mu\text{m}$ on a side, are present on the surface of the gold nugget (fig. 63B). These facets of silver, identified using the energy-dispersive microanalyzer, are raised slightly relative to the surrounding gold and are all oriented similarly. Observation of these relations at an even greater magnification (fig. 63C) shows that some of the extremely small facets of silver are even nested on one another but still retain the same overall orientation of their outlines. Energy-dispersive analysis of the silver



A 0 300 MICROMETERS



C 0 300 MICROMETERS



B 0 10 MICROMETERS



D 0 900 MICROMETERS

FIGURE 61.—Scanning electron micrographs of placer gold nuggets from Gold Basin-Lost Basin mining districts. *A*, Gold nugget from King Tut placer workings, NE $\frac{1}{4}$ sec. 9, T. 29 N., R. 17 W. Weight, 15.3 mg. Small amount of iron was detected in nugget using energy-dispersive analyzer. Rectangle indicates area shown in *B*. *B*, Enlargement of area outlined in *A* showing surface striae created during transport. *C*, Gold nugget from workings at Old Placers area (infor-

mal name), SW $\frac{1}{4}$ sec. 10, T. 29 N., R. 18 W., approximately 1.5 km northeast of Gold Hill mine. *D*, Gold nugget from site at Twin Yucca gulch (informal name), SE $\frac{1}{4}$ sec. 9, T. 29 N., R. 18 W., approximately 1 km north of Gold Hill mine. Weight, 38.9 mg. Nugget shows numerous cubic molds indicating former presence of euhedral crystals of pyrite. Small amount of silver was detected in nugget using energy-dispersive analyzer.

reveals no detectable gold, and analysis of the gold reveals no detectable silver. We suggest that the silver may reflect the following events in the placer environment: (1) Sedimentation of the detrital nugget of gold in the Quaternary gravel; (2) dissolution of silver from a nearby source in the gravels, possibly galena or cerrusite, at a relatively elevated Eh and, only locally, a somewhat acidic pH (see stability relations of gold and silver in water at 25 °C and 1 atm shown by Hallbauer and Utter, 1977); (3) final deposition of the silver on the surface of the gold, controlled largely by traces of {111} twin planes and primarily in response to a decline in the prevailing Eh of the overall system. Some experimental work suggests that such a succession of phenomena may have occurred. Sakharova and others (1979) showed that at room temperature and atmospheric pressure dislocations and other surface defects can control the actual sites where native silver precipitates onto placer minerals from silver-charged acid or alkaline solutions. Even if such a sequence of physical and (or) chemical events contributed toward what appears to be a very local and very minor accretionary phenomenon, we do not believe that a similar chemical mechanism should be used to explain "growth"

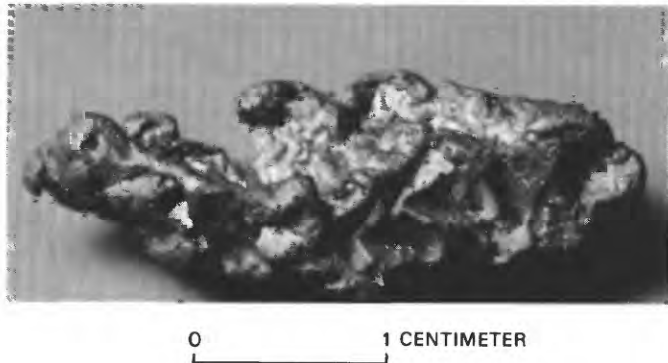
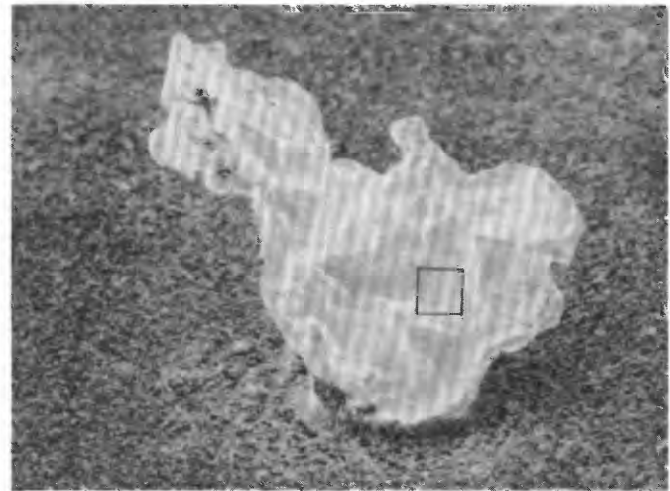
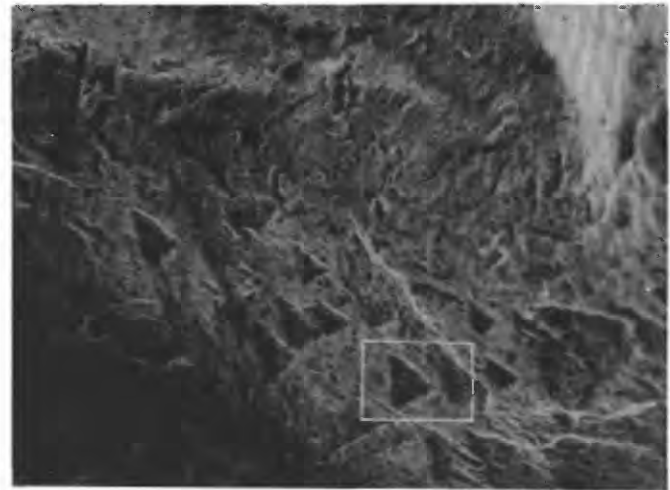


FIGURE 62.—Relatively large placer gold nugget from Lost Basin mining district showing extremely well developed rhombic molds (see text).



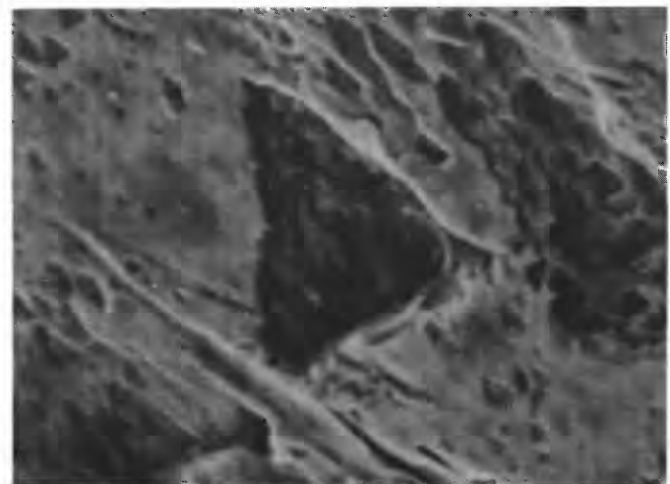
A

0 100 MICROMETERS



B

0 10 MICROMETERS



C

0 3 MICROMETERS

FIGURE 63.—Scanning electron micrographs of silver-gold relations in placer gold nugget obtained from northern part of Lost Basin mining district. Placer workings are near Golden Gate mine, NW¼ sec. 32, T. 30 N., R. 17 W. A. Overall irregular shape of entire nugget. Rectangle indicates area enlarged in B. B, Small oriented triangular facets of silver, approximately 5 μm on a side but ranging down to much less than 1 μm on a side, present on surface of gold nugget. Facets of silver are raised slightly relative to surrounding surface of gold nugget. Energy-dispersive analysis of triangular facets of silver reveals no detectable gold, and analysis of gold reveals no detectable silver. Outlined area is enlarged in C. C, Further enlargement of triangular facets of silver showing their nested or stacking relations.

of the relatively large sized nuggets in the placers from "seeds" of relatively small sized masses of lode gold observed throughout the districts. In fact, such size contrasts are fairly common in many combined lode gold and placer gold districts (see Antweiler and others, 1972; Boyle, 1979; and many others). We suggest that the relatively large placer gold nuggets were derived mostly from the upper portions of the vein systems that have been removed by erosion. The source areas probable for the placer gold will be discussed in this section.

Minor metals in seven heavy-mineral concentrates obtained from one lode site and several placer gold sites in the Gold Basin-Lost Basin mining districts were studied using cursory geochemical methods (table 20). Spectrographic methods used are those by Grimes and Marranzino (1968). An analysis (No. 1) of heavy minerals concentrated from the site of the gold-bearing episyenitic rock is included in table 20 for comparative purposes. We were not able to verify the site from which sample 3 was collected by P.M. Blacet. However, the very high concentration of tungsten (greater than 2 weight percent) in sample 3 (table 20) in contrast to a maximum 0.3 weight percent tungsten in the six other samples of placer concentrates suggests that sample 3 may be a scheelite concentrate handpicked from one of the seven others. The seven remaining samples analyzed include both magnetic and nonmagnetic fractions. Although the bulk of the samples analyzed consists of nonmagnetic portions, approximately one-tenth to one-third by volume of the concentrates include a magnetite-rich fraction that may be essentially separated magnetically using a 1-kg hand-held magnet. In addition, all relatively large fragments of gold were first removed by handpicking the heavy-mineral concentrates before the concentrates were analyzed. Those eight samples, now consisting of composited fragments of gold, were analyzed separately for palladium, platinum, and ruthenium, together with nine other gold samples similarly obtained from various placer workings throughout the districts. No palladium, platinum, or ruthenium was detected in any of these 17 gold samples at limits of determination that range between 48 and 219 ppm (Joseph Haffty and A.W. Haubert, written commun., 1978).

The drainage basins contributing material to the placer sample sites from which we obtained and analyzed the heavy-mineral concentrates are widespread, spanning the districts along their entire north-south length. As a consequence, the lode sources for these anomalous metal concentrations must also be widespread. We have not attempted to establish geochemical dispersion trains nor have we attempted to follow these metals back to their specific sources. Two analyzed samples show concentrations of 0.3 and 0.15 weight percent uranium, and 0.5 and undetected amounts of thorium, respectively. The Th:U

ratio of about 1.7 in analysis 4 (table 20) suggests a probable source in detrital grains of monazite, allanite, or euxenite derived from the Early Proterozoic metamorphic and igneous rocks. The concentration of rare-earth elements and the values of various rare-earth ratios suggest this relation also. Furthermore, Reyner (1954) described small pods of polycrase-, euxenite-, and monazite-bearing rock associated with pegmatite in SW $\frac{1}{4}$ sec. 10 and NE $\frac{1}{4}$ sec. 14, T. 28 N., R. 16 W., on the lower west flank of Garnet Mountain. Analyses of four select samples from that locality range from 0.007 to 0.533 percent eU $_3$ O $_8$.

The overall abundance of rare-earth elements and the values of various rare-earth ratios in the concentrates from five of the six placer samples are remarkably similar to the rare-earth signature of the heavy minerals concentrated from the apparently Cretaceous gold-bearing episyenitic rock (table 20). The source areas of the placer samples are mostly the Early Proterozoic rocks. These relations suggest that the hydrothermal process of episyenitic rock development may have occurred without a significant disruption of the rare-earth geochemical signature of the Proterozoic protolith of the episyenite. These inferences do not preclude the possibility that some contamination of the heavy minerals obtained from the episyenitic rock took place during the current erosion cycle.

Gold in the King Tut placer area of the Lost Basin mining district apparently is being reworked out of the upper parts of the exposed sequences of the Muddy Creek Formation. However, these predominantly fanglomeratic deposits have been derived from several source areas as fans were coalescing and filling the Miocene trough along the Grand Wash fault zone. This trough is along present-day Grapevine Mesa (see Blacet, 1975). Detailed examination by P.M. Blacet (unpub. data, 1967-72) of cobbles from the Muddy Creek Formation along the entire east flank of the Lost Basin Range revealed that granitic cobbles and boulders from the rapakivi granite of Gold Butte, which crops out north of Lake Mead, extend in the Muddy Creek Formation to approximately 1 km north of the Climax mine. Just north of the study area, granite of the Gold Butte area commonly is present as 2 to 3 m boulders throughout an at least 200-m-thick sequence of the exposed Muddy Creek Formation. West of the Meadview store, 1 km north of the study area in the adjoining southern part of the Iceberg Canyon 15-minute quadrangle, the Muddy Creek Formation also includes abundant fresh cobbles and isolated boulders of light-pinkish-gray porphyritic monzogranite that are very much like the Early Proterozoic porphyritic monzogranite cropping out in the southeastern White Hills, just east of the Cyclopic mine. In addition, subangular to moderately well rounded cobbles of medium- to coarse-grained meta-diorite are present in the Muddy Creek Formation here,

whereas the adjacent Lost Basin Range includes extremely sparse abundances of this lithology generally north of the area of the Bluebird mine. These relations suggest that the bulk of the debris being shed into the depositional trough of the Muddy Creek Formation at the northern part of the Lost Basin district was being derived from a northerly source, but that some lesser amounts of fanglomeratic material were probably coming from the southwest also.

The lithology of clasts in the lowermost sequences of the Muddy Creek Formation at its southernmost exposures in the Lost Basin district, approximately 1.5 km west-southwest of the junction of the Pierce Ferry Road and the Diamond Bar Ranch Road, also suggests derivation from a source to the southwest (P.M. Blacet, unpub. data, 1967-72). In this general area, the Muddy Creek Formation includes scattered cobbles and small boulders of basalt, unretrograded sparkling fresh garnet- and

TABLE 20.—*Semiquantitative spectrographic analyses, in weight percent, for minor metals in heavy-mineral concentrates from a selected lode occurrence and previously worked placer deposits and occurrences in the Gold Basin-Lost Basin mining districts*

[Spectrographic analyses by L.A. Bradley. Results are to be identified with geometric brackets whose boundaries are 1.2, 0.83, 0.56, 0.38, 0.26, 0.18, 0.12, and so forth, but are reported arbitrarily as midpoints of these brackets, 1, 0.7, 0.5, 0.3, 0.2, 0.15, 0.1, and so forth. The precision of a reported value is approximately plus or minus one bracket at 68-percent confidence, or two brackets at 95-percent confidence. Symbols used are: G, greater than 10 percent or value shown; N.d., not detected; L, detected but below limit of determination; ---, not looked for. Looked for but not found, Pd, Pt, Sb, Te, Ge, In, Li, Re, Ta, Il, Th, Tm, Lu]

Analysis --- Lab No. ----	1 D194818	2 D194819	3 D194820	4 D194821	5 D194822	6 D194823	7 D194824	8 D194825
Mn ----	0.7	0.15	0.2	0.15	0.5	0.03	0.15	0.15
Ag ----	.0015	.03	N.d.	.0007	.0015	.15	.0003	.00015
As ----	N.d.	.15	N.d.	N.d.	N.d.	N.d.	N.d.	N.d.
Au ----	.01	.05	.003	N.d.	N.d.	N.d.	N.d.	N.d.
B ----	N.d.	N.d.	N.d.	L	N.d.	N.d.	L	L
Ba ----	.02	.005	.003	.02	.03	7	.03	.03
Be ----	.0003	N.d.	N.d.	N.d.	N.d.	N.d.	L	L
Bi ----	N.d.	N.d.	N.d.	N.d.	N.d.	.3	N.d.	.003
Co ----	.007	.007	L	.01	.007	.005	.015	.015
Cr ----	.02	.015	.005	.015	.015	.003	.05	.03
Cu ----	.005	.002	.01	.03	.03	.03	.05	.05
La ----	1.5	.7	.007	1	1.5	.015	.3	.3
Mo ----	.01	.0003	.03	.002	.003	1.5	.003	.002
Nb ----	.07	N.d.	.03	.007	N.d.	N.d.	.007	.007
Ni ----	.0015	.007	.001	.007	.002	.003	.01	.01
Pb ----	.15	.03	.007	.15	.15	G	.07	.07
Sc ----	---	.003	.001	.002	---	.0007	.002	.0015
Sn ----	.003	.003	.005	N.d.	N.d.	N.d.	.003	N.d.
Sr ----	.015	.003	.007	.015	.015	.15	.015	.01
U ----	N.d.	N.d.	N.d.	.3	---	.15	N.d.	N.d.
V ----	.02	.07	.015	.03	.015	.02	.05	.07
W ----	N.d.	.015	G2	.3	L	N.d.	L	N.d.
Y ----	.15	.07	.007	.07	.07	.003	.05	.05
Zn ----	N.d.	.15	N.d.	N.d.	N.d.	N.d.	N.d.	N.d.
Zr ----	.15	.05	.01	.15	1	.015	.07	.07
Ce ----	1.5	1.5	N.d.	2	G2	.07	.7	.7
Ga ----	---	.03	.005	---	---	---	---	---
Hf ----	N.d.	N.d.	N.d.	N.d.	.03	N.d.	N.d.	N.d.
Th ----	---	.5	N.d.	.5	.7	N.d.	.3	.2
Yb ----	.015	---	.0005	.005	.003	---	---	.0015
Pr ----	.3	.15	---	.3	.3	N.d.	.07	.07
Nd ----	1	.7	---	1	1	.02	.3	.3
Sm ----	.15	.15	N.d.	.2	.2	N.d.	.07	.07
Eu ----	.01	.01	N.d.	L	L	N.d.	L	L
Gd ----	.05	---	---	.05	---	---	.03	.03
Dy ----	.03	L	N.d.	.03	.015	---	.005	.005
Ho ----	.01	.002	N.d.	.007	---	---	L	L
Er ----	.015	L	N.d.	.015	.015	---	.007	.005

1. Heavy-mineral concentrate from gold-bearing episyenite (fig. 50); SE1/4 sec. 27, T. 28 N., R. 18 W.
2. Drywasher concentrate. Fine gold fragments visible; SW1/4 sec. 4, T. 27 N., R. 18 W.
3. Drywasher concentrate. Location uncertain.
4. Drywasher concentrate. SW1/4 sec. 10, T. 29 N., R. 18 W.
5. Drywasher concentrate, above caliche-cemented fanglomerate. Few fine gold fragments visible; NW1/4 sec. 31, T. 29 N., R. 17 W.
6. Drywasher concentrate, includes barite, magnetite, limonite after pyrite, cerussite, galena, and traces of gold; SW1/4 sec. 8, T. 29 N., R. 17 W.
7. Drywasher concentrate, SW1/4 sec. 31, T. 30 N., R. 17 W.
8. Drywasher concentrate, SW1/4 sec. 31, T. 30 N., R. 17 W.

biotite-bearing schists, unretrograded amphibolite, pegmatoid alaskite, and aplite. The overall proportions of the lithologies of the Muddy Creek Formation suggest derivation from the southwest. Deaderick (1980, p. 96) analyzed the population of heavy minerals in concentrates from gravels along the east flank of the Lost Basin Range and concluded that the gold-bearing fanglomerates of the Muddy Creek Formation, out of which the gold placers are being reworked, must have been derived from some source to the west or southwest, more distant than the adjacent Lost Basin Range. The Early Proterozoic metamorphic complex which crops out beneath the lavas of the Table Mountain area, approximately 10 km south-southeast of the Cyclopic mine, includes lithologies in approximately the same proportions as the Proterozoic clasts in the Muddy Creek Formation at the south end of the Lost Basin Range. The source area for the Muddy Creek Formation, which crops out at the south end of the Lost Basin Range, could not have been from the Garnet Mountain tectonic block to the southeast. This block of Early Proterozoic rock includes too much porphyritic monzogranite and insufficient amounts of pegmatoid leucogranite and unretrograded metamorphic rock.

Progressively increasing abundances of lithologies derived from the Early Proterozoic terrane of the Lost Basin Range make up the sequences of the Muddy Creek Formation north from about 3.5 km southeast of the Lone Jack placer mine (P.M. Blacet, unpub. data, 1967-72). As pointed out by Deaderick (1980, p. 99), apparently only the Early Proterozoic metamorphic-clast facies of the Muddy Creek Formation contains the gold here. Furthermore, in this general area, the Muddy Creek Formation includes a considerable amount of 2.5- to 10.0-cm, rounded to subangular clasts of retrograded quartzofeldspathic gneiss. The clasts of quartzofeldspathic gneiss are yellowish gray and are well foliated to laminated. Sparse cobbles of pyrite-bearing vein quartz also are present here in the Muddy Creek Formation, as are minor amounts of retrograded amphibolite. Quartzofeldspathic gneiss is the dominant clast type in the Muddy Creek Formation from approximately 3.5 km southeast of the Lone Jack placer mine northward to several kilometers beyond the main workings of the King Tut placer area. The relations suggest derivation of the bulk of the gold from sources to the west in the Lost Basin Range, but possibly including some sources farther to the west in Hualapai Valley now covered by alluvial deposits younger than fanglomerate and tuff of the Muddy Creek Formation. Some placer gold may eventually have also come from the southwest. A probable sequence of depositional and structural events leading to the present-day geomorphologic relations is outlined in figure 3.

Quaternary fanglomeratic deposits which host the placer deposits along the west flank of the Lost Basin

Range are clearly dissected and incised, whereas those Quaternary deposits which were not worked previously for their placer gold are distinctly less dissected (P.M. Blacet, unpub. data, 1967-72; Blacet, 1975). In addition, a sharp geomorphic boundary exists between the productive Quaternary placer gold deposits and the nonproductive Quaternary deposits. This abrupt boundary is just south of the major canyon leading to the Bluebird mine. South of this boundary the alluvial fans are significantly less dissected and covered with conspicuous desert-varnish-stained trains of boulders and reddish-brown soil. Displacement(s) along a buried fault that is largely post-Quaternary in age may explain these relations. However, the overall strike of such a fault is not readily apparent. On the one hand, an east-striking normal fault, south side down, may crosscut the bajada approximately at the geomorphic transition (P.M. Blacet, unpub. data, 1967-72). Movement(s) along this hypothetical fault may have increased alluvial gradients on the north, thereby increasing both the dissection of the Quaternary deposits and the concentration of the placer gold. Alternatively, the geomorphic transition may reflect the approximate fulcrum point of very late predominantly scissors-type movements along the approximately north-south-striking fault bounding the Lost Basin Range on the west (see Blacet, 1975).

Finally, analysis of the abundance of placer gold in various dry-washer concentrates in the placers of the Gold Basin district suggested to P.M. Blacet (unpub. data, 1967-72) that the placer gold there may not be locally derived. Apparently, the placer gold in this general area was concentrated by being reworked out of erosional thin caps of older Quaternary gravels resting unconformably on the underlying Early Proterozoic gneiss. Overall production of gold from these placer deposits in the Gold Basin district was quite small and included 19 oz of gold recovered in 1942 by several operators (Woodward and Luff, 1943, p. 251).

IMPLICATIONS OF THE COMPOSITIONS OF LODE AND PLACER GOLD

By J.C. ANTWEILER and W.L. CAMPBELL

INTRODUCTION

The purpose of this chapter is to report the results and our interpretations of about 250 compositional analyses on lode gold from 48 veins or mines in the Lost Basin mining district and from 20 mines and prospects in the Gold Basin mining district and of nearly 100 compositional analyses on placer gold from the Lost Basin district. Sample localities for the two districts are shown on plate 1. Many of the analyses on placer gold were on samples from

the King Tut placer mines, but some were made on placer gold from other localities on the east side of the Lost Basin Range and from seven localities on the west slopes of the Lost Basin Range.

The compositional data are discussed with regard to how they may be useful for (1) relating the placer gold deposits to bedrock sources, (2) determining ore-deposition conditions, and (3) suggesting the possibility of relating some of the gold veins to a buried porphyry copper deposit. In previous papers (Antweiler and Sutton, 1970; Antweiler and Campbell, 1977, 1982), we suggested that compositional analyses of gold provide information that can be applied to the search for undiscovered ore deposits or to studies of ore genesis; the data presented here are examined for those possibilities.

The compositional analyses utilized mainly direct-current emission-spectrographic techniques for quantitative determination of Ag and Cu in native gold (a natural alloy composed of Au, Ag, and Cu), together with semi-quantitative determination of other elements. The gold was placed directly into graphite electrodes and analyzed by E.L. Mosier using a previously described procedure (Mosier, 1975). Supplementary analyses for Au, Ag, and Cu by electron microprobe were made by W.L. Campbell using methods described by Desborough (1970). The emission-spectrographic data provide the basis for assigning signatures (Antweiler and Campbell, 1977) to gold from each locality. Signatures consist of alloy proportions of Au, Ag, and Cu together with one or more of the following elements: Pb, Bi, Sb, As, Zn, Te, Pt, Pd, Rh, Ni, Cr, Co, V, B, Ba, and Be. Elements of high crustal abundance (Fe, Mn, Ca, Mg, Si, Ti) that are found commonly in compositional analyses and elements such as Zr, La, and Y that may be found in mineral inclusions in gold grains are not known to be useful for prospecting or ore-genesis studies and are not included herein as part of the gold signature. Mercury was found in extremely varied amounts in all samples but also is not included as part of the signature because it was found in all samples and varied greatly from one analysis to another on replicate samples. Gold content was estimated by subtracting from 100 percent the sum of the percentages of Ag and other elements found in the analyses. Gold fineness (parts per thousand Au in native gold) was estimated by dividing the Au content by the sum of the Au and Ag content and multiplying by 1,000.

We crushed and coarsely ground the lode samples from veins and mines and recovered gold grains by panning and handpicking. We avoided use of chemical, amalgamation, or roasting procedures, because those recovery procedures alter the composition of the sample (Campbell and others, 1973). Gold from the placer deposits was recovered by dry placering or panning and also was obtained without the use of procedures that might alter its composition.

Warren Mallory, president of the Apache Oro Co., Laramie, Wyo., which is reported to have mining claims in the districts, collected specimens with visible gold from many of the veins and generously donated them to us. He also gave us gold from the King Tut placer mines and from many of the other placer localities. Without his interest and generosity this work would not have been possible.

VARIATIONS IN GOLD COMPOSITION

Many papers have been published on the composition of native gold (for example, Warren and Thompson, 1944; Gay, 1963; Jones and Fleischer, 1969; Lantsev and others, 1971). Variations in composition are present even from point to point within the same grain (Desborough, 1970). Native gold in oxidized zones and in associated placers generally contains lesser amounts of Ag and other elements compared with the native gold in the corresponding primary deposits; within some specific deposits single particles of native gold are relatively homogeneous, but in other deposits the native gold is heterogeneous (Boyle, 1979). Because variations in gold composition are natural rather than analytical, they are worthy of study, particularly if their significance can be understood. In spite of the variations, gold compositional data are useful in that they help characterize conditions of ore deposition and are commonly areally distinctive for mines, districts, or regions.

To lessen uncertainties in interpreting gold compositional data that are inherently subject to natural variations, replicate analyses of gold from the same sample locality should be made if possible. As a general guide, in a district in which no prior compositional information for gold is available, we believe that at least five spectrochemical analyses of 5-mg samples of gold are desirable for a single sample site to obtain a signature in which one can place confidence. However, in the context of many other analyses from the same district, a single analysis is of value. Fortunately, at many localities in both the Lost Basin and Gold Basin districts, sample quantities were available for several analyses. At some localities, however, limited quantities of sample precluded making more than one or two analyses.

The variations in composition of Lost Basin placer samples are shown in table 21, where it can be seen that in 46 emission-spectrographic analyses of gold from the King Tut placer mines, Ag content ranges from 2.1 to 15.0 weight percent and Cu content ranges from 0.0017 to 0.07 weight percent. Standard deviation for these analyses is nearly 50 percent of the mean for Ag ($7.25 = 3.1$ percent) and nearly 60 percent of the mean for Cu ($0.0185 = 0.0114$ percent). In individual analyses, Ag ranges from 2.1 to 20 weight percent (0.1–22.3 for electron-microprobe analyses) and Cu from 0.001 to 0.097 weight percent.

TABLE 21.—*Compilation of signatures of placer gold samples, Lost Basin mining district*
[N.D., not determined]

Sample	Number of analyses	Ag (percent)			Cu (percent)			Au (fineness)				Characteristic trace elements, in order of abundance	
		Range	Mean	Standard deviation	Range	Mean	Standard deviation	Mean	$\frac{Au}{(Au+Ag)} \times 1,000$	Au/Ag	Au/Cu		Ag/Cu
HuW-1	1	N.D.	6.8	N.D.	N.D.	0.125	N.D.	93.1	932	13.7	745	54	Pb, Zn
HuW-3	1	N.D.	7.1	N.D.	N.D.	.023	N.D.	92.9	929	13.1	4,039	309	Pb, Mo
HuW-4	1	N.D.	6.5	N.D.	N.D.	.250	N.D.	93.4	935	14.4	374	26	Pb
HuW-5	1	N.D.	12.2	N.D.	N.D.	.15	N.D.	87.6	878	7.2	584	81	Pb, Mo
N33PC-7	14	4.7-8.1	5.7	1.6	.048-.08	.062	.0144	94.2	942	16.5	1,519	92	Pb, Bi, Mo, Te
34PC-1	1	N.D.	8.9	N.D.	N.D.	N.D.	.0375	91.0	911	10.2	2,426	237	None
LB-1	2	5.5-13.3	9.4	5.5	.018-.06	.039	.03	90.5	910	9.6	3,016	241	Pb, Bi
LB-2	13	18.9-19.8	19.3	.56	.038-.055	.047	.012	80.6	806	4.2	1,715	411	Pb, Te, Zn, Bi, Cd
LB-3	13	18.9-19.8	19.3	.56	.038-.055	.047	.012	80.6	806	4.2	1,715	411	Pb, Te, Zn, Bi, Cd
King Tut (analyses by microprobe)	245*	.1-22.3	11.0	5.5	*	*	*	89.0	890	8.1	*	*	N.D.
King Tut (analyses by emission spectrograph)	46	2.1-15.0	7.25	3.1	.0010-.07	.0185	.0114	92.5	926	12.8	5,000	392	Pb, Bi, Mo, Sb, Zn
10PC-4	10	4.0-20.0	11.6	5.7	.006-.078	.029	.0216	88.5	886	7.6	3,051	400	Pb, Bi
GAS	3	N.D.	13.2	N.D.	N.D.	.01	N.D.	86.7	N.D.	N.D.	N.D.	N.D.	Pb, Bi
10PC-3	1	N.D.	2.3	N.D.	N.D.	.007	N.D.	97.7	977	42.5	13,957	329	None
10PC-1	1	N.D.	10.7	N.D.	N.D.	.014	N.D.	89.2	893	8.3	6,371	764	Pb
LB-4	5	3.5-6.5	4.9	2.4	.019-.097	.053	.0325	95.0	951	19.4	1,792	92	Bi, Pb, Pd, Te
15PC-4	1	N.D.	4.3	N.D.	N.D.	.03	N.D.	95.6	957	22.2	3,187	143	Pb
14PC-2	1	N.D.	2.0	N.D.	N.D.	.0125	N.D.	98.0	980	49.0	7,840	160	Pb
22PC-1	5	15.0-20.0	17.0	2.1	.022-.03	.03	.0021	82.9	831	4.9	2,763	567	None
26PC-1	4	7.5-12.5	10.0	2.0	.005-.045	.022	.0168	89.9	900	9.0	4,086	455	Pb

¹All analyses on portions of the same nugget.

²45 individual grains were analyzed, each by 3-5 spot analyses which were then averaged for mean Au and Ag content. Copper was detected only occasionally.

At three localities (N33PC-7, LG-2, and LB-3) replicate emission-spectrographic analyses were made on portions of the same nugget. Substantial variation is evident both in Ag content and Cu content, although such variation is generally not so great as in analyses made on different grains.

The much smaller size of samples analyzed in electron-microprobe work compared with emission-spectrographic analyses (0.05-0.10 mg compared with 5 mg) resulted in greater standard deviation in Ag values (5.5 weight percent compared with 3.1 weight percent). Higher mean values for Ag content also resulted (11.0 weight percent compared with 7.25 weight percent). These higher mean values may indicate that the Ag content of grains analyzed by microprobe just happened to be higher than that of samples analyzed by spectrograph, but another explanation is that most of the microprobe analyses were made on polished interior surfaces of individual grains, whereas spectrographic analyses were made on several whole grains. Most of the grains that were analyzed by both methods were small. However, in spectrographic analyses of Lost Basin samples made earlier (Antweiler and Sutton, 1970), coarse gold (nuggets) averaged 10.4 weight percent Ag and 0.034 weight percent Cu, whereas finer gold (minus-60 mesh) averaged 5.6 weight percent Ag and 0.015 weight percent Cu. The lower Ag and Cu contents in the smaller particle-size fraction was interpreted as having resulted from more surface exposure with attendant greater Ag and Cu loss through atmospheric and ground-water leaching agents. Exterior surfaces of gold in placers commonly are depleted in Ag content (McConnell, 1907; Desborough, 1970). Electron-microprobe analyses are ideal for determining such losses because the percentages of Au and Ag can be determined at any spot including

exterior surfaces to which the microprobe beam is directed. A number of spot analyses were made on exterior surfaces of grains by microprobe; these analyses showed Ag content ranging from nil to 14 weight percent on exterior surfaces and generally from 2 to 5 weight percent less Ag than in the interior of the grains. The zone of Ag depletion (and Au enrichment) varied from grain to grain, but rarely penetrated into the interior of the grains more than a few micrometers. No attempt was made to compute the total percentage loss of Ag because the geometry of the grains varies considerably as does the Ag content. If the higher Ag content obtained in microprobe analyses is attributable to loss of Ag on grain surfaces, the Ag content obtained by microprobe should more nearly reflect the Ag content of the gold when it was in a vein, provided, of course, that no other compositional changes occurred.

The difficulty of identifying placer gold with a specific lode source is highlighted by the data (table 22), which shows the extent of variation in Ag and Cu contents in lode gold from Lost Basin and Gold Basin. Only those samples are listed for which five or more spectrographic analyses are available. The Cu content of Lost Basin lode samples ranges from 0.017 percent to 0.7 weight percent, and the standard deviation at one locality, B-B1, is nearly 100 percent of the mean. Ag content ranges from 6.6 to 31.5 weight percent, but at most localities the standard deviation approximates 20 percent of the mean value—a generally smaller percentage than in the placer samples. The Gold Basin samples also show high standard deviations for Cu; samples from locality MAS, for example, have a Cu content ranging from 0.01 to 0.28 weight percent, resulting in a standard deviation of 0.14 percent, which is 125 percent of the mean value. The standard

TABLE 22.—Variation of silver and copper content of lode gold samples from Lost Basin and Gold Basin mining districts as shown by replicate emission-spectrographic analyses

Sample	Number of analyses	Ag (percent)			Cu (percent)		
		Range	Mean	Standard deviation	Range	Mean	Standard deviation
Lost Basin							
S -----	10	20.0-29.0	22.3	3.0	0.004-0.014	0.0086	0.0033
HW -----	9	11.4-31.5	19.1	7.3	.03-.5	.18	.1510
HET -----	5	15.9-23.9	20.7	3.8	.035-.300	.15	.1110
GG -----	5	12.0-19.5	15.1	3.4	.04-.13	.092	.0480
Climax -----	8	7.5-14.0	10.4	2.2	.015-.025	.019	.0040
Golden Mile -	6	6.6-12.5	10.7	2.5	.02-.037	.035	.0149
B-J -----	10	9.7-18.0	14.4	3.0	.0175-.50	.092	.1465
B-B1 -----	10	14.0-22.5	17.5	3.4	.03-.39	.17	.1624
B-A -----	8	18.0-30.0	20.8	3.8	.014-.06	.029	.0148
B-B1W -----	6	14.5-26.0	20.9	4.2	.02-.70	.32	.2313
B-C -----	9	10.0-15.0	11.6	1.8	.028-.10	.047	.0246
Summary ---		6.6-31.5	16.7	3.5	.015-.7	.1038	.0829
Gold Basin							
AWS-M -----	7	12.0-15.0	13.7	.94	.014-.0455	.0215	.0114
GHM -----	8	14.0-25.0	19.3	3.1	.0075-.05	.0225	.0153
MAS -----	5	15.0-25.0	17.4	4.3	.0100-.28	.1120	.1400
ENW-2 -----	7	25.0-31.0	29.0	2.2	.003-.02	.008	.0056
MWS -----	5	10.0-35.0	18.0	9.8	.015-.10	.0502	.0323
OLY -----	8	14.0-30.0	20.3	4.8	.036-.07	.0495	.0140
Summary ---		10.0-35.0	19.6	4.2	.003-.28	.0440	.0364

deviations for most analyses of Ag in Gold Basin samples, like those in Lost Basin samples, tend to be 20 to 25 percent of the mean value, although some are less than that and some are more.

Because gold in placers could have more than one source and could have either a simple or a complex history in moving from a primary source to a placer site, wider variations in composition might be in placers than in lodes. Compositional variations in placers, however, are moderated to some extent by the natural refining that occurs during the transition from the environment of vein gold in bed rock to the environment of the placer gold. Although such natural refining may affect only the surface of gold grains, its net effect is an overall decrease in the content of Ag, Cu, and trace elements, with a higher percentage of Au content being the final product. If all the grains of gold in a placer deposit are uniform in composition, the chances appear favorable that all the grains came from one source area, which also would have gold of uniform composition. However, most of the lode gold in the Lost Basin and Gold Basin districts has a rather heterogeneous composition.

COMPARISON OF COMPOSITION OF PLACER GOLD IN LOST BASIN WITH THAT OF POSSIBLE LODE SOURCES

Most of the placer gold samples obtained in the Lost Basin district are not geographically relatable to a specific lode locality, but four of them are from drainages below veins from which gold was collected and analyzed (table 23). Even though this direct geographic relation does exist, gold in the placers on the east flank of the Lost Basin Range definitely was reworked out of the Muddy Creek Formation, which locally includes the bed rock from which

the alluvial placers were derived. On the west flank of the Lost Basin Range, sample GM-G1 below the Golden Mile mine must certainly have come from the Golden Mile mine vein. The small volume of alluvium in the drainage where the placer sample was collected consists entirely of locally derived material from the nearby Early Proterozoic rocks. Only enough placer gold was obtained for one analytical determination, which shows a Cu content of 0.17 weight percent compared with a mean value for six analyses of the lode sample of 0.035 weight percent. Addition of Cu to native gold during the transition from vein to placer is unlikely; therefore, the high content of Cu in the placer sample probably reflects the presence of inclusions of chalcopyrite or other Cu-bearing minerals in the gold sample analyzed. Decrease of Ag content from 10.7 to 7.1 weight percent from lode to placer gold is reasonable, as is the loss of Bi and Mo. On the east flank of the Lost Basin Range, lode-placer pair LB4-WSE2 (table 23), although geographically closely related, shows the absence of a direct kinship. The placer sample has only 4.9 weight percent Ag compared with 15.5 weight percent Ag for the lode sample. If the placer sample came directly from the lode, its Ag content should have been at least 10 weight percent, and Te should not have been present in the placer if not in the lode. The lower Ag content could be explained as the addition of Au through chemical or physical accretion, but the appearance of Te in the placer poses a mystery. A likely possibility is that some or all of the placer gold had its immediate, though secondary, source in the Muddy Creek Formation and had a more distant primary source. Alternatively, the placer sample could have come from a part of the vein at WSE2 (table 23) that is considerably different in composition from that which we analyzed.

A discrepancy also exists between placer sample N33PC7 (table 23) and the Climax vein sample (table 23). Although the Ag and trace-element contents are compatible, the greater amount of Cu in the placer sample indicates the placer sample either came from a different lode or from a part of the Climax vein containing a much higher content of Cu than that found in the part of the vein that we sampled.

Placer sample LB3 (table 23) has a composition that is compatible with derivation from lode sample BL-1 (table 23) except for the placer's Zn and Cd, which could be explained by assuming that inclusions of sphalerite containing Cd were present in the particular gold sample analyzed. Absence of Mo and Te in the placer sample is readily explainable as the result of loss from oxidation or leaching in the transition from vein to placer.

All the lode samples from the Gold Basin and Lost Basin districts were examined in terms of their Ag content and fineness as possible sources for the Lost Basin placer deposits. Histograms showing the number of samples with

TABLE 23.—Comparison of signatures of placer gold and possible lode gold sources

Sample P, placer; L, lode	Number of analyses	Percent mean				Fineness Au	Au/Ag	Au/Cu	Au/Ag Cu	Ag/Cu	Characteristic trace elements, in order of abundance
		Au	Ag	Cu							
GMG1 (P) ---	1	92.8	7.1	0.17	929	13.1	546	77	42	Pb	
GMG1 (L) ---	6	89.2	10.7	.035	893	8.3	2,549	237	306	Pb, Bi, Mo	
LB4 (P) ----	5	95.0	4.9	.053	951	19.4	1,792	366	92	Bi, Pb, Te	
WSE2 (L) ---	2	84.4	15.5	.088	845	5.4	959	61	176	Bi, Pb, Te, W	
N33PC7 (P) -	4	94.2	5.7	.062	943	16.5	1,519	266	92	Pb, Bi, Mo	
Climax (L) -	8	89.5	10.4	.019	896	8.6	4,710	452	547	Pb, Bi, Mo	
LB3 (P) ----	3	80.6	19.3	.047	807	4.2	1,715	89	411	Pb, Bi, Sb, Zn, Cd	
BL-1 (L) ---	2	76.6	23.0	.056	769	3.1	1,351	55	411	Pb, Bi, Mo, Sb, Te	

a particular level of Ag concentration (fig. 64) and the fineness of Au in Lost Basin placer samples and Lost Basin and Gold Basin lode samples (fig. 65) show an absence of strong or convincing evidence to relate the lodes to the placers. For example, no lode sample was found that contained less than 6.0 weight percent Ag, but several placer localities had gold with less than 5 weight percent Ag, and one placer gold sample contained only 2 weight percent Ag. Also, the highest mean Ag content in any placer sample was 19.3 weight percent Ag; however, the Ag content at some lodes was as high as 38 weight percent, and at 20 localities the gold samples contained more than 20 weight percent Ag. If chemical accretion of dissolved Ag around detrital gold particles occurred, as indicated by examination of some of the nuggets (see frontispiece), the local veins presumably could have provided all the gold. Nearly all the placer gold is

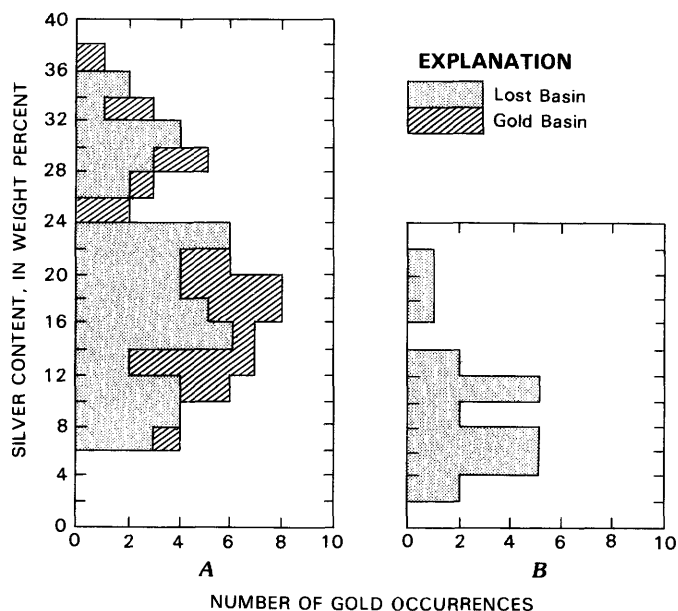


FIGURE 64.—Weight percent silver versus number of gold occurrences. A, Lode gold from Gold Basin and Lost Basin districts. B, Placer gold from Lost Basin district.

of comparatively high fineness with respect to that of the lodes (fig. 65). Therefore, although some of the placer gold probably had its origin in Lost Basin veins (and possibly in Gold Basin veins as well), more than half of it must have either had a different lode source from any of those sampled or must have come from parts of veins no longer extant; or it represents gold that was at one time in solution and was added to placer gold particles by chemical accretion or other processes. In any event, a direct source relation for gold in the Lost Basin placer deposits to gold in veins in either Lost Basin or Gold Basin appears extremely difficult, if not impossible, to determine.

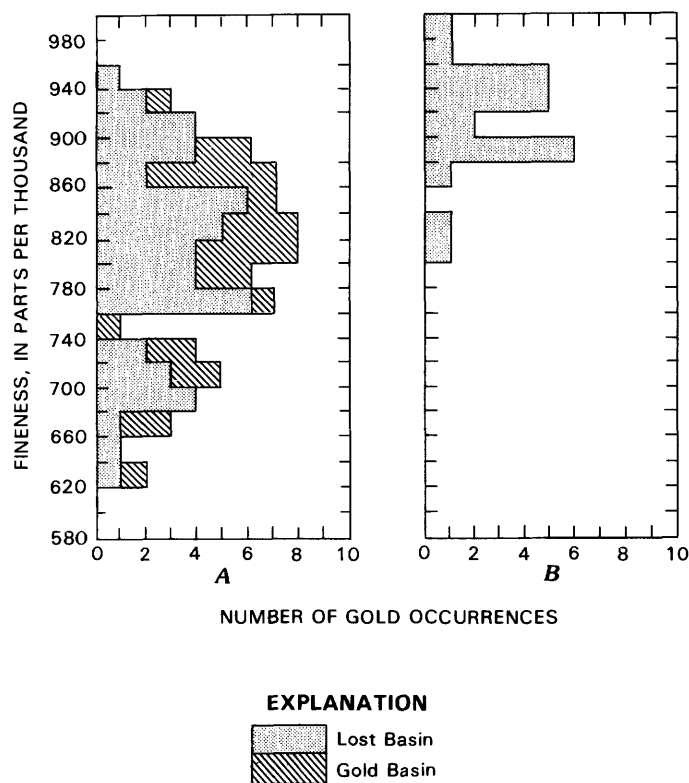


FIGURE 65.—Mean fineness (see text) versus number of gold occurrences. A, Lode gold from Gold Basin and Lost Basin districts. B, Placer gold from Lost Basin district.

COMPOSITION OF LODE GOLD FROM THE LOST BASIN DISTRICT

Signatures for lode gold samples from Lost Basin are listed in table 24 and are arranged geographically from west to east and north to south (pl. 1) and grouped according to veins that may be related because of their proximity to one another. A crude zoning relation was observed in the sulfides present in the veins. At both the southern and northern extremities of mineralization in the Lost Basin Range, galena and sphalerite were the abundant sulfides, and in some veins containing sphalerite and galena it was not possible to obtain sufficient gold for analysis. In the central part of the Lost Basin Range, chalcopyrite was the dominant sulfide, and some veins contained molybdenite and arsenopyrite, with minor amounts of galena and sphalerite. The gold signatures reflect this zoning relation only vaguely. The Climax vein samples, the samples in the vicinity of the "Blowout" (table 24, samples B1-1, B1-8), and the samples designated "Wall Street East" (table 24) appear to be near the center of the district. The trace elements in the gold signatures are dominated by Pb, Mo, and Bi, with analyses commonly showing the presence of As. Individual analyses could be singled out to suggest that gold of high fineness is present in some analyses, but the gold in nearly all the veins is extremely heterogeneous so that no convincing generalizations can be made. The vein with lowest Ag content, the TP vein, is west of most of the veins where gold was found but is about midway between the northern and southern boundaries of mineralization. The TP vein is more homogeneous than most of the other veins, and being the vein with the highest Au fineness it may represent more nearly the center of the district than any of the other veins.

The abundance of veins in the Lost Basin district suggests the desirability of prospecting further, perhaps at depth, in the Lost Basin district.

COMPOSITION OF GOLD FROM MINES IN GOLD BASIN

Signatures of lode gold from samples taken from the Gold Basin district are listed in table 25, also arranged from north to south (pl. 1). Northwest of the Gold Hill mine, a group of samples is designated with the prefix AWS. Sample AWS-M (table 25), in the center of this group, showed in replicate samples the least variation in Ag content of any of the lode samples in either the Gold Basin or Lost Basin district. The Ag content of gold from this prospect was also somewhat less than most of the other prospects in the group, thus suggesting that AWS-M may have been a local center of mineralization. The other veins in this group vary widely in composition, however; like most others in the Gold Basin and Lost

Basin districts they are mixed sulfide veins and are generally small.

Pt was found in gold samples from the Excelsior mine (table 25, sample EXC), and Pd was found in gold samples from the Excelsior mine as well as from sample AWS-W (table 25). No apparent significance is attached to these occurrences. However, minor-element analyses of amphibolite from the general area of the Bluebird mine in the Lost Basin Range revealed the presence of detectable Pt and Pd.

A gold sample of high Ag content was found south of the Malco mine at locality MOK (table 25) and had the highest Ag content found in any of the samples from both Gold Basin and Lost Basin.

The average Ag content of lodes in the Gold Basin district is greater than that of lodes in the Lost Basin district, although the Ag content varies widely in both districts. Cu content also varies widely in both districts but is generally somewhat higher in the Lost Basin district. These observations suggest that conditions of ore deposition were generally similar for both districts, but the temperature and pressure of ore deposition was probably somewhat greater in the Lost Basin district.

SIMILARITY OF SIGNATURES OF GOLD SAMPLES FROM SOME LOCALITIES IN THE DISTRICTS TO THAT OF GOLD SAMPLES FROM SOME PORPHYRY COPPER DEPOSITS

In previous work (Antweiler and Campbell, 1977, 1982), we found that gold samples from some porphyry copper deposits had an Ag content of 25 to 30 weight percent, a Cu content of 0.04 to 0.15 weight percent, and a suite of trace elements that usually included Pb, Bi, and Sb, and sometimes one or more other elements that might include Zn, As, Te, Sn, Cr, Ni, or W. Probably the most important indicator in these gold-sample signatures is the quantity of Ag and Cu. Characteristically in hydrothermal deposits, native gold includes maximum Cu and minimum Ag contents at ore depositional conditions of high temperature and pressure and minimum Cu and maximum Ag contents at low temperature and pressure (Antweiler and Campbell, 1977). Gold samples from porphyry copper deposits, however, include an Ag content that is usually characteristic of epithermal or mesothermal deposits, but a Cu content more nearly like that of hypothermal deposits. Samples that contain or exceed 0.04 weight percent Cu, and also contain at least 20 weight percent Ag, should be considered in the context of their possible relation to a porphyry copper deposit.

The Lost Basin and Gold Basin gold-sample signatures were examined to determine whether any of the signatures were similar to those obtained on gold samples from porphyry copper deposits (Antweiler and Campbell, 1977,

TABLE 24.—*Compilation of signatures*

[N.D., not

Sample	Number of analyses	Ag (percent)			Cu (percent)		
		Range	Mean	Standard deviation	Range	Mean	Standard deviation
BDN1 -----	2	27.9-35.6	31.8	5.4	N.D.	0.075	N.D.
BD -----	2	22.1-22.1	22.1	N.D.	0.042-0.085	.063	0.030
BD summary -----	4	22.1-35.6	26.95	N.D.	.042-.085	.069	N.D.
S-HW -----	2	22.6-25.1	23.9	1.3	.025-.047	.036	.016
S -----	10	20.0-29.0	22.3	3.0	.004-.014	.0086	.0033
S vein summary -----	12	20.0-29.0	22.6	N.D.	.004-.047	.013	N.D.
WB-U -----	1	N.D.	26.5	N.D.	N.D.	.019	N.D.
WB-S -----	1	N.D.	31.1	N.D.	N.D.	.070	N.D.
WB summary -----	2	26.5-31.1	28.8	N.D.	N.D.	.0445	N.D.
Ford vein -----	4	20.3-25.3	23.3	2.2	.01-.07	.033	.026
PB vein -----	1	N.D.	29.8	N.D.	N.D.	.0125	N.D.
GG (Golden Gate mine) ----	5	12.0-19.5	15.1	3.4	.04-.13	.092	.048
GGW-1 -----	1	N.D.	18.0	N.D.	N.D.	.125	N.D.
Golden Gate summary ----	6	12.0-19.5	15.6	N.D.	.04-.13	.098	N.D.
TP-1 -----	2	5.9-6.0	6.0	.07	.009-.02	.0145	.078
TP-2 -----	5	3.6-16.8	6.1	5.0	.01-.05	.0310	.0175
TP-3 -----	5	5.0-8.3	6.5	1.7	.0125-.03	.0190	.007
TP-4 -----	2	8.3-10.1	9.2	1.6	.005-.0125	.0088	.005
TP vein summary -----	14	3.6-16.8	6.7	N.D.	.005-.05	.021	N.D.
HWG -----	2	30.2-31.2	30.7	.7	N.D.	.03	N.D.
HW -----	3	30.6-40.6	34.9	5.1	.2-.4	.27	.11
HET -----	5	15.9-23.9	20.7	3.8	.035-.3	.15	.11
HW -----	9	11.4-31.5	19.1	7.3	.03-.5	.18	.15
HEE-1 -----	2	12.2-13.7	13.0	1.1	.025-.028	.027	.015
Harmon veins summary ---	21	11.4-40.6	22.3	N.D.	N.D.	.16	N.D.
Climax mine -----	8	7.5-14.0	10.4	2.2	.015-.025	.019	.004
CBW-2 -----	4	16.8-25.8	20.8	3.7	.016-.025	.02	.003
CB-C -----	3	10.9-19.4	15.1	4.3	.015-.03	.0225	.008
Climax mine summary ----	15	7.5-25.8	14.1	N.D.	.015-.03	.02	N.D.
Bl-1 -----	2	22.0-24.0	23.0	1.4	.05-.065	.058	.011
Bl-8 -----	3	19.0-39.0	29.0	10.0	.017-.025	.022	.004
Blowout summary -----	5	19.0-39.0	26.6	N.D.	.017-.065	.036	N.D.
Golden Mile mine area							
GM -----	1	N.D.	9.7	N.D.	N.D.	0.0375	N.D.
GMR -----	3	24.4-37.4	31.0	6.5	0.005-0.010	.007	0.0026
GMG1 -----	6	6.6-12.5	10.7	2.5	.02-.037	.035	.0149
Summary -----	10	6.6-37.4	16.7	N.D.	.005-.0375	.027	N.D.
Wall Street veins							
A. West veins -----							
WS-V -----	2	34.0-34.0	34.0	N.D.	.0235-.0335	.029	.007
WS-W7 -----	2	11.4-21.4	16.4	7.1	.15-.30	.225	.106
WS-W -----	3	15.5-19.5	17.8	2.1	.02-.036	.0277	.008
WS-HG2 -----	1	N.D.	8.6	N.D.	N.D.	.0200	N.D.
WS-HG3 -----	3	13.9-15.9	14.9	1.0	.018-.028	.024	.007
WS-HG5 -----	1	N.D.	23.9	N.D.	N.D.	.010	N.D.
Summary West -----	12	8.6-34.0	19.3	N.D.	N.D.	.058	N.D.
B. East veins							
WS-HVN -----	3	21.4-42.4	33.2	10.0	.0625-.0825	.0725	.010
WS-HV -----	3	26.6-28.6	27.9	7.2	.023-.10	.0510	.043
WS-E12 -----	2	13.6-18.0	15.8	3.9	.0125-.25	.1300	.168
WS-CL5 -----	1	N.D.	9.4	N.D.	N.D.	.0700	N.D.
WS-E1 -----	2	17.3-21.1	19.2	2.7	N.D.	.1500	N.D.
Summary East -----	11	9.4-42.4	23.9	N.D.	.0125-.25	.09	N.D.
Summary West, East -	23	8.6-42.4	21.5	N.D.	.0125-.25	.07	N.D.
Bluebird veins							
A. West of wash -----							
B-A -----	8	14.6-30.6	20.9	4.5	.014-.06	.031	.015
B-B1 -----	10	13.4-23.4	18.4	3.1	.03-.38	.17	.16
B-B1W -----	6	15.1-26.0	21.5	4.2	.02-.7	.31	.26
B-C -----	9	10.3-15.3	11.9	1.8	.02-.1	.046	.016
BM-9 -----	2	15.3-19.8	17.6	3.3	.006-.018	.012	.008
BM-8 -----	1	N.D.	29.2	N.D.	N.D.	.0075	N.D.
BM-3 -----	2	8.7-14.2	11.5	3.9	.034-.04	.037	.004
BM-3S -----	3	14.1-18.1	17.5	2.2	.032-.0375	.035	.003
BM-1S -----	2	8.8-15.8	12.3	4.9	.02-.025	.0225	.004
Summary -----	43	8.7-30.6	17.5	N.D.	.02-.31	.104	N.D.
B. East of wash							
B-J -----	10	9.9-18.2	14.6	2.9	.0175-.10	.0525	.032
B-20L2 -----	2	12.9-15.4	14.2	1.8	.019-.026	.0225	.005
B-JP -----	1	N.D.	17.3	N.D.	N.D.	.0250	N.D.
Summary -----	13	12.9-18.2	14.7	N.D.	N.D.	.046	N.D.

of lode gold, Lost Basin mining district
determined]

Au fineness						Characteristic trace elements, in order of abundance
Mean	$\frac{\text{Au}}{(\text{Au}+\text{Ag})} \times 1,000$	Au/Ag	Au/Cu	$\frac{\text{Au/Ag}}{\text{Cu}}$	Ag/Cu	
67.8	681	2.1	900	28	425	Pb, Bi, Ba
73.7	769	3.3	1,170	52	351	Pb, Mo, Bi, Te, Co, Ni
70.75	725	2.6	1,025	38	391	Pb, Bi, Mo, Te, Ba, Co, Ni
76.0	761	3.2	2,083	89	664	Pb, Bi
77.6	777	3.5	9,023	407	2,593	Pb, Mo, Bi, Ba
77.3	774	3.4	5,946	263	1,738	Pb, Bi, Mo, Ba
69.7	725	2.6	3,668	137	1,394	Pb, Bi
63.9	694	2.1	913	30	444	Pb, Bi, Mo, Co, V, Ba
66.8	710	2.4	2,291	84	919	Pb, Bi, Mo, Co, V, Ba
75.8	764	3.3	2,296	100	942	Pb, Bi
70.2	703	2.4	5,616	2,384	192	Pb, Bi
84.8	849	5.6	922	61	164	Pb, Bi, Sb, As, Zn, Pd, Cr, Ni
81.9	820	4.6	654	37	144	Pb, Bi, As, Zn
84.3	844	5.4	860	55	159	Pb, Bi, As, Zn, Sb, Pd, Cr, Ni
93.9	940	15.7	6,302	1,082	4,141	Pb, Bi, Pd, Mo
90.8	909	10.0	2,929	322	294	Pb, Bi, Mo, Co, Ni, Cr
93.4	935	14.4	4,916	758	342	Pb, Zn, Cd, Cr
90.7	908	9.9	10,306	1,120	1,045	Pb, Bi, Zn, Cd, Cr
92.2	923	13.8	4,388	655	319	Pb, Bi, Cr, Mo, Zn, Cd, Mo, Pd, Co
69.1	692	2.3	2,303	75	1,023	Pb, Bi, Mo, Te
61.4	638	1.8	227	6.7	129	Pb, Bi, Ba
79.2	793	3.8	528	26	138	Pb, Mo, Bi
80.8	809	4.2	449	23	106	Pb, Bi, Mo, W
86.6	869	6.7	3,207	247	481	Pb, Mo, Bi
77.1	776	3.5	482	22	139	Pb, Bi, Mo, W, Te, Ba
89.5	896	8.6	4,710	453	547	Pb, Bi, As, Mo, Zn
79.0	792	3.8	3,950	190	1,040	Pb, Mo
84.3	848	5.6	3,750	249	671	Pb, Mo, Bi, As, Te
85.7	859	6.1	4,285	305	705	Pb, Mo, Bi, As, Zn, Te
76.7	769	3.3	1,400	59	411	Pb, Mo, Bi, Sb, Zn, Cr, Ba
70.6	713	2.4	3,200	109	1,318	Pb, Mo, Bi, V, Ba, Sr
73.0	733	2.7	2,027	76	739	Pb, Mo, Bi, Sb, Zn, Ba, V, Cr
90.1	903	9.3	2,402	248	259	Pb, Bi, Ba, Cr
68.8	689	2.2	9,828	317	4,428	Pb, Mo, Bi, Ba
89.2	893	8.3	5,986	238	718	Pb, Bi, Cr, Ba
83.1	837	5.0	3,078	185	618	Pb, Bi, Ba, Cr, Mo
65.7	659	1.9	2,270	67	1,172	Pb, Bi
83.0	835	5.1	370	23	73	Pb, Bi, Ba
79.4	817	4.5	2,890	160	647	Pb, Bi, Mo, Ni, V, Ba
91.2	914	10.6	4,560	530	430	Pb, Bi, Ba
84.9	851	5.7	3,540	237	621	Pb, Bi, Te, Mo
76.0	761	3.2	7,600	320	2,390	Pb, Bi, Te, Mo, Cr, V, Ba
79.8	805	4.1	1,376	71	333	Pb, Bi, Mo, Ba, Te, V, Cr, Ni
64.7	661	1.9	890	27	458	Pb, Bi, Mo, Sn, V, Ba
71.7	720	2.6	1,405	50	558	Pb, Bi, Mo, Sn, Zn, Cr, V
83.8	841	5.3	645	41	122	Pb, Bi, Te, V
90.5	906	9.6	1,290	138	134	Pb, Bi, Mo, Ba
79.6	806	4.1	530	28	128	Pb, Bi, As
75.1	759	3.1	834	35	266	Pb, Bi, Mo, V, Ba, As, Zn, Cr, Ni
77.6	783	3.6	1,108	51	307	Pb, Bi, Mo, Ba, V, Te, As, Zn, Cr, Ni
78.7	790	3.8	2,540	120	674	Pb, Bi, Ba
79.6	804	4.3	470	25	108	Pb, Bi, Sb, Zn, Ba
77.9	782	3.6	250	12	69	Pb, Bi, Mo
87.7	881	7.4	1,900	160	259	Pb, Bi, As, Zn, Mo, Ba
81.7	823	4.6	6,808	383	1,467	Pb, Bi, Te, Cr, Ba
71.5	716	2.4	9,530	326	3,893	Pb, Bi, Te, V, Ba
88.3	885	7.6	2,390	208	311	Pb, Te
82.3	825	4.7	2,400	134	500	Pb, Bi
87.3	877	7.1	3,880	315	547	Pb, Bi
81.8	824	4.7	787	45	168	Pb, Bi, Te, Ba, Mo, Zn, Cr, V
85.2	854	5.8	1,620	110	278	Pb, Bi
85.7	859	6.0	3,800	268	631	Pb, Cr, V
82.6	827	4.8	3,300	190	692	Pb, V
85.1	853	5.8	1,850	126	320	Pb, V, Bi, Cr

TABLE 25.—*Compilation of lode gold*
[N.D., not

Sample	Number of analyses	Ag (percent)			Cu (percent)		
		Range	Mean	Standard deviation	Range	Mean	Standard deviation
SSM-W -----	1	N.D.	11.3	N.D.	N.D.	0.0215	N.D.
Prospects northwest of Gold Hill mine:							
AWS-M -----	7	12.0-15.0	13.7	0.94	0.014-0.0455	.0215	0.0114
AWS-W -----	4	13-18.4	14.9	2.4	.008-.026	.0155	.007
AWS-E -----	1	N.D.	17	N.D.	N.D.	.011	N.D.
AWS-T -----	4	9.3-14.5	11.8	2	.02-.05	.032	.015
AWS-ES -----	1	N.D.	7.5	N.D.	N.D.	.075	N.D.
AWS-TS3 -----	2	20.5-21.5	20	.7	.028-.065	.05	.026
AWS-TS2 -----	2	30-35	32.5	3.5	.2-.5	.35	.21
Summary -----	21	9.3-35	15.8	N.D.	.008-.5	.05	N.D.
Gold Hill mine -----	8	14.3-25.4	19.7	3.1	.0075-.05	.0225	.015
Senator mine -----	1	N.D.	12.8	N.D.	N.D.	.0250	N.D.
MAS -----	5	15.6-25.6	18	4.3	.01-.28	.112	.14
VVM -----	4	6.3-15.3	12.5	4	.014-.0375	.0216	.0109
ENW-2 -----	7	25-31	29	2	.003-.02	.008	.0056
ENW -----	3	14.4-18.4	16.7	2.1	.05-.07	.058	.01
EXC -----	3	28.3-42.5	36.1	7.2	.003-.0375	.023	.018
MAL-C -----	3	23-30	27	3.6	.007-.014	.0117	.004
MWT -----	4	26.5-31.5	28.5	2.4	.003-.0125	.0075	.004
MOK -----	3	46.2-54.2	49.5	4.2	.005-.006	.0057	.0006
MWS -----	5	10.5-35.5	18.5	9.8	.015-.10	.05	.0287
OLY -----	8	15.1-30.1	21.3	4.2	.036-.118	.058	.0311
OLY-SS -----	2	12.8-14.3	13.5	1	.0375-.0830	.06	.032
FLU-SS -----	3	23.8-26.8	25.5	1.5	.008-.012	.01	.002
CUR -----	1	N.D.	12.5	N.D.	N.D.	.0375	N.D.
CYE -----	3	9.6-21.5	16.8	6.4	.005-.03	.021	.0125
CYC -----	1	N.D.	24	N.D.	N.D.	.0125	N.D.
CYC SW -----	1	N.D.	18.1	N.D.	N.D.	.03	N.D.
MES4 -----	1	N.D.	32.4	N.D.	N.D.	.03	N.D.

1982). Samples with signatures that might qualify are listed in table 26 together with those from four porphyry copper deposits. The best candidates in the Lost Basin district are in a cluster northeast of the Golden Gate mine, samples BDN-1, BD, and S-HW; sample cluster WB-S, HW, and HET; on the Bluebird vein, samples B-B1W and B-B1; at the "Blowout", sample BL-1; and sample WSE-1 on one of the "Wall Street" veins. The most similar signatures are in the Gold Basin district near the Malco mine, sample MAS. However, of note is that no outcrops of Late Cretaceous and (or) early Tertiary I-type granite are known to us in either of the districts. All porphyry copper systems in North America are associated with I-type granites (Burnham, 1979).

FLUID-INCLUSION STUDIES

Initial fluid-inclusion studies of the precious- and base-metal vein deposits and occurrences and of samples containing disseminated gold in the districts were carried out in 1970-72 by J.T. Nash in conjunction with the field investigations of P.M. Blacet. These studies included quantitative tests using heating and freezing techniques, visual

estimates of approximate filling temperatures of about one-third of the studied samples, and the examination of fluid-inclusion relations in all available thin sections. Subsequently these investigations were supplemented by intensive heating and freezing tests by T.G. Theodore and T.F. Lawton of a few geologically critical samples to resolve some ambiguities remaining between mineralization and its associated fluids. About 60 doubly polished plates, approximately 0.5 to 1 mm thick, were prepared of rock and vein samples from about 40 different localities. Three different stages were used during the course of the investigations. The earlier studies by Nash used a custom-fabricated heating stage probably having a more than ± 5 °C precision. Freezing tests were accomplished using cooling equipment that utilized approximately 7 liters of rapidly circulating acetone as the heat-exchange medium (see Roedder, 1962). The later investigations by Theodore and Lawton used a commercially available Chaixmeca stage described by Poty and others (1976) and modified using insulation materials designed by Cunningham and Carollo (1980). The Chaixmeca stage uses dry nitrogen gas passed through a liquid nitrogen bath as the refrigerant. Repeated calibrations of this stage using natural

signatures, Gold Basin mining district
determined]

Au (fineness)						
Mean	$\frac{\text{Au}}{(\text{Au}+\text{Ag})} \times 1,000$	Au/Ag	Au/Cu	$\frac{\text{Au/Ag}}{\text{Cu}}$	Ag/Cu	Characteristic trace elements, in order of abundance
88.6	887	7.8	4,100	390	526	Pb
86.1	863	6.3	4,004	293	637	Pb, Bi, Mo, Co, Cr, Ni, Ba
85	851	5.7	5,484	368	961	Bi, Pb, Pd
82.9	830	4.9	7,536	445	1,545	Pb, Bi, Ba
88	882	7.5	2,750	233	369	Pb, Mo, Bi, Ba
92.4	925	12.3	1,232	164	2,846	Pb, Mo, Ni
79.7	799	4	227	154	57	Pb, Bi, Cr
67.4	675	2.1	193	6	93	Pb, Te, Mo, Bi, Co, Ni, Cr
N.D.	N.D.	N.D.	N.D.	N.D.	N.D.	N.D.
79.9	802	4.1	3,551	227	875	Pb, Bi
86.9	872	6.8	3,480	271	512	Pb
81.4	819	4.5	728	40	161	Pb, Bi, Sb, Zn, Cr, Sn, Mo
87.5	878	7.2	4,050	333	578	Pb, Bi, Mo, Co
70.4	708	2.4	8,850	300	3,625	Pb, Sb, Bi, Co
80.8	829	4.8	1,403	83	288	Pb, Bi, As, Mo
62.9	635	1.7	2,735	76	1,570	Pb, Pt, Pd, Bi, Mo, Te
72.9	730	2.7	6,230	230	2,308	Pb
71.3	714	2.5	9,506	333	3,800	Pb, Bi, Mo, W, Ba
48.6	495	.98	8,526	172	8,684	Pb, Bi, Mo, Cr
81.2	814	4.4	1,620	88	370	Pb, Bi, Mo, Cr, V, Pd
78.5	787	3.7	1,570	64	367	Pb, Bi, Zn, Mo, V
86.	864	6.4	1,430	107	225	Pb, Ba
69	730	2.7	6,900	271	2,550	Pb, Bi, Cr, Ni
87.4	875	7	2,330	187	333	Pb, Mo, V, Ba
80.1	827	4.8	3,815	227	800	Pb, As, Bi, Mo, Cr
74.7	757	3.1	5,975	249	1,920	Pb, Ba, Sr, Bi
81.6	818	4.5	2,720	150	603	Pb, Mo, Bi, Cr
67.5	676	2.1	2,250	69	1,080	Pb, Cr

and synthetic standards suggest temperature measurements are less than ± 0.1 °C in error in the range -56 to $+200$ °C and approximately ± 1.0 °C in the range 200 to 550 °C. Fluid inclusions rich in carbon dioxide were studied using the methods of Collins (1979). Daughter minerals were studied using the SEM and an attached energy-dispersive detector following the sample-preparation techniques of Metzger and others (1977).

TYPES OF FLUID INCLUSIONS

Several types of well-developed and relatively large fluid inclusions are present in quartz and fluorite that are associated spatially and temporally with gold. The fluid inclusions may be classified as follows:

1. Type I, moderate salinity type, consists of a liquid phase and a vapor phase (fig. 66A). The vapor phase of this very common inclusion type typically makes up about 15 volume percent of the inclusion at room temperature. Freezing tests show these inclusions to have salinities generally in the range 10 to 14 weight percent NaCl equivalent. Very rarely this

type of fluid inclusion also contains an extremely small crystal of hematite. However, some sulfide minerals also have been trapped in these fluid inclusions during the growth of their host mineral, mostly quartz. These sulfides include chalcopyrite, galena, and pyrite (fig. 66B, C) and are believed to be captured minerals trapped during crystallization of the quartz; they apparently are not daughter minerals. Some type-I inclusions also contain significant amounts of CO₂ because during freezing tests liquid CO₂ appears at temperatures slightly below room temperature as a thin meniscus around the vapor bubble. The moderate salinity of the liquid in the type-I fluid inclusions is reflected in the presence of extremely small rounded crystals of NaCl, about 0.25 μm wide, found near open fluid inclusions using the SEM and indicate dessication from the evaporation of the released fluid-inclusion waters.

2. Type II, a very low density, vapor-rich type, shows more than 50 volume percent vapor at room temperature. This type of inclusion is very rare in the Gold Basin-Lost Basin districts and may reflect either local boiling or secondary necking down.

TABLE 26.—*Signatures of gold from Lost Basin and Gold Basin mining districts that*
[N.D, not

Sample	Number of analyses	Ag, percent			Cu (percent)		
		Range	Mean	Standard deviation	Range	Mean	Standard deviation
Lost							
BDN-1 -----	2	27.9-35.6	31.8	5.4	N.D.	0.075	N.D.
BD -----	2	22.1-22.1	22.1	N.D.	0.042-0.085	.063	N.D.
SHW -----	2	22.6-25.1	23.9	1.3	.025-.047	.0360	0.011
WB-S -----	1	N.D.	31.1	N.D.	N.D.	.07	N.D.
HW -----	9	11.4-31.5	19.1	7.3	.03-.5	.18	.151
HET -----	5	15.9-23.9	20.7	3.8	.035-.3	.15	.111
B-B1W -----	6	15.1-20.0	21.5	4.2	.02-.7	.31	.26
B-B1 -----	10	13.4-23.4	18.4	3.1	.03-.038	.17	.16
BL-1 -----	2	22.0-24.0	23.0	1.4	.05-.065	.058	.011
WSE-1 -----	2	17.3-21.1	19.2	2.7	N.D.	.15	N.D.
Gold							
MAS -----	5	15.6-25.6	18.0	4.3	0.01-.28	0.112	0.14
ENW -----	3	14.4-18.4	16.7	2.1	.05-.07	.058	.01
NWS -----	5	10.5-35.5	18.5	9.8	.015-.10	.05	.0287
MES-4 -----	1	N.D.	32.4	N.D.	N.D.	.03	N.D.
OLY -----	8	15.1-30.1	21.3	4.2	.036-.118	.058	.0311
Gold from known copper							
Butte, Mont. -----	¹ 11	N.D.	25.9	N.D.	N.D.	0.05	N.D.
Mineral Park, Ariz. -----	¹ 5	N.D.	29.6	N.D.	N.D.	.04	N.D.
Cala Abajo, P. R. -----	¹ 1	N.D.	25.1	N.D.	N.D.	.15	N.D.
Stinkingwater, Wyo. -----	² 1	N.D.	25.0	N.D.	N.D.	.15	N.D.

¹Antweiler and Campbell (1977).²Antweiler and Campbell (1982).

3. Type III, a high salinity type, includes one or more nonopaque daughter minerals at room temperature. The most common daughter mineral is NaCl (fig. 66D, E). A highly birefringent mineral that has parallel extinction and is probably anhydrite, and a sparse carbonate mineral, probably calcite, are also present in some of this type of fluid inclusion. In addition, small crystals of opaque minerals may be present in this type of inclusion. Some type-III inclusions also show low concentrations of liquid CO₂ at room temperature. Although we do not recognize optically the presence of sylvite (KCl) in these type-III inclusions, some extremely small rounded crystals of sylvite were found using the SEM on broken surfaces of vein quartz (fig. 66E). These crystals probably formed during evaporation of liquid from the ruptured fluid inclusions. If so, these are not daughter minerals but do attest to some minor amounts of potassium in the fluid. The proportion of vapor in the type-III inclusions is about 15 volume percent. Type-III inclusions are relatively rare in the examined deposits and occurrences but seem to be

concentrated preferentially in quartz paragenetically associated with the feldspathic parts of the quartz-cored pegmatitic veins or with narrow micropegmatitic veins that did not evolve a significant quartz-carbonate ± base- and precious-metal stage.

4. Type IV comprises three-phase inclusions that at room temperatures contain mostly liquid H₂O, relatively abundant liquid CO₂, and CO₂-rich vapor. These CO₂-rich inclusions are the preeminent signature of the fluid-inclusion populations associated with the gold-bearing veins and the gold-bearing episyenite (fig. 67A-D). About 70 percent of the samples studied contain the liquid carbon dioxide-bearing fluid inclusions. Typically, the combined liquid CO₂ plus vapor proportion of these inclusions is in the 15- to 20-volume-percent range. A very few of these inclusions also show extremely small opaque to partially translucent minerals. The salinity of these type-IV inclusions also is moderate (3 to 9 weight percent NaCl equivalent). In addition, primary quartz in the Late Cretaceous two-mica monzogranite contains abundant concentrations of type-IV inclusions in

are somewhat similar to those of gold from porphyry copper deposits in other areas determined]

Au (fineness)						
Mean	Au (Au+Ag)x1,000	Au/Ag	Au/Cu	Au/Ag Cu	Ag/Cu	Characteristic trace elements, in order of abundance
Basin						
67.8	681	2.1	900	28	425	Bi, Pb, Ba
73.7	769	3.3	1,170	52	351	Pb, Mo, Bi, Te, Co, Ni
76.0	761	3.2	2,083	89	664	Pb, Bi
63.9	694	2.1	913	30	444	Pb, Bi, Mo, Co, V, Ba
80.8	809	4.2	449	23	106	Pb, Bi, Mo, W
79.2	793	3.8	528	26	138	Pb, Mo, Bi
77.9	782	3.6	250	12	69	Pb, Bi, Mo
79.6	804	4.3	470	25	108	Pb, Bi, Sb, Zn, Ba
76.7	769	3.3	1,400	59	411	Pb, Mo, Bi, Sb, Zn, Cr, Ba
79.6	806	4.1	530	27	135	Pb, Bi, Cd
Basin						
81.4	819	4.5	728	40	161	Pb, Bi, Sb, Zn, Cr, Sn, Mo
80.8	829	4.8	1,403	83	288	Pb, Bi, As, Mo
81.2	814	4.4	1,620	88	370	Pb, Bi, Mo, Cr, V, Pd
67.5	676	2.1	2,250	70	1,080	Pb, Cr
78.5	787	3.7	1,353	64	367	Pb, Bi, Zn, Mo, V
porphyry deposits						
74.0	741	2.9	1,500	58	518	Pb, Bi, Sb, Zn, Sn, Cr, Ni
70.3	704	2.4	1,800	60	740	Pb, Bi, Sb, Zn, As, Te
74.8	749	3.0	500	20	167	Pb, Bi, Sb, Zn, As, Te
75.0	750	3.0	500	20	167	Pb, W

clusters (fig. 67B, C) and in planar arrays along secondary annealed microfractures (fig. 67D). Thus, the CO₂-rich fluids are probably younger than the initial crystallization of the two-mica monzogranite from a magma.

Artificially broken cleavage surfaces in galena also were examined using the SEM to study fluid inclusions. Generally, the fluid inclusions in galena are rounded and equant in the range 1.0 to 10.0 μm , although some elongate fluid inclusions are as long as 40 μm . The fluid inclusions are apparently free of daughter minerals, although this judgment is based on the examination of only a limited number of samples of galena. Some of the inclusions contain crystals of quartz, potassium feldspar, iron sulfide (possibly marcasite because of apparently orthorhombic habit and comb structure), and an unknown silver telluride mineral. Many of these crystals are probably minerals captured during late crystallization stages of the host galena. Trace amounts of silver also were detected locally in some crystals of galena by spot qualitative analyses using the energy dispersive analyzer.

HOMOGENIZATION TEMPERATURES AND SALINITIES

Homogenization temperatures in the Gold Basin-Lost Basin districts are in the range 150 °C to about 300 °C (table 27). However, most of the homogenization temperatures are approximately 200 °C. Although the overwhelming bulk of the heating tests resulted in the fluid inclusions filling to liquid, some inclusions in two samples from the quartz + carbonate + sulfide(s) vein stage (table 27, mineralization stage B) homogenize to vapor. In addition, only one sample contains relatively abundant vapor-rich (table 27, type II) inclusions in late-stage clear quartz, a relation which suggests either that boiling occurred only locally during mineralization and most likely during the final stages of the mineralization or that these vapor-rich inclusions reflect secondary necking. A significant difference in homogenization temperatures was not apparent between the feldspar-dominant stage (table 27, mineralization stage A) and the quartz-carbonate-sulfide(s) stage (table 27, mineralization B) in which the bulk of the gold was finally deposited. However, at most only six of the

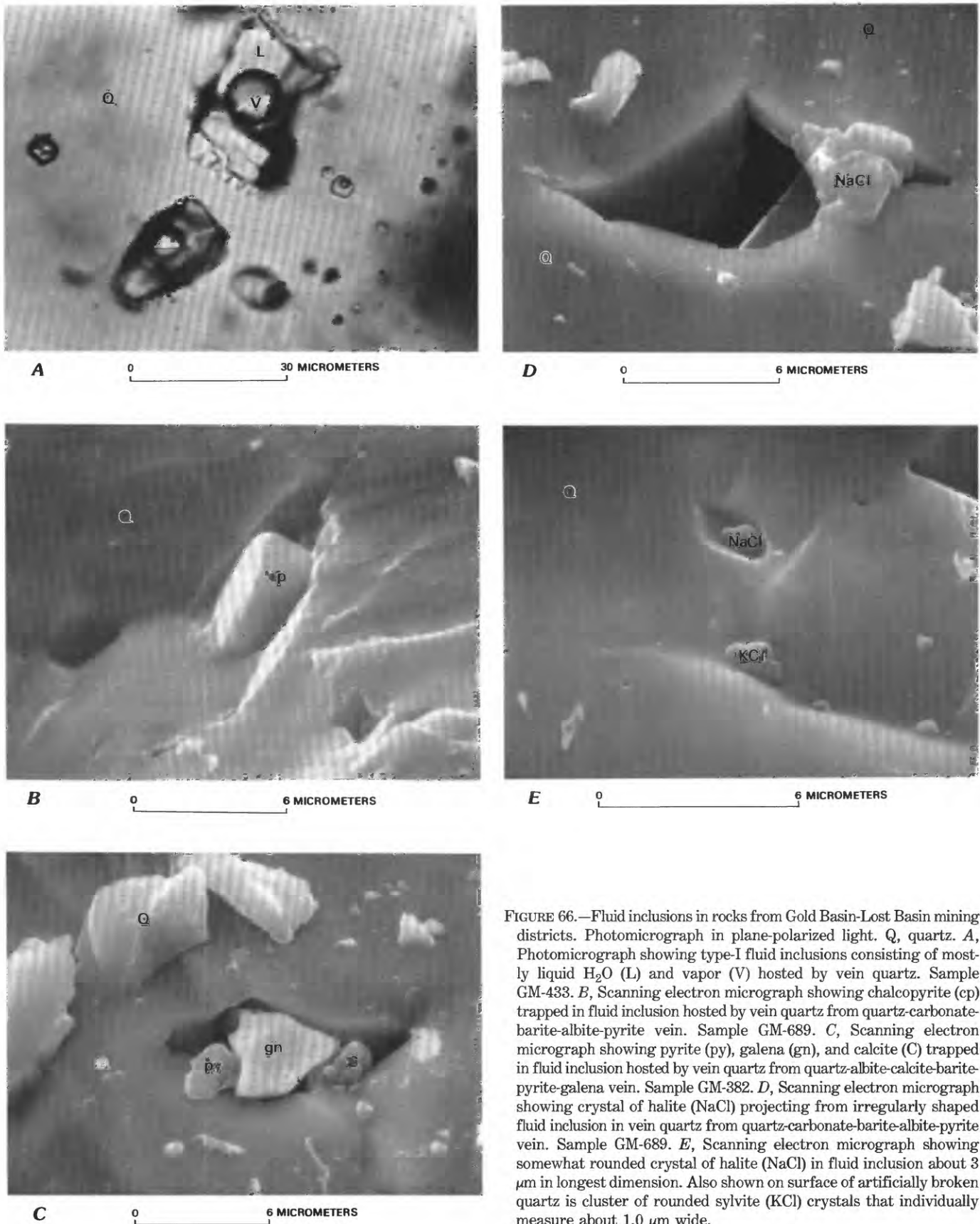


FIGURE 66.—Fluid inclusions in rocks from Gold Basin-Lost Basin mining districts. Photomicrograph in plane-polarized light. Q, quartz. A, Photomicrograph showing type-I fluid inclusions consisting of mostly liquid H_2O (L) and vapor (V) hosted by vein quartz. Sample GM-433. B, Scanning electron micrograph showing chalcopyrite (cp) trapped in fluid inclusion hosted by vein quartz from quartz-carbonate-barite-albite-pyrite vein. Sample GM-689. C, Scanning electron micrograph showing pyrite (py), galena (gn), and calcite (C) trapped in fluid inclusion hosted by vein quartz from quartz-albite-calcite-barite-pyrite-galena vein. Sample GM-382. D, Scanning electron micrograph showing crystal of halite (NaCl) projecting from irregularly shaped fluid inclusion in vein quartz from quartz-carbonate-barite-albite-pyrite vein. Sample GM-689. E, Scanning electron micrograph showing somewhat rounded crystal of halite (NaCl) in fluid inclusion about $3 \mu m$ in longest dimension. Also shown on surface of artificially broken quartz is cluster of rounded sylvite (KCl) crystals that individually measure about $1.0 \mu m$ wide.

studied samples are from the feldspar-dominant stage of mineralization and probably include some quartz paragenetically later than the feldspar (mostly albite).

The salinities of the fluid inclusions determined from the districts range from about 6 to about 35 weight percent NaCl equivalent. The measured temperatures of first melting of ice in the fluid inclusions not containing a daughter mineral of NaCl are consistently near -24°C , a value that is very close to the -21.1°C expected eutectic temperature for the system NaCl-H₂O. From this relation we infer that the inclusion fluids contain sparse concentrations of calcium or magnesium, thereby supporting

our referral of the data to the system NaCl-H₂O. The type-I inclusions generally show salinities between 10 and 14 weight percent NaCl equivalent (table 27), and their abundance in the deposits, together with type-IV inclusions, indicates the largely nonboiling nature of the mineralizing fluids. Only four of the samples studied contain NaCl daughter minerals, and the measured solution temperature (260°C) of the NaCl in one of these samples suggests that the salinities very locally were as high as 35 weight percent NaCl equivalent. However, within these overall salinity limits there is a wide range even within a single crystal of vein quartz or fluorite, suggesting the

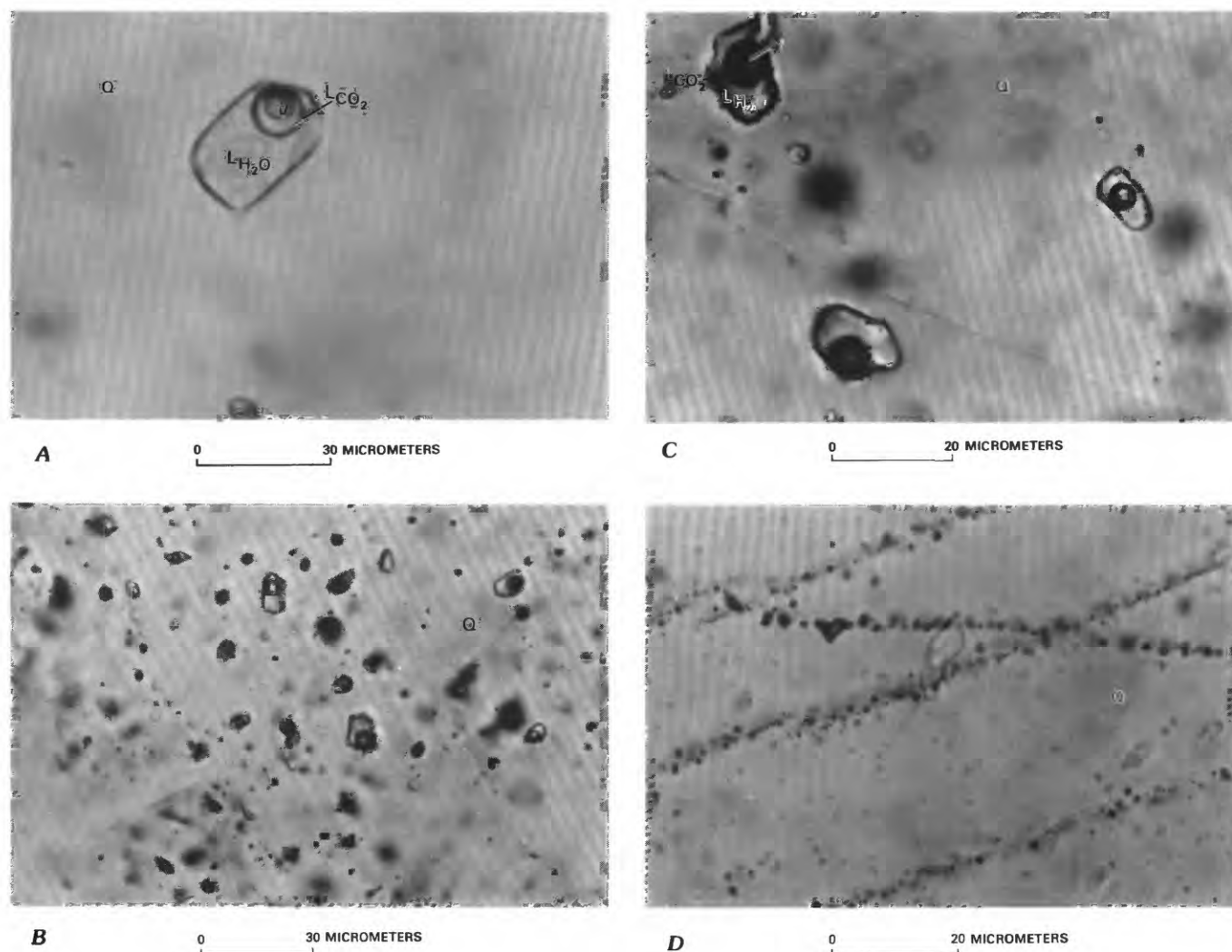


FIGURE 67.—Relations among liquid carbon dioxide-bearing (type IV) fluid inclusions. Q, quartz; L_{H₂O}, mostly liquid H₂O; L_{CO₂}, mostly liquid carbon dioxide; V, mostly CO₂ vapor. Plane-polarized light. A, Isolated, relatively large, pseudosecondary fluid inclusion containing abundant liquid carbon dioxide at room temperature. Inclusion is hosted by vein quartz from approximately 0.6-m-thick quartz-chalcopyrite-galena vein emplaced along a shallow-dipping fault. Sample GM-433. B, Typical concentration of type-IV apparently second-

ary fluid inclusions in primary quartz phenocrysts in the Late Cretaceous two-mica monzogranite. Sample GM-1089. C, Closeup view showing relative proportions of mostly liquid H₂O, liquid carbon dioxide, and mostly carbon dioxide vapor found commonly in fluid inclusions hosted by primary quartz in the Late Cretaceous two-mica monzogranite. Sample GM-1103. D, Abundant secondary type-IV fluid inclusions along annealed microfractures in primary quartz in the Late Cretaceous two-mica monzogranite. Sample GM-977.

TABLE 27.—Homogenization temperatures and salinity data from fluid-inclusion studies in the Gold Basin-Lost Basin mining districts

[A, feldspar-dominant stage (quartz + albite ± barite ± sulfide(s) ± white mica assemblage; B, quartz + carbonate + sulfide(s) ± gold ± fluorite stage; queried where uncertain. F, fluorite; Q, quartz. Salinity is expressed in equivalent weight percent NaCl using the freezing point depression method of Roedder (1962). x, liquid CO₂ present at room temperature; ---, liquid CO₂ not observed at magnifications of about ×1,000. NaCl, halite; Hm, hematite; Anh, anhydrite; Carb, carbonate; queried where identification uncertain; ---, daughter minerals not observed at magnifications of about ×1,000. N.D., not determined; e, estimated]

Sample	Mineralization stage	Mineral	Homogenization temperature (°C)	Salinity	Liquid CO ₂	Daughter minerals	Comments
GM-14	B	F	250; >260	35	x	NaCl	NaCl daughters dissolve at 260°C
GM-14a	B	Q	180-255	14.1-14.4	x	---	Contains visible gold
GM-280	B	F	251-268	8.5-9	x	---	Fluorite-bearing episyenitic rock containing disseminated gold (see text)
GM-382	A	Q	195-205	10.3	x	---	Early-stage quartz
		Q	190±10	8	---	---	Later quartz
		Q	193±5	15.8	---	---	Later quartz
GM-431	B	Q	N.D.	N.D.	x	Hm, Anh	Early-stage quartz
		Q	175e	N.D.	---	Am, Anh	Late-stage quartz
GM-433	B?	Q	250±25	12-15.5	x	---	Early stage. Some inclusions fill to vapor
		Q	N.D.	N.D.	---	---	Late stage. Relatively abundant vapor-rich inclusions
GM-436b	B	Q	220±10	11-14	x	---	Early stage
		Q	N.D.	N.D.	---	---	Late stage
GM-437	B?	Q	210-230	15.4-22	x	Anh	Early stage
		Q	205±5	12-13	---	Anh	Late stage
GM-447	B	Q	183±3	8.7-12.6	---	---	Early-stage milky quartz
		Q	167±3	8-13	---	---	Late-stage clear quartz
GM-456f	B	Q	225e	10	x	---	---
GM-466	B	Q	180-210	9.5-14	---	---	---
GM-467	B	Q	200e	N.D.	x	---	---
GM-470a	B	Q	250e	14	x	---	---
		Q	200±15	22	---	---	---
GM-479	B	Q	200±5	22	---	Anh	---
		Q	170	6-12	---	---	---
GM-482	A or B	Q	N.D.	N.D.	x	Hem	---
		Q	175	N.D.	---	---	---
GM-489	B	Q	N.D.	N.D.	x	---	Early stage
		Q	190±10	7-14	---	---	Late stage
GM-513	B	Q	205±10	13-16	---	---	---
GM-516a	B	Q	178-240	10.2-16.3	x	---	Contains visible gold in early-stage quartz
		Q	110-120	N.D.	---	---	Late-stage, secondary fluid inclusion
GM-567	B	Q	189	5.5	---	---	---
GM-569	B	Q	186	17-23	---	---	---
GM-576	B	Q	200e	N.D.	x	---	---
GM-688	A	Q	250e	>30	---	NaCl	---
		Q	250e	N.D.	x	---	---
		Q	200e	N.D.	---	---	---
GM-689	A	Q	N.D.	N.D.	x	---	---
		Q	250e	>30	---	NaCl	---
		Q	225-245	N.D.	---	Hm	---
GM-690	A	Q	250e	N.D.	---	Hm, Anh(?)	Early stage. May have some NaCl daughter minerals
		Q	176-205	N.D.	---	---	Late stage
GM-735	B	Q	186-197	10.4	---	---	Contains visible gold
GM-735-1	B	Q	178-200	N.D.	---	---	Contains visible gold
GM-802a	B	Q	225e	N.D.	x	Anh(?)	---
		Q	150	N.D.	---	---	Late secondary fluid inclusions
GM-802b	B	Q	225-230	>30	---	NaCl	---
		Q	200e	N.D.	x	---	---
		Q	200e	N.D.	---	Anh(?)	---
GM-812	B	F	<200e	N.D.	---	---	---
		Q	<200e	N.D.	---	---	---
GM-837	B	Q	250e	N.D.	---	---	---
		Q	250e	N.D.	x	---	---
GM-878	A or B	Q	250e	N.D.	x	---	Some inclusions possibly contain Anh
GM-897	B	Q	200e	N.D.	---	---	---
GM-913	B	Q	250e	N.D.	x	---	---
GM-913v	B?	Q	200e	N.D.	---	---	Vein
GM-917e	B	Q	250±10	N.D.	x	---	Some fill to vapor
		Q	250-275e	N.D.	---	Hm	---
GM-923	B	F	N.D.	N.D.	x	---	Secondary fluid inclusions
		Q	300	N.D.	x	---	Estimate 50 percent of inclusions contain CO ₂
		Q	250e	N.D.	x	---	---
		Q	255	N.D.	x	---	Quartz very milky
		Q	167	N.D.	---	---	Late stage
GM-923a	B	Q	235-240	N.D.	x	---	---
		Q	210±10	N.D.	---	---	---
GM-927	B	Q	250	N.D.	---	Carb	---
GM-1134h	B	Q	145-186	5.8-9.5	---	---	Fluorite-bearing syenitic rock containing disseminated gold (see text)

salinity of the fluids associated with gold mineralization varied widely. The overall range in salinities of the fluids associated with gold mineralization largely bridges the interval in fluid compositions between many epithermal precious-metal districts and porphyry copper deposits (fig. 68).

In an attempt to bracket closely the pressure-temperature-chemical environment(s) associated with Late Cretaceous and (or) early Tertiary precious- and base-metal mineralization in the districts, fluid-inclusion studies were focused especially on (1) samples from the episyenitic alteration pipes containing disseminated gold and on (2) a quartz-fluorite-white mica vein that cuts the Late Cretaceous two-mica monzogranite.

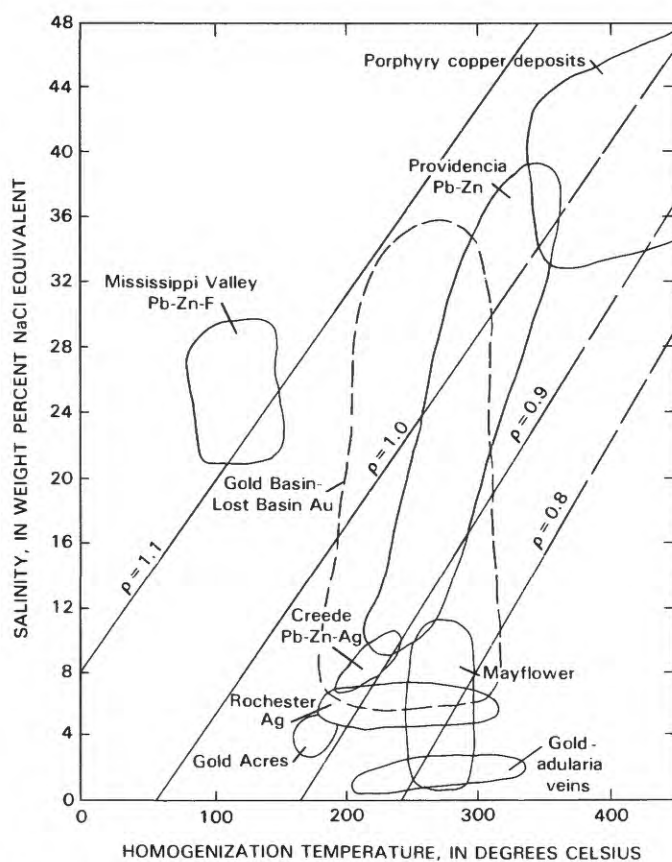


FIGURE 68.—Fluid-inclusion homogenization temperature and salinity data for various precious- and base-metal districts and deposits. Modified from Nash (1972). Data for Rochester, Nev., silver district are from Vikre (1977, 1981) and have been corrected for inferred pressures of approximately 1,000 bars during mineralization. Data for Gold Basin-Lost Basin districts are from this study. Lines of equal density (in grams per cubic centimeter) also shown; dashed where located approximately.

FLUID INCLUSIONS IN THE EPISYENITIC ALTERATION PIPES CONTAINING DISSEMINATED GOLD

Abundant type-I and type-IV fluid inclusions are present in hydrothermal quartz and purple fluorite that fill cavities in the episyenitic alteration pipes that contain disseminated gold. Two samples (table 27, GM-280 and GM-1134h) were collected from coarse-grained episyenitic rock in the interior portions of two of the alteration pipes. However, the generally small size of the fluid inclusions in these rocks restricted our quantitative studies to fluid inclusions in fluorite from sample GM-280 and to fluid inclusions in quartz from sample GM-1134h. All fluid inclusions are trapped in the fluorite along nearly planar arrays.

Type-I fluid inclusions presumed to be primary, or having formed during initial crystal growth (Roedder, 1972), are present in diffuse planar arrays that commonly contain parallel linear trains of inclusions, the effect of which is to create a cubic network (fig. 69A). These networks are inferred to reflect the cubic habit and growth planes of the host fluorite and suggest that the fluid inclusions were trapped on growth planes during early stages of the fluorite crystallization. The fluid inclusions are equant in shape, generally rhomblike to circular, and range from less than 4 μm to 14 μm . They exhibit a consistent vapor fraction, which averages 20 volume percent at room temperatures. Although these early stage or primary type-I fluid inclusions in fluorite show at magnifications of about $\times 1,000$ no liquid carbon dioxide at room temperature, they nonetheless may contain limited amounts of carbon dioxide. The solubility of carbon dioxide in H_2O at 25 $^\circ\text{C}$ and at a pressure of 50 bars is approximately 2.1 mol percent (Greenwood and Barnes, 1966), and the limit of detection optically is about 3 mol percent (Ypma, 1963).

Type-IV fluid inclusions in the fluorite are interpreted to be mostly pseudosecondary. This type of fluid inclusion is concentrated in discontinuous planar arrays that are confined to the interiors of the fluorite crystals. The fluid inclusions were trapped during the latter stages of growth of the fluorite. Crystallization of the fluorite must have continued after trapping of the fluids along these planar arrays. The type-IV inclusions consist of saline fluid (mostly H_2O), vapor (mostly carbon dioxide), and about 15 to 18 volume percent liquid carbon dioxide. In fact, one of the diagnostic features of the pseudosecondary type-IV fluid inclusions in these gold-bearing episyenitic rocks is the high proportion of liquid carbon dioxide in them at room temperature (fig. 69B). The volume ratio of liquid carbon dioxide to vapor has a value of about nine, and liquid carbon dioxide plus vapor is typically about 20

volume percent of the inclusion. These type-IV inclusions are somewhat larger, ranging from 16 to 35 μm , than the primary type-I fluid inclusions noted above. Their habits are equant to somewhat elongate. The type-I and type-IV fluid inclusions trapped together in the fluorite suggest that the fluids that circulated through the episyenitic rocks at various times during the crystallization of fluorite and thus during the introduction of gold there included wide-ranging proportions of carbon dioxide.

Secondary fluid inclusions are present in fluorite along well-defined planes that converge, diverge, and intersect at various angles and which do not have the generally orthogonal aspect of the primary inclusions. The planes commonly are broadly arcuate and cut crystal boundaries in the fluorite. Such secondary inclusions exhibit varied shapes, from smoothly elliptical to highly irregular, and varied sizes, from 10 to 48 μm in diameter. The secondary inclusions are mostly type I and show varied amounts of vapor fill at room temperature, with a range from 0 to 50 percent, although most commonly they contain between 2 to 10 volume percent vapor.

Salinities of the primary and pseudosecondary fluid inclusions in fluorite overlap significantly the salinities of the secondary fluid inclusions. Salinities of the primary type-I fluid inclusions were determined using the depression of freezing-point method (Roedder, 1962), and salinities of the pseudosecondary type-IV fluid inclusions were determined from the final melting temperature of clathrate, most likely $\text{CO}_2 \cdot 5\frac{3}{4} \text{H}_2\text{O}$ (Roedder, 1963), formed during the freezing runs (see Takenouchi and Kennedy, 1965; Bozzo and others, 1975; Collins, 1979). The overall range of salinities of the primary fluid inclusions is from approximately 3.0 to 9.0 weight percent NaCl equivalent (fig. 70A). Most salinity determinations are in the narrow range 8.5 to 9.0 weight percent NaCl, whereas the fluid inclusions containing liquid carbon dioxide at room temperature seem to show salinities at the lower end (3.0 to 8.0 weight percent NaCl equivalent) of the overall range. Salinities of obviously secondary fluid inclusions in fluorite mostly are approximately 6.5 to 7.0 weight percent NaCl equivalent (fig. 70B, C); they are approximately 2.0 weight percent NaCl, less saline than the primary inclu-

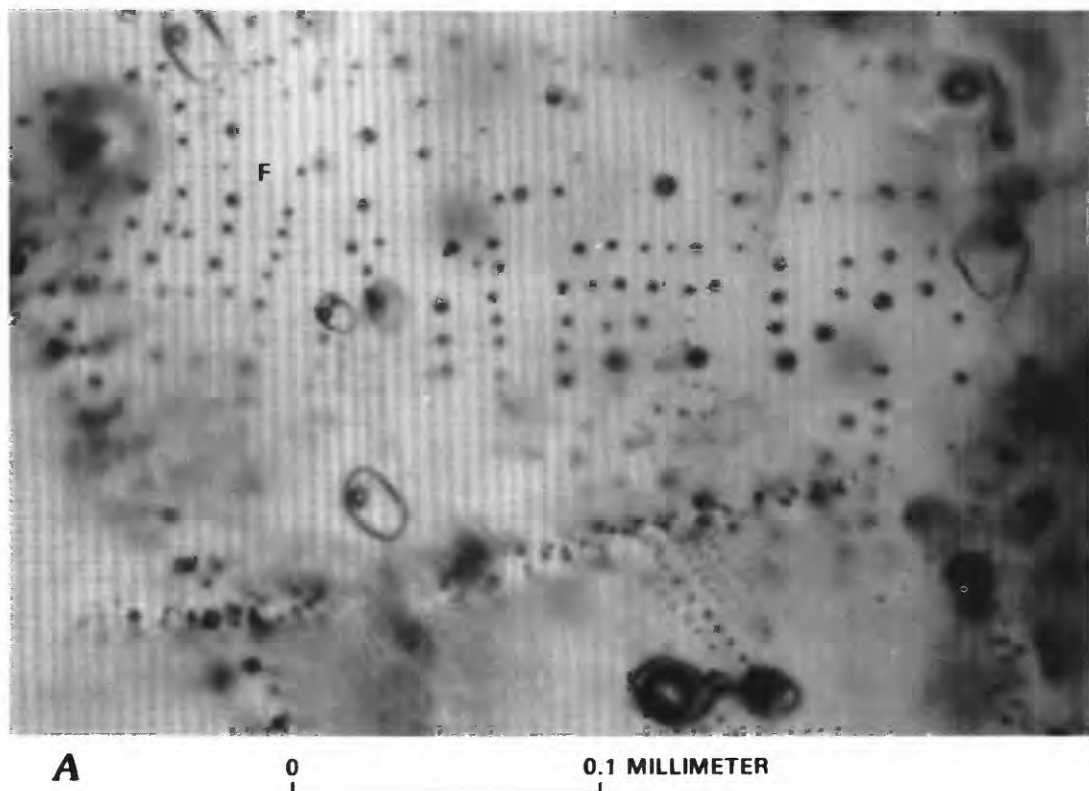


FIGURE 69.—Fluid inclusions in samples from gold-bearing episyenitic rock. Plane-polarized light. F, fluorite. A, Extremely small, primary fluid inclusions defining cubic network in fluorite. Also in field of view, discontinuous planar arrays of very small fluid inclusions and large type-IV and rare type-II fluid inclusions that are along discontinuous planes; each of these characteristics is inferred to reflect pseudosecondary relations. Sample GM-280b. B, Relatively large pseudosecondary type-IV fluid inclusion in fluorite. V, vapor; L_{CO_2} , liquid carbon dioxide; $\text{L}_{\text{H}_2\text{O}}$, mostly liquid H_2O . Sample GM-280b.

sions. However, the salinity of the secondary fluids ranges upward to slightly more than 15 weight percent NaCl equivalent.

In all, 41 filling temperatures were measured from the primary, pseudosecondary, and secondary inclusions trapped in fluorite from the gold-bearing episyenitic rocks (fig. 71). The primary type-I fluid inclusions show a very restricted range in filling temperatures between 251 °C and 268 °C (262 °C mean). The pseudosecondary type-IV fluid inclusions contain significant proportions of liquid carbon dioxide and have a lower or first homogenization wherein their vapor phase disappears between 26.9 and 28.0 °C. The average temperature of vapor-phase disappearance for these inclusions is 27.6 °C. Continued heating of four of these inclusions results in their homogenization into a single liquid phase in the temperature range 280 to 282 °C. The secondary fluid inclusions in fluorite all fill to liquid at temperatures of 130 to 167 °C, significantly less than the filling temperatures of the primary and pseudosecondary fluid inclusions (fig. 71).

Limited freezing and heating tests also were performed on type-I fluid inclusions hosted by irregular patches of secondary quartz, that fills cavities (table 27, sample GM-1134h). The quartz, which contains these fluid inclusions, typically contains some needles of rutile that are

concentrated near the margins of the quartz. The fluid inclusions range in size from less than 1 to 24 μm . Some have elliptical shapes, but many are irregular in outline and confined along planar annealed microfractures, suggesting secondary origins. Eight freezing tests yield salinities in the range 5.8 to 9.5 weight percent NaCl equivalent; the mean is 7.8 weight percent NaCl equivalent. Heating tests show 17 fluid inclusions to fill to liquid in the range 144 to 186 °C. The filling temperatures for these fluid inclusions in quartz correspond quite well the filling temperatures of the secondary fluid inclusions in fluorite; the mean filling temperature of the fluid inclusions in quartz is 159 °C, and the mean temperature of the secondary fluid inclusions in fluorite is 149 °C. Thus, much of this paragenetically late quartz, sparsely distributed through the episyenitic rock, may have been introduced after the initial deposition of fluorite there.

**FLUID INCLUSIONS IN A QUARTZ-FLUORITE-WHITE
MICA VEIN THAT CUTS THE LATE CRETACEOUS
TWO-MICA MONZOGRAHITE**

Additional fluid-inclusion studies were conducted on a sample of a carefully selected quartz-fluorite-white mica vein (table 27, sample GM-923) that unquestionably cuts

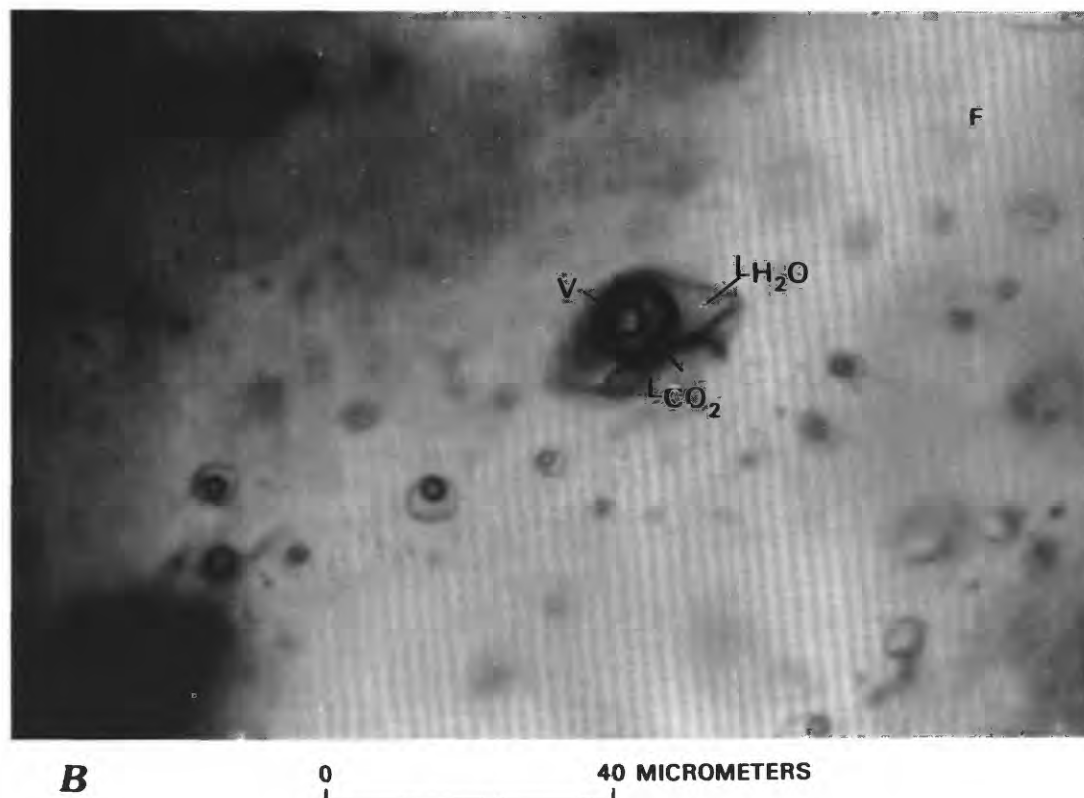


FIGURE 69.—Continued.

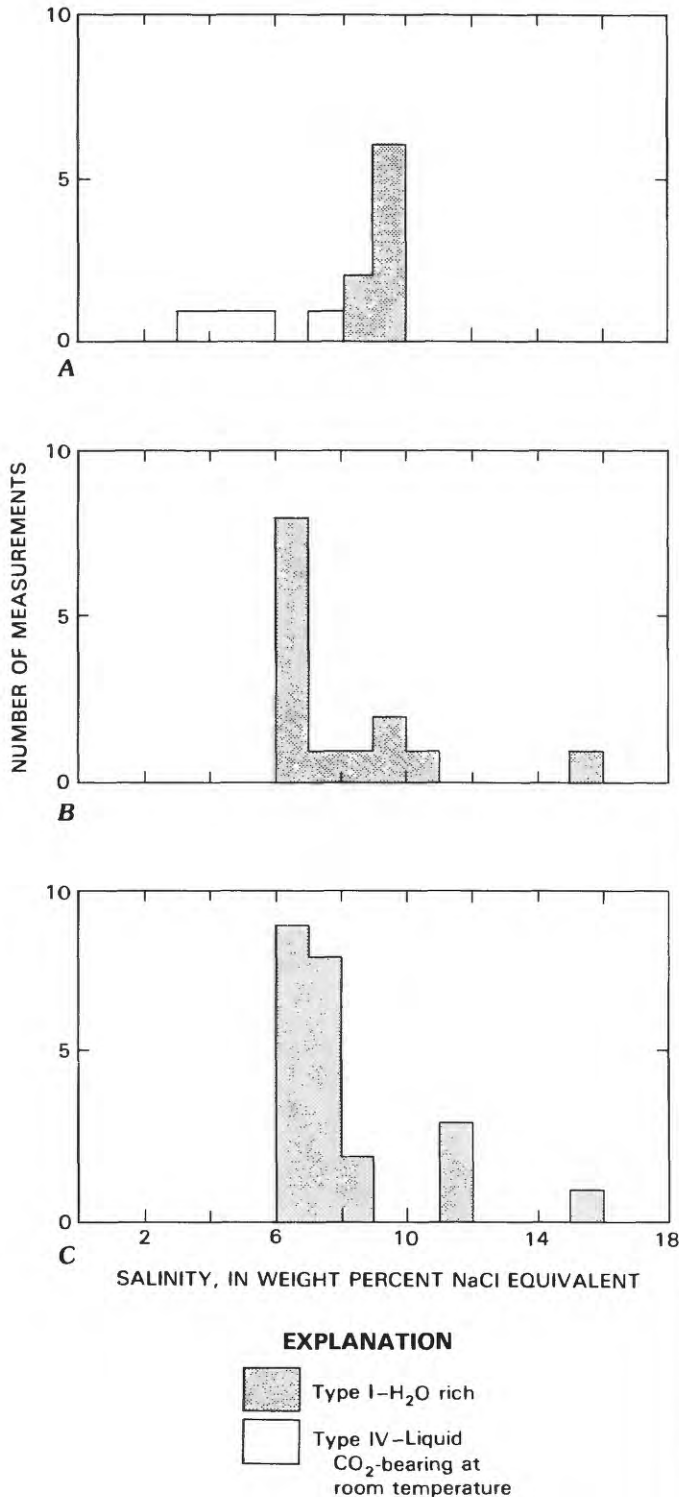


FIGURE 70.—Salinities of fluid inclusions in fluorite from gold-bearing episyenitic rocks. Sample GM-280b. A, Salinities of primary and pseudosecondary fluid inclusions determined using depression of freezing point method for type-I H₂O-rich fluid inclusions and final melting temperature of clathrate(s) for type-IV fluid inclusions (see text). B, Salinities of secondary inclusions determined using the depression of freezing point method. C, Salinities of secondary inclusions determined using final melting temperature of clathrate(s).

the Late Cretaceous two-mica monzogranite and that appears to be related genetically and temporally to it. The purposes of these detailed studies were to establish the pressure, temperature, and chemistry of fluids associated closely with the two-mica monzogranite and to compare and contrast such fluids with those in mineralized veins elsewhere in the district and with the occurrence of gold-bearing episyenitic pipes. Sample GM-923 (table 27) was obtained from a 25- to 45-cm-wide vein that cuts the Proterozoic metamorphic gneiss and the two-mica monzogranite at its east margin. Elsewhere, at the nearby Jumbo prospect (P.M. Blacet, unpub. data, 1967-72), similar veins are cut by two-mica monzogranite dikes. These complex crosscutting relations indicate that the vein is related genetically to the emplacement of the two-mica monzogranite. White mica from the vein yielded a K-Ar age of 68.8 ± 1.8 Ma. The sample selected consists of massive milky-white quartz that encloses colorless fluorite in anhedral crystals as much as 3 cm wide; the sample also includes cubes as much as 5 mm across of limonite and (or) hematite that have replaced pyrite and muscovite flakes as much as 2 mm wide.

Fluid inclusions in both quartz and fluorite consist essentially of two types: (1) liquid-rich two-phase type-I inclusions that are composed of fluid plus vapor and (2) liquid-rich type-IV inclusions that consist of saline fluid + vapor + liquid carbon dioxide. However, in very small inclusions, carbon dioxide is commonly not visible, but its presence could be determined by behavior of the phases during heating and freezing tests, following procedures outlined by Collins (1979). When cooled, the inclusions show two freezing points, the first during the development of clathrate and the second when the saline liquid itself freezes. During warming, these small inclusions

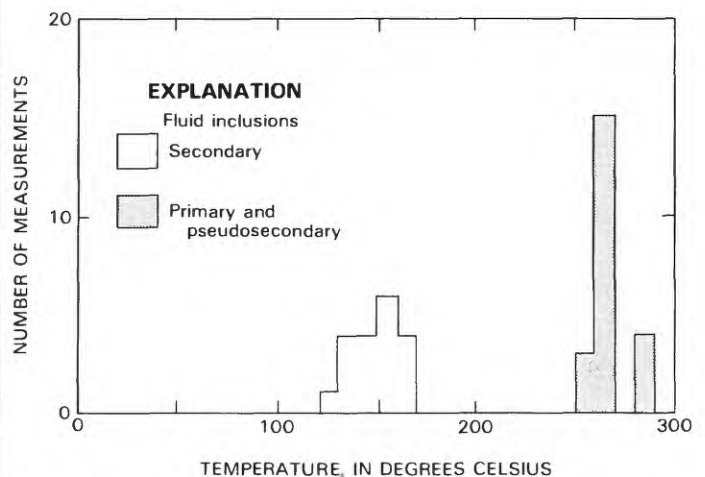


FIGURE 71.—Filling temperatures in fluorite from gold-bearing episyenitic rocks. Sample GM-280b.

generally fail to show visible melting of ice at temperatures below 0 °C because of the presence of clathrate. The first visible evidence of a phase change occurs when the clathrate melts somewhere in the temperature range between 0 and 10 °C. This melting is accompanied by rapid expansion of the vapor phase and sweeping of the vapor phase across the inclusion, commonly followed by the immediate reappearance of the third phase, liquid carbon dioxide. Fluid inclusions in quartz are slightly different from those in fluorite. Consequently, all inclusion types are described separately by host mineral.

Two-phase type-I fluid inclusions observed in fluorite occur in planar arrays. The inclusions have regular ovoid shapes that range in length from 2 to 22 μm . The percentage of vapor fill in the inclusions at 22 °C is fairly consistent at 5 to 7 volume percent; salinities range from 6.3 to 10.1 weight percent NaCl equivalent (fig. 72A) with an average of 9.0 weight percent. Type-I fluid inclusions homogenize by vapor disappearance between 149 and 206 °C, with an average of 177 °C (fig. 72B). The narrow range of salinities and homogenization temperatures for these inclusions indicates that necking and resultant changes in vapor percentage and salinity were not significant following trapping of these inclusions. However, the presence of the type-I fluid inclusions along intersecting planar arrays contrasts with the mode of occurrence of the type-IV fluid inclusions in the fluorite, and this relation suggests that the type-I fluid inclusions studied are secondary.

Type-IV liquid carbon dioxide-bearing inclusions in the fluorite do not appear to be constrained to planar arrays. Instead, they are present in restricted clusters in which individual inclusions occur along wispy rays that radiate from a vague center. The type-IV fluid inclusions are about the same size as the type-I fluid inclusions, and they also have consistently elliptical outlines. At 22 °C, about 7 percent of the volume of a typical inclusion consists of vapor plus liquid carbon dioxide; of this, 10 to 15 volume percent is vapor. The salinity of these fluid inclusions ranges from 5.5 to 6.0 weight percent NaCl equivalent and is thus somewhat lower than many of the type-I fluid inclusions (fig. 72A). The type-IV fluid inclusions homogenize to the liquid high-density carbon dioxide phase by vapor disappearance between 28.1 and 29.1 °C, with an average of 28.7 °C for nine measurements. Further increases in temperature enhance the mutual solubilities of the phases, and between 203 and 207 °C (average 206 °C) the type-IV fluid inclusions homogenize to a single phase (fig. 72B). The chemistry, habit, and higher homogenization temperatures contrast the type-IV fluid inclusions with secondary type-I fluid inclusions in the vein fluorite and indicate that fluids circulating in the environment of the vein decreased in content of carbon dioxide and increased somewhat in salinity with time.

Both primary and pseudosecondary type-I and type-IV fluid inclusions in vein quartz are randomly dispersed throughout the quartz and can be distinguished easily from planar trains of obviously secondary inclusions. The fluid inclusions tend to cluster by type, indicating that the silica-depositing fluid varied significantly in chemistry during the deposition of quartz. Type-I fluid inclusions have 4 to 7 volume percent vapor at 22 °C. They range from about 1 to 16 μm in size and have regular elliptical forms, and they show a very good correspondence of their salinities to the type-IV fluid inclusions (fig. 72C). The full range of salinities determined for both types of fluid inclusions is between 7.0 and 11.0 weight percent NaCl equivalent, averaging about 8.2 weight percent NaCl equivalent. However, almost all of the type-I fluid inclusions studied contain some carbon dioxide because they develop clathrates during freezing tests. The clathrates persist to temperatures in the range 4.6 to 6.4 °C. The type-IV fluid inclusions in quartz range in size from less

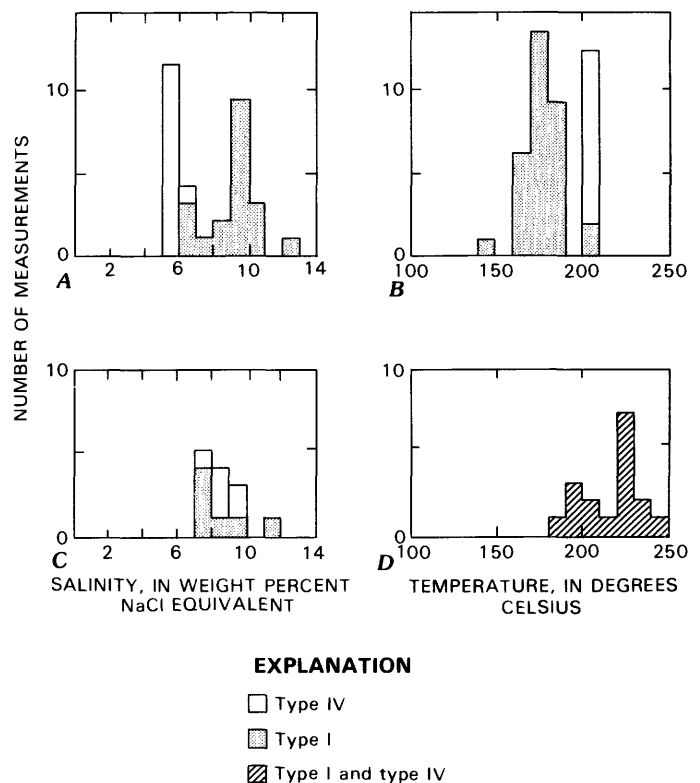


FIGURE 72.—Salinity and filling-temperature data obtained from selected quartz-fluorite-white mica vein. Sample GM-923. A, Salinities of fluid inclusions hosted by fluorite. Salinities of type-IV primary fluid inclusions determined using final melting temperature of clathrate (see text), and salinities of secondary type-I inclusions determined using depression of freezing point method. B, Filling temperatures of fluid inclusions hosted by fluorite. C, Salinities of fluid inclusions hosted by quartz. Salinities determined as in A. D, Filling temperatures of fluid inclusions hosted by quartz.

than 1 to 22 μm . The small size of the fluid inclusions commonly makes it difficult or impossible to resolve the liquid carbon dioxide meniscus even at magnifications of about $\times 1,000$. For the larger of these type-IV fluid inclusions, visual estimates suggest equal volumes of liquid carbon dioxide and vapor carbon dioxide at room temperatures. Typically, these fluid inclusions contain 80 to 90 volume percent saline liquid. The type-IV fluid inclusions homogenize by vapor disappearance between 28.3 and 30.0 $^{\circ}\text{C}$, with an average of 29.4 $^{\circ}\text{C}$. This indicates that the carbon dioxide is somewhat less dense than in the fluorite inclusions but still dense enough to homogenize to liquid carbon dioxide rather than vapor upon heating (see Kennedy, 1954; Koltun, 1965, fig. 5). Upon additional heating, the type-I and type-IV inclusions homogenize to a single phase in the range 188 to 240 $^{\circ}\text{C}$, averaging 218 $^{\circ}\text{C}$ (fig. 72D). As such, these filling temperatures are slightly higher than those measured from the primary type-IV fluid inclusions in fluorite (compare fig. 72B with 72D).

COMPARISON OF FLUIDS IN A QUARTZ-FLUORITE-WHITE MICA VEIN AND IN GOLD-BEARING EPISYENITIC PIPES

Similarities in physical and chemical properties determined by fluid-inclusion studies of a quartz-fluorite-white mica (table 27, sample GM-923) vein and the gold-bearing episyenitic pipes provide an insight into the deposition of fluorite and quartz and their accompanying gold mineralization in the districts.

Similarities include:

1. Carbon dioxide densities of fluid inclusions from the pipes and the vein, which is clearly related to the two-mica monzogranite, have very similar low densities of about 0.61 to 0.66 g/cm^3 . The fluids associated with the introduction of gold into the episyenitic pipes show a slightly greater density of carbon dioxide than fluids from the selected vein. Type-IV fluid inclusions in fluorite from the episyenitic pipes homogenize by vapor disappearance in the range 26.9 to 28.5 $^{\circ}\text{C}$, which corresponds to densities of carbon dioxide of about 0.64 to 0.66 g/cm^3 . Type-IV fluid inclusions in the well-studied vein homogenize by vapor disappearance in the range 28.1 to 30.4 $^{\circ}\text{C}$, which corresponds to densities of carbon dioxide of about 0.61 to 0.64 g/cm^3 . Visual estimates of the proportion of liquid carbon dioxide present at room temperatures in many other veins throughout the districts suggest that their carbon dioxide contents are similar to those of sample GM-923.
2. Carbon dioxide content of fluid inclusions of both the vein and the pipes, calculated from visual volume estimates of the amount of carbon dioxide in the fluid inclusions at room temperatures, ranges from about 4 to about 8 mol percent. The proportions of carbon

dioxide to saline-water solution appear to be very consistent (see above), but precise determinations are difficult to make (Roedder and Bodnar, 1980).

3. Salinities of fluids that deposited quartz and fluorite, and presumably gold, in the gold-bearing pipes and the vein are in the same range. Fluid salinities range from 3 to 16 weight percent NaCl equivalent and cluster especially in the interval from 6 to 10 weight percent NaCl equivalent, a range not common in many epithermal gold-bearing hydrothermal systems.
4. The mineral assemblages and parageneses in both the late gold-bearing stage of the pipes and the vein are very similar. Hydrothermal minerals in both include quartz, fluorite, pyrite, white mica, ferroan carbonate (ankerite), and gold. The relative amounts of quartz and fluorite, however, are variable in the two environments; quartz dominates in the vein, and fluorite is more abundant than quartz in the pipes; together the two minerals are paragenetically late minerals filling cavities. Both the pipes and the vein show decreasing activity ratios of $(\text{K}^+)/(\text{H}^+)$ over time in their alteration envelopes as the systems evolved from biotite-stable (vein) and potassium feldspar-stable (pipes) assemblages to white mica-stable assemblages.
5. Homogenization temperatures of the vein and the pipes are generally similar. Temperatures of final homogenization to a single fluid for primary type-I and pseudosecondary type-IV fluid inclusions in fluorite from the pipes are among the highest filling temperatures recorded throughout the mining districts. They range from 251 to 282 $^{\circ}\text{C}$ (table 27). Nonetheless, many of the vein occurrences are estimated to have filling temperatures close to these values, and a few were measured so (table 27). In contrast, fluid inclusions from the vein, which more probably was emplaced near the final stages of the Late Cretaceous and (or) early Tertiary mineralization in the districts (exemplified by sample GM-923, which cuts the two-mica monzogranite), show filling temperatures 45 to 60 $^{\circ}\text{C}$ less in quartz and 70 to 100 $^{\circ}\text{C}$ less in fluorite (fig. 72) than those in the pipes.

ESTIMATES OF THE PRESSURE-TEMPERATURE ENVIRONMENT OF MINERALIZATION

Fluid-inclusion data and phase relations provide useful limiting estimates for the physical and chemical environment of mineralization. Consistent proportions of saline liquid, liquid carbon dioxide, and carbon dioxide-rich vapor for most early-stage type-IV fluid inclusions in the gold-bearing episyenitic pipes suggest that they were trapped from a homogeneous fluid. Furthermore, the early-stage CO_2 -rich fluids (pseudosecondary type-IV fluid inclusions

in fluorite, see above) in the pipes most likely include about 8 mol percent CO_2 and are moderately saline, ranging from about 3 to 7 weight percent NaCl equivalent. These type-IV fluid inclusions must also contain minimal amounts of calcium and magnesium as determined from the temperatures of first melting. Thus, we can model the behavior of the fluids by referring to the system NaCl- H_2O - CO_2 . However, the episyenitic pipes also show evidence (primary type-I fluid inclusions) for early-stage circulation of CO_2 -depleted fluids that range from 8 to 10 weight percent NaCl equivalent in salinity. The early-stage fluid inclusions relatively rich in CO_2 in the episyenitic pipes homogenize to a single fluid at temperatures of about 280 to 282 °C. From this isotherm and by assuming a fluid composition including 8 mol percent CO_2 and 6 weight percent NaCl, we interpret pressures at the times of trapping were above 500 bars. In making this interpretation for these fluids, we have assumed that the miscibility gap for the 280 °C isotherm in the system H_2O - CO_2 , initially determined by Todheide and Franck (1963), expanded an amount similar to that found experimentally by Takenouchi and Kennedy (1965). Takenouchi and Kennedy (1965) showed that addition of a limited amount of salt, about 6 weight percent NaCl, to the system H_2O - CO_2 significantly widens the miscibility gap. Furthermore, at a fluid composition of about 8 mol percent CO_2 , isotherms converge tightly and are extremely sensitive to slight differences in pressure (see discussion by Roedder and Bodnar, 1980).

An upper pressure estimate during the development of the episyenitic pipes may be inferred from the experimentally determined solubilities of quartz in the system SiO_2 - H_2O (Kennedy, 1950; Fournier, 1977) and from the fact that dissolution of primary quartz was an important process in the evolution of the episyenitic pipes. Kennedy (1950) showed that a "solubility hump," or region of increasing solubility of silica for decreasing temperature at constant pressure, occurs in the system SiO_2 - H_2O at pressures less than 750 bars. Subsequently, Fournier (1977) refined these experimental results and determined the apex of the "solubility hump" is at a pressure of 715 bars, and a corresponding temperature of 480 °C.

The range in pressure 500–700 bars estimated respectively from data derived from the type-IV fluid inclusions in fluorite, and the primary quartz solubility relations may be used to establish a +50 to +70 °C temperature correction for the primary type-I fluid inclusions. Such a pressure estimate for the type-I fluid inclusions appears to be geologically reasonable because of the very close temporal relations between the two related sets of fluid-inclusion types in the fluorite. The type-I fluid inclusions were trapped from a homogeneous fluid at P - T conditions somewhere along an isochore, or line of equal volume, that originates at a temperature of 263 °C on the two-phase

or liquid-vapor curve for a solution approximately 9 weight percent NaCl equivalent (fig. 70A). This temperature is the average temperature of filling to a liquid of 18 type-I fluid inclusions (fig. 71). Then from the isochoric data for a 10-weight-percent NaCl solution, as compiled by Roedder and Bodnar (1980, fig. 4), our best estimate is that the type-I fluid inclusions in fluorite were trapped at temperatures of about 315 to 335 °C.

Pressure corrections cannot be obtained successfully from fluid-inclusion data (fig. 72) of the quartz-fluorite-white mica vein that cuts the two-mica monzogranite because of lower carbon dioxide content. But these data nonetheless indicate that pressures at the time of trapping were more than 100 bars to maintain the carbon dioxide content of the fluid and to retard effervescing. Fluorite from this vein shows an average temperature of 206 °C for the homogenization of its type-IV fluid inclusions to a single phase. This value in a P - T diagram is then the temperature of the isotherm that marks the boundary between the two-phase and one-phase regions in the system H_2O - CO_2 -NaCl (see Roedder and Bodnar, 1980, fig. 7). Yet, for a 9-weight-percent NaCl-equivalent solution containing approximately 4.5 mol percent CO_2 (values determined from the fluid inclusions), such an isotherm essentially would parallel the pressure axis and cannot be used to establish an effectual lower boundary for the pressure prevailing at the time of trapping of the fluid inclusions. At best, we only can estimate that pressures in the environment of this vein during its emplacement were greater than the pressure along the liquid-vapor curve at the point(s) of homogenization of its two-phase type-I fluid inclusions. These pressures are less than 100 bars. Therefore, we have not been able to determine well-defined limits of the pressures in the fluids associated with the final stages of precious-metal mineralization in the districts.

We judge the pressure-temperature conditions during the late-stage gold mineralization at the site of the episyenitic alteration pipes, namely more than 500 bars and 315 to 335 °C, to be reasonable values for the physical conditions prevailing during the onset of Late Cretaceous and (or) early Tertiary gold mineralization in the districts. A pressure estimate of 500 bars corresponds to a minimum depth of about 2 km under a lithostatic load and a minimum depth of about 5 km under a hydrostatic load. Assumptions involved in the calculation of the hydrostatic load are (1) a nonstratified fluid column occurs above the site(s) of the gold-depositing fluids and (2) the fluid column is open to and extends to the ground surface at the time of gold mineralization (see Roedder and Bodnar, 1980). A value somewhere between lithostatic and hydrostatic is most likely on geologic grounds; the Paleozoic formations that must have overlain the districts total approximately 2.1 km in thickness (Peirce, 1976).

DISCUSSION

Most of the fluid, mineral, and geologic observations related to gold mineralization documented during our study compare well with observations in many other mesothermal (Jensen and Bateman, 1979) districts that show generally similar geology. For example, in the Hopewell and Bromide districts of New Mexico, gold-bearing fissure veins typically are associated with siderite, chlorite, pyrite, chalcopyrite, and galena (Graton, 1910). Gold vein deposits in the Grass Valley, Calif., district yielded about \$300 million (Clark, 1970). This district, about 30 km north of the northern terminus of the Mother Lode but considered generally not to be part of the Mother Lode (Albers, 1981), shows vein and wall-rock assemblages containing quartz, iron and magnesium carbonates, white mica, chlorite, epidote, arsenopyrite, pyrite, galena, chalcopyrite, and gold (Lindgren, 1896; Johnston, 1940). The wall rocks, which consist of Paleozoic and Mesozoic units intruded by a Mesozoic granodiorite (Johnson, 1940), are variably sericitized, carbonatized, and chloritized. The bulk of the gold and galena in the veins was deposited during a quartz substage (Johnston, 1940). Further, liquid-vapor relations in fluid inclusions shown in Johnston (1940, pl. 22) suggest that the fluids associated with mineralization were trapped from homogeneous nonboiling fluids. Wall-rock alteration surrounding the gold-quartz veins in the Alleghany, Calif., district, about 30 km northeast of Grass Valley, includes carbonates (mainly ankerite), albite, mariposite, and white mica (Ferguson and Gannett, 1932). The occurrence of late-stage gold, preceded by a potassium-enriching and (or) silica-depleting stage, as in the episyenitic pipes at Gold Basin, may be comparable to gold associations reported elsewhere. Harris (1980a, p. B1; 1980b) described disseminated gold in the altered parts of a granodiorite in the Salave gold prospect in northwest Spain as occurring in a zone typified by "increased carbonatization, desilicification, sericitization, albitization, sulphidization and texture-destruction." In addition, he reports that the "introduction of CO₂ as carbonates and the loss of SiO₂ as quartz derived from the silicate-destructive alteration are petrographically obvious" (Harris, 1980b, p. B11). Furthermore, in these alteration facies, his "hongorock," secondary fluid inclusions are abundant and include liquid carbon dioxide-bearing types showing highly varied proportions of carbon dioxide possibly indicative of unmixing. The silicate-destructive phenomena together with a mineralizing environment highly enriched in carbon dioxide are very similar to the gold-bearing episyenites in the Gold Basin district. Maclaren (1908, p. 100-101) mentions several other occurrences of paragenetically late gold being present in "acidic dyke rocks." Boyle (1979, p. 296) cites several reports of gold ore bodies that are hosted mostly by syenitic rock (Dyer, 1936; Derry and others, 1948;

North and Allen, 1948). At the Young-Davidson mine in the Matachewan district of Ontario, Canada, disseminated gold-bearing pyrite makes up about 2 volume percent of an early-phase syenite; minor associated minerals are chalcopyrite, galena, molybdenite, scheelite, and specularite. Subsequent fracture-controlled mineralization there includes quartz-carbonate veins and free gold. However, all the syenitic rocks in these latter districts may not be equivalent genetically to the episyenites we describe here. Nonetheless, Dyer (1936) and Sinclair (1984) describe some pink to brick-red, gold-bearing syenite that apparently formed by potassic alteration of gray porphyritic syenite in the Young-Davidson mine. The red altered facies of these rocks includes the assemblage potassium feldspar and hematite, both of which make up a significant proportion of the episyenite in the Gold Basin district. The syenite-hosted gold deposits in the Matachewan district have yielded about 800,000 troy ounces gold from as much as five million tons ore (Sinclair, 1984). Further, Comba and others (1981) allude to a fenite (episyenite)-gold association at the Upper Canada gold mine at Dobie, Ontario.

Fluid-inclusion compositions and mineral assemblages in the veins and wall rocks provide fairly limiting constraints on the chemistry of the ore-depositing environment in the Gold Basin-Lost Basin districts, but most likely above a mass of Cretaceous two-mica monzogranite at depth. The exposed episyenitic pipes most likely reflect a mineralized level deeper than the bulk of the pegmatite-vein systems throughout the districts. At the episyenitic pipes, early stages of alteration initially must have involved a tightly confined flux of upward-streaming fluids whose (K⁺)/(Na⁺) ratios eventually exceeded the buffering capabilities of potassium feldspar and plagioclase relict from the protolith (see discussion in Poty and others, 1974). Such fluids also leached primary quartz from the Early Proterozoic monzogranite protolith and increased the porosity at the sites. Generation of silica-undersaturated fluids may reflect interaction of Early Proterozoic mafic or ultramafic rocks and fluids initially evolved from Late Cretaceous two-mica monzogranite (fig. 73). As pointed out by Burnham and Jahns (1962), magmas of pegmatitic granite, such as the two-mica monzogranite of the Gold Basin district probably contain 8 to 12 weight percent H₂O. Those fluids should be depleted significantly in silica and become quite alkaline if they were to react at elevated pressure and temperature conditions with mafic or ultramafic rocks (Fournier, 1985). Specific mineral assemblages resulting in mafic or ultramafic rocks from these chemical reactions would reflect largely the mol fraction CO₂ in the fluid(s): fluids severely depleted in CO₂ might yield serpentine-bearing assemblages, whereas fluids containing relatively abundant CO₂ might yield anthophyllite-, talc-, and (or) magnesite-bearing assemblages, (Evans and Trommsdorff, 1970;

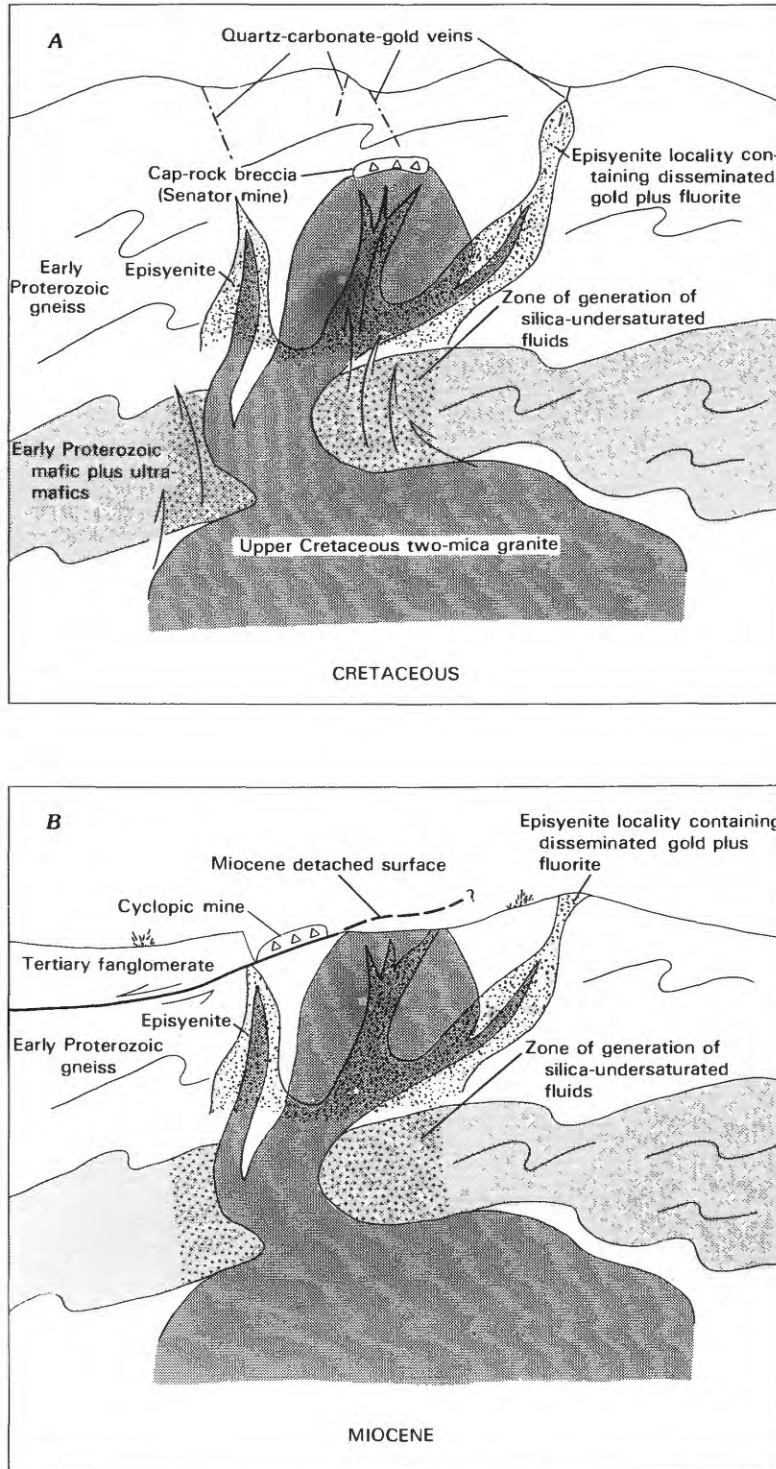
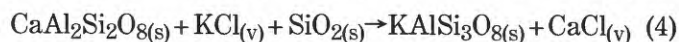
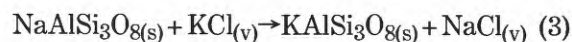
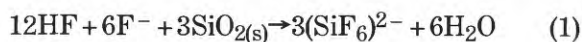


FIGURE 73.—Schematic relations among Late Cretaceous two-mica monzogranite, cap-rock breccia, episyenite, and Miocene detachment fault. *A*, Silica-undersaturated fluids (arrows) associated genetically with episyenite probably were generated by chemical interaction with Proterozoic mafic and ultramafic rocks during the Late Cretaceous as fluids evolved from two-mica monzogranite (see text). Flat-lying cap-rock breccias, such as that at Senator mine, probably represent areas of silica deposition above deep episyenite. *B*, Subsequent faulting along low-angle Miocene detachment surfaces further brecciated veins, such as those at Cyclopic mine, during tectonic transport from site(s) of original deposition. Fault, solid line; dashed where projected, queried where uncertain, arrows indicate direction of relative movement.

Winkler, 1974). The potassium feldspar stage of episyenitization at Gold Basin may be comparable to the early-alkaline high-temperature (450–600 °C) stage of microcline crystallization associated with many greisens (Shcherba, 1970). Further, some intragranitic veins associated with uranium mineralization show parageneses similar to the gold-episyenite relations at Gold Basin (see Nash and others, 1981). In the intragranitic Gunnar uranium deposit, Saskatchewan, Evoy (1961) showed that albitization there preceded ore mineralization and that albitization produced a so-called syenite by leaching primary quartz from the syenite's protolith. However, we have no fluid-inclusion data documenting the chemistry of the fluids at Gold Basin during the onset of flooding by potassium feldspar and dissolving of quartz. Early-stage fluids probably contained some fluorine and carbon dioxide, although partition of fluorine toward a vapor or aqueous phase in equilibrium with a granitic magma is low (Burnham, 1967, 1979; Koster van Groos and Wyllie, 1969; Carmichael and others, 1974, p. 314–316). However, with progressive differentiation of granitic rocks, there is a tendency for coexisting very late fluids to show a buildup in their fluorine contents (see Bailey (1977) for discussion of such relations). The overall HF content in these fluids must be subordinate to their HCl content because of the very large partition coefficients of HCl in favor of the aqueous phase (Burnham, 1979). In such a supercritical late-magmatic environment, fluorine probably combines into very soluble complexes, possibly including $(\text{SiF}_6)^{2-}$ (Shcherba, 1970), which may be related to the early stages of development of the episyenitic pipes. Subsolidus consumption of primary quartz and replacement of plagioclase by potassium feldspar there may have occurred by a coupling of reaction (1) or reaction (2) to the alkali exchange reactions (3) and (4) proposed by Burnham (1979):



Eventually, fluorite and gold were deposited in the pore spaces within the episyenitic pipes at temperatures of 315 to 335 °C and at pressures between 500 and 700 bars. Solubility studies of gold (Baranova and Ryzhenko, 1981; see also Lewis, 1982) suggest that free gold has a wide-ranging stability field in terms of pH and temperature. Thus, oxidation resulting from the dissociation of H_2O may be one way to precipitate gold in a relatively deep-seated geologic environment. As a comparison, the depths of such an environment in the Gold Basin-Lost Basin

districts appear to be similar to that of the more deeply seated porphyry copper deposits (Nash, 1976). At these temperatures, deposition of fluorite may have occurred in response to a combination of interrelated factors (see Richardson and Holland, 1979; Holland and Malinin, 1979), including a common-ion effect with $\text{NaF}(\text{aq})$ as the system evolved and possibly a decrease in salinity. However, the fluids associated with mineralization in the districts show no compelling evidence requiring a salinity decrease as an important component during deposition of the ores. Early- and late-stage fluids in quartz and fluorite of the pipes and vein both are correspondingly moderately saline in contrast to the early fluids at other fluorite deposits, which are extremely saline (for example, see Nash and Cunningham, 1973). Furthermore, such trapping temperatures (315 to 335 °C) are quite common in mesothermal environments, which led Barnes (1979) to suggest that cooling of postmagmatic fluids is an important ore-depositing mechanism that must be considered also.

The prevailing high pressures in the mesothermal environment at the sites of the pipes and the vein during early and late stages of mineralization precluded boiling of the fluids with a concomitant loss of carbon dioxide. Loss of carbon dioxide can lead to a decrease in the solubility of carbonate (Ellis, 1963; Holland and Malinin, 1979). However, in the Gold Basin-Lost Basin districts fluid-inclusion relations apparently do not suggest significant boiling of fluids occurred during the quartz, carbonate (ferroan carbonate or ankerite), white mica, fluorite, sulfide, and gold stages of mineralization. Some rocks may contain apparently nonboiling relations, although the associated fluids were boiling (Roedder, 1984). The fact that the fluids circulating at the pipes and in the vein apparently were not boiling indicate a fairly widespread high fugacity of carbon dioxide in the fluids. In addition, the nonboiling of these fluids must have retarded the physical separation and removal of acid components (including mostly carbon dioxide) from the circulating fluids and thereby enhanced the stability of white mica during the ore-depositing stage. This relation is in marked contrast to the preceding potassium feldspar-stable stage in the episyenitic pipes. The increased abundance of white mica both laterally toward the so-called pegmatitic-vein systems and temporally as they and the episyenitic pipes evolved demonstrates a transition from high $(\text{K}^+)/(\text{H}^+)$ fluids to ones with lower $(\text{K}^+)/(\text{H}^+)$ (Hemley and Jones, 1964) and probably somewhat more acidic conditions. Seward (1982) has shown experimentally that at 300 °C the solubility of gold increases with increasing alkalinity of a fluid in the stability field of pyrite and chalcopyrite. Thus, deposition of gold may reflect partly a response in the change from an alkaline to an acidic chemical environment.

The association in the Gold Basin-Lost Basin districts of Late Cretaceous and (or) early Tertiary gold mineralization with fluids related to two-mica magmatism is apparently more widespread in the southern cordillera than most geologists previously realized (Keith, 1986). Many two-mica peraluminous granites of Arizona and California are not associated with any significant ore deposits, although a few commercial tungsten deposits are present locally in wall rocks adjacent to some two-mica plutons (Reynolds and others, 1982), gold mineralization in the Cargo Muchacho Mountains, California, may be associated with two-mica magmatism, and 19 districts in Arizona and adjacent regions show production of gold, silver, copper, lead, and zinc from mines associated apparently with two-mica plutons (Keith, 1986). Furthermore, Reynolds and others (1982) note that all two-mica peraluminous granitoids must incorporate significant crustal components because of their uniformly high initial $^{87}\text{Sr}/^{86}\text{Sr}$ isotopic ratios. Therefore, we suggest that the gold and base metals and possibly fluorine in the districts may also have a crustal source and may have been recycled from Early Proterozoic rocks. These crustal sources may include some near-surface Proterozoic rocks in the districts, possibly including some of the Early Proterozoic metabasites described above (fig. 73; see also Moiseenko and Fatyanov, 1972). However, some of the gold in the Late Cretaceous and (or) early Tertiary occurrences also may have been incorporated in the magmatic stages of the two-mica monzogranite and thus reflect anatexis of deep crustal rocks.

The Proterozoic rocks in the districts and elsewhere in the region include some gold and fluorine that may be considered as potential sources for the Late Cretaceous and (or) early Tertiary occurrences and deposits. In this report, we have described mineralized veins in Proterozoic rocks that have a fabric and mineral assemblage that seem to date from the Proterozoic greenschist metamorphic event. In addition, some of the gold-bearing veins of the districts may have been emplaced at about the same time as the copper, lead, and gold veining in the Gold Butte district, which apparently is Proterozoic in age (Wasserman and Lanphere, 1965). Early Proterozoic gold is present elsewhere in the southwest, as exemplified by an occurrence of stratiform gold in Early Proterozoic rocks of Yavapai County, Ariz. (Swan and others, 1981). Fluorine in the veins and episyenitic pipes in the Gold Basin-Lost Basin districts also may have been recycled from a Proterozoic protolith. Our analyses, for example, of the Early Proterozoic porphyritic monzogranite of Garnet Mountain in the districts show contents of fluorine in the range of 0.06 to 0.17 weight percent (table 14). Remobilization of fluorite from Proterozoic igneous rocks into Late Cretaceous and (or) early Tertiary veins has been postulated by Snyder (1978) at the Park Range,

Colorado; Antweiler and others (1972) suggested somewhat similar relations for gold at Han's Peak, Colorado. Furthermore, Stephenson and Ehmann (1971) showed the depletion of gold from hydrothermally altered country rock and the apparent migration of gold into veins at the Rice Lake-Beresford Lake area, southeastern Manitoba, Canada. On the other hand, metal ratios in Late Cretaceous and (or) early Tertiary and Tertiary ore deposits in Yavapai County, Ariz., apparently do not reflect the metal ratios of the Proterozoic crust (DeWitt, 1982). Nonetheless, Boyle (1979, p. 65) maintains that transport and, by implication, remobilization of gold as gold-sulfide complexes by near-neutral to moderately alkaline carbonate-depositing fluids must occur. Many experimental studies have confirmed the transport of gold as a sulfide complex in a largely reducing environment showing relatively high contents of total sulfur (Baranova and Ryzhenko, 1981; Seward, 1982). Deposition of gold would most likely occur by a chemical reaction(s) that results in an increase of the oxidation potential of the fluids. On the other hand, the experimental studies of Henley (1973) also reveal an inflection or solubility hump for gold that culminates in the range 300 to 350 °C in 3M potassium chloride solution (approximately 18 weight percent KCl) at pressures less than 1,000 bars. Certainly the early-stage fluids at the episyenite pipes and at many of the veins in the Gold Basin-Lost Basin districts must have had high K/Na ratios because of their associated potassic alteration. We suggest that such fluids may have been primarily responsible for the remobilization and extraction during the Cretaceous of the bulk of the known gold from shallow Proterozoic, possibly metabasite, sources, whereas some of the gold probably was emplaced during the Cretaceous after having been incorporated into the magmas of the two-mica monzogranite. Experimental studies suggest that the gold-carrying capacity of the fluids associated with the final crystallization of the Cretaceous two-mica monzogranite would be more than adequate to account for all the known gold in the districts. Ten cubic kilometers of such monzogranite (equivalent to the exposed two-mica monzogranite extending to a depth of about 0.5 km) would have the capacity to deposit or extract about 64 t (70 tons) of gold, on the basis of experimental data of Ryabchikov (1981). Further, Korobeynikov (1976) reported a significant amount of gold to be soluble in the fluid-inclusion waters of minerals associated with skarn- and vein-type gold deposits.

SUGGESTIONS FOR EXPLORATORY PROGRAMS

The known and inferred relations of gold mineralization in the Gold Basin-Lost Basin districts suggest several geologic environments that should be evaluated carefully in exploratory programs. Certainly the most obvious

would be any remaining high-grade ore shoots in the veins themselves. However, such occurrences most likely would not yield the relatively large tonnages of ore needed for a commercial mining operation. Five environments should be considered. (1) Sequences of rock that might form favorable replacement zones adjacent to or near any of the gold-bearing veins that crop out should be evaluated. Such sequences might include Early Proterozoic carbonate, amphibolite, or any zones of porous rock that occurred before mineralization. Such favorable zones could include any rocks shattered tectonically prior to the major mineralizing event in the Late Cretaceous. (2) If the occurrence of disseminated free gold in the fluorite-bearing episyenitic alteration pipes in the Gold Basin district evolved as we described above, then such an environment must reflect a mineralized level geologically deeper than the bulk of the veins that crop out elsewhere in the districts. Thus, all quartz-fluorite-bearing veins should be evaluated as to whether or not they reflect the upper quartz-depositing parts of a system which at depth includes early quartz-dissolving and late gold-depositing parageneses. Similarly, the two-mica monzogranite that crops out in the Gold Basin district might include some disseminated gold-bearing episyenitic facies at depth (fig. 73). (3) The entire trace of the low-angle detachment surface or glide surface should be evaluated for the occurrence of Cyclopic-type deposits (see fig. 2). Much of the trace or inferred trace of this structure as mapped by P.M. Blacet along the west flank of the White Hills is poorly exposed, partly because it is locally covered by Quaternary sand and gravel. However, the increased abundance of tectonically polished or striated vein quartz along some of the poorly exposed parts of its trace might be indicative of gold-bearing Cretaceous veins caught up tectonically along the detachment surface. Furthermore, detailed geologic mapping along the general trace of the detachment surface might reveal other fault strands that should be evaluated similarly. (4) The Early Proterozoic metamorphic rocks in the districts should be considered as potential hosts for syngenetic, stratiform deposits. Certainly, as we described above, some indications in the rocks suggest that boron-enriched fluids were important in the paragenesis of tourmaline-bearing schists. Such rocks might reflect emanations of boron-bearing fluids expelled from exhalative centers in the protolith of the metamorphic rocks. Tourmalinite makes up the major part of the ore in the gold deposit of Passagem de Mariana, Brazil, and this deposit yielded more than 60 tons of gold (Fleischer and Routhier, 1973). The exploration implications of tourmalinite horizons are exceptionally well described by Slack (1980, 1981, 1982) and Nicholson (1980). In fact, Nicholson (1980, fig. 1) shows a striking correlation between tourmalinite horizons and gold deposits. However, in the Early Proterozoic metamorphic

rocks of the Gold Basin-Lost Basin districts, some horizons of tourmalinite may be mistaken for amphibolite. Nonetheless, detailed mapping of all tourmalinite horizons in the Proterozoic might yield some additional targets worthy of further exploratory efforts. Last, the oxide-facies iron formations known in the Proterozoic also should be considered as potential guides to sea-floor volcanogenic-type gold deposits (see Hodgson and others, 1982). We envision that such oxide-facies iron formations, if they prove to be anomalous in syngenetic gold, might be indicative of facies distal to disseminated gold either in an intermediate pyritic facies of iron formation mostly along the same horizon or in the immediate area of the vent. (5) The minor-element signatures of native lode gold (mostly the content of silver and copper) from several localities in the Gold Basin and Lost Basin districts should be evaluated with respect to their potential relation to a buried porphyry copper system.

REFERENCES

- Ackermand, D., and Morteani, G., 1977, Der chemismus der granate, chlorite, biotite und turmaline in den steinogelschiefern (Laud Salzburg, Oesterreich); ein beitrag zur geologischen Geschichte des Mittelostalpins. [The chemistry of the garnets, chlorite, biotite and tourmaline in the Steinkogel Schist (Salzburg, Austria); the geologic history of the central Eastern Alps]: *Neues Jahrbuch für Geologie und Paläontologie Abhandlungen*, v. 154, no. 3, p. 367-385 [incl. English summary].
- Albers, J.P., 1981, A lithologic-tectonic framework for the metallogenic provinces of California: *Economic Geology*, v. 76, no. 4, p. 765-790.
- Allen, Percival, Sutton, John, and Watson, J.V., 1974, Torridonian tourmaline-quartz pebbles and the Precambrian crust northwest of Britain: *Geological Society of London Journal*, v. 130, no. 1, p. 85-91.
- Anderson, C.A., 1968, Arizona and adjacent New Mexico, in Ridge, J.D., ed., *Ore deposits of the United States, 1933-1967, The Graton-Sales Volume II*: New York, American Institute of Mining, Metallurgical, and Petroleum Engineers, p. 1163-1190.
- Anderson, C.A., Blacet, P.M., Silver, L.T., and Stern, T.W., 1971, Revision of Precambrian stratigraphy in the Prescott-Jerome area, Yavapai County, Arizona: *U.S. Geological Survey Bulletin* 1324-C.
- Anderson, J.L., and Cullers, R.L., 1978, Geochemistry and evolution of the Wolf River batholith, a late Precambrian rapakivi massif in north Wisconsin, U.S.A.: *Precambrian Research*, v. 7, p. 287-324.
- Anderson, J.L., and Rowley, M.C., 1981, Synkinematic intrusion of peraluminous and associated metaluminous granitic magmas, Whipple Mountains, California: *Canadian Mineralogist*, v. 19, p. 83-101.
- Anderson, P.M., and Guilbert, J.M., 1979, The Precambrian massive-sulfide deposits of Arizona—a distinct metallogenic epoch and province, in Ridge, J.D., ed., *Papers on mineral deposits of western North America: International Association on the Genesis of Ore Deposits, Quadrennial Symposium, 5th, Snowbird, Utah, 1978, Proceedings: Nevada Bureau of Mines and Geology Report* 33, v. 2, p. 39-48.
- Anderson, R.E., 1971, Thin skin distension in Tertiary rocks of southeastern Nevada: *Geological Society of America Bulletin*, v. 82, no. 1, p. 43-58.
- 1973, Large-magnitude Late Tertiary strike-slip faulting north of Lake Mead, Nevada: *U.S. Geological Survey Professional Paper* 794, 18 p.

- _____. 1977, Geologic map of the Boulder City 15-minute quadrangle, Clark County, Nevada: U.S. Geological Survey Geologic Quadrangle Map GQ-1395, 1 sheet, scale 1:62,500.
- _____. 1978, Geologic map of the Black Canyon 15-minute quadrangle, Mohave County, Arizona, and Clark County, Nevada: U.S. Geological Survey Geologic Quadrangle Map GQ-1394, 1 sheet, scale 1:62,500.
- Anderson, R.E., and Laney, R.L., 1975, The influence of Late Cenozoic stratigraphy on distribution of impoundment-related seismicity at Lake Mead, Nevada-Arizona: U.S. Geological Survey Journal of Research, v. 3, no. 3, p. 337-343.
- Anderson, R.E., Longwell, C.R., Armstrong, R.L., and Marvin, R.F., 1972, Significance of K-Ar ages of Tertiary rocks from the Lake Mead region, Nevada-Arizona: Geological Society of America Bulletin, v. 83, no. 2, p. 273-288.
- Angelier, Jacques, Colletta, Bernard, and Anderson, R.E., 1985, Neogene paleostress changes in the Basin and Range: A case study at Hoover Dam, Nevada-Arizona: Geological Society of America Bulletin, v. 96, no. 3, p. 347-361.
- Antweiler, J.C., and Campbell, W.L., 1977, Application of gold compositional analyses to mineral exploration in the United States: Journal of Geochemical Exploration, v. 8, no. 1-2, p. 17-29.
- _____. 1982, Gold in exploration geochemistry, in Levinson, A.A., ed., Precious metals in the northern cordillera: Association of Exploration Geochemists Special Publication 10, p. 33-44.
- Antweiler, J.C., Doe, B.R., and Delevaux, M.H., 1972, Lead isotope and other evidence on the bedrock source of placer gold at Hahns Peak, Colorado: Economic Geology, v. 67, no. 3, p. 302-314.
- Antweiler, J.C., and Sutton, A.L., 1970, Spectrochemical analysis of native gold samples: U.S. Clearinghouse Federal Science Technical Information, P B Report 194809, 32 p.
- Armbrustmacher, T.J., and Simons, F.S., 1977, Geochemistry of amphibolites from the central Beartooth Mountains, Montana-Wyoming: U.S. Geological Survey Journal of Research, v. 5, no. 1, p. 53-60.
- Bailey, J.C., 1977, Fluorine in granitic rocks and melts: A review: Chemical Geology, v. 19, p. 1-42.
- Baranova, N.N., and Ryzhenko, B.N., 1981, Computer simulation of the Au-Cl-S-Na-H₂O system in relation to the transport and deposition of gold in hydrothermal processes: Geochemistry International, v. 18, no. 4, p. 46-60.
- Barnes, H.L., 1979, Solubilities of ore minerals, in Barnes, H.L., ed., Geochemistry of hydrothermal ore deposits (2d ed.): New York, John Wiley and Sons, p. 404-460.
- Bateman, P.C., 1961, Granitic formations in the east-central Sierra Nevada near Bishop, California: Geological Society of America Bulletin, v. 72, no. 10, p. 1521-1538.
- Beal, L.H., 1965, Geology and mineral deposits of the Bunkerville mining district, Clark County, Nevada: Nevada Bureau of Mines Bulletin 63, 96 p.
- Beane, R.E., and Titley, S.R., 1981, Porphyry copper deposits, Part II. Hydrothermal alteration and mineralization, in Skinner, B.J., ed., Seventy-fifth anniversary volume, Economic Geology, 1905-1980: New Haven, Conn., Economic Geology Publishing Co., p. 235-269.
- Binns, R.A., 1965a, Hornblendes from some basic hornfels in the New England region, New South Wales: Mineralogical Magazine, v. 34, no. 268, p. 52-65.
- _____. 1965b, The mineralogy of metamorphosed basic rocks from the Willyama complex, Broken Hill district, New South Wales. Part I. Hornblendes: Mineralogical Magazine, v. 35, no. 269, p. 306-326.
- _____. 1965c, The mineralogy of metamorphosed basic rocks from the Willyama complex, Broken Hill district, New South Wales. Part II: Mineralogical Magazine, v. 35, no. 272, p. 561-587.
- Blacet, P.M., 1969, Gold placer and lode deposits, Gold Basin-Lost Basin, in Geological Survey research 1969: U.S. Geological Survey Professional Paper 600-A, p. A1-A2.
- _____. 1972, Late Cretaceous plutonism and metallization south of Lake Mead, in Geological Survey research 1972: U.S. Geological Survey Professional Paper 800-A, p. A44.
- _____. 1975, Preliminary geologic map of the Garnet Mountain quadrangle, Mojave County, Arizona: U.S. Geological Survey Open-File Map 75-93, scale 1:48,000.
- Blair, W.N., 1978, Gulf of California in Lake Mead area of Arizona and Nevada during late Miocene time: American Association of Petroleum Geologists Bulletin, v. 62, no. 7, p. 1159-1170.
- Blair, W.N., and Armstrong, A.K., 1979, Hualapai Limestone Member of the Muddy Creek Formation: The youngest deposit predating the Grand Canyon, southeastern Nevada and northwestern Arizona: U.S. Geological Survey Professional Paper 1111, 14 p.
- Blair, W.N., McKee, E.H., and Armstrong, A.K., 1977, Age and environment of deposition—Hualapai Limestone Member of the Muddy Creek Formation [abs.]: Geological Society of America Abstracts with Programs, v. 9, no. 4, p. 390-391.
- Bohannon, R.G., 1984, Nonmarine sedimentary rocks of Tertiary age in the Lake Mead region, southeastern Nevada and northwestern Arizona: U.S. Geological Survey Professional Paper 1259, 72 p.
- Boyle, R.W., 1979, The geochemistry of gold and its deposits: Geological Survey of Canada Bulletin 280, 584 p.
- Bozzo, A.T., Chen, H.-S., Kass, J.R., and Barduhn, A.J., 1975, The properties of the hydrates of chlorine and carbon dioxide: Desalination, v. 16, p. 303-320.
- Brown, E.H., Babcock, R.S., Clark, M.D., and Livingston, D.E., 1979, Geology of the older Precambrian rocks of the Grand Canyon, part I. Petrology and structure of the Vishnu Complex: Precambrian Research, v. 8, p. 219-241.
- Burchard, H.C., 1882, Report of the director of the mint upon the statistics of the production of the precious metals in the United States [1881]: Washington, U.S. Government Printing Office, 765 p.
- _____. 1883, Report of the director of the mint upon the statistics of the production of the precious metals in the United States [1882]: Washington, U.S. Government Printing Office, 873 p.
- Burchfiel, B.C., 1979, Geologic history of the central Western United States, in Ridge, J.D., ed., Papers on mineral deposits of western North America: International Association on the Genesis of Ore Deposits, Quadrennial Symposium, 5th, Snowbird, Utah, 1978, Proceedings: Nevada Bureau of Mines and Geology Report 33, v. 2, p. 1-11.
- Burnham, C.W., 1967, Hydrothermal fluids at the magmatic stage, in Barnes, H.L., ed., Geochemistry of hydrothermal ore deposits: New York, Holt, Rinehart and Winston, p. 34-76.
- _____. 1979, Magmas and hydrothermal fluids, in Barnes, H.L., ed., Geochemistry of hydrothermal ore deposits (2d ed.): New York, John Wiley and Sons, p. 71-136.
- Burnham, C.W., and Jahns, R.H., 1962, A method for determining the solubility of water in silicate melts: American Journal of Science, v. 260, p. 721-745.
- Büsch, W., 1966, Petrographie und Abfolge der Granitisation im Schwarzwald. V [Petrography and the sequence of granitization in the Black Forest, Part 5]: Neues Jahrbuch für Mineralogie Abhandlungen, v. 104, p. 190-258.
- Callaghan, Eugene, 1939, Geology of the Searchlight district, Clark County, Nevada: U.S. Geological Survey Bulletin 906-D, p. 135-188.
- Campbell, W.L., Mosier, E.L., and Antweiler, J.C., 1973, Effects of laboratory treatments on silver and other elements in native gold: U.S. Geological Survey Journal of Research, v. 1, no. 2, p. 211-220.
- Carmichael, D.M., 1969, On the mechanism of prograde metamorphic reactions in quartz-bearing pelitic rocks: Contributions to Mineralogy and Petrology, v. 20, p. 244-267.
- _____. 1978, Metamorphic bathozones and bathograds: A measure of the depth of post-metamorphic uplift and erosion on the regional

- scale: American Journal of Science, v. 278, no. 6, p. 769-797.
- Carmichael, I.S.E., Turner, F.J., and Verhoogen, John, 1974, Igneous petrology: New York, McGraw-Hill, 739 p.
- Chappell, B.W., and White, A.J.R., 1974, Two contrasting granite types: Pacific Geology, v. 8, p. 173-174.
- Christiansen, R.L., and Lipman, P.W., 1972, Cenozoic volcanism and plate tectonic evolution of the Western United States; II, Late Cenozoic, in A discussion on volcanism and the structure of the Earth: Royal Society of London Philosophical Transactions, ser. A, v. 271, no. 1213, p. 249-284.
- Clark, M.D., 1979, Geology of the older Precambrian rocks of the Grand Canyon. Part III. Petrology of mafic schists and amphibolites: Precambrian Research, v. 8, p. 277-302.
- Clark, W.B., 1970, Gold districts of California: California Division of Mines and Geology Bulletin 193, 186 p.
- Clarke, F.W., 1924, Data of geochemistry (5th ed.): U.S. Geological Survey Bulletin 770, 841 p.
- Clifton, C.G., Durning, P.W., and Buchanan, L.J., 1980, Controls of mineralization and exploration procedure in the Oatman mining district, Oatman, Arizona [abs.]: American Institute of Mining, Metallurgical, and Petroleum Engineers Annual Meeting, Las Vegas, Nev., 1980, Program with Abstracts, p. 24.
- Collins, P.L.F., 1979, Gas hydrates in CO₂-bearing fluid inclusions and the use of freezing data for estimation of salinity: Economic Geology, v. 74, no. 6, p. 1435-1444.
- Comba, C.D.A., Gibson, H.L., and Lichtblau, A., 1981, Four Corners fenite: Noranda, Quebec, Canada: Economic Geology, v. 76, no. 5, p. 1202-1205.
- Condie, K.C., 1982, Plate-tectonics model for Proterozoic continental accretion in the southwestern United States: Geology, v. 10, no. 1, p. 37-42.
- Coney, P.J., and Reynolds, S.J., 1977, Cordilleran Benioff zones: Nature, v. 270, no. 5636, p. 403-406.
- Creasey, S.C., 1966, Hydrothermal alteration, in Titley, S.R., and Hicks, C.L., eds., Geology of the porphyry copper deposits, southwestern North America: Tucson, Arizona University Press, p. 51-85.
- Crittenden, M.D., Jr., Coney, P.J., and Davis, G.H., eds., 1980, Cordilleran metamorphic core complexes: Geological Society of America Memoir 153, 490 p.
- Cunningham, C.G., and Carollo, Clyde, 1980, Modification of a fluid-inclusion heating/freezing stage: Economic Geology, v. 75, no. 2, p. 335-337.
- Davis, G.A., Anderson, J.L., Frost, E.G., and Shackelford, T.J., 1979, Regional Miocene detachment faulting and early Tertiary(?) mylonitization, Whipple-Buckskin-Rawhide Mountains, southeastern California and western Arizona, in Abbott, P.L., ed., Geological excursions in the southern California area: Geological Society of America Annual Meeting, 92d, San Diego, Calif., p. 75-108.
- Deaderick, A.J., 1980, Geologic investigation of the Apache Oro mining claims, Lost Basin Range, Mohave County, Arizona: Socorro, New Mexico Institute of Mining and Technology, 273 p.
- Deans, T., Sukheswala, R.N., Sethna, S.F., and Viladkar, S.G., 1972, Metasomatic feldspar rocks (potash fenites) associated with the fluorite deposits and carbonates of Amba Dongar, Gujarat, India: Institution of Mining and Metallurgy Transactions, Section B, v. 81, 1972, Bulletin 783, p. B1-B9.
- Deer, W.A., Howie, R.A., and Zussman, J., 1962a, Rock-forming minerals. Volume 1. Ortho- and ring silicates: London, Longmans, Green and Co., 333 p.
- 1962b, Rock-forming minerals. Volume 3. Sheet silicates: London, Longmans, Green and Co., 270 p.
- 1962c, Rock-forming minerals. Volume 5. Non-silicates: London, Longmans, Green and Co., 371 p.
- 1963, Rock-forming minerals. Volume 2. Chain silicates: London, Longmans, Green and Co., 379 p.
- Derry, D.R., Hopper, C.H., and McGowan, H.S., 1948, Matachewan Consolidated mine, in Structural geology of Canadian ore deposits: Canadian Institute of Mining and Metallurgy, v. 1, p. 638-643.
- Desborough, G.A., 1970, Silver depletion indicated by microanalysis of gold from placer occurrences, Western United States: Economic Geology, v. 65, no. 3, p. 304-311.
- DeWitt, Ed, 1982, The geochemistry of Precambrian crust and its effect on younger metallogenesis, Yavapai County, Arizona [abs.]: Geological Society of America Abstracts with Programs, v. 14, no. 4, p. 159.
- Dickinson, W.R., 1975, Potash-depth (*K-h*) relations in continental margin and intra-oceanic magmatic arcs: Geology, v. 3, no. 2, p. 53-56.
- 1981, Plate tectonic evolution of the southern cordillera, in Dickinson, W.R., and Payne, W.D., eds., Relations of tectonics to ore deposits in the southern cordillera: Arizona Geological Society Digest, v. 14, p. 113-135.
- Dickinson, W.R., and Hatherton, T., 1967, Andesitic volcanism and seismicity around the Pacific: Science, v. 157, no. 3790, p. 801-803.
- Diman, E.N., 1976, On the minimum fineness of gold associated with pyrite: Geochemistry International 1976, v. 13, no. 2, p. 63-70.
- Donnelly, M.E., and Hahn, G.A., 1981, A review of the Precambrian volcanogenic massive sulfide deposits in central Arizona and the relationship to their depositional environment, in Dickinson, W.R., and Payne, W.D., eds., Relations of tectonics to ore deposits in the southern cordillera: Arizona Geological Society Digest, v. 14, p. 11-22.
- Dusel-Bacon, Cynthia, and Foster, H.L., 1983, A sillimanite gneiss dome in the Yukon crystalline terrane, east-central Alaska: Petrography and garnet-biotite geothermometry: U.S. Geological Survey Professional Paper 1170-E, p. E1-E25.
- Dyer, W.S., 1936, Geology and ore deposits of the Matachewan-Kenogami area: Ontario Department of Mines, v. 44, pt. 2, p. 1-55.
- Ellis, A.J., 1963, The solubility of calcite in sodium chloride solutions at high temperatures: American Journal of Science, v. 261, no. 3, p. 259-267.
- Engineering and Mining Journal, 1939, Arizona: Engineering and Mining Journal, v. 140, no. 13, p. 70.
- 1984, Arizona: Engineering and Mining Journal, v. 185, no. 2, p. 67.
- Espenshade, G.H., 1969, Kyanite and related minerals, pt. 1, Geology and mineral resources, in Mineral and water resources of Arizona: Arizona Bureau of Mines Bulletin 180, p. 382-385.
- Ethier, V.G., and Campbell, F.A., 1977, Tourmaline concentrations in Proterozoic sediments of the southern cordillera of Canada and their economic significance: Canadian Journal of Earth Sciences, v. 14, no. 10, p. 2348-2363.
- Evans, B.W., and Leake, B.E., 1960, The composition and origin of the striped amphibolites of Connemara, Ireland: Journal of Petrology, v. 1, no. 3, p. 337-363.
- Evans, B.W., and Trommsdorff, Volkmar, 1970, Regional metamorphism of ultramafic rocks in the central Alps: Parageneses in the system CaO-MgO-SiO₂-H₂O: Schweizerische Mineralogische und Petrographische Mitteilungen, v. 50, p. 481-492.
- Evoy, E.F., 1961, Geology of the Gunnar uranium deposit, Beaverlodge area, Saskatchewan: Madison, University of Wisconsin, Ph. D. thesis, 80 p.
- Ferguson, H.G., and Gannett, R.W., 1932, Gold quartz veins of the Alleghany district, California: U.S. Geological Survey Professional Paper 172, 139 p.
- Fleischer, Ronald, and Routhier, Pierre, 1973, The "consanguineous" origin of a tourmaline-bearing gold deposit: Passagem de Mariana (Brazil): Economic Geology, v. 68, no. 1, p. 11-22.
- Fournier, R.O., 1977, Constraints on the circulation of meteoric water in hydrothermal systems imposed by the solubility of quartz [abs.]:

- Geological Society of America Abstracts with Programs, v. 9, no. 7, p. 979.
- _____. 1985, Silica minerals as indicators of conditions during gold deposition, in Tooker, E.W., ed., *Geologic characteristics of sediment- and volcanic-hosted disseminated gold deposits—search for an occurrence model*: U.S. Geological Survey Bulletin 1646, p. 15–26.
- Galbraith, F.W., and Brennan, D.J., 1970, *Minerals of Arizona*: Arizona Bureau of Mines Bulletin 181, 116 p.
- Gallagher, David, 1940, Albite and gold: *Economic Geology*, v. 35, no. 6, p. 698–736.
- Gay, N.C., 1963, A review of geochemical characteristics of gold in ore deposits: University of Witwatersrand, *Economical Geological Research Unit Information Circular 12*, 70 p.
- Gerry, C.N., and Miller, T.H., 1935, Gold, silver, copper, lead, and zinc in Arizona: U.S. Bureau of Mines *Minerals Yearbook*, 1934, *Statistical Appendix*, p. 153–178.
- Glazner, A.F., 1983, Paleoconvergence rates determined from K_2O/SiO_2 ratios in magmatic rocks and their application to Cretaceous and Tertiary tectonic patterns in southwestern North America: Discussion: *Geological Society of America Bulletin*, v. 94, p. 1032.
- Glen, R.A., 1979, Evidence for cyclic reactions between andalusite, "sericite" and sillimanite, Mount Franks area, Willyama Complex, New South Wales: *Tectonophysics*, v. 58, no. 1–2, p. 97–112.
- Goetz, A.F.H., Billingsley, F.C., Gillespie, A.R., Abrams, M.J., Squires, R.L., Shoemaker, E.M., Lucchitta, Ivo, and Elston, D.P., 1975, Application of ERTS images and image processing to regional geologic problems and geologic mapping in northern Arizona: *National Aeronautics and Space Administration Technical Report 32–1597*, 188 p.
- Graton, L.C., 1910, Rio Arriba County, in Lindgren, W., Graton, L.C., and Gordon, C.H., *The ore deposits of New Mexico*: U.S. Geological Survey Professional Paper 68, p. 124–133.
- Greenwood, H.J., and Barnes, H.L., 1966, Binary mixture of volatile components, in Clark, S.P., Jr., ed., *Handbook of physical constants* (rev. ed.): *Geological Society of America Memoir 97*, p. 385–400.
- Gregnanin, Arrigo, and Piccirillo, E.M., 1969, Indagini preliminari geologico-petrografiche sulla zona compresa fra la Valle de Plan e Val Clava (Alto Adige) [Geology and petrography of the zone between Plan and Clava valleys, Alto Adige]: *Rendiconti della Societa Italiana di Mineralogia e Petrologia*, v. 25, no. 2, p. 439–473 [in Italian with English summary].
- Griggs, D.T., and Blacic, J.D., 1965, Quartz: anomalous weakness of synthetic crystals: *Science*, v. 147, no. 3655, p. 292–295.
- Grimes, D.J., and Marranzino, A.P., 1968, Direct-current arc and alternating-current spark emission spectrographic field methods for the semiquantitative analysis of geologic materials: U.S. Geological Survey Circular 591, 6 p.
- Gross, G.A., 1980, A classification of iron formations based on depositional environments: *Canadian Mineralogist*, v. 18, p. 215–222.
- Groves, D.I., and McCarthy, T.S., 1978, Fractional crystallization and the origin of tin deposits in granitoids: *Mineralium Deposita*, v. 13, no. 1, p. 11–26.
- Haffty, Joseph, Haubert, A.W., and Page, N.J., 1980, Determination of iridium and ruthenium in geological samples by fire assay and emission spectrography, in *Shorter contributions to geochemistry*, 1979: U.S. Geological Survey Professional Paper 1129, p. G1–G4.
- Haffty, Joseph, and Riley, L.B., 1968, Determination of palladium, platinum and rhodium in geologic materials by fire assay and emission spectrography: *Talanta*, v. 15, no. 1, p. 111–117.
- Hallbauer, D.K., and Utter, T., 1977, Geochemical and morphological characteristics of gold particles from Recent river deposits and the fossil placers of the Witwatersrand: *Mineralium Deposita*, v. 12, p. 293–306.
- Hamblin, W.K., 1984, Direction of absolute movement along the boundary faults of the Basin and Range–Colorado Plateau margin: *Geology*, v. 12, no. 2, p. 116–119.
- Hanekom, H.J., Staden, C.M.v.H. van, Smit, P.J., and Pike, D.R., 1965, *The geology of the Palabora igneous complex*: Geological Survey of South Africa *Memoir 54*, 185 p.
- Harris, M., 1980a, Gold mineralization at the Salave gold prospect, north-west Spain: *Institution of Mining and Metallurgy (London), Transactions, Applied Earth Sciences*, sec. B, v. 89, p. B1–B4.
- _____. 1980b, Hydrothermal alteration at Salave gold prospect, north-west Spain: *Institution of Mining and Metallurgy (London), Transactions, Applied Earth Sciences*, sec. B, v. 89, p. B5–B15.
- Hatherton, T., and Dickinson, W.R., 1969, The relationship between andesitic volcanism and seismicity in Indonesia, the Lesser Antilles, and other island arcs: *Journal of Geophysical Research*, v. 74, no. 22, p. 5301–5310.
- Haxel, G.B., Tosdal, R.M., May, D.J., and Wright, J.E., 1984, Latest Cretaceous and early Tertiary orogenesis in south-central Arizona: Thrust faulting, regional metamorphism, and granitic plutonism: *Geological Society of America Bulletin*, v. 95, no. 6, p. 631–653.
- Helgeson, H.C., Delany, J.M., Nesbitt, H.W., and Bird, D.K., 1978, Summary and critique of the thermodynamic properties of rock-forming minerals: *American Journal of Science*, v. 278–A, 229 p.
- Hemley, J.J., and Jones, W.R., 1964, Chemical aspects of hydrothermal alteration with emphasis on hydrogen metasomatism: *Economic Geology*, v. 59, no. 4, p. 538–569.
- Henley, R.W., 1973, Solubility of gold in hydrothermal chloride solutions: *Chemical Geology*, v. 11, no. 2, p. 73–87.
- Hernon, R.M., 1938, Cerbat Mountains, Pt. 2, Mining districts, in Butler, G.M., ed., *Some Arizona ore deposits*: Arizona Bureau of Mines Bulletin 145, *Geological Series 12*, p. 110–117.
- Hess, P.C., 1969, The metamorphic paragenesis of cordierite in pelitic rocks: *Contributions to Mineralogy and Petrology*, v. 24, p. 191–207.
- Hewett, D.F., Callaghan, Eugene, Moore, B.N., Nolan, T.B., Rubey, W.W., and Schaller, W.T., 1936, *Mineral resources of the region around Boulder Dam*: U.S. Geological Survey Bulletin 871, 197 p.
- Hewitt, D.A., 1973, The metamorphism of micaceous limestones from south-central Connecticut: *American Journal of Science, Cooper Volume 273–A*, p. 444–467.
- Hietanen, Anna, 1973, *Geology of the Pulga and Bucks Lake quadrangles, Butte and Plumas Counties, California*: U.S. Geological Survey Professional Paper 731, 66 p.
- Hine, R., Williams, I.S., Chappell, B.W., and White, A.J.R., 1978, Contrasts between I- and S-type granitoids of the Kosciusko batholith: *Geological Society of Australia Journal*, v. 25, no. 3, p. 219–234.
- Hodgson, C.J., Chapman, R.S.G., MacGeehan, P.J., 1982, Application of exploration criteria for gold deposits in the Superior province of the Canadian Shield to gold exploration in the cordillera, in Levinson, A.A., ed., *Precious metals in the northern cordillera: The Association of Exploration Geochemists Symposium*, Vancouver, British Columbia, Canada, 1981, *Proceedings*, p. 173–206.
- Holdaway, M.J., 1971, Stability of andalusite and the aluminum silicate phase diagram: *American Journal of Science*, v. 271, no. 2, p. 97–131.
- Holdaway, M.J., and Lee, S.M., 1977, Fe-Mg cordierite stability in high-grade pelitic rocks based on experimental, theoretical, and natural observations: *Contributions to Mineralogy and Petrology*, v. 63, p. 175–198.
- Holland, H.D., and Malinin, S.D., 1979, The solubility and occurrence of non-ore minerals, in Barnes, H.L., ed., *Geochemistry of hydrothermal ore deposits* (2d ed.): New York, John Wiley and Sons, p. 461–508.
- Holser, W.T., 1970, Bromide geochemistry of some non-marine salt deposits in the southern Great Basin, in Morgan, B.A., ed., *Fiftieth anniversary symposia: Symposium on the mineralogy and geochemistry of non-marine evaporites*: *Mineralogical Society of America Special Paper 3*, p. 307–319.

- Hoschek, G., 1969, The stability of staurolite and chloritoid and their significance in metamorphism of pelitic rocks: *Contributions to Mineralogy and Petrology*, v. 22, p. 208-232.
- Hotz, P.E., 1979, Regional metamorphism in the Condrey Mountain quadrangle, north-central Klamath Mountains, California: U.S. Geological Survey Professional Paper 1086, 25 p.
- Ishihara, Shunso, Sawata, Hidaho, Shibata, Ken, Terashima, Shigeru, Arrykul, Surapon, and Sato, Kohei, 1980, Granites and Sn-W deposits of Peninsular Thailand, in Ishihara, S., and Takenouchi, S., eds., *Granitic magmatism and related mineralization: Mining Geology Symposium*, Tokyo, Japan, 1979, Special Issue 8, p. 223-241.
- Jakes, P., and White A.J.R., 1972, Major and trace element abundances in volcanic rocks of orogenic areas: *Geological Society of America Bulletin*, v. 83, no. 1, p. 29-40.
- James, H.L., 1981, Bedded Precambrian iron deposits of the Tobacco Root Mountains, southwestern Montana: U.S. Geological Survey Professional Paper 1187, 16 p.
- James, R.S., and Hamilton, D.L., 1969, Phase relations in the system $\text{NaAlSi}_3\text{O}_8$ - KAlSi_3O_8 - $\text{CaAl}_2\text{Si}_2\text{O}_8$ - SiO_2 at 1 kilobar water vapour pressure: *Contributions to Mineralogy and Petrology*, v. 21, p. 111-141.
- Jensen, L.S., 1976, A new cation plot for classifying subalkalic volcanic rocks: Ontario Division of Mines Miscellaneous Paper 62, 22 p.
- Jensen, M.L., and Bateman, A.M., 1979, Economic mineral deposits (3d ed.): New York, John Wiley and Sons, 593 p.
- Johnson, M.G., 1972, Placer gold deposits of Arizona: U.S. Geological Survey Bulletin 1355, 103 p.
- Johnston, W.D., Jr., 1940, The gold quartz veins of Grass Valley, California: U.S. Geological Survey Professional Paper 194, 101 p.
- Jones, Bob, 1979, Tourmaline, its colors and its occurrences are truly legion: *Rock and Gem*, p. 56-58, 61-62, 85-88.
- Jones, R.S., and Fleischer, Michael, 1969, Gold in minerals and the composition of native gold: U.S. Geological Survey Circular 612, 17 p.
- Keith, S.B., 1978, Paleosubduction geometries inferred from Cretaceous and Tertiary magmatic patterns in southwestern North America: *Geology*, v. 6, no. 9, p. 516-521.
- 1984, Map of outcrops of Laramide (Cretaceous-Tertiary) rocks in Arizona and adjacent regions: Arizona Bureau of Geology and Mineral Technology, scale 1:1,000,000, 1 sheet.
- (in press), Petrochemical variations in Laramide magmatism and their relationship to Laramide tectonic and metallogenic evolution in Arizona and adjacent regions: *Arizona Geological Society Digest*.
- Keith, S.B., and Reynolds, S.J., 1980, Geochemistry of cordilleran metamorphic core complexes, in Coney, P.J., and Reynolds, S.J., eds., *Cordilleran metamorphic core complexes and their uranium favorability; final report: Grand Junction, Colo.*, U.S. Department of Energy Report GJBX-258-80, p. 247-310.
- Keith, S.B., and Wilt, J.C., 1985, Late Cretaceous and Cenozoic orogenesis of Arizona and adjacent regions: A stato-tectonic approach, in Flores, R.M., and Kaplan, S.S., eds., *Cenozoic paleogeography of the west-central United States: The Rocky Mountain Section of the Society of Economic Paleontologists and Mineralogists, Rocky Mountain Paleogeography, 3d Symposium, 1985, Denver, Colo.*, p. 403-437.
- Kennedy, G.C., 1950, A portion of the system silica-water: *Economic Geology*, v. 45, no. 7, p. 629-653.
- 1954, Pressure-volume-temperature relations in CO_2 at elevated temperatures and pressures: *American Journal of Science*, v. 252, no. 4, p. 225-241.
- Kepezhinskas, K.B., and Khlestov, V.V., 1977, The petrogenetic grid and sub-facies for middle-temperature metapelites: *Journal of Petrology*, v. 18, pt. 1, p. 114-143.
- Kimberley, M.M., 1983, Constraints on genetic modeling of Proterozoic iron formations, in Medaris, L.G., Jr., Byers, C.W., Mickelson, D.M., and Shanks, W.C., eds., *Proterozoic geology: Selected papers from an international Proterozoic symposium: Geological Society of America Memoir 161*, p. 227-235.
- King, P.B., 1969, The tectonics of North America—A discussion to accompany the tectonic map of North America, scale 1:5,000,000: U.S. Geological Survey Professional Paper 628, 95 p.
- Kistler, R.W., 1974, Phanerozoic batholiths in western North America, in Donath, F.A., ed., *Annual Review of Earth and Planetary Sciences*, v. 2, p. 403-418.
- Koltun, L.I., 1965, Application of mineralothermometric analysis in studies of the origins of certain gold ore deposits in Ural, in Yermakov, N.P., ed., *Research on the nature of mineral-forming solutions: New York, Pergamon Press*, p. 426-457.
- Korobeynikov, A.F., 1976, Gold in gas-liquid inclusions in minerals [abs.]: All-Union Conference in Thermobarogeochemistry, 5th, Ufa, U.S.S.R., 1976: Ufa, U.S.S.R., Academy of Sciences, Bashkir Section, Institute of Geology, Abstracts, p. 189-190 [in Russian].
- Koschmann, A.H., and Bergendahl, M.H., 1968, Principal gold-producing districts of the United States: U.S. Geological Survey Professional Paper 610, 283 p.
- Koster van Groos, A.F., and Wyllie, P.J., 1969, Melting relationships in the system $\text{NaAlSi}_3\text{O}_8$ - NaCl - H_2O at one kilobar pressure, with petrological applications: *Journal of Geology*, v. 77, no. 5, p. 581-605.
- Krish, E.J., 1974, Relationship of trace element distribution to level of erosion in some porphyry copper deposits and prospects, southwestern U.S. and northwestern Mexico: Golden, Colorado School of Mines, M.S. thesis, 156 p.
- Lantsev, I.P., Nikolaeva, L.A., Badalova, R.P., and Denisova, L.K., 1971, Distribution of trace elements in native gold from different deposits: *Trudy Nauchno-Issledovatel'skogo Instituta Geologii Artiki (Leningrad, U.S.S.R.)*, no. 96, pt. 1, p. 130-137.
- Lausen, Carl, 1931, Geology and ore deposits of the Oatman and Katherine districts, Arizona: Arizona Bureau of Mines Bulletin 131, Geological Series 6, 126 p.
- Leake, B.E., 1964, The chemical distinction between ortho- and para- amphibolites: *Journal of Petrology*, v. 5, no. 2, p. 238-254.
- Lebedev, M.M., Tararin, I.A., and Lagovskaya, E.A., 1967, Metamorphic zones of Kamchatka as an example of the metamorphic assemblages of the inner part of the Pacific belt: *Tectonophysics*, v. 4, no. 4-6, p. 445-461.
- Lee, W.T., 1908, Geologic reconnaissance of a part of western Arizona: U.S. Geological Survey Bulletin 352, 96 p.
- Le Maitre, R.W., 1976, The chemical variability of some common igneous rocks: *Journal of Petrology*, v. 17, no. 4, p. 589-637.
- Leroy, Jacques, 1978, The Margnac and Fanay uranium deposits of the La Crouzille district (western Massif Central, France): *Geologic and fluid inclusion studies: Economic Geology*, v. 73, no. 8, p. 1611-1634.
- Lewis, Alvin, 1982, Gold Geochemistry: *Engineering and Mining Journal*, v. 183, no. 12, p. 56-60.
- Liggett, M.A., and Childs, J.F., 1977, An application of satellite imagery to mineral exploration, in Woll, P.W., and Fischer, W.A., eds., *Proceedings of the first annual William T. Pecora memorial symposium, Sioux Falls, S. Dak.*, 1975: U.S. Geological Survey Professional Paper 1015, p. 253-270.
- Liggett, M.A., and others, 1974, A reconnaissance space sensing investigation of crustal structure for a strip from the eastern Sierra Nevada to the Colorado Plateau, Final report: U.S. National Aeronautics and Space Administration, NASA-CR-139434, 156 p.
- Lindgren, Waldemar, 1896, The gold quartz veins of Nevada City and Grass Valley districts, California: U.S. Geological Survey Annual Report, 17th, part 2, p. 1-262.
- Lindgren, Waldemar, and Davy, W.M., 1924, Nickel ores from the Key West mine, Nevada: *Economic Geology*, v. 19, no. 4, p. 309-319.
- Livingston, D.E., 1973, A plate tectonic hypothesis for the genesis of porphyry copper deposits of the southern Basin and Range province:

- Earth and Planetary Science Letters, v. 20, p. 171-179.
- Longwell, C.R., 1936, Geology of the Boulder Reservoir floor, Arizona-Nevada: Geological Society of America Bulletin, v. 47, no. 9, p. 1393-1476.
- 1963, Reconnaissance geology between Lake Mead and Davis Dam, Arizona-Nevada, in *Shorter contributions to general geology, 1960*: U.S. Geological Survey Professional Paper 374, p. E1-E51.
- Longwell, C.R., Pampeyan, E.H., Bowyer, Ben, and Roberts, R.J., 1965, Geology and mineral deposits of Clark County, Nevada: Nevada Bureau of Mines Bulletin 62, 218 p.
- Loomis, T.P., 1979, A natural example of metastable reactions involving garnet and sillimanite: *Journal of Petrology*, v. 20, no. 2, p. 271-292.
- Lucchitta, Ivo, 1966, Cenozoic geology of the upper Lake Mead area adjacent to the Grand Wash Cliffs, Arizona: University Park, Pennsylvania State University, Ph.D. dissertation, 218 p.
- 1972, Early history of the Colorado River in the Basin and Range province: Geological Society of America Bulletin, v. 83, no. 7, p. 1933-1948.
- 1979, Late Cenozoic uplift of the southwestern Colorado Plateau and adjacent lower Colorado River region: *Tectonophysics*, v. 61, no. 1-3, p. 63-95.
- Ludwig, K.R., 1973, Precambrian geology of the central Mazatzal Mountains, Arizona, Part I: Pasadena, California Institute of Technology, Ph.D. dissertation, 303 p.
- Luth, W.C., 1969, The systems $\text{NaAlSi}_3\text{O}_8\text{-SiO}_2$ and $\text{KAlSi}_3\text{O}_8\text{-SiO}_2$ to 20 kb and the relationship between H_2O content, $\text{P}_{\text{H}_2\text{O}}$ and P_{total} in granitic magmas: *American Journal of Science*, v. 267-A (Schairer volume), p. 325-341.
- Maclaren, J.M., 1908, Gold: Its geological occurrence and geographical distribution: *Mining Journal* (London), 687 p.
- Manson, Vincent, 1967, Geochemistry of basaltic rocks: Major elements, in Hess, H.H., and Poldervaart, Arie, eds., *Basalts: The Poldervaart treatise on rocks of basaltic composition*, v. 1: New York, Interscience Publishers, p. 215-269.
- Mariano, A.N., 1979, Enhancement and classification of fentization by cathodoluminescence [abs.]: Geological Association of Canada-Mineralogical Association of Canada, Joint Annual Meeting, University Laval, Quebec, 1979, Program with Abstracts, v. 4, p. 65.
- Mason, Roger, 1978, *Petrology of the metamorphic rocks*: London, George Allen and Unwin, 254 p.
- McBride, E.F., 1963, A classification of common sandstones: *Journal of Sedimentary Petrology*, v. 33, no. 3, p. 664-669.
- McConnell, R.G., 1907, Report on gold values in the Klondike high level gravels: Geological Survey of Canada Report 979, 34 p.
- McCurry, Patricia, 1971, A pseudomorphic quartz-tourmaline relationship from northern Nigeria: *American Mineralogist*, v. 56, no. 7-8, p. 1474-1476.
- Mehnert, K.R., 1968, *Migmatites and the origin of granitic rocks*: Amsterdam, Elsevier Publishing Co., 393 p.
- Metzger, F.W., Kelly, W.C., Nesbitt, B.E., and Essene, E.J., 1977, Scanning electron microscopy of daughter minerals in fluid inclusions: *Economic Geology*, v. 72, no. 2, p. 141-152.
- Middlemost, E.A.K., 1980, A contribution to the nomenclature and classification of volcanic rocks: *Geological Magazine*, v. 117, no. 1, p. 51-57.
- Middleton, G.V., 1960, Chemical composition of sandstones: Geological Society of America Bulletin, v. 71, no. 7, p. 1011-1026.
- Miller, C.F., 1981, Cordilleran peraluminous granites: An ancient quartzofeldspathic source [abs.], in Howard, K.A., Carr, M.D., and Miller, D.M., eds., *Tectonic framework of the Mojave and Sonoran Deserts, California and Arizona*: U.S. Geological Survey Open-File Report 81-503, p. 70-72.
- Miller, C.F., and Bradfish, L.J., 1980, An inner cordilleran belt of muscovite-bearing plutons: *Geology*, v. 8, no. 9, p. 412-416.
- Miller, D.M., 1980, Structural geology of the northern Albion Mountains, south-central Idaho, in Crittenden, M.D., Jr., Coney, P.J., and Davis G.H., eds., *Cordilleran metamorphic core complexes*: Geological Society of America Memoir 153, p. 399-423.
- Mining Journal, 1929, Mining activities of the southwest: *Mining Journal* (Phoenix), v. 12, no. 18, p. 25-26.
- 1933, Mill heads from western states: *Mining Journal* (Phoenix), v. 17, no. 9, p. 10.
- 1938, Concentrates from western states: *Mining Journal* (Phoenix), v. 22, no. 14, p. 21.
- Miyashiro, Akiho, 1958, Regional metamorphism of the Gosaisyo-Takanuki district in the central Abukuma Plateau: *Tokyo University Faculty of Sciences Journal*, sec. 2, v. 11, pt. 2, p. 219-272.
- 1973, *Metamorphism and metamorphic belts*: London, George Allen and Unwin, 492 p.
- Moiseenko, V.G., and Fatyanov, I.I., 1972, Geokhimiya zolota [Geochemistry of gold]: International Geological Congress, 24th, Montreal, Canada, 1972, sec. 10, p. 159-165.
- Moreau, Marcel, and Ranchin, Guy, 1973, Altérations hydrothermales et contrôles tectoniques dans les gîtes filoniens d'uranium intragranitiques du massif Central Français [Hydrothermal alteration and tectonic controls in the uranium intragranitic vein deposits of the French Central Massif], in Morin, Philippe, ed., *Les roches plutoniques dans leurs rapports avec les gîtes minéraux*: Paris, Masson and Cie, p. 77-100.
- Mosier, E.L., 1975, Use of emission spectroscopy for the semi-quantitative analysis of trace elements and silver in native gold, in Ward, F.N., ed., *New and refined methods of trace analysis useful in geochemical exploration*: U.S. Geological Survey Bulletin 1408, p. 97-105.
- Myers, I.A., and Smith, E.I., 1984, Relationship of mineralization to detachment faulting at the Cyclopic mine, Mohave County, northwestern Arizona [abs.]: Geological Society of America, Abstracts with Programs, v. 16, no. 5, p. 324.
- Nash, J.T., 1972, Fluid-inclusion studies of some gold deposits in Nevada, in Geological Survey research 1972: U.S. Geological Survey Professional Paper 800-C, p. C15-C19.
- 1976, Fluid-inclusion petrology—data from porphyry copper deposits and applications to exploration: U.S. Geological Survey Professional Paper 907-D, p. D1-D16.
- Nash, J.T., and Cunningham, C.G., Jr., 1973, Fluid-inclusion studies of the fluorspar and gold deposits, Jamestown district, Colorado: *Economic Geology*, v. 68, no. 8, p. 1247-1262.
- Nash, J.T., Granger, H.C., and Adams, S.S., 1981, Geology and concepts of genesis of important types of uranium deposits, in Skinner, B.J., ed., *Seventy-fifth anniversary volume, Economic Geology, 1905-1980*: New Haven, Conn., The Economic Geology Publishing Co., p. 63-116.
- Neuerburg, G.J., 1961, A method of mineral separation using hydrofluoric acid: *American Mineralogist*, v. 46, no. 11-12, p. 1498-1501.
- 1975, A procedure, using hydrofluoric acid, for quantitative mineral separations from silicate rocks: *U.S. Geological Survey Journal of Research*, v. 3, no. 3, p. 377-378.
- Newton, R.C., 1966, Kyanite-andalusite equilibrium from 700° to 800 °C: *Science*, v. 153, no. 3732, p. 170-172.
- Nicholson, P.M., 1980, The geology and economic significance of the Golden Dyke Dome, Northern Territory, in Ferguson, John, and Goleby, A.B., eds., *Uranium in the Pine Creek geosyncline*: International Atomic Energy Agency, International Uranium Symposium on the Pine Creek Geosyncline, Sydney, Australia, 1979, Proceedings: Serial STI/PUB/555, p. 319-334.
- Nitsch, K.H., 1970, Experimentelle Bestimmung der oberen stabilitäts-grenze von stülpnomenlan [Experimental determination of the upper stability limit of stülpnomenlane] [abs.]: Fortschritte der Mineralogie,

- v. 47, supplement 1, p. 48-49.
- North, H.H., and Allen, C.C., 1948, Young-Davidson mine, in *Structural geology of Canadian ore deposits*: Canadian Institute of Mining and Metallurgy, v. 1, p. 839-845.
- Odikadze, G.L., 1971, Distribution of fluorine in the granitoids of the Greater Caucasus and Dzirul' Massif: *Geochemistry International*, v. 8, no. 3, p. 314-323.
- Page, N.J., Theodore, T.G., and Bradley, L.A., 1986, Discussion of ultramafic and mafic rocks and platinum-group element analyses from the Lost Basin mining district, northwestern Arizona: U.S. Geological Survey Open-File Report 86-33, 13 p.
- Peacock, M.A., 1931, Classification of igneous rock series: *Journal of Geology*, v. 39, no. 1, p. 54-67.
- Peirce, H.W., 1976, Elements of Paleozoic tectonics in Arizona: *Arizona Geological Society Digest*, v. 10, p. 37-58.
- Petro, W.L., Vogel, T.A., and Wilband, J.T., 1979, Major-element chemistry of plutonic rock suites from compressional and extensional plate boundaries: *Chemical Geology*, v. 26, p. 217-235.
- Pettijohn, F.J., 1949, *Sedimentary rocks*: New York, Harper and Brothers, 718 p.
- 1963, Chemical composition of sandstones—excluding carbonate and volcanic sands: U.S. Geological Survey Professional Paper 440-S, 21 p.
- Pitcher, W.S., 1979, The nature, ascent and emplacement of granitic magmas: *Geological Society of London Journal*, v. 136, p. 627-662.
- Plimer, I.R., 1980, Exhalative Sn and W deposits associated with mafic volcanism as precursors to Sn and W deposits associated with granites: *Mineralium Deposita*, v. 15, p. 275-289.
- Poty, B.P., Leroy, Jacques, and Jachimowicz, Leon, 1976, Un nouvel appareil pour la mesure des températures sous le microscope: l'installation de microthermometrie Chaixmecca [A new apparatus for the measurement of temperatures under the microscope: the installation of a Chaixmecca microthermometer]: *Société Française Minéralogie et Cristallographie Bulletin*, v. 99, no. 2-3, p. 182-186.
- Poty, B.P., Stalder, H.A., and Weisbrod, A.M., 1974, Fluid inclusions studies in quartz from fissures of Western and Central Alps: *Schweizerische Mineralogische und Petrographische Mitteilungen*, v. 54, no. 2-3, p. 717-752.
- Reinhardt, E.W., 1968, Phase relations in cordierite-bearing gneisses from the Gananoque area, Ontario: *Canadian Journal of Earth Sciences*, v. 5, no. 3, pt. 1, p. 455-482.
- Rehrig, W.A., and Heidrick, T.L., 1976, Regional tectonic stress during the Laramide and late Tertiary intrusive periods, Basin and Range province, Arizona: *Arizona Geological Society Digest*, v. 10, p. 205-228.
- Reyner, M.L., 1954, Preliminary reconnaissance report, in U.S. Atomic Energy Commission preliminary reconnaissance for uranium in Mohave County, Arizona, 1952 to 1956: Grand Junction, Colo., U.S. Atomic Energy Commission, Report RME-158, p. 43.
- Reynolds, R.C., Jr., 1965, Geochemical behavior of boron during the metamorphism of carbonate rocks: *Geochimica et Cosmochimica Acta*, v. 29, no. 9, p. 1101-1114.
- Reynolds, S.J., 1980, A conceptual basis for the occurrence of uranium in cordilleran metamorphic core complexes, in Coney, P.J., and Reynolds, S.J., eds., *Cordilleran metamorphic core complexes and their uranium favorability*, final report: Grand Junction, Colo., U.S. Department of Energy, Report GJBX-258-80, p. 187-245.
- Reynolds, S.J., Keith, S.B., and DeWitt, Ed, 1982, Late Cretaceous-early Tertiary peraluminous granitoids of Arizona-California and their related mineral deposits [abs.]: *Geological Society of America Abstracts with Programs*, v. 14, no. 4, p. 227.
- Richardson, C.K., and Holland, H.D., 1979, Fluorite deposition in hydrothermal systems: *Geochimica et Cosmochimica Acta*, v. 43, no. 9, p. 1327-1335.
- Robbins, C.R., and Yoder, H.S., Jr., 1962, Stability relations of dravite, a tourmaline: *Carnegie Institution of Washington Year Book* 61, p. 106-107.
- Roberts, W.L., Rapp, G.R., Jr., and Weber, Julius, 1974, *Encyclopedia of minerals*: New York, Van Nostrand Reinhold Co., 693 p.
- Roedder, Edwin, 1962, Studies of fluid inclusions I: Low-temperature application of a dual-purpose freezing and heating stage: *Economic Geology*, v. 57, no. 7, p. 1045-1061.
- 1963, Studies of fluid inclusions II: Freezing data and their interpretation: *Economic Geology*, v. 58, no. 2, p. 167-211.
- 1972, *Composition of fluid inclusions* (6th ed.): U.S. Geological Survey Professional Paper 440-JJ, 164 p.
- 1984, Fluid inclusions: *Mineralogical Society of America, Reviews in Mineralogy*, v. 12, 644 p.
- Roedder, Edwin, and Bodnar, R.J., 1980, Geologic pressure determinations from fluid inclusion studies, in Donath, F.A., ed., *Annual Review of Earth and Planetary Sciences*, v. 8, p. 263-301.
- Rubie, D.C., and Gunter, W.D., 1983, The role of speciation in alkaline igneous fluids during fenite metasomatism: *Contributions to Mineralogy and Petrology*, v. 82, p. 165-175.
- Rumble, Douglas, III, 1978, Mineralogy, petrology, and oxygen isotopic geochemistry of the Clough Formation, Black Mountain, western New Hampshire, U.S.A.: *Journal of Petrology*, v. 19, no. 2, p. 317-340.
- Ryabchikov, I.D., 1981, Mobilization of ore metals by supercritical fluids from crystallizing magmas, in Rickard, D.T., and Wickman, F.E., eds., *Chemistry and geochemistry of solutions at high temperatures and pressures*: Oxford, Pergamon Press, p. 529-535.
- Sakharova, M.S., Batrakova, Y.A., and Posukhova, T.V., 1979, Causes of differentiation of gold and silver during their precipitation on natural minerals: *Moscow University Geology Bulletin*, v. 34, no. 4, New York, Allerton Press, p. 36-44 [translation].
- Schrader, F.C., 1909, Mineral deposits of the Cerbat Range, Black Mountains, and Grand Wash Cliffs, Mohave County, Arizona: U.S. Geological Survey Bulletin 397, 226 p.
- 1917, Geology and ore deposits of Mohave County, Arizona: *American Institute of Mining Engineers Transactions*, v. 56, p. 195-227.
- Seward, T.M., 1982, Hydrothermal transport and deposition of gold, in Glover, J.E., and Groves, D.I., eds., *Gold mineralization: University of West Australia, Geology Department and Extension Service Publications*, p. 45-55.
- Shapiro, Leonard, 1967, Rapid analysis of rocks and minerals by a single solution method, in *Geological Survey research 1967: U.S. Geological Survey Professional Paper 575-B*, p. B187-B191.
- Shapiro, Leonard, and Brannock, W.W., 1962, Rapid analysis of silicate, carbonate, and phosphate rocks: *U.S. Geological Survey Bulletin* 1144-A, p. A1-A56.
- Sharp, J.E., 1980, Gold breccia pipe southwest of Las Vegas, Nevada [abs.]: *American Institute of Mining, Metallurgical, and Petroleum Engineers Annual Meeting, Las Vegas, Nev., 1980, Program with Abstracts*, p. 24.
- Shcherba, G.N., 1970, Greisens: *International Geology Review*, v. 12, no. 2, p. 114-150; v. 12, no. 3, p. 239-255. Translated from Shcherba, G.N., 1968, *Greyzenovyye mestorozhdeniya*, chapter 6 of *Genезis endozennykh rudnykh mestorozhdeniy* [Genesis of endogenic ore deposits]: Moscow, Nedra Press, 720 p.
- Silver, L.T., 1960, Age determinations on Precambrian diabase differentiates in the Sierra Ancha, Gila County, Arizona [abs.]: *Geological Society of America Bulletin*, v. 71, no. 12, pt. 2, p. 1973-1974.
- 1963, The uses of cogenetic uranium-lead isotope systems in zircons in geochronology, in *Radioactive dating; Symposium on Radioactive Dating*, Athens, 1962: Vienna, International Atomic Energy Agency, p. 279-287.
- 1964, Mazatzal orogeny and tectonic episodicity [abs.]: *Geological Society of America Special Paper* 82, p. 185-186.

- 1966, U-Pb isotope relations and their historical implications in Precambrian zircons from Bagdad, Arizona [abs.]: Geological Society of America Special Paper 101, p. 420.
- 1967, Apparent age relations in the older Precambrian stratigraphy of Arizona [abs.], in Burwash, R.A., and Morton, R.D., eds., Geochronology of Precambrian stratified rocks: University Alberta, Edmonton, Canada, Conference, June 1967, p. 87.
- Silver, L.T., Bickford, M.E., Van Schmus, W.R., Anderson, J.L., Anderson, T.H., and Medaris, L.G., Jr., 1977, The 1.4–1.5 b.y. transcontinental anorogenic plutonic perforation of North America [abs.]: Geological Society of America Abstracts with Programs, v. 9, no. 7, p. 1176–1177.
- Sinclair, W.D., 1984, Gold deposits of the Matachewan area, Ontario, in Hodder, R.W., and Petruk, William, eds., Geology of Canadian gold deposits: Canadian Institute of Mining and Metallurgy Special Volume 24, p. 83–93.
- Skippen, G.B., 1971, Experimental data for reactions in siliceous marbles: *Journal of Geology*, v. 79, no. 4, p. 457–481.
- Slack, J.F., 1980, Tourmaline—a prospecting guide for massive base-metal sulfide deposits in the Penobscot Bay area, Maine: Maine Geological Survey, Special Economic Studies Series 8, 25 p.
- 1981, Prospecting with tourmaline for stratabound massive sulfide deposits: Examples from the Appalachian-Caledonide orogen [abs.]: Institution of Mining and Metallurgy Transactions (London), sec. B, Applied Earth Science, v. 90, p. B56.
- 1982, Tourmaline in Appalachian-Caledonian massive sulfide deposits and its exploration significance: Institution of Mining and Metallurgy Transactions (London), sec. B, Applied Earth Sciences, v. 91, p. B81–B89.
- Slack, J.F., and Annis, M.P., 1981, Time-space relations of tourmaline-rich rocks at the Elizabeth mine and vicinity, Vermont Copper Belt [abs.]: Geological Society of America Abstracts with Programs, v. 3, p. 177.
- Smirnov, V.I., 1976, Geology of mineral deposits: Moscow, Mir, 520 p.
- Smith, J.V., 1974, Feldspar minerals [vol.] 2, Chemical and textural properties: New York, Springer-Verlag, 690 p.
- Snyder, G.L., 1978, Intrusive rocks northeast of Steamboat Springs, Park Range, Colorado, with a section on Geochronology by C.E. Hedge: U.S. Geological Survey Professional Paper 1041, 42 p.
- Stanton, R.L., 1972, Ore petrology: New York, McGraw-Hill, 713 p.
- Steiner, J.C., Jahns, R.H., and Luth, W.C., 1975, Crystallization of alkali feldspar and quartz in the haplogranite system $\text{NaAlSi}_3\text{O}_8\text{-KAlSi}_3\text{O}_8\text{-SiO}_2\text{-H}_2\text{O}$ at 4 kb: Geological Society of America Bulletin, v. 86, no. 1, p. 83–97.
- Stephenson, J.F., and Ehmann, W.D., 1971, Neutron activation analysis of gold in Archean igneous and metamorphic rocks of the Rice Lake-Beresford Lake area, southeastern Manitoba: *Economic Geology*, v. 66, no. 6, p. 933–939.
- Streckeisen, A.L., and others, 1973, Plutonic rocks; classification and nomenclature recommended by the IUGS Subcommittee on the Systematics of Igneous Rocks: *Geotimes*, v. 18, no. 10, p. 26–30.
- Suk, Milos, 1964, Material characteristics of the metamorphism and migmatization of Moldanubian paragneisses in central Bohemia: Prague, Krystalinikum, v. 2, p. 71–105.
- Sutherland, D.S., 1965a, Potash-trachytes and ultra-potassic rocks associated with the carbonatite complex of the Toror Hills, Uganda: *Mineralogical Magazine*, v. 35, no. 270, p. 363–378.
- 1965b, Nomenclature of the potassic-feldspathic rocks associated with carbonatites: Geological Society of America Bulletin, v. 76, no. 12, p. 1409–1412.
- Swan, M.M., Hausen, D.M., and Newell, R.A., 1981, Lithological, structural, chemical, and mineralogical patterns in a Precambrian stratiform gold occurrence, Yavapai County, Arizona, in Hausen, D.M., and Park, W.C., eds., Process mineralogy: Extractive metallurgy, mineral exploration, energy resources: The Metallurgical Society of the American Institute of Mining, Metallurgical, and Petroleum Engineers Process Mineralogy Committee, Symposium, American Institute of Mining, Metallurgical and Petroleum Engineers Annual Meeting, 110th, Chicago, Ill., 1981, Conference Proceedings, p. 143–157.
- Takenouchi, Sukune, and Kennedy, G.C., 1965, Dissociation pressures of the phase $\text{CO}_2 \cdot 5\frac{3}{4} \text{H}_2\text{O}$: *Journal of Geology*, v. 73, no. 2, p. 383–390.
- Theodore, T.G., Keith, W.J., Till, A.B., and Peterson, J.A., 1978, Preliminary geologic map of the Mineral Mountain $7\frac{1}{2}$ -minute quadrangle, Arizona: U.S. Geological Survey Open-File Report 78–468, 1 sheet.
- Thomas, B.E., 1949, Ore deposits of the Wallapai district, Arizona: *Economic Geology*, v. 44, no. 8, p. 663–705.
- Thompson, J.B., Jr., 1957, The graphical analysis of mineral assemblages in pelitic schists: *American Mineralogist*, v. 42, nos. 11–12, p. 842–858.
- Thornton, C.P., and Tuttle, O.F., 1960, Chemistry of igneous rocks I. Differentiation index: *American Journal of Science*, v. 258, no. 9, p. 664–684.
- Thorson, J.P., 1971, Igneous petrology of the Oatman district, Mohave County, Arizona: Santa Barbara, University of California, Ph.D. thesis, 189 p.
- Tischendorf, Gerhard, 1977, Geochemical and petrographic characteristics of silicic magmatic rocks associated with rare-element mineralization, in Stempok, M., Burnol, L., and Tischendorf, G., eds., Metallization associated with acid magmatism: International Geological Correlation Programme, Symposium on Metallization Associated with Acid Magmatism, Prague, 1974, v. 2, p. 41–96.
- Todheide, K., and Franck, E.U., 1963, Das Zweiphasengebiet und die kritische Kurve in System Kohlendioxid-Wasser bis zu Drucken von 3500 bar [The two-phase field and the critical curve in the system carbon dioxide-water to 3500 bars]: *Zeitschrift fur physikalische Chemie*, v. 37, p. 388–401.
- Turekian, K.K., and Wedepohl, K.H., 1961, Distribution of the elements in some major units of the Earth's crust: Geological Society of America Bulletin, v. 72, no. 2, p. 175–192.
- Tuttle, O.F., and Bowen, N.L., 1958, Origin of granite in the light of experimental studies in the system $\text{NaAlSi}_3\text{O}_8\text{-KAlSi}_3\text{O}_8\text{-SiO}_2\text{-H}_2\text{O}$: Geological Society of America Memoir 74, 153 p.
- van de Kamp, P.C., 1969, Origin of amphibolites in the Beartooth Mountains, Wyoming and Montana: New data and interpretation: Geological Society of America Bulletin, v. 80, no. 6, p. 1127–1136.
- Vidale, R.J., 1969, Metasomatism in a chemical gradient and the formation of calc-silicate bands: *American Journal of Science*, v. 267, no. 8, p. 857–874.
- Vidale, R.J., and Hewitt, D.A., 1973, "Mobile" components in the formation of calc-silicate bands: *American Mineralogist*, v. 58, no. 11–12, p. 991–997.
- Vikre, P.G., 1977, Gold and silver mineralization of the Rochester district, Pershing County, Nevada: Stanford, Calif., Stanford University, Ph.D. dissertation, 404 p.
- 1981, Silver mineralization in the Rochester district, Pershing County, Nevada: *Economic Geology*, v. 76, no. 3, p. 580–609.
- Viladkar, S.G., 1980, The fenitized aureole of the Newania carbonatite, Rajasthan: *Geological Magazine*, v. 117, no. 3, p. 285–292.
- Vinogradov, A.P., 1962, Average contents of chemical elements in the principal types of igneous rocks of the earth's crust: *Geochemistry*, no. 7, p. 641–664.
- Warren, H.V., and Thompson, R.M., 1944, Minor elements in gold: *Economic Geology*, v. 39, no. 7, p. 457–471.
- Wasserburg, G.J., and Lanphere, M.A., 1965, Age determinations in the Precambrian of Arizona and Nevada: Geological Society of America Bulletin, v. 76, no. 7, p. 735–758.
- Welty, J.W., Reynolds, S.J., Keith, S.B., Gest, D.E., Trapp, R.A., and

- DeWitt, E., 1985, Mine index for metallic mineral districts of Arizona: Arizona Bureau of Geology and Mineral Technology Bulletin 196, 92 p.
- Wenk, Eduard, 1954, Berechnung von Stoffaustauschvorgängen [Calculation of matter-exchange reactions]: Schweizerische Mineralogische und Petrographische Mitteilungen, v. 34, no. 2, p. 309-318.
- White, A.J.R., Clemens, J.D., Holloway, J.R., Silver, L.T., Chappell, B.W., and Wall, V.J., 1986, S-type granites and their probable absence in southwestern North America: *Geology*, v. 14, p. 115-118.
- White, A.J.R., Williams, I.S., and Chappell, B.W., 1977, Geology of the Berridale 1:100,000 sheet 8625: New South Wales [Australia] Geological Survey, 138 p.
- Wilcox, R.E., 1979, The liquid line of descent and variation diagrams, in Yoder, H.S., Jr., ed., *The evolution of the igneous rocks, fiftieth anniversary perspectives*: Princeton, N.J., Princeton University Press, p. 205-232.
- Wilkins, Joe, Jr., and Heidrick, T.L., 1982, Base and precious metal mineralization related to low-angle tectonic features in the Whipple Mountains, California and Buckskin Mountains, Arizona [abs.]: Geological Society of America Abstracts with Programs, v. 14, no. 4, p. 245.
- Williams, S.A., 1963, Oxidation of sulfide ores in the Mildren and Steppe mining districts, Pima County, Arizona: *Economic Geology*, v. 58, no. 7, p. 1119-1125.
- Wilson, E.D., 1939, Pre-Cambrian Mazatzal revolution in central Arizona: Geological Society of America Bulletin, v. 50, no. 7, p. 1113-1164.
- 1962, A resume of the geology of Arizona: Arizona Bureau of Mines Bulletin 171, 140 p.
- Wilson, E.D., Cunningham, J.B., and Butler, G.M., 1934, Arizona lode—gold mines and gold mining: Arizona Bureau of Mines Bulletin 137, Mining Technology series 37, 261 p.
- Wilt, J.C., 1980, Arizona molybdenum minerals as keys to metallogenic types: Geological Society of America Abstracts with Programs, v. 12, no. 6, p. 309.
- Wilt, J.C., and Keith, S.B., 1980, Molybdenum in Arizona: Arizona Bureau of Geology and Mineral Technology, Fieldnotes, v. 10, no. 3, p. 1-3, 7-9, 12.
- Winkler, H.G.F., 1974, Petrogenesis of metamorphic rocks: New York, Springer-Verlag, 320 p.
- Woodward, G.E., and Luff, Paul, 1943, Gold, silver, copper, lead, and zinc in Arizona, in Needham, C.E., ed., *Minerals yearbook 1942*: Washington, U.S. Government Printing Office, p. 231-259.
- Wright, J.E., and Haxel, Gordon, 1982, A garnet-two-mica granite, Coyote Mountains, southern Arizona: Geologic setting, uranium-lead isotopic systematics of zircon, and nature of the granite source region: Geological Society of America Bulletin, v. 93, no. 11, p. 1176-1188.
- Wyllie, P.J., 1981, Magma sources in cordilleran settings, in Dickinson, W.R., and Payne, W.D., eds., *Relations of tectonics to ore deposits in the southern cordillera*: Arizona Geological Society Digest, v. 14, p. 39-48.
- Wyman, R.V., 1974, The relationship of ore exploration targets to regional structure in the Lake Mead metallogenic province: Tucson, University of Arizona, Ph.D. dissertation, 103 p.
- Yeend, Warren, 1975, Experimental abrasion of detrital gold: U.S. Geological Survey Journal of Research, v. 3, no. 2, p. 203-212.
- Ypma, P.J.M., 1963, Rejuvenation of ore deposits as exemplified by the Belledonne metaliferous province: Leiden, The Netherlands, University of Leiden, Ph.D. dissertation, 212 p.

TABLE 11

TABLE 11.—*Notable occurrences of commodities in the Gold Basin-Lost Basin mining districts*
 [Modified from P. M. Blacet, unpub. data, 1967-72; ?, presence of commodity inferred]

Locality (pl. 1)	Name	Approximate location (UTM 10,000-m grid, zone 11)	Commodities present	Comments
11	Golden Gate mine	NW1/4 sec. 32, T. 30 N., R. 17 W.	Au, Cu	Free gold occurs in yellowish- to red-stained quartz characterized by empty pyrite molds and cellular hematite vugs. Gold usually is in very intricate sheaves that are so fragile that they wave in the wind. Some rather solid gold pieces as much as 1 mm in diameter are present also. Veins as much as 1 m thick, but many of the veins consist of massive quartz containing little sulfide. Relatively abundant free gold on the dump so early miners must really have high-graded the deposit. First workings probably date before 1900. Chalcopyrite, cuprite, malachite, and pyrite noted.
12	L.P.M. mine	NW1/4 sec. 4, T. 27 N., R. 18 W.	Cu, Au	Country rocks are very coarse grained, porphyritic monzogranite, including potassium feldspar phenocrysts as much as 5 cm. Altered schist crops out in pit 60 m northwest of old headframe. Sparse secondary copper found. Low sulfide content and absence of coarse vein material suggests general alteration zone with many small quartzose seams. A zone of steeply north dipping to vertical quartz veins and veinlets have an average strike of N. 50° E. The veins are not persistent and the majority are stringers less than 2.5 cm, while a few are 20 to 30 cm long. No chalcopyrite, galena, fluorite, or carbonate was observed. A trace of gold was found in fine- to medium-grained quartz. Ore probably was hosted by silicified granite and schistose metamorphic rocks.
13	Red Norse mine	NE1/4 sec. 32, T. 28 N., R. 18 W.	Au, Cu, Pb, Mo	Vein 20 cm wide at the collar of 60° inclined shaft. Vein strikes N. 15° E., dips 60° E. Country rock is Early Proterozoic porphyritic monzogranite. Free gold coarse and abundant in cellular vuggy quartz containing limonitic and hematitic cavity fills. Some secondary copper minerals and wulfenite. Quartz, galena, chalcopyrite (minor), pyrite (trace), and relatively abundant wulfenite in vein exposed in shallow open-cut trending N. 30° E. Vein strikes approximately N. 30°-35° E. and dips 85° southeast. Some masses of partially oxidized pyrite show irregularly shaped blebs of free gold
14	Junction mine	SE1/4 sec. 29, T. 28 N., R. 18 W.	Au, Cu, Pb, Mo	

16	Cyclopic mine	SW1/4 sec. 30, T. 28 N., R. 18 W.	Au, Pb, Mo,	<p>approximately 1 to 2 mm across. Exposed segment of the vein is approximately 1 m and includes some septa of granitic rock from the surrounding Early Proterozoic porphyritic monzogranite. Opencut is about 30 m southwest of two shallow shafts, each 15 to 30 m deep.</p> <p>Series of northwest opencuts and pits along Miocene detachment fault breccia which is exposed in place at several localities. Free gold in at least one hand sample picked up in southern half of series of cuts. Abundant angular fragments contain milky-white quartz with dark-reddish-gray matrix. Considerable cellular gossan, with wulfenite common. Old underground workings intersected in some of the opencuts; none accessible. Numerous prospects, pits, and trenches in the lower(?) gouge zone. Vein quartz is brecciated and widely scattered in the gouge as blocks 0.6 m long and approximately 0.3 m thick. Veins contain galena, pyrite, ferrocaldite, malachite (alteration of chalcocopyrite(?)), wulfenite, gold, cerussite. Brilliant crimson mineral may be cuprite. Red, brown, and black Fe and Mn(?) oxides.</p>
17	Eldorado mine	SW1/4 sec. 21, T. 28 N., R. 18 W.	Cu, Pb, Mo, Au	<p>The mineralized vein seems to average 1 m thick and dips 25°-30° E.-SE. on west side of workings and shallowing to nearly horizontal at the tunnel portals on the east side of the ridge. The workings generally dip 20° E.-SE. parallel to the vein. The country rock is intensely sheared, cataclastic medium-grained Early Proterozoic gneissic granodiorite. The mineralized vein(s) is occupying an intensely sheared zone that is of probable Late Cretaceous and (or) early Tertiary age. Although the vein quartz is fractured (locally intensely), it is not brecciated. Some veins crosscut highly foliated gneissic granodiorite, but generally they approximately parallel the schistosity. No red or other clay gouge and no indication of notable Tertiary movement. The main vein parallels also the pegmatite, and, in part, the 2-m thickness of quartz probably reflects the quartz-core stage of the pegmatite. The quartz vein lies between a crumpled and kinkbanded schistose granodiorite and an overlying sill of leucogranite pegmatite.</p> <p>Abundant chrysocolla; moderate galena; but no chalcocopyrite seen. Some wulfenite and cerussite present also.</p> <p>In the irregular surface cut 10 m northwest of the opening at the northwest end of the underground stopes, altered biotite lamprophyre has consistent chilled margins against the mineralized vein quartz. This indicates the mafic dikes and sills are postmineralization. Intensely sericitized leucogranitic sills occur below the vein here,</p>

TABLE 11.—Notable occurrences of commodities in the Gold Basin-Lost Basin mining districts—Continued

Locality (pl. 1)	Name	Approximate location (UTM 10,000-m grid, zone 11)	Commodities present	Comments
17	Eldorado mine—Continued			
19	Unnamed prospect	SE1/4 sec. 27, T. 28 N., R. 18 W.	Au, F	indicating a somewhat crosscutting relationship. Numerous veins 2 cm to 1 m thick are concentrated in an intensely sheared zone, which dips very gently but is undulating overall. Fluorite-gold-pyrite-bearing episyenitic rocks, which cut fine- to medium-grained biotite monzogranite. Gold occurs in leached cavities in these episyenitic rocks (see text). In outcrop, the episyenitic rock occurs in four small pipelike masses, the largest of which measures about 8 m across (see fig. 50). Two shallow prospect pits have been dug on the pipes most likely because of the color anomaly resulting from the oxidation of pyrite. Portal initially trends N. 10° W., then bends to N. 15° E. and extends 100 to 150 m intersecting raise and winze. Winze continues 10 m below level of main drift. Workings follow shear zone. Quartz vein as much as 1.5 m thick, exposed in back, contains thin seams of chalcopyrite oxidizing to chalcocite, cuprite, malachite, and azurite; and a trace of galena. Some fine gold seen in yellow-brown lacy quartzose gossan. Vein ends by interfingering with altered and sheared amphibolite.
24	Ford mine	SW1/4 sec. 33, T. 30 N., R. 17 W.	Au, Cu, Pb	Vertical shaft 30 ft deep in opencut made in garnet-epidote-quartz skarn composing a small roof pendant or septum in Early Proterozoic porphyritic monzogranite. Pendant is approximately 50 m long and trends N. 45°-55° W.
25	Unnamed prospect	SE1/4 sec. 19, T. 28 N., R. 16 W.	W	Horizontal adit 800 m along northwest-striking shear zone dipping 65° SW. Damp clay gouge is contorted and locally contains some quartz veinlets which mushroom into quartz stringers making as much as 0.5 m of the adit width.
26	Blue Bird mine	NE1/4 sec. 19, T. 29 N., R. 17 W.	Au	Two pegmatite dikes, both apparently claimed but unmined. The dikes are muscovite bearing with books as much as 15 cm in diameter and 5 to 8 cm thick. One dike trends approximately N. 10° W. and is about 3 m wide. Small prospect pit at second dike.
138	Unnamed prospect	SE1/4 sec. 26, T. 28 N., R. 17 W.	Mica	
139	M. P. Mica mine	SE1/4 sec. 26, T. 28 N., R. 17 W.	Mica	A series of north-northwest-striking pegmatite lenses 3 to 5 m thick with well-defined bull quartz cores. Coarse muscovite is common, transparent in thin cleavage sheets, but inclusions of other minerals

205	Unnamed prospect	NE1/4 sec. 28, T. 30 N., R. 17 W.	Au?	<p>are common. The books are less than 10 to 15 cm across. This series of pegmatites possibly is continuous with a series of several muscovite-bearing pegmatites to the northwest. Early Proterozoic leucocratic monzogranite makes up the country rock. The main mine workings are open-cut. Prospect pit just west of contact between Muddy Creek Formation and Early Proterozoic gneiss. The pit exposes an alternating sequence of amphibolite and biotitic quartzite and (or) quartzofeldspathic gneiss. The rocks here also show abundant iron oxide-stained cubic molds after pyrite. No gold or secondary copper minerals observed. Locally, coarse-grained granitic dikes or sills are abundant in some of the schistose sequences. Metaclinopyroxene contains very sparse concentrations of chromite.</p>
213	Unnamed locality	SE1/4 sec. 29, T. 29 N., R. 17 W.	Cr	Banded jasper-magnetite beds associated with laminated or foliated quartzite. Foliation strikes N. 30° W. and dips 65°-70° SW. Quartzite includes vitreous white and micaceous pink types.
216	Valley View	NW1/4 sec. 32, T. 29 N., R. 17 W.	Fe	Inclined shaft plunging 45°-55° (30° below third main level) parallel to a conspicuous shear zone which strikes N. 45° E. Mineralized quartz veins are parallel to the shear zone. There are three major levels, about evenly spaced, from which irregular raises follow ore shoots. Overall workings are close to a contact between Early Proterozoic gneissic granodiorite and gneiss.
217	Malco mine	SE1/4 sec. 21, T. 28 N., R. 18 W.	Au	Prospect pit exposing complexly intermixed quartz-pyrite rock and apparently genetically related and intermixed quartz-calcite-pyrite and feldspar-calcite-quartz-pyrite rock very similar to the episyenitic rocks containing visible gold in the East White Hills (loc. 19, above). Although oxidized, pyrite-rich rocks were examined carefully, no free gold was seen.
259	Unnamed prospect	SE1/4 sec. 20, T. 29 N., R. 17 W.	Au?	In one of the prospect pits, a pyrite-bearing aplitic dike strikes east-northeast and dips 40°-45° S. A large amount of weathered pyrite is associated with the dike. In addition, nearby there is a coarse-grained magnetite-rich pegmatite which may have a genetic connection with the pyrite-bearing dike. The dike is about 0.5 m wide and has rather sharp contacts with altered and silicified feldspathic gneiss.
274	Unnamed prospects	NE1/4 sec. 20, T. 29 N., R. 17 W.	Au?	Prospect contained a very altered feldspar-quartz-pyrite vein several centimeters thick, judging from rock samples on the upper "ore" pile. Generally similar to rocks at location 274. The aplitic feldspar rock usually bounds the quartz vein on the north side, and the quartz-rich portions contain most of the sulfide. Gold was seen in the boxwork. No indications of copper were seen.
275	Unnamed prospect	SE1/4 sec. 20, T. 29 N., R. 17 W.	Au	

TABLE 11.—Notable occurrences of commodities in the Gold Basin-Lost Basin mining districts—Continued

Locality (pl. 1)	Name	Approximate location (UTM 10,000-m grid, zone 11)	Commodities present	Comments
276	Unnamed adit and prospect pit	NW1/4 sec. 20, T. 29 N., R. 17 W.	Au?	Small adit driven straight in for about 9 m along a fault zone varying about 0.6 to 1.2 m wide. Slickensides are well developed with the wall rock altered to an ochre-orange color. The slickensides plunge westward at about 50° in the fault zone, which strikes N. 50° W., and dips about 60° W. An irregular vein zone of crushed- and carbonate-cemented (ankeritic) white milky quartz, ranging from 0 to 23 cm thick can be seen locally at the back of the adit. A small prospect also is located along the fault about 60 m to the southeast. No copper staining, sulfides, or pyrite-type boxworks present. A newspaper found inside suggests work was before or during the 1920's.
277	Unnamed adit	NW1/4 sec. 20, T. 29 N., R. 17 W.	Au?	This adit is similar to location 276. The adit is driven at about N. 50° W. along the same fault as in location 276 for about 10 to 12 m. The fault dips about 60°-65° SW., and it contains oblique mullions and slickensides plunging about 55° W. The fault zone, which is about 0.3 m to 0.9 m wide, is composed of highly sheared gouge and brecciated lenses of white milky quartz. The quartz vein observed at location 276 is not continuous through this adit. An orange-ochre color from weathering ankeritic calcite was also observed at this locality. This adit also intersects a raise to the surface about 9 m from the portal. No sulfides or copper staining were observed.
279	Unnamed prospect	NW1/4 sec. 20, T. 29 N., R. 17 W.	F, Au?	The prospect pits are along feldspathic veins which contain quartz, potassium feldspar, carbonate, and pyrite. The veins are about 0.6 m thick and strike irregularly N. 55° W. roughly paralleling the vertical layering in the surrounding banded gneiss. On the dump there are samples of fluorite and topaz. Gold was not observed but may be present in the vuggy (pyrite molds) quartz at the pits. There is also abundant ankeritic carbonate commonly containing large pyrite cubes about 1.3 cm. The pyrite is generally altered. No copper staining or galena was observed.
284	Unnamed drywasher site	NW1/4 sec. 19, T. 29 N., R. 17 W.	Au	The sample was taken from above the caliche-cemented fanglomerate just west of mine road leading to the adit and shaft at locality 285. A few fine-sand-size frosted colors were found. From their

285	No name opencut and adit	SW1/4 sec. 18, T. 29 N., R. 17 W.	Au?	condition, they are probably some distance from their source. The first 6 m along the adit consists of Quaternary fanglomerate which has been faulted against amphibolitic, banded gneiss. The fault strikes north-south and dips 60° W. The brecciated amphibolite and banded gneiss generally have their layering striking N. 15° E. and dipping 50° W. Well-developed striations trend N. 85° W. and plunge 43° W. The fanglomerate, gravel, and breccia generally are poorly cemented except in certain spots where they have been case-hardened by caliche. About 50 m from the portal, the adit apparently was filled subsequently with waste rock from a shaft. No vein material seen in place, but the dump contains vein material similar to that of the Bluebird vein.
286	Unnamed drywasher site	SW1/4 sec. 18, T. 29 N., R. 17 W.	Au	Drywasher concentrate from irregular surface consisting of amphibolite bed rock about 6 m upstream from highest Quaternary fanglomerate and fault. One small color was observed with abundant garnet.
291	Unnamed prospects	SW1/4 sec. 17, T. 29 N., R. 17 W.	Cu, Au?	This locality consists of two prospect pits approximately 3 m apart along a shear zone striking N. 30° E. and dipping 65° E. and about 1 to 1.5 m wide. Although the fault may be relatively important, and somewhat like the one at the Bluebird mine, it could not be traced because of talus- and debris-covered slopes. In the pits, the veins consist of pyrite and chalcopyrite together with milky quartz and ferruginous carbonate. Generally the veins are thin stringers, less than 3 cm wide, although one pod reached as much as 25 cm across and had a well-developed sericitic envelope.
297	Unnamed prospect	NE1/4 sec. 20, T. 29 N., R. 17 W.	Cu	An approximately 8-m-thick syenitic micropegmatite contains abundant quartz associated with red-brown, presumably iron-rich carbonate and pyrite. This locality is approximately 30 m N. 35° E. of the two prospects known as the Jumbo (loc. 913, this table). The feldspar in the micropegmatite is microcline, and only traces of secondary copper minerals were noted to stain the rocks.
300	Unnamed adit	SE1/4 sec. 17, T. 29 N., R. 17 W.	Au?	An approximately 35-m-long adit initially driven N. 40° E. on a black quartz-rich lens. Exposed in the workings are a series of three northeast-striking quartz veins or stringers that are as much abundant yellow or reddish-brown carbonate and sparse amounts of weathered pyrite. Country rock consists of strongly lineated feldspathic gneiss.
303	Unnamed shaft	NE1/4 sec. 17, T. 29 N., R. 17 W.	Fe	A N. 30° W.-striking oxide facies, banded iron formation. An approximately 20-m deep vertical shaft has been sunk on the iron formation; the shaft is 13 cm wide. Associated with these veins are shaft probably follows a minor fault zone. Another shaft, approximately 100 m N. 70° W. of this

TABLE 11.—Notable occurrences of commodities in the Gold Basin-Lost Basin mining districts—Continued

Locality (pl. 1)	Name	Approximate location (UTM 10,000-m grid, zone 11)	Commodities present	Comments
303	Unnamed shaft	NE1/4 sec. 17, T. 29 N., R. 17 W.	Pb, Cu, Au	locality, has been put down on dark, manganeseiferous gossanlike stringers in brecciated and highly altered granitoid pegmatite. See figure 22 (this report) for a photomicrograph of quartz-iron oxide relations in the banded iron formation.
305	Unnamed shaft	NE1/4 sec. 17, T. 29 N., R. 17 W.	Pb, Cu, Au	Shaft along a N. 35° W.-striking, 55° NE.-dipping approximately 0.6-m-wide quartz-carbonate vein. Downward the vein feathers into a series of veinlets measuring from 2 to 8 cm wide. Yellow-brown carbonate fills the center of the veins, but much of the carbonate is intergrown with quartz. The primary minerals observed in the veins include galena, chalcopyrite, pyrite, and free gold. Secondary minerals include chrysocolla and malachite.
307	Ideas Lode 30	NE1/4 sec. 17, T. 29 N., R. 17 W.	Au?	Workings along nearly flat lying shear zone which includes irregularly distributed quartz-yellow-brown-carbonate veins nearly parallel to the shallow-dipping foliation. Some evidence for the flooding of nearby rock by yellow-brown carbonate.
308	Unnamed prospect	NE1/4 sec. 17, T. 29 N., R. 17 W.	Au?	Episyenitic apite exposed in the prospect pit. Disseminated pyrite, but relatively little carbonate and no fluorite were seen. The episyenitic apite crops out in an approximately 9-m ² area. The upper parts of the gulch in this general area include many small, irregular dikes of similar episyenitic apite.
310	Vanadinite mine (Van-Wulf)	NE1/4 sec 17, T. 29 N., R. 17 W.	V, Pb, Mo, Cu	The adit is about 15 m long, driven along a fault zone striking S. 15° E. and dipping about 70° NE. Slickensides have a variable orientation but generally they plunge moderately (50°-60°) to the north. Vanadinite and wulfenite are especially abundant in brecciated vein material and in adjacent wall rock just inside the portal. Rocks across the opencut show at least 3 m of offset. At east end of opencut is an 8-cm-thick quartz-carbonate vein, containing sporadically distributed interstitial chlorite. Minerals observed in the vein include galena, chrysocolla, wulfenite, vanadinite, red-brown carbonate, quartz, mottramite(?), chlorite, minor greenish clear calcite, and sericite. Little or no altered pyrite, no gold seen. Minor seams of episyenitic apite were observed also.

311	Unnamed adit	SE1/4 sec. 32, T. 30 N., R. 17 W.	Pb, Au, Cu	<p>A lower adit follows a well-defined fault zone 15 cm thick striking N. 80° E. and dipping 45°-50° S. Galena is rather abundant in quartz-carbonate gangue.</p> <p>Upper workings consist mostly of dump material derived by stripping overburden from vein lying along a N. 75° E., 45°-50° S.-dipping fault. No vein material ranges from 0 to 30 cm thick. No vein material seen in lower workings, which follows the fault, and the quartz+minor carbonate vein occupied a steeply plunging mullionlike opening along the fault which had no lateral extent. Some gold, but minor chrysocolla, a little unoxidized pyrite, and galena. Quartz is the major gangue together with yellow-brown carbonate. Wall rock alteration appears to be mostly introduction of carbonate. One speck of gold found in the samples.</p>
316	Unnamed drywasher site	NW1/4 sec. 23, T. 28 N., R. 18 W.	Au	<p>From approximately 12 hoppers processed through the drywasher, only a few colors were obtained</p>
319	Unnamed drywasher site	NW1/4 sec. 27, T. 28 N., R. 18 W.	Au	<p>Only one color obtained from gravelly, reddish soil which overlies hard caliche-cemented false bed rock in the Quaternary fanglomerate.</p>
324	Unnamed drywasher site	NE1/4 sec. 24, T. 29 N., R. 18 W.	Au	<p>Moderate amount of fine gold.</p>
325	Unnamed drywasher site	SW1/4 sec. 7, T. 29 N., R. 17 W.	Au	<p>Moderate amount of gold.</p>
327	Golden Mile mine	NW1/4 sec. 8, T. 29 N., R. 17 W.	Pb, Cu, Au?	<p>1-2-m-thick prominent quartz vein exposed in face west of road approximately 20 m northwest of small shack; vein strikes N. 70° W. and dips 20°-25° SW. It is offset in a reverse sense approximately 1 m by an intensely clay-altered shear zone striking east-west and dipping 40° N. Fe-bearing calcite occurs in coarsely crystalline irregular masses which are markedly tabular and form lenses striking N. 20° W. and dipping 30° SW. These lenticular and irregularly shaped calcite pods definitely are oriented obliquely to the plane of the vein and may represent replacement of earlier quartz along opened gash fractures. The bulk of this carbonate occurs along the central zone of the vein, but it is sporadically distributed throughout the length of the examined vein. A poorly developed alteration zone in the vein's walls seems to include albite and pyrite+galena and a little chalcocopyrite. A second oblique slip fault offsets the vein 1 m west of the incline. Slickensides plunge N. 65° E. at 25°.</p> <p>Crystals of feldspar (albite?), quartz, and calcite commonly reach 10 to 15 cm across in optically continuous, irregular, intergrown masses. Galena can be seen to vein or crosscut calcite, feldspar, and quartz--probably the</p>

TABLE 11.—Notable occurrences of commodities in the Gold Basin-Lost Basin mining districts—Continued

Locality (pl. 1)	Name	Approximate location (UTM 10,000-m grid, zone 11)	Commodities present	Comments
327	Golden Mile mine—Continued			galena, pyrite, and trace of chalcopyrite are somewhat later than the coarse crystalline material although all are probably related to transition pegmatite-vein processes. The vein exposed 15 m south of the portal is about 1 m thick and rather clearly the extension of the vein exposed in the small inclined shaft. Numerous east-northeast or easterly faults offset the vein, which strikes N. 70° W., 25° SW. No stipes in the adit. A trace of weathered pyrite was observed along the footwall in the adit. The prospect exposes approximately 2-m-thick pegmatite containing well-defined crudely tabular masses of fine-grained green sericite in potassium feldspar in its 15-cm-wide alteration wall zones. A specimen found on the dump of the small cut shows a remnant of a white mica book, with cleavage faces 1 cm across. Pegmatite strikes N. 40° E. and dips 80°-85° SE. No sulfides except rare pyrite pseudomorphs near the walls. Gold as much as matchhead size especially in upper reaches of small gulch.
329	Unnamed prospect	NW1/4 sec. 8, T. 29 N., R. 17 W.	Au?	
330	Unnamed drywasher site	SW1/4 sec. 31, T. 30 N., R. 17 W. (location uncertain)	Au	
341	Unnamed prospect	SE1/4 sec. 7, T. 29 N., R. 17 W.	Au?	A prospect cut poorly exposing a small quartz-carbonate-feldspar-sulfide vein of the Golden Mile type. Vein strikes north-south and is vertical. Maximum width about 0.6 m.
356	Glow in the Dark 8	SW1/4 sec. 8, T. 29 N., R. 17 W.	Pb, Cu, Au?	Prospects along wash about 0.8 km southeast of Golden Mile cabins. Open-cut on side exposes for about 8 m 15- to 25-cm-wide quartz vein striking N. 15°-20° W. and dipping 50° NE. in a shear zone of approximately the same attitude. Maximum depth of vein exposed in cut is about 5 m. The shear zone separates vertically dipping inter-layered quartzfeldspathic gneiss from amphibolite to the east. The vein pinches and swells averaging 25 to 30 cm in thickness. Galena and chalcopyrite appear disseminated in knots throughout quartz; sparse carbonate. No gold seen, but a trace has been reported. Another nearby prospect is on coarse magnetite-bearing highly fractured pegmatite containing galena and chalcopyrite (some altered to malachite). The sulfides in this pegmatite are scattered widely in white quartz as vug fillings. Somewhat anomalous radioactivity, approximately three times background.

372	Miss Texas 2	NE1/4 sec 17, T. 29 N., R. 17 W.	Au?	<p>Pyritized zone now limonitic striking N. 60° W. and parallel to foliation in the surrounding gneiss. Several quartz veins cut this 10- to 15-m-wide altered zone which can be followed toward the southeast for at least 0.3 km. Location of zone about 100 m S. 25° E. from stone monument of the Miss Texas 2.</p> <p>Two veinlets generally 2 to 8 cm thick but locally as much as 15 cm thick, striking nearly east and dipping steeply south. Abundant galena, but sparse pyrite noted. Veins cut amphibolite and gneiss. Broad open fold in amphibolite, plunging approximately 35° NW. just north of prospect. Some pyrite and altered feldspar in border alteration zone, which measures about 2 to 8 cm in thickness.</p>
374	Bluebird 17-16	NW1/4 sec 17, T. 29 N., R. 17 W.	Pb	<p>A 10-m shaft along the road 300 m south-southwest of Golden Mile cabins. Barren-looking veins, little carbonate, pyrite, and feldspar. No galena or copper minerals noted. The vein is about 0.6 m thick. A group of prospects near the west base of Lost Basin Range, approximately 1.5 km north-northwest of the Golden Mile mine. Intensely altered mylonitic coarse-grained granite or alaskite dike striking N. 20° E. and dipping 55°-60° W. parallels the adjacent well-layered quartzofeldspathic gneiss which contains abundant thin well-defined amphibolite layers. Abundant hematite with some limonite. Pyrite molds are abundant in hematitic masses along shear zone. An inclined shaft south of the wash is 10 m deep. A gneissoid very coarse grained biotite granite dike forms the footwall. There is parallel layering in quartzofeldspathic gneiss which forms the hanging wall.</p>
375	Unnamed prospect	SE1/4 sec. 7, T. 29 N., R. 17 W.	Au?	<p>North of Salt Springs Wash road. This general area shows evidence of old placering possibly in the 1930's and much more recent scraping using a small bulldozer. Possibly part of the early Summit Mining Company work. Good placer gold as much as 2 mm obtained using a drywasher. The gold is not well concentrated on bed rock but instead is distributed throughout 20 to 35 cm of dirt above earliest Proterozoic outcrop. Proterozoic rocks are quartz-mica schist and gneiss.</p>
389	Unnamed prospects	NE1/4 sec. 6, T. 29 N., R. 17 W.	Au?	<p>Some fine placer gold in heavily dug gulch. High percentage of granitoid clasts in the general area of this locality is distinctly out of proportion with the amount of granitoid rocks exposed in the Lost Basin Range.</p>
405	Twin yucca gulch	SE1/4 sec. 9, T. 29 N., R. 18 W.	Au	<p>Prospect adit about 150 m southwest of lower dump of the Golden Gate mine. The adit essentially follows a well-developed, vertical, N. 50° E.-striking fault. Conspicuous cross faults include an east-west fault dipping 5° S. A little copper staining</p>
409	Unnamed drywasher site	NW1/4 sec. 22, T. 30 N., R. 17 W.	Au	
436	Unnamed prospect	NW1/4 sec. 32, T. 30 N., R. 17 W.	Cu, Au	

TABLE 11.—Notable occurrences of commodities in the Gold Basin-Lost Basin mining districts—Continued

Locality (pl. 1)	Name	Approximate location (UTM 10,000-m grid, zone 11)	Commodities present	Comments
436	Unnamed prospect			occurs on brecciated blocks of quartz-carbonate-minor chalcocopyrite blocks. Considerable sericitization and carbonatization of the country rock. No vein material observed. A short adit directly up the ridge to the south exposes a prominent fault striking north-south to N. 10° E. This fault occurs between the brecciated footwall of an east-dipping quartz-carbonate vein which is as much as 0.6 m thick. The faulting postdates the quartz-carbonate vein whose footwall it follows. There is abundant sericitization and carbonate flooding of the quartzofeldspathic gneiss within a few meters of the vein. The brecciated vein material locally looks like that at the Cyclopic mine. A shaft at the top of the ridge is vertical and includes abundant broken-up vein quartz. Some free gold noted.
442	Unnamed prospect	NW1/4 sec. 32, T. 30 N., R. 17 W.	Pb	Small veinlets, approximately 5 to 20 cm wide, cut medium-grained quartzofeldspathic gneiss and minor amphibolite. Veins include minor galena, pyrite, carbonate, and chlorite. In addition, these veins locally develop a comb structure.
443	Unnamed prospect	NW1/4 sec. 32, T. 30 N., R. 17 W.	Cu, Au?	A small prospect pit on ridge crest at bend in ridge. A trace of copper stain occurs on an approximately 10-cm-thick vein including quartz, carbonate, some chlorite, pyrite, and possibly some gold.
444	Unnamed prospect	SW1/4 sec. 29, T. 30 N., R. 17 W.	Au?	A small prospect pit along major 10-m-wide range-front fault between iron oxide-stained quartzofeldspathic gneiss and interlayered amphibolite and caliche-cemented fanglomerate or talus. Clearly quartz-carbonate vein material is broken up in the zone, suggesting the fault zone may have followed locally an already emplaced vein system. The fault zone also shows evidence of having originally contained a lot of highly sericitized, chloritized, and carbonate-altered gneissic fragments. No sulfides or gold seen; little weathered pyrite noted.
445	Clipper	SE1/4 sec. 29, T. 30 N., R. 17 W.	Au?	Joins north endline of claims at Troy prospect and lies approximately 1 km southwest from the Scanlon mine. The quartz mass at this locality is bounded by two shear zones 15 cm thick dipping east approximately 75°. The shearing has been localized along the steep east-dipping northeast limb of a

446	Troy	SE1/4 sec. 29, T. 30 N., R. 17 W.	Cu, Au	<p>northwest-plunging fold. Gneissic-rock inclusions are sericitized and altered by carbonate. Little indication of sulfide mineralization.</p> <p>Lower adit contains a splendid example of a quartz-carbonate vein disrupted and sheared out by later faulting. Lower adit driven almost due south beneath quartz vein outcrop; adit length is about 30 m, and the vein is sheared off 15 m from portal. Footwall bounded by fault, as is hanging wall. This occurrence is a brecciated quartz vein sliver in a low-angle oblique slip fault, similar to that in the vein just west of the Golden Gate. Total vein exposed in the lower adit is about 10 m long, and it has a maximum thickness of about 1 m. No sulfides seen in lower adit.</p> <p>In main adit or Troy vein, small amount of Cu staining (malachite) and some coarse anhedral pyrite oxidizing to cellular drusy boxworks. A few small flecks of gold seen in cellular drusy "high grade." The upper prospect pit shows four vein slivers in a nearly vertical shear zone. Overall strike of the vein is N. 5°-10° E. and dips 65°-85° E. A little orange-brown carbonate occurs in the mostly quartz vein. Very little stopping. Probably no production. Prospect probably was worked in the 1930's. Veins show sheared margins containing gouge and contain milky-white quartz that is brecciated. Country rock consists of complexly and tightly folded quartz-feldspar gneiss. Wulfenite and anglesite noted.</p>
453	Scanlon mine	SW1/4 sec. 28, T. 30 N., R. 17 W.	Au, Pb, Cu, Mo	<p>Vein cutting amphibolite consists of milky quartz with irregularly distributed orange-brown carbonate with some granular chlorite in distinct irregular masses. Approximately 30 to 50 m west, other prospects show flat-lying similar veins approximately 0.3 m wide, containing traces of galena and secondary copper minerals. Workings along the same vein system as exposed at the Scanlon mine (loc. 453). At adit number 1, complexly layered folded quartzofeldspathic gneiss is exposed directly north of portal. In adit, quartz-cored pegmatite containing microcline crystals as much as 30 cm across in its outer zones crops out. No sulfides seen in rocks on the dump, but malachite occurs as minute crystals in some boxworks showing cellular structures. No stopes in adit.</p> <p>Adit number 2 is short and straight and strikes N. 15° E. Fine gold seen at several points along vein outcrop. Here, the vein apparently cuts the pegmatite as does the fault zone. Average strike of Scanlon fault-vein in the workings is north-south to N. 3° E. dipping 85° E. Some malachite, galena, and wulfenite noted in samples on dump.</p>
456	Unnamed prospects	SE1/4 sec. 29, T. 30 N., R. 17 W.	Au?, Cu, Pb	<p>Vein cutting amphibolite consists of milky quartz with irregularly distributed orange-brown carbonate with some granular chlorite in distinct irregular masses. Approximately 30 to 50 m west, other prospects show flat-lying similar veins approximately 0.3 m wide, containing traces of galena and secondary copper minerals. Workings along the same vein system as exposed at the Scanlon mine (loc. 453). At adit number 1, complexly layered folded quartzofeldspathic gneiss is exposed directly north of portal. In adit, quartz-cored pegmatite containing microcline crystals as much as 30 cm across in its outer zones crops out. No sulfides seen in rocks on the dump, but malachite occurs as minute crystals in some boxworks showing cellular structures. No stopes in adit.</p> <p>Adit number 2 is short and straight and strikes N. 15° E. Fine gold seen at several points along vein outcrop. Here, the vein apparently cuts the pegmatite as does the fault zone. Average strike of Scanlon fault-vein in the workings is north-south to N. 3° E. dipping 85° E. Some malachite, galena, and wulfenite noted in samples on dump.</p>
457	Eagle Nest	SW1/4 sec. 28, T. 30 N., R. 17 W.	Au, Cu, Pb, Mo	<p>Vein cutting amphibolite consists of milky quartz with irregularly distributed orange-brown carbonate with some granular chlorite in distinct irregular masses. Approximately 30 to 50 m west, other prospects show flat-lying similar veins approximately 0.3 m wide, containing traces of galena and secondary copper minerals. Workings along the same vein system as exposed at the Scanlon mine (loc. 453). At adit number 1, complexly layered folded quartzofeldspathic gneiss is exposed directly north of portal. In adit, quartz-cored pegmatite containing microcline crystals as much as 30 cm across in its outer zones crops out. No sulfides seen in rocks on the dump, but malachite occurs as minute crystals in some boxworks showing cellular structures. No stopes in adit.</p> <p>Adit number 2 is short and straight and strikes N. 15° E. Fine gold seen at several points along vein outcrop. Here, the vein apparently cuts the pegmatite as does the fault zone. Average strike of Scanlon fault-vein in the workings is north-south to N. 3° E. dipping 85° E. Some malachite, galena, and wulfenite noted in samples on dump.</p>

TABLE 11.—Notable occurrences of commodities in the Gold Basin-Lost Basin mining districts—Continued

Locality (pl. 1)	Name	Approximate location (UTM 10,000-m grid, zone 11)	Commodities present	Comments
464	Unnamed adit	NE1/4 sec. 32, T. 30 N., R. 17 W.	Au, Cu	Approximately 15-m-long adit driven due south. A little highly cellular boxworks on dump is presumed to be ore from this vein system. Gold seen in several samples. Some specular hematite may reflect an alteration of carbonate or pyrite. Another nearby short adit driven along a steep west-dipping shear zone shows sparse amounts of chalcopyrite associated with iron-bearing calcite. Abundant galena, wulfenite, malachite in N. 15° W.—striking vein.
466	Warren Lode 5 (Cumberland)	NW1/4 sec. 33, T. 30 N., R. 17 W.	Pb, Cu	Poorly exposed 1-m-thick feldspar-rich dikes (albite?) containing sparse amounts of quartz, iron-bearing carbonate, and pyrite. Quartzofeldspathic gneiss makes up the wall rock of this dike and within about 5 to 15 m of it the wall rock shows veining by quartz and some evidence of prophylic alteration. Numerous quartz veinlets are the range 2.5 to 10 cm wide and locally they show abundant amounts of galena, especially concentrated in the central portions.
470	Warren Lode 10	SW1/4 sec. 28, T. 30 N., R. 17 W.	Pb	Small 1-m-deep pit on ridge and main 6-m-across open trench to the northeast. The prospect is in layered amphibolite and biotite schist. No scheelite noted. Some tourmaline seen in quartz-feldspar-biotite pegmatitic-gneiss stringer. Some quartz-carbonate-pyrite-albite(?) veinlets as much as 8 cm thick. Euhedral tablets of albite(?) at extreme margins of vein. Main prospect is on southeast side of ridge 30 m northeast of small pit. The main prospect consists of an opencut 6 m long. Skarnlike amphibolite associated with quartz pods or stringers as much as 18 cm thick is exposed here. Pegmatoid gneiss also occurs in crosscutting dike as much as 8 cm thick which strikes N. 30° W. and dips 25° SW.
480	"BaBa" prospect ("Tungstake" on one 1955 claim notice)	SW1/4 sec. 4, T. 29 N., R. 18 W.	W?	Prospect across gulch to east-southeast contains more skarnlike calc-silicate rock apparently owing to the silicification of limy amphibolite or limy quartzofeldspathic gneiss. Well-layered amphibolitic gneiss strikes north-northwest dipping 30°-35° SW.
482	Unnamed prospect	NW1/4 sec. 33, T. 30 N., R. 17 W.	Au, Cu, Pb, Mo	An exposed feldspathic vein here is 45 to 60 cm thick and shows a well-developed quartz core. The vein strikes N. 55° W. and has an almost vertical dip.

Quartz-carbonate-pyrite-chalcopyrite stringers cut the south end of the vein. They are as much as 5 cm thick and strike north-south, dipping 70°-75° E. The northeast wall of the vein is a 5-cm-thick crumbly fault gouge; whereas the southwest wall of the vein is healed to country rock. A second quartz-carbonate vein strikes N. 10°-15° E. approximately one-half of the way to the top of the hill from this locality and approximately 60 m S. 10° E. of the termination of the first vein described above. The second vein is 10 to 20 cm thick, locally brecciated, and shows no apparent copper staining or sulfides. No prospects on this second vein. Rock fragments included in the second vein are intensely sericitized. There are several pegmatites of the quartz-cored and related types which strike N. 50°-60° W. and are also cut by quartz-carbonate veins.

A partial list of minerals identified in the veins includes: galena, wulfenite, malachite, chalcocite, gold (fine, fernlike in quartz and oxidized chalcopyrite), ferruginous carbonate, tenorite-cuprite(?), chrysocolla, opal, specular hematite, goethite.

483	Unnamed drywasher site	SE1/4 sec. 30, T. 30 N., R. 17 W.	Au	One moderate-sized color obtained from approximately 10 to 12 hoppers of gravel taken from two localities about 8 m apart.
498	Climax mine	SE1/4 sec. 33, T. 30 N., R. 17 W.	Pb	Vein strikes N. 18° E., dips 80° W.-NW. and swells to at least 2 m thick about 15 m south of the headframe. Massive milky quartz is present with some brecciated and recemented zones. A little carbonate, galena, pyrite molds, and honeycombed quartz showing cubic molds and elongate molds were noted. The host rocks are a sequence of granitoid gneiss within the mapped paragneiss unit.
505	Unnamed drywasher site	NE1/4 sec. 9, T. 29 N., R. 17 W.	Au	Sample of relatively small volume, approximately three hoppers, of red soil. Sample was not obtained from a good caliche horizon. One pinhead-sized color obtained.
509	Unnamed prospect	SE1/4 sec. 32, T. 30 N., R. 17 W.	Au, Cu	Prospect pit 3 m deep on lenticular, discontinuous quartz-carbonate-chalcopyrite-pyrite-gold vein. Lenticular masses of chalcopyrite and pyrite are largely altered to limonitic boxwork. No galena was noted. Gneissic inclusions are sericitized. Gold occurs along boundaries of chalcopyrite boxwork and quartz.
513	Unnamed prospect	SE1/4 sec. 32, T. 30 N., R. 17 W.	Au	Prospect in 3-cm-thick vein, showing mullionlike striae plunging 20° N.-NE. along footwall. Gold seen as fine dendritic foil in quartz. Webbed boxwork similar to that at the Golden Gate. Massive granular chlorite and sericitized quartz-feldspathic gneiss inclusions occur in the vein. Some are lined by quartz crystals and calcite. Pyrite is rather abundant but no chalcopyrite,

TABLE II.—Notable occurrences of commodities in the Gold Basin-Lost Basin mining districts—Continued

Locality (pl. 1)	Name	Approximate location (UTM 10,000-m grid, zone 11)	Commodities present	Comments
513	Unnamed prospect—Continued			galena, or copper stain observed. A second nearby prospect contains a 45- to 60-cm-thick vein including intense sericitization of the wall rock. Small crosscut adit. Massive anhedral pyrite is the only sulfide observed. There was no galena, chalcopyrite, or malachite seen at any of these largely echelon quartz veins. Numerous small quartz-carbonate stringers cut quartzfeldspathic host. Small prospect pit in chalcopyrite-quartz bodies in coarse-grained granite pegmatite. The chalcopyrite occurs locally in the feldspathic portion of the pegmatite, and mineralization is probably co-genetic with the late hydrothermal stages of the pegmatite.
546	Unnamed prospect	SE 1/4 sec. 35, T. 30 N., R. 18 W.	Cu	Breccia cemented with manganese oxide and calcite. Maximum amount of vein exposed is 20 cm. The vein cuts Proterozoic gneiss. Prospect is approximately 3 m long.
552	Unnamed prospect	(In Iceberg Canyon quadrangle) UTM: 752,500 m E., 3,987,670 m N.	Mn	Gold-bearing quartz stringers about 15 cm thick, poorly exposed in prospect pit, where they are seen to occupy a shear zone in biotite gneiss. Quartz, galena, iron-bearing calcite, albite, chlorite, pyrite pseudomorphs; trace copper stain. Free gold associated with pyrite and red chalcopyrite boxwork observed in three samples.
604	Gold Barr	NE 1/4 sec. 16, T. 29 N., R. 18 W.	Au, Pb, Cu	Sample collected from alluvial gravels along a present arroyo bottom. Collected to a depth of about 20 cm, and approximately 1 ft ³ of material put through drywasher. Few colors were obtained.
608	Unnamed drywasher site	UTM: 749,800 m E., 3,978,540 m N.	Au	Thin east-west-striking quartz vein containing fine-grained albite along its walls, orange-brown-weathering iron-bearing calcite in knots, a moderate amount of pyrite, and some galena and secondary copper minerals. Not prospected.
609	Unnamed site	UTM: 749,800 m E., 3,978,540 m N.	Pb, Cu, Au?	Abundant scheelite in crystalline masses as much as about 3 cm across. Scheelite occurs in narrow west-dipping skarn zones, developed as small pods less than 0.3 m thick adjacent to a 10-cm-thick granitic pegmatite stringer.
611	Mead Tungsten	UTM: 749,770 m E., 3,979,070 m N.	W	Trace of gold associated with oxidized blebs of chalcopyrite in quartz stringers. Stringers cut a fine-grained porphyritic granite dike exposed at southeast end of small open-cut.
623	Marihauna	NE 1/4 sec. 16, T. 29 N., R. 18 W.	Au, Cu, Pb	Microcline(?)-bearing alteration assemblages are

626	Unnamed drywasher site	SW1/4 sec. 21, T. 29 N., R. 18 W.	Au	<p>apparently similar to that noted previously at locality 19 (this table), but no fluorite was found here.</p> <p>Ferrocalsite and galena in quartz occur in surficial rubble.</p> <p>Over the hill from the highest cut, galena found in place as sparsely scattered blebs and irregular grains as much as 0.6 cm in diameter together with minor chalcopyrite. An open trench exposes vein apparently striking N. 10° W. that cuts gently east dipping gneiss. Approximately 9 m west of north end of northern prospect cut, a quartz vein is at least 12 to 15 cm thick and contains abundant galena and chalcopyrite. Narrow alteration zones and quartz seams cut a granite dike here striking most likely N. 10° W. and dipping 55° E.</p> <p>There is a moderate amount of surface scraping by bulldozer in this general area. Bed rock in this placer area consists of weathered and caliche-encrusted gently dipping gneiss. The gold and some rounded pebbles of magnetite appear to be coming off the low ridge to the northwest. Swept bed rock at head of the gulch at this site yielded not one single color, suggesting that the placer gold that was found is not local.</p> <p>Rather fair showing of placer gold in concentrates from drywasher. Some gold is approximately 1 mm across in longest dimension.</p> <p>Gold concentrated in coarse quartz gravel at scoured and winnowed head of delta in previously worked placer gravels.</p> <p>Only a trace of gold, one color, obtained in concentrate from gravels excavated from deep cracks in outcrops along main gulch. Concentrate included abundant lavender zircon and some fresh garnet.</p> <p>Two veins, approximately 6 m apart, follow shear zones developed along the schistosity in the surrounding gneiss. Quartz is the predominant mineral in the veins and only trace amounts of secondary copper minerals and galena were noted in one of the veins. In an incline, one of the veins pinches and swells along the shear zone. Adjacent to the veins where they cut amphibolite, there is a marked development of chlorite and carbonate for about 1 m.</p> <p>Vein is approximately 0 to 0.6 m thick, and it has been explored by a shaft approximately 15 m deep. Gold occurs in fine honeycomb and pyrite(?) boxwork. Minerals in the vein also include quartz, ferrocalsite, and chlorite. Chlorite most likely reflects altered fragments of country rock picked up by the vein.</p> <p>Abundant staining by secondary copper minerals occurs at this adit driven approximately N. 20° E. Another prospect approximately 20 m</p>
627	Unnamed drywasher site	SW1/4 sec. 21, T. 29 N., R. 18 W.	Au	
629	Unnamed drywasher site	SW1/4 sec. 20, T. 29 N., R. 18 W.	Au	
635	Unnamed drywasher site	UTM: 749,230 m E., 3,977,500 m N.	Au	
636	Unnamed prospects	UTM: 750,310 m E., 3,977,500 m N.	Pb, Cu	
637	Red Rattler or Richman	UTM: 749,150 m E., 3,977,170 m N.	Au	
639	Unnamed adit	UTM: 748,950 m E., 3,977,060 m N.	Cu	

TABLE 11.—Notable occurrences of commodities in the Gold Basin-Lost Basin mining districts—Continued

Locality (pl. 1)	Name	Approximate location (UTM 10,000-m grid, zone 11)	Commodities present	Comments
639	Unnamed adit—Continued			
640	Unnamed prospect	UTM: 748,670 m E., 3,977,530 m N.	Cu	north-northeast of this locality shows gneissic biotite granite cut by a 0.6-m-wide vein which is in turn cut off by a N. 10° E.—striking fault. Prospect in gently north-dipping granite gneiss. Honeycomb quartz; trace of copper stain in quartz-pyrite-chalcopyrite(?) vein. No gold observed.
641	Songbird	UTM: 749,850 m E., 3,976,890 m N.	Au, Cu, Pb	Late irregular patches of chalcopyrite, galena, pyrite pseudomorphs in irregular quartz vein; thickness approximately 0.3 to 0.6 m. Very minute gold specks associated with chrysocolla in late fractures.
642	Summit	NE1/4 sec. 16, T. 29 N., R. 18 W.	Cu	Mullion structure on footwall. Quartz vein approximately 30 to 45 cm thick, traced laterally about 1 m using float. Trace of malachite, chrysocolla, and dark-red cuprite(?). Generally poor in sulfides.
643	Pick 'N' Pan Originally named: Intention to Gold	NW1/4 sec. 16, T. 29 N., R. 18 W.	Au, Cu	Two parallel veins dip approximately 45° to 50° E., parallel to layering in surrounding gneiss. Lower vein explored by an incline sunk along the vein which is 0.3 to 0.45 m thick. Trace of gold occurs as minute inclusions in oxidized chalcopyrite. A sheared alteration zone above and below lower vein consists of orange carbonate. A third vein is poorly exposed in upper portion of the prospect and includes very minor amounts of chalcopyrite. Very fine gold, some quite flakey, collected at this locality.
644	Unnamed drywasher site	NW1/4 sec. 15, T. 29 N., R. 18 W.	Au	Prospect pit on 20- to 50-cm-thick quartz vein, containing minor pyrite, chalcopyrite, and carbonate. Considerable chlorite and carbonate alteration of the gneissic diorite country rock.
645	Unnamed prospect pit	SW1/4 sec. 15, T. 29 N., R. 18 W.	Cu	Sparsely scattered patches of altered chalcopyrite and pyrite are included in milky-quartz vein. Trace amounts of gold occur as minute platelike inclusions in pyrite and possibly in chalcopyrite.
646	Merrieta	SW1/4 sec. 15, T. 29 N., R. 18 W.	Au, Cu	Open stope along vein and inclined shaft suggest that gold was once much more plentiful than may be inferred from samples now available. Very few sulfides overall, however.
647	Unnamed prospect (part of Gold Hill workings)	NE1/4 sec. 16, T. 29 N., R. 18 W.	Cu, Au?	Swarm of veins and associated altered country rock exposed in prospect cut. Overall shear zone strikes about N. 35° W. dips approximately 40° NE. Irregular main vein contains pyrite and patches of chalcopyrite generally less than 2 cm across almost completely altered to dark-red

648	Gold Hill mine	NE1/4 sec. 16, T. 29 N., R. 18 W.	Au	Intermittent production of gold from 1930 to 1942 (see text, this report).	mineral and chrysocolla. No gold observed. Country rock is altered diorite gneiss. In uppermost portion of prospect, a vein approximately 10 to 15 cm thick cuts a gently dipping leucogranite pegmatite dike. Minor amounts of carbonate pyrite and oxidized chalcopyrite are included within this vein.
651	Smoky (or Highline)	NW1/4 sec. 16, T. 29 N., R. 18 W.	Cu, Au, Pb	Irregular and brecciated vein approximately 10 to 15 cm thick, dips gently to the northeast. Six adits are driven to intersect the vein, in total, they aggregate approximately 90 m of workings. Minor oxidized chalcopyrite occurs as late fracture fillings and irregular patches. Minor galena, mostly altered to cerussite, occurs as blebs filling quartz-lined vugs. Gold occurs as minute grains in oxidized pyrite and quartz.	
653	Unnamed prospects	UTM: 749,440 m E., 3,977,060 m N.	Au, P, Cu, Ba	A series of pods and stringers of quartz veins emplaced along what appears to be a N. 80° W.-striking and 35°-50° N.-dipping shear zone. An early quartz-carbonate-pyrite-galena-chalcopyrite-gold assemblage in the veins has been brecciated and cut by subsequent seams of white calcite, limonite, and barite. Bladed groups of thin barite crystals fill vugs from which the early carbonate has been leached. Considerable free gold found along pyritic seams in large quartz blocks on the easternmost dump along these workings. Galena and chalcopyrite are also abundant. Country rock consists of an altered granitic gneiss sequence within the gneiss unit.	
654	Unnamed adit	UTM: 748,710 m E., 3,978,170 m N.	Au?	An approximately 1.5-m-long adit underlies a 40-cm-thick milky-quartz vein. The close association of an altered pegmatite beneath the vein may indicate that the vein itself may be the quartz-core portion of a small pegmatite-vein system here. No sulfides or secondary copper minerals were observed. A quartz pod approximately 1.2 m thick is exposed 30.5 m northeast of the prospect; it also may be related to the pegmatite.	
657	Gold Bond	UTM: 748,650 m E., 3,977,450 m N.	Au, Pb, Cu	Massive milky-quartz veins are cut by many low-angle faults. Along the Gold Bond incline, several quartz veins approximately 1.7 m thick do not show significant alteration of the adjoining country rock. However, seams of pyrite voids and boxworks honeycombed by quartz are distributed throughout the vein parallel to its surface. Unaltered pyrite, chalcopyrite, and galena found in trace amounts. No gold was observed in place within the workings, although chalcopyrite and associated gold were found in an ore sample at the miners' camp. Mine predominantly worked during 1910-20. A second period of occupation of the workings occurred during the following depression.	

TABLE 11.—Notable occurrences of commodities in the Gold Basin-Lost Basin mining districts—Continued

Locality (pl. 1)	Name	Approximate location (UTM 10,000-m grid, zone 11)	Commodities present	Comments
659	Solomon	UTM: 748,590 m E., 3,976,540 m N.	Au?	A simple, massive, milky-quartz vein about 0.6 m thick. An approximately 3-m-deep prospect shaft penetrates the vein at approximately 1.5 m below the surface. Cubic pyrite boxwork, partially filled by jarosite(?), is present in outcrop. No sulfides were observed.
664	Unnamed site	SW1/4 sec. 4, T. 29 N., R. 18 W.	Fe	An approximately 20-cm-thick sequence of highly magnetic iron-formation crops out at this locality. The iron-formation is conformable with the surrounding amphibolite and mafic schist. In this general area, there are also some centimeter-sized tourmaline-bearing pegmatitic dikes which crosscut sharply the layering in the amphibolite and quartzofeldspathic gneiss.
668	Unnamed prospect	UTM: 749,660 m E., 3,978,160 m N.	Cu	A 20-cm-wide quartz-ankerite-pyrite vein contains trace amounts of secondary copper, and honeycomb partings. No gold was observed.
675	Unnamed site	UTM: 749,650 m E., 3,981,510 m N.	W	Calc-silicate rock and stringers of marble occur in a zone as much as 0.6 m thick, largely adjacent to 2- to 15-cm-thick sills and pods of quartz-rich leucogranitic pegmatite. Generally, the overall zone of calc-silicate rock and marble is enclosed within laminated amphibolite. The presence of scheelite in the calc-silicate rocks was verified using a black light. In addition, approximately 30 m north of the locality there is a post-regional-metamorphic granite dike striking approximately N. 10° W.
676	Unnamed site	UTM: 749,560 m E., 3,981,030 m N.	Cu	A 20-cm-wide quartz-ankerite (or siderite)-chalcocopyrite vein crops out here. No gold or galena found.
678	Unnamed prospects	NW1/4 sec. 34, T. 30 N., R. 18 W.	Cu, Au?	Prospects at top of peak show quartz-ankerite-sericite-pyrite veins. Trace secondary copper present, and some gold was observed. The remoteness and amount of past work done at the site suggest that some gold must have been found here previously.
687	Unnamed site	SE1/4 sec. 28, T. 30 N., R. 18 W.	Ba	Group of approximately N. 10° W.-striking veins which dip 30°-35° NE. crop out here. Irregular stringers and elongate masses of coarsely crystalline barite are somewhat abundant in this general area as late fillings of echelon gashes. Ankerite is associated with the barite, and an albite-pyrite-ankerite assemblage is common along the walls of individual veins.

689	Unnamed site	NE1/4 sec. 28, T. 30 N., R. 18 W.	Ba	<p>Veins showing an assemblage of quartz, carbonate, barite, albite, and pyrite crop out here. There is considerable albite along the wall zone of the veins. The main vein here measures about 20 cm thick, but several others are about 2 to 5 cm thick.</p>
690	Unnamed site	NE1/4 sec. 29, T. 30 N., R. 18 W.	Ba, Cu	<p>A 0.6-m-thick vein here includes chalcopyrite in its quartz-carbonate-barite-albite-pyrite assemblage.</p>
735	Unnamed prospects	UTM: 747,180 m E., 3,984,640 m N.	Au	<p>Gold was observed at five different prospects in this general area. A deep vertical shaft approximately 30 m deep had the largest amount of secondary(?) gold (see fig. 41). The veins generally pinch and swell irregularly and are composed essentially of quartz, carbonate, pyrite, and gold. They may be Proterozoic in age (see text).</p>
754	Unnamed prospect	UTM: 746,850 m E., 3,984,420 m N.	Hg?	<p>An adit approximately 9 m long intersects a gently south-dipping shear zone. Apparently, the prospect was for mercury, as the remains of an old hearth and a stockpile of hematitic schist suggests that the early prospectors mistook this for cinnabar.</p>
800	Unnamed site	SW1/4 sec. 35, T. 28 N., R. 18 W.	Au?	<p>Leucosyenitic pipe, elongate in a northeasterly direction crops out at this locality. Its overall dimensions at the surface are about 20 by 60 m. The pipe contains a quartz-free central zone which also shows fairly abundant concentrations of fluffy orange iron oxide(s) replacing iron carbonate. The outer portion of the pipe shows increasing concentrations of quartz in irregularly distributed stringers and veinlets. Although this locality shows no fluorite or obvious pyrite, the pipe here is nonetheless similar to that at locality 19 which contains visible disseminated gold.</p>
802	Unnamed site	SE1/4 sec. 34, T. 28 N., R. 18 W.	F	<p>Quartz-fluorite vein crops out here and shows an average thickness of about 20 cm. The quartz is intergrown with the variably colored fluorite, which ranges from colorless to deep purple.</p>
803	Unnamed site	SE1/4 sec. 34, T. 28 N., R. 18 W.	F, Au?	<p>An approximately 2-cm-wide quartz-fluorite-specularite-pyrite vein crops out here. One possible speck of free gold observed in limonitic boxworks after pyrite. Bleaching and the possible introduction of feldspar extends into the country rock for about 2 cm adjacent to the vein.</p>
804	Unnamed site	SE1/4 sec. 34, T. 28 N., R. 18 W.	F	<p>Fluorite occurs as coarsely crystalline knots in a quartz-fluorite-chlorite-iron carbonate-hematite-pyrite vein. The vein has a maximum observed thickness of about 20 cm.</p>
810	Unnamed site	SW1/4 sec. 34, T. 28 N., R. 18 W.	F, Pb	<p>A quartz-carbonate-fluorite-chlorite-galena vein system cuts a mixed zone of Early Proterozoic biotite monzogranite and porphyritic monzogranite. Most of the veinlets in the system measure about 0.6 cm thick, and they contain colorless fluorite.</p>
811	Unnamed site	SW1/4 sec. 34, T. 28 N., R. 18 W.	F	<p>A quartz-purple fluorite veinlet parallels the local northwest-striking joint set in the porphyritic monzogranite.</p>

TABLE 11.—Notable occurrences of commodities in the Gold Basin-Lost Basin mining districts—Continued

Locality (p. 1)	Name	Approximate location (UTM 10,000-m grid, zone 11)	Commodities present	Comments
812	Unnamed site	NW1/4 sec. 34, T. 28 N., R. 18 W.	F	Quartz-fluorite-iron carbonate-pyrite-chlorite veinlets fill northeast-striking joints.
815	Unnamed site	NW1/4 sec. 34, T. 28 N., R. 18 W.	F	Quartz-fluorite-pyrite and quartz-pyrite veinlets as much as 15 cm thick fill northeast-striking steeply dipping joints.
817	Unnamed site	NW1/4 sec. 34, T. 28 N., R. 18 W.	Cu	An approximately N. 15° E.-striking and 75° NW.-dipping vein includes quartz, pyrite, chlorite, and secondary copper mineral(s).
820	Lady Mary	SW1/4 sec. 27, T. 28 N., R. 18 W.	F, Pb, Cu, Au	Numerous parallel veins and veinlets, less than or equal to 15 cm thick parallel the jointing in coarse-grained porphyritic monzogranite. Pale-lavender fluorite is in association with brown carbonate in quartz-lined cavities. There are abundant indications of galena and alteration products of chalcopyrite; numerous zones of small (less than 2 mm) pyrite molds and pseudomorphs; and minor unaltered pyrite. These veins were explored by three small inclines, but apparently the veins pinch out with depth as they are exposed only in the opencuts.
821	Unnamed prospect	SW1/4 sec. 27, T. 28 N., R. 18 W.	F	Vein cuts coarse-grained porphyritic monzogranite. Purple fluorite occurs with pyrite along late hypogene fractures and in masses about 1.0 cm across in milky quartz. No galena, gold, or copper stain was observed. The vein probably was emplaced along a northeast-striking fault as suggested by an intensely altered and friable zone at least 0.6 m thick along the footwall of the vein.
823	Unnamed site	SE1/4 sec. 28, T. 28 N., R. 18 W.	F	A quartz-fluorite-pyrite-chlorite-bearing vein strikes approximately N. 50° E., and dips 35°-40° NW. The vein is as much as 0.3 m thick and can be traced at the surface for a distance of about 30 m along strike. The fluorite in the vein consists of coarsely crystalline masses as much as 6 cm across.
824	Unnamed drywasher site	SW1/4 sec. 4, T. 27 N., R. 18 W.	Au	Fine particles of detrital gold are moderately abundant in gravel on a somewhat consolidated, reddish-brown clay soil. This soil fills irregularities developed in the true bed rock here. However, the reddish-brown soil does not itself contain placer gold particles.
828	Unnamed prospect	NW1/4 sec. 4, T. 27 N., R. 18 W.	Cu	Relatively abundant iron oxides replacing chalcopyrite in wispy quartz stringers following a N. 70° E.-striking and north-dipping shear zone. Considerable silicification along the zone.

831	Unnamed site	SE1/4 sec. 32, T. 28 N., R. 18 W.	F	An approximately 3-cm-thick quartz-pyrite-fluorite-carbonate vein cuts porphyritic monzogranite at this locality. The vein strikes N. 65° E. and dips 70° SE.
832	Unnamed site	SE1/4 sec. 32, T. 28 N., R. 18 W.	F	At this locality, two veins crop out about 1 m apart. The mineralogy of the veins includes quartz, pyrite, pale-lavender fluorite, carbonate, white mica, and possibly potassium feldspar.
834	Unnamed shaft	SW1/4 sec. 33, T. 28 N., R. 18 W.	Pb, Cu, Au	Quartz veins, as much as 20 cm wide, appear to parallel a strongly developed foliation in a N. 35° E.-striking shear zone in cataclastically deformed porphyritic monzogranite. The porphyritic monzogranite contains some scattered patches of galena and secondary copper minerals. One small grain of gold was noted.
835	Unnamed site	NW1/4 sec. 33, T. 28 N., R. 18 W.	Cu, Pb, Au	Several quartz-pyrite-carbonate-chalcopyrite-galenite (trace) veins cut coarse-grained porphyritic monzogranite. Gold occurs as minute grains in iron oxide-stained cavities possibly reflecting the former presence of chalcopyrite. In addition, a hornblende porphyry dike crops out at this locality and strikes northeasterly.
836	Unnamed prospect	SE1/4 sec. 33, T. 28 N., R. 18 W.	F, Pb	A quartz-fluorite-pyrite-galena (trace) vein strikes N. 25° E. and dips 80° NW. Fluorite in the vein is as much as 4-cm-across and varies from colorless to dark purple.
837	Unnamed site	SW1/4 sec. 32, T. 28 N., R. 18 W.	F	Two quartz-fluorite-white mica veins crop out here approximately 3 m apart. The veins strike approximately N. 65° E. Greisen occur in the surrounding coarse-grained porphyritic monzogranite and includes some pyrite and feldspar. A potassium-argon age determination of white mica from these veins yielded an age of 65.4 Ma (see table 3).
838	Unnamed site	NE1/4 sec. 32, T. 29 N., R. 18 W.	F	Quartz-pyrite-fluorite veinlets in porphyritic monzogranite strike N. 20°-25° E. and dip 70° NW. In addition, several mafic dikes at this locality parallel the trend of the veins, but no veins were observed to cut the mafic dikes.
856	Unnamed prospect	SE1/4 sec. 30, T. 28 N., R. 18 W.	Au?	Prospect sunk on a 15- to 20-cm-thick, brecciated quartz-carbonate-pyrite vein. Further, a nearly flat lying shear zone is exposed throughout the prospect pit. The shear zone includes abundant sericitized and broken-up schist.
858	Red Cloud	NW1/4 sec. 31, T. 28 N., R. 18 W.	Cu	Approximately 30-m-long adit and 5-m raise to surface along quartz-pyrite-carbonate-chalcopyrite (trace) veins cutting porphyritic monzogranite. Numerous minor faults in the workings show shallow dips.
868	Cyclopic 6 prospects	NE1/4 sec. 25, T. 28 N., R. 19 W.	Au?	Major splay of detachment-fault zone containing red-brown gouge and comminuted monzogranite cuts through the prospects. A minor fault strikes N. 10°-15° E., and dips approximately 40° W.; it is possibly parallel to the main fault system. Quartz-carbonate-pyrite veins and recemented quartz breccia of the Cyclopic type occur in the gouge zone.

TABLE 11.—Notable occurrences of commodities in the Gold Basin-Lost Basin mining districts—Continued

Locality (pl. 1)	Name	Approximate location (UTM 10,000-m grid, zone 11)	Commodities present	Comments
868	Cyclopic 6 prospects—Continued		Pb, Cu, Au, Mo	Approximately 150 to 300 m southeast of this locality, there are numerous prospects, pits, and trenches in the lower gouge zone. Vein quartz is brecciated and widely scattered in the gouge as blocks 0.6 m long and approximately 0.3 m thick. Veins contain galena, pyrite, iron carbonate, malachite (alteration of chalcopyrite(?)), wulfenite, gold, and cerussite. Brilliant crimson mineral may be cuprite. Red, brown, and black iron and manganese(?) oxides are relatively abundant. Two prospect pits expose approximately 2 m of friable, coarse-grained, porphyritic monzogranite. The entire ridge to the east has similar lithology. Several thin seams of gouge dip gently to the southwest.
869	Unnamed prospect	NE1/4 sec. 25, T. 28 N., R. 19 W.	Au?	A shaft is sunk on a late Tertiary fault zone and sheared Proterozoic rocks and Miocene and (or) Pliocene fanglomerate.
871	Fry mine	NE1/4 sec. 25, T. 28 N., R. 19 W.	Au?	Fine-grained granular quartz veins containing numerous thin seams of pyrite in cubes. Several minor shear zones are present, yet there is no brecciation of the veins themselves. Country rock is foliated and sericitized, coarse-grained porphyritic monzogranite.
872	Beppo	SE1/4 sec. 32, T. 28 N., R. 18 W.	Au?	Quartz-carbonate (minor)-pyrite-fluorite-white mica veins cut the Late Cretaceous two-mica monzogranite. Abundant quartz-white mica-fluorite veins and veinlets cut the Late Cretaceous two-mica monzogranite. The fluorite in these veins is colorless and as much as 8 cm thick.
876	Unnamed site	NE1/4 sec. 24, T. 28 N., R. 19 W.	F	A local swarm of nearly vertical, quartz-pyrite-white mica veinlets shows white mica-fluorite-quartz-potassium feldspar alteration assemblages in the adjacent two-mica monzogranite. In addition, small cubes of pyrite are oxidizing to red and yellow iron oxide(s) in some of the fluorite-bearing assemblages.
877	Unnamed site	NE1/4 sec. 24, T. 28 N., R. 19 W.	F	Prospect adit driven into a major splay of the detachment-fault zone which crops out at the Cyclopic mine area. In the adit, friable and cemented Cyclopic-type quartz is exposed. The quartz vein is oxidized and contains abundant cerussite.
878	Unnamed site	NE1/4 sec. 24, T. 28 N., R. 19 W.	F	Quartz-pyrite-chalcopyrite-white mica-potassium feldspar-specular hematite vein, approximately 5 to
885	Unnamed adit	NE1/4 sec. 25, T. 28 N., R. 19 W.	Pb	
887	Unnamed prospect	SW1/4 sec. 19, T. 28 N., R. 18 W.	Cu	

889	Unnamed shaft	SW1/4 sec. 29, T. 28 N., R. 18 W.	Au?	45 cm thick. Immediate country rock consists of a septum of metamorphic rocks that have been engulfed by the two-mica monzogranite. Shallow, 8-m-deep shaft is sunk in gneiss intruded by numerous biotite minette(?) and fine-grained andesite dikes. No obvious signs of mineralization present.
891	Unnamed prospects	NE1/4 sec. 30, T. 28 N., R. 18 W.	Pb	Series of prospects along generally east-west-striking structures crop out in the vicinity of this locality. One quartz vein (probably 15 to 30 cm thick) lies along a N. 85° E.-striking fault. Movement along the fault probably is premineralization. Abundant cerussite, minor galena, and some pyrite molds were noted locally. Numerous quartz veins and pods occur along a sericitized and deformed contact zone between medium-grained gneissic biotite granodiorite and leucocratic granite-bearing metamorphic complex. The easternmost prospect pits were sunk on two quartz-pyrite-galena-cerussite veins 15 to 30 cm thick.
897	Golden Rule mine (Gold Day mine)	NW1/4 sec. 29, T. 28 N., R. 18 W	Au, Pb	At top of hill, a shaft 6 m deep is sunk on a quartz vein 0.9 to 1.2 m thick, striking N. 20° E. and dipping 45° SE. Pyrite and other sulfides are concentrated along late hypogene fractures parallel to the overall strike of the vein. Only a small percentage of the vein is mineralized. Downhill to the east, the vein strikes N. 35° E., dips 20° SE. and is from 0.15 to 1.2 m thick. Here, the vein pinches and swells, cutting strongly sheared gneiss or medium-grained granodiorite, and it includes a quartz-iron carbonate-chlorite-pyrite-galena-sphalerite(?) -chalcopyrite(?) assemblage. Chrysocolla is abundant; no chalcopyrite was observed, although it may be present. Mineralogy of the north-northeast-striking, gently to moderately southeast dipping vein includes quartz, pyrite, galena, and cerussite. Trace amounts of secondary copper minerals were noted. Gold was found in the dump of the main shaft, approximately 30 m north-northeast of the hilltop. Veinlets locally cut hydrothermally altered alaskite. A fine-grained granular quartz-galena vein includes a trace of copper stain.
900	Mountain View 2	SE1/4 sec. 20, T. 28 N., R. 18 W.	Cu, Pb	Incline workings have a maximum depth of about 12 m, and include a short, approximately 7-m-long drift along a minor fault. Traces of galena and secondary copper minerals were noted.
902	Unnamed shaft	SE1/4 sec. 20, T. 28 N., R. 18 W.	Cu, Pb	Uppermost working is a 9-m-long, 0.6- to 3.1-m-deep opencut; along a N. 50° E. striking, 75° SE.-dipping fault vein. The vein contains minor chalcopyrite, galena, and pyrite.
903	Ridgetop prospect (Never-get-left)	SE1/4 sec. 20, T. 28 N., R. 18 W.	Cu, Pb	The prospect pit is approximately 1.5 m deep and cuts an irregular quartz-galena-sphalerite(?) -chalcopyrite-pyrite vein. Wulfenite is abundant; chalcopyrite and pyrite are rare. No free gold was found after an extensive search.
904	Unnamed prospect	SW1/4 sec. 28, T. 28 N., R. 18 W.	Zn?, Pb, Cu, Mo	

TABLE 11.—Notable occurrences of commodities in the Gold Basin-Lost Basin mining districts—Continued

Locality (pl. 1)	Name	Approximate location (UTM 10,000-m grid, zone 11)	Commodities present	Comments
909	Unnamed prospect	SW1/4 sec. 20, T. 28 N., R. 18 W.	Cu, Pb	A 0.6-m-thick quartz-galena-chalcopyrite vein here dips about 45° S. and strikes N. 85° E.
911	Unnamed adit	Location uncertain	Pb, Cu, Au, Mo	Irregular sulfide-bearing quartz pods and stringers, parallel to foliation in sheared mafic gneiss. The veins have been deformed by the regional metamorphic events (see text). Sulfides include galena, chalcopyrite, pyrite, minor secondary cerussite, wulfenite, and green-blue copper stains.
913	Jumbo prospect	SW1/4 sec. 19, T. 28 N., R. 18 W.	Au?	Main vein is 2.4 to 3 m thick, strikes N. 10° W., and has a vertical dip. The vein crops out continuously for approximately 140 m and appears to branch out into several veins at its north end. In the main prospect pit, which is about 3 m deep, the vein is 3.1 m thick and dips 80° E., cutting the gently northeast dipping gneiss.
913a	Unnamed prospect	SW1/4 sec. 19, T. 28 N., R. 18 W.	F	A second vein, 2 to 3 m thick, lies 30 m to the west and crops out for 30 m. The strike is N. 10° W., dip vertical. Veins consist of quartz, minor pyrite, trace sericite, and trace ferrocyanate. No copper, lead ore, fluorite, or gold was observed, however.
917	Unnamed site	NW1/4 sec. 19, T. 28 N., R. 18 W.	F	Massive quartz vein appears to dip 30° SE. and is intimately associated with two-mica monzogranite and pegmatite. Feldspar, muscovite, fluorite, and minor pyrite occur as thin seams less than 2.5 cm thick. The veins cut and are mutually cut by the monzogranite, suggesting a genetic relation.
920	Patsy (Neglected)	NW1/4 sec. 20, T. 28 N., R. 18 W.	Pb, Cu	Quartz-pyrite-white mica-fluorite veinlets as much as 5 cm thick cut a fine-grained facies of the two-mica monzogranite.
921	Unnamed prospect	SW1/4 sec. 17, T. 28 N., R. 18 W.	Pb, Ag	Several prospect pits on a gently southwest dipping quartz-pyrite-galena-chalcopyrite vein, 0.9 to 1.2 m thick. Also present are cerussite, chrysocolla, pyrite voids, and boxworks.
923	Unnamed site	NW1/4 sec. 19, T. 28 N., R. 18 W.	F	Considerable galena and cerussite exposed in a small pit. Country rock consists of quartzofeldspathic gneiss, amphibolite, and biotite sequences of the paragneiss unit.
				An approximately east-west-striking vertical vein cuts the two-mica monzogranite and the adjoining gneiss. The vein includes quartz, pyrite, white mica, and fluorite. Some of the fluorite cubes are 5 cm on a side. A potassium-argon age determination on white mica from this vein yielded an age of 68.8 Ma (see text and table 3, this report).

927	Shelby mine (Harmonica)	NW1/4 sec. 17, T. 28 N., R. 18 W.	Au, Pb, Cu, V, Mo	Hilltop prospect pit exposes a pod of quartz-chalcopyrite-galena that is approximately 1.8 m thick. Examination of mineralogy on samples from dump revealed abundant gold approximately 1 mm in diameter; galena, minor altered chalcopyrite, pyrite, wulfenite, vanadinite, chrysocolla, copper stain.
928	Unnamed adit	SE1/4 sec. 17, T. 28 N., R. 18 W.	Au, Pb, Cu	Lower adit is approximately 14 to 15 m long. Workings are along a quartz-galena-cerussite-gold-altered chalcopyrite (malachite) vein, approximately 0.9 m thick.
929	Gold Street (also titled Climax group)	NE1/4 sec. 17, T. 28 N., R. 18 W.	Pb, Cu, V, Mo	Main shaft inaccessible but was approximately 9 m deep. A quartz-pyrite-iron carbonate-galena-chalcopyrite-chlorite vein is poorly exposed. It appears to strike N. 25°-30° W. Some vanadinite, wulfenite, and copper stain were observed also.
931	Big Lease	NW1/4 sec. 8, T. 28 N., R. 18 W.	Trace Cu	Prospect pit is approximately 3 m deep on a zone of quartz-pyrite-chlorite-sparse chalcopyrite veins, 1.5 m thick. The veins are fractured, brecciated, and recemented somewhat similar to ore at the Cyclopic mine workings.
931a	Unnamed prospect	NW1/4 sec. 8, T. 28 N., R. 18 W.	Au	A small opencut, about 3 m deep and 12 m long, lies in a zone of brecciated quartz lenses in a northwest-striking shear zone. Float suggests that this system of veining is the continuation of the zone of quartz veins extending through the Shelby mine (loc. 927). Vein includes quartz, pyrite, carbonate, chlorite, and gold.
933	Unnamed prospect	NW1/4 sec. 5, T. 28 N., R. 18 W.	Trace Cu	Pit on quartz-pyrite-carbonate-chlorite vein, approximately 2.4 m thick. A trace of copper stain was observed on float. The vein strikes approximately east-west and dips 35° N.
934	Star Extension 2	SW1/4 sec. 16, T. 28 N., R. 18 W.	Cu, Pb, Mo, Au?	Upper pit is on a quartz-pyrite-chalcopyrite-galena vein that ranges from 2.5 to 25 cm(?) thick. Minor chrysocolla and wulfenite present. No gold was observed. The vein strikes N. 25° E. and dips 75° SW. A mafic dike approximately 3 m thick is in the hanging wall of the vein and has a chilled margin against the vein.
935	Morning Star	SW1/4 sec. 16, T. 28 N., R. 18 W.	Au?	Morning Star is a shaft with a short connecting adit.
935a	Saint Charles	SE1/4 sec. 16, T. 28 N., R. 18 W.	Pb, trace Cu, Au?	Quartz-pyrite-galena-trace copper-bearing vein, 7 to 25 cm thick, strikes N. 10° E., and dips 35° E.
938	Round Top	NW1/4 sec. 22, T. 28 N., R. 18 W.	Pb, Cu, Au?	Quartz-pyrite-galena-chrysocolla vein occurs in a lens less than 0.9 m thick. Also present are cerussite and malachite.
938a	Unnamed adit	NW1/4 sec. 22, T. 28 N., R. 18 W.	Au, Pb, Cu	Vein and veinlets are concentrated in a shear zone. Country rock includes gneissic granodiorite below shear zone and paragneiss above the shear zone. At this locality, a prospect pit in lower plate of gneissic granodiorite has been dug on rocks cut by numerous small quartz veinlets. This pit lies approximately 15.2 m below a N. 65° E., 25° SE.-dipping fault zone. The main quartz-pyrite-galena-chalcopyrite (cerussite-malachite)-gold vein near

TABLE 11.—Notable occurrences of commodities in the Gold Basin-Lost Basin mining districts—Continued

Locality (pl. 1)	Name	Approximate location (UTM 10,000-m grid, zone 11)	Commodities present	Comments
938a	Unnamed adit—Continued			
940	Claude (Eastside)	NW1/4 sec. 22, T. 28 N., R. 18 W.	Au, Cu, Pb	here, however, is less than 7.6 cm thick and lies within the fault zone. Adit is 1.2 m in length. Quartz-iron carbonate-pyrite-galena-chalcopyrite (minor)-gold vein is hosted by gneiss. Vein strikes N. 75° E. and dips 50° NW.
941	Lester 1 and 2	SW1/4 sec. 15, T. 28 N., R. 18 W.	Pb, Au	An approximately 8-m-long adit is driven along a southeast-dipping fault zone in gneiss. The quartz vein is fragmented and recemented, and overall is not notably mineralized except at the north end where galena, cerussite, pyrite, and trace gold were observed.
942	Ridge Lode (For Years)	SE1/4 sec. 16, T. 28 N., R. 18 W.	Pb, Cu, Au	A quartz-pyrite-galena-carbonate-chalcopyrite-gold-bearing vein is 0.3 m thick here; it strikes approximately N. 45° E. and dips 40° SE.
947	Unnamed prospect	NW1/4 sec. 28, T. 28 N., R. 18 W.	Pb, Cu	Galena and copper stain noted in a small prospect pit dug on the ridge line, approximately 30 m south of the contact between gneissic granodiorite and porphyritic monzogranite.
948	Grand View	SE1/4 sec. 10, T. 28 N., R. 18 W.	Au, Cu, Pb	Prospects and opencuts lie on group of echelon veins striking N. 55°-75° W. and dipping 55°-70° NE. Lower adit is approximately 7 m long and includes a 7-m opencut driven on a N. 45° W.-striking, 65° W.-dipping fracture zone containing irregular quartz, iron carbonate, and pyrite veinlets. The fracture zone is 5 cm wide in the gneissic granodiorite. A second adit uphill is about 13 m long and was driven along a quartz vein system varying from 1 to 60 cm in thickness; it occupies a N. 55° W.-striking, 55° NE.-dipping fault in the gneissic granodiorite. The system consists mostly of a zone 8 cm to 0.6 m wide that is made up of branching quartz veinlets. A third prospect here explores a fracture-vein system which strikes N. 75° W. and includes individual quartz veinlets as much as 8 cm wide. Sericitization of the gneissic granodiorite extends about 3 m out from the fracture-vein system. Free gold was noted in oxidized vein material on the dump. Individual veins may include variable amounts of galena, chalcopyrite, quartz, carbonate, pyrite, cerussite, and limonite.
949	Valley View 2	SW1/4 sec. 10, T. 28 N., R. 18 W.	Cu, Pb, Au?	Two prospect shafts approximately 5 to 6 m deep explore a 75-cm-wide vein of white quartz containing less than 1 percent overall pyrite, chalcopyrite, iron carbonate, and gold(?).

952	Valley View	SW1/4 sec. 10, T. 28 N., R. 18 W.	Au?	There are two shafts near this locality. Southern shaft exposes 3-m-wide contorted gouge zone containing blocks of vein quartz as much as 1 m long. The mineralogy of the veins includes quartz, carbonate, and pyrite.
957	Unnamed placer workings	SE1/4 sec. 28, T. 29 N., R. 18 W.	Au?	Gulches in this general area have been placered very heavily during several intervals of what appears to have been prolonged occupations.
964	Unnamed placer workings	NW1/4 sec. 29, T. 29 N., R. 18 W.	Au?	Gulches on both sides of the road in this general area were worked extensively for their placer gold content. Apparently the placer gold was concentrated on fractured but coherent gneissic basement rocks.
967	Unnamed prospects	NE1/4 sec. 31, T. 29 N., R. 18 W.	Cu, Pb, Au?	Four shallow prospect pits, the deepest of which is about 4 m, explore a series of northeast-striking southeast-dipping milky quartz veins. The veins contain local concentrations of chalcopyrite, galena, and carbonate. The veins are lenticular and branch approximately parallel to foliation in the paragneiss country rock.
968	Unnamed drywasher site	NE1/4 sec. 32, T. 29 N., R. 18 W.	Au	Placer gold occurs in particles approximately 1 mm across. The gold is hosted widely by the slopewash debris and is associated with relatively sparse concentrations of magnetite.
971	Unnamed drywasher site	NW1/4 sec. 31, T. 29 N., R. 18 W.	Au	Several small colors and one cerussite-encrusted pebble of galena were obtained from material collected from a small gully cut in Tertiary and (or) Quaternary gravel. False bed rock is not well-cemented by caliche but instead consists of gravel cemented by a red clay-rich matrix.
972	Unnamed drywasher site	NW1/4 sec. 1, T. 29 N., R. 19 W.	Au	Some relatively coarse placer gold, with particles measuring more than 1 mm across, was obtained from a heavily worked gulch approximately 200 m northeast of the cabin at Owens mine.
973	Owens mine	NW1/4 sec. 1, T. 28 N., R. 19 W.	Cu, Fe	Underground workings at the mine probably measured at least 100 m. Headframes and ladders have been removed. Considerable chrysocolla and malachite occur as staining along a narrow fault zone which parallels the gneissic layering in its hanging wall. There is a slight discordance of the fault plane with the attitude of the layering in the footwall gneiss. Amphibolite and biotite gneiss are the main rock types in the mine area, but at least one 0.6-m-thick bed of laminated iron formation crops out at several points southwest and west of the main shaft. Calc-silicate rock is cut locally by quartzose veins or pegmatitic alaskite. The veins include fine-grained granular quartz, iron carbonate, specularite, pyrite, and secondary copper minerals. Sericitization is intense and widespread.
973a	Hope	NW1/4 sec. 1, T. 28 N., R. 19 W.	Cu	A shallow 3-m pit shows altered and copper-stained schistose cataclastic gneiss. Malachite, cuprite(?), and chalcopyrite occur in veinlets as

TABLE 11.—Notable occurrences of commodities in the Gold Basin-Lost Basin mining districts—Continued

Locality (pl. 1)	Name	Approximate location (UTM 10,000-m grid, zone 11)	Commodities present	Comments
973a	Hope---Continued			
974	Unnamed drywasher site	SE1/4 sec. 36, T. 29 N., R. 19 W.	Au	much as 2.5 cm wide. They parallel foliation and layering. Brecciated zones in the gneiss are cemented by iron and copper oxide minerals. Relatively abundant and moderately coarse fragments of detrital gold obtained entirely from Tertiary and (or) Quaternary gravel. The bulk of the gold at this locality is concentrated on caliche-cemented false bed rock.
976	Unnamed drywasher site	NE1/4 sec. 12, T. 28 N., R. 19 W.	Au	Very few colors were obtained from this site. One fragment of gold measured 0.5 mm across. In addition, the overall abundance of magnetite in the sand at this site is relatively low.
980	Unnamed drywasher site	NW1/4 sec. 17, T. 28 N., R. 19 W.	Au	Relatively abundant concentrations of magnetite occur in the Tertiary and (or) Quaternary gravel, but only one color was found.
988	Excelsior mine	NW1/4 sec. 22, T. 28 N., R. 18 W.	Pb, Au?	Thin quartz-carbonate veinlets parallel foliation in a highly foliated zone that strikes N. 35°-40° E. The highly foliated shear zone shows silicification, sericitization, and flooding by carbonate; the zone occurs between gneiss and porphyritic monzogranite. The bulk of the alteration and quartz veinlets are concentrated in a zone approximately 7 m wide. The veins include quartz-carbonate-chlorite-pyrite-galena (trace)-gold(?) assemblages.
990	O.D. 1	SW1/4 sec. 22, T. 28 N., R. 18 W.	Pb, Cu, Au?	As much as 0.6 m of well-mineralized quartz occupies a west-northwest-dipping fault zone--possibly the extension of the Excelsior vein system. Abundant cerussite after galena, local concentrations of malachite and chrysocolla staining, and iron oxide pseudomorphs after pyrite.
992	Unnamed prospect	SW1/4 sec. 22, T. 28 N., R. 18 W.	Pb	Shaft 15 m deep shows stoping to that depth along a 0.3- to 1.0-m-thick vertical quartz vein occupying a N. 10° E.-striking sericitized shear zone. Two biotite lamprophyre dikes are visible in main shaft. One dike 15 cm thick crosscuts the vein, and the other, which is 40 cm thick, lies 0.6 m east of the vein. Galena and weathered pyrite occur in the vein quartz.
1031	Unnamed drywasher site	SE1/4 sec. 7, T. 29 N., R. 17 W.	Au	Considerable coarse-grained and fine-grained fragments of gold are associated with a moderate amount of magnetite, some barite, and a considerable amount of cerussite-encrusted galena. The coarse fragments of gold are moderately rounded, whereas the fine fragments are angular.

1036	Unnamed prospects	SW1/4 sec. 8, T. 29 N., R. 17 W.	U?, W?	<p>Radioactivity is as much as seven times background locally in some hot spots. At this prospect a magnetite-bearing leucogranite pegmatite contains cataclastic margins characterized by fine-grained magnetite. The margins of the pegmatite have the highest counts in areas along the hanging wall.</p> <p>A block of skarn occurs in the wash at the prospect. Some calcite, quartz, garnet, pyrite, amphibole, and scheelite(?) were noted in the skarn.</p>
1043	Unnamed prospect	UTM: 756,030 m E., 3,988,780 m N.	Cu	<p>Prospect is east of Burro Springs in the Iceberg Canyon quadrangle. A 1-m-wide quartz vein contains some knots of brown-weathering carbonate, rather abundant pyrite, and a trace of secondary copper staining. The vein occupies a narrow augen gneiss cataclastic zone in an otherwise fresh porphyritic coarse-grained monzogranite.</p>
1071	Lone Jack placer	SW1/4 sec. 15, T. 29 N., R. 17 W.	Au	<p>Yellow-gray distinctly foliated to laminated quartzofeldspathic gneiss (medium grained) is the dominant clast type. Subangular to subrounded boulders as much as 0.6 m in diameter are common. Pyritic vein quartz is present but uncommon, and some pyritic and feldspathic altered wall rock of quartzofeldspathic gneiss is present. Gold and limonite pseudomorphs after pyrite were found northward. Heavily worked in the late 1950's; reportedly fragments of gold greater than 1 mm were very common.</p>
1086	Unnamed prospect	SW1/4 sec. 1, T. 28 N., R. 19 W.	Pb, Cu, Ba?, Fe	<p>A 0.3-m-thick quartz vein containing some iron carbonate, albite, and some minor seams of barite(?) crops out here. Considerable late galena and oxidation products of chalcocopyrite also occur in the vein. The vein occupies a minor normal(?) fault in predominantly amphibolite paragneiss, which includes a lens of well-laminated iron formation, approximately 100 m north-northwest of the 2-m-deep pit at this site.</p>
1087	Unnamed prospects	NW1/4 sec. 1, T. 28 N., R. 19 W.	Cu, Pb?	<p>These workings include approximately 10 m of vertical and inclined shafts. There is considerable chrysocolla, but very little galena, if any. Iron oxides after pyrite are rather abundant.</p>
1095	Senator mine	NW1/4 sec. 14, T. 28 N., R. 19 W.	Cu, Au?	<p>An approximately 100-m-long adit has been driven to crosscut an approximately 0.6-m-thick breccia zone along a shallow-dipping fault zone. The fault zone dips 5°-10° E.-NE. and has a hanging wall of brecciated gneiss and a footwall of two-mica monzogranite. Only traces of secondary copper minerals were noted to occur in the fault zone, approximately 20 m from the portal. The fault zone in the adit also includes some vein quartz.</p>
1096	Buena Vista	SE1/4 sec. 11, T. 28 N., R. 19 W.	Au?	<p>Two quartz lenses as much as 2 m thick and 25 m along strike appear to lie on either side of a shear zone poorly exposed in a small prospect pit at the north end of the lenses. Indications of mineralization are very sparse. Faulting along the shear zone may</p>

TABLE 11.—Notable occurrences of commodities in the Gold Basin-Lost Basin mining districts—Continued

Locality (pl. 1)	Name	Approximate location (UTM 10,000-m grid, zone 11)	Commodities present	Comments
1096	Buena Vista—Continued			
1097	Unnamed site	SE1/4 sec. 11, T. 28 N., R. 19 W.	Cu	have repeated a single lens. There are a few barren-appearing quartz veins in this general area, but no other prospects were noted. Altered amphibolite here shows silicification and flooding by carbonate. In addition, a quartz-carbonate-hematite-pyrite vein crops out here and includes some secondary copper mineral(s). Quartz-white mica-pyrite veins cutting two-mica monzogranite locally include relatively abundant concentrations of galena and trace amounts of secondary copper minerals(?).
1100	Unnamed site	NE1/4 sec. 15, T. 28 N., R. 19 W.	Pb, Cu	Prospect exposing fanglomerate of the Muddy Creek Formation in fault contact with paragneiss. The deep-brick-red and red-brown gouge of the fault zone, however, is not well exposed. The rocks in the lower plate here sporadically include tectonic blocks of crushed and recemented vein quartz similar to the Cyclopic-type ore.
1105	Unnamed prospect	NW1/4 sec. 14, T. 28 N., R. 19 W.	Au?	A lens of crushed quartz as much as 15 cm thick crops out in a prospect here. The prospect exposes these veins as gently east-dipping crosscutting bodies enclosed in crushed, brecciated, and intricately faulted Proterozoic gneiss. The brecciated ore is restricted entirely to a tectonic sliver of gneiss between two-mica monzogranite and fanglomerate.
1106	Unnamed prospect	NW1/4 sec. 14, T. 28 N., R. 19 W.	Au?	Horizontal adit penetrates a low-angle fault, which is in turn offset about 1 m by a high-angle normal fault. An upper prospect nearby is an opencut 15 m long, entirely in mangled gneiss, containing commonly isolated blocks and lenses of crushed quartz. A trace of pyrite was found on one vein fragment.
1107	Unnamed adit	NW1/4 sec. 14, T. 28 N., R. 19 W.	Au?	A 10-cm-thick vein of quartz, epidote, calcite, and fluorite crops out in a sheared and brecciated zone within the granodioritic border facies of the porphyritic monzogranite. Fluorite varies from colorless to purple and occurs together with white coarsely crystalline calcite in veinlets which cut the quartz- and epidote-bearing vein.
1127	Unnamed site	NW1/4 sec. 32, T. 28 N., R. 16 W.	F	Gold-bearing quartz+pyrite+carbonate vein material occurring in a coarse, angular landslide breccia. Trace of gold visible.
1225	Unnamed prospect	NE1/4 sec. 26, T. 28 N., R. 20 W.	Au	Two prospects occur at this locality. In the first prospect, hematitic gossan is apparently associated here with a 30-cm-wide quartz vein
1356	Unnamed prospect	NW1/4 sec. 9, T. 29 N., R. 17 W.	Cu	

originally carrying abundant sulfides, including chalcopyrite. The vein dips moderately and parallels the dip of layering in the enclosing gneiss and leucogranite complex. In the second prospect, a trace of chrysocolla was noted associated with a 1-m-wide quartz vein occupying a minor fault in nearly flat lying amphibolite gneiss.

Gentle inclined adit exposes a 2- to 25-cm-thick zone of massive goethite-hematite lying parallel to the rounding, undulating foliation. Some malachite and chrysocolla on dump. Another shaft is vertical and about 10 m deep; it passes through a flat-lying hematite-goethite-malachite-chrysocolla gossan exposed at the surface by cuts. The country rock is gently dipping amphibole-quartzofeldspathic gneiss and alaskite. This area seems to be dominated by a series of gently dipping quartz sulfide lenses parallel to layering in interlayered amphibole-quartzofeldspathic gneiss. Mineralization in this general area is referred to as Copper Blowout ridge in Deaderick (1980) and Krish (1974). Geochemical studies of minor elements in rocks in this area suggested to Krish that if there is a porphyry copper system buried here, the exposed rocks are above the outermost propylitic fringes of the system.

A vein as much as 25 cm thick contains abundant cerussite, malachite, chrysocolla, and bornite(?).

Cu

NW1/4 sec. 9, T. 29 N., R. 17 W.

Copper Glance 2
(Copper Blowout)

1357

Pb, Cu

SW1/4 sec. 9, T. 29 N., R. 17 W.

White Beauty
(High Voltage)

1359